SOFTENING COAL PYROLYSIS

by

Myongsook Susan Oh

B.S. in Chemical Engineering
University of California, Berkeley (1978)

Submitted to the Department of Chemical Engineering
in Partial Fulfillment of the requirements for the
Degree of

DOCTOR OF SCIENCE

at the

MASSACHUSETTS INSTITUTE OF TECHNOLOGY

March, 1985

Signature of Author _____
Department of Chemical Engineering
March 19, 1985

Certified by _____
Prof. Jack B. Howard
Thesis Supervisor

Certified by _____
Dr. William A. Peters
Thesis Supervisor

Accepted by _____
Prof. William M. Deen
Chairman, Committee on Graduate Students

SOFTENING COAL PYROLYSIS

by

Myongsook Susan Oh

Submitted to the Department of Chemical Engineering
in Partial Fulfillment of the requirements for the
Degree of

DOCTOR OF SCIENCE

at the

MASSACHUSETTS INSTITUTE OF TECHNOLOGY

March, 1985

Thesis Supervisors: Prof. J. B. Howard
Department of Chemical Engineering

Dr. W. A. Peters
Energy Laboratory

Softening Coal Pyrolysis

by

Myongsook S. Oh

Submitted to the Department of Chemical Engineering at the Massachusetts Institute of Technology in March 1985, in partial fulfillment of the requirements for the degree of Doctor of Science.

ABSTRACT

Both experimental and theoretical studies were performed to obtain improved understanding of the pyrolysis behavior of softening coals. Experiments were geared to provide better quantitative information on metaplast formation and depletion kinetics, and to determine the molecular weight distribution (MWD) of metaplast and tar at various stages of pyrolysis. A model was developed to describe the coupled effects of primary and secondary chemical reactions, volatiles transport, and transient plastic behavior during softening coal pyrolysis.

Experiments were performed to measure the yields of volatiles, and of metaplast (the hypothesized plasticizing agent in softening coals) remaining in coal, and to measure the MWD's of metaplast and tar (transported metaplast). The approach was to pyrolyze samples of Pittsburgh No. 8 seam bituminous coal under known time-temperature histories and then to determine the yields of volatiles and the MWD of tar, and the amount and MWD of pyridine extractable material recoverable from the resulting chars. The yield of extract was taken as a measure of the amount of metaplast within the coal at that stage of pyrolysis. The MWD's of the extract and pyrolysis tars were measured by gel permeation chromatograph (GPC). The results show components of similar MW in both the tar and extract, with the latter enriched in high MW components. The number average MW of 1 atm tar is about 350 and the vacuum tar is about 50 gm/mole heavier than 1 atm tar, while that of extracts from 1 atm and vacuum varies between 450 and 500. The volatiles yields, especially tar yield, are higher at lower pressures. However, in context to plasticity, the yields of extracts do not change significantly with pressure.

In the present model, initial decomposition of coal generates gas, char, and metaplast within the coal particle. Some metaplast pre-exists in coal and its amount is estimated from the yield of pyridine extract of untreated coal. Metaplast undergoes further decomposition to form gases and char, and at the same time, is transported to bubbles and to the particle surface. Metaplast vapor in bubbles (also identified as tar) undergoes cracking reactions at high temperatures.

Both gases and metaplast are transported through the melt by growth of bubbles, and by direct diffusion to the particle surface. Bubbles may originate from macropores in solid coal and may also be nucleated from the molten coal. However, bubble nucleation is not a rate-limiting step. The

bubbles grow due to diffusive flux of volatiles and the growth rate is a function of the internal and external pressures of the bubble, the surface tension and viscosity of the coal melt, and the rate of volatiles transfer into the bubble. Expansion of some bubbles sufficiently close to the particle surface causes interfacial rupture and, therefore, release of their contents from the coal. The onset and duration of coal plasticity is modeled as a function of temperature and the metaplast inventory in the molten phase. The increase in melt viscosity inhibits the growth of bubbles and reduces the rate of volatiles diffusion. The swelling of the particle is obtained by calculating the total volume of bubbles and the volume of the molten phase in a particle.

At the onset of plasticity, most of the bubbles originating from micro and intermediate size pores quickly dissolve in the molten phase. Stable size bubbles originate from macropores. In the absence of coalescence, here neglected because of mathematical tractability, bubble growth occurs by diffusion of volatiles from the melt, and the growth of smaller bubbles is faster, causing the bubble size distribution to grow into a narrow size range and allowing it to be approximated as a single size.

Application of the model requires estimating physical properties which are not readily available at present: (1) the more reasonable estimation of metaplast vapor pressure is given by Maiorella's model at low temperatures and by Suuberg's model at high temperatures; (2) the viscosity correlation which models the viscosity as a function of temperature and metaplast concentration at low temperatures and as a function of solely metaplast concentration at high temperatures does a good job of describing the change in plasticity during pyrolysis and predicting volatiles yields; (3) the initial number density of bubbles is best left as a fitted parameter. The best fitting kinetic parameters derived with Maiorella's vapor pressure model give a slightly better fit to the experimental data on volatiles and extract yields than those with Suuberg's vapor pressure model, while the latter more closely predicts measured variations in plasticity during pyrolysis.

Despite the lack of knowledge of many physical properties of molten coal, the modeling of transport in the softened coal in terms of bubble motions along with secondary reactions in both bubbles and the liquid phase predicts the trends in volatiles yields, plasticity, and extent of swelling under various temperatures, pressures, particle sizes and heating rates, thereby strongly support the picture that bubbles play an important role in intra-particle volatiles transport. Improved understanding of the physical properties will help improve the quantitative model predictions.

Thesis supervisors:
Professor Jack B. Howard, Department of Chemical Engineering.
Dr. William A. Peters, Energy Laboratory

Acknowledgements

I am deeply grateful to both of my advisors, Prof. Jack B. Howard and Dr. William A. Peters for their guidance, and continued support and encouragement during the course of this work. Prof. Howard introduced me to the topic and subsquently guided me through many difficult times with extreme patience. Dr. Peters was always generous with his time, and his encouragement at the last phase of this work is deeply appreciated.

Next to my advisors, I thank my thesis commitee members. Prof. J. P. Longwell's helpful comments were invaluable and Prof. R. Brown's advice on the numerical side of this research always saved me from the days of work. Dr. F. Gelbard gave his time generously during his short stay at MIT and his continued interest in this work is gratefully appreciated.

I am grateful to Prof. A. P. Sarofim for the use of the HP plotter, and Prof. E. M. Suuberg of the Div. of Eng., Brown University, for the use of their laboratory and his helpful comments.

My sincere appreciations are due to Dr. Michael Serio, William Fong, and Dr. Georg Schaub for numerous discussions which impoved this thesis significantly and for their friendship. I am specially grateful to Dr. Serio for his invaluable assiatance when I first started this thesis work and also during the course of my experimental work. I also like to thank Dr. Hisham Ettouney for his assistance in numerical and computer problems, and Steve C. K. Lai and C-S Chang for their assistance in experimental work. Thanks are also due to undergraduates who were involved in the experimental work, LaVern Smith, Thomas Lo, and Paul Soltys.

I also like to thank all my friends at MIT and two of my best friends Percila Ip and Joanna Wu Kuriyama. Their love and friendship meant a lot to me all through my stay at MIT.

The financial support of this work and personal support by the U.S. Department of Energy under Contract No's. EX-76-A-01-2295 (Task Order 26), DE-AC21-82MC-19207, and DE-FG22-83PC-60799 are gratefully acknowledged along with personal support by the M.I.T. Department of Chemical Engineering.

Finally, I like to thank my family: my husband, my parents and parents-in-law, and my brothers and sisters, for their love and support. I am especially grateful to my husband whose love and encouragement kept me going in many difficult times, and to my parents, to whom I dedicate this thesis, whose enthusiasm for higher education and for this degree made me go for it first place.

TO MY PARENTS

Table of Contents

List of Figures

List of Tables

1. SUMMARY

1.1. BACKGROUND AND OBJECTIVES

Volatiles products of coal pyrolysis are generated within the coal matrix and their transport out of the particle is accompanied by secondary reactions. In the thermal conversion processes of coal, the intraparticle transport and secondary reactions of volatiles can significantly influence the distribution and yield of pyrolysis products. Quantitative modeling of these processes requires analysis of the transport-kinetics coupling and treatment of the physical structure of the decomposing coal matrix.

The modes of volatiles transport depend upon the plastic behavior of the coal. For non-plastic coals, volatiles are transported by diffusion and hydrodynamic flow through pores. Plastic coals soften to form a fluid-like viscous mass in which volatiles from the primary decomposition form bubbles. Because of the high viscosity of molten coal, bubbles are approximately stationary but they grow by volatiles transport into them. Heavy hydrocarbons or tar species diffuse through the molten coal and evaporate into the bubbles or at the particle surface, and some of these species may undergo secondary reactions to form both lighter and heavier products.

Considerable progress has been made modeling volatiles transport in coal pyrolysis in the case of non-softening coals (Russel et al., 1979; Chen and Wen, 1979; Gavalas and Wilks, 1980), but there has been much less progress in the case of softening coals, despite valuable contributions (Lewellen, 1975; Mills et al., 1976; James and Mills, 1976). The physical structure of softening coals undergoes radical changes during pyrolysis. The decomposing coal is a reacting medium that proceeds successively through solid, solid-liquid-gas, and finally resolidified stages. Mathema-

tical formulation of the coupled effects of transport and chemistry under such conditions is difficult. Futhermore, there is a severe lack of experimental data on the physico-chemical phenomena contributing to the structural modifications, including the rheological behavior of softened coal, volatiles secondary reactions, and the effects of reaction conditions on the intraparticle inventory of coal plasticizing agent, which is called 'metaplast' (Van Krevelen, 1961; Neavel, 1975, 1982).

This thesis work addresses these information deficiencies. The overall objective was to obtain improved understanding of the pyrolysis behavior of softening coals. Specific objectives were the following:

- To obtain kinetic information on metaplast formation and decomposition reactions by recovering metaplast as well as measuring volatiles yields.
- To obtain molecular weight distribution of metaplast, both transported and remaining in the particle, in order to characterize processes which are responsible for metaplast transport.
- To develop a model for softening coal pyrolysis that provides or allows:
  - A better understanding of pyrolytic reactions and the modes of volatiles transport including transport via bubbles.
  - Predictions of volatiles yields and product distribution, changes in plasticity, and the extent of swelling during pyrolysis.
  - Prediction of the independent effects of temperature, pressure, particle size, and heating rate on the yields and composition of pyrolysis products, plasticity, and the extent of swelling.

1.2. EXPERIMENTAL

The experimental objectives were to provide better quantitative information on metaplast formation and depletion kinetics, and to determine the molecular weight distribution of metaplast and tar at various stages of pyrolysis. In this work, tar produced by pyrolysis is viewed as metaplast that has escaped the particles following the work of Unger and Suuberg (1981, 1982). Because the equilibrium vapor pressure of complex organic compounds can be estimated, approximately, from a correlation of temperature and molecular weight, information on the molecular weight distribution of metaplast and tar throughout the pyrolysis cycle is important in modeling the transport of metaplast and, therefore, in modeling the mass balance of metaplast within the softened coal particle.

The weight of material recoverable by solvent extraction of char particles after the coal had undergone pyrolysis via a known time-temperature history is taken as a measure of the amount of metaplast remaining within the coal at that stage of pyrolysis. Similarly, the molecular weight distribution (MWD) of the extracted material is taken as the MWD of metaplast.

1.2.1. Experimental Facilities and Procedures

Pyrolysis: A schematic view of the apparatus is shown in Fig. 1.2.1. The reactor is a batch electrical screen-heater reactor which is designed for pyrolysis measurements of relatively large samples (compared to previous screen-heater experiments on coal) at atmospheric pressure and also at vacuum. Thin layer of about 35 - 40 mg of powdered Pittsburgh #8 seam coal (75-90 μm particle size) were pyrolyzed between the bottom folds of pre-weighed 325 mesh stainless steel screen. The time-temperature history of

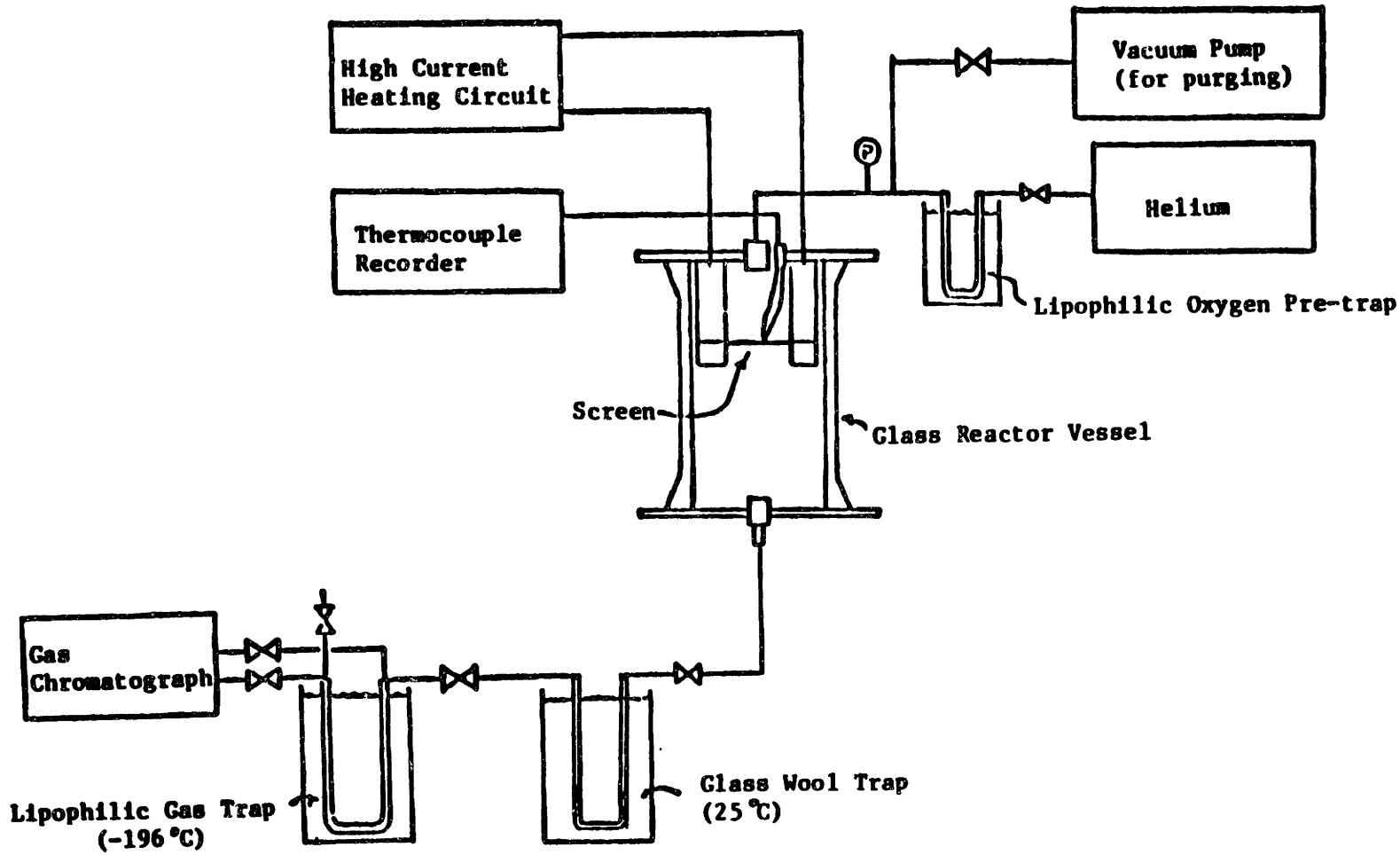

Fig. 1.2.1. **Captive Sample Apparatus**

the coal particles is measured by a chromel-alumel thermocouple (24 μm wire dia. and 75 μm bead dia.) placed within the screen and connected to a fast response recorder. A typical time-temperature history is shown in Fig. 1.2.2. and consists of a linear heating period followed by natural cooling through radiation, conduction and convection.

The screen is reweighed to determine char yield. In previous studies, char as a product has been defined as the condensed phase material retained on the screen upon the completion of the run. In the present work, char is further separated into a solvent extractable material and an unextracted residue. Tar is collected on a piece of filter paper at the reactor outlet and on other reactor surfaces. Some of the tar is dissolved in pyridine as soon as possible for the molecular weight analyses.

Gas products heavier than hydrogen are collected outside the reactor in a trap, consisting of a tube packed with Porapak QS immersed in a dewer flask of liquid nitrogen (-196 °C). Gas and condensible products are analyzed on a Perkin Elmer Sigma 2 chromatograph with dual flame ionization/thermal conductivity detectors. This system is connected to a Sigma 10 data station. Individual yields of CO, CH_4, CO_2, C_2H_2, C_2H_4, and H_2O, and of total C_3's and total C_4+ yields are obtained. The experimetal conditions employed and the product analysis systems are summerized in Fig. 1.2.3.

Solvent Extraction: Extractions of char produced at various peak temperatures are carried out in a Soxhlet extraction apparatus. Pyridine (MW= 79.10, and BP= 115 °C) was chosen to dissolve tar and for extraction of char. The 25 ml of extract solution is removed from the round flask after 2 hours of extraction. After adding 50 ml of new solvent, the char sample undergoes another 16 hours of extraction to ensure complete removal of the

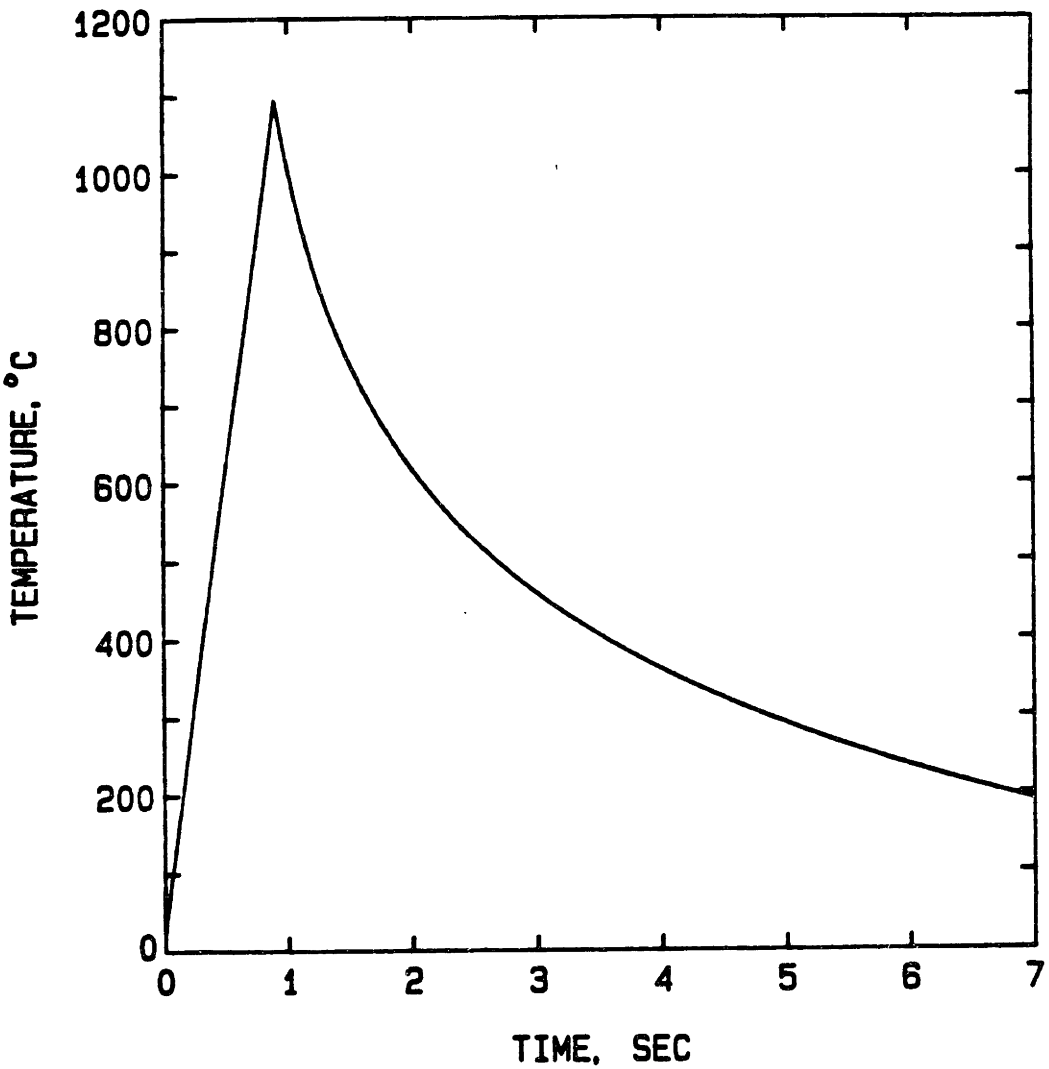

Fig. 1.2.2. Example of typical time-temperature history.
From run 6SA: Peak Temperature = 1100 °C, Pressure = 1 atm

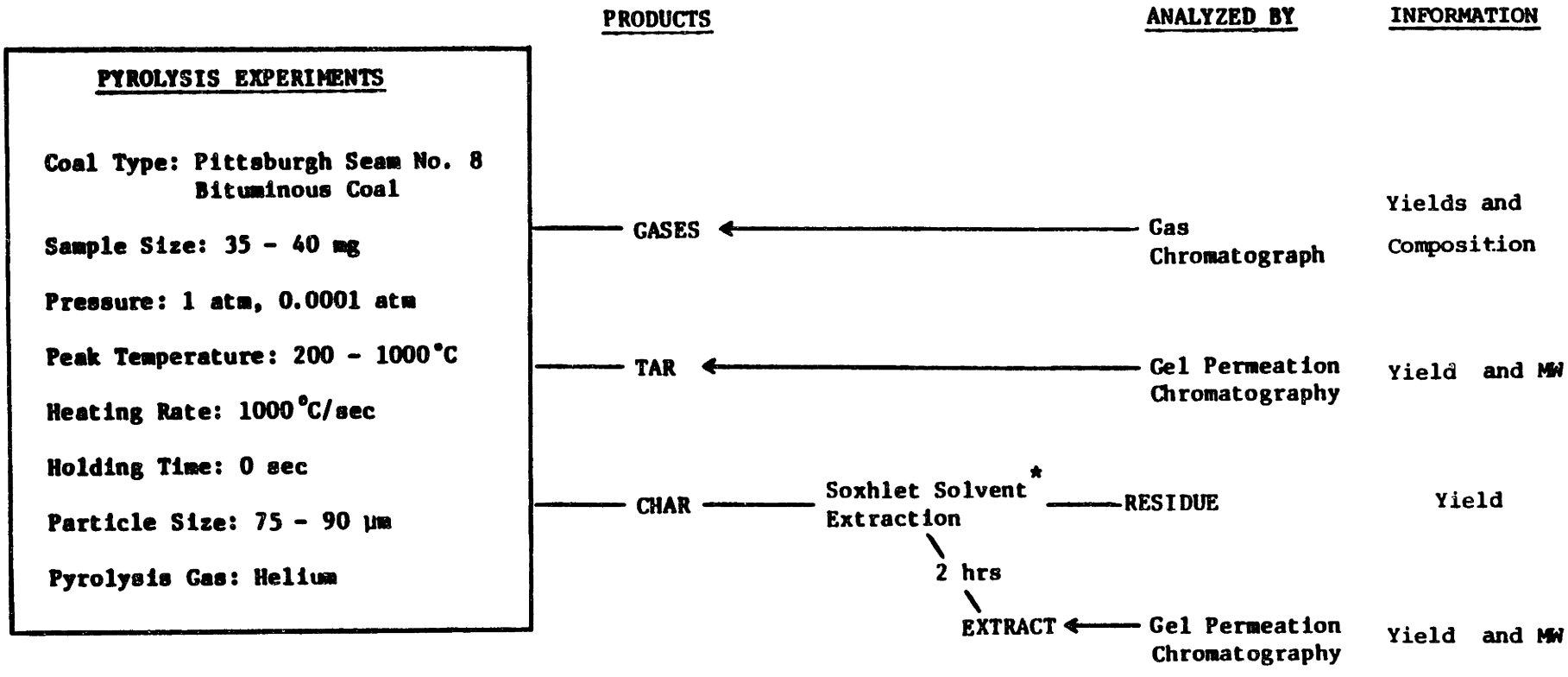

Fig. 1.2.3. Experimental Conditions and Product Analysis Techniques

pyridine soluble material from the char. After the thimble containing the screen and char is dried, the weight loss is determined. The tar solutions and the extracts removed at the 2 hour stage of the extraction are stored in dark bottles and kept in a refrigerator until the analysis of the molecular weight distribution.

Molecular Weight Analysis (Gel Permeation Chromatography): Gel Permeation Chromatography (GPC) has been employed for the analysis of MWD of tar and pyridine extract. GPC separates molecules in solution by molecular size. The chromatograhic system used was a Waters Associates ALC/GPC 201 Gel Permeation Chromatography systems with 500 and 100 $A^{o}\mu$.-syragel columns. The columes were calibrated with tar samples of which the molecular weight is determined using vapor pressure osmometery.

1.2.2. Yields of Volatiles and Extraction Yield

Figures 1.2.4 and 1.2.5 show the total volatiles and tar yields (top) and the yield of pyridine extracts (bottom) as a function of peak temperature at 1 atm and at vacuum (~ 0.0001 atm), respectively. The yields of tar and the total volatiles increase with peak temperature at both pressures and the yields are higher at vacuum. These trends are in agreement with previous studies (Suuberg, 1978).

Extraction of the raw coal yields 30 % weight loss on an as-received basis. The yield of extract decreases with increasing pyrolysis temperature up to ~ 400°C. As the coal starts to soften, the extract yield starts to increase and shows a maximum at ~550°C and then decreases rapidly with further temperature increases. At temperatures between about 650 - 800°C, the rate of depletion of pyridine extract appears somewhat faster at 1 atm than at vacuum.

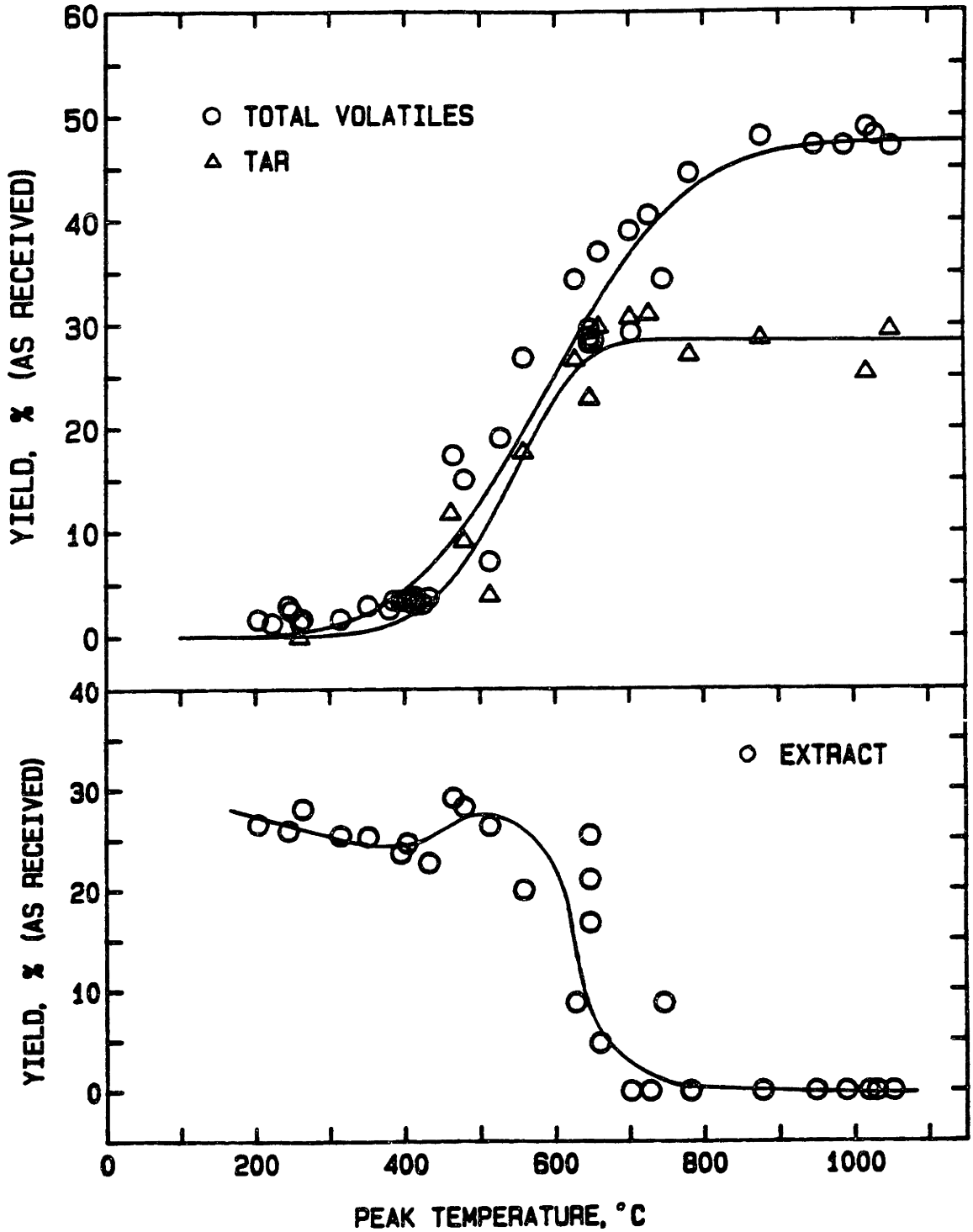

Fig. 1.2.4. Yields of total volatiles and tar (top) and yield of pyridine extracts (bottom) from pyrolysis at 1 atm as a function of peak temperature.

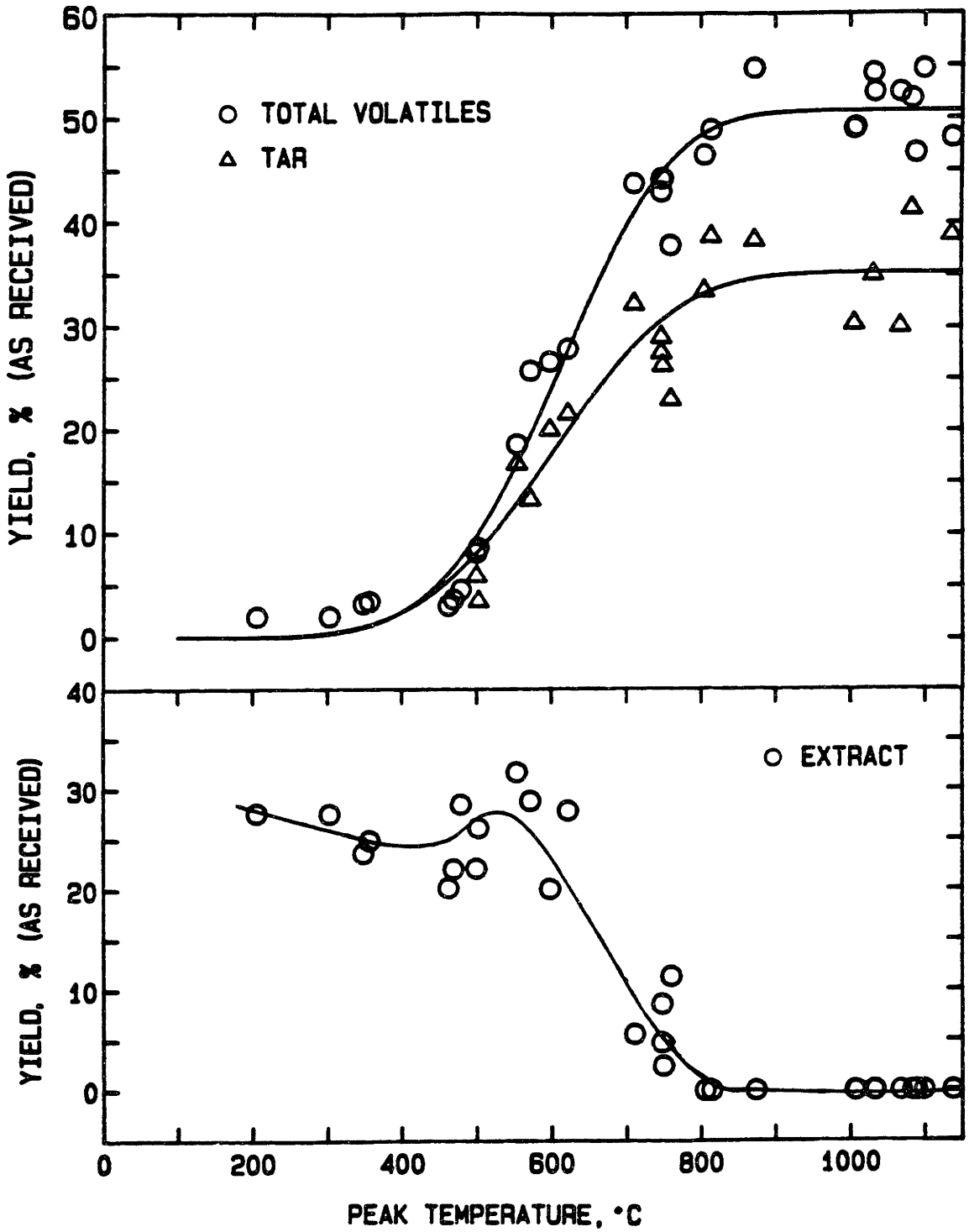

Fig. 1.2.5. Yields of total volatiles and tar (top) and yield of pyridine extracts (bottom) from pyrolysis at vacuum as a function of peak temperature.

These observations can be interpreted as follows. The initial decrease in the extract yield at low temperatures is due to the loss of lower MW molecules (H_2O, CO_2, and CO) as volatiles and to the absence of significant formation of metaplast. As the temperature increases, thermal cleavage of chemical bonds causes an increase in the extract yield and at the same time one also observes a noticible tar yield, i.e. metaplast molecules are now escaping from the reacting medium, allowing them to be 'counted' as tar molecules. At temperatures greater than 550 °C, the formation reactions approach completion, the rate of tar transport becomes faster, and the pyridine extractables are also diminished by secondary cracking and repolymerization reactions within the coal particles. Therefore, rapid depletion of extractible materials is observed and there is no extract yield at temperatures greater than 800°C at 1 atm and 900°C at vacuum. However, the yields of pyridine extract do not reflect pressure effect on transient plasticity.

1.2.3. Molecular Weight Distribution (MWD) of Pyridine Extract and Tar

Examples of the MWD of tar and extract from 1 atm pyrolysis at a peak temperature of 625°C and that of tar from vacuum pyrolysis at a peak temperature of 600°C, are shown in Fig. 1.2.6. 1 atm tar is lower in MWD than the extract, and than vacuum tar. The upper limit of the molecular weight of tar is about 1200 while that of extract is about 1500. However, the fraction of extract material having molecular weight greater 1200 is just a few percent of the total extract. Thus, it is safe to assume that the most of extract and tar have the same range of molecular weight but tar has more of the lighter fractions while extract has more of the heavier fractions. These molecular weight data are consistant with our conceptua-

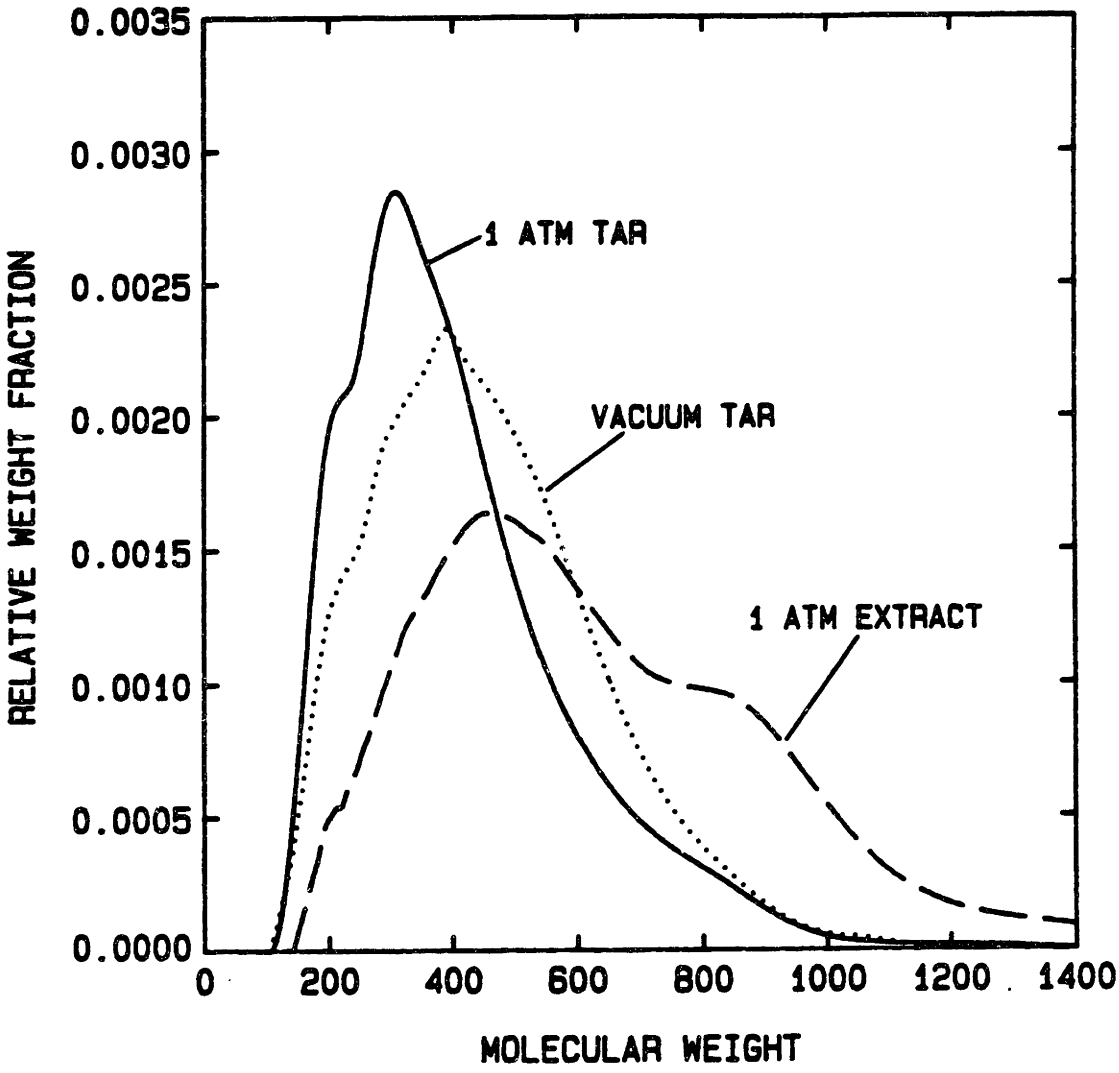

Fig. 1.2.6. Normalized molecular weight distributions of 1 atm tar and extract (Peak Temp = 626°C) and of vacuum tar (Peak Temp = 600°C).

lization of metaplast as unevaporated tar and support (but do not prove) our hypothesis that the yield of pyridine extract is a good estimate of the amount of metaplast remaining in char.

Figures 1.2.7 and 1.2.8 plot the number average molecular weight (MN) of tar and pyridine extract as a function of peak temperature (PT) at 1 atm and at vacuum, respectively. Since no tar is obtained at temperatures below 400°C and no extract at temperatures greater than 800°C at 1 atm and 950°C at vacuum, the data points are restricted to certain temperature ranges. The number average molecular weight of 1 atm tar initially increases, stays about the same and then decreases slightly at PT > 800°C, while the MN of vacuum tar continues to increase as a function of peak temperature. The trends shown in the MN data for the extracts are more interesting; 1 atm extract displays a maximum around 550°C while the MN of the vacuum extracts shows no significant change with increasing PT above 400°C. The MN of vacuum tars are about 50 gm/mole higher than those of 1 atm tars. This observation is in agreement with the evaporation model which predicts that heavier fractions of metaplast are more readily transported at vacuum than at 1 atm. The heavy fraction which is missing in 1 atm tar but present in vacuum tar remains in the char at 1 atm pyrolysis and causes the extract to have a higher MN at around 550°C until this portion is transported or depleted by secondary reactions at high temperatures.

1.3. MODEL DEVELOPMENT

1.3.1. Overall Model Description

As defined earlier, metaplast is the material responsible for the coal

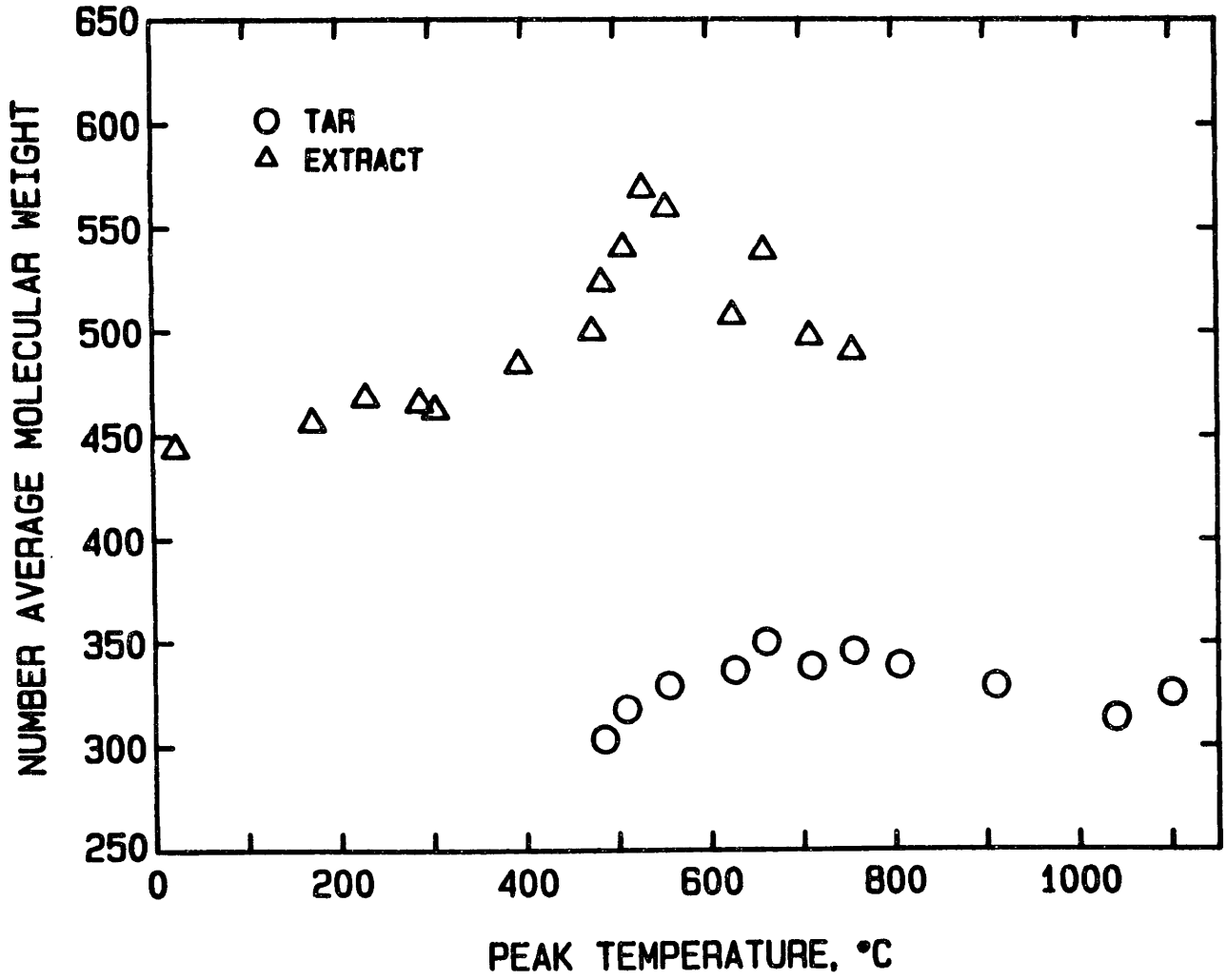

Fig. 1.2.7. Number average molecular weight of 1 atm tar and extract.

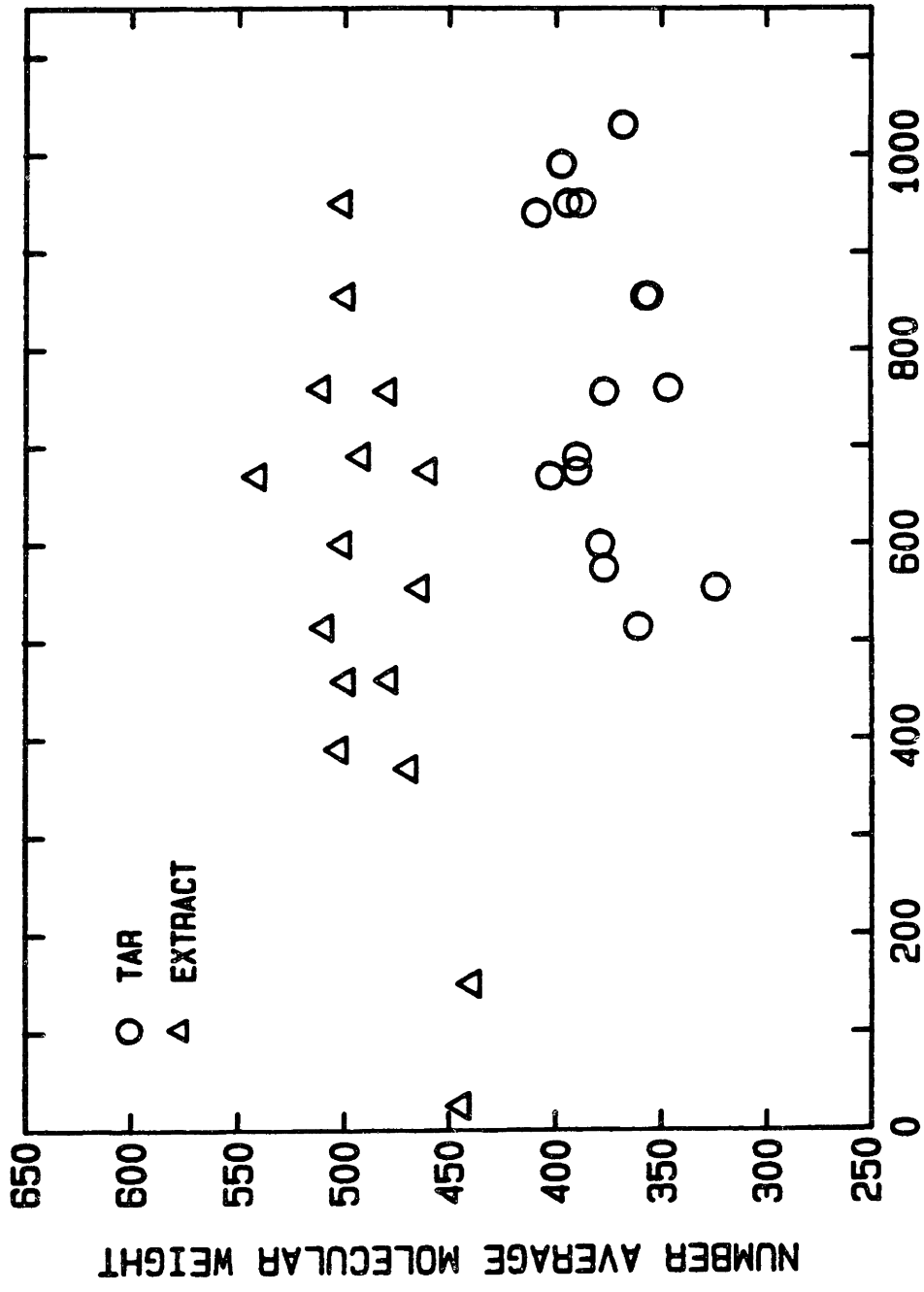

Fig. 1.2.8. Number average molecular weight of vacuum tar and extract.

fluidity. Some of metaplast is assumed to be pre-existing in coal ('bitumen') and as coal is heated to a certain temperature, which is referred as the softening point, the bitumens melt and the coal softens. Further increase of coal temperature causes additional metaplast to form and modifies the plasticity of coal. Therefore, the development of softening is assumed to be both physical transformation ('melting') and pyrolysis. At high temperatures, however, depletion of metaplast due to transport, decomposition, or polymerization reactions causes the coal to be resolidified.

Once coal develops fluidity, viscous flow closes pore mouths and the open pore structure collapses. The volatiles diffuse either to the particle surface or to existing bubbles through viscous melt. The characteristic time for volatiles dissolved in the molten phase to diffuse from the centroid to the surface of a 70 μm diameter particle is of order 100 sec, which is too slow to explain experimentally observed transport behavior of volatiles. The characteristic time for volatiles dissolved in the molten phase to diffuse into existing bubbles is ~ 0.1 sec for a 1-μm bubble radius or less for smaller bubbles. Then volatiles formed at a point in the melt may diffuse into bubbles rather than diffusing to the particle surface. Thus, one can conclude that bubbles may be the primary mechanism by which volatiles leave the particle. The growth of bubbles would also explain swelling behavior.

In modeling the transport of the heavy fraction of metaplast (MW > 1000), the maximum amount that can be transported by bubbles is limited by the vapor pressure of these species, and then diffusion to the particle surface may still be important. Also, transport outside the particle can be rate-limiting for this heavy fraction of metaplast, for example, at high pressure (~ 70 atm) and low temperature (~ 400°C).

Fundamentals of the model are depicted schematically in Fig. 1.3.1.

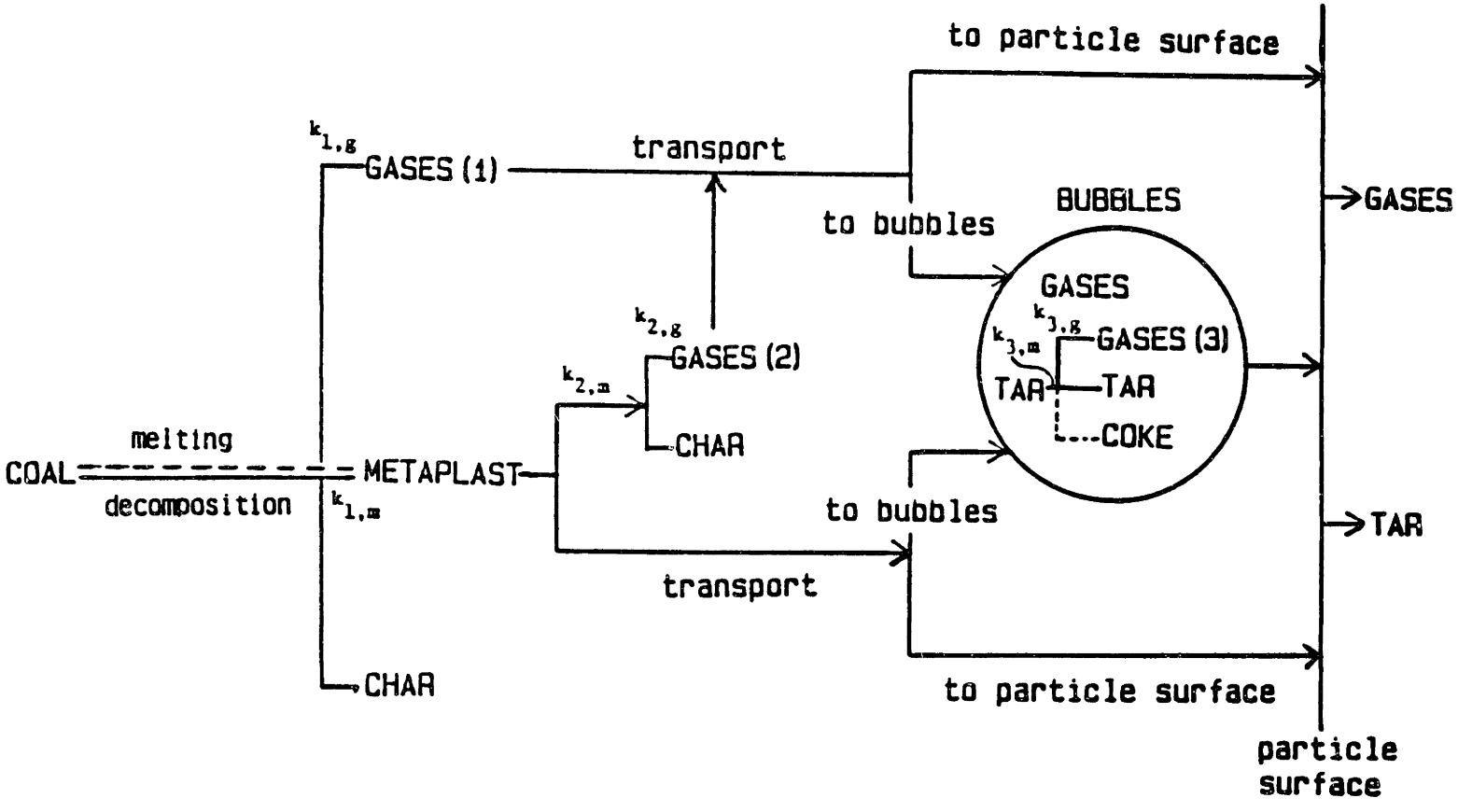

Fig. 1.3.1. Schematic of chemical and transport rate processes contributing to volatiles evolution during pyrolysis of softened coal.

Initial decomposition of coal generates gases, char and metaplast within coal particles. Metaplast further decomposes or polymerizes to form more stable and more aromatic materials as well as light gaseous components. Physical transformation (melting) of pre-existing metaplast to liquid with increasing temperature is denoted by a dotted line. Since vaporized metaplast no longer functions as a plasticizing agent, metaplast vapor in bubbles of the particle is also characterized as tar as well as metaplast transported away from the particle.

The transport of volatiles is assumed to involve diffusion of species dissolved in the coal melt and expansion of bubbles originating from pores in the initial coal or nucleated from the gas, super-saturated in the coal melt. Once bubbles are formed, species formed at a point in the melt may diffuse to bubbles or to the outer surface of the particle. When the surface of an expanding bubble reaches the particle surface, the bubble contents are assumed to be released into the ambient gas, thus simulating the rupturing of bubbles.

1.3.2. Chemical Kinetics

The formation of gases(1) and metaplast is modeled as unimolecular decompositions first-order in the amount of the given material yet to be formed:

$$\frac{dV_i}{dt} = k_i \left(V_i^* - V_i \right) \qquad (1.3\text{-}1)$$

where V_i and V_i^* are amounts of gases(1) or metaplast formed at time t and $t=\infty$, respectively. At t=0, V_i for gases(1) is zero and V_i for metaplast is estimated as the yields of pyridine extractables from raw coal. The formation of gases(1) originates from pre-existing metaplast in coal

and is completed at a low temperature.

The rates of metaplast depletion in the liquid and in bubbles due to secondary reactions and, therefore, the rate of formation of gases(2) and gases(3), respectively, are also modeled as first-order in the amount of metaplast available in each phase:

Metaplast secondary reactions:

In condensed phase: $k_{2,m}\, C_m$ (1.3-2)

In bubbles: $k_{3,m}\, B_m$ (1.3-3)

Gases(2) and gases(3) formation rates:

$$\frac{dV_{g,2}}{dt} = f_{g,2}\, k_{2,m}\, C_m \qquad (1.3\text{-}4)$$

$$\frac{dV_{g,3}}{dt} = f_{g,3}\, k_{3,m}\, B_m \qquad (1.3\text{-}5)$$

where $f_{g,j}$, j=2 or 3, is the fraction of metaplast converted to gases and C_m and B_m are metaplast concentrations in the liquid and in bubbles, respectively, expressed as gm metaplast/gm original coal.

The reaction rate constants, k, with appropriate subscripts, are each expressed as k_o exp(-E/RT) assuming a single-reaction model.

1.3.3. Conservation Equations

To formulate the conservation equations, the particles are assumed to be spatially isothermal and to have a spatially uniform bubble concentration. These assumptions are considered valid for small particles (~ 70 μm) at heating rates less than 1000°C/s.

Bubble Balance

The pores in solid coal are assumed to become bubbles in molten coal and bubbles can be generated by nucleation in the molten coal when the

concentration of gases and vapors exceeds the saturation limit.

Once a bubble is formed, it will grow and coalesce through the following mechanisms: addition of gas molecules by diffusion from the condensed phase; chemical reactions inside or at the surface of the bubble, which include secondary reactions of tar if the concentration of its vapor within the bubble is significant; gross physical force changes such as changes in internal or external pressures; and coalescence with other bubbles.

The growth and coalescence of bubbles is described mathematically as follows. Let n_j be the number of bubbles containing j molecules per unit mass of original coal. Then, the bubble conservation equations are

$$\frac{dn_j}{dt} = K_{j-1}n_{j-1}n_1 - K_j n_j n_1 + \frac{1}{2}\sum_{i=2}^{N-j} P_{i,j-i}n_i n_{j-i} - \sum_{i=2}^{N} P_{ij}n_i n_j - E_{bj}n_j \qquad (1.3\text{-}6)$$

forj from 2 to N, where K_j describes the rate of volatiles diffusion to bubbles; P_{ij} is the rate of coalescence of two bubbles; and E_{bj} is a bubble escape term.

The first two terms in Eq. 1.3-6 are from the growth due to diffusion and $K_j\ n_1$ is the same as the rate of volatiles transport to a bubble where the concentration of monomers is expressed in terms of number of molecules/gm orig. coal. Therefore,

$$K_j = \rho_o\ 4\ \pi a\ D_{v,L}\ Sh\ (\ n_1 - n_{eq}\ )\ /\ n_1 \qquad (1.3\text{-}7)$$

where a = bubble radius; $D_{v,L}$ = diffusivity of the volatiles in the liquid; Sh = Sherwood number of mass transfer; n_{eq} = equilibrium concentration of volatiles at the interface between the molten coal phase and the bubble; and ρ_o = density of condensed phase. The small variations in Sherwood number and ρ_o are ignored; i.e., they are assumed to be constants.

Assuming an ideal solution of gases in molten coal, the equilibrium concentration of gaseous volatiles at the interface is determined by Henry's law, $C_{eq} = P_g/H$, while C_{eq} for metaplast is determined from Raoult's law, $C_{eq} = P_{t,i}/P_v$. P_g and $P_{t,i}$ are the partial pressure of gases and metaplast component in bubbles and P_v is the vapor pressure of metaplast.

The coalescence of two bubbles is assumed to occur due to the expansion of two adjacent bubbles. For the spherical bubbles with radii a_i and a_j, of which the centers are stationary because of high melt viscosity, while the surfaces expand radially with the velocity of $\dot{a}_i$ and $\dot{a}_j$, the rate constant, P_{ij}, is

$$P_{ij} = \rho_o 4\pi (a + b)^2 (|\dot{a}| + |\dot{b}|) \qquad (1.3\text{-}8)$$

where the bubble concentration is based on gm original coal.

The rate of bubble expansion, $\dot{a}$, is affected by mechanical forces such as the internal and external pressures of the bubble, surface tension, and inertial and viscous forces, as well as by the rate of mass transfer into the bubble, and is derived assuming: a constant fluid density, viscosity and surface tension; the liquid behaves as a Newtonian fluid; liquid density>>gas density; and bubble radius << distance between bubbles (Scriven, 1959; Barlow and Longlois, 1962). In a very viscous liquid like molten coal, the inertial terms are small compared to the viscous term and the bubble growth rate is

$$\dot{a} = \frac{da}{dt} = \frac{a}{4\mu} \left(P_b - P - \frac{2\sigma}{a} \right) \qquad (1.3\text{-}9)$$

where P_b = total bubble pressure, i.e., the sum of gas pressure and vapor pressure of metaplast$_i$; P = ambient pressure; μ = fluid viscosity; σ = surface tension. The coal may swell to an extreme extent and form a

cenosphere. Then, Eq. 1.3-9 is an oversimplification. However, within the uncertainties in the knowledge of melt viscosity, the viscous force is a dominant term. The above simplified equation with a reasonable description of viscosity provides a first approximation to the bubble growth rate.

Assuming all the bubbles colliding with the particle surface break through the surface and escape from the particle, the collision rate to the particle surface is

$$4\pi (R_p - a_j)^2 \; \dot{a}_j \; C_j \qquad (1.3\text{-}10)$$

The bubble escape rate of bubbles sized a_j per gm original coal is

$$E_j = \frac{4\pi (R_p - a_j)^2 \; \dot{a}_j}{\frac{4\pi}{3} R_{p,o}^3} \qquad (1.3\text{-}11)$$

where R_p and R_{po} are the coal particle radius at t and t=0, respectively.

Even though the mass is conserved, the number of molecules in bubbles may vary owing to secondary reactions. However, for simplicity, this effect is not included in the above bubble conservation equation but will be included in a simplified bubble conservation equation.

Mass Balance of Gases and Metaplast

The material balance of either gases or metaplast in the condensed phase includes the rate of formation and the rate of transport to bubbles and to the particle surface. An additional term is included for metaplast to account for its depletion by secondary reactions. Let C_g and C_m be the gas and metaplast concentration in the melt, and let $K_{j,g}$ and $K_{j,m\,i}$ be K_j for gases and metaplast component i, respectively. Assume that all gases have the same molecular weight and that the rates of formation and secondary reactions are the same for all molecular

weights of metaplast. The mass balance of gases is

$$\frac{dC_g}{dt} = k_{1,g}\,(V_g^* - V_{g,1}) + f_{g,2}\,k_{m,2}\sum_{i=1}^{N_{tar}} C_{m,i} - \sum_{j=2}^{N} K_{j,g} n_{1,g} n_j - E_g\,C_g \qquad (1.3\text{-}12)$$

and for metaplast

$$\frac{dC_{m,i}}{dt} = k_{1,m}\,(V_{m,i}^* - V_{m,i}) - k_{1,g}\,(V_{g,1}^* - V_{g,1}) - k_{m,2}\,C_{m,i} - \sum_{j=2}^{N} K_{j,m} n_{1,j} n_j - E_{m,i}\,C_{m,i} \qquad (1.3\text{-}13)$$

for $i = 1, \ldots N_{tar}$, where N_{tar} is the total number of metaplast components of different molecular weight. E_g, the rate of gaseous volatiles diffusion from the particle surface is obtained from the steady-state balance of gases dissolved in the coal melt by taking the flux at the particle surface:

$$E_g = \frac{3R_p^2}{R_{po}^3}\,D_{g,L}\left[\frac{K_j\,n_j}{D_{g,L}}\right]^{\frac{1}{2}} \qquad (1.3\text{-}14)$$

Since the rate of mass transfer to bubbles is relatively fast and the gas concentration in the molten phase is around its saturation level, which corresponds to an amount that is small compared to the amount of gases formed, the above pseudo steady-state approach is appropriate to derive the rate equation for gaseous volatiles transport to the particle surface. However, the amount of metaplast transported to bubbles varies significantly with temperature and the steady-state approach is not suitable for metaplast. The rate of diffusion through the melt is derived assuming a parabolic concentration profile which satisfies the appropriate boundary conditions.

$$-D_{m,L} \left.\frac{dC}{dr}\right|_{r = R_p} = \frac{5\, D_{m,L}}{R_p} (C_m - C_s) \qquad (1.3\text{-}15)$$

where C_s is the concentration of metaplast at the particle surface. Since the external mass transport of metaplast can be important, for example, for the case of low temperature and 70 atm, both mass transfer resistances of metaplast, outside and inside the particle, are included in this study in order to allow the model to be applied to a wide range of molecular weights, i.e., MW > 1500, and at various temperatures and pressures.

$$E_{m,i} = \frac{3\, R_p}{R_{po}^3} \frac{1}{\frac{1}{D_{m,g}} \frac{P}{P_{v,i}} \frac{\rho_L}{\rho_g} + \frac{1}{5\, D_{m,L}}} \qquad (1.3\text{-}16)$$

The yields of volatiles are obtained from E_g, E_m, and E_b:

$$\text{Gas Yield} = \int (E_g\, C_g + \sum_{j=2}^{N} B_{g,j}\, E_{b,j}\, n_j)\ dt \qquad (1.3\text{-}17)$$

$$\text{Tar Yield} = \int (\sum_{i=1}^{N_{tar}} E_{m,i}\, C_{m,i} + \sum_{j=2}^{N} \sum_{i=1}^{N_{tar}} B_{mi,j}\, E_{b,j}\, n_j)\ dt \qquad (1.3\text{-}18)$$

$B_{g,i}$ and $B_{mi,j}$ are the mass of gases and metaplast i in bubble size j. The extent of swelling is calculated from the number density of bubbles and bubble radii assuming the density of the liquid phase stays constant.

The models for physical properties are summarized in Table 1.3.1.

1.4. RESULTS AND DISCUSSION

1.4.1. Model simplifications

The bubbles were assumed to grow solely by diffusive influx of vola-

Table 1.3.1. Summary of correlations for physical properties[1]

Melt viscosity[2]:

Model A: $$\mu = \frac{1 \times 10^{-10} \exp(45{,}000/RT')}{(1 - \phi)^{-1/3} - 1.0}$$

Model B: $$\mu = \frac{1 \times 10^{-7} \exp(45{,}000/RT)}{(1 - \phi)^{-1/3} - 1.0}$$

where ϕ = wt fraction of metaplast
T' = T (K) at temperatures < 450°C
T' = 723 K at temperatures > 450°C

Diffusivity of volatiles in molten coal:

$$D_v = \frac{1 \times 10^{-7} \cdot T}{\mu^q}$$

q = 0.5 for gases and 2/3 for metaplast

Vapor pressure of Metaplst

Maiorella's Model[3]:

$$P_v = 6.311 \times 10^{11} \exp(-561\ MW^{0.474} / T) \quad [dyne/cm^2]$$

Suuberg's Model[4]:

$$P_v = 5.814 \times 10^{9} \exp(-255\ MW^{0.576} / T) \quad [dyne/cm^2]$$

Surface tension[5]: 30 erg/cm^2

Solubility of gas in molten coal: $$H = \frac{2.792 \times 10^{7} \exp(314/T)}{\rho_L'}$$

ρ_L' = molar density of molten phase

Molecular weight distribution of metaplast at formation: See Fig. 1.3.2

Macropore volume[6]: 0.04 cm^3/gm coal

---

1. Unless otherwise noted, the correlations are developed in this study.
2. Nazem (1980), Frankel and Acrivos (1967), and this study
3. Maiorella (1978)
4. Suuberg and Unger (1981)
5. Attar (1978)
6. Gan et al. (1972)

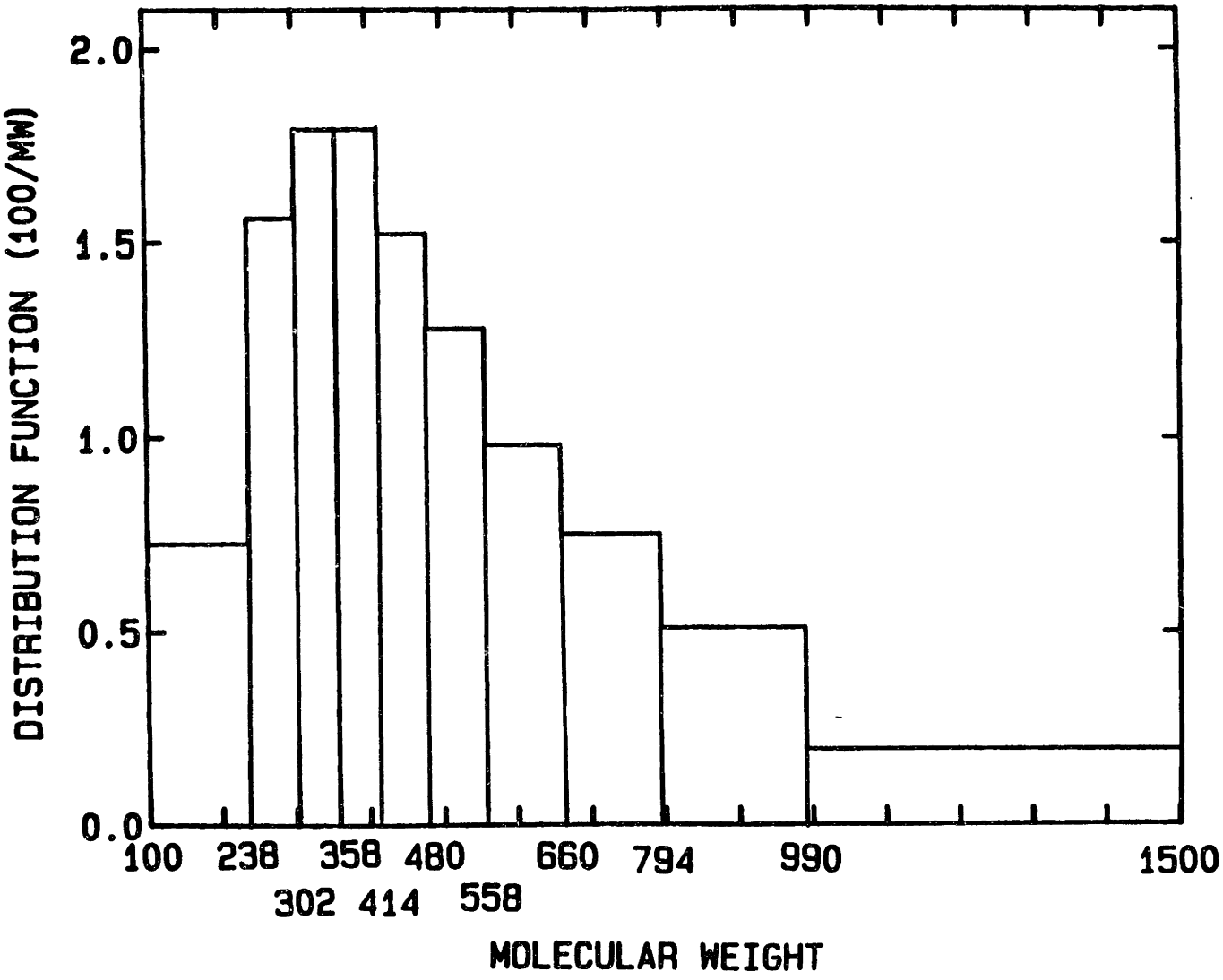

Fig. 1.3.2. Molecular weight distribution of metaplast at formation. Inferred from MWD of tar and pyridine extract from low temperature pyrolysis at 1 atm.

tiles because of numerical complications arising from the coagulation kinetics. Fig. 1.4.1 plots the changes in the bubble size distribution at various time and shows that the growth of the bubbles shifts the bubble size distribution to the larger bubble sizes and the rapid growth of smaller bubbles leads to a large fraction of the volatiles mass being in bubbles near the minimum size. Thus, one can conclude that even though a wide spectrum of bubble sizes is considered, the bubbles grow into practically one size and essentially all the mass transport to bubbles is associated with the smallest stable size bubbles. This important result allows the governing equation of bubbles to be simplified by eliminating the bubble size distribution, thereby considering only uniformly sized bubbles.

1.4.2. Bubble Generation

The model treats pores in the solid coal as one source of bubbles. Some of the pores, more likely the macropores, are assumed to have survived the coal softening, and to grow by accepting volatiles from the pyrolyzing medium.

The other mechanism considered is nucleation of bubbles. Application of nucleation rate theory to provide the bubble generation rate is considered to be not justified, due to the large uncertainties involved in the rate function for the inhomogeneous medium of molten coal. Instead, calculations were made to test whether the nucleation of bubbles can be a rate-limiting step in the transport processes for the pyrolysis conditions of interest. It was concluded that within the uncertainties in the solubilities of volatiles in the molten coal, the nucleation of bubbles is not a rate limiting process. Thus, one can assume that the nucleated bubbles as well as the ones originating from the pores are already present in the

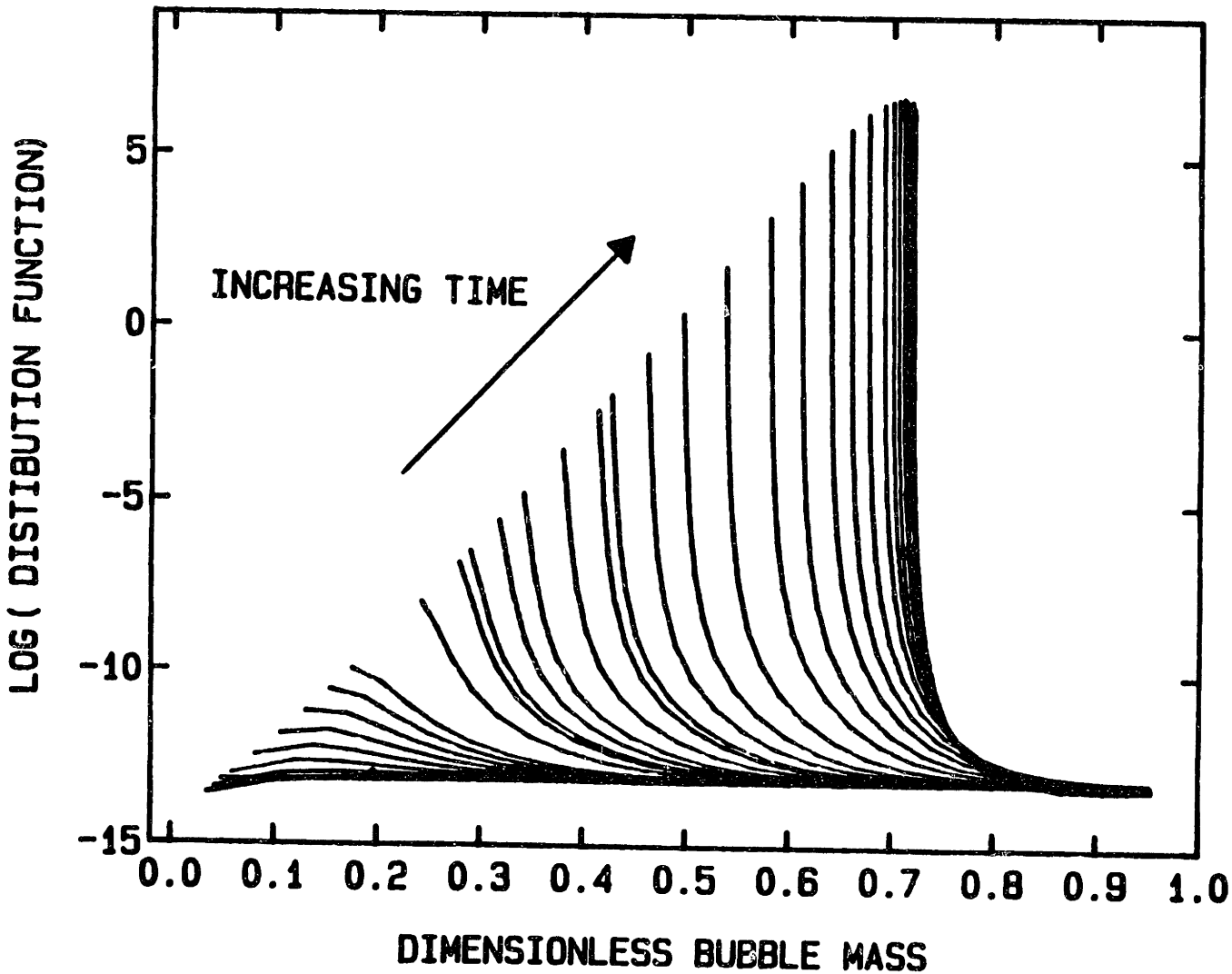

Fig. 1.4.1. Time dependant variations in bubble size distribution. Growth of bubbles at section boundaries as a function of time. Single molecular weight volatiles, constant temperature and viscosity, and no coagulation of bubbles are assumed. Dimensionless bubble mass = $\ln(v/v_{min})/\ln(v_{max}/v_{min})$ where v is the mass of a bubble.

molten coal at the onset of softening. The number density of bubbles then decreases as bubbles are released from the particle.

1.4.3. Calculation of Kinetic Parameters and Model Predictions

Since gases(1) are assumed to be formed at low temperatures (< 400°C) from pre-existing metaplast, the parameters, $k_{o1,g}$, $E_{1,g}$, and V_g^*, are obtained from the volatiles yields at peak temperatures lower than 400°C from both 1 atm and vacuum pyrolysis, without any transport model.

The parameters for tar craking reactions in bubbles and the formation of gases(3) are obtained from the work by Serio (1984).

The kinetic parameters for metaplast formation and decomposition reactions and formation of Gases(2) ($E_{1,m}$, $k_{o1,g}$, $E_{2,m}$, $k_{o2,g}$, and $f_{g,2}$) were determined form the complete transport model and the pyrolysis data at peak temperatures > 400°C at 1 atm. The ultimate amount of metaplast that can be formed, V_m^*, was treated as a fixed value (V_m^*=0.7 gm/gm orig. coal).

In addition to the 5 kinetic parameters, the initial number density of bubbles is also left as a variable. In the calculation of kinetic parameters, the initial number density of bubbles plays an important role. A high number density results in fast metaplast formation and slow liquid phase decomposition reactions, while a low number density gives slow metaplast formation rate and fast liquid phase secondary reactions at high temperatures. Since not much is understood about the initial number density of bubbles and its generation rate at different conditions of pyrolysis, the initial number density of bubbles at the onset of softening is left as a variable to be fitted.

The best fitting model parameters were calculated for the following three different cases, each distinguished by the vapor pressure model or viscosity model employed (See Table 1.3.1 for details):

Case	Vapor Pressure Model		Viscosity Model	
	Maiorella	Suuberg	Temp-Restricted (Model A)	No Temp Restriction (Model B)
A	X		X	
B		X	X	
C	X			X

Table 1.4.1 summarizes all kinetic parameters including 6-parameters obtained using Maiorella's vapor pressure model (Case A). The 3 sets of the 6-best fitting parameters for the three cases listed above are compared in Table 1.4.2. Figs. 1.4.2 through 1.4.4 plot the model predictions of total volatiles yields, tar yields, and the amount of metaplast remaining in the particle, repectively, with the experimental data. The model predictions made with Maiorella's vapor pressure model (Case A) are in the best agreement with experimental data among the three cases considered. However, the correlation by Maiorella seems to overpredict the vapor pressure of metaplast at high temperatures and to cause a large fraction of metaplast to vaporize into bubbles, resulting a low concentration of metaplast in liquid and thus, resolidification of coal. Also, most of the secondary gases are formed by tar cracking in bubbles, and the model predicts a large fraction of the secondary gases is trapped in bubbles (~ 7 wt % at peak temperature 1000°C). Since the model does not treat the transport through pores after the coal resolidifies, any gas trapped in bubbles upon resolidification is assumed eventually to diffuse out of the particle and is included in the yield of gases.

The correlation by Suuberg does not predict a high enough vapor pressure to explain the tar yields at low temperatures. As a result, the

Table 1.4.1. Summary of model kinetic parameters: both input kinetic parameters (regular type) and 6-best fitting parameters (bold type) for Case A[1].

Gases(1) formation reactions[2]	
Amount of gases(1) formed at $t=\infty$ (V_g^*)	0.0285 gm/gm orig coal
Activation Energy ($E_{1,g}$)	26,755 cal/mole
Pre-exponential constant ($k_{o1,g}$)	1×10^{13} 1/sec
Metaplast formation reactions	
Amount of metaplast formed at $t=\infty$ (V_m^*) [3]	0.7 gm/gm orig coal
Activation energy ($E_{1,m}$)	**21,690 cal/mole**
Pre-exponential constant ($k_{o1,m}$)	**2.875×10^6 1/sec**
Liquid phase decomposition reactions of metaplast	
Activation energy ($E_{2,m}$)	**18,803 cal/mole**
Pre-exponential constant ($k_{o2,m}$)	**2.976×10^5 1/sec**
Fraction of metaplast converted to gases(2) ($f_{g,2}$)	0.053
Tar cracking reactions in bubbles[4]	
Activation energy ($E_{3,m}$)	15,400 cal/mole
Pre-exponential constant ($k_{o3,m}$)	9.96×10^2 1/sec
Fraction of metaplast converted to gases(3) ($f_{g,3}$)	1
Pore size (a_{pore})	**0.0757** μm

1. Employs Maiorella's vapor pressure model and the viscosity model with temperature restrictions (Model A). Pyrolysis data at peak temperature > 400 C are used.
2. Obtained form pyrolysis data at low peak temperatures. $k_{o1,g}$ is a fixed parameter.
3. Fong (1984)
4. Serio (1984)

Table 1.4.2. Effect of vapor pressure and viscosity correlations on kinetic parameters: Comparison of kinetic parameters from two vapor pressure models and two viscosity models.

	(A)[1]	(B)[2]	(C)[3]	
$E_{1,m}$	21,690	16,083	43,759	cal/mole
$k_{o1,m}$	2.875×10^6	3.195×10^4	1×10^{13}	1/sec
$E_{2,m}$	18,803	16,860	25,853	cal/mole
$k_{o2,m}$	2.976×10^5	2.964×10^4	3.476×10^7	1/sec
$f_{g,2}$	0.053	0.284	0.205	
a_{pore}	0.0757	0.0799	0.0936	μm

1. Case A: Maiorella's vapor pressure model and the viscosity model with temperature restriction (Model A)
2. Case B: Suuberg's vapor pressure model and the viscosity model with temperature restriction (Model A)
3. Case C: Maiorella's vapor pressure model and the viscosity model with no temperature restriction (Model B)

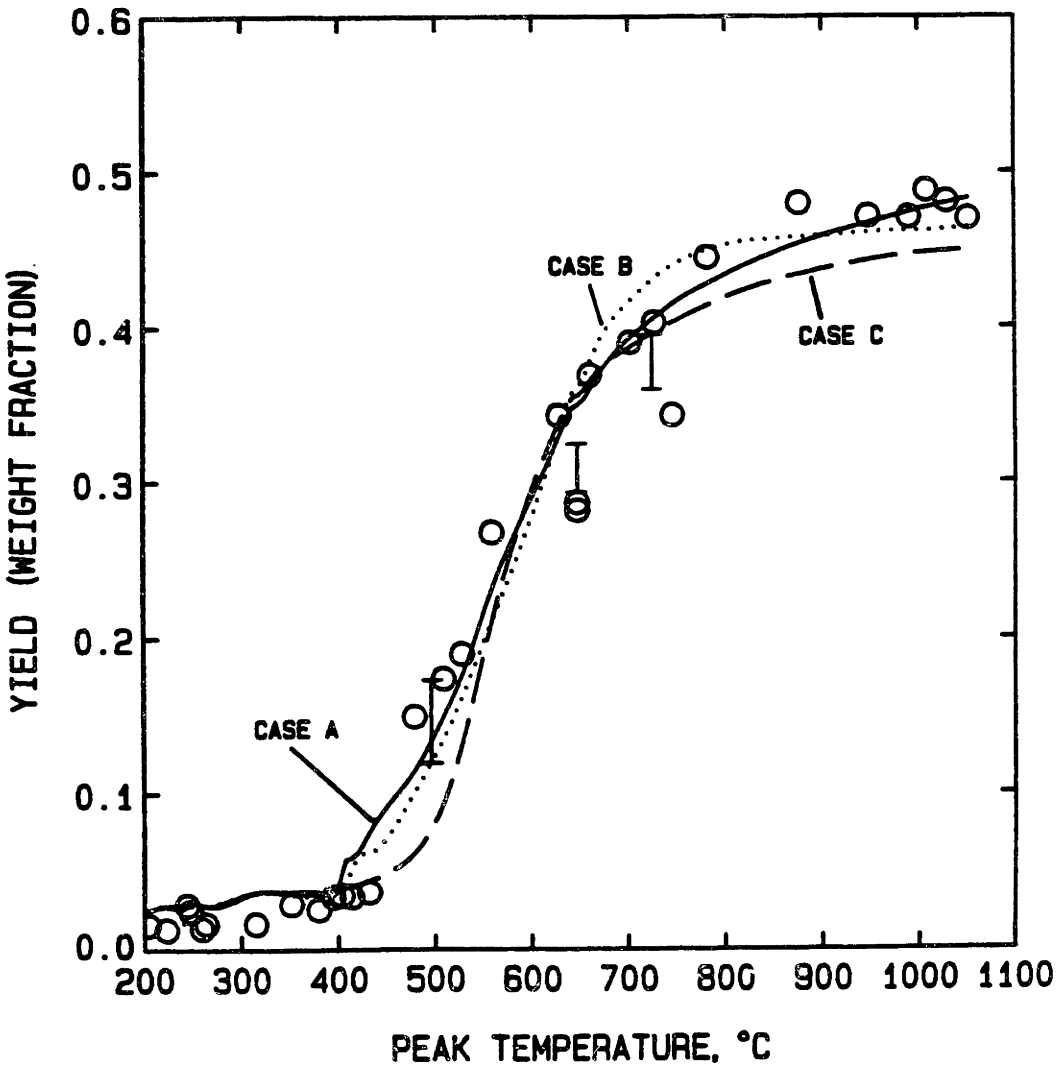

Fig. 1.4.2. Yields of total volatiles from pyrolysis of Pittsburgh Seam bituminous coal heated to different peak temperatures at 1 atm with model predictions for three different cases, each distinguished by vapor pressure model and viscosity model employed. Vapor pressure model, viscosity model and model kientic parameters for each case are listed in Table 1.4.2.

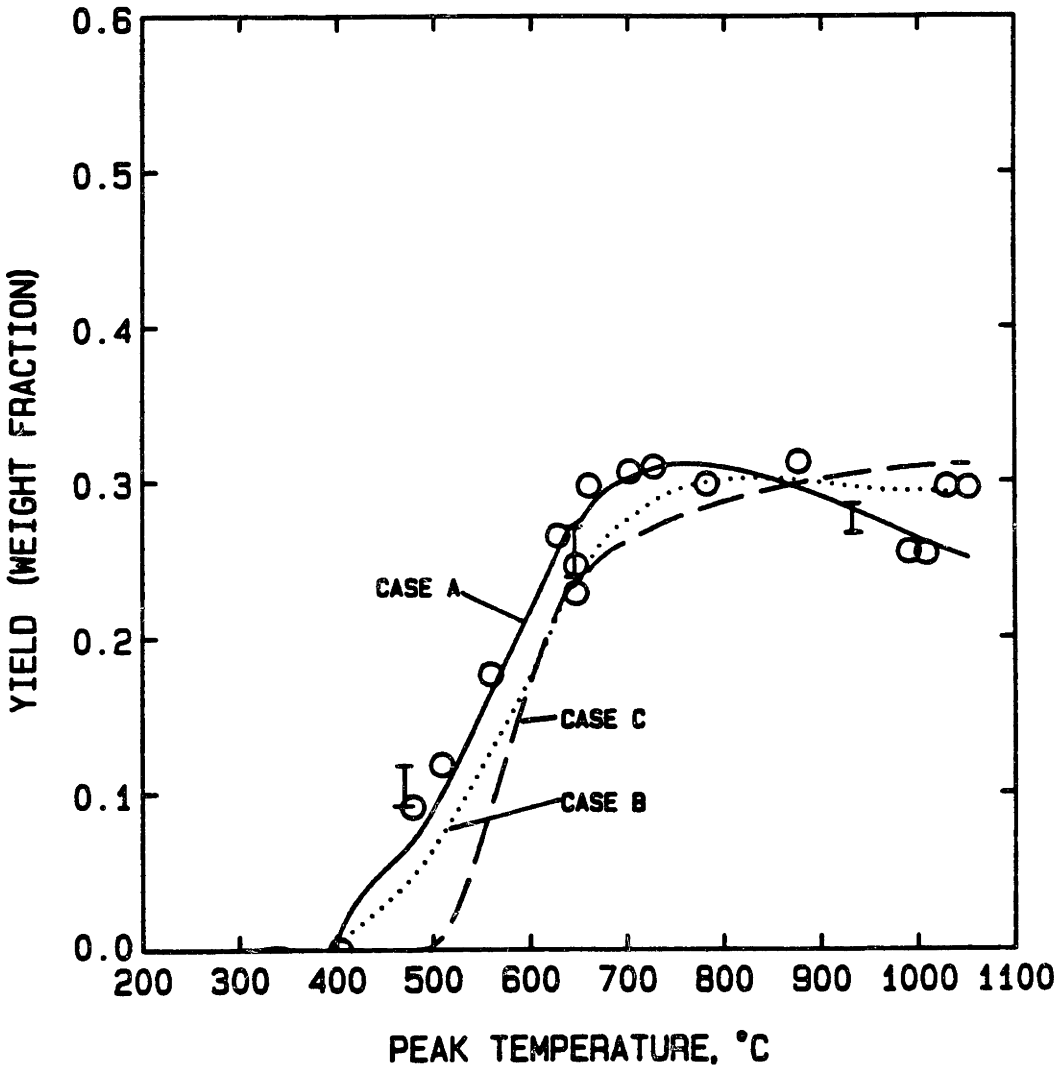

Fig. 1.4.3. **Yields of tar from pyrolysis of Pittsburgh Seam bituminous coal heated to different peak temperatures at 1 atm with model predictions for three different cases.** See Table 1.4.2 for details.

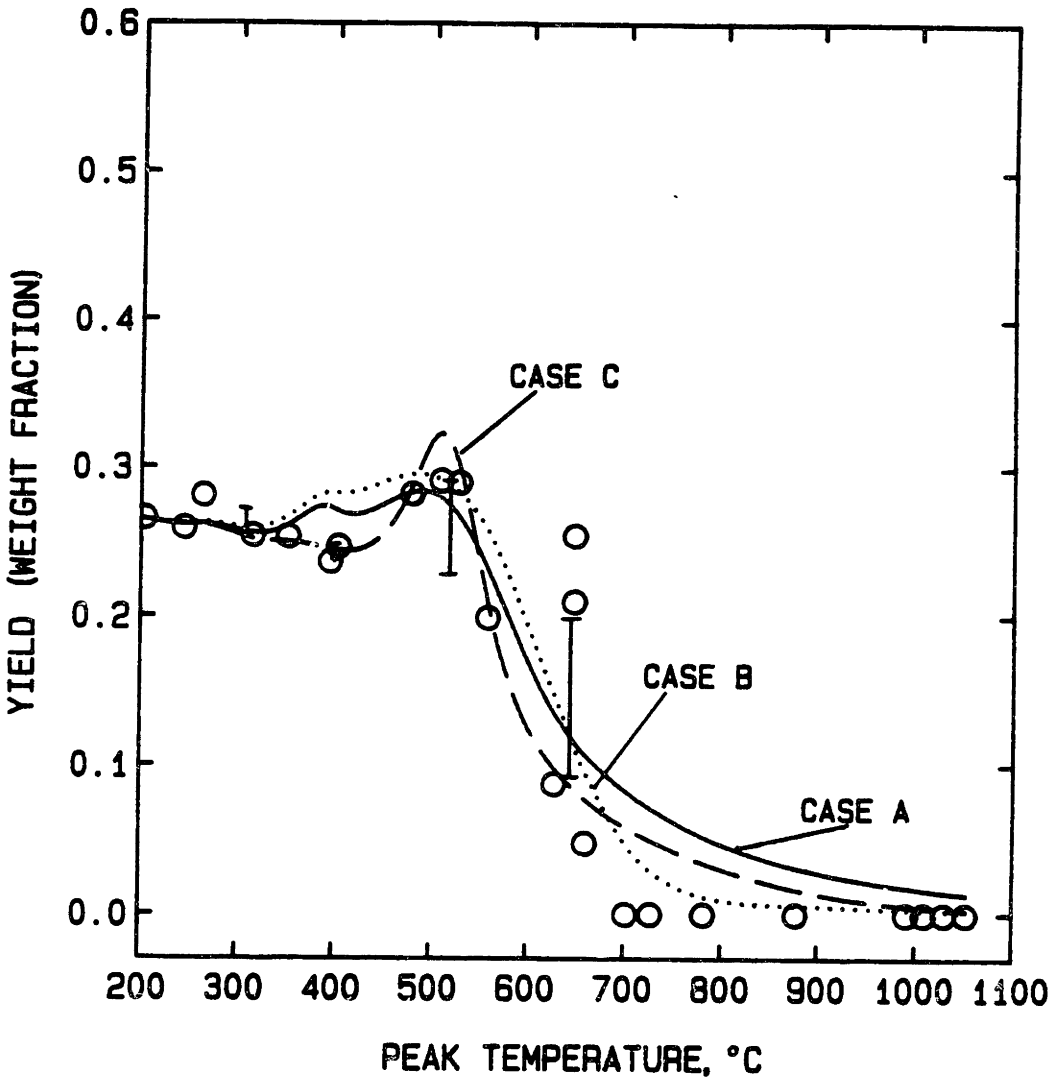

Fig. 1.4.4. Yields of pyridine extract ('metaplast surrogate') of the solid residue produced from pyrolysis of Pittsburgh Seam bituminous coal heated to different peak temperatures at 1 atm with model predictions for three different cases. See Table 1.4.2 for details.

model predictions of integral yields of pyrolysis products at different peak temperatures do not fit the data as well as Case A. The predicted vapor prssure at high temperatures, however, seems to be more reasonable than that by Maiorella's model. In this case, the metaplast depletion results from both transport and decomposition reactions, and more of the secondary gases are formed from the liquid phase reactions.

With the viscosity correlations which includes temperature dependence at all temperatures (Model B), the model predictions show poor fits to all three sets of data. This behavior can be explained by the variations in the melt viscosity. The predicted melt viscosities at a heating rate of 448°C/s and a peak temperature of 760°C are plotted as a function of time in Fig. 1.4.5. This particular time-temperature history was chosen to compare the model predictions with the measured viscosity, shown in Fig. 1.4.6. The μ predictions for Case C show a sharp minimum at 1.27 sec and the plastic period is much shorter than the other two cases. Thus, the higher viscosities at both low and high temperatures inhibit the growth of bubbles and, therefore, the model predicts lower volatiles yields. It is encouraging to see that the model's ability to predict the viscosity parallels with its ability to fit volatiles yields, to some extent.

In the viscosity predictions for Case A, the resolidification of the coal occurs as soon as the peak temperature is reached because the depletion of metaplast occurs due to the overpredicted transport of metaplast to bubbles. The predicted plastic period is shorter than the measured value. The predictions of viscosity with Suuberg's vapor pressure model agrees well with the measured viscosity.

The model predictions of the extent of swelling for the same time-temperature history are a bit higher than expected. Whereas, the observed swelling ratio of a single particle varies between 0.9 and 4 (Sung, 1978;

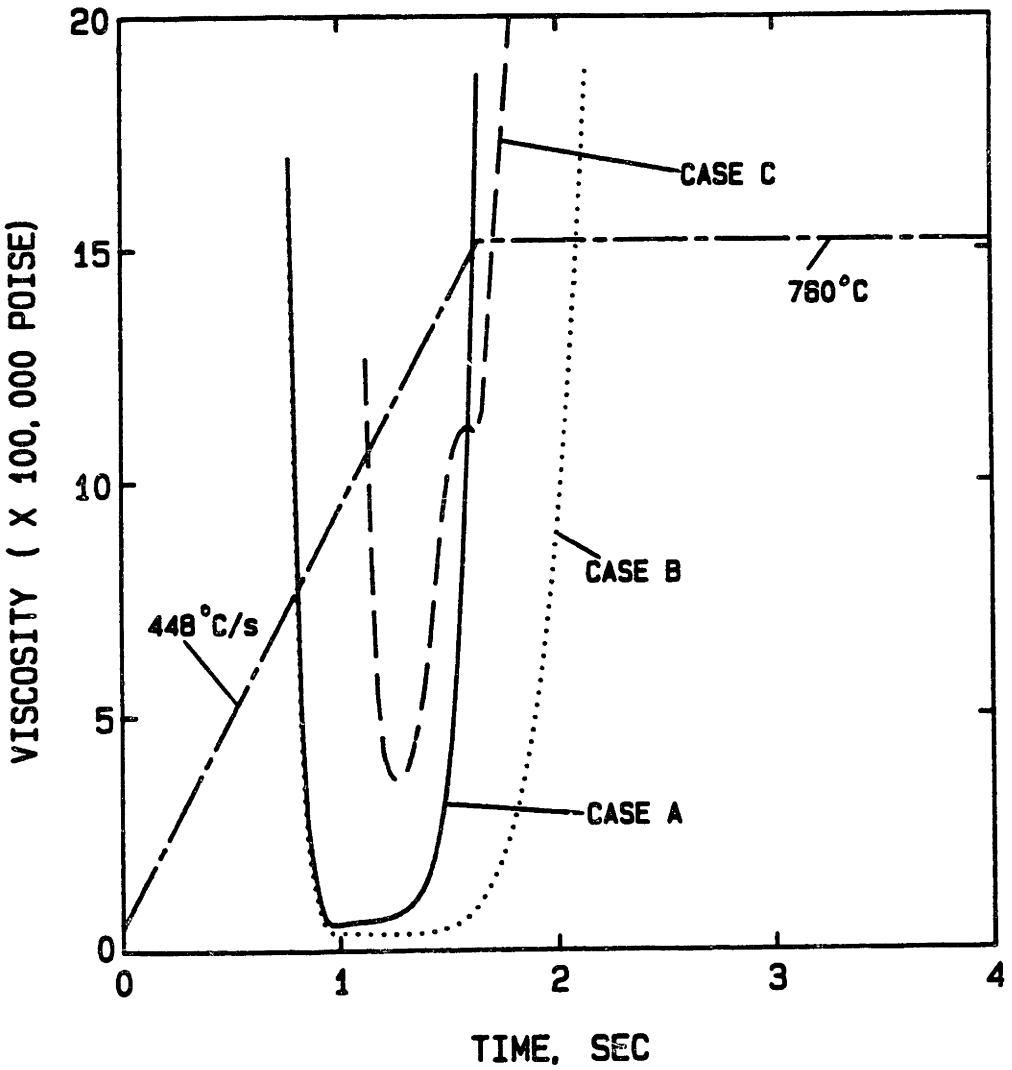

Fig. 1.4.5. Predicted variations of viscosity of coal melt at 1 atm as coal is heated to 760°C at 448°C/s and held at that temperature.

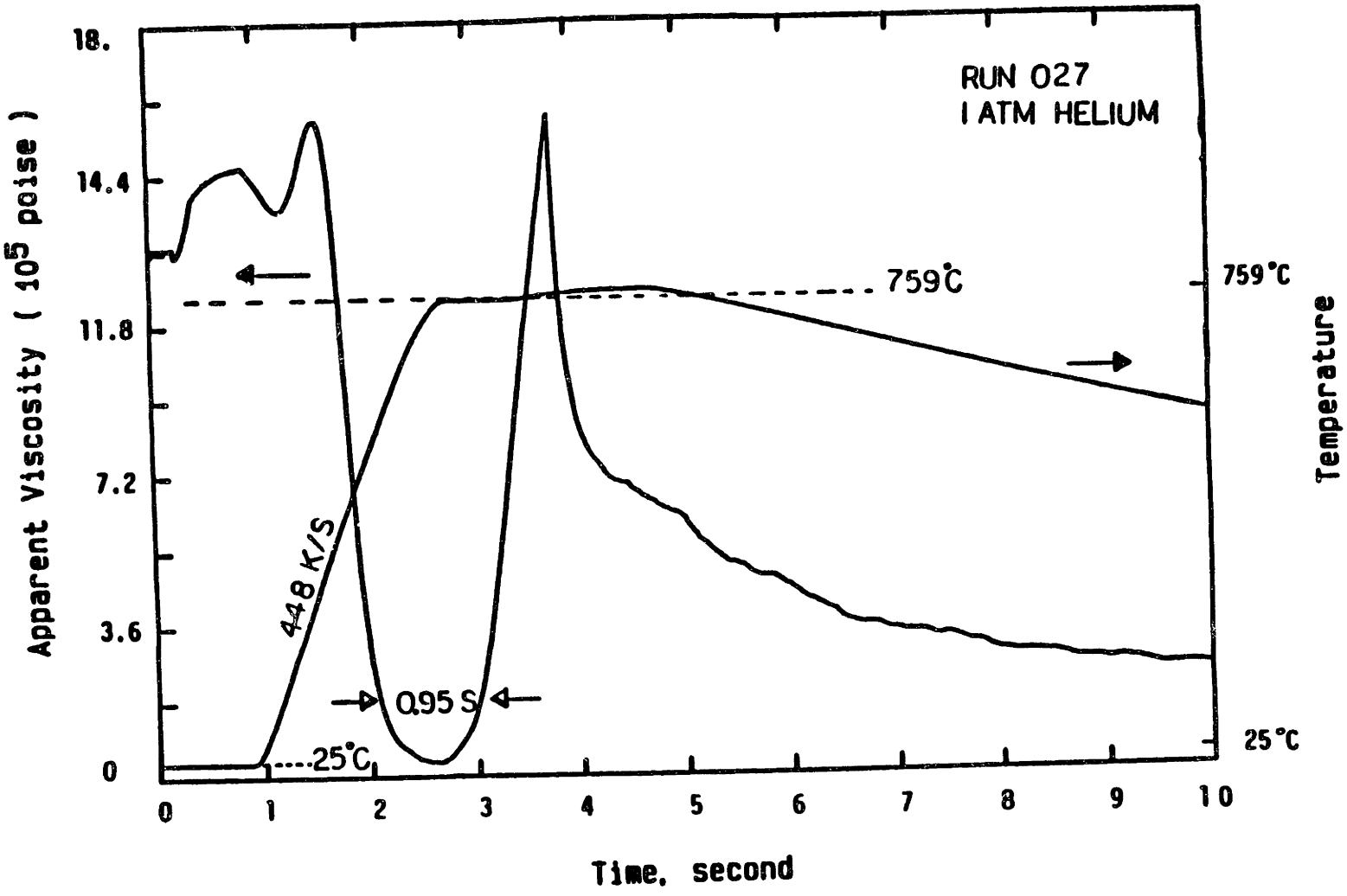

Fig. 1.4.6. Measured apparent viscosity of Pittsburgh seam #8 bituminous coal under rapid heating during 1 atm pyrolysis by a new coal plastometer. (Fong, 1985)

Matsugna, 1978; Dolan, 1980), the model predictions for all three cases are between 4 and 4.4.

1.4.4. Model Predictions of Pressure, Particle Size and Heating Rate Effects

Pressure effect: It is known that softening coals show stronger pressure effects on volatiles yield than non-softening coals. For example, the volatiles yield decreases with increasing pressure in bituminous coal pyrolysis, most of the effect being seen in the tar yield. The predicted volatiles yields and tar yields at different peak temperatures and at 3 different pressures are plotted in Fig. 1.4.7. As pressure increases, the mole fraction of metaplast in bubbles decreases and at the same time, slow growth of bubbles causes the inhibition of the net transport. More metaplast is consumed in secondary reactions and the total tar yield decreases. This result agrees with experimental observations (Howard, 1981).

The model with the same initial bubble number density at all pressures does not predict the pressure effect on plasticity. Modeling the initial number density as a function of pressure (i. e., decreasing number density with increasing pressure) will not only predict enhancement of plasticity at higher pressures but also will improve the quantitative prediction of volatiles yields at different pressures.

The model predictions of swelling ratio (R_p/R_{po}) reveal that the swelling is lower at 0.0001 atm due to larger number of bubbles released from the particle and is also lower at 69 atm due to the large compression effect.

Heating rate effect: The model predicts that increasing heating rate from 100°C/s to 1000°C/s has small effect on volatiles yields but it does shift

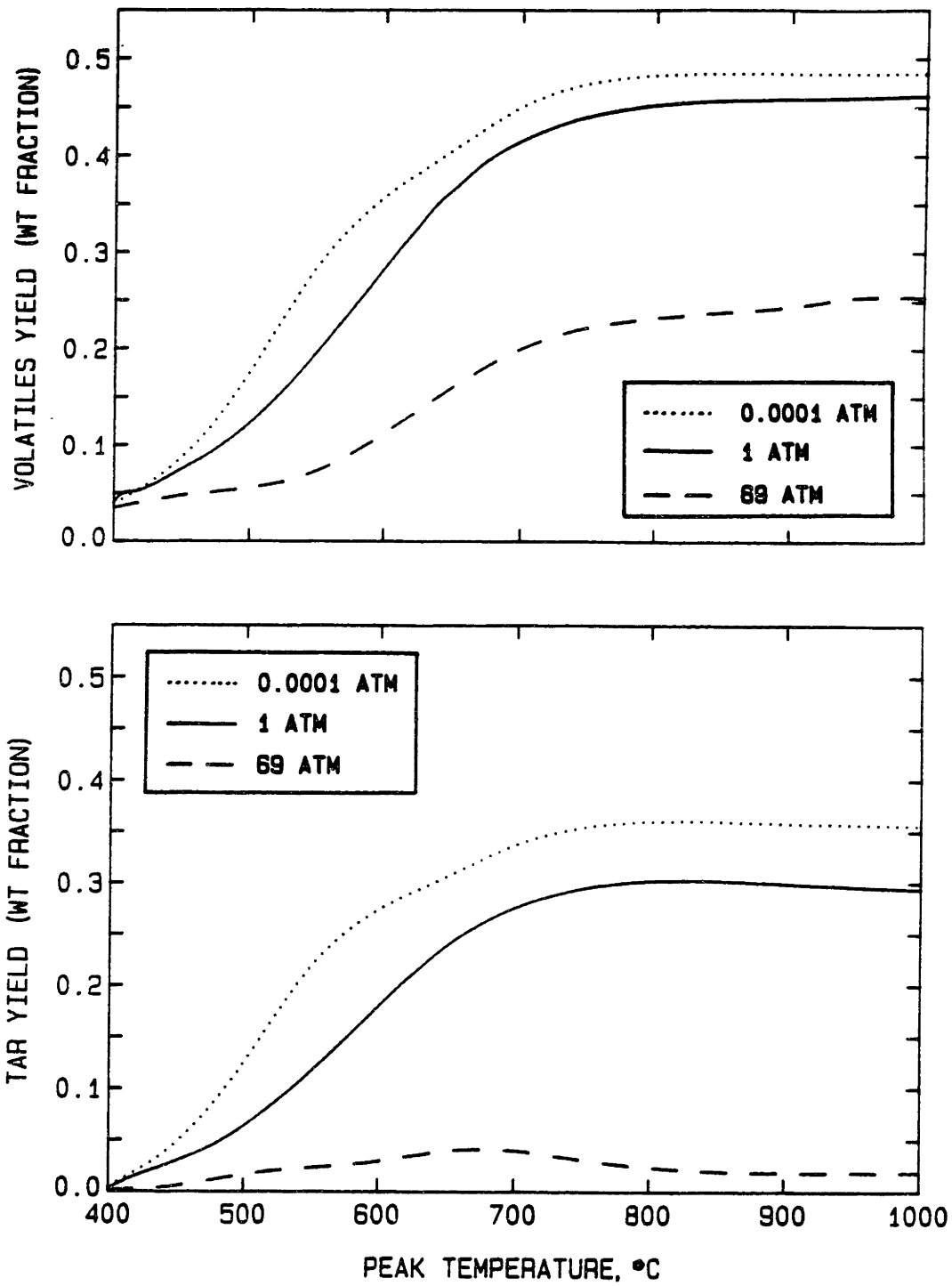

Fig. 1.4.7. Model predictions of the effect of pressure on total volatiles yields (top) and tar yields (bottom) for pyrolysis of softening coal heated to different peak temperatures.

the resolidification point to a higher temperature as seen is Fig. 1.4.8. These predictions agree with experimental observations.

Particle size effect: The smaller the particle size, the larger is the particle surface areas per gm coal available for the release of bubbles. Therefore, larger volatiles yields are predicted for smaller particles, which is also in agreement with experimental data.

1.5. CONCLUSIONS

1. Based on MW data of tar and pyridine extract, pyridine extract is a reasonable estimate of metaplast. The yield of pyridine extract of untreated coal gives an estimate of the amount of pre-existing metaplast in coal.
2. The number average molecular weight of 1 atm tar is about 350 and the vacuum tar is about 50 gm/mole heavier than 1 atm tar, while that of extracts from both 1 atm and vacuum varies between 450 and 500.
3. Transport via bubbles is a possible mechanism for both gases and tar. Bubbles may originate form pores in solid coal and may also be nucleated from the molten coal. However, bubble nucleation is not a rate limiting step in the transport process. In the absence of bubble coalescences, the bubble size distribution grows into a narrow size range and can be simplified as a single size.
4. Application of the model developed requires estimation of physical properties which are not readily available at present: (1) the more reasonable estimation of metaplast vapor pressure is given by Maiorella's model at low temperatures and by Suuberg's model at high temperatures; (2) The viscosity correlation proposed in this study with temperature restriction describes the variations in viscosity

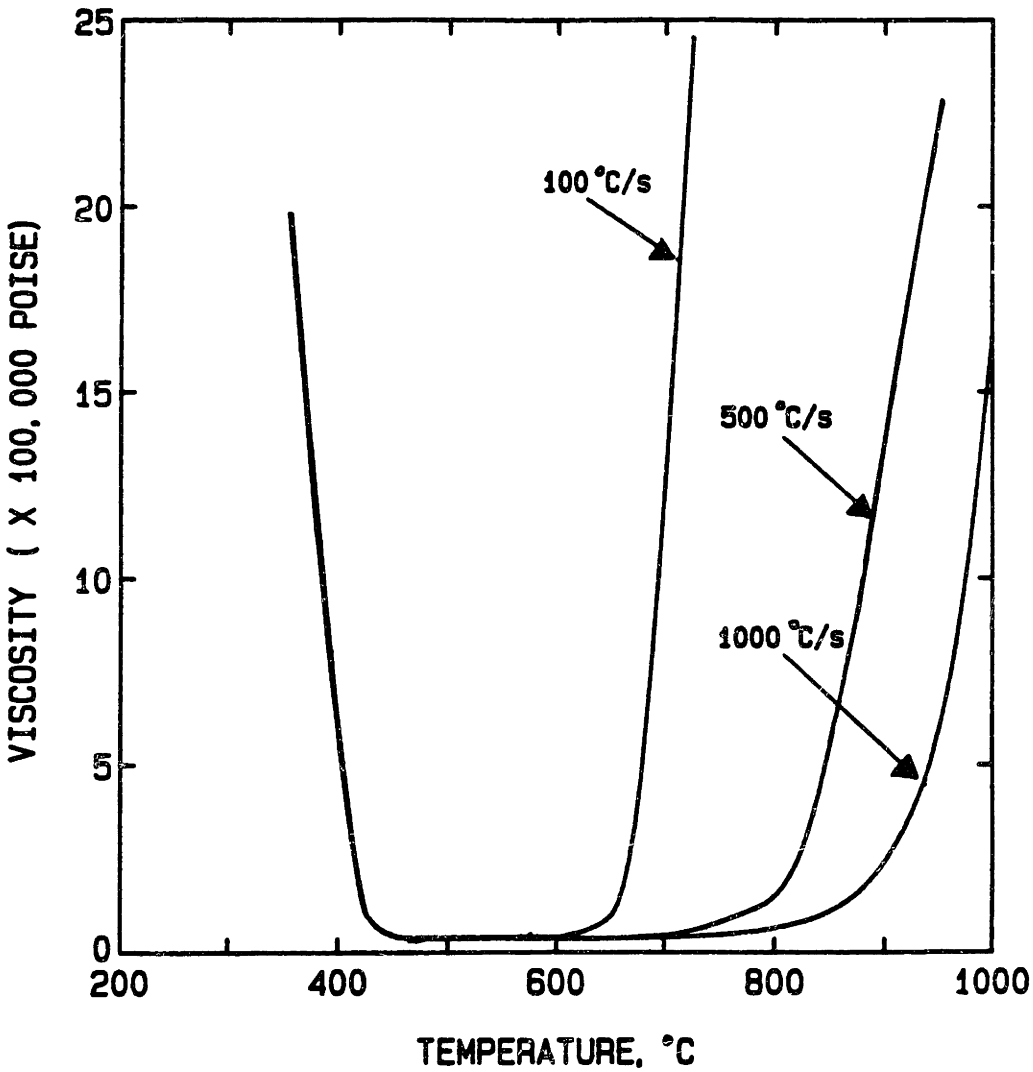

Fig. 1.4.8. Heating rate effect on plastic period as coal is heated to 1000°C at 1 atm at 100°C/s; 500°C/s; and 1000°C/s.

well; (3) the initial number density of bubbles is best left as a fitted parameter.

5. Despite the lack of knowledge of many physical properties of molten coal, the modeling of the transport in softened coal in terms of bubble motion along with secondary reactions in both bubbles and the liquid phase predicts the trends in volatiles yields, plasticity, and extent of swelling under various temperatures, pressures, particle sizes and heating rates, thereby confirming the important role that bubbles play in transport. Improved understanding of the physcial properties of molten coal will help to impove the model predictions.

1.6. REFERENCES FOR THIS SECTION

Attar, A., "Bubble Nucleation in Viscous Material Due to Gas Formation by a Chemical Reaction, Application to Coal Pyrolysis," A.I.Ch.E. J., Vol. 24, 106 (1978)

Barlow, E. J., and W. E. Langlois, "diffusion of Gas from a Liquid into an Expanding Bubbles," IBM J., 329-337 (1962)

Chen, L. H. and C. Y. Wen, "A Model for Coal Pyrolysis," ACS Div. Fuel Chem. Prepr., Vol. 24, 141 (1979)

Dolan, J., "Swelling and Agglomeration Effects for Bituminous Coal in a Lamimar Flow Reactor," B. S. Thesis. M.I.T., Cambridge (1980)

Fong, W. S., Y. F. Khalil, W. A. Peters, and J. B. Howard, "Plastic Behavior of Coal under Rapid-Heating High-Temperature Conditions", will be presented at ACS Spring Meeting, Miami, Fla., April (1985)

Fong, W. S., Sc. D. Thesis in preparation, Dept. Chem. Eng., M. I. T., Cambridge, MA (1985)

Frankel, N. a., and A. Acrivos, "On the Viscosity of a Concentrated Suspension of Solid Sphere," Chem. Eng. Sci., Vol. 22, 847 (1967)

Gan. H., S. P. Nandi, and P. L. Walker Jr., "Nature of the Porosity in American Coals," Fuel, Vol. 51, 272 (1972)

Gavalas, B. R. and K. Wilks, "Intraparticle Mass Transfer in Coal Pyrolysis," AIChE J., Vol. 26, 201 (1980)

Howard, J. B., "Fundamentals of Coal Pyrolysis and Hydropyrolysis," Chapter 12 in The Chemistry of Coal Utilization - Second supplementary Volume, M. A. Elliot, Ed., J. Wiley and Sons (1981)

James, R. K. and A. F. Mills, "Analysis of Coal Particle Pyrolysis," Letters in Heat and Mass Transfer, Vol. 3, 1 (1976)

Lewellen, P. C., "Product Decomposition Effects in Coal Pyrolysis," M. S. Thesis, Dept. of Chem. Eng., M.I.T., Cambridge (1975)

Maiorella, B. L., "Behavior of Liquid Subbituminous Coal Tars Upon Heating, as it Relates to In-Situ Gasification," B. S. Thesis, Dept. Chem. Eng., M. I. T., Cambridge, MA (1975)

Matsunaga, T., "Gasification of Coals Treated with Non-aqueous Solvent and Swelling Behavior of a Single Coal Particle," Fuel, Vol. 57, 562 (1978)

Mills, A. F., R. K. James, and D. Antonink, in Future Energy Production Series, J. C. Denton and N. Afgan, Eds., Hemisphere Publishing Co., Washingtion, D. C. (1976)

Nazem, F. F., "Rheology of Carbonaceous Mesophase Pitch," Fuel, Vol. 54, 851 (1980)

Neavel, R. C., "Coal Plasticity Mechanism; Inferences from Liquefaction Studies," Symposium on Plasticity and Agglomeration of Coal, U.S. Energy Research and Development Administration, Morgantown, W, Va (1975); Coal Science, Vol. 1, 1, M. L. Gorbaty, J. W. Larsen, and I. Wender, Eds., Academic Press, NY (1982)

Russel, W. B., D. A. Saville, and M. I. Greene, "A Modeling for Short Residence Time Hydropyrolysis of Single Coal Particles," AIChE J., Vol. 25, 65 (1979)

Serio, M. A., "Secondary Reactions of Tar in Coal Pyrolysis," Ph. D. Thesis, Dept. Chem. Eng., M.I.T., Cambridge, Mass (1984)

Sung, W. F., "The Study of the Swelling Property of Bituminous Coal," M. S. Thesis, Dept. of Chem. Eng., M.I.T., Cambridge (1978)

Suuberg, E., "Rapid Pyrolysis and Hydropyrolysis of Coal," Sc. D. Thesis, Dept. Chem. Eng., M.I.T., Cambridge (1977)

Unger, P. E. and Suberg, E. M., "Modeling the Devolatilization Behavior of a softening Bituminous Coal," Eighteenth Symposium (International) on Combustion, The Combustion Institute, Pittsburgh, PA 1203 (1981)

Unger, P. E. and E. M. Suuberg, "Internal and External Mass Transfer Limitations in Coal Pyrolysis," ACS Div. Fuel Chem. Prepr., Vol. 28, 4, 278 (1983)

Van Krevelen, D. W., Coal, Elsevier Publishing Co., Armsterdam (1961)

Ward, C. A., A. Balakrishnan, F. C. Hooper, "On the Thermodynamics of Nucleation in Weak Gas-Liquid Solutions," J. Basic Eng., 695 (1970)

Zacharias, M. W., "Analysis of Product Yields from Rapid Pyrolysis of Bituminous Coal," M.S. Thesis, Dept. Chem. Eng., M.I.T., Cambridge (1979)

2. INTRODUCTION

2.1. MOTIVATIONS

In recent years, the needs for the research to understand the basic state of coal and its reactions are becoming more and more obvious, as one realizes that natural reserves of petroleum and natural gas are limited and that a major proportion of our energy needs may have to be supplied from our vast coal reserves. Considering the fact that our fuels market is geared to the utilization of liquid and gaseous fuels, the necessity of converting some of our coal to liquid and gaseous fuels is obvious if a major portion of our energy needs is supplied by coal.

In most coal conversion processes, coal particles are heated to high temperatures. As coal is heated, some degree of decomposition occurs prior to, or concurrently with, other chemical reactions, and coal undergoes extensive thermal degradation to form a char and other volatile products. The series of chemical and physical reactions which are starting and accompanying reactions of all thermal processes of coal are included under pyrolysis. The reaction products formed at pyrolysis stage go through further chemical reactions and make important contributions to the final products. Therefore, it is necessary to study the kinetics and transport mechanism of pyrolysis for the better understanding of overall coal conversion processes and furthermore for the development of more effective ways of coal utilization.

An important factor affecting coal pyrolysis pathways is whether or not the coal exhibits plastic behavior (or in stricter terms, thermosetting behavior, i.e., softening and becoming deformed, followed by resolidifica-

tion to form a char upon being heated) during pyrolysis. Non-plastic coals undergo thermal decomposition maintaining their physical integrity and leave solid organic residues consisting almost exclusively of carbon. Volatile products leave the particle through pores by diffusion and hydrodynamic flow. Plastic coals soften and become more or less plastic. The particles form a bubbly compact plastic mass which swells. Volatiles formed in a platic melt form bubbles which grow and break through the surface. The melt ultimately resolidifies, resulting in a frothy, swollen coke. The swelling is a result of plastic properties (i.e., deformability) of the coal and the volatile hold-up as bubbles. The coal may swell to an extreme extent in which a particle consists of a thin outer shell surrounding a cellular structure of membrane-like walls, much like one element in a foam. Such a structure is known as a cenosphere. Fig. 2.1.1 shows an example of cenosphere, produced from a pyrolysis experiment in a laminar flow reactor at very high heating rate (Sung, 1978).

Studies of plastic coal pyrolysis are of particular interest because of the following:

a. Plastic coals are highly abundant in the industrialized eastern portion of the United States

b. The plastic behavior and the potential of these coals to give large yields of liquid products have particular industrial applications. Metallurgical coke production depends on coal plasticity for its success.

c. Plastic coal conversion is a more complicated process than that of non-plastic coals. Agglomeration and swelling due to plasticity affect the behavior of the coal in gasifiers and may cause a lot of trouble.

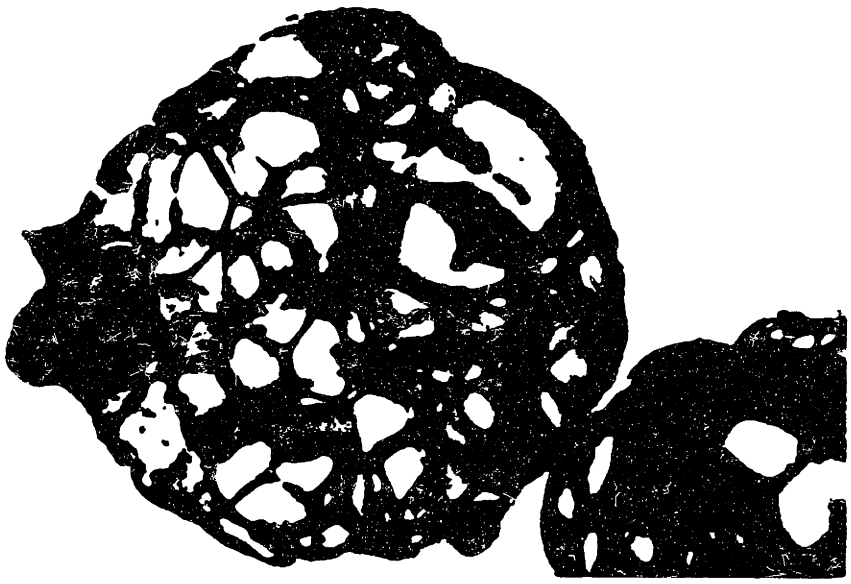

Fig. 2.1.1. Cenosphere (Sung, 1978)

The important role that pyrolysis plays in coal combustion, gasification, and liquefaction systems has long been recognized, and there has been a great deal of research done on the topic of pyrolysis (Howard, 1981). Nonetheless, the processes involved in pyrolysis have never been completely characterized. Significant headway has been made in improving the basic understanding of how process variables such as temperature, heating rate, pressure, and particle size affect pyrolysis product yields and compositions (Anthony and Howard,1976; Howard, 1981). The results from pyrolysis experiments in an inert atmoshpere suggest the influence of several interacting rate processes such as heat transfer, primary chemical reactions, gas-solid and gas phase secondary reactions, and transport of volatile products. Since pyrolysis involves coupled effects of several rate processes, predictive models for pyrolysis have been forced to address the transient state of coal during pyrolysis. Considerable success has been possible in this regard for non-plastic coals (Russel and Saville, 1979; Gavalas and Wilks, 1980; Wen and Chen, 1979). Since each particle retains a solid porous structure throughout pyrolysis, volatile products can be assumed to escape the coal particle by diffusion and hydrodynamic flow through pores and fissures permeating the particle.

The modes of volatile transport in plastic coals are different from those of non-plastic coals. Plastic coals soften to form a fluid-like viscous mass. Gaseous volatiles and relatively low molecular weight hydrocarbons (i.e., MW ~ 500) produced from the primary decomposition form bubbles. Because of a high viscosity of molten coal, bubbles are stationary but grow by the volatile transport from the molten phase and by coalescence with other bubbles. The bubble growth rate is governed by the rate of volatiles transport into the bubble as well as by the mechanical forces such as viscous forces. At one atmosphere and higher pressures,

the content of heavy hydrocarbons (i.e., MW ~ 1000) is small because the vapor pressure of heavy hydrocarbons is not high enough to vaporize into bubbles. Heavy hydrocarbons formed from decomposition diffuse through the molten coal to the particle surface, and escape from the particle. At the same time, these hydrocarbons go through secondary reactions, both in bubbles and in a condensed phase, to form lighter and heavier products. The loss of these materials through transport and secondary reactions causes the loss of fluidity. The fluidity, which is an important parameter in describing bubble transport, varies as a function of the concentration of mobile hydrocarbons in a molten coal.

Despite its importance, coal plasticity is still very poorly understood. Industrial calculations on coal plastic behavior rely on highly empirical tests such as Free Swelling Index, whose applicability to the pressures and other conditions of coal conversion reactors is questionable. In contrast to the situation with non-plastic coals, little progress has been made in quantitative description of the coupled effects of physical transport and chemical reactions in pyrolyzing particles of softening coals. The lack of progress is especially troublesome since it is precisely the softening coals for which the physical-chemical interactions are most important, as evidenced by the substantial effects of pressure and (to a lesser extent) particle size on pyrolysis product yields and compositions for these coals. Further study of coal pyrolysis, coal plastic behavior, and the agglomeration and swelling is clearly called for.

This thesis work addresses these information deficiencies. Detailed theoretical and experimental studies were preformed on coupled effects of primary and secondary chemical reactions and volatiles mass transfer within single coal particle to determine transient plasticity, swelling, and

volatile product yields. The predictions were tested by comparison with experimentally measured volatile product yields, compositions and formation kinetics as well as extents of swelling of pyrolyzing coal particles.

2.2. THESIS OBJECTIVES

The overall objective is to obtain improved quantitative understanding of the pyrolysis behavior of softening coals. Detailed theoretcial and experimental studies were made on the coupled effects of primary and secondary chemical reactions and volatiles mass transfer within single coal particles to answer how, for operating conditions of practical interest, these phenomena influence the plasticity and swelling behavior of the coal, and the yields and compositions of the pyrolysis products. It is emphasized that the present thesis is a new thrust focused on the basic physics and chemistry of the transient plastic stage of coal pyrolysis which to date has been relatively unexplored.

The specific objectives are as the following:

1. To characterize processes which are responsible for the transport of volatile products, including gases, volatile low molecular weight hydrocarbons, and relatively non-volatile heavy hydrocarbons, within and to the surface of softened coal particles.
2. To determine the role of bubbles in the transport described in 1., and to clarify the mechanisms which are responsible for bubble nucleation, growth, destruction, and escape from the softened coal particles.
3. To make predictions of the rates and extents of swelling of a pyrolyzing softening coal particle, using a model that accounts for

primary and secondary chemical reactions of pyrolysis products and allows for contributions to intra-particle volatiles transport and escape by the motion of pyrolysis-derived bubbles.

4. To predict the plasticity of individual coal particles as a function of pyrolysis conditions and to relate this predicted plasticity to that measured experimentally.

5. To predict the independent effects of temperature, total pressure, particle diameter and heating rate on the yields, compositions, and rates of formation of products from the pyrolysis of softening coals, and to understand importance of the plastic stage of pyrolysis in determining the yield and the overall product spectrum.

6. To obtain intrinsic chemical parameters for primary pyrolysis or intra-particle secondary reactions.

7. To obtain new information on the relationship between coal plasticity and metaplast concentration, and between the amount of tar obtained as a pyrolysis product and the concentration of metaplast within the coal particle and to develop a simple functional relationship between plasticity and metaplast concentration.

3. BACKGROUND

3.1. PYROLYSIS YIELDS AND PRODUCT DISTRIBUTION

Temperature effect

Many studies have been done at MIT over the past few years on the pyrolysis of a Pittsburgh Seam #8 bituminous coal, which exhibits strong plastic behavior. Anthony(1974) conducted the first systematic investigation of the weight loss from bituminous coal pyrolysis as a function of temperature, heating rate, pressure and particle size. Suuberg(1977) extended Anthony's work to obtain product distributions from coal pyrolysis. Fig. 3.1.1. shows the products distribution as a function of peak temperature for 74 μm bituminous coal particles pyrolyzed in 1 atm. He. These data were taken using a batch reactor which allows rapid heat up of coal particles. The volatile products of coal devolatilization include CO, CO_2, H_2O, CH_4, other hydrocarbon gases (C_2H_4, C_2H_6, etc.), light oils, and heavier liquids usually lumped in species called tar. The top curve denoted with T represents total measured weight loss and the difference between curves represents the yields of the products indicated. The overall yield increases with temperature and gives approximately 47 % of weight loss at 1000 °C and that each product has a different rate of formation at a given temperature. The formation of water is completed at lower temperature region (<400 °C), while tar, a dominant product of bituminous coal pyrolysis, and hydrocarbon formation occur at temperatures between 400 and 900°C. Carbon oxides have a broad temperature region of formation. At temperatures well beyond 1000 °C, the additional devolatilizaton occurs in a relatively short time. Kobayashi (1976) reported a yield

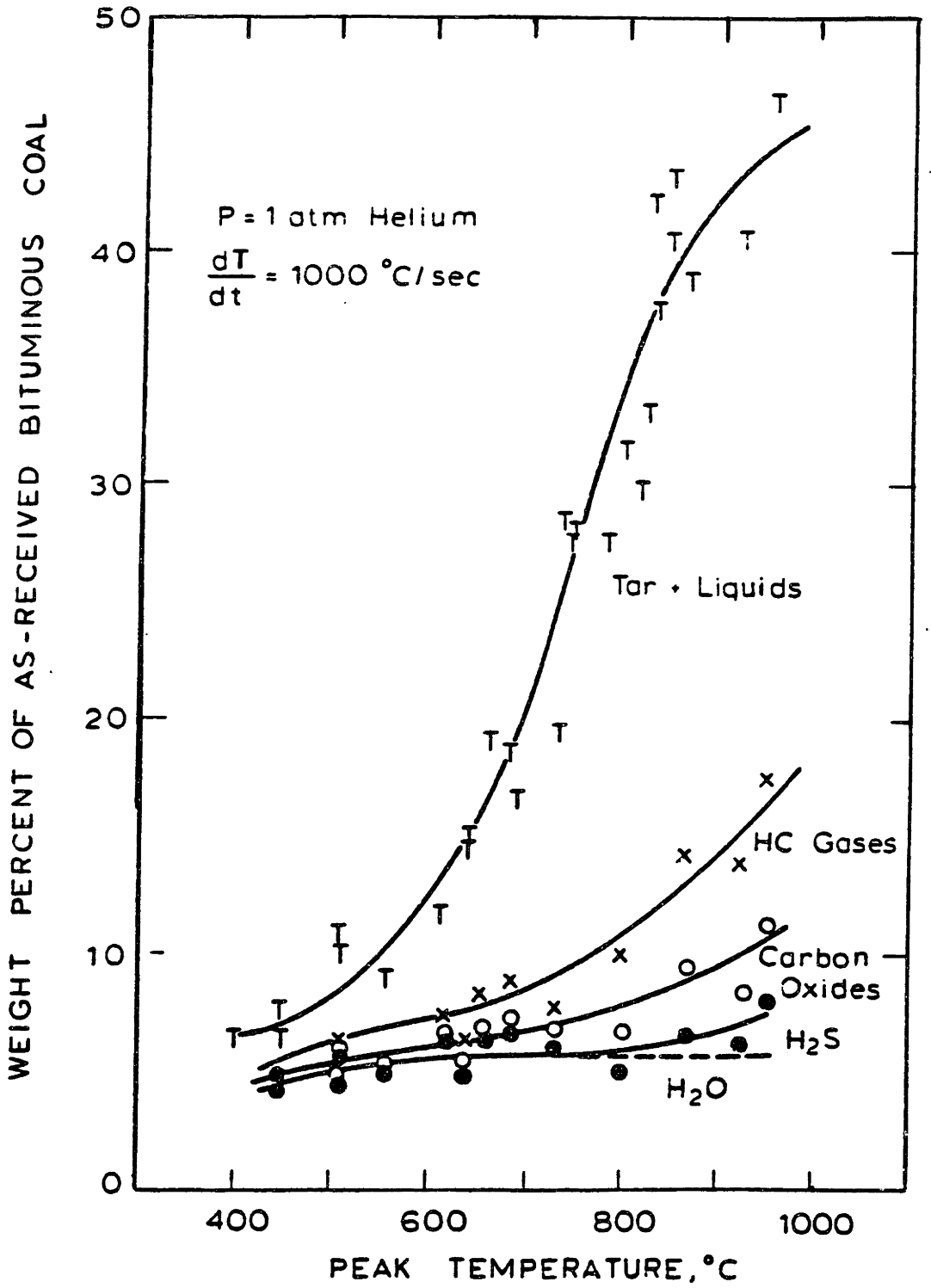

Fig. 3.1.1. **Pyrolysis product distributions from bituminous coal heated to various peak temperatures. (Suuberg, 1978)**

of 63 % at 1800°C in a laminar flow reactor. But the true ultimate measureable yield of volatiles remains unknown. Menster et al. (1974) reported that above 1000°C, tar is no longer the dominant product and the yields of gases exceed the yield of tar. This behavior presumably reflects the secondary reactions in this temperature region.

Heating rate effect

Whether or not the heating rate affects volatile yields has been debated in literature. Under carbonization conditions where packed beds of coal are heated at lower heating rate such as 1 - 10°C/min, the volatile yields are less than those from the ASTM test, where coal is heated in a crucible at the rate of about 15°C/sec to 950°C and held for a total heating time of seven minutes (Gregory and Littlejohn,1965). Under rapid heating rates, the volatile yields exceed the proximate volatile matter content(Loison and Chauvin, 1964; Badzoich, 1967; Kimber and Grey, 1967 a,b).

In carbonization studies, higher heating rates result in higher volatile yields during coal pyrolysis (Warren, 1935 a,b; Juettner, 1934; Van Krevelen, 1956) and the heating rate effects are shown in the yield of tar. Warren reasoned that the increase in tar yield with the increase of heating rate is due to the competition existing between the evaporation and decomposition reactions of tar. At fast rates of heating, much of the unaltered tar escapes by evaporation, whereas at slow rates much of the tar may disproportionate into gas and char rather than evaporate. However, Mazumar and Chatterjee (1973) reported that a variation in heating rate for a packed bed of coal from 1 to 5°C/min effected 1 % increase in weight loss which was attributed to an increase in tar yield, but the progressive increase in the thickness of coal bed from 0.75 mm to 100 mm

resulted in the increase in coke yield from 71.5 % to 78 % which appeared to follow a smooth parabolic curve. They concluded that bed depth rather than heating rate was primarily responsible for the difference between results under different heating rates from the coke oven.

Even under gasification conditions, Wen et al.(1974) observed enhencement of volatile yield at higher heating rate(0.1 - 100,000°C/sec) from the experiments of pyrolysis of Elkol coal of 635 um from a fluidized bed at 1 atm. Graff et al.(1976) obtained similar results. As heating rate increased from 20°C/sec to 650°C/sec, the yields of heavier material decreased and the yields of light hydrocarbons yields increased. They interpret this as a result of the competition between fragmentation and repolymerization which was strongly influenced by time and temperature, not mentioning any mass transfer effect. Flash heating to higher temperatures resulted in fragmentation of coal structure to lighter species before stabilization or crosslinking of the fragments to larger structure. With low heating rates, extensive repolymerization occurred before the high temperature is reached. In contrast, doubling heating rate to 1400°C/sec did not substantially alter product yields. They concluded that a heating rate of 640°C/sec was high enough for evolution of lighter species to predominate over competing processes forming heavy components.

In contrast to the foregoing, other researchers in rapid heat-up pyrolysis have found no dependence of volatile yields on heating rate. Van Heek and Juntgen found that the higher the heating rate, the higher was the temperature at which the maximum rate occurred, and the wider was the temperature range over which a given fraction of the devolatilization occured. But the interesting thing was that the integrated yield was not affected by the heating rate. This observation by Van Heek and Juntgen is

supported by the data of Anthony(1974) and Suuberg(1977). Anthony found that the volatile yields increased only slightly with increasing heating rate. For example, using coal particles of about 70 μm at 1 atm He, the increase was about 2 % where the heating rate increased from 750 to 10,000 °C/sec. Suuberg confirmed this result and extended it to include the composition as well as the total amount of volatiles.

Conflicts of heating rate effects on volatile yields appear to have arisen mainly as a result of comparison of results, without due regard to different experimental conditions such as particle size, the ranges of heating rate, and the type of reactor. Howard et al. (1980), in a literature review, concluded that over a wide range of heating rate(250 - 100,000 °C/sec) the total yield of products from pyrolysis is substantially independent of heating rate. For a lower range of heating rate (0.01 to 250 °C/sec.), data from packed bed would suggest that there is a small but significant apparent effect of heating rate due to secondary reactions in packed beds. The increase in yields which is sometimes attributed to heating rate probably results primarily from the associated experimental conditions employed to achieve faster heating.

Pressure and particle size effects

Effects of pressure and particle size effect are very important because they suggest that mass transfer of volatiles affects the pyrolysis process and that pyrolysis cannot be modeled solely by chemical kinetics. Anthony (1974) investigated the pressure effect on weight loss over a wide range of total pressure (10^{-4} to 10^{2} atm) and found that, at heating rate > 650 °C/s, the pressure effects are not shown before 600 °C but at temperatures above 600 °C the pressure effect on volatile yields is significant. The weight loss of 70 μm bituminous coal heated to 1000 °C increased signi-

ficantly with decreasing pressure. The weight loss under atmospheric pressure was 50.0 % of the as-received coal, while the loss was 54.2 % under vacuum and 34.2 % at 100 atm. The weight loss seemed to approach limiting values at both vacuum and at high pressures. The work of Suuberg (1977) revealed that the yields of tar and heavy hydrocarbons decreased with increasing pressure, while the yields of light hydrocarbons and carbon oxides (not shown) increased with increasing pressure, as shown in Fig. 3.1.2. This behavior is generally attributed to cracking and carbon deposition of tar as the residence time of tar increases at higher pressures. These results support the view that tar is the most reactive volatile species and emphasize the importance of transport of tar which is in competition with secondary reactions occurring within and outside the particles.

Some of the increase in yields of lighter volatiles such as CH_4 at temperature higher than 600°C may be due to a well known phenomena, so-called 'auto-hydrogenation', which is the formation of methane by reactions between char and hydrogen evolved from pyrolysis (Makino and Toda, 1978; Fitzgerald and Van Krevelen, 1959).

The particle size effects in overall yield are similar but smaller than those for varying pressure: the total volatiles yields decreases with increasing particle size. The yield of tar also decreases, while the yields of light cracking products increase with a increase in particle size as shown in Fig. 3.1.2. However, these data shown in Fig. 3.1.2 are somewhat questionable because the nature of the screen heater reactor is not adequate to investigate the particle size effects of plastic coal which fuses between the screen folds while it goes through the plastic stage and thereby tends to mask the effect of the dimension of individual particles.

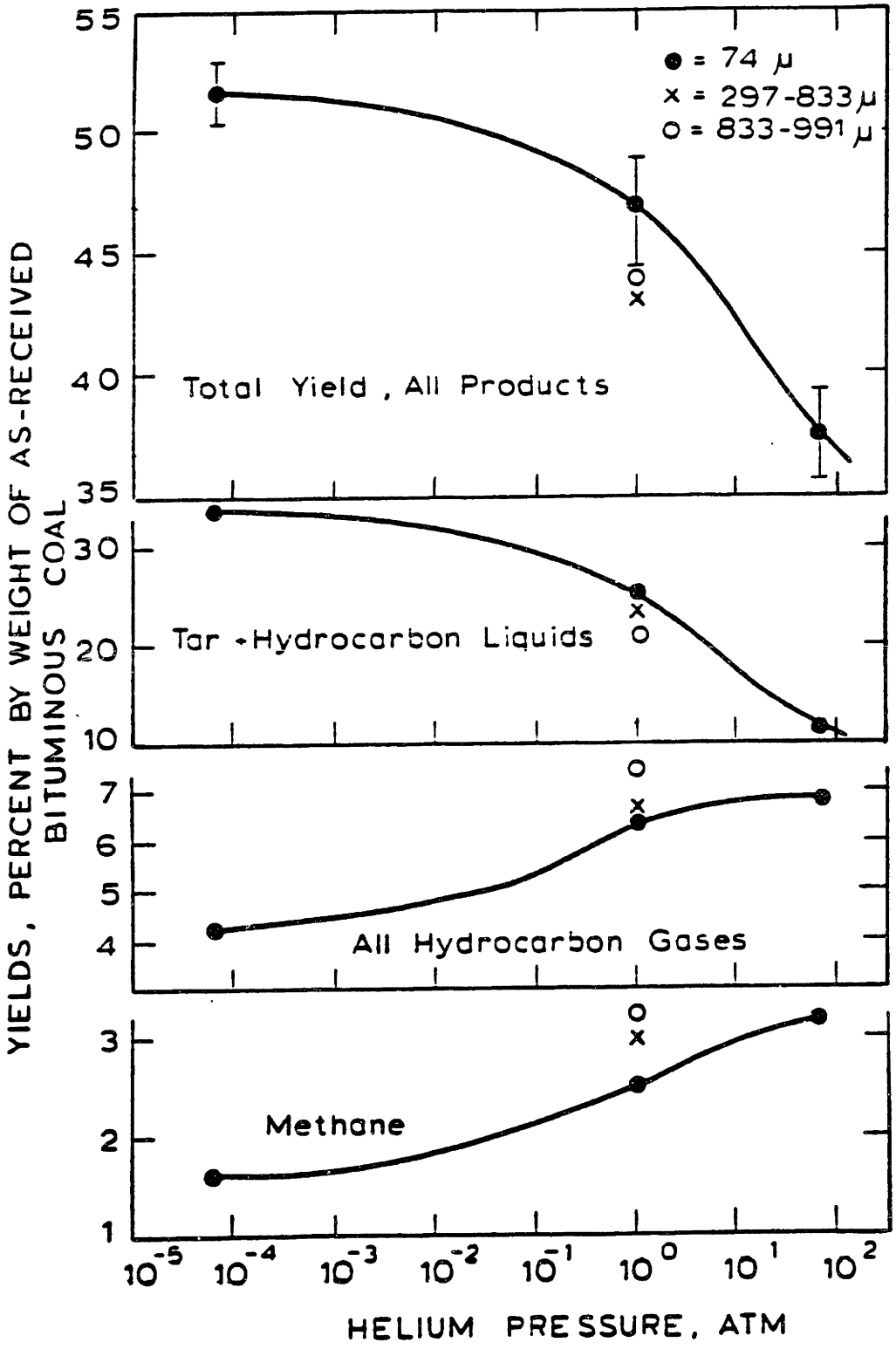

Fig. 3.1.2. Effect of pressure on product yields from bituminous coal pyrolysis. Coal is heated to 1000 °C at 1000°C/s and held for 2 - 10 sec. (Suuberg, 1978)

3.2. Solvent Extraction

The chemical composition and many physico-chemical characteristics of coal extracts are very similiar to those of the parent coal, particularly in the case of high extract yields. Because of this, solvent extraction of coal is a long estabilished method for the study of the constitution of coal much effort has been made to relate the information derived from the study of the structure of coal extracts to the structure of parent coal (Dryden, 1962). The other major area of application of solvent extraction was to relate the coking properties to the yields of chloroform extract on chloroform-soluble fraction of pyridine extract (γfraction) (Dryden, 1962; Brown et al., 1966) and, therefore, to study the plastic behavior of softening coal upon heating.

The yields and the nature of extract vary considerably depending on coal and its preparation, solvent, and conditions of extraction such as time, temperature, pressure, particle size and atmosphere. Coal extraction methods and solvents can be classified into the following groups: non-specific extraction, specific extraction, extractive disintegration, and extractive chemical disintegration. In this section, each extraction method is discussed, while emphasizing specific extraction which is the one of interest in this thesis because of its extraction power and its correlation, even though qualitative, between the extract yields and the fluidity of softening coals.

Non-specific extraction (Non-specific solvent)

Only a small amount, generally 5 - 8 % of coal, is dissolved, preferably at low and moderate temperatures (up to 150°C). Common non-specific solvents are benzene, ethanol, acetone, and chloroform. Most of

the work on non-specific extraction have dealt with chloroform extraction (Dryden and Pankhurst, 1955; Dryden and Joy, 1961; Brown and Waters, 1966). The extracts do not form a major part of the coal structure. However, the extract yields are known to correlated with the fluidity and weight loss under carbonization conditions because of the following:

1. Non-coking coals do not yield the chloroform soluble product upon heating.
2. The yields of chloroform extract increases markedly on preheating coking coal to temperatures near the onset of decomposition and the development of fluidity.
3. The residue after chloroform extraction of the heated coking coal no longer softens or swells on further heating.
4. The rapid decrease in extract yield is associated with the hardening of fluid coal.

However, the presence of chloroform extract does not gurantee softening behavior: Chakrabartty and Berkowitz (1972) found that the treatment of softening coal with boron trifluoride suppressed the fluidity but did not lower the yield of chloroform extract.

Extractive Disintegration (Degrading Solvent)

This operation is carried out at rather high temperatures (near 400 °C) which causes chemical bonds to break to form smaller and soluble fragments. The extractibility is correlated with the solvent's boiling temperature and typical degrading solvents are high boiling aromatic hydrocarbons such as phenanthrene and anthracene oil. Eventhough the nature of the solvent remains the same, it is believed the solvent plays a role as a free radical carrier. For example, a free radical formed from solvent is

attached the coal structure, generating an unstable coal radical while the solvent itself returns to an original molecule.

Extractive chemical disintegration (Reacting Solvent)

As the name implies, reacting solvents react with coal. For example, tetralin serves as a hydrogen donor to stablize the thermally generated free radicals by donating its hydrogen and becoming napthalene. This technique yields high percentages of extract.

Specific extraction (Specific solvent)

Specific solvents are distinguished by the property of being able to dissolve an appreciable amount of coal at temperatures below their normal boiling point and, thus, specific extraction is the most suitable extraction technique to study coal constituents. Specific solvents typically consist of a molecule with an oxygen and or a nitrogen atom, possessing an unshared pair of electrons. They have the power to swell the raw coal and to stablize coal extract in the liquid phase. Typical specific solvents are pyridine, tetrahydrofuran, and ethylenediamine.

Dryden et al. (1951) tested the solvent power of about 100 solvents in coal extraction and concluded that the solvent power of specific solvents is reduced when

1. There is excessive hydrogen bonding
2. There is a lone pair in resonance with the molecular nucleus.
3. There is the presence of an alkyl group which offers the steric interference between chemical groups in solvent and coal.

The yield of extact generally increases with temperature up the boiling point of the solvent (Dormans et al., 1960; Dryden et al., 1951), but heating to beyond the boiling point in an autoclave does not give any

increase in extract yield. Two other factors which govern the extract yield are the rank of the coal to be extracted and the solvent. Van Krevelen (1960) found that some solvents have an optimum extracting effect at a very specific degree of coalification. He recommended that for coals with more than 85 % carbon, pyridine was a more suitable solvent than ethylene diamine; for coal containing less than 85 % carbon, the latter was preferred. However, Van Krevelen recommended pyidine as the only solvent to yield extracts whose molecular weight could be measured with reasonable accuracy. Fig 3.2.1 plots extraction yield vs. rank of coal for three solvents.

The swelling and agglutinating properties are correlated well with the yield of non-specific solvent and & fraction (chloroform-soluble) of pyridine extract but not with the toal pyridine extract yield (Dryden, 1962). However, in later studies, Pierron and Rees (1960) found a qualitative correlation between the yields of pyridine extract of different rank coals and levels of fluidity. Fig. 3.2.2 shows the yields of pyridine extracts as a function of Gieseler maximum fluidities for eight coals. As the rank of the coal increases, the yields of pyridine extract increases and maximum fluidities increases up to a maximum, then as the rank continues to increase, the yield of extract and maximum fluidity decrease. One can also observe both the ascending and descending parts of the curve appears to approach a straight-line relationship.

Lloyd et al. also observed that the both THF and DMF (N,N-dimethyl-formide) extraction yields exhibited a systematic relationship to ASTM maximum fluidity. The average relationship to the THF- and DMF-extracts of coals with maximum ASTM fluidities below 100 ddpm, between 100 and 1,000 ddpm, and above 1,000 ddpm were

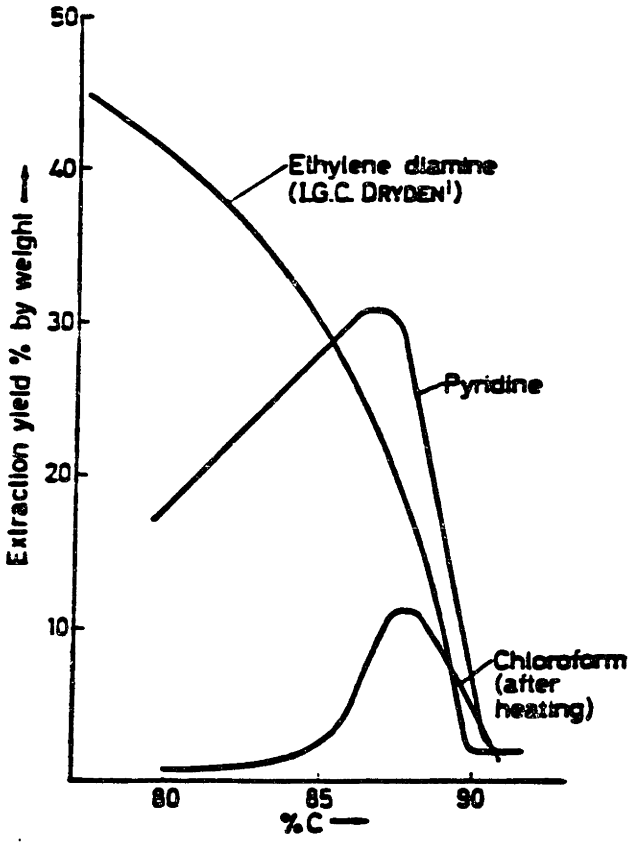

Fig. 3.2.1. Effect of type of solvent on extraction yield (Dolmans and van Krevelen, 1960)

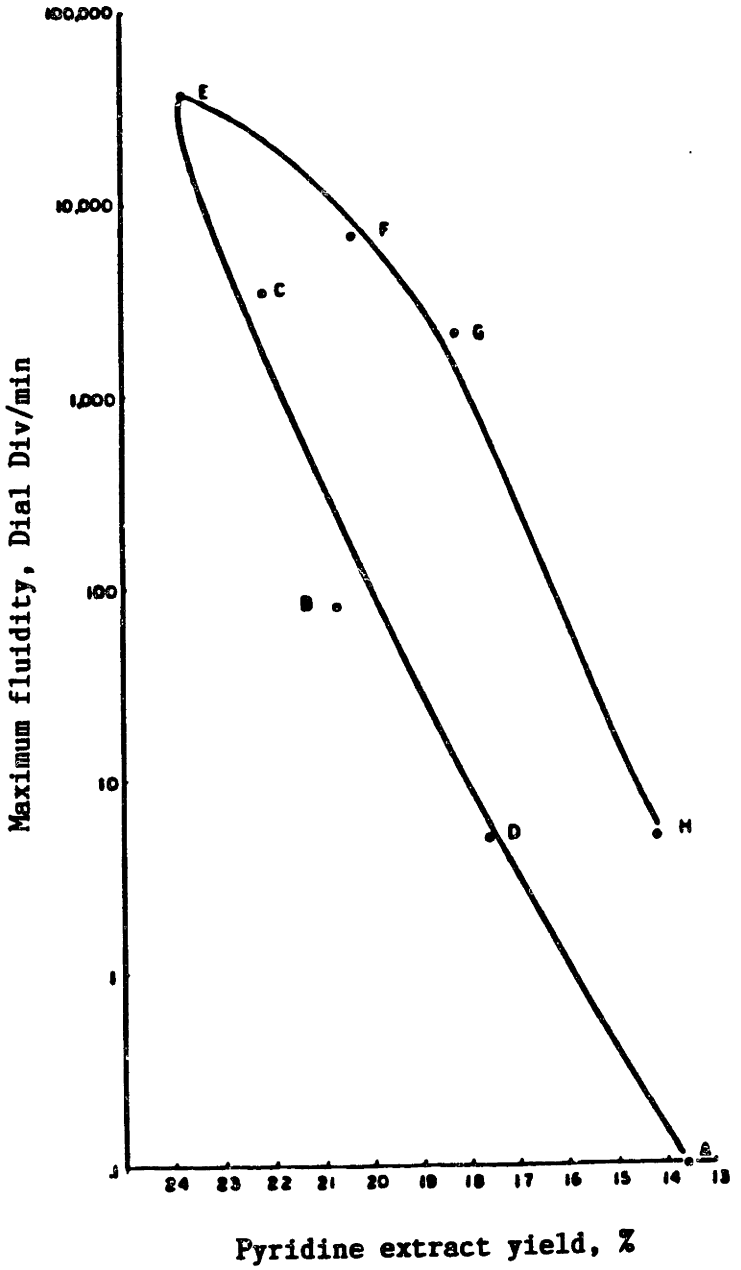

Fig. 3.2.2. Maximum Gieseler fluidity vs. yields of pyridine extract. Order of increasing rank: A — H. Fixed carbon content varies from 59.5 to 81.5 % by ASTM method. (Pierron and Rees, 1960)

	THF	DMF
Below 100 ddpm:	13.5 ± 1.4 %	23.0 ± 1.7 %
100 - 1,000 ddpm:	14.2 ± 2.3 %	24.5 ± 2.3 %
Above 1,000 ddpm:	15.9 ± 2.3 %	30.0 ± 4.0 %

These groupings show some trends, but are not highly sensitive predictors of maximum fluidity. A similar conclusion was made by Ouchi et al.(1983); they found that the yield of pyridine extract was only approximately proportional to the maximum fluidity.

3.3. PLASTIC PROPERTIES

3.3.1. Mechanism of Plasticity Development

The mechanism of softening has been described by many authors. The homogeneous melting theory (Audibert, 1926) suggests that coal undergoes true melting through the entire mass, but decomposes at the same time, giving rise to solid infusible products and gas or vapor. This theory explains why the softening point of coal, as measured by Giessler plastometer, does not vary much with heating rate and also accounts for the fact that, at least for certain coal, the commencement of softening is a reversible phenomenon (Waters, 1962). But it does not account for the fluidity change at constant temperature and the pressure effect on the fluidity, and this homogeneous melting theory no longer finds any support.

In the partial melting theory, on the other hand, soften coal is described as a mixture of solid and melted fractions. Bangham (1945) described coal as an assemblage of large molecules with diameters of about 200 A (micellae) and smaller molecules. He indentified smaller molecules as a fusible fraction and micellae as a non-melting fraction. At low

temperatures, these molecules are linked by van der Walls forces and the mass is solid. When the temperature rises, these forces of attraction are weakened, the small molecules become mobile, and the coal becomes plastic.

In a more advanced partial melting theory, it is supposed that softening is initially and essentially a physical process of melting of the coal substance into a fused mass, of which the rheological properties were subsequently modified by chemical reactions (Brown and Waters, 1962). The development of fluidity is, thus, believed to be the result of both physical and chemical processes. It assumes that the smallest molecules in the coal substance become mobile on heating and act as plasticizer. The fusible fraction has often been identifed with the fraction of coal soluble in non-specific solvent, such as benzene and chloroform, and termed 'bitumen'. Brown and Waters also identified the additional fusible fraction as 'humins' of colloidal dimensions which is pyridine soluble fraction but insoluble in non-specific solvent. They assumed that the extraction of the chloroform- and pyridine- soluble materials from raw coal does not involve the breakage of covalent bonds to any appreciable extent. At temperatures above 350°C, the fusible fraction is sufficient in volume to suspend the larger particles, 'humins' of macro molecular dimensions, and, as a result, the whole mass exhibits fluid behavior.

A theory closely related to this idea is based on X-ray studies (Riley, 1945). In the model, coal is composed of lamellae stacked more or less upon each other and forming crystallites. The fusible fraction is identified with the smallest crystal units, which are soluble in organic solvents and which become mobile when the temperature rises and gives plasticity to coal by acting like a lubricating agent.

Based on the fact that coals only attain a plastic stage when the

pyrolytic reactions develop at a sufficient rate, many researchers have suggested that softening is a consequence of pyrolysis. While the partial melting theory believes in the bitumens already present in coal, the thermobitumen theory (Oele, 1953) or the metaplast theory (van Krevelen, 1956) believed in thermal decomposition of coal to form the initial plasticizer, called 'thermobitumens' or 'metaplast'. This metaplast is decomposed, in turn, by cracking reactions into volatile matter and solid residue. The decomposition of the coal and cracking of the metaplast overlap in time. The plasticity is proportional to the concentration of metaplast and the disappearance of metaplast leads to resolidification.

The metaplast theory explains the following experimental observations:

1. Enchancement of plasticity at high pressures is due to the fact that the transport of metaplast is inhibited, the residence time of metaplast inside a particle is longer, and its concentration is higher.
2. The slow heating rates minimize the plastic behavior, because slowly increasing temperature allows ample time for initially formed plasticizers or thermobitumens to repolymerize into a larger structures which cannot act as solvating agents.
3. It is well known that swelling is caused by plastic properties during pyrolysis. No swelling is observed at very high temperatures due to the fact that secondary reactions are very fast and, therefore, the metaplast is consumed in secondary reactions before the particles go through the plastic stage.

However, the metaplast theory does not explain the fact that after solvent extraction, for example with pyridine, coal no longer show softens, although according to the theory, metaplast must be produced by heating even after solvent extraction.

Recently, the concepts of the metaplast theory and the melting theory have been combined and modified. The leading theory holds that parallel to the fusion of pre-existing metaplast, or 'bitumen', pyrolysis develops and modifies the fusibility, independently (Loison, 1963; Neavel, 1982; Lloyd et al., 1984). Neavel suggested three conditions which appeared to be necessary and sufficient for the development of plasticity in coal: the presence of lamellae bridging structures that could be thermally ruptured, a supply of hydroaromatic hydrogen, and an initial intrinsic potential for micellar and lamellar mobility which provides hydrogen to free radicals formed by pyrolysis. He also described the softening mechanism of bituminous coal as the following. In bituminous coal, it is known that vitrinite, one of the major petrographic constituents, is responsible for plastic behavior. As shown in Fig. 3.3.1, vitrinite is made up of packets (micelles, or crystallites in X-ray studies) of layers of molecular units (lamellae), which consist of condensed ring structures. Various functional grous are attached to the rings (=O, -COOH, -OH, $-C_nH_m$). Some of the ring carbons may be saturated with hydrogen. The lamallae are bound together by hydrogen bonds, van der Waals forces, and covalent bridges. There also exist about 20 % or less of unbonded, relatively low molecular weight material (bitumen) which is readily extracted by solvent. As coal is heated, bitumens become fusible and serve as the initial plasticizer to solvate the micelles. Bitumens also serve as initial hydrogen donor to free radicals produced by pyrolysis when they become thermally loosened. The rupture of lamellae bridging structures gives mobility to the lamellar units, which can also serve as hydrogen donors to stabilize free radicals. At that point, the role of original bitumen in maintaining plasticity is of less importance. Without the initial plasticizer, however, there would be no transiently necessary solvating agent and hydrogen donor, and no

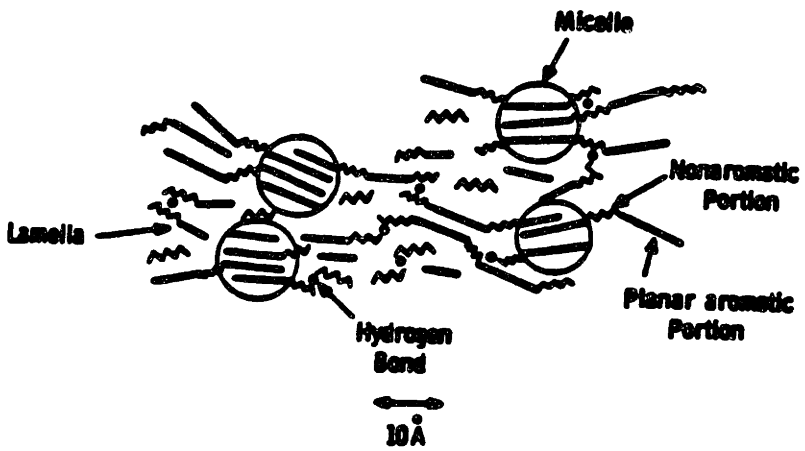

Fig. 3.3.1. Representation of idealized molecular structure of vitrinite in bituminous coal: Composite alignment of layers (Neavel, 1982)

softening would be observed. At higher temperatures, stabilization of free radicals by hydrogen is preferred if hydrogen donors are available. If not, aromatic and hydroaromatic fragments will stabilize by disproportionation to more condensed aromatic structures. In summary, bitumens and mobile lamellar units cause the fluid-like behavior of bituminous coal and the loss of these materials by transport and secondary reactions leads to resolidification.

3.3.2. Plasticity Measurements

Plasticity has been measured using plastometers (Loison, 1962) which operate mostly at low heating rate and at relatively low temperatures. The measurements are made on large coal masses rather than single particles. As with pyrolysis yields, the plasticity is affected by measurement conditions such as temperature, pressure, and heating rate. The results are summarized as the following:

a. The maximum plasticity increases with temperature up a certain temperature.

b. Higher heating rates enhance fluidity. The softening point of coal does not vary much with heating rate but increasing heating rate shifts the resolidification point to a higher temperature, therefore broadening the plastic range of the coal. The temperatures of maximum plasticity are also displaced to the higher temperature, at higher heating rates.

c. The plasticity also increases with pressure under helium atmosphere, but the variations in maximum (with rising temperature) fluidity with pressure differ remarkably with the gaseous atmosphere (Kaiho and

Toda, 1979).

d. An increase in particle size enhances fluidity. For example, 500 μm particles heated at 0.1°C/s become plastic and form cenoshperes like those formed from 100 μm particles heated at 1°C/s. Particles of 100 um diameter, heated at 0.1°C/s are almost non-plastic (Hamilton, 1979).

Recently, a plastometer which allows rapid heating (up to several hundreds °C/s) was designed (Fong, 1985). The measurements from the new plastometer are in qualitative accord with those from Giesler platometers at different operating conditions. The minimum observed viscosity is of order 10^4 poise.

3.4. SWELLING

The swelling is a result of the development of plasticity and the bubble growth due to pyrolysis generated gases, thus the parameters affecting pyrolysis and plasticity are also important in studying the swelling behavior.

The extent of swelling has been measured using dilatometers (Loison, 1982). As in the conventional plastometers, dilatometers operate mostly at low heating rates and at low temperatures. Measurements are made on large coal masses. The results from dilatometers are summarized as the following:

1. The maximum degree of swelling increases with temperature.
2. The rate of both expansion and contraction are greater at high temperatre.
3. Increasing heating rate enhances swelling.

The extent of swelling of a single particle under the rapid heating is

observed by phtomicrographs from regular microscopes and electron microscopes. The quantitative measurements are often confounded by the occurrence of both swelling and agglomerations. However, the general trends are are summarized here.

Temperature effect: The swelling ratio (particle radius/original particle radius) genrally increases with temperature up to around 650°C, after which swelling decreases with increasing temperature (Sung, 1977; Dolan, 1980). Lightman et al.(1968) found that cenosphere formation progressed up to temperatures around 1300°C for particles of 60 or 70 μm diameter and Pohl et al. (1978) observed no swelling at temperatures higher than 1470°C.

Heating rate effect: The swelling ratio generally increases with an increasing heating rate. Nsakala et al. (1978) found significant differences in chars produced following slow and rapid heatings to the same maximum temperature. Rapid heating yields chars of larger open pore volume, lower pore surface area, and lower density. This result is due to rapid heating which retards particle contraction. At a high heating rate (i.e., 10,000°C/s), cenospheres are probably formed transiently, but may not be preserved all the time. At a very high heating rate (i.e., 10^5°C/s or higher), the coal particles exploded into many particles (Hamilton, 1979).

Particle size effect: Feldman et al. (1969) claimed that there is a minimum particle size for given pyrolysis conditions, below which a cenosphere will not develop. Generally, the swelling ratio is increasing for larger particles (Sung, 1979; Dolan, 1980; Street et al., 1969).

Pressure effect: Even though not much work has been done on the pressure effect on swelling, high pressure seemed to supress the swelling (Lightman et al., 1968). Increased pressure, however, reduces the melt viscosity and

increases the amount of gases formed from secondary reactions and available to swell the molten coal. However, at the same time, the total volume of gases in a swollen coal decreases because of larger compression. Therefore, at moderately high pressures, the swelling can increase as pressure increases (Culrose, et al., 1984)

Others: The other factors worth mentioning are particle residence time (Mason et al., 1967), pyrolysis gas composition (Street et al., 1969), and coal maceral composition (Lightman et al., 1968).

Recently, the time dependant swelling ratio of a single particle has been measured by taking movies of pyrolysis experiments (Matsunaga, 1978; Arendt, 1980).

3.5. PREVIOUS MODELING EFFORTS

Comprehensive decomposition and pyrolysis models have been considered by several investigators. Van Krevelen (1956) first used the term metaplast, to mean a metastable intermediate product which is assumed to act as an unstable plasticizer. He used the concept of metaplast and modelled the pyrolysis of plastic coal as a three step process including metaplast production and decompostion:

Coking coal ——————> Metaplast

Metaplast ——————> Semi-Coke + Primary Volatiles + Tar

Semi-Coke ——————> Coke + Secondary Volatiles

He assumed first-order reactions with an Arrhenius type rate law. A mathematical model proposed with many simplifications gave only qualitative results. The plasticity, which was correlated with the concentration of

metaplast, was a function of the rates of the above chemical reactions. Fitzgerald (1956) also derived an early model which included coal going through a plastic stage in pyrolysis. In his model, coal decomposes into gas and fluid coal with the latter also undergoing further decomposition:

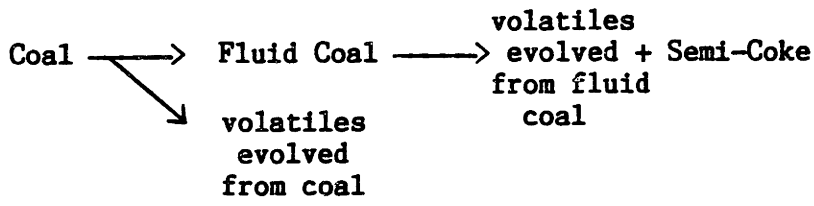

He also assumed first order reactions with the Arrhenius type rate constants and modeled the change in viscosity of coal, while in plastic stage, in terms of the concentration of fluid coal:

$$\text{Relative Fluidity} = \left[\frac{\text{fluid coal}}{\text{total mass}}\right]^{2.5}$$

In both models mentioned above, pyrolysis was modelled with kinetic equations only, and mass transport effects were completely ignored. In modeling mass transport, Anthony included a simple mass transfer coefficent in a model for the pyrolysis weight loss behavior of a highly softening bituminous coal. In his model, he introduced secondary decomposition reactions of a reactive part of volatiles, which compete with the transport. A material balance on the reactive volatile species present in a coal particle gives:

$$\frac{dV_r}{dt} - k_c (C - C_\infty) - k_1 C = \frac{dC}{dt}$$

where dV_r/dt is the formation rate of reactive volatiles and C and C_∞ are vapor phase concentrations of reactive volatiles in the void volume of the coal particle and in the ambient gas, respectively. k_c is the overall

mass transfer coefficient and k_1 is the overall rate constant of the secondary decomposition reactions, here assumed first order. Reaction kinetics were modeled using a multiple parallel reaction model which could fit the experimental data with a statistically distributed activation energy but with a constant frequency factor:

$$\frac{V^* - V}{V^*} = \int_0^\infty \exp\left(-\int_0^t k\, dt \right) f(E)\, dE$$

$$f(E) = \left(\sigma (2\pi)^{1/2} \right)^{-1} \exp(-(E - E_o)^2 / 2\sigma^2)$$

where V^* and V are volatile lose at time $t = \infty$ and t, respectively.

Other recent models considering mass transfer effects include those by Russel et al. (1979), Gavalas and Wilks (1980), and Wen and Chen (1980). The model by Russel et al. was aimed at hydropyrolysis of which pyrolysis is a special case of zero hydrogen partial pressure. The kinetics of their pyrolysis model was the same as Anthony's. They considered two types of volatile transports: diffusion and hydrodynamic flow through pores. The pore structure was caracterized by a single size, corresponding to macropores. The component fluxes are described by the dusty gas model. They expressed their model in terms of four dimensionless parameters which compare the devolatilization to four other processes: deposition of reactive volatiles as coke, diffusion, bulk flow, and direct hydrogenation reactions. They assumed isothermal processes and pseudo-steady pressure gradient inside of pores. In comparing the model prediction with experimental data, Russel et al. chose Anthony's bituminous coal pyrolysis data with the assumption of instantenous heat-up, ignoring time-temperature history. Since the open pore structure assumption does not apply to bituminous coals, the model needs to be re-evaluated with a new set of

parameters for non-softening coals.

Gavalas and Wilks proposed a model describing volatiles transport through pores by taking coal porosity into account. They believed that the roles of pores of different sizes must be carefully accessed in the analysis of combined diffusion and chemical reactions. They divided coal pores into five ranges, varying in diameter from 4A to 100,000 A. The pore connectivities were described by the number of intersections between different size pores. The model predicted that product yields depend on particle size alone, at low pressures, while they depend on both pressure and particle size at high pressures. The model, in general, shows a good fit to sub-bituminous coal but a poor fit to bituminous coal, which is an expected result.

Wen and Chen took a similar but simpler approach to Russel et al.: they assumed pseudo-steady state concentration profile, negligible increase in internal pressure, and equal binary diffusivities. Again, the mass flux of each component was expresed as the sum of the diffusion and the bulk flow through pores. They included the mass transfer outside a particle by using a film theory. The improvement over the model by Russel et al. lies in taking non-isothermal conditions into consideration by analyzing heat transfer between a coal particle and its surroundings. In modeling kinetics, the model included separate pathways for tar deposition and cracking. The model predicted that the pressure effect was related to the rate of tar deposition. However, the sucesses of the model seemed to depend on the number of fitted parameters (7 parameters) in the kinetic model.

The three models above, however, assumed that coal maintained its physical shape and internal pore structure during pyrolysis. These models

are more suitable for non-plastic coals which maintain an open pore structure during pyrolysis rather than for bituminous coals.

James and Mills (1976) described in a qualitative sense some of the important features of plastic coal pyrolysis without rigorous treatment of transport of volatiles. The voids in coal are viewed as pores when the coal is solid, and as bubbles when coal becomes fluid. The bubbles grow and foam the metaplast. Volatile products in voids are divided into two groups: gases formed from condensed phase decomposition and vapors in local equilibrium with a condensed phase. The authors recognized the importance of viscosity in governing the transport phenomena. A complicating factor was that viscosity varied with solid concentration in the coal system, and the solid concentration was a function of pyrolysis reaction and transport rates. The actual modelling of transport was not quite convincing. The transport was based on two types of gradients: the temperature gradient caused by heat of pyrolysis and rapid heating, and the pressure gradient which they claimed to exist due to the restricted diffusion path. Any temperature gradient would cause a void concentration gradient. Bubbles and gases moved under the action of the pressure gradient. However, there is no way for this model to predict the behavior of 70 um diameter particle which is isothermal (Lee, 1979) and yet shows foaming behavior.

Recently, Zacharias (1979) and Unger and Suuberg (1980) presented similar tar transport models based on evaporative diffusion away from the surface of the coal. Without a comparison of mass transfer resistances inside and outside the coal particles, Zacharias assumed that tar formed during the primary coal decomposition evaporated from the surface of the particle. To be able to test the model predictions with the pyrolysis data from a screen heater reactor, Zacharias chose a thin film geometry and the

thickness of the boundary layer for mass transfer was calculated from the rate of flow of bulk gas. The bulk gas flow near the surface was assumed as stagnation flow near a flat plane (Schlichting, 1979), rather than simulating bulk flow due to natural convection. Assuming there are no cracking reactions of tar occurring in vacuum, tar formation rate was obtained from the tar yield at vacuum. Zacharias also recognized the importance of MWD of tar in the model and he included a gaussian distributed MWD of tar and predicted that the mean molecular weight should be 584. Using the parameters predicted by the atmospheric pressure data, the model underpredicted tar yields at high pressure (69 atm).

Calculations by Unger and Suuberg suggest that at pressures of 1 atm and higher the mass transfer resistance is primarily external and hence that it is reasonable to treat tar evaporation from the coal surface as the rate limiting process for overall tar production. However, with an estimated value of tar diffusivities in molten coal, this assumption is valid if (1) particle size is sufficiently small, (2) external pressure is sufficiently high, and (3) the secondary reaction rate is sufficiently fast. At pressures of 10^{-4} to 100 atm and temperatures of 200°C to 1000°C for particles of 70 μm diameter, tar evaporation rate varies several orders of magnitude and it is difficult to conclude which mass transfer resistance dominate the rate equation. A more detailed discussion is given in Ch. 5.1.1.

None of the models mentioned so far describes the change in viscosity of the coal melt, or the growth and escape of gas filled bubbles which are considered as important modes of volatile transport in plastic coal. The only bubble transport model existing is one by Lewellen (1975). He concluded that the bubble generation mechanism was not well understood at the

time and therefore employed a stochastic method to account for bubble generation at specific sites with an initial size. The model then allowed these bubbles to grow by the receipt of volatiles instantaneously transported from the condensed phase. The growth rate of bubble was governed by momentum conservation equations, in which the viscous term had the greatest importance. By keeping account of each bubble site, size, and relative distance from neighboring bubbles and from the particle surface, and the growth rate, coalescense and bubble escape through the particle surface were simulated. For example, the bubble escape was simulated when the thickness of the bubble shell near the particle surface falled below a certain critical value. Correlations of viscosity were proposed as a function of pyrolysis rate and the pressure gradient in the particle. However, the treatment of bubble generation was highly empirical and required a great deal of computer time (many factors affecting bubble generation were chosen at random). The model also required large computer storage space to keep account of all necessary information for each bubble. In addition, because of the limitation in number of bubbles that can be treated, the model predictions were not always a smooth function of time, especially when the rapid growth of the bubbles were allowed.

4. EXPERIMENTAL

4.1. INTRODUCTION

As stated in the previsous section, metaplast, which is hypothesized to be responsible for the plastic behavior of softening coal, is a poorly understood material, whose chemical and physical nature are as yet unknown. The objectives of experiments in this thesis were to provide better quantitative information on metaplast formation and depletion kinetics, and to determine the molecular weight distribution of metaplast and tar at various stages of pyrolysis. Because the equilibrium vapor pressure of complex organic compounds can be estimated from a correlation of temperature and molecular weight, information on the molecular weight distribution of metaplast and tar throughout the pyrolysis cycle is important in modeling the transport of metaplast and, therefore, in modeling the mass balance of metaplast within the softened coal particle.

The weight of material recoverable by solvent extraction of char particles after the coal had undergone pyrolysis via a known time-temperature history is taken as a measure of the amount of metaplast remaining within the coal at that stage of pyrolysis. Similarly, the molecular weight distribution of the extracted material is taken as the molecular weight distribution of metaplast.

4.2. EXPERIMENTAL FACILITIES AND PROCEDURES

4.2.1. Pyrolysis

Coal selection

The coal used in this study was a Pittsburgh seam No. 8 bituminous coal from the Ireland mine of the Consolidation coal company, which is a typical high-caking eastern U. S. bituminous coal. This same coal type was used by Anthony (1974) and Suuberg (1977) in investigations of rapid pyrolysis behavior, by Franklin (1980) in a study of mineral matter effects during pyrolysis and by Serio (1984) in a study of secondary reactions of tar.

The Pittsbrugh seam coal is a good candidate for this study because of the following:

(1) There is the kinetic information available on volatiles yields and secondary reactions of tar in helium (Zacharias, 1979; Serio, 1984).

(2) Suuberg's investigations found that pyrolysis of Pittsburg seam bituminous coal exhibits the mass transfer effect which causes different volatiles yields at different pressures.

(3) Pittsburgh seam coal has been a good candidate for plasticity studies using conventional plastometers because of its highly softening properties.

The particular batch of the Pittsbugh No. 8 coal used in the present study was received at MIT in 1975 and sealed under nitrogen in 30 lb. buckets in early 1976. It was the same batch that was used by Franklin and Serio. An ultimate analysis of the coal is shown in Table 4.2.1 along with similar data on the sample used in the previous studies.

Apparatus

The apparatus employed was the captive sample apparatus which was first designed by Anthony (1974) and later modified and enlarged by Caron

Table 4.2.1. Characteristics of Coal Examined

Coal Type: Pittsburgh Seam (No. 8) Bituminous Coal

Ultimate Analysis (wt %, Dry)

	This Study[a]	Serio (1984)	Franklin (1980)	Suuberg (1977)
Carbon	71.95	73.59	71.74	68.8
Hydrogen	5.17	5.16	4.84	4.9
Oxygen	9.28	7.07	6.22[b]	8.2[b]
Nitrogen	1.22	1.29	1.14	1.3
Sulfur	4.80	5.32	5.77	5.4
Ash	9.36	10.26	10.80	11.5

Proximate Analysis (wt %, Dry)

Moisture	1.30[d]	0.55[c]	2.0[d]	1.4[d]
Volatile Matter	42.68	41.60	36.9	39.4
Fixed Carbon	47.96	48.1[b]	52.0[b]	49.1[b]
Ash	9.36	10.26	10.8	11.5

Heating Value (Btu/lb)

	13333	13201	-	-

(a) analyzed by Huffman Laboratories, Inc.
(b) by difference.
(c) dried basis.
(d) as-received basis.

and Hajaligol (1979). A schematic view of the apparatus is shown in Fig. 4.2.1. The apparatus consists of the reactor, the electrical system, the time-temperature monitoring system and the product collection system.

The reactor is designed for pyrolysis measurements at atmospheric pressure and also at vacuum. A detail of the reactor design is given in elsewhere (Caron, 1979). The reactor vessel is a cylindrical pipe made of corning pyrex, 22.86 cm in diameter and 22.86 cm long. The top and bottom of the reactor are 3/8" thick stainless steel plates which seals the reactor vessel with wing nuts and O rings. The top plate is equipped with electrical feeds, thermocouple feed, and gas inlet/outlet port. The bottom plate has one 1.5 inch pipe threaded in the center in which a 2.6 inch pipe nipple is threaded. The pipe nipple supports a perforated plate upon which the cap with a filter is placed.

The coal sample is placed on a piece of 325 mesh stainless steel screen (13 x 14 cm), which is then folded on itself twice and clamped between the two brass electrodes as shown in Fig. 4.2.2. The screen is heated by high current power supplies: the heating variac during heat-up and the holding variac when the sample is maintained at a desired temperature. The peak temperature and the holding time at the peak temperature are controlled by industrial timers (1 s and 60 s units respectively). The heating rate is controlled by changing the setting on the heating variac and a desired holding temperature is achieved by adjusting the setting on the holding variac. The quenching of the sample occurs by natural cooling through radiation, conduction and convection. The time-temperature history of the coal particles is measured by a chromel-alumel thermocouple (24 μm wire dia. and 75 μm bead dia.) placed within the screen and connected to a fast response recorder.

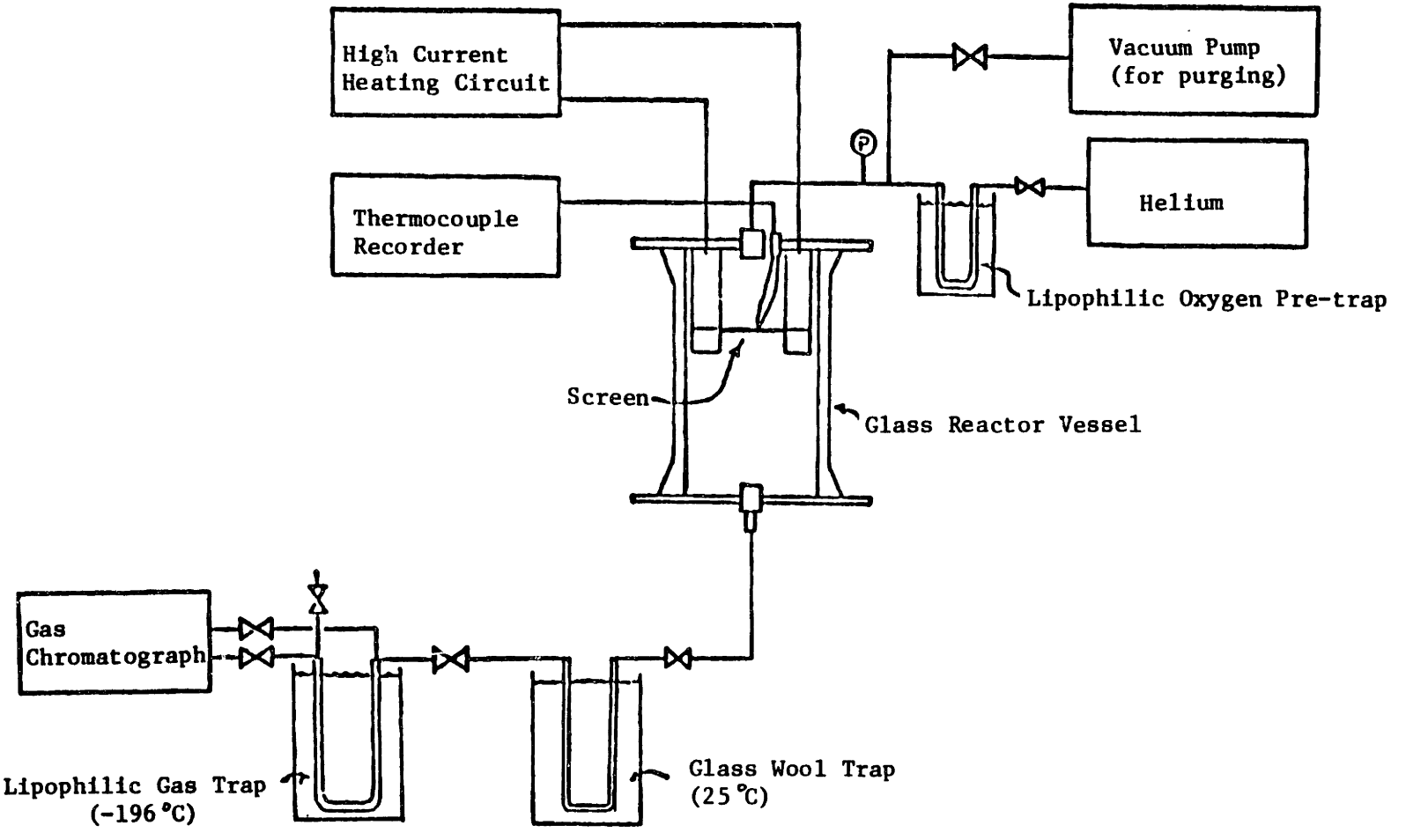

Fig. 4.2.1. Captive Sample Apparatus

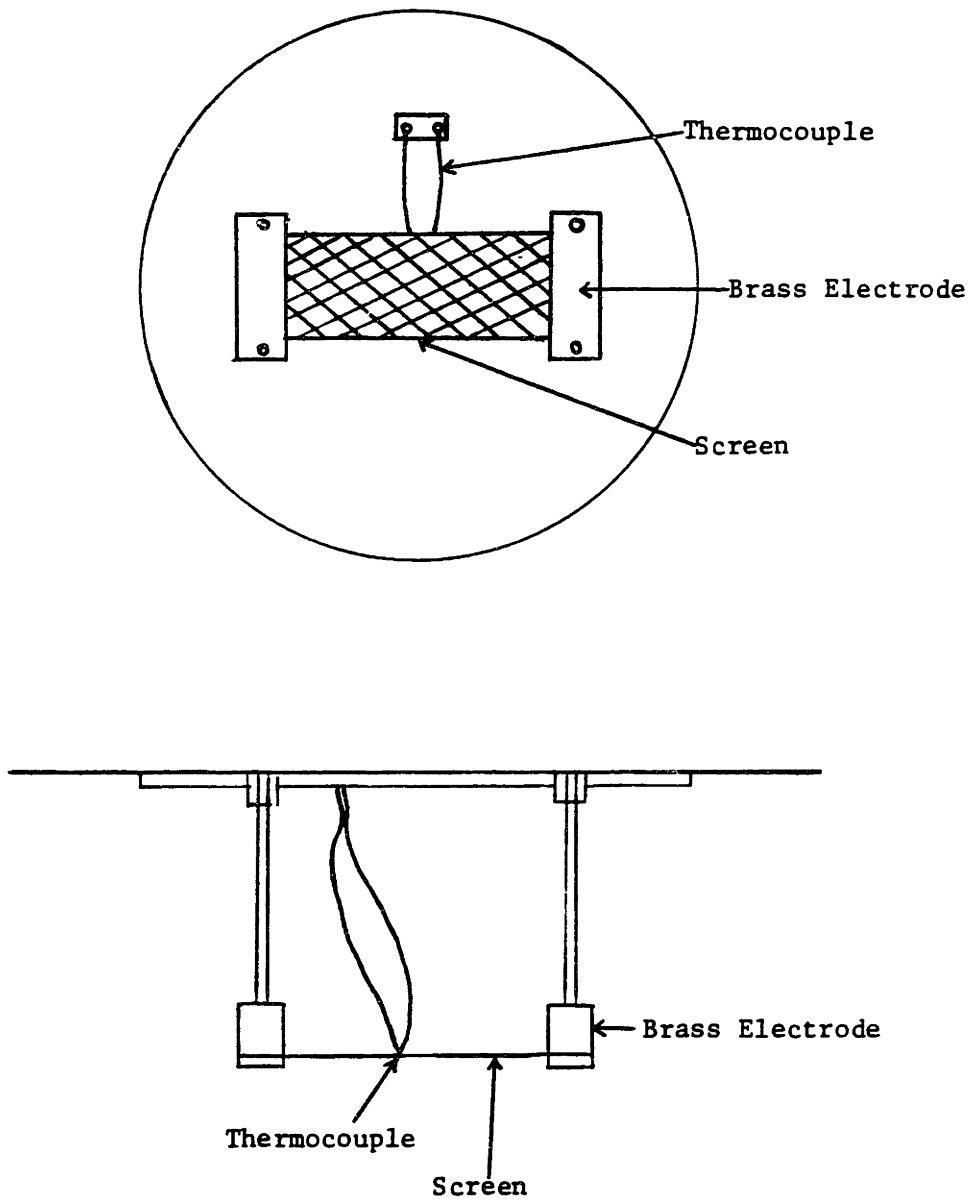

Fig. 4.2.2. Captive Sample Reactor Details

The product collection system is also shown in Fig. 4.2.1. In previous studies, char as a product has been defined as the condensed phase material retained on the screen upon the completion of the run. In the present work, char is further separated into solvent extractible material and a condensed phase (i.e. unextracted) residue. Tar is collected on a piece of filter paper at the reactor outlet and on other reactor surfaces. The latter fraction is collected by washing the reactor internals using glass fiber filters soaked in methylene chloride.

Gas products heavier than hydrogen are collected in a trap, consisting of a tube packed with Porapak QS immersed in a Dewar flask of liquid nitrogen (-196°C). Gas and condensible products are analyzed on a Perkin Elmer Sigma 2 chromatograph with dual flame ionization/thermal conductivity detectors. This system is connected to a Sigma 10 data station. Individual yields of CO, CH_4, CO_2, C_2H_2, C_2H_4, and H_2O are obtained, as are total C_3's and total C_4+ yields. Hydrogen as a product has to be determined in an independant set of runs by using nitrogen as pyrolysis gas and as a carrier gas in Gas Chromatography analysis, instead of helium. Previous pyrolysis work with the same bituminous coal (Suuberg, 1977) showed the maximum hydrogen yield of 1 %. The hydrogen analysis was not attemted here.

Coal sample preparation

A batch of coal of U. S. standard mesh (< 212 μm) was dry-sieved through a stack of 3 trays for about 2 hours using a Ro-tap machine. The -170+200 mesh (90 - 75 μm) mesh was used here. After dry-sieving, the particles were wet-sieved in order to remove fine ash and coal particles which adhere to the larger ones (Tejpar, 1978; Franklin, 1980). This was done by putting distilled water until the effluent was clear. The coal was then dried in air until it became free flowing (~2 hrs) and stored in a

dessicator.

Experimental Conditions

The studies by Anthony and Suuberg revealed that temperature and pressure along with particle size are the important variables in studying the kinetics and the mass transfer effect of pyrolysis but heating rate does not affect the ultimate pyrolysis yield. However, the study of the particle size effect in the screen heater reactor with a caking coal is difficult because the particles soften upon heating and form a thin slab at 1 atm and higher pressures. Therefore, the particle size and heating rate are fixed in this study while temperature and pressure are varied. The high heating rate previously employed in many gasification studies in this labroratory, 1000°C/sec, is chosen and the particle sizes of 75 - 90 μm are used to ensure no temperature gradient inside the particle at the chosen heating rate. Temperatures are varied from 200 to 1000°C at pressures of 0.0001 atm and 1 atm. High pressure experiments are not attempted due to the pressure limitation of the reactor vessel.

Sample size

The size of the screen is relatively large compared to the ones used in the old reactor by Anthony and there exists a temperature gradient across the screen. As the screen is heated, the electrodes, the reactor walls, and the helium atmosphere remain at room temperatures except the region in the immediate neighborhood of the screen. Therefore, there are conductive heat losses at both ends of the screen and the center temperature of the screen is expected to be higher than that at the ends. The

actual measurements of temperatures at the two spots of the screen, one at the center and the other at 2/3 of way to the electrode from the center, are shown in Fig. 4.2.3. The temperature at the center is actually higher by 87°C than the one at the side when the peak temperature (877°C at the center) is reached.

In pyrolysis experiments, coal particles have to be spread on the screen in monolayer (if possible) to minimize secondary reactions. However, the area on which the coal particles are spread has to be limited to the center of the screen to ensure that the particles are uniformly heated. Eventhough the screen is sized to handle as much as 100 mg of coal of 75 - 90 μm particle diameter, the use of only 35-40 mg of coal, thinly spread in the center area, is recommended.

Run Procedure

About 35 - 40 mg of coal particles are spreaded out on a preweighed screen which is reweighed and clamped between the brass electrodes. A preweighed aluminum foil is placed in the bottom of the reactor and also a preweighed cap with a filter is screwed into the gas inlet/outlet port on the bottom plate. The reactor is then bolted up, evacuated to ~ 0.0001 atm, flushed several times with helium, and then set at vacuum (~ 0.0001 atm) or at 1 atm absolute pressure. The heating circuit is activated to bring the coal through the desired time-temperature history. Upon the completion of a run, the system is purged with helium at ~2 ℓ/min for 1.5 hours. This procedure has been shown to provide good material balances, implying that most of the product has been trapped and recovered for analysis.

A typicial time-temperature history, shown in Fig. 4.2.4, consists of a linear heating period which is followed by the natural cooling period.

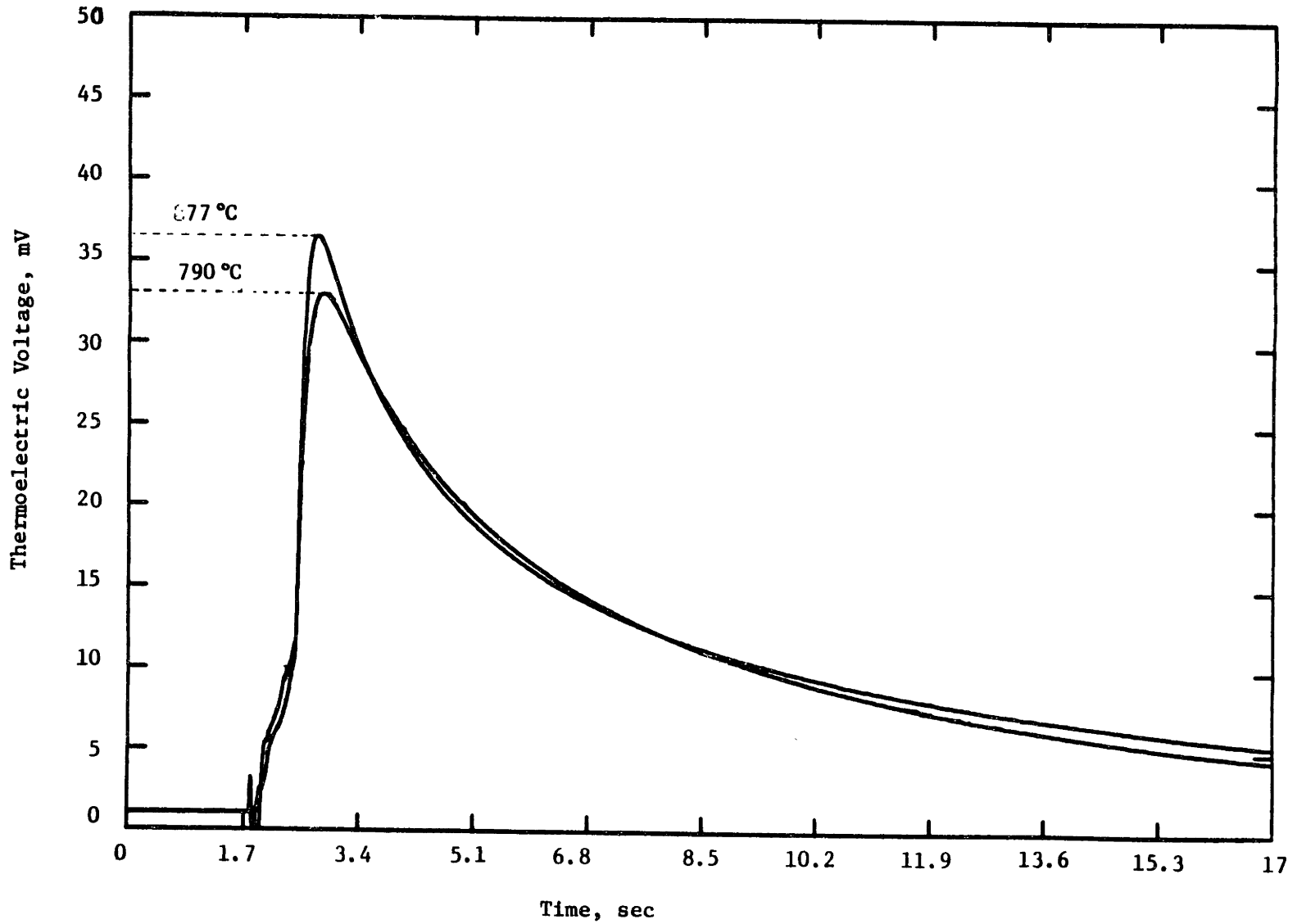

Fig. 4.2.3. Temperatures at two spots of the screen, as a function of time; (a) at the center and (b) at the side, measured by Chromel-Alumel thermocouples and recorded by Bascom-Turner electronic recorder.

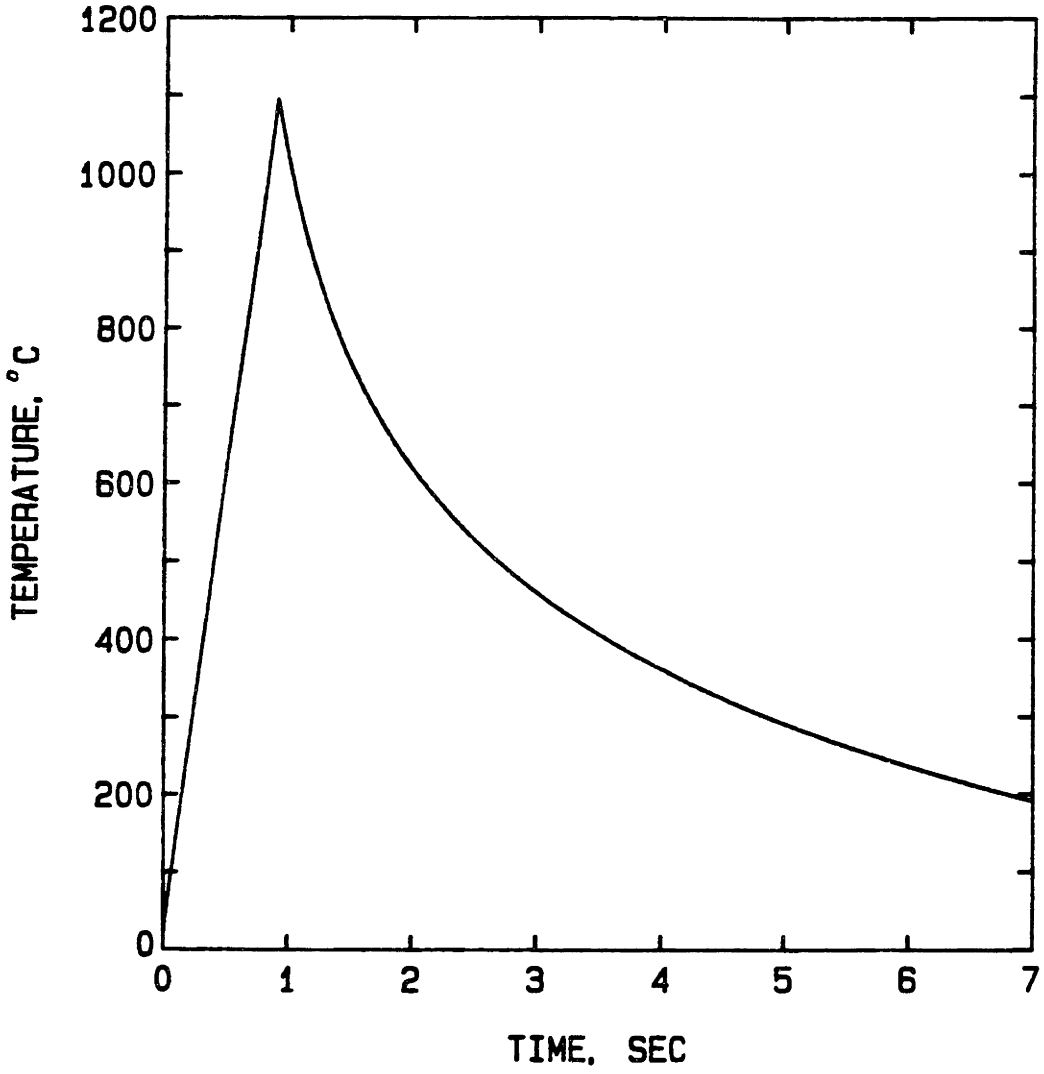

Fig. 4.2.4. Example of typical time-temperature history.
From run 6SA: Peak Temperature = 1100 °C, Pressure = 1 atm

Since the quenching of the screen occurs naturally, there is a slight variation in cooling behavior from run to run. The actual time-temperature history recorded for each run is accounted for in the kinetic analysis.

The screen is reweighed to determine char yield. The char is saved for the extraction experiments. Tar is collected from the reactor surface by wiping with preweighed glass fiber filters soaked with methylene chloride. The tissues (i.e., Kimwipes) which had been used previouly for this purpose(Gaosh, 1983) were not used here because they were found to be highly hydroscopic. However, loss of fibers from the filters is a potential problem, which is minimized by gently wiping the reactor surfaces with only the shiny side of the filter. The solvent on the filter is evaporated at room temperature in a hood, and the filters are reweighed, along with an aluminum foil liner from the bottom of the reactor and the filter from the reactor outlet, to determine tar yield. Tar collected on the exit filter and on the aluminum foil is dissolved in pyridine as soon as possible for the molecular weight analyses (see Section 4.2.4). The porapak trap with gas products is placed in boiling water to drive off the gas products, which are analyzed on the gas chromatograph (see Section 4.2.3).

The experimental conditions and the product analysis systems are summerized in Fig. 4.2.5.

4.2.2. Solvent Extraction

Choice of Solvent

Pyridine(MW= 79.10, and BP= 115°C) was chosen to dissolve tar and for extraction of char because of its ability to dissolve tar almost completely and to dissolve appreciable amounts of coal at temperatures much lower than

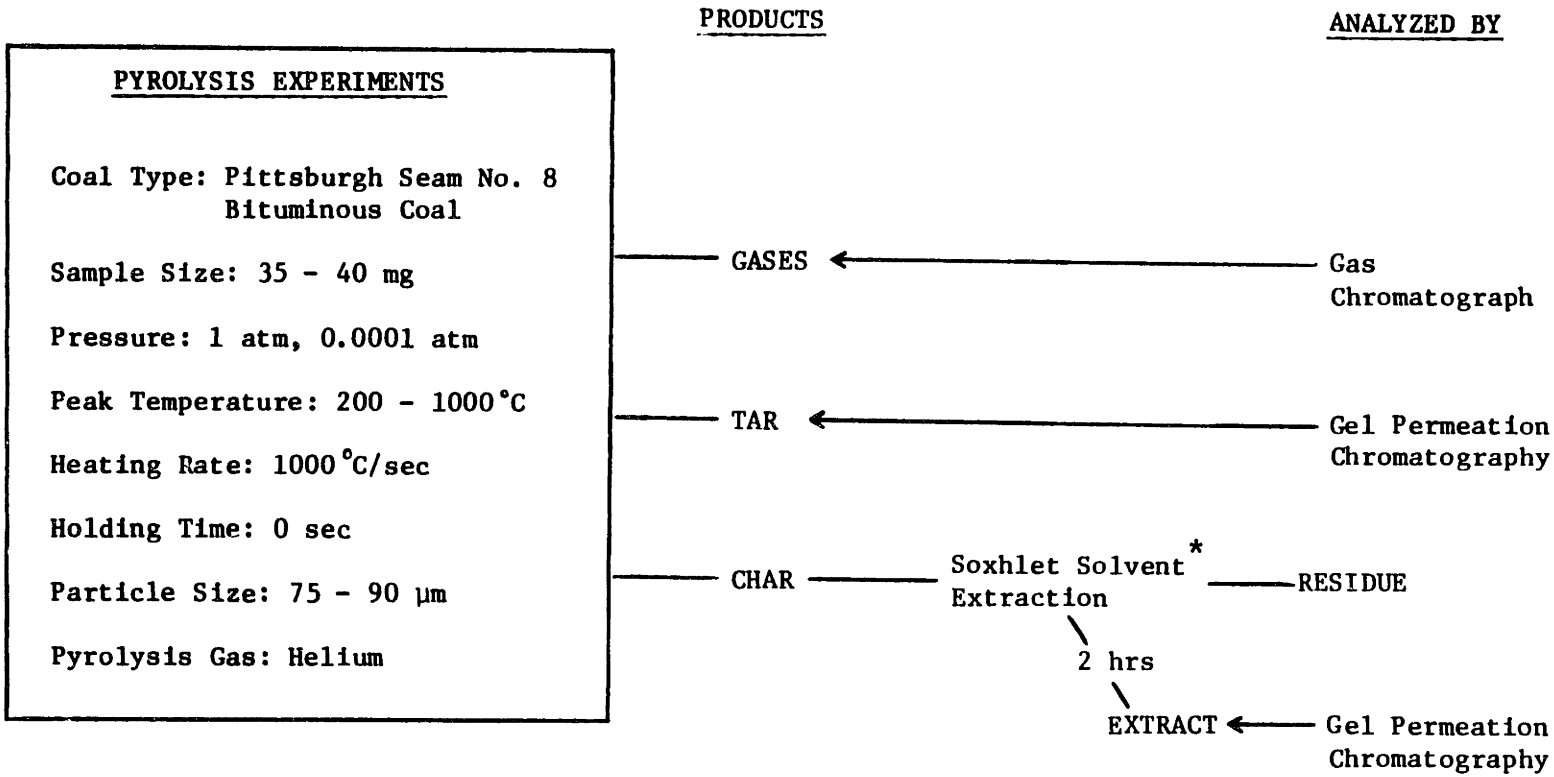

* Solvent: Pyridine

Fig. 4.2.5. Experimental Conditions and Product Analysis Techniques

pyrolysis temperatures. Also pyridine does not react with coal and, the yield of pyridine extract has been shown to correlate qualitatively with coal plasicity as measured by a Gieseler plastometer. More detailed discussions are given in Chapter 3 in the review of the solvent extraction of coal and in section 4.2.4 which discusses the solvent selection for Gel Permeation Chromatography.

Apparatus and Run Procedures

Extractions of char produced at various peak temperatures are carried out in a Soxhlet extraction apparatus. The screen with char particles is placed in the porous thimble and the latter is placed in the inner tube of the Soxhlet apparatus. The apparatus is then fitted to a round-bottomed flask containing about 100 ml of pyridine and to a reflux condenser. The solvent is boiled gently and the vapor passes up through the side tube and is condensed by the condenser. The condensed solvent falls into the thimble and slowly fills the body of the Soxhlet. When the solvent reaches to the overflow level, it siphons over into the flask, and thus removes that portion of the substance which it has extracted in the thimble. The process is repeated automatically.

The 25 ml of extract solution is removed from the round flask after 2 hours of extraction for molecular weight distribution (MWD) analysis. After adding 50 ml of new solvent, the char sample undergoes another 16 hours of extraction to ensure complete removal of the pyridine soluble material from the char. Then, the thimble is removed and dried at room temperature for a day and for 2 hours at 90°C in a vacuum oven to evaporate the solvent. The weight loss is determined by weighing the thimble containing the screen and char before and after the extraction. The tar

solutions and the extracts removed at the 2 hour stage of the extraction are stored in dark bottles and kept in a refrigerator until the analysis of the molecular weight distribution.

As stated ealier, the extracts to be analyzed for MWD are removed at the 2-hour stage of extraction to prevent it from being degraded in the boiling solution (115°C). To investigate the changes in the extract solution due to boiling, extracts are removed after 2, 4, and 6 hours of extraction. And then the sample is removed from the soxhlet and the solution is left to boil for another 12 hours. Fig. 4.2.6 compares the GPC Chromatograms of 2-hour, 4-hour, and 6-hour extract solutions (Curves A, B, and C, respectively) along with the solution subjected to an additional 12 hours of boiling (Curve D). Comparing curves C and D, one can see that boiling causes the solution to lose the lighter fractions and to gain the heavy fractions. Changes in curves A to C may also be caused by boiling or by extracting more of heavy fractions from char at the later stage of extraction.

Friedel et al.(1968) studied the chemical composition of pyridine extract at room temperature from a Pittsburgh seam coal. Extracts are removed after 5 minutes, 30 minutes, and 17 hours of extraction and analyzed by a mass spectrometer. They found that 1 and 2 ring aromatics predominate in the 5-min extract and higher aromatics predominate with longer extraction. However, the composition of 30-min and 17-hour extracts were essentially the same; the 30-min extract contains slightly higher concentration of 3-ring (0.5 % higher) and smaller aromatics (1 % higher) while the 17-hour extract contains slightly greater amount of 4-ring (0.5 % higher) and the larger component (0.5 % higher). In the light of Friedel's study, one can conclude that the changes in the GPC chromatogram of 4-hour

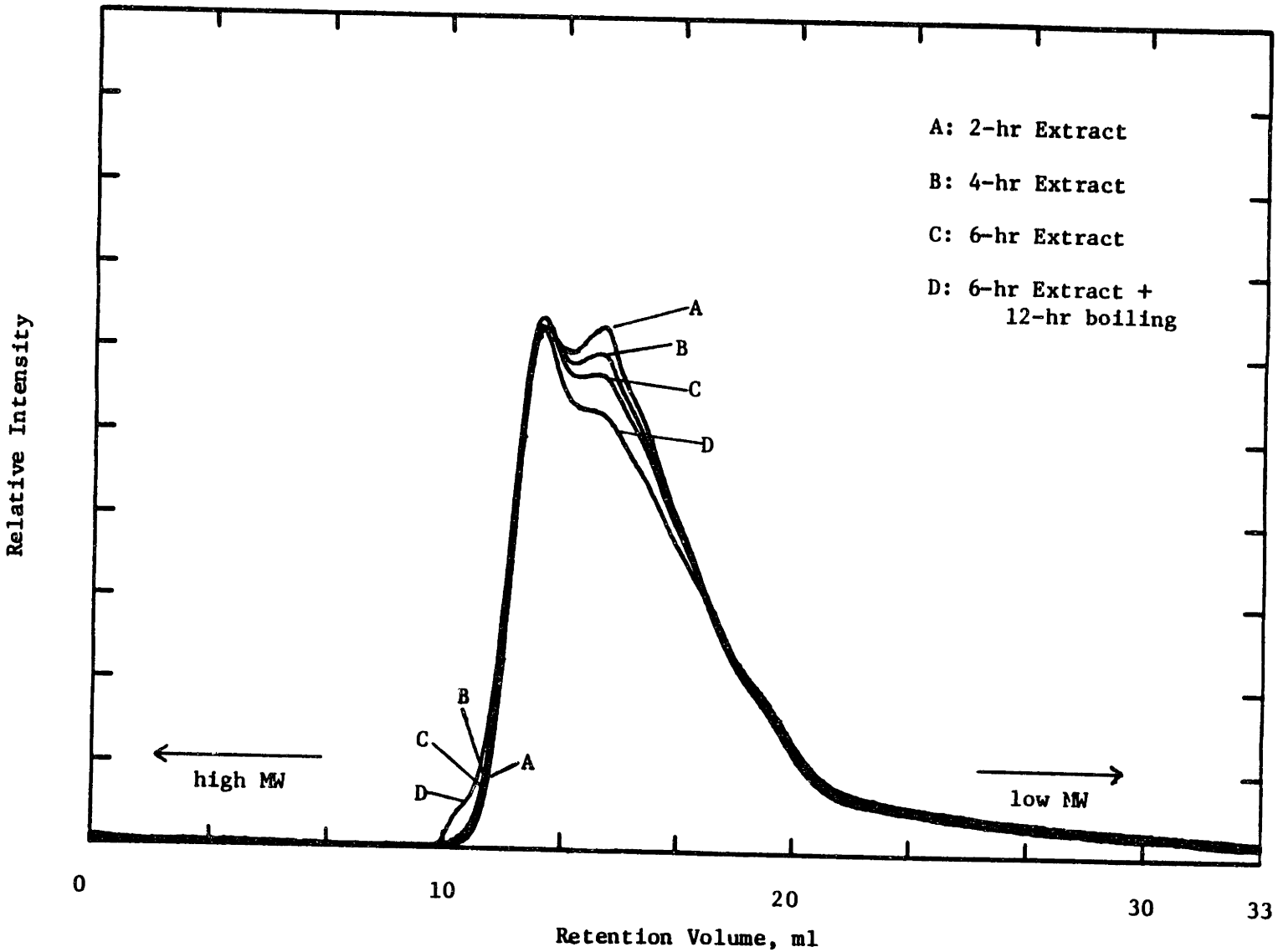

Fig. 4.2.6. Changes in molecular weight distibution of pyridine extracts with extraction time and with boiling at 115 °C

and 6-hour extracts are caused mainly by boiling rather than extraction of heavy substances.

4.2.3. Gas Analysis (Gas Chromatography)

Column system

A gas analysis system was developed for analysis of light hydrocarbons (CH_4, C_2H_4, C_2H_6, C_3's, and C_4's) and light oxygenated species (CO, CO_2, and H_2O). This was accomplished by using two columns, a 12' x 1/4" column packed with 50/80 mesh Poropak QS (Waters Assoc.) and a 10" x 1/4" column packed with 60/80 mesh Molecular Sieve 5A (Alltech #5604). The columns are connected with a Valco 10 port column switching valve (CSV), which allows the sequence of the column to be reversed (see Fig. 4.2.7a). Injection of the sample occurs CSV in position A. Here the carrier gas is directed through the porapak gas trap. At the beginning of an analysis, the contents of the porapak trap are swept out by the carrier gas onto porapak QS (PQ) column.. The light gases (H_2O, N_2 and O_2) proceed quickly through the PQ column and are separated primarily on the molecular sieve(MS) column. Immediately after the nitrogen peak exits from the MS column, the CSV is switched to position B. This reverses the order of the columns, putting the PQ column closest to the detectors. Consequently, the heavier components are never on the MS column. At the time of switching, the carbon monoxide peak has left the PQ column and is on the MS column. It has to travel across the PQ column again to get to the detectors. The methane peak is near the end of the PQ column, prior to switching. It is eluted to the detectors shortly after the switch is made. The CO_2, C_2's C_3's, etc are always on the PQ column and are largely unaffected by the switch.

Fig. 4.2.7. Gas Chromatography System

(a) Column Sequence Reversal System

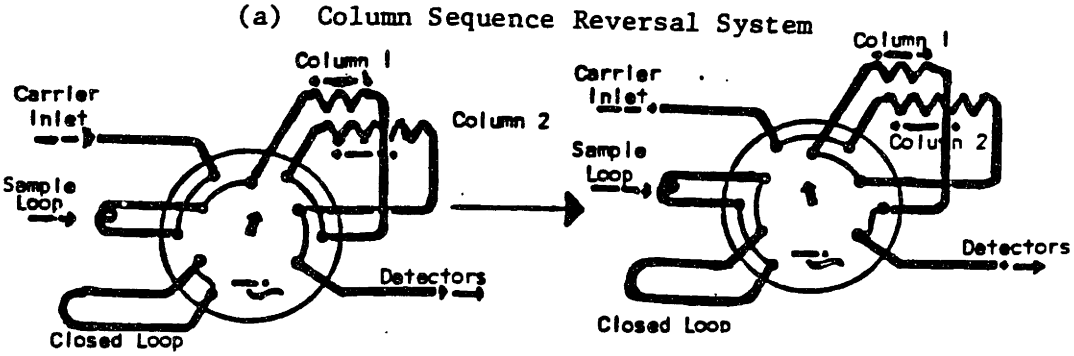

Valve Position A Valve Position B

Column 1 (Porapak QS) = 12"
Column 2 (Molecular Sieve) = 10.8"

(b) Detector System

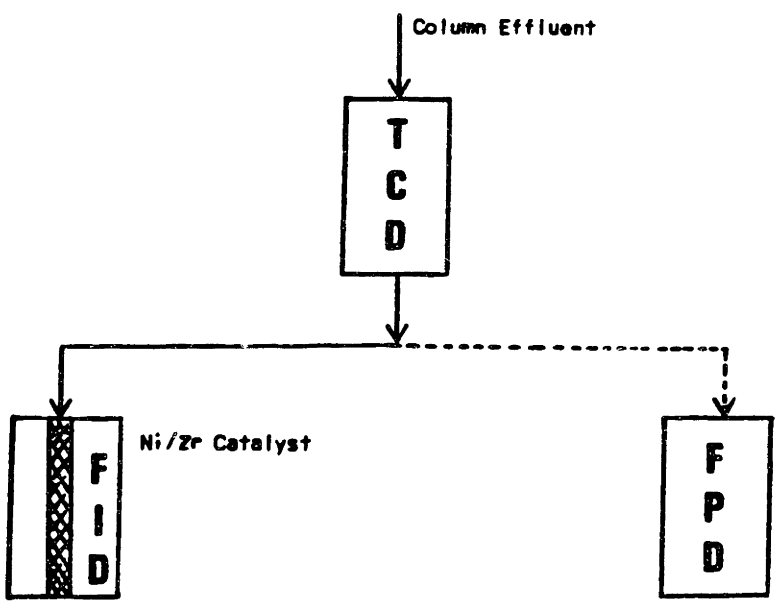

The purpose of switching two columns is to separate CO, CH_4, O_2, and N_2 without resorting to subambient tempertures, which is necessary if only the PQ column is used (e.g., Suuberg, 1977).

Detectors

After components leave the last column, they enter a thermal conductivity detector (TCD) followed by a flame ionization detector (FID) as shown in Fig. 4.2.7b. A flame photometric detector (FPD) which is sensitive to sulfur compounds is not employed in this study.

In some of the gas analyses, a nickel/zirconia catalyst bed which was installed in FID was employed to convert CO and CO_2 into CH_4 in the presence of H_2. This procedure allows these oxygenated gases to be analyzed on the FID, which is about 60 times more sensitive for CH_4 than the TCD is for CO or CO_2. The use of a catalyst bed adds some backpressure to the column system which affects the length of the MS column and the elution and switching times. However, the conversion efficiency is not very good for large amount of CO or CO_2 and sulfur compounds in pyrolysis gas (mostly H_2S) deactivated the catalyst bed constantly and it was dropped in later stage of the work.

Chromatography system

The chromatography system consists of a Perkin-Elmer Sigma 2 chromatograph with a Sigma 10 data station, both of which are microprocessor based. When the chromatograph reaches the initial conditions for an analysis, it activates a relay which automatically initiates the start of its temperature program. After 0.1 minutes another relay is activated to turn on the data station. At the end of the analysis both instruments are reset auto-

matically. During an analysis the columns are held at 55°C for 7 minutes, heated to 120°C at 10°C/min and then heated to 240°C at 25°C/min and held for 30 minutes.

Calibration and data analysis

In every gas analysis, 0.5 CC of methane (99.97 % purity) was injected 3 or 4 times and was used as the standard calibration gas. For gases other than methane, the response factors were used to calculate the amount of gas i:

$$mg_i = R_i \cdot A_i \cdot \left(\frac{mg_{CH_4}}{A_{CH_4}}\right)$$

where mg_i = Amount of gas species i

A_i = Response factor or i

mg_{CH_4} = Mass of methane of 0.5 cc

A_{CH_4} = TCD of FID peak area of 0.5 cc methane

A_i = TCD or FID peak area of gas i

A series of calibration runs were made to determine the response factors and the calibration procedures and results are summerized in Appendix A.

4.2.4. Gel Premeation Chromatography

Gel Permeation Chromatography involves the size separation of molecules in solution. The separation of sample molecules is based upon differences in their effective sizes in solution and the effective size is closely related to molecular weight (MW). Separation is accomplished by a

column packed with porous particles of which the pore sizes are closely controlled. Molecules with small effectives sizes (low MW) will penetrate more pores than molecules with larger effective sizes and, therefore, take longer to emerge from the column. Each column has a total exclusion limit, a size above which all molecules are excluded, and a total permeation limit, a size below which all molecules will equally penetrate the porous network.

The effecti e size usually correlates well with molecular weight, particularly for a homologous series of compounds. For this reason, GPC is well suited for polymer solutions and it is widely used as a characterization tool in the development and manufacture of polymers. However, in recent years the technique has been used freqently in the analysis of petroleum fractions and coal liquids.

Equipment

The GPC system used is a Waters Assoc. ALC/GPC 201, which is shown in schematic form in Fig. 4.2.8. The basic system consists of a U6K injector, an M-45 pump, two detectors (R401 differential refractormeter and Waters Assoc. Model 440 UV aborbance detector) and recording systems (a Fisher No. B5217-51 chart recorder and a Bascom Turner No. 4120T electronic recorder). The electronic recorder was used to automatically digitize and store the detector output signals. This information was then transferred to a computer and was converted to molecular weight distribution curve using calibration line (log(MW) vs. elution volume). Subsequently, the average molecular weights were calculated.

Columns: The analyses were done on a set of two Microstyragel columns, of 100 and 500 A. The 500 A column has an exclusion limit of 10,000 MW, which

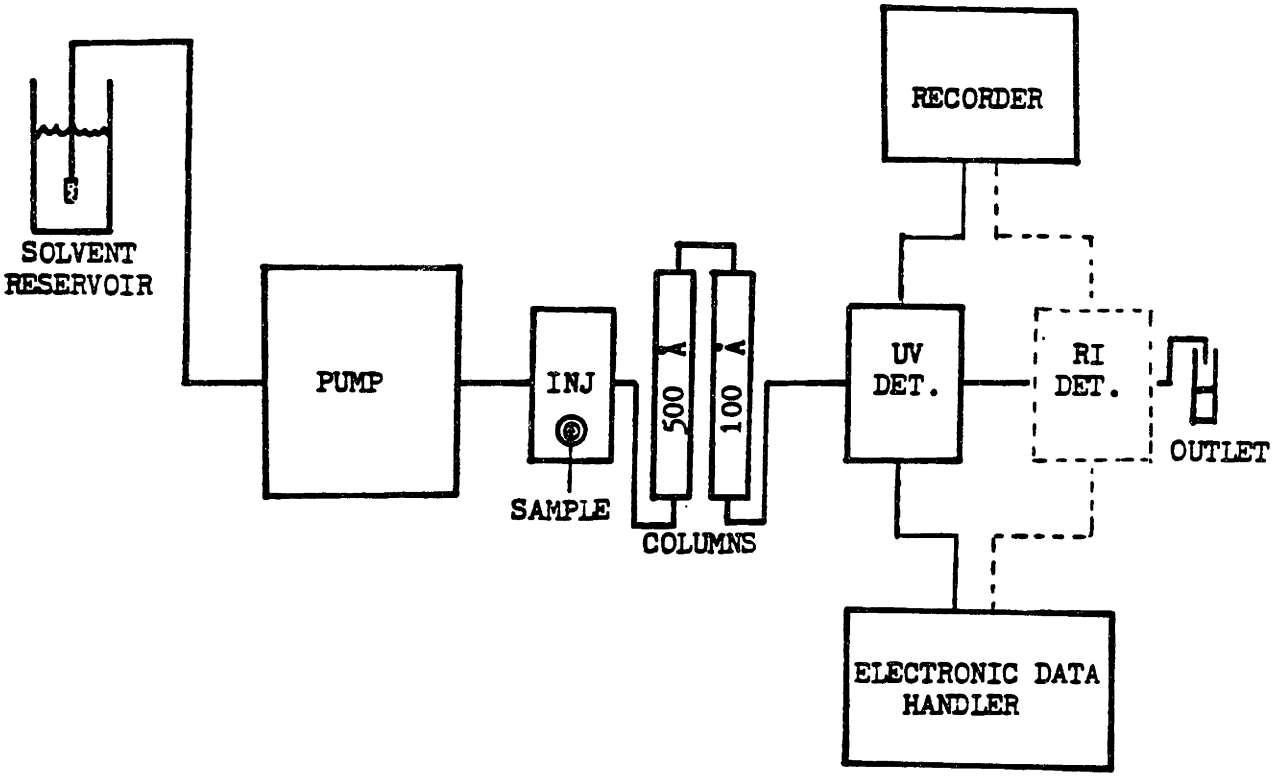

Fig. 4.2.8. Schematic of Gel Permeation Chromatography System (Montero-Garcia, 1983)

is well above the values reported for coal tars in the literature (150 - 3000). The actual separation is done in the second column, 100 A column, which has the separation range of 2000 - 100 MW.

Detectors: R401 differential Refractormeter (RI detector) continuously measures the difference in refractive index between the mobile phase and the mobil phase containing the sample. The RI device reponds whenever the solute differs in refractive index from the mobile phase by typically > 0.05 RI units. Thus, for maximum sensitivity the solvent and solute should differ in RI as much as possible. Particular care must be taken to keep a stable base line and reference cells should be flushed periodically with the mobile phase. A big disadvantage of RI detector with coal tar and extract is its low sensitivity. The concentrations of some of extract solutions were too low to be detected by the RI detector. The other problem is the water content of the sample. Depending upon the water content, the chromatogram has either a large positive or negative peak of water associated with the solvent, which actually create a discontinuity in the chromatogram. RI detector is not employed in this work.

UV absorbance detector (UV detector) measures the UV absorption (at one or more wavelengths) of the solute in a solvent which is reasonably UV transparent. UV detector has higher sensitivity than RI detector with coal samples. Other advantages of UV detector are that it is relatively insensitive to mobile phase flow rate and temperature changes, and it is reliable, repeatable, and easy to operate. Since the UV wave length is chosen where the solvent gives the minimum response, the water associated with solvent does not appear in the UV chromatogram. The sensitivity of the UV detector is higher at shorter wavelength but the linearity of detector response with concenrations is much better at longer wavelength.

The detector response with the concentration could vary with molecular weight. Frederickson and Morris (1979) found the response of UV detectors is also quite variable in the lower MW range. Snyder (1969) and Briggs and Smith (1976) also found the high response for the high and low MW species and a minimum response at intermediate values (600 - 1000 amu). However, Unger and Suuberg (1983) found that the response of their UV detector (at 330 nm) per unit mass of tar was uniform over the entire molecular weight range studied.

Choice of Solvent

Yau et al. (1979) gives the following criteria for selecting solvent for the mobile phase in GPC:

(1) The solvent must completely dissolve the sample.

(2) The solvent must permit adequate detection of solute in eluent; with UV detector, the solvent should transmit more than 10 % of the incident energy at the chosen wavelength.

(3) The solvent must not degrade the sample during dissolution.

(4) The solvent also must not corrode any of the components of the chromatograph.

(5) To be effective with μ-styragel, the solvent must swell the packing.

(6) A solvent of low viscosity is preferred.

(7) A solvent is required to help minimize the molecular association and interactions between solute and column.

In our experiments, the solvent for the mobile phase is also used to dissove tar and for solvent extraction to remove metaplast remaining in char. It is important to use the same solvent not to change the property

of tar and extract when they are introduced to GPC. Therefore, the additional requirements are

(8) The solvent must dissolve appreciable amount of coal at temperatures much lower than pyrolysis temperature.

(9) Solvent must not react with coal.

(10) The yield of extract must have a quantitative or a qualitative correlation with the plasticity.

Only solvents satisfying the solubility criteria (1, 3, 9, and 10) contain a hetroatom such as oxygen or nitrogen (See Chapter 3). Typical solvents in this catagory and their properties are

	MW	B.P., C	Viscosity	UV cut-off
Pyridine	79.10	115 C	0.974	305
Tetrahydrofuran	72.12	66	0.55	220
Ethylenediamine	60.11	119	1.61	?

Ethylenediamine is not a common solvent to use with μ-styragel and is not recommonded for MW measurement. Tetrahydorfuran is favored by secondary criteria like viscosity, volatility, and ease of handling (Unger and Suuberg, 1983). However, the extraction capability of pyridine is much stronger than THF. Furthermore, special safety precautions are needed in handling THF because of its tendency to form highly explosive peroxides. Therefore, pyridine was chosen in this work.

Calibration

The term 'effective molecular size' is diffucult to define because there are many size parameters that can be used to describe molecules or particles of different shapes and configurations. With the samples of complicated mixture like coal tar and extract, it is best to find a unique

calibration curve using its own sample so that the GPC elution curve will be transformed into a MWD curve. Two calibration methods are employed. The peak position method requires the tar sample to be fractionated into narrow molecular weight ranges. The MW of each fraction is obtained using a vapor pressure osmometer (VPO) and is related to the average retention volume of the GPC chromatogram of each fraction. The linear calibration method has an advantage of not requiring fractionation. It assumes a log-linear calibration line ($\log(MW) = D_1 - D_2 \cdot V$), where D_1 and D_2 are constants and V is the retention volume. From the GPC chromatograms of two known molecular weight samples, the two constants, D_1 and D_2, are evaluated. The molecular weights of the samples can also be obtained using VPO. The detailed discussions of VPO and two calibration methods are given in Appendix B.

Sample preparation and analysis conditions

Tar collected from the bottom of the reactor and the exit filter is dissolved in approximately 10 ml of dry pyridine. 25 ml of pyridine extract removed at 2 hours stage of extraction is also saved. No drying is attempted not to change the property of the samples. The tar solutions and extracts are saved in dark bottles and kept in the refrigerator till GPC analysis. Analysis conditions are

Detector = UV detector, wavelength 405 nm
Sample size = 100 ~ 250 µl
Temperature = 23°C (room temperature)
Inlet pressure = 1100 - 1500 psia
Flow rate = 1.0 ml/min
Data aquisition rate = 1 point/sec

4.3. RESULTS AND DISCUSSION

4.3.1. Yields of Volatiles and Extract Yield

Total volatiles, tar and extract yields

Figures 4.3.1 and 4.3.2 show the total volatiles yield, tar yield (top) and the yield of pyridine extracts (bottom) as a function of peak temperature (PT) at 1 atm and at vacuum(~ 0.0001 atm), respectively. Each data point at a peak temperature represents an integral yield as the coal is heated to a peak temperature at 1000 °C/s and then immediately subjected to quenching by natural cooling. All results in this section are reported on an as-received basis.

The yields of total volatiles and tar increases with the increasing peak temperature showing asymptotic yields of 47 % and 28.1 % at 1 atm and 51 % and 33 % at vacuum, respectively. At temperatures up to 400°C, the volatiles yield is a few percent of the coal. At temperatures around 400 °C, tar starts to evolve and the total volatiles yield rapidly increases till they reach the asymptotic value. These trends, increasing volatiles yields with PT and higher volatiles and tar yields at vacuum, are in agreement with previous studies (Howard, 1981).

Extraction of the raw coal yields 30 % weight loss on an as-received basis. The yield of extract decreases with increasing pyrolysis temperature up to ~ 400 °C. As the coal starts to soften and tar starts to evolve, the extract yield starts to increase and shows a maximum at ~550°C and then decreases rapidly with further temperature increases. At temperatures between about 650 - 800 °C, the rate of depletion of pyridine extract appears somewhat faster at 1 atm than at vacuum.

These observations can be interpreted as follows. The initial

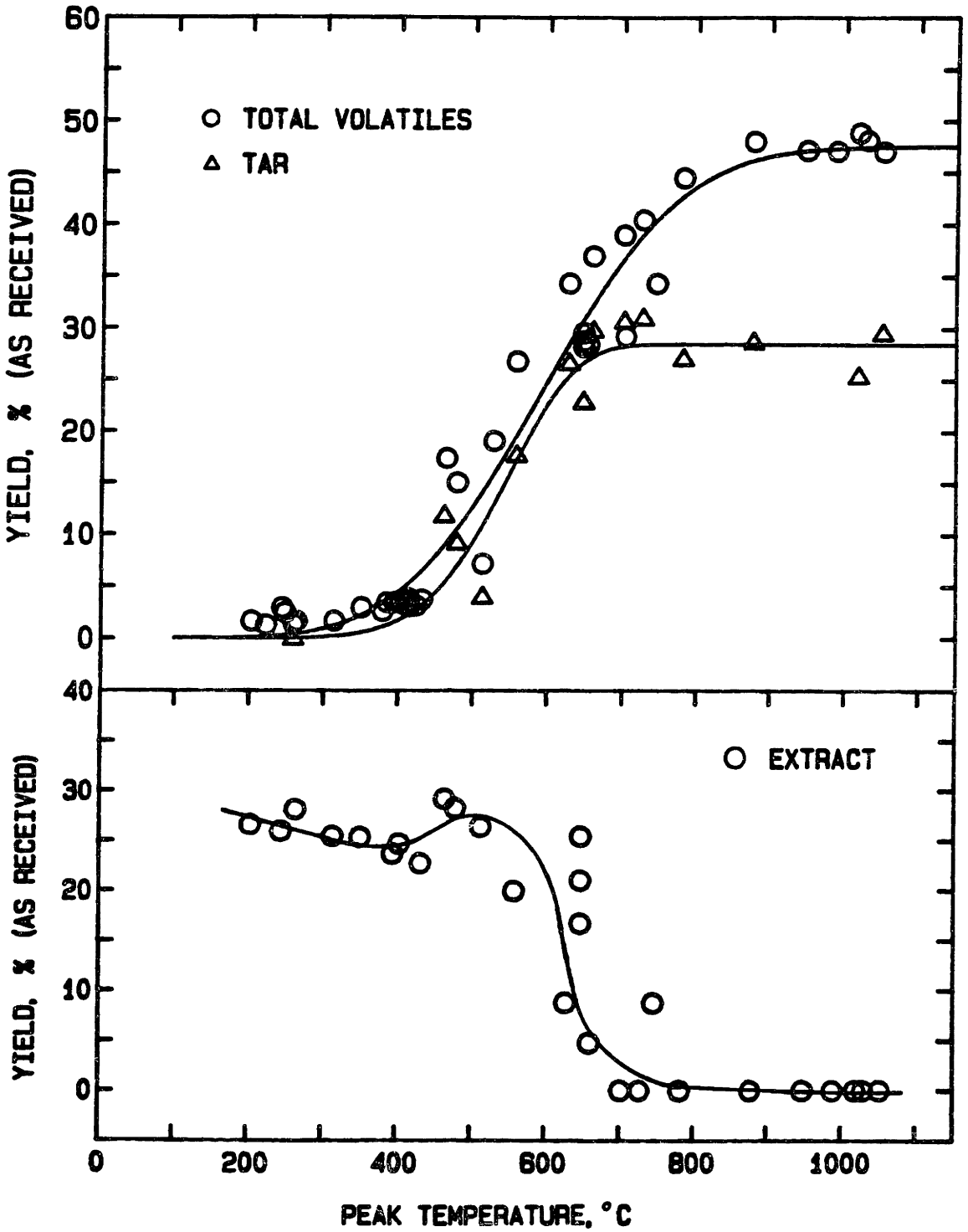

Fig. 4.3.1. Yields of total volatiles and tar (top) and yield of pyridine extracts (bottom) from pyrolysis at 1 atm as a function of peak temperature.

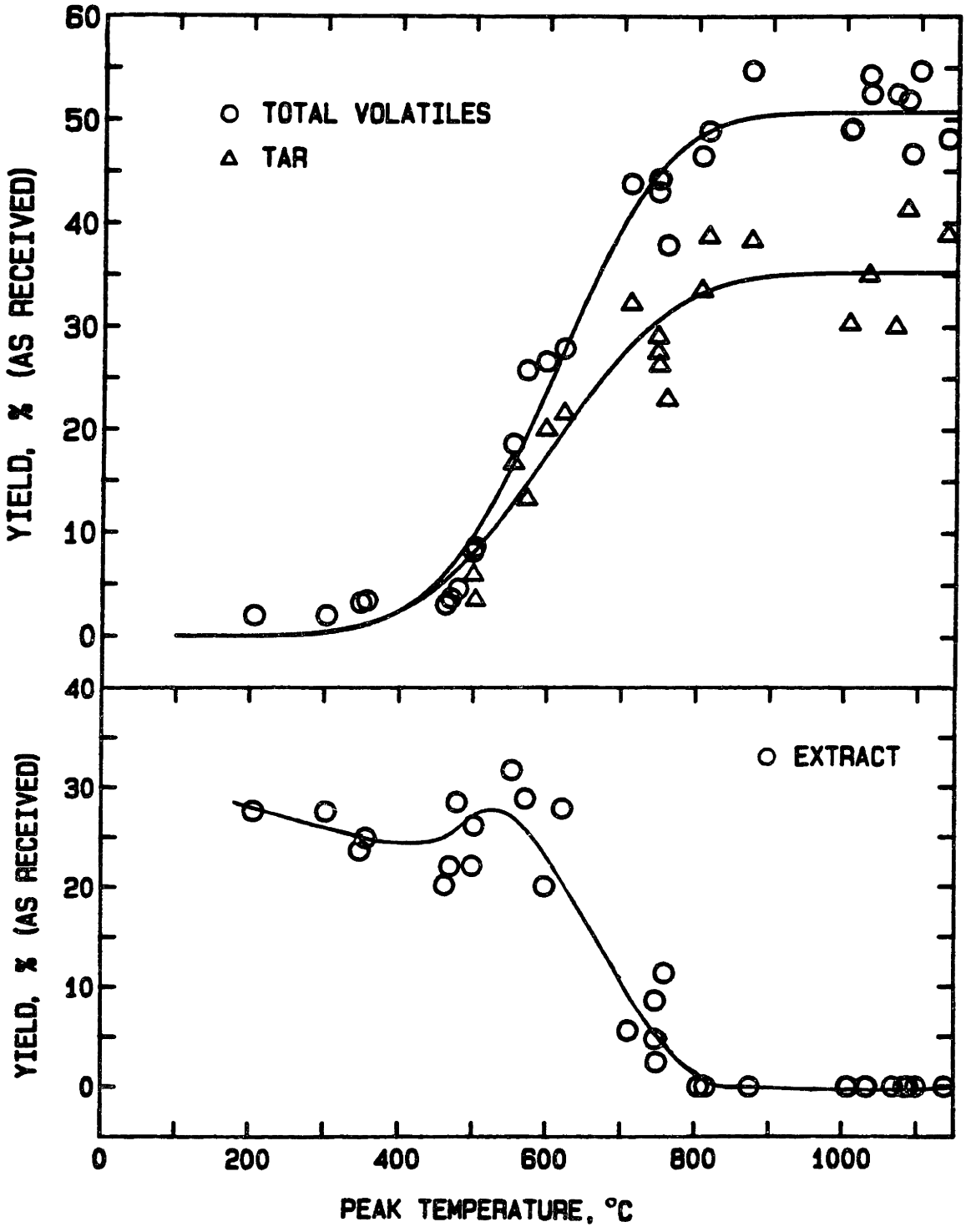

Fig. 4.3.2. Yields of total volatiles and tar (top) and yield of pyridine extracts (bottom) from pyrolysis at vacuum as a function of peak temperature.

decrease in the extract yield at low temperatures is due to the loss of lower MW molecules (H_2O, CO_2, and CO) as volatiles and to the absence of significant formation of metaplast. Figures 4.3.3 plots the sum of total volatiles and extracts yields as a function of peak temperature, from 1 atm and vacuum pyrolysis. At both pressures, the sum stays the same within the experimental error at low temperatures (PT < 400°C). As the temperature increases, thermal cleavage of chemical bonds causes an increase in the extract yield and at the same time one also observes a noticeable tar yield, i.e. metaplast molecules are now escaping from the reacting medium, allowing them to be 'counted' as tar molecules. The sum of volatiles and extract rapidly increases. At temperatures greater than 550°C, the formation reactions become slower as they approach completion, while the rate of tar transport becomes faster, and the pyridine extractables are also lost by secondary cracking and repolymerization reactions within the coal particles. Therefore, rapid depletion of extractible materials is observed and there is no extract yield at temperatures greater than 800°C at 1 atm and 900°C at vacuum.

Gas yields

The yields of hydrocarbon gases (CH_4, C_2H_4, C_2H_6, and C_3H_8), carbon oxides (CO and CO_2) and water are plotted in Figures 4.3.4 (1 atm) and 4.3.5 (at vacuum). Again, each data point represents an integral yield of pyrolysis at a given peak temperature.

The gas yields at two pressures as a function of peak temperature are similiar. At both cases, water is the first volatile component evolved which is followed by CO_2 and then CO. The formation of water is completed by 400°C. The carbon monoxide peak starts to appear at PT around 400°C and

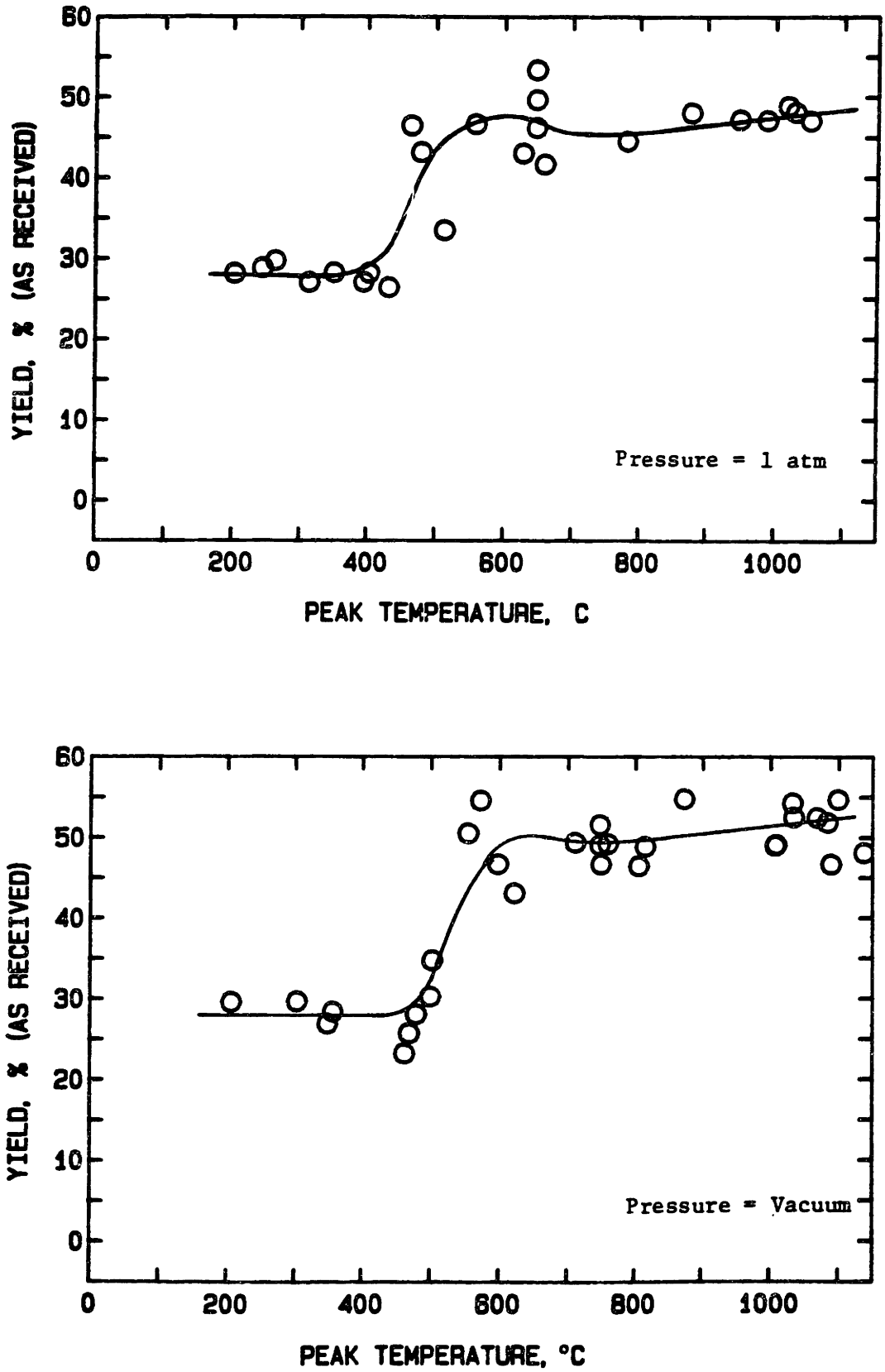

Fig. 4.3.3. Total yield of volatiles and extract as a function of peak temperature at 1 atm (top) and at vacuum (bottom).

increases with the temperature while the yield of CO_2 reaches the asymptote at ~ 600°C. The hydrocarbon gases also start to evolve at ~ 400 °C and increase rapidly with temperature. The major component is methane which shows the asymptotic yield of 3 %. The yield of ethane is higher than ethylene yield at temperatures < 800 or 900°C. However, the yield of ethylene is higher at very high temperatures (Temperature > 900°C). Figures 4.3.4 and 4.3.5 plot the sum of ethane and ethylene yields.

The yield of water is somewhat less accurate than other gases due to the moisture leaking into the porapak trap from air. The water yield at vacuum seemed to be affected more by the moisture in air since the most of vacuum experiments were done in summer. At PT < 400°C the volatiles are composed of water and CO_2. Therefore, from the weight loss data and the yield of CO_2, the correct water yield can be calculated. Fig. 4.3.5c shows the corrected water yield at low temperatures along with the measured values which show the difference of 3 to 4 % by weight of coal.

Heat transfer from screen to coal particles

Comparing the volatiles yields at 1 atm and vacuum (0.0001 atm), one can observe the larger scatter in the data from vacuum pyrolysis. The main souce of scatter in the volatiles yields seemed to be caused by the uncertainties in time-temperature history due to poor heat transfer. Appendix C shows the derivation and discussion of the heat transfer from the screen to the coal particles of which the temperature is measured by a Chromel-Alumel thermocouple.

Because of the differences in heat transfer mechanisms, the solutions to the heat transfer equations are worked out separeatly for the case of atmospheric pressure and for vacuum. At atmospheric and higher pressures,

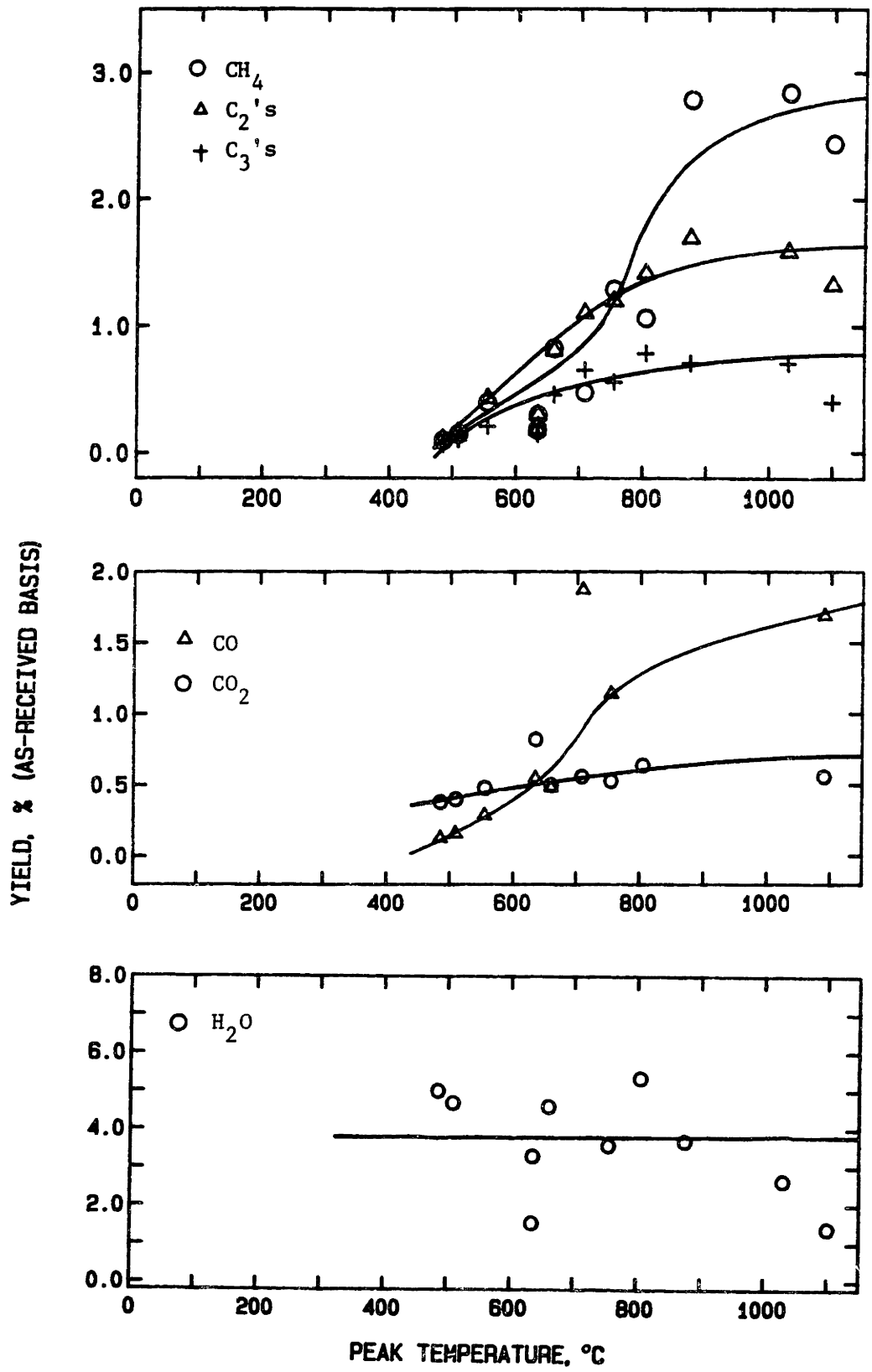

Fig. 4.3.4. Yields of gases from 1 atm pyrolysis: hydrocarbon gases (top), carbon oxides (middle), and water (bottom).

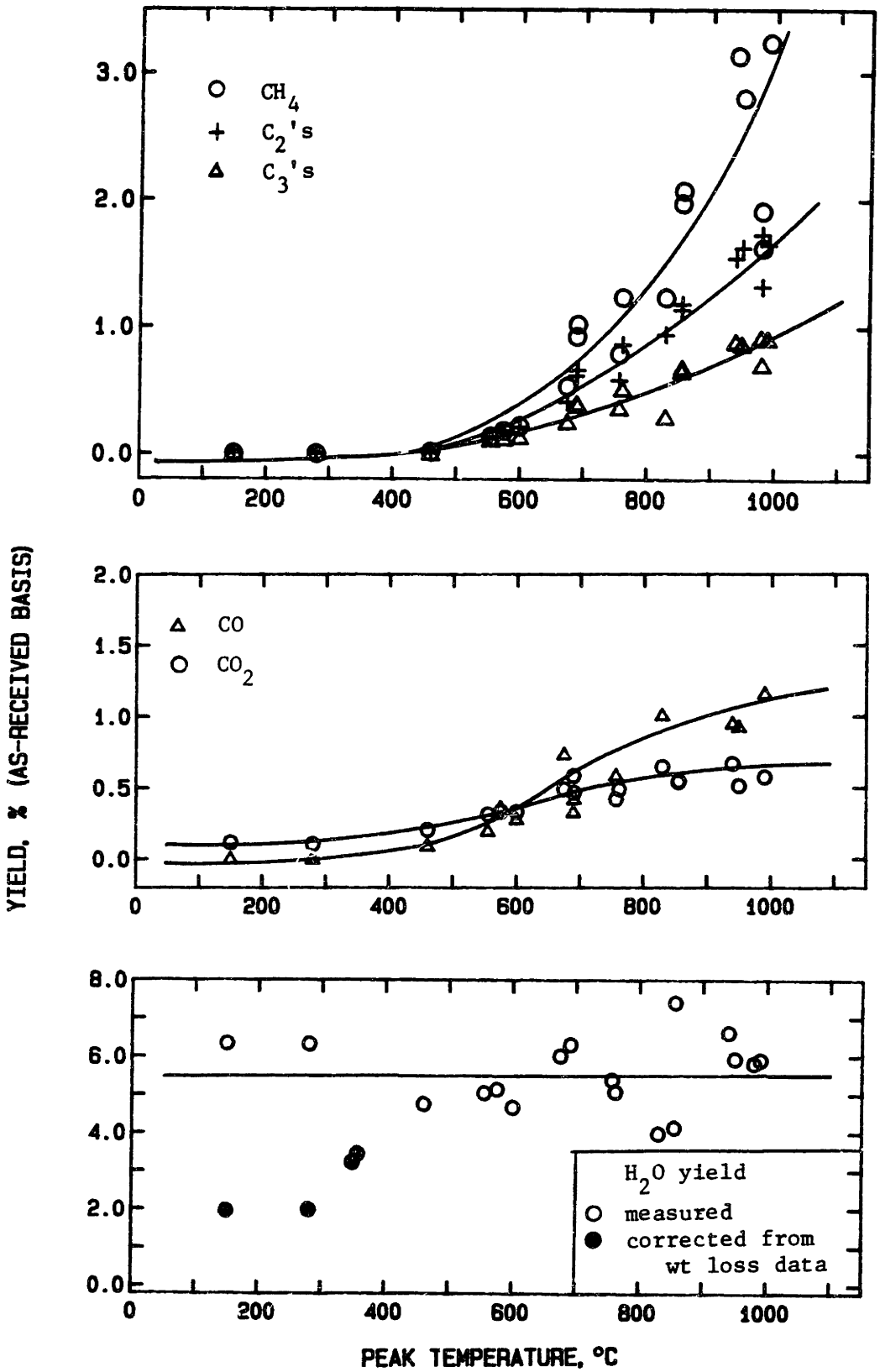

Fig. 4.3.5. Yields of gases from vacuum pyrolysis: hydrocarbon gases (top), carbon oxides (middle), and water (bottom).

convective heat transfer from the surrounding gases dominates. The thermocouple and coal particles tempertures are very close and the coal particle temperature is not affected by either the heat of pyrolysis or the value for heat transfer coefficients at the heating rate of 1000°C/sec.

Under the vacuum conditions, the contribution of the convective heat transfer is not important and the radiation and the direct conduction from the screen play important roles. The agreement between the coal and thermocouple temperatures depends on physical properties such as thermal properties and emissivities, and also depends on the thickness of the sample load on the screen.

Difficulties in tar collection at vacuum and extent of secondary reactions of tar outside the screen

Tar collection after the pyrolysis at vacuum is more difficult than at higher pressures. The heated screen at 1 atm causes natural convective currents inside the reactor which tend to deposit a considerable amount of tar into certain areas of the reactor, i.e., at the off-center of the reactor top and the bottom plates. However, tar is diffused away from the screen at the vacuum and gets evenly deposited all over the reactor internal surfaces including electrodes, thus making tar collection more difficult.

At 1 atm, tar collected may also have been affected by the secondary reactions outside the particle. Since tar is a reactive substance, its residence near the hot screen could cause tar to undergo cracking reactions. To estimate the extent of tar secondary reactions, one needs to understand the velocity of the flow inside the reactor as well as the

temperature gradient around the screen. Obtaining rigorous analysis is very difficult because of the nature of the convective flow which combines the non-linear momentum balance with heat transfer equations. Simplified analysis is presented in Appendix D. According to the analysis presented in Appendix D, the thickness of the thermal boundary layer at which the temperature is high enough to expect secondary reactions is on the order of a few centimeters when the screen temperature is 1000°C. The amount of tar converted in this hot zone is just a few percent of the total primary tar evolved, and amounts to on the order of 1 % of the weight of original coal.

Retention of pyridine in coal extract and residue

One major problem of using pyridine as an extracting solvent is that significant amounts of pyridine are retained in coal extracts as well as in the residue. Collins et al. (1981) found that both extracts and the solid residue from extraction of Illinois No. 6 coal with pyridine-^{14}C retained large quantities (10 % on ash free basis) of the solvent, even after drying under vacuum at room temperature.

In the extraction work in this thesis, the samples were dried at 90 C under vacuum after extraction. The amount of pyridine retained at this drying temperature is unknown. However, one can estimate that from the char samples resulted from the pyrolysis at peak temperatures greater than 900 °C. At these temperatures, one can assume all metaplast has been transported or has been converted to heavier MW substances. The samples obtained from the pyrolysis at PT > 900 °C at both pressures show the average weight gain of 2.33 % based on weight of char and 1.21 % based on the weight of original coal. Surface properties of char (i.e., total surface area and reactivity) produced from pyrolysis at different tempera-

tures will be quite different from each other. Assuming all solid residue of different char sample retain the same amount of pyridine may be erroneous. However, without sophisticated experimental set-up such as a super-critical CO_2 extractor (Smith et al., 1982), it is difficult to remove or measure the pyridine retained in residue. Therefore, all the experimental data of extraction plotted in Figures 4.3.1 and 4.3.2 are assumed to have error bars of on the order of one percent due to the pyridine retained.

4.3.2. Molecular Weight Distribution (MWD) of Pyridine Extract and Tar

Examples of the normalized MWD's of tar and extract from 1 atm pyrolysis at a PT of 625°C and of tar from vacuum pyrolysis at a PT of 600 °C are shown in Fig. 4.3.6. Both the atmospheric and vacuum tars are lower in MWD than the extract. The upper limit of the molecular weight of tar at either pressure is about 1200 while that of extract is about 1500. However, the fraction of extract material having molecular weight greater 1200 is just a few percent of the total extract. Thus, it is safe to assume that the most of extract and tar have the same range of molecular weight but tar has more of the lighter fractions while extract has more of the heavier fractions. These molecular weight data are consistant with the conceptualization of metaplast as unevaporated tar and support (but do not prove) the hypothesis that the yield of pyridine extract is a good estimate of the amount of metaplast remaining in char. Vacuum tars also have the same range of molecular weights as 1 atm tars but are lighter than extracts and have more of the fractions of molecular weights between 400 and 800 than 1 atm tars.

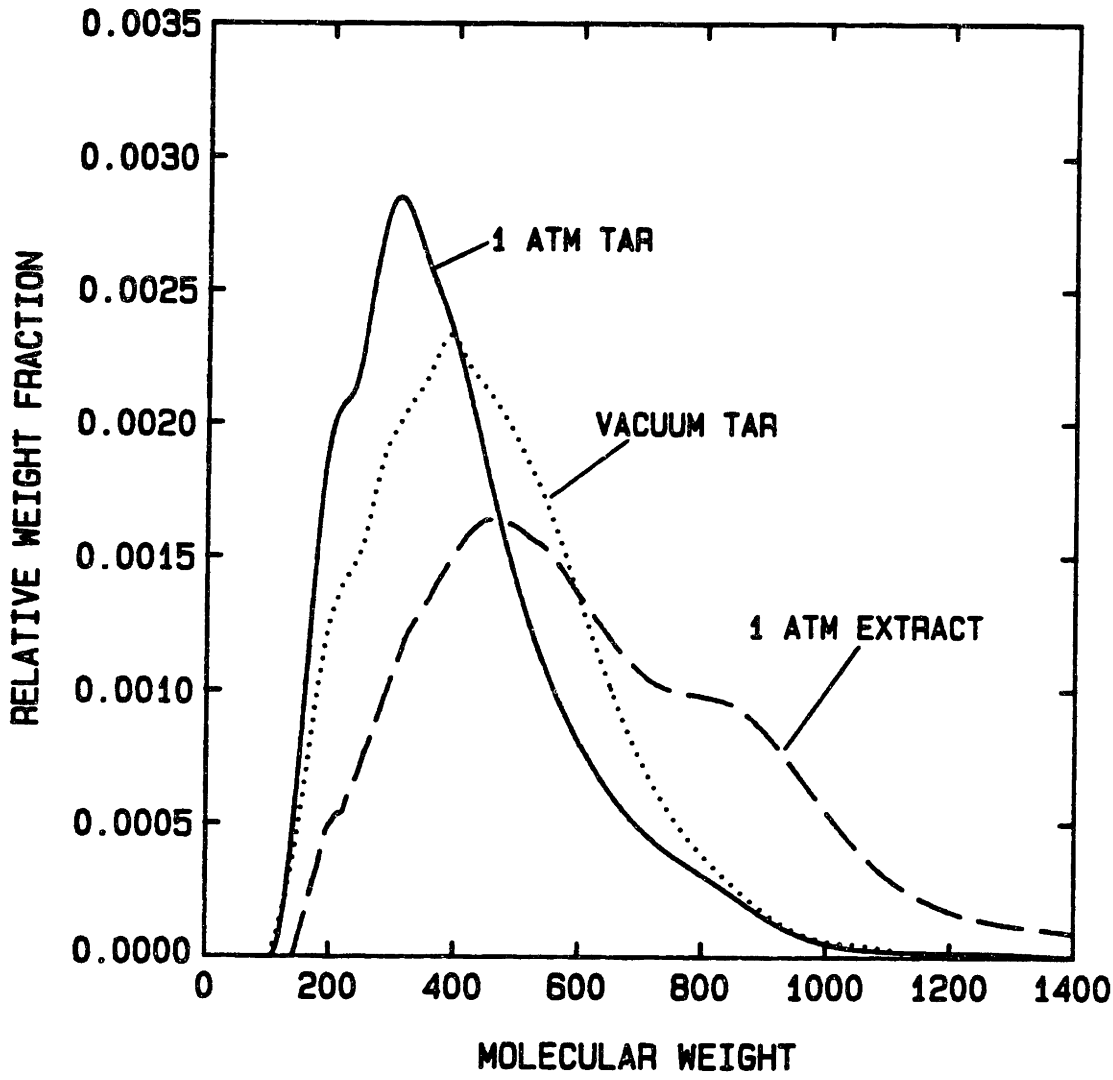

Fig. 4.3.6. Normalized molecular weight distributions of 1 atm tar and extract (Peak Temp = 626 °C) and of vacuum tar (Peak Temp = 600 °C).

The changes in MWD with the peak temperature is described in terms of the number average molecular weight (MN) which is defined as the following:

$$MN = \frac{\sum_{j=1}^{N} h_j}{\sum_{j=1}^{N} h_j/MW_j}$$

where the whole MWD is devided into N sections of MW_1 to MW_N respectively, and h_j is the average peak intensity in section j.

Figures 4.3.7 and 4.3.8 plot the number average molecular weight of tar and pyridine extract as a function of peak temperature at 1 atm and at vacuum, respectively. Since no tar is obtained at temperatures below 400°C and no extract at temperatures greater than 800°C at 1 atm and 950°C at vacuum, the data points are restricted to certain temperature ranges. The number average molecular weight of 1 atm tar initially increases, stays about the same and then decreases slightly at PT > 800°C, while the MN of vacuum tar continues to increase as a function of peak temperature. As discussed earlier, vacuum tars have more of the heavy fraction than 1 atm tars and as a result, the MN of vacuum tars are about 50 gm/mole higher than those of 1 atm tars. This observation is in agreement with the evaporation model (Zacharias, 1979; Unger and Suuberg, 1980) which predicts that the heavier fractions of metaplast are more readily transported at vacuum than at 1 atm. However, the evaporation model does not predict the temperature dependance of the MN of 1 atm tars correctly; The evaporation model predicts increasing MN of tars with increasing PT at 1 atm.

The trends shown in the MN data for the extracts are more interesting; 1 atm extract displays higher MN at around 550°C while the MN of the vacuum extracts shows no significant changes with increasing PT above 400°C. Except the PT at around 550°C at 1 atm, the MN of the extracts from two pressures are about the same (~500 gm/mole) which is 150 gm/mole heavier

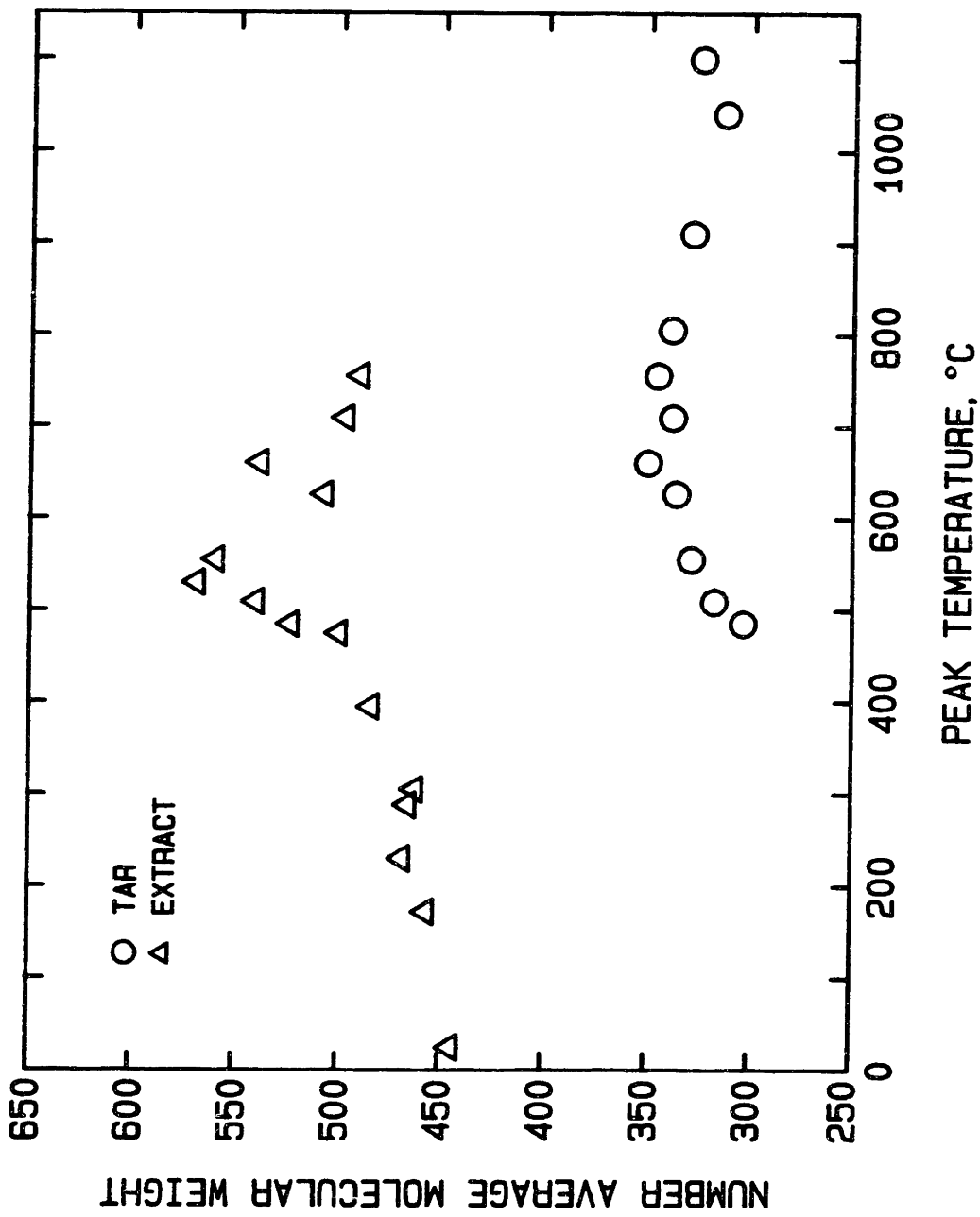

Fig. 4.3.7. Number average molecular weight of 1 atm tar and extract.

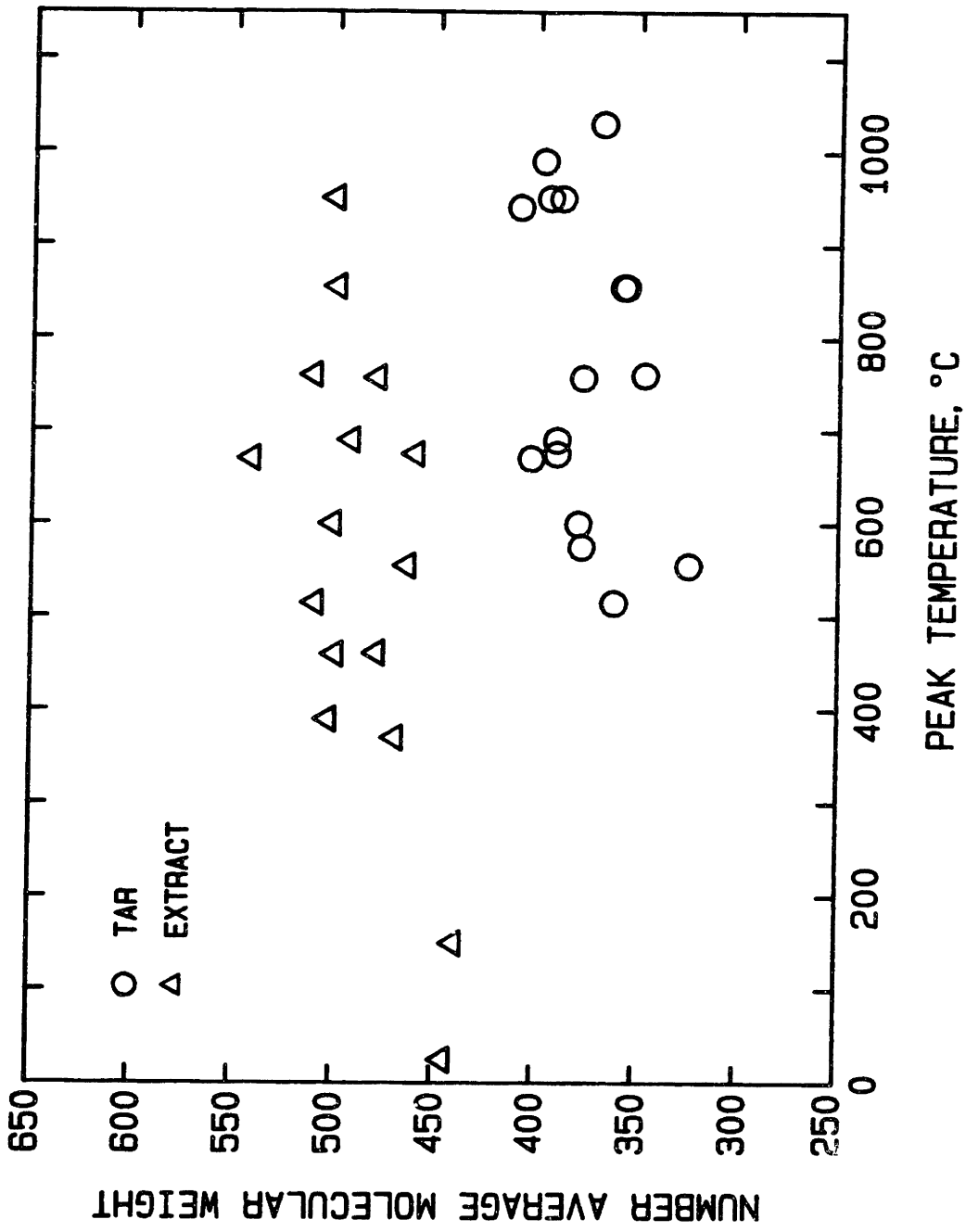

Fig. 4.3.8. Number average molecular weight of vacuum tar and extract.

than 1 atm tars and 100 gm/mole than vacuum tars. The higher MN of 1 atm extract at around PT 550°C can be explained as follows. The heavy fraction (MW between 400 and 800) which is missing in 1 atm tar but present in vacuum tar remains in the char at 1 atm pyrolysis, but is removed as extracts, and causes the extract to have a higher MN at around 550°C. However, at higher temperatures (> 600°C), this portion is transported from the coal or depleted by secondary reactions. In Figures 4.3.9 and 4.3.10, extracts are divided into 3 fractions; low MW fraction where MW < 500, medium MW fraction where 500 < MW < 1000, and high MW fraction where MW > 1000, and the yield of each fraction is plotted as a function of peak temperature at 1 atm and at vacuum, respectively. At 1 atm, eventhough the total extract yield is increasing with the temperature between PT 400 and 550°C, the yield of low MW fraction undergoes an overall decreas with PT, while the yields of all three fractions of vacuum extract show the same trends shown in the total extract yield. Therefore, one can see that there is more selective transport of low MW substances at 1 atm than at vacuum, resulting in lighter tar and heavier extract.

To support the above argument further, the MN of the sum of extract and tar at PT < 600°C is calculated:

$$MN_{sum} = \frac{\text{Yield of Tar} + \text{Yield of Extract}}{\frac{\text{Yield of Tar}}{\text{MN tar}} + \frac{\text{Yield of Extract}}{\text{MN extract}}}$$

The result is

Pressure	PT, °C	MN sum
1 atm	485	444.06
	509	449.6
	555	421.0

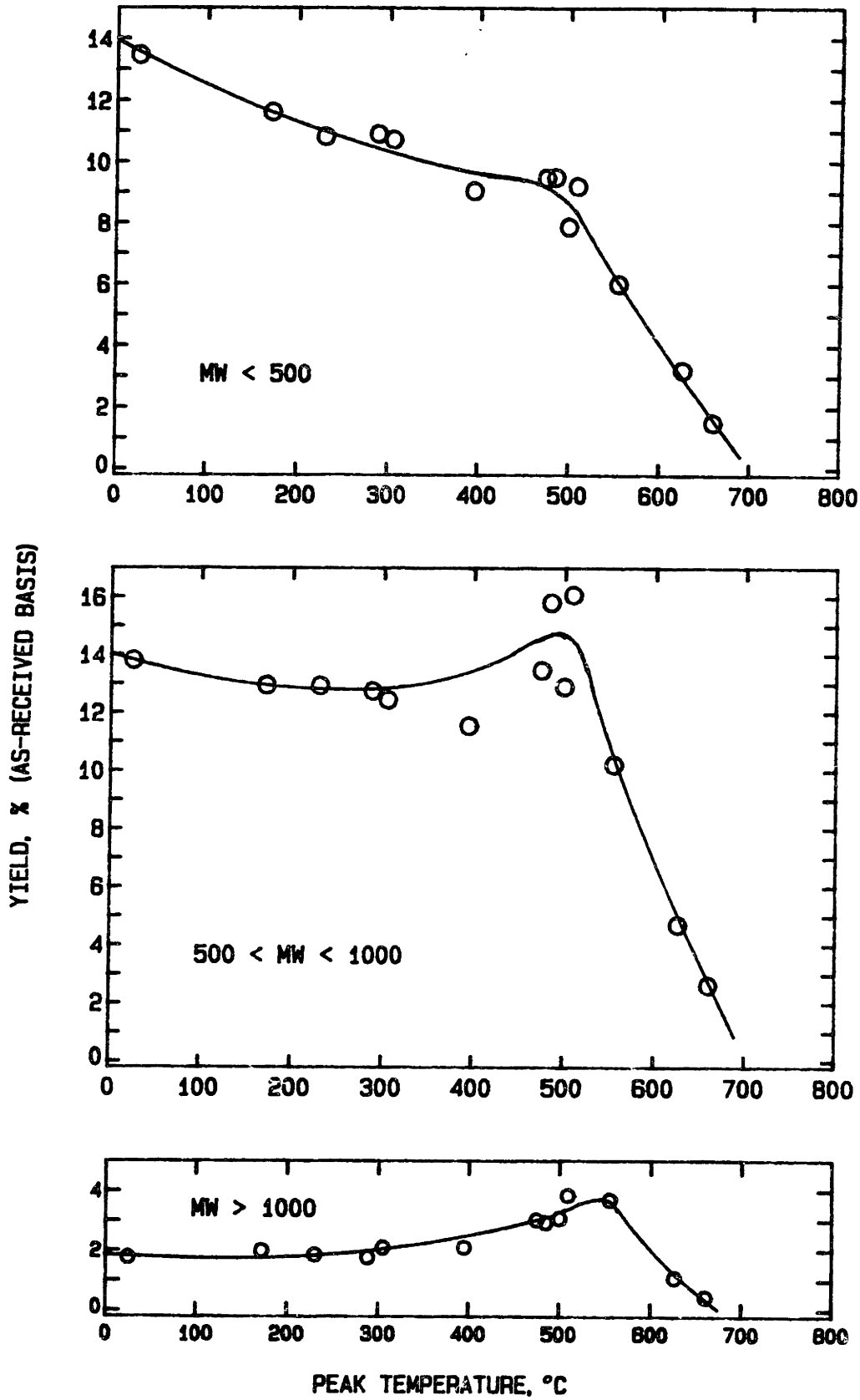

Fig. 4.3.9. Yields of pyridine extract, divided into three fractions; MW <500 (top), 500< MW <1000 (middle), and MW>1000 (bottom), as a function of peak temperature. Pressure = 1 atm.

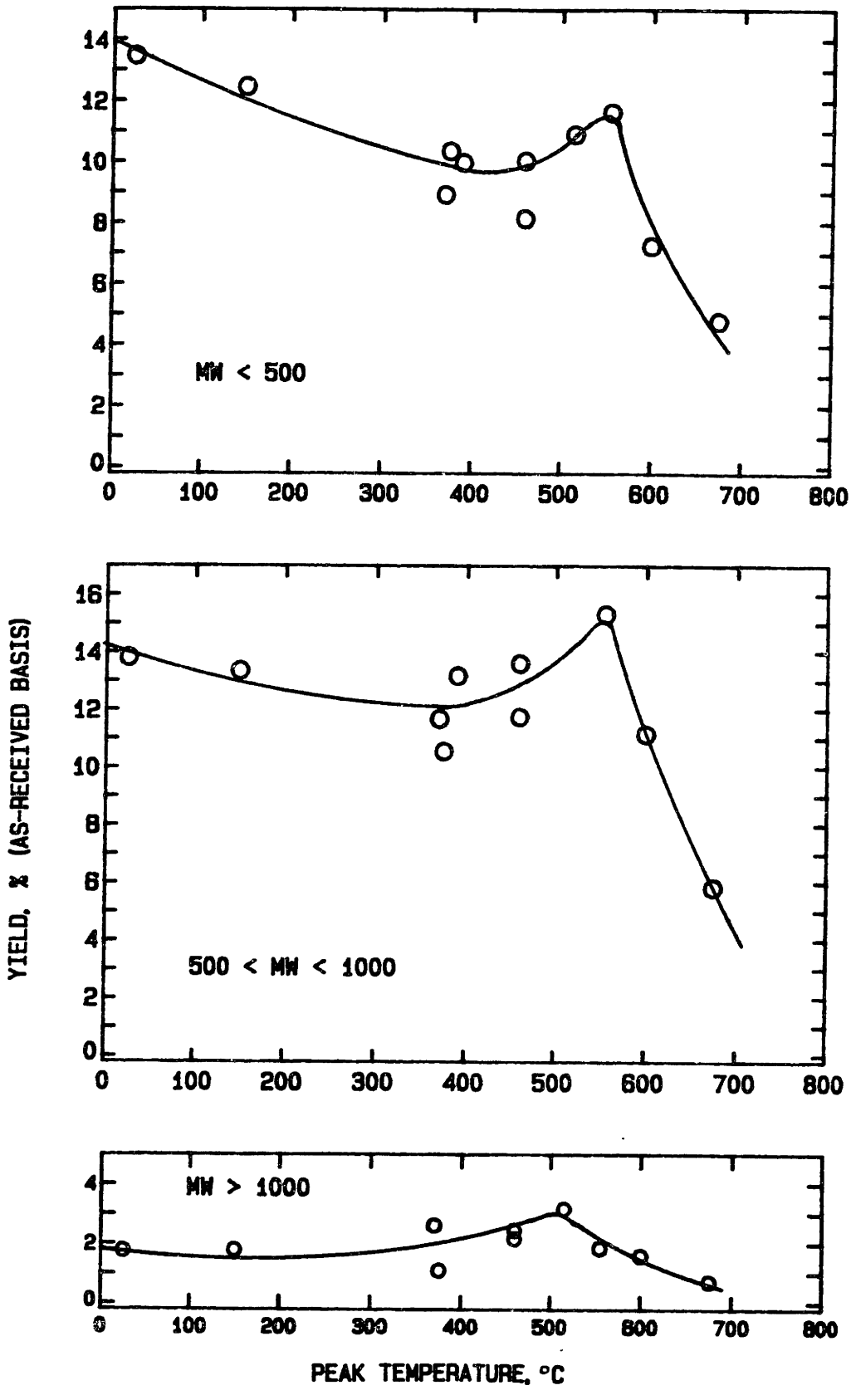

Fig. 4.3.10. Yields of pyridine extract, divided into three fractions; MW < 500 (top), 500 < MW < 1000 (middle), and MW > 1000 (bottom), as a function of peak temperature, Pressure = Vacuum.

Vacuum	515	445.96
	600	421.33

From the table above, one can see that the MN of the sum of extract and tar from both pressures at PT < 600°C are indeed similar.

Figures 4.3.11a and b show the changes in actual molecular weight distributions of tar from 1 atm and vacuum pyrolysis. The MWD's of 1 atm tars change very little with temperature while the MWD's of vacuum tars show higher percentages of the heavier substances at higher temperatures. Compared to the MWD's of tars, the changes in the MWD's of extracts appear at low temperatures (Figures 4.3.12a and b).

4.3.3. Comparison with Previous Studies

The total volatiles yields from 1 atm pyrolysis are compared with the work of Suuberg (1977) and Franklin (1980) at peak temperatue = 600°C and at an asymptotic point (PT > 1000°C). The comparison is possible because the same coal type is used in all three works.

	Total Volatiles Yield, as received basis		
PT, °C	Suuberg	Frankline	This work
600	12 %	14%	25 %
> 1000	46 %	45.34%	47.5 %

* from the pyrolysis of demineralizd coal. Numbers are converted back to as received basis..

Suuberg and Franklin had used the same screen heater reactor with strips of the folded screen of 1.5 x 5 cm which had 10 - 15 mg of coal sample. The amount of coal used per unit area of the screen (center area, only) in this thesis work is much smaller than those in Suuberg and Franklin's work.

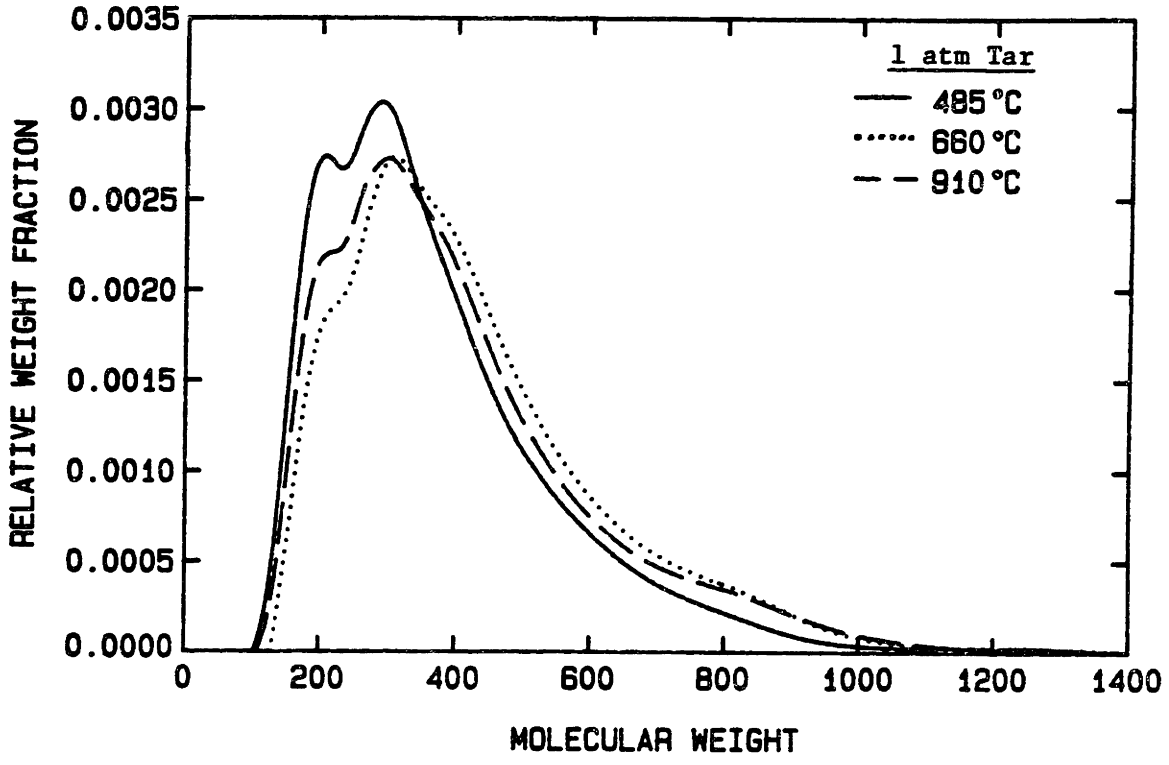

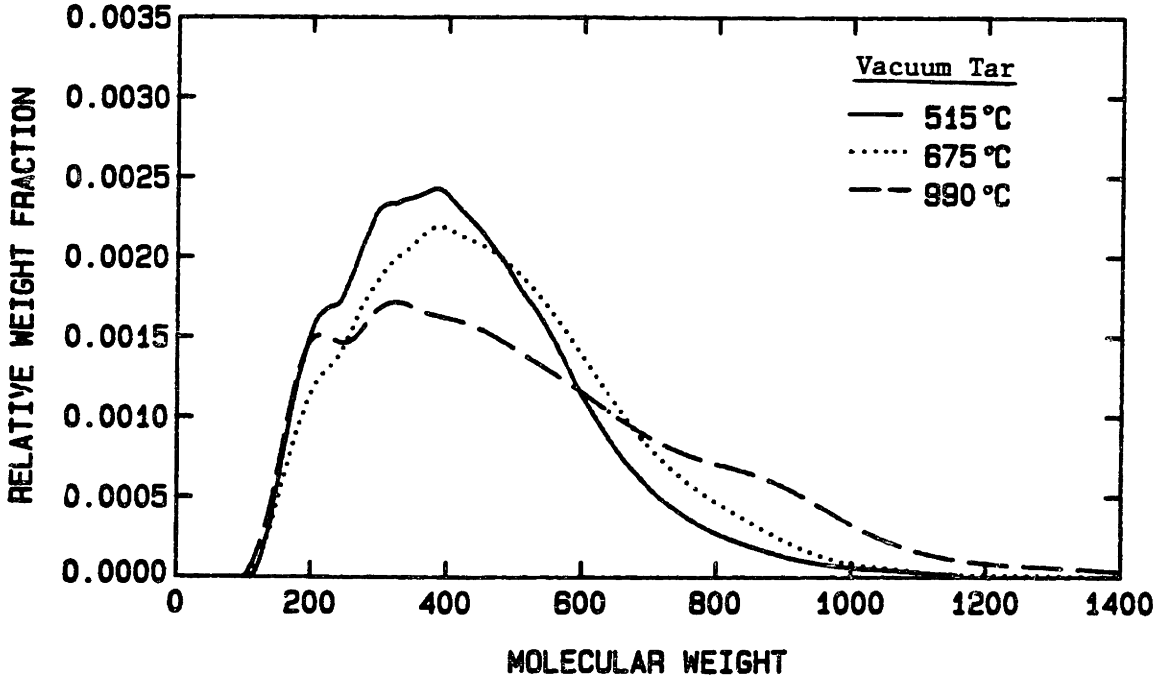

Fig. 4.3.11. Normalized molecular weight distribution of 1 atm (top) and vacuum tars (bottom) at various peak temperatures.

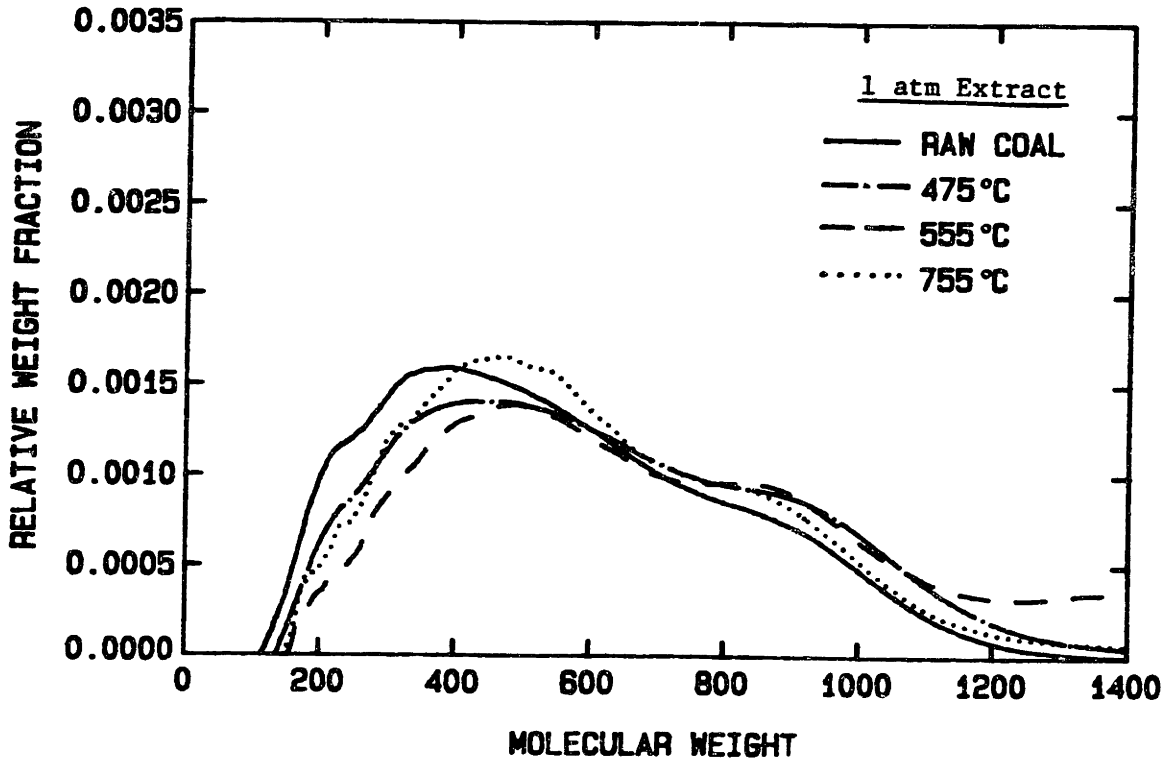

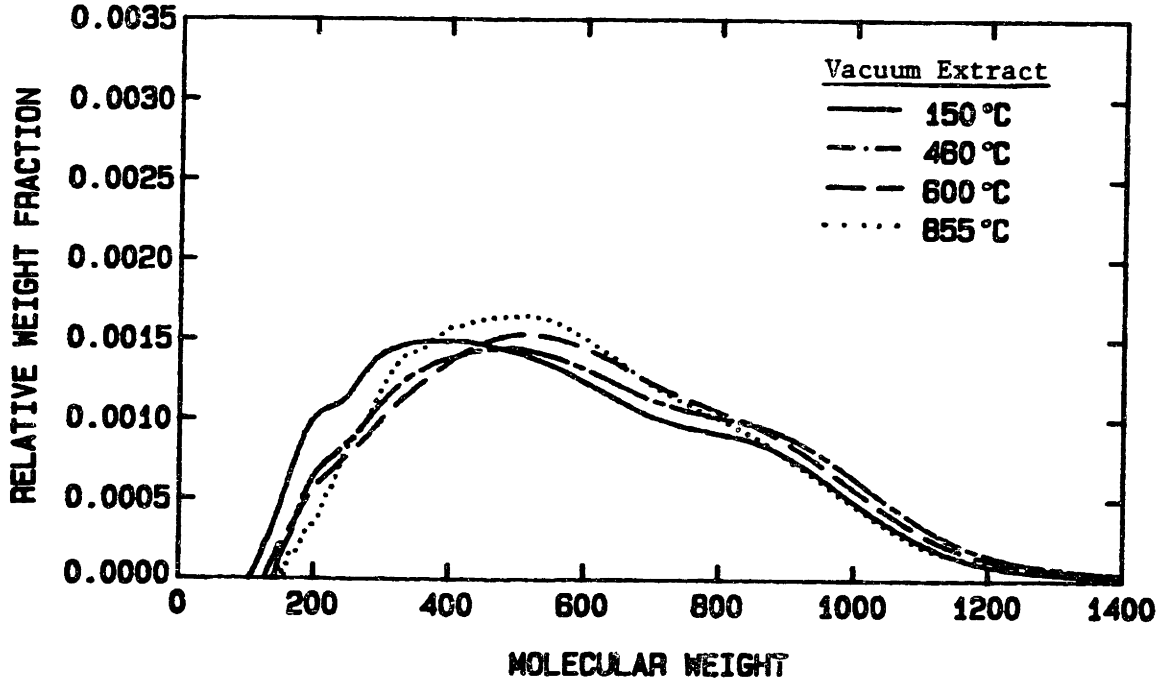

Fig. 4.3.12. Normalized molecular weight distribution of 1 atm (top) and vacuum extracts (bottom) at various peak temperatures.

Thus, it is expected that the coal samples have different time temperature history which cause a quite different yield at 600 °C. However, the asymptotic volatiles yields are in a better agreement, within ± 2 % of each other.

The direct comparison of the extract yield and the MWD's of tar and extract with others is difficult because of different coal type, extracting solvent, and different extraction conditions employed in reported experiments. Only qualatative comparisons are attempted.

The increase in extract yields with the pyrolysis temperature is observed earlier by Dormans and Van Krevelen (1960) in various types of coals. In Fig. 4.3.13, Dormans et al. describe the preheating effect on extract yield. The graphs in the top row, which show the pyridine extract yield as a function of preheating temperature for Faulquemont coal (VM = daf 36.9 % and % C = daf 80.1), show much the same behavior as the coal in this study (VM = daf 47 % and % C = daf 78.81 %). They also gave the plots of the rank vs the yield of pyridine extract and the rank vs the molecular weight of the extracts. Figures 4.3.14a and b are taken from their work with the addition of the data from this thesis work. The extract yield falls far above the curve while the MW falls a little below the generalized curve. However, considering the scattering of the data presented, the deviation of our data from the generalized curve does not imply much significance.

Badzok and Marzec (1981) analyzed the solvent (pyridine/ethylenediamine) extract of a high volatile bituminous coal (extract yield = 38 %) from Poland by FI mass spectrometry and found that the volatile part of the extract (75 - 80 wt % of the extract) is composed of substances between 70 - 800 amu. The highest contibution comes from

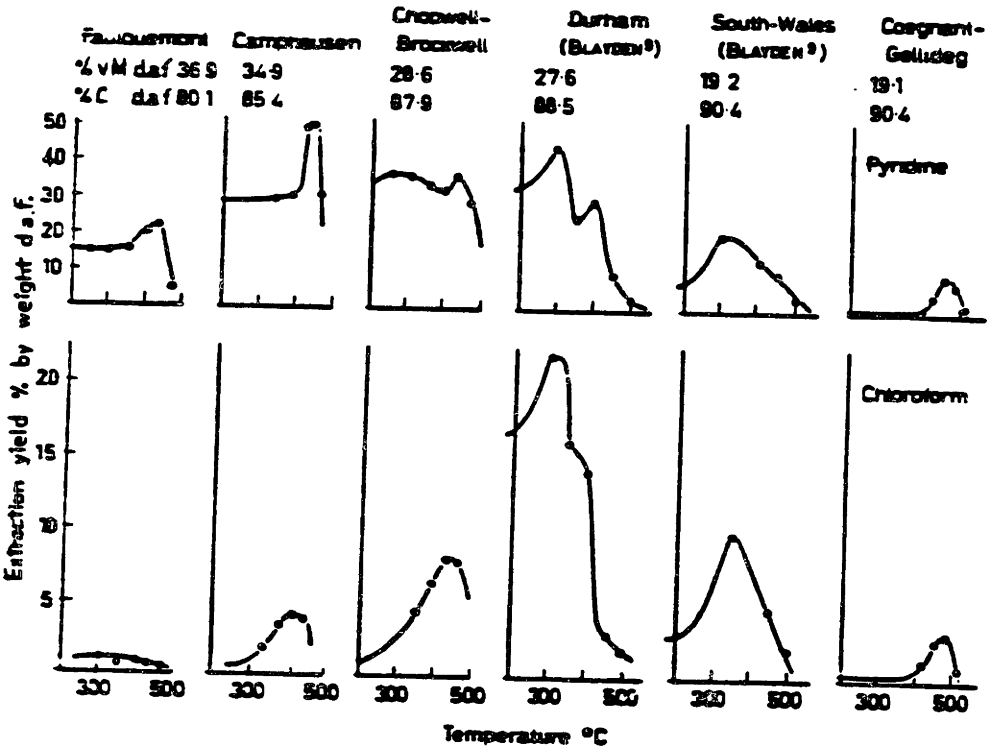

Fig. 4.3.13. Extraction yield vs. preheating temperature. (Dormans and van Krevelen, 1960)

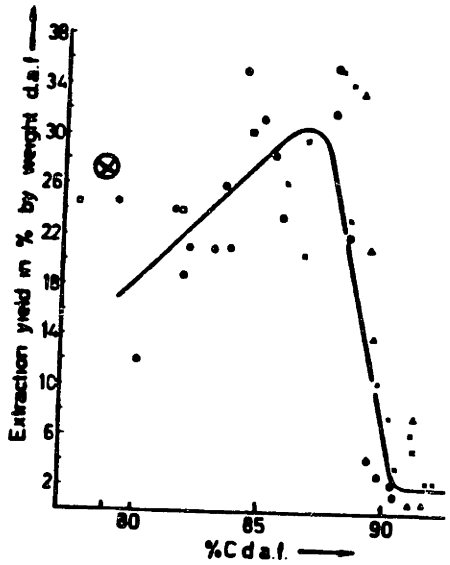

O Dormans and van Krevelen, 1960
× W. F. K. Wynne-Jones et al., 1952
O C. Kroger, 1956
□ I. G. C. Dryden, 1952
△ S. R. Illingworth, 1922
⊗ this work

Fig. 4.3.14a. Extraction yield in pyridine at 115 C vs. rank. (Dormans and van Krevelen, 1960)

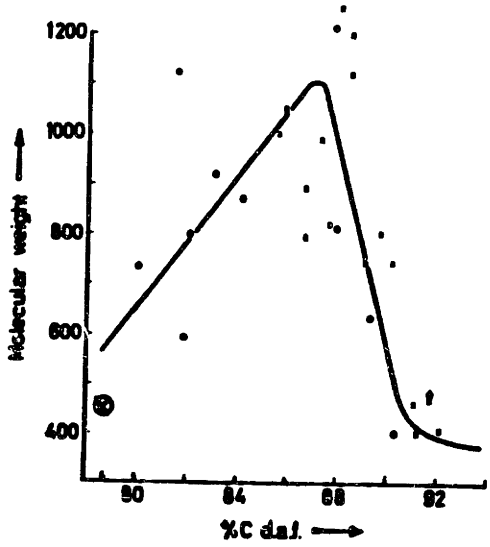

O Dormans and van Krevelen, 1960
× W. F. K. Wynne-Jones et al., 1952
⊗ this work

Fig. 4.3.14b. Molecular weight of pyridine extracts vs. rank of parent coal. (Dormans and van Krevelen, 1960)

substances in the range of 200 - 600 amu. Their result is in good agreement with this work.

Pyridine extracts of Illinois No. 6 coal show quite different number average molecular weights: the MN of the fraction only soluble in pyridine was 1214 and those of the fractions of pyridine extract soluble in toluene and in hexane were 427 and 332, respectively (Mayo and Kirshen, 1978). The molecular weight measurements were made with GPC using tetrahydrofuran (THF) as a mobile phase. Since not all of the fraction only soluble in pyridine is entirely soluble in THF, the measurement 1214 is questionable.

Unger and Suuberg (1984) also studied the yields of extract and the MWD of tar and extract as a function of pyrolysis temperature using a Pittsburg seam coal (Bruceton mine; % C = 80.4 on a dry basis). They used THF as an extracting solvent as well as a mobile phase in GPC. The maximum extract yield was around 10 % on an as received basis. The trends in the MWD of tar and extract are the same as observed here; extracts are heavier than tars; vacuum tars are heavier than 1 atm tars; and the MN of vacuum tars changes with the pyrolysis temperature more than 1 atm tars. However, the range of the molecular weight of tar and extract is much broader than the one reported here (the upper limit is 3500) and the reason for this difference in the molecular weight range are still under investigation.

5. MODEL DEVELOPMENT

5.1. INTRODUCTION

5.1.1. Softening Development

The mechanism of softening development is assumed to be both physical transformation ('melting') and pyrolysis. Metaplast is the material assumed to be responsible for the coal fluidity (Van Krevelen, 1961; Neavel, 1975, 1982) and depletion of metaplast due to transport, decomposition, or polymerization causes coal to be resolidified. Metaplast can be identified with thermobitumens in thermobitumen theory, bitumens in melting theory, or small crystalites in X-ray studies. Non-softening materials which identify with micelles, large crystallites, or large molecules which are stable and too large to be volatilized at temperatures of interest (< 1100 C in the present study) would be called char. Some of metaplast is assumed to be pre-existing in coal ('bitumen') and its amount is estimated from the yield of pyridine extract from untreated coal following the definition by Brown and Waters (1966). As coal is heated to a certain temperature, which is referred as softening point, bitumens melt and act as initial plasticizer. Further increase of coal temperature causes thermal cracking of functional groups and bridging atoms between lamillar units to form additional metaplast. Evidence for the formation of additional amount of metaplast is found in the increase of the sum of tar and pyridine extract yields at temperatures above softening point.

When hydrogen donors such as hydrogen atoms, bitumens, and mobile lamillar units are available, free radicals are stablized by accepting hydrogens. At high temperatures, however, further decomposition of meta-

plast occurs and, at the same time, free radicals are stablized via polymerization reactions, forming large stable molecules. Loss of metaplast also occurs due to transport to outside the particle.

When there is enough residence time at high temperatures, metaplast is depleted due to chemical reactions and transport. However, a rapid quench of coal particle from a high temperature causes metaplast to remain inside the particle and to be solidified.

5.1.2. Role of Bubbles in Volatiles Transport

When coal maintains porous structure during pyolysis, the volatiles are transported by diffusion or hydrodynamic flow through pores. Once coal develops fluidity, viscous flow closes pore mouths and the open pore structure collapses. The volatiles diffuse either to the particle surface or to existing bubbles through viscous melt.

The characteristic time for volatiles dissolved in the molten phase to diffuse from the centroid to the surface of a 70 μm diameter particle is

$$t_{c,s} \sim \frac{R_p^2}{D} = \frac{(0.0035\ \text{cm})^2}{10^{-7}\ \text{cm}^2/\text{sec}} \sim 100\ \text{sec} \qquad (5.1\text{-}1)$$

Since the experimentally observed characteristic time for gas release from the same size particles is of order 1 sec or less, the diffusion through the melt does not explain transport behavior of gaseous volatiles.

The characteristic time for volatiles dissolved in the molten phase to diffuse into existing bubbles is calculated assuming 1 μm for bubble radius:

$$t_{c,b} \sim 0.1\ \text{sec} \qquad (5.1\text{-}2)$$

Most of bubbles, either originated from pores or nucleated from supersaturated volatiles in molten phase, are smaller than 1 um diameter and,

therefore, $t_{c,b}$ is much smaller than 0.1 sec. Thus, one can conclude that the time for volatiles diffusion into bubbles is small enough so that bubble may be the mechanism by which volatiles leave the particle. The growth of bubbles during pyrolysis of softening coals not only suggest a mechanism for volatiles transport but also explains swelling behavior (See Ch. 3.3), formation of cenospheres, and the increase of macropore sizes and pore volume during pyrolysis (Franklin, 1949; Marsh et al., 1971; Toda, 1971; Miure, 1980; Singla, 1983).

In modeling transport of metaplast, evaporation models (Suuberg et al., 1980; Zacharias, 1979), which assume all mass transfer resistances lie outside the particle, have been well accepted. However, the magnitude of external mass transfer resistance is very sensitive to molecular weight of tar, and the validity of evaporation models needs to be checked with new information on MWD of metaplast and tar, reported in Ch 4.3. Using a film theory of mass transfer, the flux of metaplast at the particle surface is given as the following:

$$N_m' = \frac{D_{m,L}}{\delta_L} \rho_L (x_m - x_s) = \frac{D_{m,G}}{\delta_G} \rho_G (y_s - 0) \qquad (5.1\text{-}3)$$

where N_m' = molar flux of metaplast at the particle surface

ρ_L, ρ_G = molar densities of gaseous and liquid phases

δ_L, δ_G = boundary layer thicknesses inside and outside the particle

x, y = mole fractions of metaplast in liquid and gaseous phases

Using Roault's law, at equilibrium, $P\ y_s = P_v\ x_s$, where P and P_v are total pressure and the vapor pressure of pure metaplast, y_s and x_s are eliminated. Then N_m' becomes

$$N_m' = \frac{\rho_L \, x_m}{\frac{\delta_G}{D_{m,G}} \frac{\rho_L}{\rho_G} \frac{P}{P_v} + \frac{\delta_L}{D_{m,L}}} \qquad (5.1\text{-}4)$$

where the first and second terms in the denominator represent the relative mass transfer resistance outside, $(MR)_G$, and inside, $(MR)_L$, the particle. If the ratio of the two terms, $(MR)_L/(MR)_G$, is much less than 1, the external mass transfer resistance dominates, and the evaporation model can successfully describe the transport of metaplast.

The parameters in Eq. 5.1-4 are estimated as the following:

$\delta_G = R$

$\delta_L = R$

$$D_{m,G} = 0.1 \; \frac{T}{273} \; \frac{1}{P, \text{ atm}} \qquad \{cm^2/sec\}$$

$$P_v = 6.23 \times 10^5 \; \exp\left(\frac{561 \; MW^{0.474}}{T}\right) \qquad \{atm\}$$

$\rho_G = P/RT$

R = Gas Constant

$D_{m,L} = 10^{-7}$ cm^2/sec

$\rho_L = 1.3$ gm/cm^3 / MW_i

Note that ρ_L is slightly over-estimated. Average MW of liquid should be (wt fraction of char/MW_{char} + wt fraction of metaplast/MW_i)$^{-1}$. Table 5.1.1 presents $(MR)_L/(MR)_g$ at 1 atm, 0.0001 atm, and 70 atm and at various temperatures using metaplast MW 500 and 1000. At vacuum and 1 atm, $(MR)_L/(MR)_G >> 1$ at all temperatures and the mass transfer inside the particle is clearly the rate-limiting step. Even at the high pressure, i.e.,70 atm, the internal mass transfer resistance dominates except at around 400°C, at which tar starts to evolve.

Table 5.1.1. Comparison of mass transfer resistances of tar at various temperatures and pressures.

Pressure (atm)	0.0001		1		70	
MW / Temp	500	1000	500	1000	500	1000
400°C	2.85×10^{6}	5.93×10^{3}	2.84×10^{2}	9.53	4.06	0.0136
600°C	5.29×10^{7}	7.66×10^{5}	5.29×10^{3}	7.67×10^{1}	7.56×10^{1}	1.095
800°C	3.30×10^{8}	1.20×10^{7}	3.31×10^{4}	1.20×10^{3}	4.72×10^{2}	1.71×10^{1}
900°C	6.55×10^{8}	3.34×10^{7}	6.55×10^{4}	3.34×10^{3}	9.35×10^{2}	4.78×10^{1}
1000°C	1.16×10^{9}	7.93×10^{7}	1.16×10^{5}	7.93×10^{3}	1.66×10^{3}	1.13×10^{2}

The molecular weight information on metaplast also ables one to explore the possibility of tar transport via bubbles by calculating maximum weight fraction of tar transported by bubbles and by comparing it with experimental observations. Figs. 4.3.1 and 4.3.2 show that volatiles consist of at least 50 wt % of tar at temperatures greater than approximately 500°C. When 0.01 μm bubbles are saturated with the tar of MW=500, the mole fraction of tar in bubbles at 800°C is roughly

$$\frac{P_v(MW=500,\ T=500°C)}{P + \frac{2\sigma}{a}} = \frac{0.6284}{60.230} - 0.0104 \qquad (5.1\text{-}5)$$

and the weight fraction is ~ 15.8 % assuming 28 for MW of gaseous volatiles. The tar fraction in bubbles will be higher for larger bubbles and at higher temperatures. This result suggest the possibility of low MW metaplast transport (MW < 500) via bubbles. For heavier fractions of metaplast (i.e., MW = 1000), however, the maximum amount that can be transported via 0.01 μm radius bubbles is about 0.173 wt % at 500 °C, which implies that diffusion to the particle surface may still be important for these heavier fractions of mataplast.

5.1.3. Overall Model Description

Intraparticle transport of volatiles is assumed to contribute to pyrolysis product evolution via a set of coupled rate phenomena depicted schematically in Fig. 5.1.1. Initial decomposition of coal generates gases, char and metaplast within coal particles. Metaplast further decomposes or polymerizes to form more stable and more aromatic materials as well as light gaseous components. Physical transformation (melting) of pre-existing metaplast to liquid with increasing temperature is denoted as

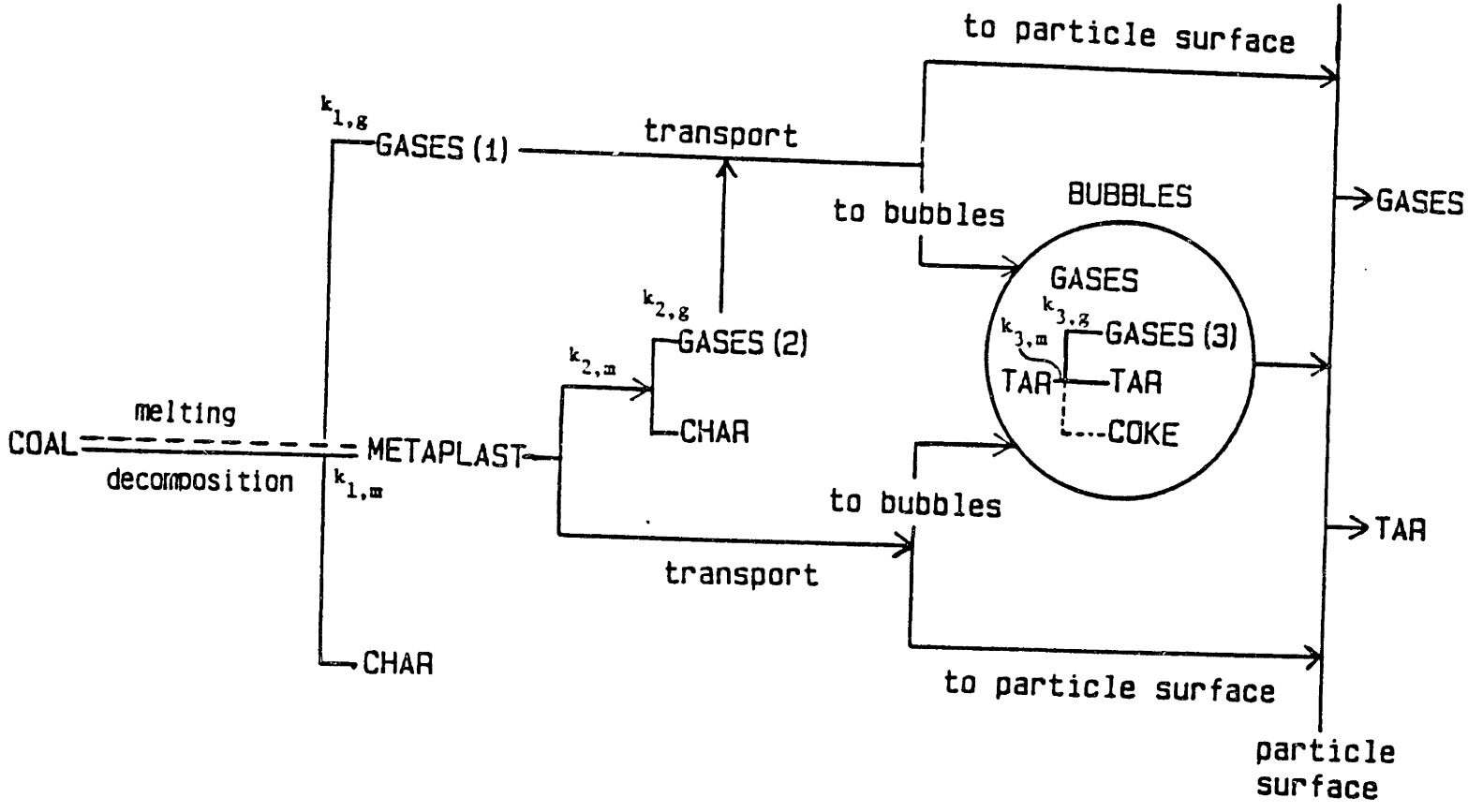

Fig. 5.1.1. Schematic of chemical and transport rate processes contributing to volatiles evolution during pyrolysis of softened coal.

dotted line. Gases include H_2, H_2O, CO, CO_2, CH_4, C_2H_4, C_2H_6, C_3's, C_4's and C_5's and light hydrocarbon liquids. Metaplast transported from the particle is characterized as tar following the work of Unger and Suuberg(1981, 1982), and metaplast vapor in bubbles of the particle is also characterized as tar. The tar is assumed to be room temperature condensibles.

The transport of volatiles from the particle is assumed to involve the diffusion of species dissolved in the coal melt and the expansion of bubbles originating from pores in the initial coal or nucleated from the gas, super-saturated in the coal melt. Once bubbles are formed, species formed at a point in the melt may diffuse to bubbles or to the outer surface of the particle. When the surface of an expanding bubble reaches the particle surface, the bubble contents are assumed to be released into the ambient gas, thus simulating the rupturing of bubbles and the formation of volatiles jets observable in high-speed photography of pyrolyzing particles. Again, the transport by diffusion through the melt directly to the particle surface is especially important for higher molecular weight metaplast components since their low vapor pressure (below 1000°C) precludes significant transport as bubble components. Conversely, the expansion and release of bubbles are important modes of transport for the species appearing as gaseous volatiles and lower molecular weight tar components.

5.2. CHEMICAL KINETICS

As shown in Fig. 5.1.1, the reactants and products are lumped into 5 species; coal, gases, metaplast, char and tar. The gases are assumed

to originate from decomposition of initial coal structures (gases(1)), metaplast (gases(2)) and tar (gases(3)). The formation of gases(1) is, more specifically, originated from pre-existing metaplast in coal (or from 'bitumen') and its formation is completed at low temperature. This simplification is necessary to make metaplast balane and support the initial decrease in the yield of pyridine extracts at temperatures lower than 400°C, as reported in Figures 4.3.1 and 4.3.2. Therefore, gases(1) include all of H_2O, most of CO_2 and some of CO. The kinetic informations can be obtained from the weight loss data at peak temperatures lower than 400°C. The formation of gases(1) and metaplast from the initial decomposition of the coal is modeled as unimolecular decompositions first order in the amount of the given material yet to be formed:

$$\frac{dV_i}{dt} = k_i \left(V_i^* - V_i \right) \qquad (5.2\text{-}1)$$

where V_i and V_i^* are amounts of gases(1) or metaplast formed at time t and $t=\infty$, respectively. At t=0, V_i for gases(1) is zero and V_i for metaplast is estimated as the pyridine extract yield of raw coal.

The mechanism of metaplast reactions is unclear, but would be the mixture of polymerization followed by deposition as coke, and cracking to char and gases. The rates of metaplast depletion in the liquid and in bubbles due to secondary reaction and, therefore, the rate of formation of gases(2) and gases(3), respectively, are also modeled as first order in the amount of metaplast available in each phase:

Metaplast secondary reactions:

In condensed phase: $k_{2,m} C_m$ (5.2-2)

In bubbles: $k_{3,m} B_m$ (5.2-3)

Gases(2) and gases(3) formation rate:

$$\frac{dV_{g,2}}{dt} = f_{g,2}\, k_{2,m}\, C_m \qquad (5.2\text{-}4)$$

$$\frac{dV_{g,3}}{dt} = f_{g,3}\, k_{3,m}\, B_m \qquad (5.2\text{-}5)$$

where $f_{g,j}$, j=2 or 3, is the fraction of metaplast converted to gases and C_m and B_m are metaplast concentrations in the liquid and in bubbles, respectively, expressed as gm metaplast/gm original coal. Gases(2) and gases(3) are formed at similar temperatures and are difficult to be distinguished from each other. They include some CO_2, most of CO and all of light hydrocarbon gases and light liquids.

The kinetic information of tar conversion in bubbles, $f_{g,3}$ and $k_{3,m}$, can be obtained from the work on homogeneous secondary reactions of tar (Serio, 1984). Fig. 5.2.1. shows tar conversion data for tar decomposition reactions in helium compared with predictions from a single-reaction first-order model. Serio showed that a three lump model, which employs two first-order parallel reactions, fits the tar conversion data better than the single reaction model. However, the single reaction model is used here for simplicity. The mass balance for homogeneous cracking experiments also reveals that most of tar cracked become light hydrocarbon gases, carbon oxides and light oils, and only a few percent is deposited as solid. Therefore, in this bubble model, all tar cracked in bubbles is assumed to be converted to gases, which means $f_{g,3} = 1$.

The kinetic constant for metaplast decomposition in the molten phase, $k_{m,2}$, is obtained from the experimental data on tar and extract yields at various peak temperatures and at two pressures, and $f_{g,2}$ will be inferred from the yields of gases at high temperatures (> 400°C).

The reaction rate constants, k, with appropriate subscripts, are

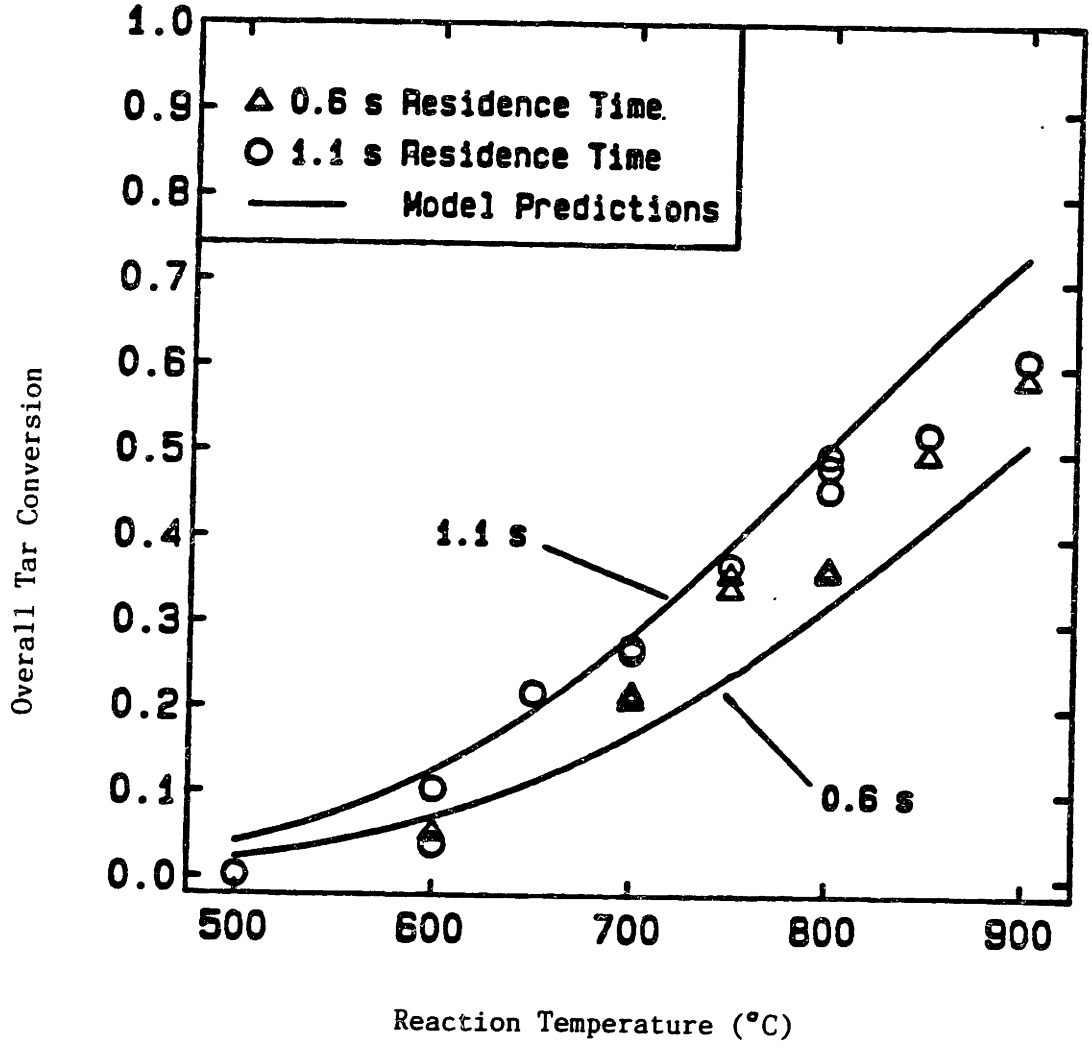

Fig. 5.2.1. Tar conversion data for homogeneous reaction experiments 1.1 s and 0.6 s residence time compared with predictions from single reaction model. Model parameters; k_o = 996 /s, E = 15.4 Kcal/mole, and V^* = 100 %. (Serio, 1984)

each expressed as $k_o \exp(-E/RT)$ assuming a single reaction model. The more complicated but more reasonable approach is a multiple-reaction model, where the decomposition is modeled as a set of independant, first-order reactions with a distribution of activation energies,

$$k = k_o \int_0^\infty f(E) \exp(-E/RT) \, dE$$

The distributed activation energies reflect different bond strengths in coal molecules. The multiple reaction model is widely used in coal pyrolysis studies. However, the single-reaction model is preferred when the model deals with the combined complexity of kinetics and transport because of its relative simlicity.

5.3. CONSERVATION EQUATIONS

To formulate the conservation equations for gaseous volatiles, metaplast, and bubbles in a coal particle, the particles are assumed to be spatially isothermal and to have a spatially uniform bubble concentration. These assumptions are considered valid for small particles ($\bar{}$ 70 μm) at heating rates less than 1000°C/s. (See Appendix C)

5.3.1. Bubble Generation

The pores in solid coal are assumed to become bubbles in molten coal as suggested by James and Mills (1976). The initial bubble distribution is thus determined by the pore size distribution of the original coal.

The other mechanism of bubble generation is bubble nucleation. As in the case of the nucleation of bubbles in pure liquids, the formation of

gas-vapor nuclei occurs in a gas-liquid solution if the concentration of gases and vapors exceeds the saturation limit. In the system of coal melt, if all pores are collapsed due to softening, there are no free surfaces which the gaseous volatiles or metaplast vapors can diffuse into, except the outer surface of the softened particle. Then, the excess of the gases and vapors over the saturation concentration are removed by bubble formation during a certain initial period. Once bubbles become available, the excess is removed by diffusion to the bubbles. Detailed derivations for the critical radius and for the rate of bubble generation are found in literature (Reid, 1973; Blander and Katz, 1975 and 1971; Kagan, 1960; Tucker et al., 1975; Wards et al., 1970). In this section, The critical radius and the rate of nucleation are defined for the hypothetical coal system, in which all pores disappear upon softening.

The Critical Radius

The critical radius, r_c is the minimum radius of a spherical bubble which can grow to a macroscopic size. Nuclei of radius smaller than r_c tend to decay while those of the radius larger than r_c tend to grow. The nuclei with the critical radius are in equilibrium, even though unstable equilibrium, with the surrounding liquid and r_c is given by

$$r_c = \frac{2\sigma}{(P_b - P)} \qquad (5.3\text{-}1)$$

where P_b is the pressure inside of the bubble, P is the pressure of the surrounding liquid and σ is the surface tension of the liquid. For a single component system, P_b is simply the vapor pressure of the liquid corrected for the curvature of the vapor-liquid interface:

$$P_b = P_v \exp\left(\frac{(P - P_v)\, V^L}{RT}\right) \qquad (5.3\text{-}2)$$

where P_v is the vapor pressure of the liquid and V^L is the molar volume. However, for a multiple component system, the bubble pressure is

$$P_b = \sum_{i=1}^{N} P_{v,i} + \sum_{j=1}^{M} P_{I,j} \qquad (5.3\text{-}3)$$

where $P_{v,i}$ = Partial pressure of vapor i

$P_{I,j}$ = Partial pressure of gas j

Wards et al. (1970) considered the non-ideal behavior of gases in a multicomponent system and defined the critical radius as follows. The bubble pressure is again the sum of the partial pressure of vapors and inert gases:

$$\text{For vapors :} \quad y_i P_b = \frac{P_{v,i}\,\eta}{\nu_i}$$

$$\text{For gases :} \quad y_j P_b = \frac{P\,C_j}{\nu_j\,C_{jo}}$$

where $\eta = \exp\left(\frac{V^L}{RT}(P - P_v) - C\right)$

C = Concentration of gases in a liquid, gm mole/mole of liquid

C_o = Saturation concentration of gas j in a liquid across a flat surface, mole/mole of liquid

y_i, y_j = Mole fraction of component i or j in the gas-vapor mixture

ν_i, ν_j = Activity coefficient of component i or j in the gas-vapor mixture and is 1 in an ideal mixture.

Then, the critical radius is

$$r_c = \frac{2\sigma}{\sum_{i=1}^{N} \frac{P_{v,i}\,\eta}{\nu_i} + \sum_{j=1}^{M} \frac{P\,C_j}{\nu_j\,C_{o,j}} - P} \qquad (5.3\text{-}6)$$

Rate Equation

The formation rate of nuclei, J, is usually expressed as number of nuclei formed/unit volume/unit time. The literature contains several different expressions for J_p which are derived for the evaporation and condensation processes. Among these, one of the most widely used rate equations for a pure liquid is presented here without detailed derivation. Factors correcting the rate equation for a viscous multicomponent system will then be discussed.

Reid (1973) and Blander and Katz (1975) give the following rate equation for nucleation from a pure liquid:

$$J = N \left(\frac{2\sigma\beta}{\pi m B}\right)^{0.5} \exp\left(-\frac{4\pi\sigma r_c^2}{3 k T}\right) \qquad (5.3\text{-}7)$$

where N = Total number of liquid molecules per unit volume

σ = Surface Tension

k = Boltzman's constant

r_c = critical radius

m = Mass of a molecule

$B = 1 - (1 - P_L/P_v)/3$

β = Condensation coefficient

The condensation coefficient, β, is taken as 1 following the work of Blander et al. (1971).

Blander et al. (1971) also suggested a correction factor for the impedance arising from the diffusion of volatile components through the mixture. The corrected rate of nucleation, J_D, is

$$J_D = \frac{J}{1 + \delta_D} \tag{5.3-8}$$

where J is the nucleation rate shown in Eq. 5.3-7 and δ_D is

$$\delta_D = \frac{2\sigma}{D\,(2\pi\, m\, kT)^{1/2}\,(C_o - C_L)} \tag{5.3-8a}$$

where C_L is the bulk concentration of volatile solute and C_o is the equilibrium concentration at the interface, both having units of # molecules/cm^3. For typical values of the parameters for molten coal (σ ~ 30 erg/cm^2, D ~ 10^{-7} cm^2/s, m ~ 10^{-22} gm, and C ~ 10^{17}), δ_D is much larger than unity and this correction factor makes a difference of 9 orders of magnitude on the nucleation rate.

For the effect of viscosity, the work of Kagan (1960) is employed with a small modification. Kagan (1960) presented an important extension of nucleation theory which takes into account hydrodynamic and transport constraints on the rate of nucleation. When inertial terms are relatively small and when the viscosity is high enough, the rate of nucleation becomes

$$J = 3\,N\frac{\sqrt{\frac{8kT}{\pi\, m}}}{1 + \delta_D}\sqrt{\frac{\sigma}{kT}}\,\frac{\exp\left(-\frac{4\sigma\pi r_c^2}{3kT}\right)}{2\left(w + (3+b)/b\right)} \tag{5.3-9}$$

where

$$w = \frac{3\,\mu}{\sigma\,(1 + \delta_D)}\sqrt{\frac{2kT}{\pi\, m}} \tag{5.3-9a}$$

$$b = 1 - \frac{P_L}{P_v} \tag{5.3-9b}$$

and μ is the viscosity of the fluid. In the original form by Kagan, the

correction factor for the process limited by heat transfer was included instead of δ_D in Eq's 5.3-9 and 5.3-9a. When the rate of growth of the bubble near the critical size is controlled by the viscous term, the pressure inside the bubble is usually much higher than P_L, and b becomes 1. And since $\delta_D >> 1$, the above equation is simplified into

$$J = N\sqrt{\frac{18\sigma}{\pi m}}\left(\frac{1}{\delta_D}\right)\frac{1}{w+4}\exp\left(-\frac{4\sigma\pi r_c^2}{3kT}\right) \qquad (5.3\text{-}10)$$

where

$$\delta_D = \frac{2}{D\,(2\pi mkT)^{1/2}\,(C_o - C_L)} \qquad (5.3\text{-}10a)$$

$$w = \frac{\mu}{\sigma\delta_D}\sqrt{\frac{18kT}{\pi m}} \qquad (5.3\text{-}10b)$$

and again N is the total number of molecules of volatiles and inert gases dissolved in the molten coal per unit volume.

5.3.2. Bubble Growth and Bubble Conservation Equations

Once a bubble is formed, it will grow and coalesce through the following mechanisms:

1. Addition of gas molecules by diffusion from the condensed phase.
2. Chemical reactions inside or at the surface of the bubble. These include secondary reactions of tar if the concentration of its vapor within the bubble is significant.
3. Gross physical force changes such as changes in internal or external pressures.
4. Coalescence with another bubbles.

Bubble coalescence may arise when two bubbles physically contact each other or approach each other to within a certain critical distance. When actual contacting occurs, the two bubbles are combined into one large one. These bubble-bubble interactions are caused by the growth of bubbles dueto the mechanism (1) and by diffusive bubble motion. Coalescence due to diffusive motion of bubbles is analogous to the coagulation of colloidal particles exhibiting brownian motion and the apparent diffusivities of two colliding bubbles may be related to their corresponding diameters at the moment of impact (Chandrasekhar, 1943). However the contribution from this process is very small because of the small apparent diffusivities of bubbles and can be neglected.

A phenomenon known as inter-bubble gas diffusion may also cause bubble coalescence. This process usually occurs in foams when bubbles exist in close proximity to each other with only a thin layer of liquid between them. Since the pressure inside a smaller bubble is higher than that of a larger bubble, the gas diffuses from the smaller to the larger bubble. As a result, the larger bubble grows and the smaller one shrinks to the point of disappearance. Inter-bubble gas diffusion is visualized as a two step process. The first step is gas diffusion from the smaller bubble to the liquid layer between two bubbles and the second step is transport from the liquid to the larger bubble. Since the mechanism (1) describes the net rate of diffusion, the model treats inter-bubble gas diffusion as part of (1).

As bubbles expand, bubbles sufficiently close to the particle surface will eventually break through the particle surface and the contents of bubbles will be released from the particle. The growth and coalescence of bubbles is described mathematically as follows. Let n_j be the number

concentration of bubbles containing j molecules, i.e., the number of bubbles per unit mass of original coal. Then, growth from molecular diffusion is described by the following kinetic scheme:

$$n_1 + n_j \xrightarrow{K_j} n_{j+1} \qquad (5.3\text{-}11a)$$

for j from 2 to N - 1, where N is the number of molecules in the largest size bubble. The rate constant, K_j, describes the rate of volatiles diffusion to bubbles. The coalescence of two bubbles is also expressed in terms of kinetic equation:

$$n_i + n_j \xrightarrow{P_{ij}} n_{i+j} \qquad (5.3\text{-}11b)$$

for j from 2 to N - 2. From the above equations, the bubble conservation equations are

$$\frac{dn_j}{dt} = K_{j-1}n_{j-1}n_1 - K_j n_j n_1 + \frac{1}{2}\sum_{i=2}^{N-j} P_{i,j-i}n_i n_{j-i} - \sum_{i=2}^{N} P_{ij}n_i n_j - E_j n_j \qquad (5.3\text{-}12)$$

for j from 2 to N, where E_j is a bubble escape term, and P_{ij} and K_j are kinetic constants defined in Eq's 5.3-11a and 5.3-11b. The detailed derivation will be shown in the following section (Ch 5.4). The resulting kinetic expressions for K_j, P_{ij}, and E_j are

$$P_{ij} = P_{ji} = \rho_o 4\pi (a_i + a_j)^2 (a_i' + a_j') \qquad (5.3\text{-}12a)$$

$$K_j = \rho_o 4 \pi a D_{v,L} Sh (n_1 - n_{eq}) / n_1 \qquad (5.3\text{-}12b)$$

$$E_j = \frac{3 (R_p - a_j)^2}{R_{po}^3} a_j' \qquad (5.3\text{-}12c)$$

where ρ_o = liquid density

a_i = radius of a bubble containing i molecules

$\dot{a}_i$ = da/dt = growth rate of the bubble radius

R_p = coal particle radius at time t

R_{po} = radius of the unpyrolyzed coal particle

Assuming an ideal solution of gases in molten coal, the equilibrium concentration of gaseous volatiles at the interface is determined by Henry's law:

$$C_{eq} = P_g / H$$

while C_{eq} for metaplast is determined from Raoult's law:

$$C_{eq} = P_{t,i} / P_v$$

P_g and $P_{t,i}$ are the partial pressure of gases and metaplast component in bubbles and P_v is the vapor pressure of metaplast. n_{eq} is the equilibrium concentration of gases or metaplast interms of # molecules/gm orig. coal. The bubble growth rate, $\dot{a}_i$, will be also derived in Ch 5.4.1.

Even though the mass is conserved, the number of molecules in bubbles may vary owing to secondary reactions. However, for simplicity, this effect is not included in the above bubble conservation equation and will be included later in a simplified bubble conservation equation.

5.3.3. Mass Balance of Gases and Metaplast

The material balance of either gases or metaplast in the condensed phase includes the rate of formation and the rate of transport to bubbles and to the particle surface. An additional term is included for metaplast to account for its depletion by secondary reactions. Let C_g and C_m be the gas and metaplast concentration in the melt, and let $K_{j,g}$ and

$K_{j,m\ i}$ be K_j for gases and metaplast component i, respectively. Assume that all gases have the same molecular weight and that the rates of formation and secondary reactions are the same for all molecular weight metaplast. The mass balance of gases is

$$\frac{dC_g}{dt} = \begin{matrix}\text{formation}\\ \text{rate of}\\ \text{Gases(1)}\end{matrix} + \begin{matrix}\text{formation}\\ \text{rate of}\\ \text{Gases(2)}\end{matrix} - \begin{matrix}\text{rate of}\\ \text{transport}\\ \text{to bubbles}\end{matrix} - \begin{matrix}\text{rate of}\\ \text{transport to}\\ \text{particle surface}\end{matrix}$$

$$\frac{dC_g}{dt} = k_{1,g}\,(V_g^* - V_{g,1}) + f_{g,2}\,k_{m,2}\sum_{i=1}^{N_{tar}} C_{m,i} - \sum_{j=2}^{N} K_{j,g} n_{1,g} n_j - E_g\,C_g \qquad (5.3\text{-}13)$$

and for metaplast is

$$\frac{dC_m}{dt} = \begin{matrix}\text{formation}\\ \text{rate}\end{matrix} - \begin{matrix}\text{reaction}\\ \text{to form}\\ \text{Gases(1)}\end{matrix} - \begin{matrix}\text{secondary}\\ \text{reactions}\\ \text{rate}\end{matrix} - \begin{matrix}\text{transport}\\ \text{to}\\ \text{bubbles}\end{matrix} - \begin{matrix}\text{transport}\\ \text{to particle}\\ \text{surface}\end{matrix}$$

$$\frac{dC_{m,i}}{dt} = k_{1,m}\,(V_{m,i}^* - V_{m,i}) - k_{1,g}\,(V_{g,1}^* - V_{g,1}) - k_{m,2}\,C_{m,i} - \sum_{j=2}^{N} K_{j,m} n_{1,j} n_j - E_{m,i}\,C_{m,i} \qquad (5.3\text{-}14)$$

for i = 1, ... N_{tar}, where N_{tar} is the total number of metaplast components of different molecular weight. E_g and E_m are the coefficients of diffusion through the melt and are derived later in Ch 5.4.4. The resulting escape coefficients are

$$E_g = \frac{3R_p^{\,2}}{R_{po}^{\,3}}\,D_{g,L}\,\left[\frac{K_j\,n_j}{D_{g,L}}\right]^{0.5} \qquad (5.3\text{-}15)$$

$$E_{m,i} = \frac{3\,R_p}{R_{po}^3} \frac{1}{\frac{1}{D_{m,g}} \frac{P}{P_{v,i}} \frac{\rho_L}{\rho_g} + \frac{1}{5\,D_{m,L}}} \qquad (5.3\text{-}16)$$

The yields of volatiles are obtained from the E's:

$$\text{Gas Yield} = \int \left(E_g\, C_g + \sum_{j=2}^{N} v_{g,j}\, E_{b,j}\, n_j \right) dt \qquad (5.3\text{-}17)$$

$$\text{Tar Yield} = \int \left(\sum_{i=1}^{N_{tar}} E_{m,i}\, C_{m,i} + \sum_{j=2}^{N} \sum_{i=1}^{N_{tar}} v_{mi,j}\, E_{bj}\, n_j \right) dt \qquad (5.3\text{-}18)$$

$v_{g,i}$ and $v_{mi,j}$ are the mass of gases and metaplast i in bubble size j. The extent of swelling is calculated from the number density of bubbles and bubble radii assuming the density of the liquid phase stays constant.

5.4. DERIVATION OF RATE CONSTANTS IN CONSERVATION EQUATIONS

5.4.1. Transport of Volatiles to Bubbles and Bubble Growth rate

According to the film theory of mass transfer, the rate of volatiles transport to a bubble is

$$\frac{dv}{dt} = 4\pi a\, D_{v,L}\, Sh\, (C - C_{eq}) \qquad (5.4\text{-}1)$$

where v = mass of a bubble, i.e. the mass of gases and vapors confined within the bubble

a = bubble radius

$D_{v,L}$ = diffusivity of the volatiles in the liquid

Sh = Sherwood number of mass transfer

C = concentration for volatiles (gases or metaplast) in liquid phase

C_{eq} = equilibrium concentration of volatiles at the interface between the molten coal phase and the bubble

The Sherwood number can vary from 1 to 2 (Appendix E). However, the magnitude of the diffusivity varies several orders of magnitude because of the changes in coal viscosity. Furthermore, there are one to two powers of ten uncertainty in the diffusivity, with direct measurements for gases in molten coal being unavailable and values for $D_{v,L}$ thus having to be estimated from the literature on diffusivities of various gases and vapors in hydrocarbon liquids. Therefore, the small variation in Sherwood number is ignored, i.e., Sh is assumed to be a constant.

Since the first two terms of the bubble balance (Eq. 5.3-12) are from the growth due to diffusion, $K_j\ n_1$ is the same as Eq. 5.4-1, except the concentration of monomers is expressed in terms of # molecules/gm orig. coal. Therefore,

$$K_j = \rho_o\ 4\pi a\ D_{v,L}\ Sh\ (\ n_1 - n_{eq}\ )\ /\ n_1 \qquad (5.3\text{-}12b)$$

where ρ_o is the density of condensed phase and is assumed to be a constant.

As volatiles from the molten phase are added to bubbles, the bubbles grow with a rate that is affected by mechanical forces such as the internal and external pressures of the bubble, surface tension, and inertial and viscous forces, as well as by the rate of mass transfer into the bubble. The bubble growth rate, $\dot{a}$, is derived assuming: a constant fluid density, viscosity and surface tension; the liquid behaves as a Newtonian fluid; liquid density>>gas density; and bubble radius << distance between bubbles (Scriven, 1959; Barlow and Longlois, 1962).

$$\frac{P_b - P - 2\sigma/a}{\rho} = a\ddot{a} + \frac{3}{2}\dot{a}^2 + \frac{4\mu\dot{a}}{\rho a} \qquad (5.4\text{-}2)$$

where P_b = total bubble pressure, i.e., the sum of gas pressure and vapor pressure of metaplast$_i$

P = ambient pressure

μ = fluid viscosity

σ = surface tension

ρ = fluid density

In a very viscous liquid like molten coal, the inertial terms are small compared to the viscous term and the above equation is simplified into

$$\dot{a} = \frac{da}{dt} = \frac{a}{4\mu}\left(P_b - P - \frac{2\sigma}{a} \right) \qquad (5.4\text{-}3)$$

The coal may swell to an extreme extent and form a cenoshpere in which a particle consists of a thin outer shell surrounding a cellular structure of membrane-like walls, much like a foam. When the molten coal approaches the cenosphere configuration, the above equation is an oversimplification. However, within the uncertainties in the knowledge of melt viscosity, the viscous force is a dominant term. The above simplified equation with a reasonable description of viscosity provides a first approximation to the bubble growth rate.

5.4.2. Coalescences of Bubbles and Bubble Escape

The coalescence of two bubbles is assumed to occur due to the expansion of two adjacent bubbles. One can visualize this process as two bubble surfaces making a point contact and further as two particles colliding with each other. By drawing an analogy from simple hard sphere collision theory, consider a particle, A, moving with the velocity $\mathbf{v}$, through the column uniformly packed with particles, B, with the particle packed density C_B. During the time interval of Δt, assuming the particle A

moves along a straight line even after collisions, the number of collisions made is

$$\begin{matrix}\text{cross-}\\ \text{sectional}\\ \text{area}\end{matrix} \cdot \begin{matrix}\text{distance}\\ \text{travelled}\end{matrix} \cdot \frac{\#\ \text{particle}}{\text{volume}} = \pi\ (\ r_A + r_B\ )^2\ \Delta t\ v_A\ C_B \qquad (5.4\text{-}4)$$

The collision rate for C_A particles is

$$\pi\ (\ r_A\ +\ r_B\ )^2\ v_A\ C_B \qquad (5.4\text{-}5)$$

If the particles B move with the velocity **u**, relative to B, the particle A is moving with the velocity **u** - **v**. Then, the collision rate would be

$$\pi\ (\ r_A + r_B\ )^2\ (\ \mathbf{u} - \mathbf{v}\ )\ C_A\ C_B \qquad (5.4\text{-}6)$$

For the spherical bubbles with radii a_i and a_j, of which the centers are stationary because of high medium viscosity, while the surfaces expand radially with the velocity of $\dot{a}_i$ and $\dot{a}_j$, the rate of collision is

$$4\pi\ (\ a_i + a_j\ )^2\ (|\dot{a}_i| + |\dot{a}_j|)\ C_i\ C_j \qquad (5.4\text{-}7)$$

Then, the rate constant, P_{ij} due to the bubble expansion is

$$P_{ij} = 4\pi\ (\ a + b\ )^2\ (\ \dot{a} + \dot{b}\ ) \qquad (5.4\text{-}8)$$

When the bubble concentration is based on gm original coal, the correction is made on the P_{ij};

$$P_{ij} = 4\pi\ \rho_o\ (\ a + b\ )^2\ (\ \dot{a} + \dot{b}\ ) \qquad (5.3\text{-}12a)$$

The last remaining term is the bubble escape term. Assume all the bubbles colliding with the particle surface break through the surface and escape from the particle. As in coalescence, the bubble expansion is visualized as bubble moving velocity of $\dot{a}_j$ and bubble escape as bubbles

colliding to the particle surface. The collision rate is

$$4\pi(R_p - a_j)^2 \; a'_j \; C_j \qquad (5.4\text{-}9)$$

And the bubble escape rate of bubbles sized a_j per gm original coal is

$$E_j = \frac{4\pi (R_p - a_j)^2 \; a'_j}{\frac{4\pi}{3} R_{p,o}^3} \qquad (5.3\text{-}12c)$$

5.4.3. Gaseous Volatile Transport to the Particle Surface

Before determining the mass transfer rate at the particle surface, the mass transfer resistance inside and outside the particle are compared. Assuming steady state, the flux of gaseous volatiles at the particle surface is expressed using a film theory:

$$N_g = \frac{D_{g,L}}{d_L} (C_g - C_s) = \frac{D_{g,G}}{d_G} \frac{P}{RT} (y_s - 0) \qquad (5.4\text{-}10)$$

where C_g = Average gas concentration in the particle

C_s = Gas concentration at the surface

y_s = Equilibrium gas concentration at the surface, C_s H / P

d_L, d_G= Boundary layer thickness inside and outside the particle

$D_{g,L}$, $D_{g,G}$= Diffusivities of gases inside and outside the particle

R = Gas constant

For a spherical particle in an infinite medium, d_G is the particle radius, R_p. By substituting appropriate values for the above parameters ($D_{g,L}$ ~ 10^{-7} cm^2/s, $D_{g,G}$ ~ 1 cm^2/s, R_p ~ 3 x10^{-3} cm, T ~ 1000 K, H ~ 1 x 10^{-10} $(dyne/cm^2)/(gm\ gas/cm^3)$, MW_g ~ 28), one can compare the mass transfer

resistances inside and outside the particle.

$$\frac{(MR)_L}{(MR)_G} = \frac{\dfrac{d_L}{D_{g,L}}}{\dfrac{R_p}{D_{g,G}}\,\dfrac{RT}{H\,MW_g}} = \frac{10^7\, d_L}{10^{-1}\, R_p} \qquad (5.4\text{-}11)$$

Unless $d_L << 1 \times 10^{-8}\ R_p$, the mass transfer resistance for gaseous volatiles is inside the particle.

The rate of gaseous volatiles diffusion from the particle surface is obtained from the steady-state balance of gases dissolved in the coal melt by taking the flux at the particle surface. The mass balance and the boundary conditions are as the following:

$$\frac{D_{g,L}}{r^2}\,\frac{d}{dr}\,r^2\,\frac{dC}{dt} + \rho_c\, R_f - K \cdot C = 0 \qquad (5.4\text{-}12)$$

$$\text{B. C.:} \quad r = 0 \qquad \frac{dC}{dr} = 0$$

$$r = R_p \qquad C = 0$$

where C = Mass concentration of gas dissolved in the particle

ρ_c = Density of coal

R_f = Rate of gas formation, gm/gm original coal sec

$K \cdot C$ = Rate of volatiles transport from the liquid into bubbles (see Eq 5.3-13)

Now let $\alpha = \dfrac{\rho_c\, R_f}{D_{g,L}}$ and $\beta = \dfrac{K}{D_{g,L}}$. The flux at the particle surface is

$$- D_{g,L} \left. \frac{dC}{dr} \right|_{r = R_p} = - \frac{\alpha}{\beta} \frac{D_{g,L}}{R_p} \left(1 - \sqrt{\beta} R \coth(\sqrt{\beta} R_p) \right) \quad (5.4\text{-}13)$$

The above equation can be simplified by an order of magnitude analysis of the three terms in the governing equation.

$$\frac{O\{ R_f / D_{g,L} \}}{O\{ C / R_p^2 \}} \sim 10^6 \gg 1, \quad O\{ \sqrt{\beta} R \} \sim 10^{-2} \quad (5.4\text{-}14)$$

Therefore, $\alpha / \beta \sim C$ and $\coth(\sqrt{\beta} R) \sim 1$. Eq. 5.4-13 is simplified to

$$- D_{g,L} \left. \frac{dC}{dr} \right|_{r = R_p} = D_{g,L} \, C \sqrt{\beta} \quad (5.4\text{-}15)$$

$\alpha \sim \beta$ implies that the rate of mass transfer to bubbles is relatively fast and the gases generated due to pyrolysis reactions are quickly transported to bubbles. Therefore the gas concentration in the molten phase is around its saturation level which is small compared to the amount of gases formed and the above pseudo steady-state approach is appropriate to derive the rate equation for gaseous volatiles transport to the particle surface.

5.4.4. Metaplast Transport by Diffusion

Again, using the film theory, the flux of metaplast at the particle surface is given as the following:

$$N_m = \frac{C_m}{\dfrac{\delta_G}{D_{m,G} \left(\dfrac{\rho_G}{\rho_L} \right) \left(\dfrac{P_v}{P} \right)} + \dfrac{\delta_L}{D_{m,L}}} \quad (5.4\text{-}16)$$

where C_m = average metaplast concentration inside the particle expressed in gm/gm original coal

δ_L, δ_G = boundary layer thicknesses inside and outside the particle

P_v = vapor pressure of metaplst

ρ_G, ρ_L = molar densities of the gas phase and the liquid phase

Two terms in the denominator of Eq 5.4-16, again, represent the mass transfer resistances of metaplast, outside and inside the particle. Except for the case at low temperatures at 70 atm, the mass transfer resistance inside the particle dominates as shown earlier. However, to apply the model to a wide range of molecular weight, i.e., MW > 1500, and at various temperatures and pressures, both terms are included in this study.

Again, δ_G for the pyrolyzing single particle in infinite medium is the particle radius (Suuberg, 1981) and δ_L can be estimated in the same manner as for gaseous volatiles where $\beta = K + k_{m,2}$. However, the amount of metaplast tranported to bubbles is limited by the vapor pressure of metaplast and the amount of metaplast transported to bubbles varies a lot with temperature. And also, the rate of secondary reactions is very slow where the formation rate is fast, while the formation reactions are almost completed when $k_{m,2}$ becomes large at typically high heating rates(1000 °C/sec). In this case, an order of magnitude comparison shows that α and β do not balance each other and the steay-state approach is no longer suitable. For a first approximation of δ_L, a parabolic concentration profile is assumed which satisfies the boundary conditions of $\partial C/\partial r = 0$ at r=0 and $C = C_s$ at $r=R_p$:

$$C(r,t) = g(t) \left(r^2 - R_p^2 \right) + C_s \qquad (5.4\text{-}17)$$

The average concentration of metaplast at time t is also obtained from

the above concentration profile:

$$C_m(t) = \frac{\int_0^{R_p} r^2 \; C(r,t) \; dr}{\int_0^{R_p} r^2 \; dr} = -\frac{2}{5} g(t) \; R_p^2 + C_s \qquad (5.4\text{-}18)$$

and the flux at the particle surface as a function of the average metaplast conctration inside the particle, C_m, is

$$-D_{m,L} \left.\frac{dC}{dr}\right|_{r = R_p} = 2 \; g \; D_{m,L} \; R_p = \frac{5 \; D_{m,L}}{R_p} (C_m - C_s) \qquad (5.4\text{-}19)$$

and, therefore,

$$\delta_L = \frac{R_p}{5} \qquad (5.4\text{-}20)$$

5.5. MODEL FOR MELT VISCOSITY AND VISCOSITY RELATED PROPERTIES

5.5.1. Melt Viscosity

The melt viscosity is modeled as a function of temperature, T, and the mass fraction of metaplast in the coal melt, ϕ :

$$\mu = C_v \; \exp (E_\mu / RT) \; f(\phi) \qquad (5.5\text{-}1)$$

where C_v is a constant. Activation energy, E_μ = 43 Kcal/mole is obtained from the viscosity data on carbonaceous pitch consisting of 55% Pyridine insolubles and 93% mesophase (Nazem, 1980). Similarly, E_μ=45.5 Kcal/mole can be derived from data on the viscosity of H-coal liquids at two different temperatures (Chao, 1980). However, Nazem also found that Eu is strongly temperature dependant and E_μ = 43 Kcal/mole is valid in a very narrow region at low temperatures. As the temperature increases, Eu decreases. In this study, the temperature dependance of the melt viscosity is employed only at low temperatures (< 450°C) to explain melting of pre-

existing metaplast and resolidification of the softened coal where both repolymerization reactions and the transport of the metaplast are negligible.

Studies on the viscosity of coal liquids also suggest that the viscosity of the liquid increases as the concentration of high molecular weight components increases (Schiller et al., 1977; Bockrath, et al., 1978) and that the change of viscosity can be modeled as a function of the high molecular weight content and therefore, as a function of metaplast concentration. There are several correlations which have been proposed for describing the relation between relative viscosity of dispersed systems and concentration of the dispersed phase (Rutgers, 1962). Some of these correlations had been applied to the system of molten coal. In the efforts of obtaining the coking rate from the viscosity of four coking coals, measured by a Giesseler plastometer, Bronowski et al.(1953) modeled the relative fluidity, Θ, which is the ratio of the viscosity of the liquid/solid mixture to that of pure liquid as

$$\Theta = 1 + \lambda (1 - \phi)$$

and concluded that λ was a constant in the range $0.8 < \lambda < 1.2$. Fitzgerald (1956) modeled the change in coal viscosity during resolidification as a function of the solids content $(1 - \phi)$ and he used $f(\phi) = \phi^{-2.5}$ taken from the Einstein equation which describes the viscosity of an infinitely dilute suspension of solid spheres.

The opposite of the Einstein equation is proposed by Frankel and Acrivos (1967). Where the solid fraction approaches 1, their assymptotic solution for the relative viscosity, θ, is

$$\theta \sim C' \left[\frac{(\psi / \psi_m)^{1/3}}{1 - (\psi/\psi_m)^{1/3}}\right] \quad \text{as } (\frac{\psi}{\psi_m}) \longrightarrow 0 \qquad (5.5\text{-}2)$$

where ψ is the volumeric concentration of spheres in the suspension, ψ_m is the maximum attainable concentration, and C' is a constant.

In pyrolyzing bituminous coal, the fraction of pyridine insolubles is greater than 50 % even at temperatures showing the minimum viscosity as shown in Figures 4.3.1 and 4.3.2. Therefore, the latter solution seems more appropriate for molten coal than the Einstein equation and is used here assuming $\psi_m = 1$ and where $\phi = 1 - \psi$,

$$\theta = \frac{1}{(1 - \phi)^{-1/3} + 1}$$

as $\phi \longrightarrow 0$, $f(\phi) \sim 1/(1 + \phi/3 - 1) \sim \phi^{-1}$.

Coal viscosity data obtained from conventional or modified Giesseler plastometers give qualitative information on how the coal viscosity varies with pyrolysis conditions but the quantitative information is not directly useful to the model because the Giesseler instrument is typified by low heating rates, low temperatures, and poorly defined flow field in the melt. Using a viscometer designed especially for molten coal, Fong (1985) has recently measured a minimum viscosity of 10^4 poise at heating rates of several hundreds °C/sec and peak tempratures exceeding 500 °C for a Pittsburgh Seam coal. The value of the constant, C_v is adjusted so that Eq 5.5-1 gives the correct order of magnitude of this minimum viscosity. An example of the measured apparent viscosity at a high heating rate as a function of time is shown in Fig. 5.5.1.

5.5.2 Diffusivities of Volatiles

Diffusivity of the volatiles in the coal melt is estimated from the simple correlation of temperature and viscosity:

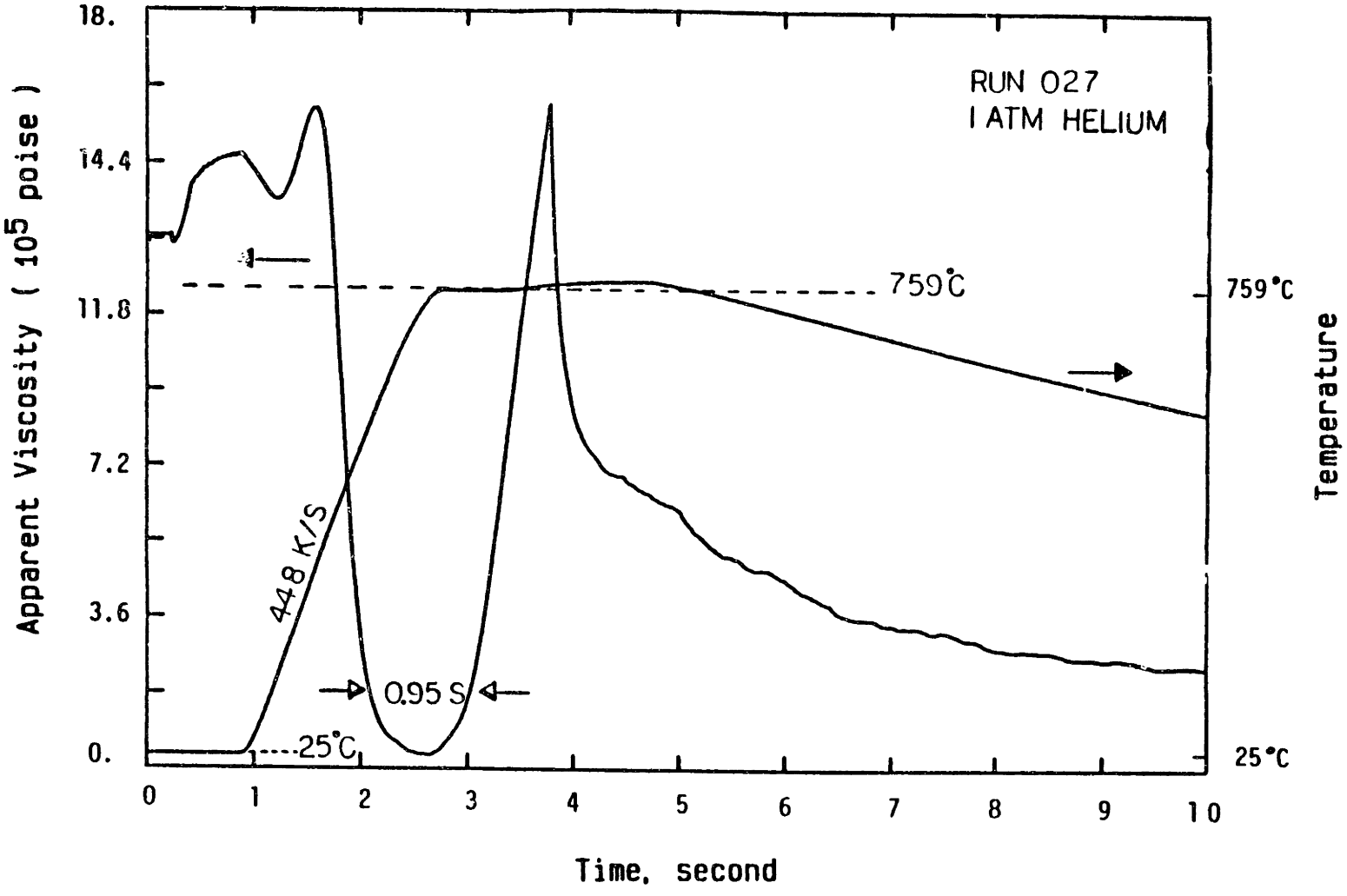

Fig. 5.5.1. Measured apparent viscosity of Pittsburgh seam #8 bituminous coal under rapid heating during 1 atm pyrolysis by a new coal plastometer. (Fong, 1985)

$$D_{v,L} = \frac{C_D\, T}{\mu^q} \qquad (5.5\text{-}4)$$

The linear dependance on temperature is taken from several theoretical correlations of diffusivity in liquids such as Arnold's, Wilke and Chang's, and Akgerman and Gainer's correlations (reviewed in Reid et al., 1977). The last two correlations also predict the inverse proportionality to viscosity (q = 1) which originates from the Stokes-Einstein relation, while Arnold's correlation predicts q=1/2.

Several experimental studies show that q is solute dependant. For example, q is 0.44-0.47 for CO_2; 0.49 for ethane; 0.88 for benzene; 2/3 for n-hexane and naphthalene; and 0.545 for propane (Hayduk and Chang, 1973; Hayduk et al., 1971; McManamey et al., 1973; Hiss et al., 1973). Based on this information, q in this study is assumed to be 0.5 for gaseous volatiles and 2/3 for metaplast of all molecular weight.

Since a typical diffusivity of a solute in a hydrocarbon liquid at room temperatures is around 1 x 10^{-5} cm^2/s when the viscosity is of order 1 cp, and since the minimum viscosity of the coal melt of interest is 10^4 poise at temperatures around 500°C, the constant, C_D, is adjusted to give a maximum diffusivity of 1 x 10^{-7} cm^2/s.

5.5.3 Surface tension

Surface tension of a coal melt, σ, is poorly understood, but probably varies with temperature, pressure and viscosity. For example, experimental data on coal liquids show that the surface tention, in general, decreases with increasing temperature and pressure but the magnitude of the decrease is small compared to that of the viscosity or the diffusivity. For

example, surface tension varies from 30 to 10 dyne/cm at temperatures and pressures in the ranges 93°C - 370°C and 67 - 136 atm while the viscosity varies from 2.71 to 0.196 cp (Hwang et al., 1982). Surface tension of pure liquid increases with the increasing viscosity. However, an emperical correlation of surface tension-viscosity for pure liquids (Pelofsky, 1966) suggest a constant surface tension at the region of high viscosities ($> 10^4$ poise):

$$\ln \sigma = -\frac{B}{\mu} + \ln A, \quad \text{as } \mu \longrightarrow \text{large}, \quad \sigma = A \qquad (5.5\text{-}5)$$

where A and B are constants. The surface tension of the coal melt is assumed to be a constant in the present work.

5.6. OTHER PHYSICAL PROPERTIES

The other physical properties which are not related to the viscosity but are necessary for implementation of the model are the gas solubility in the melt, vapor pressure of metaplast, and the molecular weight distribution of metaplast.

5.6.1. Vapor Pressure of Metaplast

The equilibrium vapor pressure of metaplast has been estimated by simple emperical models using only the component molecular weight, which is first proposed by Homann (1976) and later modified by Maiorella (1978) and by Suuberg et al. (1981):

$$\text{Maiorella's}: \quad P_v \text{ (atm)} = 6.23 \times 10^5 \exp\left(-\frac{561\ MW^{0.474}}{T}\right) \qquad (5.6\text{-}1)$$

$$\text{Suuberg's}: \quad P_v \text{ (atm)} = 5756 \exp\left(-\frac{255\ MW^{0.576}}{T}\right) \qquad (5.6\text{-}2)$$

Recently, experimental and theoretical studies were made on the vapor pressure of coal liquids: Grey et al. (1983) and Wilson et al. (1981) measured the vapor pressure of narrow boiling fractions of coal liquids and fitted the data to an existing correlation which uses critical properties. The molecular weight of the heaviest fraction was ~ 350, of which the boiling point was 515°C. The vapor pressure was estimated by the following equations:

$$\ln (P_r^o) = f_o + w f_1 \qquad (5.6\text{-}3)$$

where $f_o = 5.671845 - 5.809839/T_r - 0.86751 \ln(T_r) + 0.13835 T_r^6$

$f_1 = 12.4396 - 12.7560/T_r - 9.6542 \ln(T_r) + 0.31637 T_r^6$

$P_r^o = P_v / P_c$

$T_r = T / T_c$

Eq. 5.6-3 satisfies (1) the definition of acentric factor, $w = - \log(P_r^s) - 1$, at $T_r = 0.7$; (2) the Reidel condition, $d\alpha/dT_r = 0$ at $T_r = 1.0$ where $\alpha = d(\ln P_r)/d(\ln T_r)$; and (3) the critical point requirement, $P_r^s = 1.0$ at $T_r = 1.0$(Lee et al., 1975). The critical temperature, T_c and the critical pressure, P_c, are estimated from correlations using molecular weight, MW, and specific gravity, SG. For T_c:

$$\log(T_c, K) = 0.30293 \log(MW) + 0.68568 \log(SG) + 2.22185 \qquad (5.6\text{-}4)$$

For P_c:

$$\log(T_b, K) = 0.4541 \log(MW) + 0.4451 \log(SG) + 1.7238 \qquad (5.6\text{-}5a)$$

$$K_w = (T_b, R)^{1/3}/SG \qquad (5.6\text{-}5b)$$

$$\log(P_{c,corr}) = 4.86609 - 0.20833 K_w \qquad (5.6\text{-}5c)$$

$$(1 - T_b/T_c)_{corr} = 0.84579 - 0.04923 K_w \qquad (5.6\text{-}5d)$$

$$\Delta = (1 - T_b/T_c)_{actual} - (1 - T_b/T_c)_{corr} \qquad (5.6\text{-}5d)$$

$$\log(P_{c,act}/P_{c,corr}) = -0.00167 + 3.12579 \Delta \qquad (5.6\text{-}5)$$

Different Correlations estimating Critical properties of coal liquids were also proposed by Brule et al. (1982) and their correlations are much more complicated.

Tremper et al. (1981) proposed the correlations of vapor pressure using structural information such as fraction of aromaticity, naphthenicity, branching, and heteroaromaticity, instead of critical properties. Their correlation includes 15 empirical constants and requires one datum of temperature and vapor pressure. The correlation also has the molecular weight limitation which is the largest drawback of applying this correlation to metaplast: the model is good only for MW < ~475.

Even though there are inadequecies due to the MW range which the model is derived from, Grey and Wilson's model is employed to see which of the two simple emperical models, Eq's 5.6-1 and 5.6-2, gives more realistic predictions of metaplast vapor pressure. Figure 5.6.1 plots the calculated vapor pressures as a function of MW at 1000 °C and shows Maiorella's model predicts much higher vapor pressure than the other two. The heaviest fraction of the coal liquid (MW = ~360) in Grey's work (1983) has the H/C ratio of 0.84. The coal of which the number average MW is about 350 (see Ch 4.3) has the H/C ratio of 1.05 - 1.11 (Suuberg, 1978; Serio, 1984). Considering the fact that the molecules with higher hydrogen content has higher vapor pressure (for example, phenanthren (MW = 178.24) boils at 340 °C at 1 atm, which 9,10-dihydrophenanthrene boils at 169 °C at 1 atm), Maiorella's model seems to be more realistic than Suuberg's. In addition, Suuberg's model gives too low vapor pressure to predict theexpected tar yield at temperatures between 450 - 600°C. However, Maiorella's model seems to overpredict vapor pressure of metaplast at high temperatures (i.e., at 1000 °C and MW = 500, P_v = 42 atm vs P_v = 4.4 atm by Suuberg's

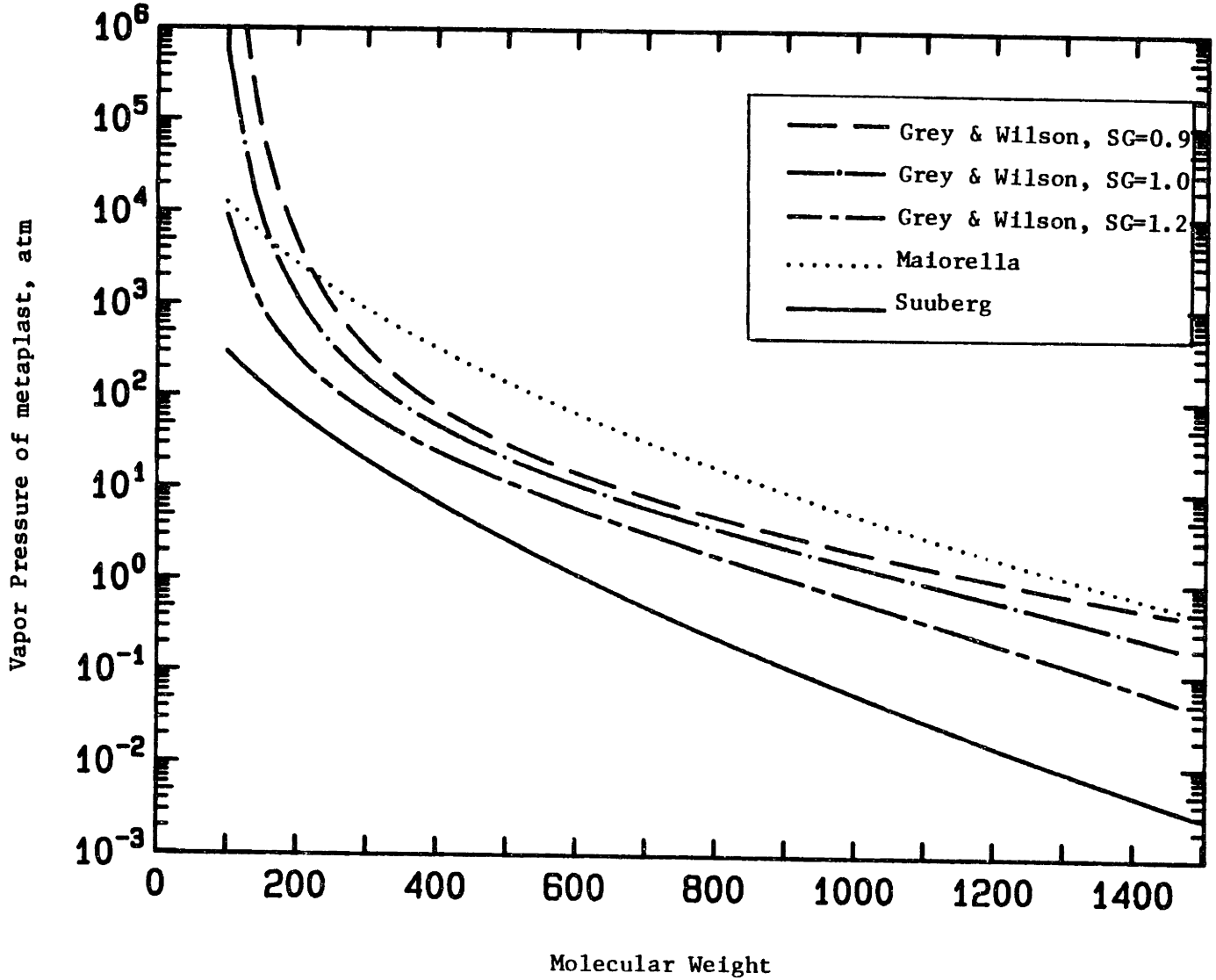

Fig. 5.6.1. Comaprison of Vapor Pressure predictions of metaplast at 1000°C

model). Both vapor pressure correlations are employed in the calculations of kinetic parameters and the resulting model parameters are compared.

The molecular weight information which is required in vapor pressure correlation is obtained from experimental data on the MWD of both pyridine extracts of char and coal tar from low temperature pyrolysis experiments. Since it is assumed that the formation rates of each MW fractions of metaplast are the same, the MWD of metaplast generated due to decomposition of coal stays constant regardless the formation temperature.

5.6.2. Solubility of Gaseous Volatiles in Molten Coal

At modest pressures, most gas solubilities in typical liquids are low and the solubilities are on the order of 1×10^{-4} (mole fraction). While there are some exceptions (i.e., hydrogen), the solubilility of a gas usually decreases with rising temperature. However, at temperatures close to the critical temperature of solvent, the solubility of gas usually rise with temperature. When the solubility is small, Henry's law provides a good approximation. Assuming ideal gas, Henry's law is written

$$P\, y_i = H\, x_i \qquad (5.6\text{-}6)$$

where x_i and y_i are mole fractions of gas i in liquid and in gas phase and H_i is the Henry's law constant for gas i. The effect of temperature on Henry's law constant can be accounted by the form of the Arrhenius equation

$$H = H_o \exp(- E_s / RT) \qquad (5.6\text{-}7)$$

where H_o is a constant and E_s is the heat of solution. Strictly speaking, E_s is also a function of temperature bue is treated as a constant for simplicity.

For the average solubilities (1/H) of gaseous volatiles in molten coal

as a function of temperature, the best one can do in this stage is to obtain the right order of magnitude for Henry's law constant from the gas solubilities in hydrocarbon liquids. Experimentally determined solubilities have been reported in chemical literature for over 100 years. Among those, solubilities of H_2, CH_4, and CO_2 in aromatic hydrocarbon liquids such as toluene, 1-methylnaphthalene and coal liquids were reviewed to estimate gas solubility in molten coal.

Most of solubility data quoted here were reported by H. M. Sebastian, H-M Lin, J. J. Simnick, and K-C Chao at Prudue University and of which the experiments were performed at relatively high pressures. To take the effect of pressure on Henry's law constant into consideration, the reported solubilities at high pressures were fitted to the following equation:

$$\ln\left(\frac{f_i}{x_i}\right)_p = \ln\left(\frac{f_i}{x_i}\right)_{x_i \to 0} + \frac{V^{\infty}_{s,i}\,(P - P_v)}{RT} \qquad (5.6\text{-}8)$$

where f_i = Fugacity of gas i, P_i for ideal gas

$V^{\infty}_{s,i}$ = Partial molar volume of gas i at infinite dilution in the liquid phase

P_v = Vapor pressure of solvent

Assume $V^{\infty}_{s,i}$ is independant of pressure in the interval $P - P_v$. Then the linear regression of $\ln(f_i/x_i)_p$ vs $(P - P_{vp})$ gives an intercept of $\ln(f_i/x_i)_{x\to 0}$, which is the definition of Henry's law constant. For coal liquids, vapor pressure was calculated by the empirical correlations by Gery et al., which are given in Eq's 5.6-3 to 5.6-5.

The Henry's law constants derived from the above equation along with the ones reported in literature are summerized in Table 5.6.1 and Table 5.6.2 gives the properties of the solvent in Table 5.6.1. The solubility of methane, in general, as well as that of H_2 seems to increase with

Table 5.6.1. Henry's law constant of H_2, CH_4, and CO_2 in hydrocarbon solvents at various temperatures: Temperature, C, first line and ln(Henry's law constant, atm), second line.

5.6.1a. Gas: Hydrogen

Solvent	Temperature/ln(H)				Reference
Toluene	189	229	269	302	Simnick et al., 1978
	7.0788	6.7223	6.3277	5.8990	
EDS-I	189		269		Lin et al., 1981
	7.1555		6.8627		
EDs-II	189		269		"
	2.2463		7.0083		
SRC-I	189		269		"
	7.2580		6.9018		
SRC-II	189		269		"
	7.3454		7.0498		
SRC-III			269		"
			7.1433		
Creosote Oil[a]	100	200	300	400	Guin et al., 1977
	7.2042	7.0503	6.9399	6.7206	

5.6.1b. Gas: Methane

Toluene	149	189	228	270	Lin et al., 1979
	6.1939	6.2363	6.0487	5.8508	
1-Methyl-naphthalene	191	270	351	431	Sebastian et al., 1979
	6.5890	6.5073	6.3130	5.9736	
EDS-I	189	268			Lin et al., 1981
	6.2333	6.1099			
EDS-II	189	268			"
	6.2082	6.2661			
SRC-I		268			"
		6.1860			
SRC-II		268			"
		6.3132			

5.6.1c. Gas: Carbon Dioxide

Toluene	120	149	204	230	Sebastian et al., 1980
	5.3635	5.4740	5.5066	5.5145	
1-Methyl-naphthalene	27	57	77	102	Tremper et al., 1976
	4.8442	5.1059	5.3279	5.5094	
	127	152	177	202	
	5.5654	5.7398	5.7869	5.7430	

a) The original data were reported in gm H_2/gm oil-psia. To convert the data into the above unit, MW of 170 for creosote oil is assumed. Creosote oil consists of mostly 2-3 ring hydrocarbons.

Table 5.6.2. Physical properties of solvents in Table 5.6.1.

	MW	b. p., C	SG(gm/cm^3)	ΔH_{vp}	T_c, °C
Toluene	92.15	110.6	0.8669	8333	318.7
1-Methylnaphthalene	142.20	244.64	1.0202	11000	499
EDS-I[a]	154.34	180.4 - 257	0.9320	-	430.1
EDS-II	182.3	240.9 - 352.6	0.9844	-	510.1
SRC-I[b]	182	224.9 - 292.2	0.9826	-	481.4
SRC-II	212	297.7 - 348.9	1.0306	-	549.6
SRC-III	252	355.6 - 392.2	1.091	-	609.7
Creosote Oil	170	175 - 350	1.10	-	-

a) Distillate cuts from Exxon Donor Solvent(EDS); I:400-450 F cut; II:500-600 F cut.
b) Distillate cuts from Solvent Refined Coal II(SRC) Process: I:500-528 F cut; II:600-632 cut; III:700-750 cut.

Table 5.6.3. Average composition of gaseous volatiles

	% mole	% weight
H_2O	21.32	29.48
CO	6.77	16.58
CO_2	0.18	6.24
CH_4	17.35	21.35
C_2H_4	3.74	8.06
C_2H_6	2.10	4.84
C_3's	1.85	6.27
H_2	45.75	7.03

temperature, while the solubility of CO_2 decreases. Therefore, the average solubility of a mixture of these gases is expected to change a little with temperature. Except the methane solubility in 1-methylnaphthalene, solubilities seem to decrease with increasing molecular weight of solvent.

For the average solubility of gaseous volatiles as a function of temperature, assume (1) solubilities of CO and H_2O are the same as CO_2 and (2) solubilities of hydrocarbon gases are the same as CH_4. Since higher hydrocarbons (C_2+) are more soluble than methane, while CO is less soluble than CO_2, the error expected in the average solubility from the above assumptions would be cancelled in a certain degree. Table 5.6.3 gives the composition of gaseous volatiles produced at peak temperatures > 900°C.

The solubilities H2-SRCII, methane - 1-methylnaphthalene, and carbon dioxide - 1-methylnaphthalene are chosen to model the solubilities of volatile gases in molten coal.

$$H_{He} = 390 \exp(1267 / RT) \qquad (5.6\text{-}9)$$

$$H_{CH_4} = 128 \exp (1665 / RT) \qquad (5.6\text{-}10)$$

$$H_{CO_2} = 1801 \exp (- 1579 / RT) \qquad (5.6\text{-}11)$$

Then, the total amount of gases dissolved in molten coal is

$$x = \sum_{i=1}^{N} x_i = \sum_{i=1}^{N} \frac{P_g\, y_i}{H_i} = P_g \sum_{i=1}^{N} \frac{y_i}{H_i} \qquad (5.6\text{-}12)$$

where P_g is the total gas pressure. The average Henry's law constant is

$$H = \left(\sum_{i=1}^{N} \frac{y_i}{H_i} \right)^{-1} \qquad (5.6\text{-}13)$$

Since the amount of gas dissolved in liquid is usually small, one can assume

$$x_i \sim \frac{\text{mole gas}}{\text{mole solvent}} \sim \frac{\text{gm. gas dissolved}}{\text{mole solution}} \cdot \left(\frac{1}{MW_i} \right) \qquad (5.6\text{-}14)$$

In terms of gm gas dissolved/mole of solvent, the Henry's law constant becomes

$$H' = \left[\sum MW_i \frac{y_i}{H_i} \right]^{-1} \quad \{atm/gm\ gas \cdot mole\ solvent\} \qquad (5.6\text{-}15)$$

By substituting Eq's 5.6-9 to 5.6-11 into Eq. 5.6-15 for gases listed in Table 5.6.3, the modified Henry's law constant, H', at various temperatures are calculated:

Temperature, K	H'
700	43.189
800	41.635
900	39.943
1000	38.348
1100	36.918
1200	35.661

Fig. 5.6.1 plots ln(H') vs 1/Temp(K), and H' is written as the following:

$$H' = 27.566 \exp (624 / RT) \quad \{atm/gm\ gas \cdot mole\ solvent\} \qquad (5.6\text{-}16)$$

Sebastian et al (1981) also proposed empirical correlations for the solubilities of H_2, CH_4, and CO_2 in hydrocarbon solvents. Henry's law constants are correlated as a function of solubility parameter and temperature. Each correlation is unique for a gas and it has 5 or 6 emperical constants. Their correlation seems to work well for single gas component dissolved in a pure hydrocarbon or in a mixture. However, because of difficulties in estimating solubility parameter for molten coal and the number of emperical constants involved for each gas component, the correlations were not used here.

The correlations used to estimate the melt viscosity, diffusivities of volatiles in molten coal, surface tension, gas solubility, and the vapor pressure of metaplast are summerized in Table 5.6.4.

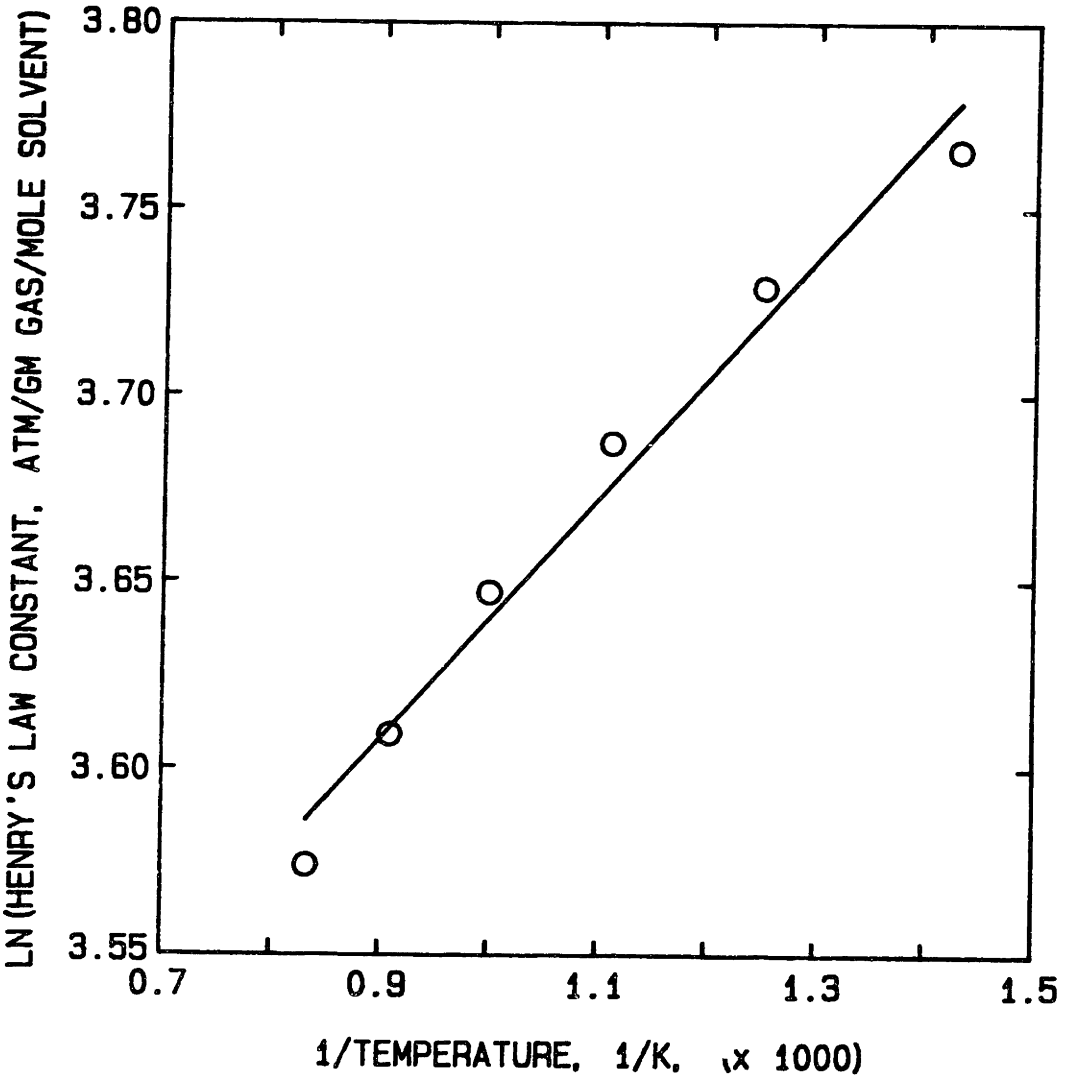

Fig. 5.6.2. Henry's law constant for gaseous volatiles in molten coal as a function of temperature

Table 5.6.4. Correlations to estimate melt viscosity and other physical properties.[1]

Melt viscosity[2]: $$\mu = \frac{C_\mu \exp(-E_\mu/RT')}{(1 - \phi)^{-1/3} - 1.0}$$

where ϕ = wt fraction of metaplast
T' = T (K) at temperatures < 450°C
T' = 723 K at temperatures > 450°C

Diffusivity of volatiles in molten coal:

$$D_v = \frac{C_D\, T}{\mu^q}$$

q = 0.5 for gases and
2/3 for metaplast

Vapor pressure of metaplast:

Maiorella's model[3]: $P_v = 6.311 \times 10^{11} \exp(-561\ MW^{0.474}/T)$ [dyne/cm^2]

Suuberg's model[4]: $P_v = 5.813 \times 10^{9} \exp(-255\ MW^{0.586}/T)$ [dyne/cm^2]

Surface tension: Constant

Gas Solubility in molten coal: $$H = H_o \cdot \exp(-E_s / RT)$$

---

1. Unless otherwise noted, this study.
2. Nazem (1980), Frankel and Acrivos (1967), and this study.
3. Maiorella (1978)
4. Suuberg and Unger (1981)

6. RESULTS AND DISCUSSION

6.1. MODEL SIMPLIFICATIONS

The model presented in Ch 5 has three independant variables: time, metaplast molecular weight and size of bubbles. Since the bubbles grow due to the influx of pyrolysis generated volatiles, modeling the changes of the bubble size distribution as a function of time requires monitoring the growth of different size bubbles, independantly. Different size bubbles also have different tar and gas compositions and, furthermore, coagulation between bubbles makes the calculation of mass balances extremely complicated. Numerical problems arising from the three-dimensional problem and from the kinetic equations of coagulation, such as computer storage space and long cpu times, hinder routine applications of the model at this stage of modeling softening coal pyrolysis. Therefore, it is necessary to simplify the model.

As discussed in Ch 5.1, molecular weight of metaplast plays an important role in determining the mode of metaplast transport and, therefore, the MWD of metaplast must be included. As for the bubble size distribution, one expects to see the growth of bubbles as seen in microphotographs of cenospheres formed at various temperatures, which show bubbles as large as a few microns in diameter. However, not much is known about the initial size distribution and about the changes as a function of time during the plastic period. Attempts were made to simplify the bubble size distribution and yet to predict the growth of bubbles to micron size, which seem to play an important role in volatiles transport.

6.1.1. No Bubble Coalescence

Bubble coalescence was considered to occur when two growing bubbles physically contact each other as described in Ch 5.3.2 and the coalescence coefficient, P_{ij}, was modeled as a function of the bubble growth rate. Since the bubble growth rate is a function of viscosity, volatiles generation rate, concentration of volatiles dissolved in the molten coal and total bubble concentration, the rate constant, P_{ij}, is not only a function of time, but also releated to a dependant variable, the bubble concentration.

The problem of coagulation kinetics has been around for a long time in modeling particle coagulation. The degree of difficulty of solving coagulation equations varies depending on how the rate constant, P_{ij}, is formulated and on the initial size distribution of particles. Analytical solutions are possible when P_{ij} is a constant or is proportional to the product $v_i v_j$, where v is a conserved property between coagulations, and the initial distribution is described by some particular functions. For Brownian coagulations, assymptotic solutions were obtained by means of a similarity transformation, assuming that the particle size distribution becomes self-preserving, independant of the initial distribution, after a sufficiently long time (Friedlander, 1966).

For a non-linear coalescence rate constant, which varies not only with time but also with the dependant variable, there seems to be no simple numerical method to solve the kinetic equation. In the present work, two numerical methods were tried unsuccessfully. In the method of the sectional representation of particle population balance (Gelbard, 1978), the coagulation coefficient, P_{ij}, is transformed to sectional coagulation,

β_{ij}, which involves evaluating double integrals. The minimum number of sectional coagulation coefficient required is $(3m^2 - m)/2$ where m is the number of sections. More about this method will be discussed in the following section. The sectional balance works best when the sectional coagulation coefficient were independant of time or when interpolation of β_{ij} is possible if β's vary with time. This technique gives an excellent mass balance between coagulations. However, for the model presented in this thesis, the bubble sizes change with time and the number of β's required was $(m^3 + 6m^2 - m)/6$. The evaluation of β's for each time step of integration was very costly.

The second method employed was the finite element approximation of particle size distribution, where the element boundaries were modeled to vary with time. The size distribution function was transformed to a log function and then was approximated with a linear basis function. The numerical formulation of coagulation terms were less complicated than the sectional balance method but the finite element approximation fails to give a closed mass balance at each step of integration.

To incorporate the coagulation term into the present model, the rate constant, P_{ij}, needs to be simplified while, at the same time, retaining adequate description of the coagulation mechanisms. The bubble growth rate, described by Eq 5.4-3, was derived for a bubble which is sufficiently far away from the next bubble. Therefore, Eq. 5.4-3 is not adequate to discribe the growth of two bubbles extremely close to each other. In an effort to simplify the model and to avoid the complication arising from the coagulation kinetics, the coalescence terms were not included in further development of the model.

6.1.2. Changes in Bubble Size Distribution

Now, the bubbles were assumed to grow solely by diffusive influx of volatiles, and the predicted changes in the bubble size distibution in the model were studied. The molten coal is treated as a homogeneous medium, which means that the inhomogeneties which might enhance or reduce gas formation such as mineral matter or maceral composition were not taken into consideration. Volatiles were assumed to be gases of a single molecular weight and constant melt viscosity and temperature were assumed.

Without coagulation terms, Eq. 5.3-12 becomes

$$\frac{dn_j}{dt} = K_{j-1}n_{j-1}n_1 - K_jn_jn_1 - E_jn_j \qquad (6.1\text{-}1)$$

The size of bubbles, j, varies from j=2 to 10^{11}. With the assumption that all gaseous volatiles have the same molecular weight, j can be transformed to a continuous variable. Let v be the mass of bubble (v = j x mass of a molecule) and n(v,t) be the bubble size distibution function, defined such that n(v,t)dv is the number of bubbles of mass between v and v + dv at time t. In terms of the continuous variable v, the number balance of bubbles becomes

$$\frac{\partial n(v,t)}{\partial t} = - \frac{dv}{dt}\frac{\partial n}{\partial v} - E(v,t)\, n(v,t) \qquad (6.1\text{-}2)$$

Eq. 6.1-2 can be transformed to ordinary differential equations using the concept of characteristic equations. since

$$\frac{dn}{dt} = \frac{\partial n}{\partial t} + \frac{\partial n}{\partial v}\frac{dv}{dt} \qquad (6.1\text{-}3)$$

Eq. 6.1-2 becomes

$$\frac{dn}{dt} = - E(v,t)\ n(v,t) \qquad (6.1\text{-}4)$$

and Eq. 6.1-4 has to be solved with Eq. 5.4-1 for several $v = v_o$ values at $t = 0$. In other words, the number balance of bubbles which has mass v_o at t=0 varies only due to the loss to the outside of the particle (Eq. 6.1-4), while the mass of the bubble varies according to Eq. 5.4-1.

Eq. 6.1-4 appears to be simple. However, prediction of the time dependant bubble size distribution is still difficult because bubbles of different size have different growth rates. To obtain a good mass balance of volatiles (for example, total amount of volatiles generated + inital amount of gases in the particle = volatiles escaped + volatiles in bubbles + volatiles in the molten phase), Eq's 6.1-4 and 5.4-1 have to be solved for a large number of $v=v_o$ values at t=0. To avoid this problem, sectional representation, the numerical technique of Gelbard et al. (1978) mentioned earlier for computing size distributions in aerosol dynamics, was employed. The method is based on dividing the bubble size domain into m arbitrary sections and assigning one integral quantity, for example, mass, to each section. This technique has the advantages of reducing the number of equations and conserving the integral quantity within the computational domain.

To make a mass balance on the total mass of bubbles in a section, the bubble size domain, v, is divided into m sections, and the total bubble mass of the section k, Q_k, is taken to be the integral quantity of section k:

$$Q_k(t) = \int_{v_k}^{v_{k+1}} v \cdot n(v,t)\ dv \qquad k = 1,2,.....m \qquad (6.1\text{-}5)$$

where v_{k+1} and v_k are the sizes of the smallest and largest bubbles in

section k. To express n(v,t) in terms of Q_k, assume that q(v,t) within each section k can be written as

$$q(v,t) = v \cdot n(v,t) = q_k(t) \cdot f'(v) \qquad (6.1\text{-}6)$$

where $f'(v) = df/dv$ and q(t) is a constant within each section. Substituting Eq. 6.1-6 to Eq. 6.1-5 results in

$$Q_k(t) = q_k(t) \cdot (f(v_k) - f(v_{k+1})) \qquad (6.1\text{-}7)$$

By eliminating $q_k(t)$ from Eq's 6.1-6 and 7, n(v,t) is writen as the following:

$$n(v,t) = \frac{Q_k(t) \cdot f'(v)}{v \, (w_{k+1} - w_k)} \qquad (6.1\text{-}8)$$

where $w = f(v) = \ln(v/v_{min}) \; / \; \ln(v_{max}/v_{min})$.

The bubble population balance is then transformed to m sectional balances in terms of Q_k:

$$\frac{dQ_k}{dt} = \frac{Q_k}{w_{k+1} - w_k} \int_{w_k}^{w_{k+1}} \left[\frac{\frac{dw}{dt}}{\ln(v_{max}/v_{min})} - E(w,t) \right] dw \qquad (6.1\text{-}9)$$

and Eq's 5.4-1 and 5.4-3 are also non-dimensionalized into dw/dt and $d\Upsilon/dt$ where $\Upsilon = \ln(a/a_{min}) \; / \; \ln(a_{max}/a_{min})$. The dimensionless domain w is defined intially from 0 to 1, and divided into 20 equal size sections. The bubble growth rates, dw/dt and $d\Upsilon/dt$, are solved at section boundaries along with the 20 sectional bubble mass balances (Eq. 6.1-9) and the balance of gases in the molten phase (Eq 5.3-13). The growth rates of the bubbles within a section are estimated by linear interpolation of the growth rates at the section boundaries. The total mass balance of gases is

checked at every time step of integration to insure the accuracy of the solution.

Fig. 6.1.1 describes the growth of bubbles at section boundaries as a function of time. At time = 0, the dimensionless size domain, w, is equally divided form 0 to 1. Once the simulation begins, bubbles may, depending on their size, either grow or shrink as the gases within them equilibrate with gases dissolved in the molten coal. Bubbles smaller than a critical size are completely dissolved and those larger than the critical size bubbles continue to grow by accepting volatiles from the reacting medium. At constant viscosity and temperature, the minimum required size for stable bubbles is a function of the initial concentration of gases in liquid as well as the rate of gas formation. For example, bubbles smaller than w=0.05 at t = 0 are completely dissolved in a very short time and bubbles in the second section (between w=0.05 and 0.1 at t=0) lose their contents initially and then start to grow as the concentration of gas in liquid increases due to the gas formation reactions.

The rate of mass transfer to the smaller of the bubbles above the critical size is much faster than the rate to the larger ones. Therefore, the smaller bubbles grow faster than the larger bubbles. As shown in Fig. 6.1.1, the bubbles at the boundaries of the section 2, w_1 and w_2, become about the same size at time t=0.03, and $w_1 \tilde{} w_2 \tilde{} w_3$ at t= 0.05 while the size of the larger bubbles is hardly changed. As time progresses, the bubble size distibution becomes very narrow. This behavior is seen more vividly in Fig. 6.1.2 which plots the changes in q(v,t) at various times and shows that even though the initial bubble size distribution is uniform, the growth of the bubbles shifts the bubble size distribution to the larger bubble sizes. The rapid growth of smaller bubbles leads to a large fraction of the volatiles mass being in bubbles near the minimum size.

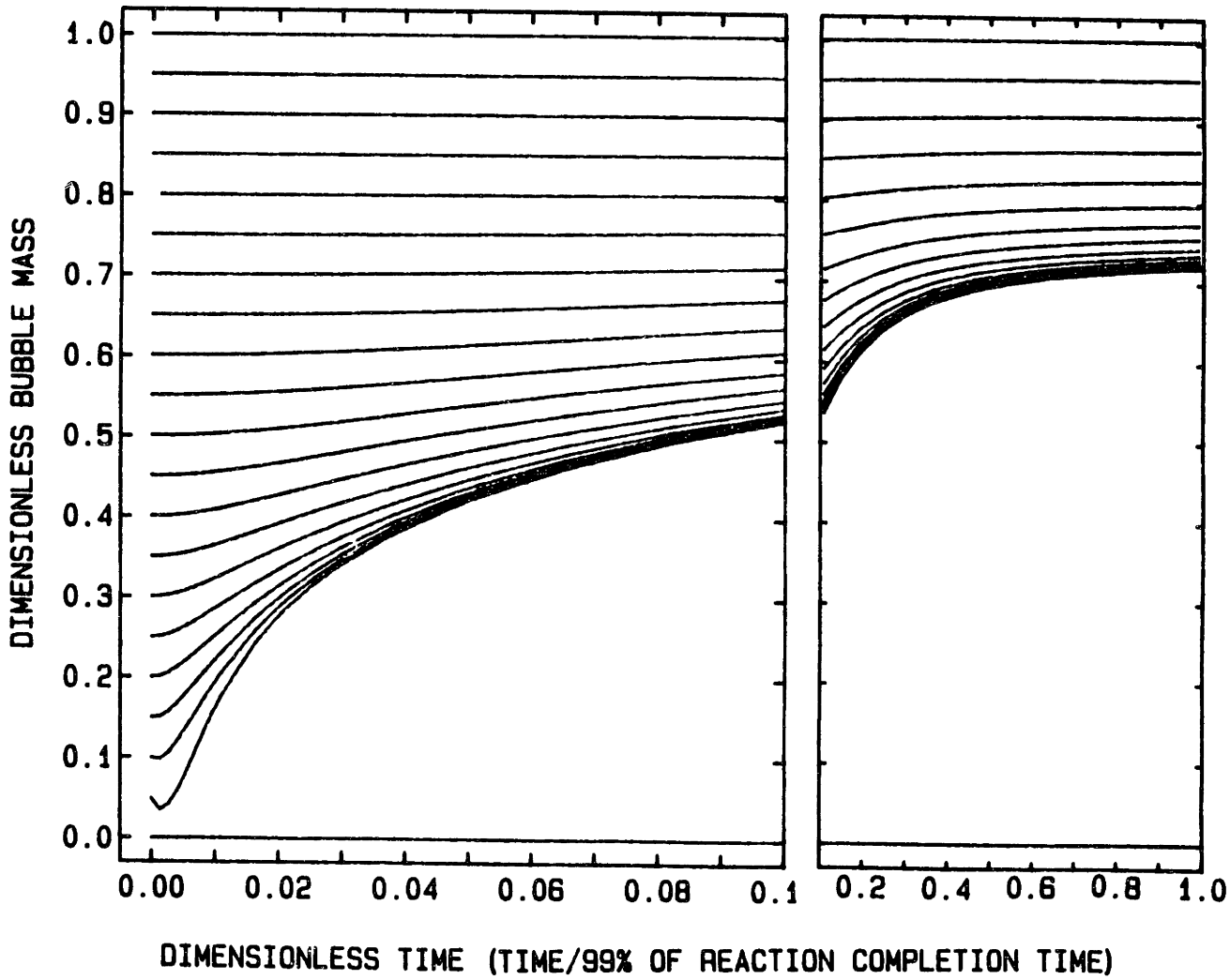

Fig. 6.1.1. Growth of bubbles at section boundaries as a function of time. Single molecular weight volatiles, constant temperature and viscosity, and no coagulation of bubbles are assumed. Dimensionless bubble mass = $\ln(v/v_{min})/\ln(v_{max}/v_{min})$ where v is the mass of a bubble.

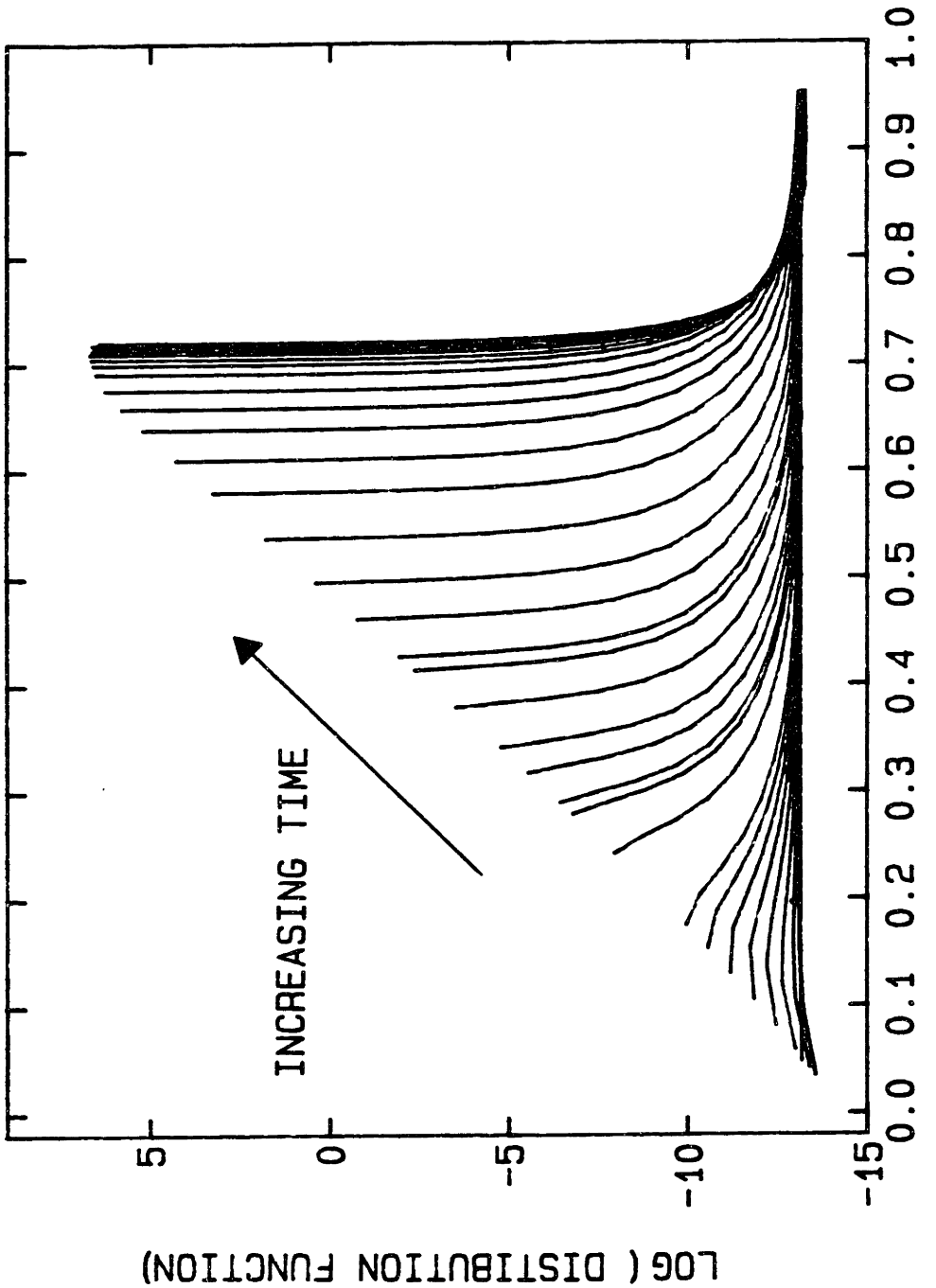

Fig. 6.1.2. Time dependant variations in bubble size distribution.

From Figs. 6.1.1 and 2, one can conclude that even though a wide spectrum of bubble sizes is considered, the bubbles grow into practically one size and essentially all the mass transport to bubbles is associated with the smallest stable size bubbles. Therefore, it is these small bubbles that account for essentially all of the volatiles transport by bubbles and the larger bubbles do not play an important role in mass transport. This important result allows the governing equation of bubbles to be simplified by eliminating the bubble size distribution and by just considering only uniformly sized bubbles.

Different values of melt viscosity, gas diffusivity in liquids and initial bubble size distribution do not change the above result but they do affect the rate of bubble escape, the gas yield, and the extent of swelling.

6.1.3. Model with Single Size Bubbles

The transport model was transformed assuming that all bubbles initially have the same size and, therefore, that they grow by the same diffusive flux of volatiles. Thus all bubbles have the same growth rate, and the number balance of bubbles is simplified into

$$\frac{dn}{dt} = -E_b\, n \qquad (6.1\text{-}10)$$

The rate of bubble expansion, da/dt, is again calculated by Eq. 5.3-4 to monitor the growth of bubbles. However, for the growth in bubble mass, the mass of metaplast and that of gases are monitored separately. Let $B_{m,i}$ and B_g be the mass of tar component i and the mass of gases in bubbles, respectively. Then the total bubble mass, v, is

$$v = \sum_{i=1}^{N_{tar}} B_{m,i} + B_g \qquad (6.1\text{-}11)$$

The mass balance of $B_{m,i}$ is

$$\frac{dB_{m,i}}{dt} = \begin{array}{c}\text{rate of} \\ \text{transport into} \\ \text{the bubble}\end{array} - \begin{array}{l}\text{loss due to} \\ \text{secondary} \\ \text{reactions}\end{array}$$

$$\frac{dB_{m,i}}{dt} = \rho_0 4\pi a\, D_{m,L}\, Sh\, (C_{m,i} - C_{eq,m,i}) - k_{3,m} B_{m,i} \qquad (6.1\text{-}12)$$

and that of B_g is

$$\frac{dB_g}{dt} = \begin{array}{c}\text{rate of} \\ \text{transport into} \\ \text{the bubble}\end{array} - \begin{array}{l}\text{formation of gases(3)} \\ \text{due to secondary} \\ \text{reactions of tar}\end{array}$$

$$\frac{dB_g}{dt} = \rho_0 4\pi a\, D_{g,L}\, Sh\, (C_g - C_{eq,g}) - f_{g,3}\, k_{3,m} B_{m,i} \qquad (6.1\text{-}13)$$

The balance of gases and metaplast in the condensed phase are the same as Eq's 5.3-13 and 14, except the summation on different bubble sizes are now unnecessary.

6.2. BUBBLE GENERATION

6.2.1. Bubble Nucleation in a Molten Coal

In a bubble transport model, it is important to understand the source of bubbles and their generation rate, related to volatiles formation and decomposition reactions. Unfortunately, not much is understood in this area. The model assumes pores in the solid coal as one source of bubbles

and that some of them survive upon softening and grow by accepting volatiles from the pyrolyzing medium. The other mechanism considered is nucleation of bubbles. Attar (1978) has claimed that the bubble nucleation from the volatiles, supersaturated in a molten coal can be a rate-limiting for volatiles transport via bubbles. If it is true, the bubble model proposed here would be invalid since it assumes that bubble generation is very fast compared to other kinetic processes and bubbles are already present in the melt upon coal softening. To resolve this issue, calculations were made to test whether the nucleation of bubbles can be a rate-limiting step in the transport processes for the pyrolysis conditions of present interest.

To calculate the critical concentration of dissolved gases, N^*, which is required for the homogeneous nucleation of bubbles, assume J^* to be 1:

$$J^* = 1 \text{ bubble/cm}^3 \text{ sec}$$

Because the nucleation rate function, J (Eq. 5.3-10), is dominated by the exponential term, the exact value chosen for J will have a very small effect on the critical concentration at the onset of nucleation (Attar, 1978; Cole, 1975). One can also assume that the pressure inside a critical size bubble at the formation stage is much larger than the external pressure, and then

$$P_b - P \simeq P_b \qquad (6.2\text{-}1)$$

and

$$N_o - N \simeq N^* \qquad (6.2\text{-}2)$$

Since the concentration of the gases in the molten coal is small, Henry's law is employed to describe the equilibrium relationship between gases dissolved in liquid and gaseous phase:

$$P_b = H \cdot N^* \qquad (6.2\text{-}3)$$

Apply the above assumption to Eq's (5.3-10), (5.3-10a), and (5.3-10b) and substitute appropriate values for parameters (σ = 30 erg/cm^2, m = 10^{-22} gm, k = 1.38 x 10^{-16} erg/K, T=670 K, μ = 10^5 dyne s/gm, D = 10^{-7} cm^2/s, H = 5.07 x 10^{10} (dyne/cm^2)/(gm/cm^3), and ρ_{coal} = 1.3 gm/cm^3). The Eq's (5.3-10), (5.3-10a), and (5.3-10b) become

$$1. = N^* (2.8202 \times 10^{34}) \left(\frac{1}{\delta_D}\right) \left(\frac{1}{w+1}\right) \exp\left(\frac{-1.9022 \times 10^{-3}}{N^{*2}}\right) \qquad (6.2\text{-}4)$$

$$\delta_D = 3.3054 \times 10^3 / N^* \qquad (6.2\text{-}4a)$$

$$w = 2.4625 \times 10^8 / \delta_D \qquad (6.2\text{-}4b)$$

where N^* is in gm volatiles/cm^3. Eq's 6.2-4, 4a, and 4b are solved interatively using Newton's interation method and give N^* = 5.89 x 10^{-3} gm/cm^3 (4.52 x 10^{-3} gm/gm coal). As disscussed above, the value for J^* makes only a small difference in N^*. For example, N^* is 5.33 x 10^{-3} gm/gm coal when J = 5 x 10^6, which is about 1 bubble/70 μ particle, and 5.59 x 10^{-3} gm/gm coal when J = 1 x 10^{10}.

Assume that at the nucleation stage, volatiles consist only of gases. The gas formation rate at temperatures less than 800°C is obtained from the gas yield from 1 atm pyrolysis (Fig. 4.3-1). The yields of gases at various peak temperatures are fitted to a single reaction model, and the resulting curve and the experimental data are shown in Fig. 6.2.1:

$$\frac{dV_g}{dt} = k_o \exp(-E/RT)\,(V_g^* - V_g) \qquad (6.2\text{-}5)$$

The kinetics parameters are k_o = 11.4 sec^{-1}, E = 5561 cal/mole, and V_g^* =

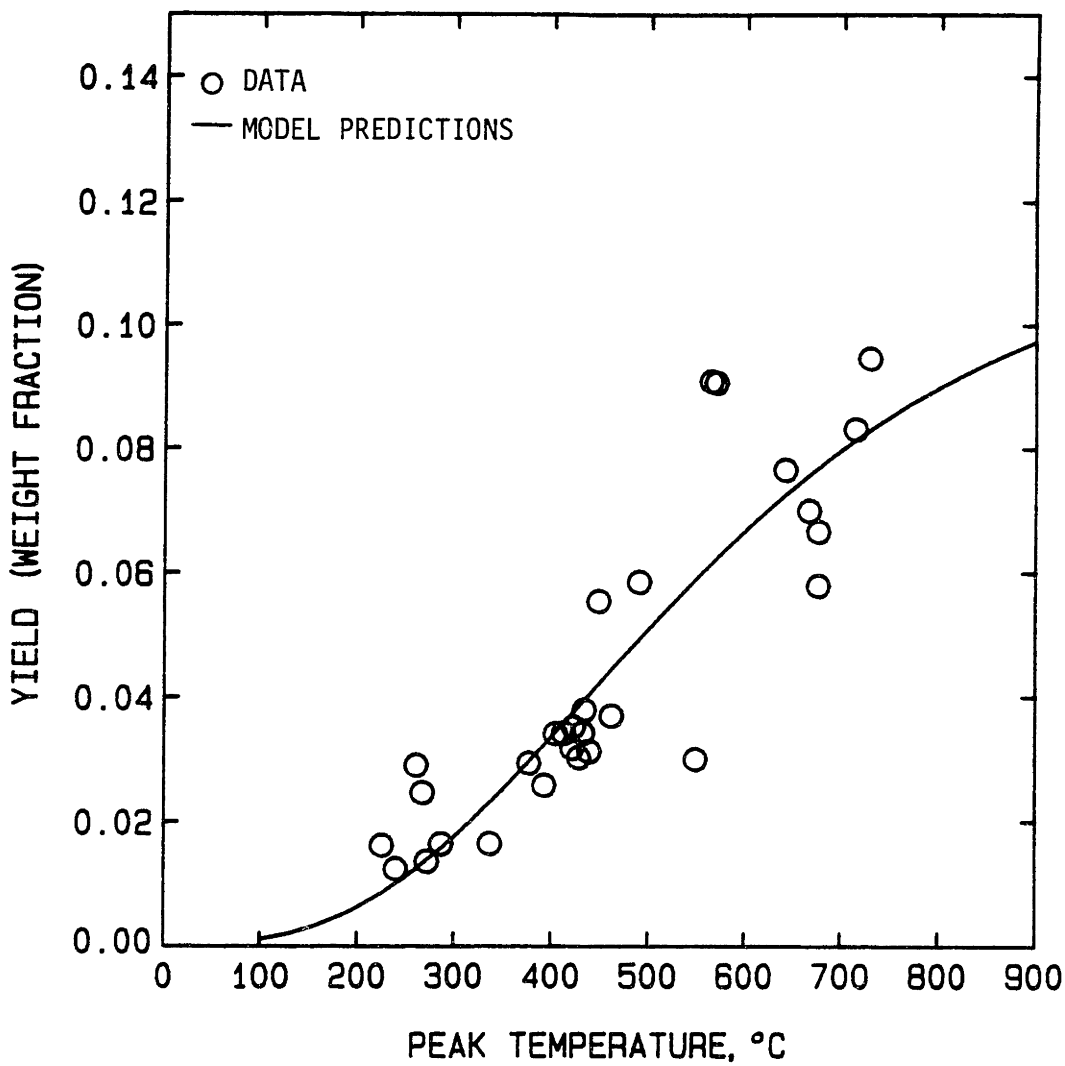

Fig. 6.2.1. Yields of gases from pyrolysis of Pittsburgh seam bituminous coal heated to different peak temperatures with the model predictions from a single reaction model.

0.119 gm/gm coal. At around the softening temperature (i.e., T=420 °C), the time required to observe the bubble formation is

$$t_c = -\frac{1}{k_o \exp(-E/RT)} \ln\left(1 - \frac{V_g}{V_g^*}\right) = 0.194 \text{ sec} \qquad (6.2\text{-}6)$$

As the temperature increases, the rate of gas formation also increases which results in a smaller t^*.

As the coal particles are heated at 1000°C/s from room temperature, the amount of volatiles generated in the molten coal is as follows:

Temperature, °C	$V_g \times 10^3$, gm/gm orig coal
300	1.19
350	2.08
400	3.37
420	4.02
430	4.37
440	4.75
450	5.14
460	5.56
470	6.00

The characteristic time for gases to diffuse through the molten coal to the particle surface is ~ 100 sec for particles of radius ~ 0.0035 cm. Therefore, the amount of gases depleted due to the diffusion to the particle surface is small. At the heating rate of 1000 °C/sec, the softening is observed at around 400 °C . According to the table above, the bubble generation is observed at around 440 °C, only 0.04 seconds after the softening. Therefore, the nucleation of bubbles does not appear to be a rate limiting process.

The critical concentration, N^*, however, is very sensitive to the solubility parameter (the Henry's law constant). Attar used H = 4800 atm/(mole/l). Assuming the average gas molecular weight is 28 and the coal

density is 1.3 gm/cm^3, H = 1.7366 x 10^{11} (dyn/cm^2)/(gm/cm^3), which gives N^* = 1.68 x 10^{-3} gm/cm^3 (1.2923 x 10^{-3} gm/gm coal). At this critical concentration, the bubble formation is observed at t_c = 0.054 sec at 420°C and at 310°C when coal is heated from room temperature at the heating rate of 1000 °C/sec if the coal is softened.

The above analysis of the rate of bubble nucleation is quite similar to that by Attar. However, the conclusion is quite different. Attar concluded that the bubble nucleation can be a rate limiting step in bubble transport (i.e., t_c ~ 54 min at 420°C). The improvement made in this analysis over the work by Attar is using the total gas generation rate for gas generation instead of methane generation rate. At temperatures around the softening point, the methane generation rate is low and most of the pyrolysis gases consist of H_2O, CO_2 and some CO. Therefore, it is more appropriate to use the overall gas generation rate than just that of methane.

Application of the nucleation rate theory to the molten coal to provide the bubble generation rate is avoided in this stage of modeling due to the following reasons:

1. J function has a several orders of magnitudes uncertainty. For example, when the correction for diffusion resistance is added, J is changed by 9 orders of magnitudes.
2. In an inhomogeneous medium like molten coal, heterogeneities such as different macerals or mineral matter could serve as nucleation sites and add even more uncertainty to the prediction of the rate of bubble nucleation.
3. If some pores in solid coal survive through softening and become voids, diffusion to the existing bubbles will be fast and the critical

concentration to nucleate bubbles will never be reached until all bubbles have been lost due to growth and escape through the particle surface.

6.2.2. Bubbles Originating from Pores in Solid Structure

Changes in Pore Structure Associated with Pyrolysis

Coals have significant pore volume with porosities varying from 2.5 to 18.0 % and pores which have openings of from 4 - 5 Å to the order of several microns. The International Union of Pure and Applied Chemisty (IUPAC) has proposed the following limits to standardized pore sizes. Macropores have a diameter greater than 500 Å. Mesopores often referred to as transitional pores, range from 20 - 500 Å. Micropores range from 8 - 20 Å, and sub- or super-micropores are less than 8 Å. The dimensions correspond roughly to different adsorption phenomenon and supermicropores are considered to be inaccesible to adsorbates and can only be measured by X-ray diffraction. However, the divisions frequently differ in the literature. Most sorption data on coals is considered to measure total pore volume, even though closed pores are not included. Closed pores (or inaccessible pores) can only be measured by X-ray diffraction or electron microscopy.

Gan et al. (1972) studied the pore size distribution of various ranks of American coals and Table 6.2.1 shows the total open pore volume distribution. The different pore volumes in the indicated pore diameter range are defined as

V_T : total open pore volume for pores accessible to helium at 32.5 °C.

V_1 : pore volume for pores in diameter > 300 Å

Table 6.2.1. Gross pore distribution in American coals (Gan et al., 1972)

Sample	Rank	V_T (cm³/g)	V_1 (cm³/g)	V_2 (cm³/g)	V_3 (cm³/g)	V_3 (%)	V_2 (%)	V_1 (%)
PSOC-80	Anthracite	0·076	0·009	0·010	0·057	75·0	13·1	11·9
PSOC-127	LV Bit.	0·052	0·014	0·000	0·038	73·0	nil	27·0
PSOC-135	MV Bit.	0·042	0·016	0·000	0·026	61·9	nil	38·1
PSOC-4	HVA Bit.	0·033	0·017	0·000	0·016	48·5	nil	51·5
PSOC-105A	HVB Bit.	0·144	0·036	0·065	0·043	29·9	45·1	25·0
Rand	HVC Bit.	0·083	0·017	0·027	0·039	47·0	32·5	20·5
PSOC-26	HVC Bit.	0·158	0·031	0·061	0·066	41·8	38·6	19·6
POC-197	HVB Bit.	0·105	0·022	0·013	0·070	66·7	12·4	20·9
PSOC-190	HVC Bit.	0·232	0·040	0·122	0·070	30·2	52·6	17·2
PSOC-141	Lignite	0·114	0·088	0·004	0·022	19·3	3·5	77·2
PSOC-87	Lignite	0·105	0·062	0·000	0·043	40·9	nil	59·1
PSOC-89	Lignite	0·073	0·064	0·000	0·009	12·3	nil	87·7

V_2 : pore volume for pores in diameter between 300 and 12 A°

V_3 : pore volume for pores in diameter < 12 A°, ($V_3=V_T - (V_1 + V_2)$)

In general, all coals show significant fractions of micropores. The anthracite sample has the highest proportion of micropores, V_3, and the lignite sample has the lowest. In high volatile bituminous coal samples, it can be seen that the volume of macropores varies from 0.02 - 0.04 cm^3/gm.

Changes in pore structure with heating have been studied extensively by porosimetry, sorption and density measurements. Many of the pore development studies were done under carbonization conditions. The configuration of the fine pores which include micro and some of mesopores, are related to the way in which the coal micelles are bound together (Franklin, 1949a) and the micropore volume increases with heating to 600 °C and decreased after a certain temperature, i.e., 800 °C (Toda, 1970; Miura, 1980) or 1000 °C (Franklin, 1949b). Increase of fine pore volume can be explained by the opening of new micropores and the decrease results from shrinkage which collapses the final pores (Toda, 1971).

Macro pore volume also goes through a maximum between 600 °C and 800 °C (Cameron et al., 1958; Miura et al., 1980; Singla et al., 1982) during carbonizations. Figs. 6.2.2a and b show macropore volume and the mean pore diameter obtained at two heating rates for coking and non-coking coals. For two coking coals, Jewel No. 2 and Pittsburgh high-volatile coal, both macropores volume and the mean pore diameter exhibit maximums which indicate pore growth. The decrease of volume and diameter between 800 and 1000 °C can be explained by the shrinkage of pore structure.

Muira et al. (1980) reported simultaneous changes in the micro and macro pores using differential pore volume distribution curves for four

(A)

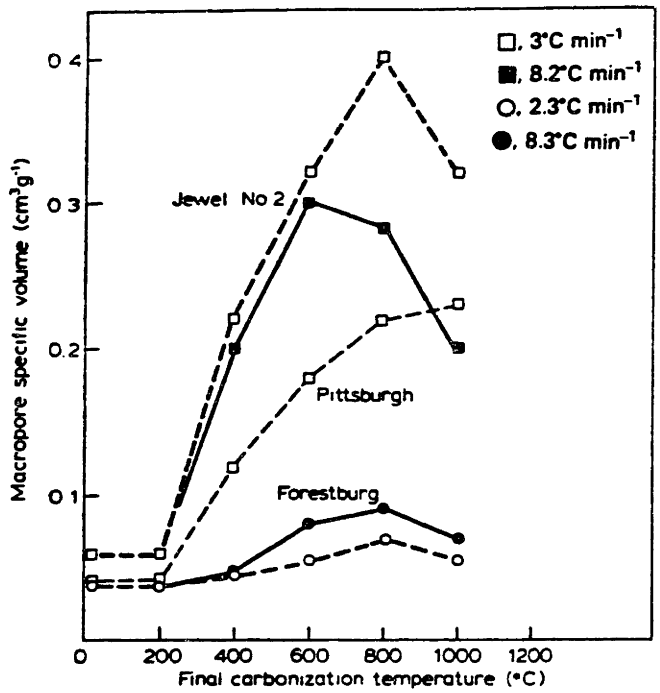

(B)

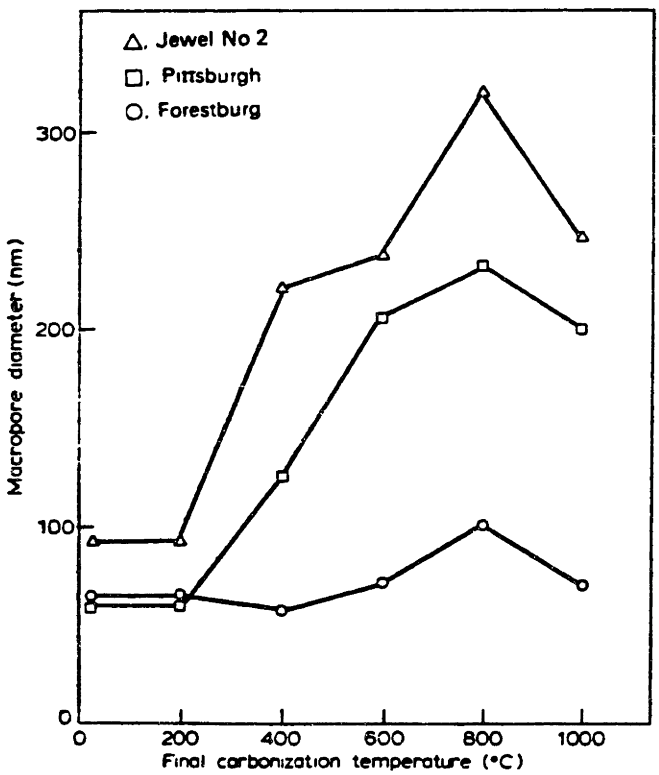

Fig. 6.2.2. Development of macropore volume (A) and mean pore diameter (B) as a function of final carbonization temperatures for coking and non-coking coals, heated at 2.3 - 8.3°C/min (A) and 2.3 - 3.0°C/min (B). (Singla, 1983)

final carbonization temperatures. These curves are shown in Fig. 6.2.3a for Jewel No. 2 coal and in Fig. 6.2.3b for Pittsburgh hv B coal. Higher peaks at low temperatures are explained by new pore initiation and the shift of the peak towards larger pore radius is attributed to the growth of pores. On the other hand, the shift of the peak toward smaller pores at high temperatures is due probably to pore shrinkage. It can be seen that macropores in both coals grow into larger pores of which the volume distribution is dominated by the peak at 10 μm at the given heating rate.

Once the plasticity develops, the direct observation of macropore development shows bubble formation in a molten phase which leads to macropores (Mackowsky et al., 1966). Woods et al. (1967) made qualitative observations on three separate types of pores in determining the porosities of chars of different maceral composition: rounded holes, angular holes and natural holes. They claimed that the rounded holes were formed as the gases resulting from the decomposition of exinite and vitrinite attempted to escape through the plastic phase, and that the angular holes were cracks formed after carbonization when the material contracted on cooling. The third classification of holes, natural holes, occurred in fusinite and semi-fusinite grains. Similar observations of rounded holes can be made on photographs from a regular microscope (Hays et al., 1976) and a scanning electron microscope (Adair et al., 1972). However, there are lack of data on the actual bubble size distribution derived from the photomicrographs. Even though photomicrographs have an advantage of detecting closed pores, the bubbles reported have diameters of microns or larger (Hays et al., 1976; Adair et al., 1972; Lightman et al., 1968) and no size distribution data are reported from the work on photomicrographs of char.

Development of bubbles and cenosphere structure is also observed under high heating rates as reviewed in Ch 3.3.

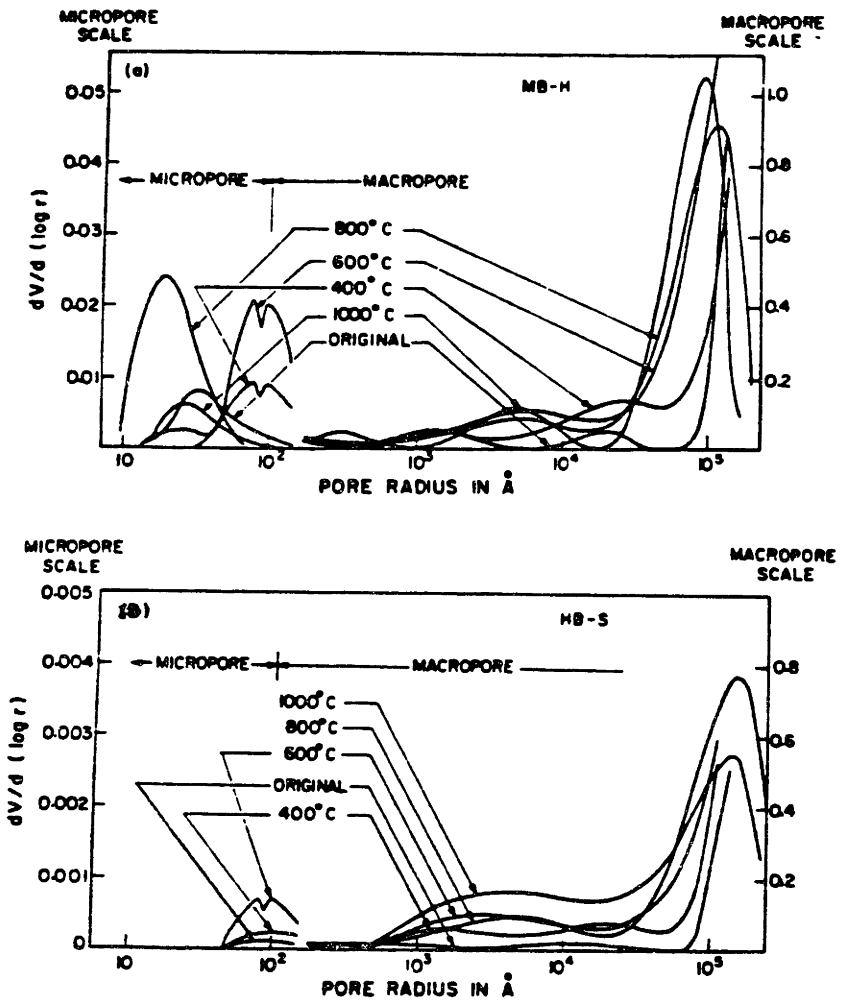

Fig. 6.2.3. Distribution of pore volume as a function of final carbonization temperature. (a). Jewel No. 2 (MB) coal, heating rate = 8.2°C/min; (b). Pittsburgh (HB) coal. (Miura et al., 1980)

Initial Size and Number Density of Bubbles

In the transport model, a number balance for bubbles in the particle of molten coal was maintained along with the mass balances of pyrolysis products. In the bubble number conservation equation, the loss of bubbles was modeled by simulating the rupture of bubbles at the particles surface. However, modeling bubble generation is difficult because not much is understood about the size and the rate of bubble generation as a function of pyrolysis conditions. As explained earlier, bubbles can be generated due to nucleation but a large number of uncertainties regarding the specific generation mechanisms and physico-chemical properties of a complex inhomogeneous medium like a molten coal precludes use of this rate theory. One conclusion that can be drawn from the analysis of nucleation, however, is that as long as the nucleation of bubbles is not a rate limiting step, one can assume for the purpose of the present model that nucleated bubbles as well as bubbles originating from the pores in solid structure before softening are already present in the molten coal at the onset of softening. The number density of bubbles, then, decreases as bubbles are released from the particle.

The initial number density of bubbles can be calculated from reasonable approximations of a bubble size and of the pore volume of the coal. The initial size has to be large enough so that bubbles will not dissolve at the initial stage of softening. As pointed out in the previous section, coal has a significant fraction of micropores (pore diameter < 20 Å) and the amount of fine pores varies with pyrolysis temperature. However, the existance of fine pores and their participation in transport during the plastic period are questionable. Pores of diameter 20 Å in

solid coal would become bubbles of diameter 0.82 Å, for which the pressure inside the bubble would be 1.44×10^4 atm when the external pressure and the surface tension of molten coal are 1 atm and 30 erg/cm^2, respectively. This hypothetical bubble pressure and bubble size suggest that bubbles originating from micropores are most likely to dissolve in the molten phase and disappear. As the coal resolidifies and contracts, the fine pores reappear due to the way that coal micelles are stacked aganist each other as shown in Fig. 6.2.4 (Franklin, 1949; Hirsh, 1954). Increase and decrease of fine pore volume with temperature may indicate the extent of decomposition and polymerization reactions during pyrolysis. The same argument can be applied to transitional size pores. Bubbles originating from pores of 200 Å diameter has the inital diameter and bubble pressure of 26 Å and 454 atm. These bubbles probably dissolve upon softening unless volatiles generation reactions and tranport to bubbles are extremely fast.

The above argument leads to the conclusion that the bubbles which survive the coal softening should come from macropores. For example, pores of 300 Å radius become bubbles of 67 Å raduis and 89 atm bubble pressure and pores of 1500 Å become 714 Å radius and 9.3 atm bubble pressure at 1 atm external pressure.

Thus, one can limit the initial size of bubbles to those originating from macropores, but determination of the initial size and the number density is still difficult. Since most of gaseous volatiles are transported to bubbles upon formation due to their small solubility in the melt and to their rapid rate of transport to bubbles, higher bubble number density means a smaller amount of gaseous volatiles transported to each bubble and thus a slower bubble growth rate. Therefore, the volatiles yields are reduced and the swelling is increased. However, the amount of

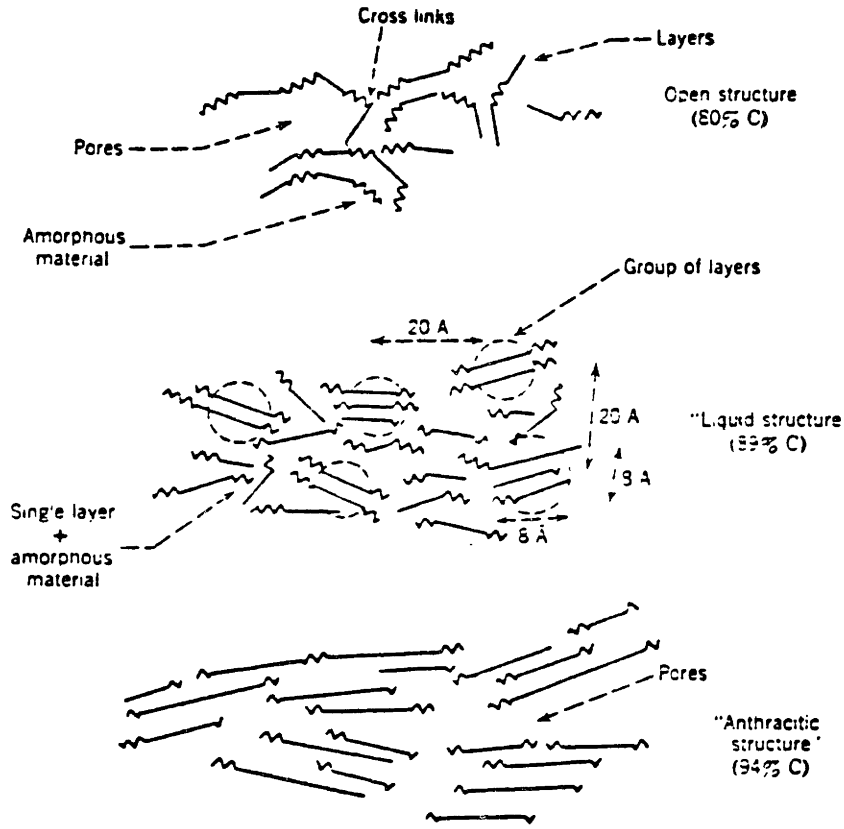

Fig. 6.2.4. Origin of pores (Hirsch in Dryden, 1963)

tar in each bubble is limited by its vapor pressure at a given temperature and the total amount of tar in bubbles actually increases with a higher number density, except at high temperatures, where all metaplast is vaporized. One can also expect more secondary reactions of tar to occur in bubbles if the number density of bubbles is higher.

The choice of initial number density of bubbles has a strong effect in applying the model to derive best fitting kinetic parameters. For example, in calculations of kinetic parameters, where several kinetic parameters are varied to give the best fit between the model predictions and the experimental data on total volatiles yields, tar yields and yields of pyridine extract, the initial number density of bubbles clearly plays an important role. A high number density results in rapid metaplast formation and slow liquid phase decomposition reactions. Since the total amount of tar in bubbles increases at higher number density, a large fraction of the metaplast is vaporized into bubbles even at moderately high temperatures (~ 500 - 550°C) and almost all the metaplast is vaporized into bubbles at high temperatures. Most of the secondary gases formed are gases(3) which result in a large swelling number, and some of gases(3) are formed even after coal is resolidified. However, a low number density gives slow metaplast formation rate and fast liquid phase secondary reactions at high temperatures. The resulting parameters give poor fit to extract yields and some of the metaplast is formed during the cooling period for which temperatures are too low for any significant liquid phase secondary reactions to occur.

It seems to be best that the initial number density of bubbles at the onset of softening is left as a variable to be fitted to predict volatiles yields and extract yields, and to give reasonable predictions of the extent of swelling.

6.3. CALCULATION OF MODEL KINETIC PARAMETERS

6.3.1. Kinetic Parameters for Gases(1)

Gases(1) are assumed to be formed at low temperatures (< 400°C) from pre-existing metaplast. At these temperatures, the total volatiles yields are the same as the yields of gases(1) since tar starts to evolve approximately at 400°C. Also, coal maintains its pore structure which presents small transport resistances at these low temperatures. Therefore, the parameters, $k_{o1,g}$, $E_{1,g}$, and V_g^*, are obtained from the volatiles yields at peak temperatures lower than 400°C from both 1 atm and vacuum pyrolysis, without any transport model. The residual function, R, is defined as the following:

$$R = \sum_{i=1}^{N_{data}} (\text{Volatiles yield,i} - \text{Calculated Volatiles Yield,i})^2 \qquad (6.3\text{-}1)$$

The minimization of the above residual function is relatively simple. A routine known as Powell, available in the Data General Eclipse computer is employed in a modified form, in order to incorporate the time-temperature history of each data point. The modified Powell and subsequent subroutines (modified 'Calfun' and 'Pplot', and user-provided 'Fun') are listed in Appendix G. The actual minimization routine, SSQMIN, is unchanged.

Both 3-parameter fitting, in which all three kinetic parameters were varied, and 2-parameter fitting, in which $E_{1,g}$ and V_g^* were varied, were attempted. For 2-parameter fitting, the pre-exponential factor, $k_{o1,g}$, was fixed as 1×10^{13} sec^{-1} which is representative of the order of magnitude of pre-exponential constants for many organic decomposition reactions. The resulting parameters are

	3-parameter fit	2-parameter fit	
$k_{o1,g}$	7.824	1×10^{13}	sec^{-1}
$E_{1,g}$	3,872	26,755	cal/mole
v_g^*	0.045	0.029	gm/gm orig. coal

Fig. 6.3.1. shows volatiles yields at low temperatures as a function of peak temperature along with the model predictions using the parameters from 2- and 3-paramter fitting and also using the idealized time-temperature history. The idealized time-temperature history is described by Eq. C-7 for heating period where the heating rate is 1000°C/s, and by Eq. C-8 for cooling period. The time-temperature history of each data point is different from the others and also from the idealized time-temperature history used to calculate model predictions. Therefore, the actual time-temperature histories were normalized as follows. First, the total volatiles yield is calculated using the kinetic parameters from 3-parameter fit and the actual time-temperature history. Then, the new smoothed peak temperature was found as the temperature that gives the same calculated volatiles yield when the ideal time-temperature history is used. The yield data are then plotted as a function of their corresponding smoothed peak temperature. Because low temperature vacuum experiments have slower cooling rates than 1 atm runs, normalization of those time-temperature histories resulted in a higher peak temperatures. It is for this reason that a few data points in Fig. 6.3.1 are at peak temperatures > 400°C.

The additional degree of freedom of the 3-parameter fit gives a much better fit to the data than the model prediction from the 2-parameter fit. However, the parameters from 3-parameter fit predicts slow formation of gases(1) with increasing temperature. Fig. 6.3.1a plots the amount of gases formed when coal is heated to 1000°C at the rate of 1000°C/s as a

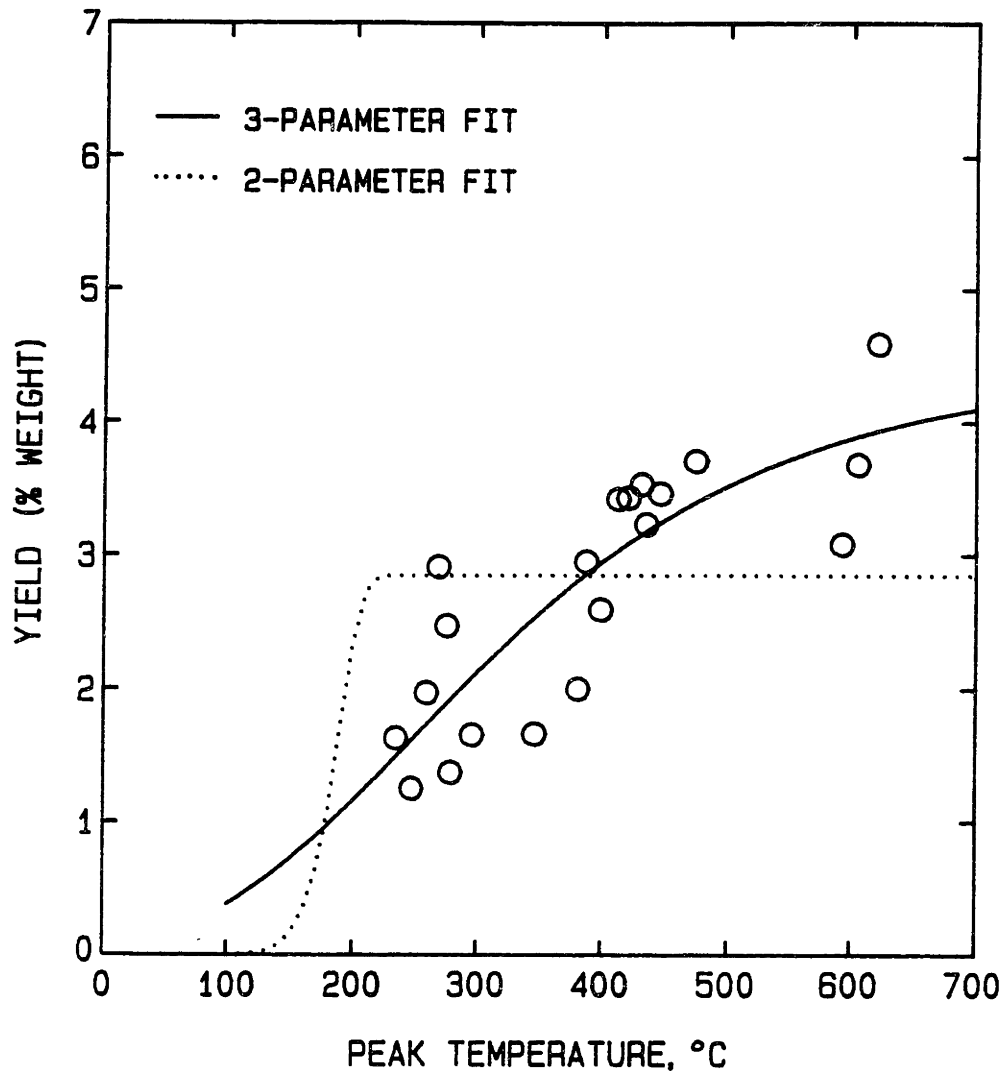

Fig. 6.3.1. Yields of volatiles from low temperature pyrolysis of Pittsburgh seam bituminous coal heated to different peak temperatures with the model predictions from 3-parameter fit (solid line) and from 2-parameter fit (dotted line).

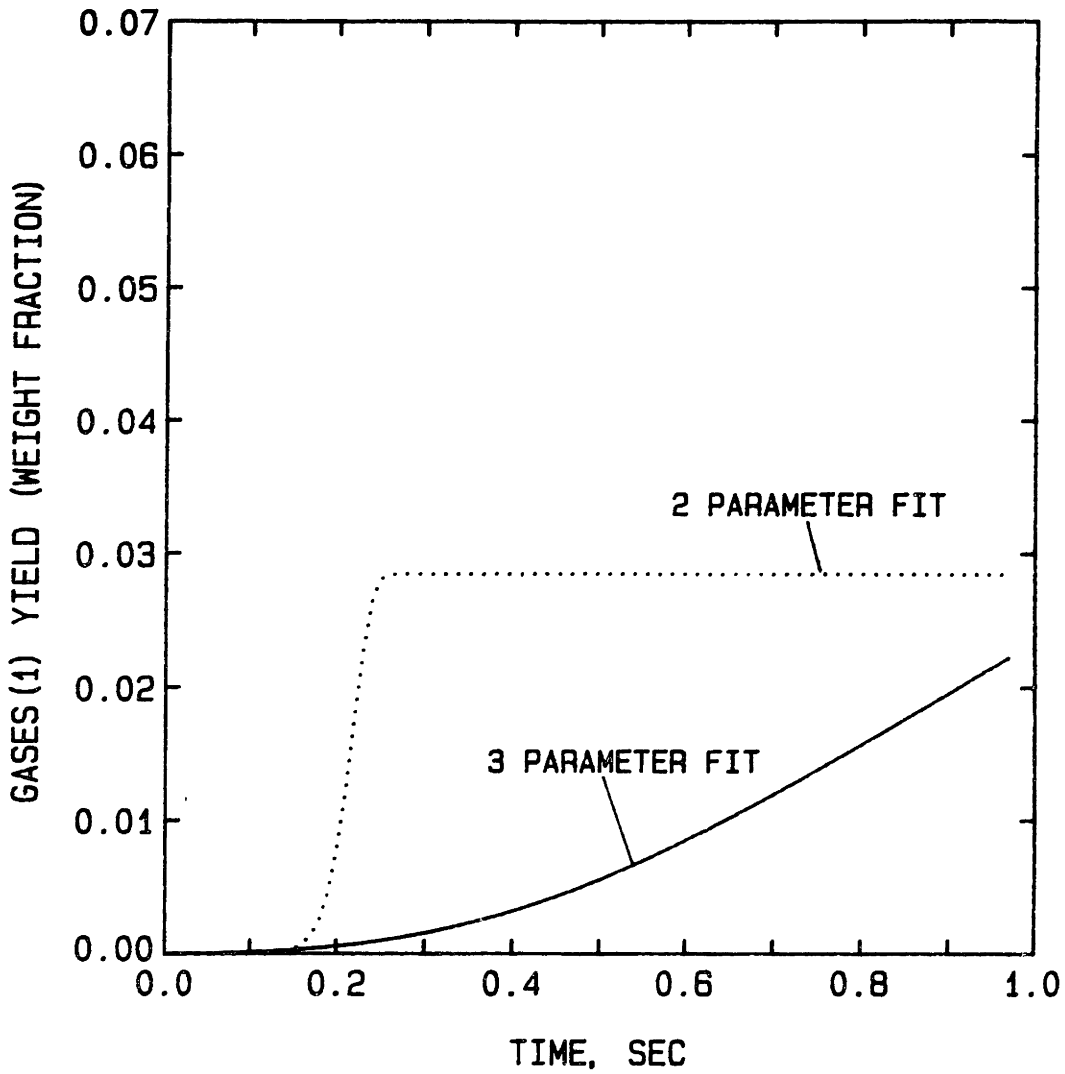

Fig. 6.3.1a. Amount of gas formed during heating period when the coal is heated at 1000°C/s to 1000°C, predicted by a single reaction model with the kinetic parameters obtained from 3-parameter (solid line) and 2-parameter fit (dotted line).

function of time, predicted with the parameters from 3- and 2-parameter fits. As can be seen, the model with 2 fitted parameters predicts a stepwise formation of gases(1) at low temperature, while the model with 3 fitted parameters predicts continuous formation of gases(1) and the formation reactions have not been completed during heating period. The parameters from the 2-parameter fit were employed in the transport model during plastic period.

6.3.2. Formation of Gases(3) and Tar Cracking Reactions in Bubbles

The parameters for tar craking reactions in bubbles and the formation of gases(3) are obtained from the work by Serio (1984) as mentioned in Ch 5.2. The parameters are

$k_{o3,m}$ = 996 sec^{-1}

$E_{3,m}$ = 15,400 cal/mole

$f_{g,3}$ = 1

6.3.3. Metaplast Formation and Decomposition Reactions and Formation of Gases(3)

Other remaining kinetic parameters are for

Metaplast formation reactions: $k_{o1,m}$, $E_{1,m}$, V_m^*

Metaplast decomposition reactions: $k_{o2,m}$, $E_{2,m}$

Formation of gases(2): $f_{g,2}$

The ultimate amount of metaplast that can be formed, V_m^*, was treated as a fixed value. V_m^*=0.7 gm/gm orig. coal is obtained from the work by Fong (1984) who found that the maximum of pyridine extract plus volatiles yields varies between 0.65 and 0.76 when coal is pyrolyzed at low temperatures and

rapidly quenched by introducing liquid-N_2 to the reactor.

The complete transport model was employed at temperatures > 400°C to calculate the yields of gases, tar, and char, and the balance of metaplast. The calculated yields of gases, tar, and char are compared with the experimental data on the yields of gases, tar, and char, and the amount of metaplast remaining in coal is compared with the data on pyridine extract. The residual function is defined as follows:

$$\begin{aligned} R = & \sum(\text{Gas yield,i} - \text{Calculated gas yield, i})^2 \\ & + \sum(\text{Tar yield,i} - \text{Calculated tar yield,i})^2 \\ & + \sum(\text{Ext yield,i} - \text{Calculated amount of metaplast remaining in the particle,i})^2 \\ & + \sum(\text{Char yield,i} - \text{Calculated char yield,i})^2 \end{aligned} \qquad (6.3\text{-}2)$$

The total volatiles yields from 1 atm pyrolysis with the individual time-temperture histories are first fitted to a single reaction model to normalize the time-temperature history. Then, the data obtained from peak temperautures > 400°C with the normalized time-temperature history were employed to minimize the above residual function.

As the formation reactions approach completion and the coal starts to resolidify, transport by the bubble motion becomes less important. Metaplast remaining in the particle is either consumed in secondary reactions, if there is sufficient residence time at high temperatures, or condensed as the coal particles cool down. Some of the gas release occurs by diffusion of dissolved gases through the melt or through fixed pores after the coal resolidifies. Since the present model describes the transport of volatiles in a softened coal and does not treat volatiles transport through pores, one does not know how much of the gases was released during the softened period or after the coal is resolidified, from the data obtained in the

batch screen-heater reactor. If all gases generated in the particle were transported during the plastic period, the last term in Eq. 6.3-2 is unnecessary. However, to minimize the amount of gases trapped in bubbles upon resolidification, the differences between calculated and measured char yield are included in the residual function.

In addition to the 5 kinetic parameters mentioned above, the initial number density of bubbles is also left as a variable. Since it is concluded (Ch 6.2.3) that bubbles which survive through softening probably originate from macropores, the initial number density of bubbles is calculated by assuming a fixed pore volume and by changing the pore radius, within the range of the macropore sizes. At the same time, the initial bubble size in molten the coal is also calculated, assuming spherical geometry and the mass of the bubble to be the same before and after softening. Table 6.2.1 shows that the volume of macropores varies from 0.02 to 0.04 cm^3/gm coal in bituminous rank coals and thus the pore volume is fixed as 0.04 cm^3/gm in the model.

Routine E04JBF from National Algorithms Group Library (NAG) was employed for the evaluation of the best fitting parameters. E04JBF is a comprehensive quasi-Newton algorithm for finding a minimum of a function of several variables subject to fixed boundaries. The direction of search for the minimum is obtained by calculating derivatives of the residual function with respect to each variable. Since there were no analytical form for the derivatives of the above residual function, the derivatives were calculated by finite-difference approximations. Evaluating Eq. 6.3-2 for 21 selected data points at peak temperatures > 400°C takes about 3-5 cpu mins in a Honeywell Multics computer, which makes the calculation of the best fitting kinetic parameters very expensive.

The resulting parameters are

$E_{1,m}$ = 21,690 cal/mole

$k_{o1,m}$ = 2.875×10^6 sec^{-1}

$E_{2,m}$ = 18,800 cal/mole

$k_{o2,m}$ = 2.976×10^5 sec^{-1}

$f_{g,2}$ = 0.053

a_{pore} = 0.076 μm

Even though the number of parameters varied (i.e., 6) is rather large, the model utilizes three sets of data in the fitting procedure: gas yield, tar yield and extract yield. This corresponds to deriving 2 fitted parameters per data set, rather than the three per data set usually fitted when using a single reaction model.

The activation energies for metaplast formation and decomposition reactions are quite similiar (different by ~ 3 kcal/mole) and suggest the reactions forming additional metaplast and those decomposing the metaplast occur approximately in the same temperature range. Since the pre-exponential constants for the formation reactions are roughly 10 times larger than those for the decomposition reactions, the formation reactions occur faster than the latter. If secondary gases (gases(2) and gases(3)) are formed solely from the liquid phase decomposition reactions, $f_{g,2}$ will be about 0.4; the closer $f_{g,2}$ is to 0.4, the more metaplast decomposition reactions occur in the liquid phase rather than in bubbles. In this case, the best fitting $f_{g,2}$ is 0.053, which suggests that most of secondary gases are formed due to tar cracking in bubbles. This result is a consequence of the vapor pressure correlation employed in this calculation. As discussed in Ch 5.6, the correlation by Maiorella seems to overpredict the vapor pressure of metaplast at high temperatures and to cause a large fraction of

metaplast to be evaporated into bubbles.

All the model kinetic parameters along with input correlations for estimating the melt viscosity and other physical properties are summarized in Table 6.3.1. Figs. 6.3.3a and b plot the model predictions of total volatiles yields and tar yields and compare them to experimental data. The solid line and the dotted line in Fig. 6.3.3a show the total volatiles yields with and without the amount of gases trapped in bubbles upon resolidification, respectively. Fig. 6.3.3c plots the amount of metaplast remaining in char and the measured pyridine extract yields as a function of peak temperature. As can be seen in Figs. 6.3.3a thru c, the model predictions are in good agreement with experimental data at 1 atm in all three sets of data.

6.3.4. Alternative Residual Function

As discussed earlier, it is difficult to decide how much of gases generated are released during the softened stage from the data obtained in the batch reactor. The best fit to the yields of gases will be obtained when the calculated gas yield includes the amount trapped in bubbles and compared with the experimental data. In that case, the mass balance of products gives char yield = 100 - (gas yield + tar yield + metaplast yield) and the yield of char is no longer independant. Then, the last term in Eq. 6.3-2, must not be included in the residual function:

$$R = \sum (\text{Gas yield},i - \text{Calculated gas formed},i)^2 + \sum (\text{Tar yield},i - \text{Calculated tar yield},i)^2 + \sum (\text{Ext yield},i - \text{Calculated amount of metaplast remaining in the particle},i)^2 \qquad (6.3\text{-}3)$$

The resulting kinetic parameters from the modified residual function

Table 6.3.1. Summary of model parameters

Table 6.3.1a. Correlations for physical properties[1]

Melt viscosity[2]: $$\mu = \frac{1 \times 10^{-10} \exp(45{,}000/RT')}{(1 - \phi)^{-1/3} - 1.0}$$

where ϕ = wt fraction of metaplast
T' = T (K) at temperatures < 450 °C
T' = 723 K at temperatures > 450 °C

Diffusivity of volatiles in molten coal:

$$D_v = \frac{1 \times 10^{-7} \; T}{\mu^q}$$

q = 0.5 for gases and 2/3 for metaplast

Vapor pressure of metaplast[3]: $P_v = 6.311 \times 10^{11} \exp(-561 \; MW^{0.474} / T)$ [dyne/cm^2]

Surface tension[4]: 30 erg/cm^2

Solubility of gas in molten coal: $$H = \frac{2.792 \times 10^7 \exp(314/T)}{\rho'_L}$$

ρ'_L = molar density of molten phase

Molecular weight distribution of metaplast at formation: See Fig. 6.3.2

Macropore volume[5]: 0.04 cm^3/gm coal

---

1. Unless otherwise noted, the correlations are developed in this study.
2. Nazem (1980), Frankel and Acrivos (1967) and this study
3. Maiorella(1978)
4. Attar (1978)
5. Gan et al. (1972)

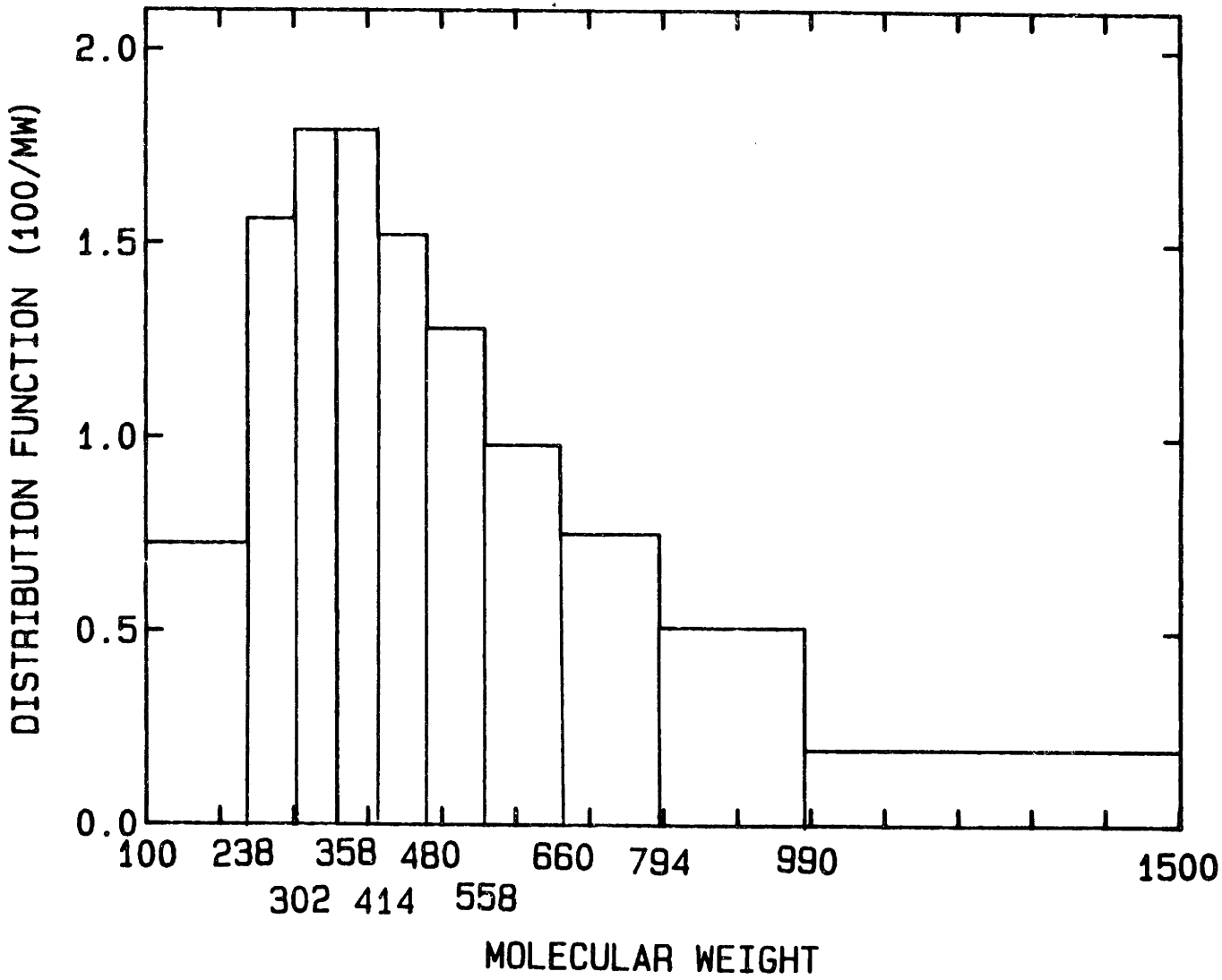

Fig. 6.3.2. Molecular weight distribution of metaplast at formation. Inferred from MWD of tar and pyridine extract from low temperature pyrolysis at 1 atm.

6.3.1b. Model kinetic parameters.
Input kinetic parameters are in regular type and 6-best fitting parameters are in **bold type.**

Gases(1) formation reactions[1]	
Amount of gases(1) formed at t = ∞ (V_g^*)	0.0285 gm/gm orig coal
Activation Energy ($E_{1,g}$)	26,755 cal/mole
Pre-exponential constant ($k_{o1,g}$)	1×10^{13} sec^{-1}
Metaplast formation reactions	
Amount of metaplast formed at t = ∞ (V_m^*)	0.7 gm/gm orig coal
Activation energy ($E_{1,m}$)	**21,690** cal/mole
Pre-exponential constant ($k_{o1,m}$)	**2.875×10^6** sec^{-1}
Liquid phase decomposition reactions of metaplast	
Activation energy ($E_{2,m}$)	**18,803** cal/mole
Pre-exponential constant ($k_{o2,m}$)	**2.976×10^5** sec^{-1}
Fraction of metaplast converted to gases(2) ($f_{g,2}$)	**0.053**
Tar cracking reactions in bubbles[2]	
Activation energy ($E_{3,m}$)	15,400 cal/mole
Pre-exponential constant ($k_{o3,m}$)	9.96×10^2 sec^{-1}
Fraction of metaplast converted to gases(3) ($f_{g,3}$)	1
Pore size (a_{pore})	**0.0757** μm

1. Obtained from pyrolysis data at low peak temperatures. $k_{o1,g}$ is a fixed parameter.
2. Serio (1984)

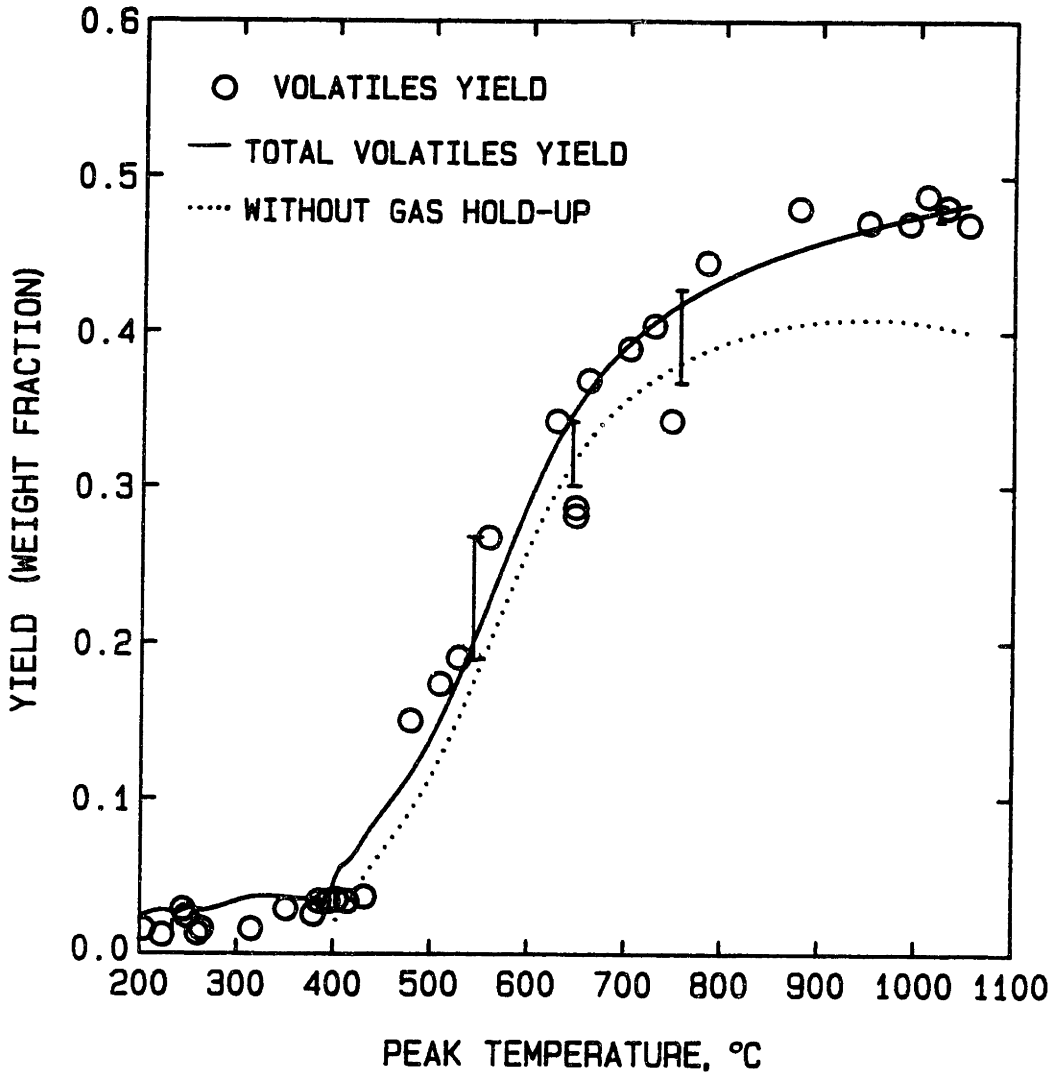

Fig. 6.3.3a. Yields of total volatiles from pyrolysis of Pittsburgh seam bituminous coal heated to different peak temperatures at 1 atm with model predictions. Parameters are listed in Table 6.3.1.

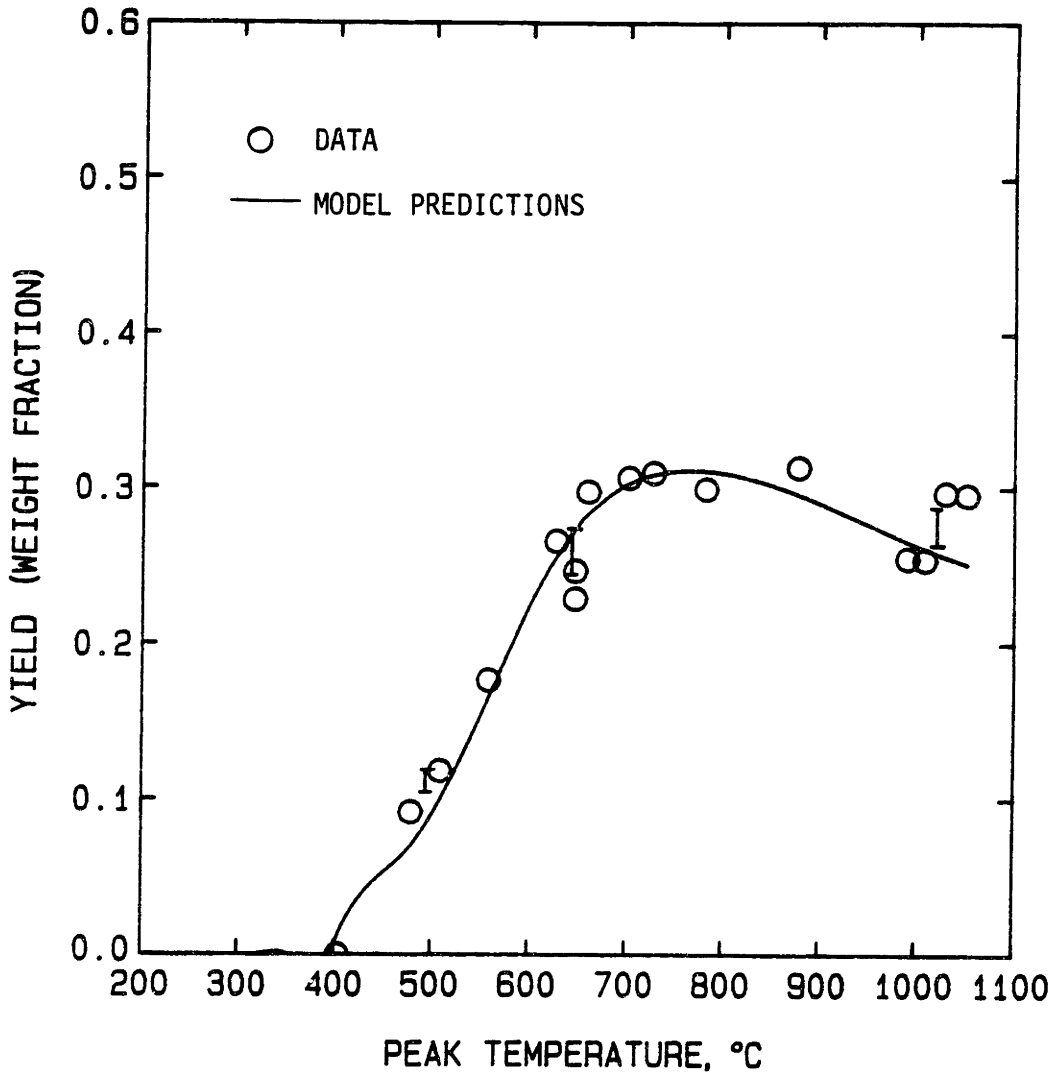

Fig. 6.3.3b. Yields of tar from pyrolysis of Pittsburgh seam bituminous coal heated to different peak temperatures at 1 atm with model predictions. Parameters are listed in Table 6.3.1.

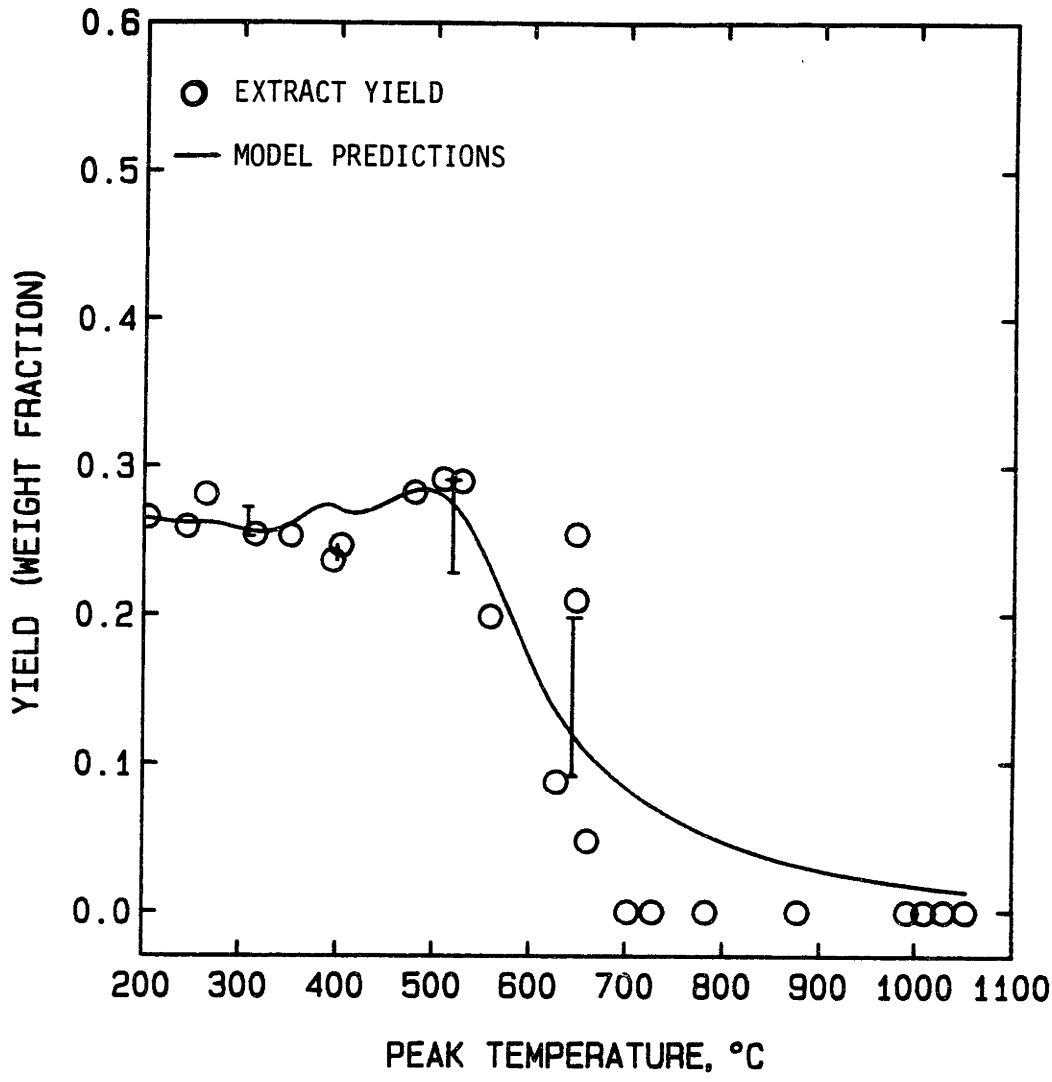

Fig. 6.3.3c. Yields of pyridine extract ('metaplast surrogate') of the solid residue produced from pyrolysis of Pittsburgh seam bituminous coal heated to different peak temperatures at 1 atm with the model predictions of the amount of metaplast remaining in a pyrolyzed coal particle. Parameters are listed in Table 6.3.1.

are listed in Table 6.3.2 with the parameters from the original residual function (Eq. 6.3-2) and the model predictions along with experimetnal data are shown in Figs. 6.3.4a and b. Again, the dotted line represents the volatiles yields without accounting for gas hold-up in bubbles.

The activation energy for metaplast formation reactions is larger by 10 kcal/mole than that of decomposition reactions, and thus, the formation will occur at a narrower temperature range. While the kinetic parameters for formation reactions are quite different from the ones from the original residual function, the parameters for decompositions reactions are similar. These kinetic parameters fit the extract data slightly better at peak temperatures between 350 - 400°C but the overall model predictions are not much different from those in Figs. 6.3.3a thru c. The predicted time dependant viscosity was also quite similar.

6.3.5. Predictions of the Extent of Swelling and Time Dependant Viscosity

To obtain a better understanding of time dependant pyrolysis behavior, the predicted product distribution during pyrolysis at 1 atm is plotted as a function of time in Fig. 6.3.5. The heating rate of 448°C/sec, peak temperature of 760°C, and the holding time of 5 sec are chosen to compare the model predictions of viscosity variation with the experimental data. The measured viscosity at the above time-temperature history is shown in Fig. 6.3.7 (Same as Fig. 5.5.1). At around 400°C, the coal starts to soften (predicted viscosity = 4×10^5 poise), and essentially all of the gas formed is immediately transported into bubbles because the equilibrium amount of dissolved gases in the melt is small compared to the amount of pyrolysis gas being formed, and the transport rate into bubbles is fast.

Table 6.3.2. Comparison of kinetic parameters from two residual functions: (A) Eq. 6.3-2 and (B) Eq. 6.3-3.

	(A)[1]	(B)[2]	
$E_{1,m}$	21,690	27,354	cal/mole
$k_{o1,m}$	2.875×10^6	1.905×10^9	sec^{-1}
$E_{2,m}$	18,803	17,915	cal/mole
$k_{o2,m}$	2.976×10^5	1.755×10^5	sec^{-1}
$f_{g,2}$	0.053	0.019	
a_{pore}	0.0757	0.0756	μm
standard error of estimate	0.039	0.032	

1. Same as listed in Table 6.3.1b.
   Calculated gas yield = gases released from the particle during softened period. Differences between calculated and experimental char yields are included.
2. Calculated gas yield = gases generated during pyrolysis.
   Residuals in char yield must not be included.

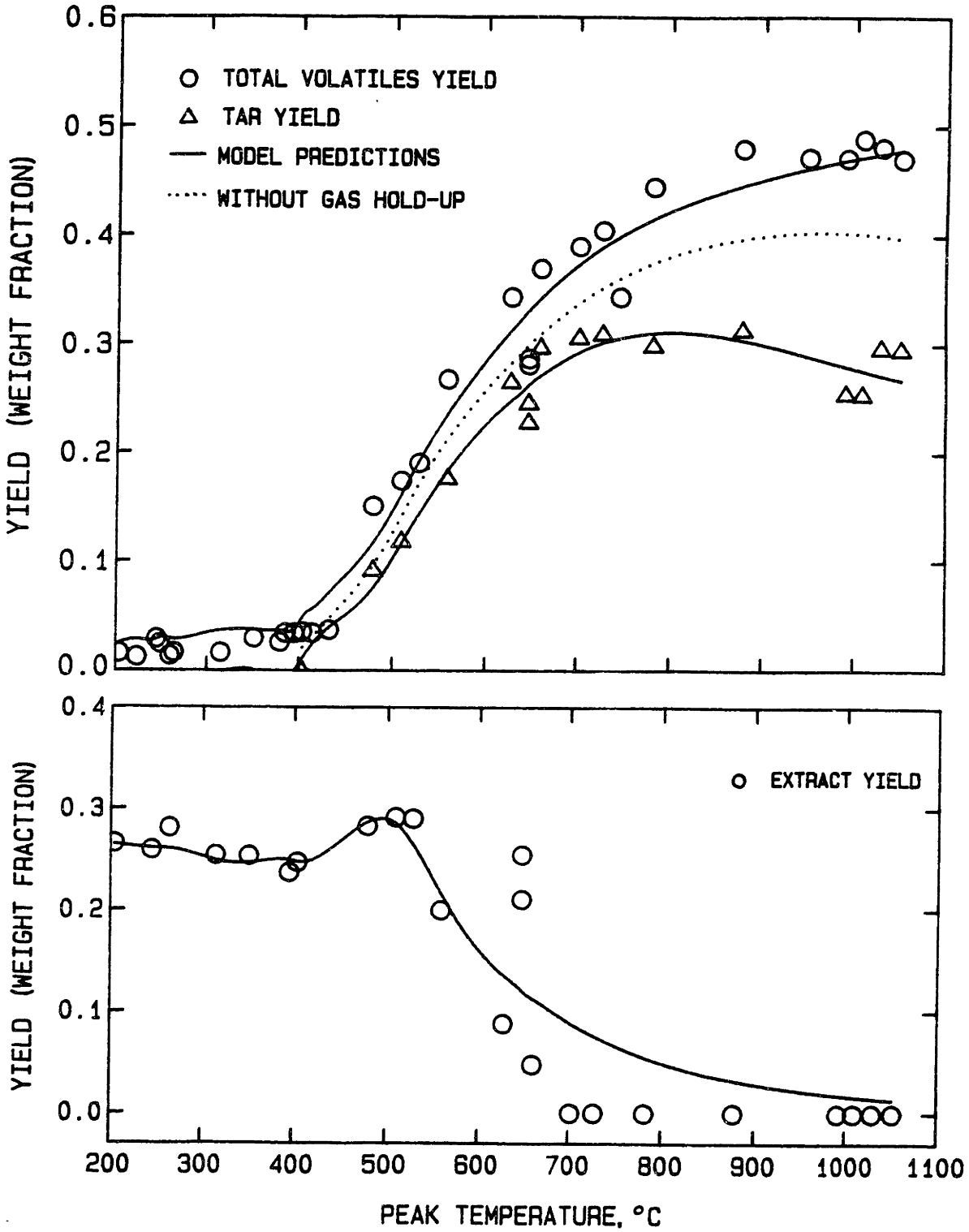

Fig. 6.3.4. Yields of total volatiles and tar (top) and yields of extract (bottom) at 1 atm as a function of peak temperature with the model predictions using the kinetic parameters obtained from the modified residual function, Eq. 6.3-3. Kinetic parameters are listed in Table 6.3.2 (B).

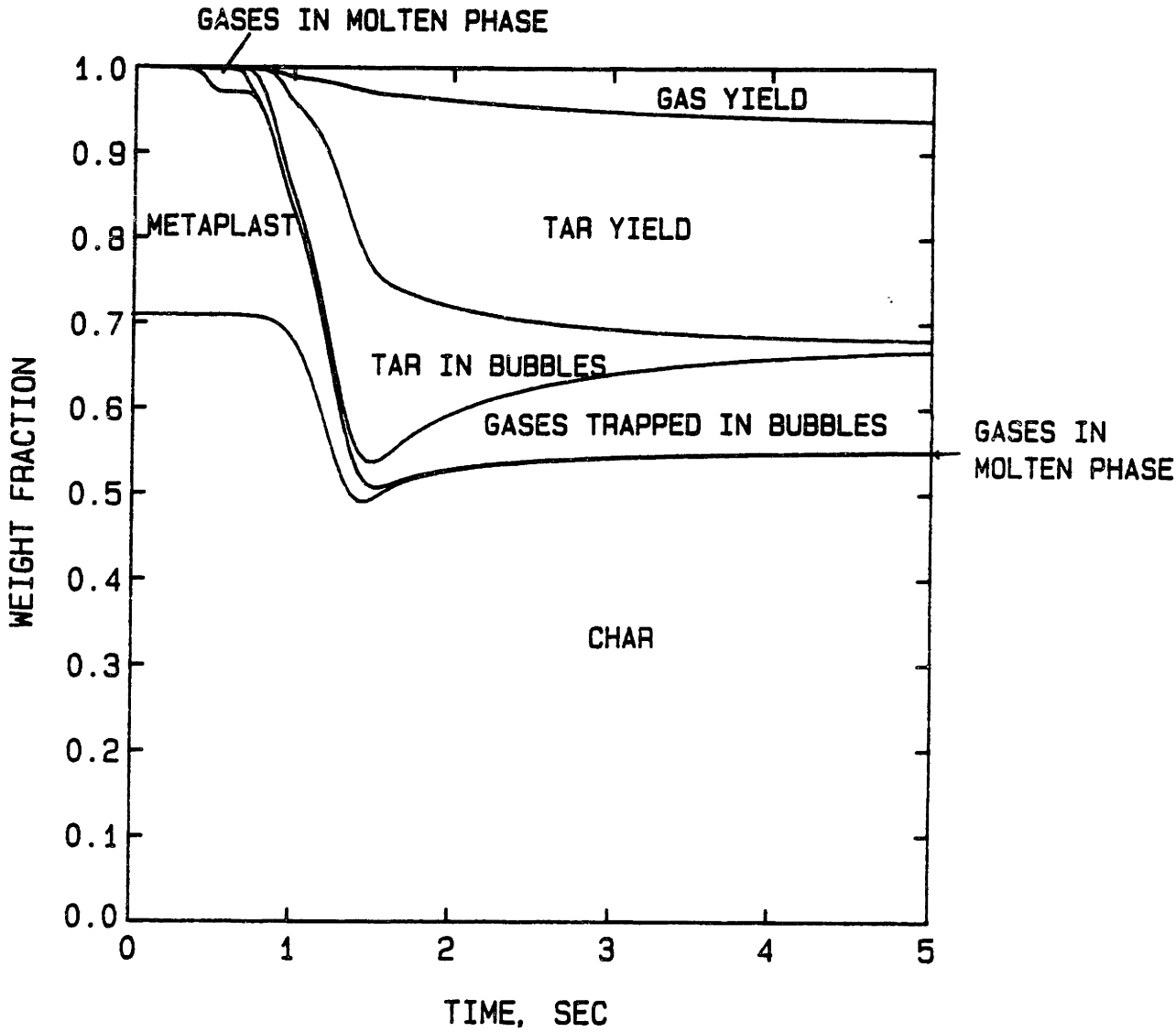

Fig. 6.3.5. Predicted product distribution during coal pyrolysis at 1 atm. (heating rate = 448°C/s and holding temperature = 760°C). The model parameters are listed in Table 6.3.1.

Compared to gaseous volatiles, the tar content in bubbles is limited by its vapor pressure. The transport of metaplast from the melt into bubbles is sufficiently fast to justify the assumption that the tar in bubbles (i.e., metaplast vapor in bubbles) is in equilibrium with the molten phase. As temperature increases, metaplast evaporates into bubbles more rapidly due to high vapor pressure, predicted by Maiorella's model. One can see a sharp decrease in metaplast concentration (15.2 to 0.6 wt %) between 600°C (1.28 sec) and the peak temperature (760°C, 1.64 sec) and, at the same time, the yields of gases and tar, and the tar concentration in bubbles increase rapidly. Under the given time-temperature history, 99 % of metaplast formation reactions are completed before the peak temperature is reached. Then, once the peak temperature is reached, the low concentration of metaplast, and thus higher melt viscosity, inhibits the bubble growth and most of the tar in bubbles is decomposed to gases, forming large gas-hold up in bubbles.

The reason for using Eq. 6.3-2 instead of Eq. 6.3-3 was to minimize the amount of gases trapped in bubbles and to maximize the amount of gases released during the softened period. However, the amount of gas hold-up in bubbles, which is represented by the space between the solid and dotted lines in both Figs. 6.3-3a and 6.3-4a, is about the same in both cases and it is quite large at high temperatures (~ 7 wt % at peak temperatures around 1000°C), which is one of the reasons that the model overpredicts the extent of swelling.

The predicted variations in viscosity and the swelling ratio are shown in Fig. 6.3.6. The time-temperature history is shown in a dotted line. The melt viscosity starts to increase at ~ 1.5 sec and the coal starts to solidify. However, the predicted plastic period, where the melt viscosity is less than 2×10^5 poise, is ~ 0.59 sec, which is much shorter than the

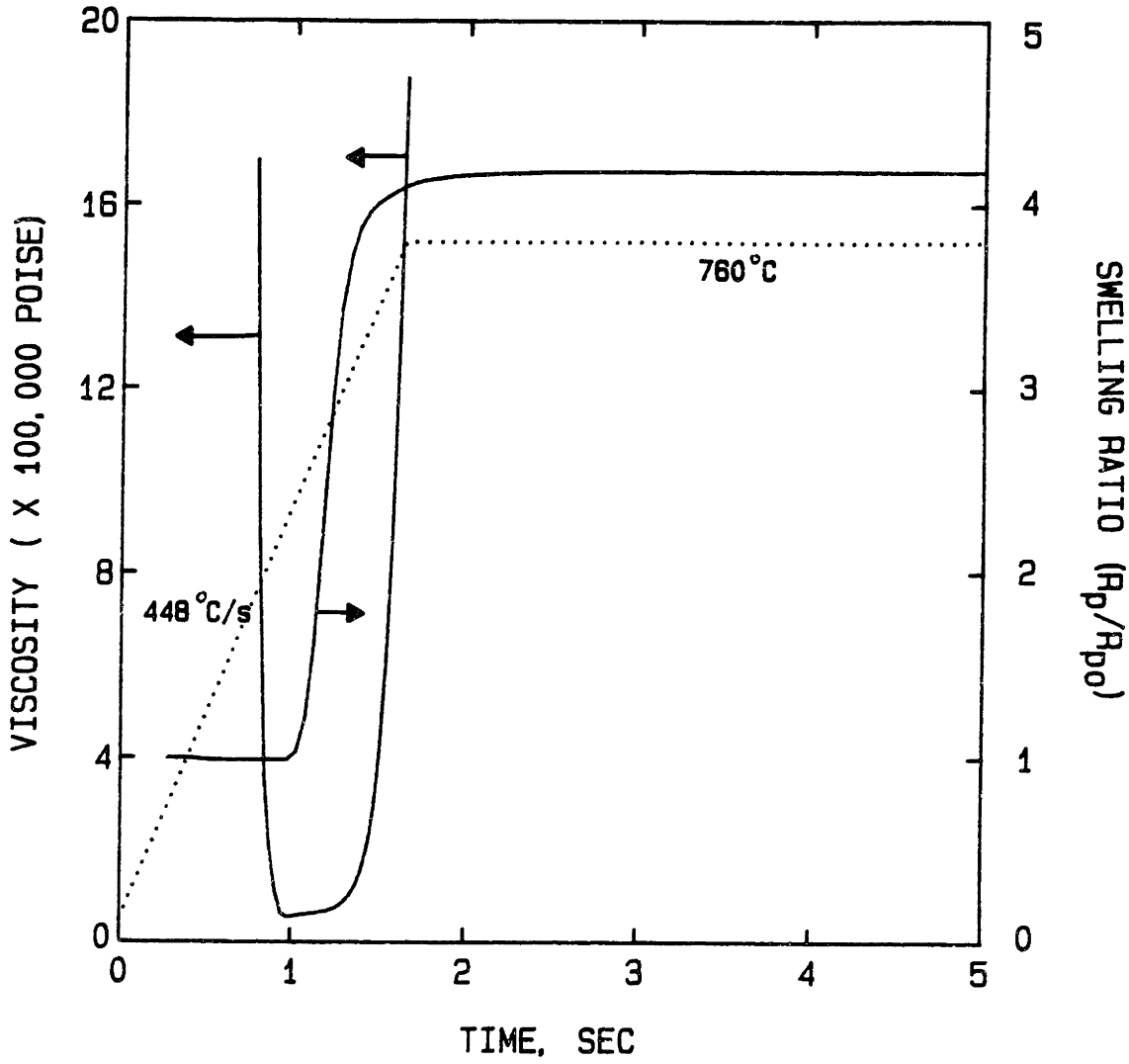

Fig. 6.3.6. Predicted variations of viscosity of coal melt and swelling ratio during pyrolysis at 1 atm with the model parameters listed in Table 6.3.1. Heating rate = 448°C/sec and Holding temperature = 760°C.

measured plastic period under essentially identical conditions (Fig. 6.3.7). Since the depletion of metaplast occurs due to excessive transport to bubbles rather than due to secondary reactions, the shorter predicted plastic period suggests that the vapor pressure of metaplast is overestimated at temperatures higher than 600°C.

Since the swelling is a result of bubble growth and plasticity, the rapid build-up of bubble mass during the plastic period causes the swelling ratio (R_p/R_{po}) to increase. However, after the peak temperature is reached, the high viscosity inhibits continued bubble growth as well as bubble release. Therefore, the swelling ratio stays constant at 4.2 even though the bubble pressure is increasing due to higher gas concentration. The predicted final swelling ratio is about twice as large as what is expected from the available experimental data. Sung (1978) and Dolan (1980) measured the swelling of particles under rapid heat-up, using a laminar flow reactor (10^4 - 10^5°C/sec). Even though the swelling measurements were confounded by the occurrence of both swelling and agglomeration, the measured swelling ratio varied between 0.9 - 4. Further by counting the number of particles pyrolyized, Dolan was able to conclude that the true swelling ratio was around 2. Matsugna (1978) measured the swelling ratio of a single particle (200 μm, heated at 16°C/sec), and found to be between 2 and 3.

It is already concluded that the high vapor pressure of metaplast, predicted by Maiorella's model causes the large gas hold-up in bubbles and thus the high swelling ratio. Model predictions with Suuberg's vapor pressure correlation, which predicts a lower vapor pressure of metaplast at higher temperatures, will be discussed in the following section (Ch 6.4.2). The other factors related to this problem are the initial number density of

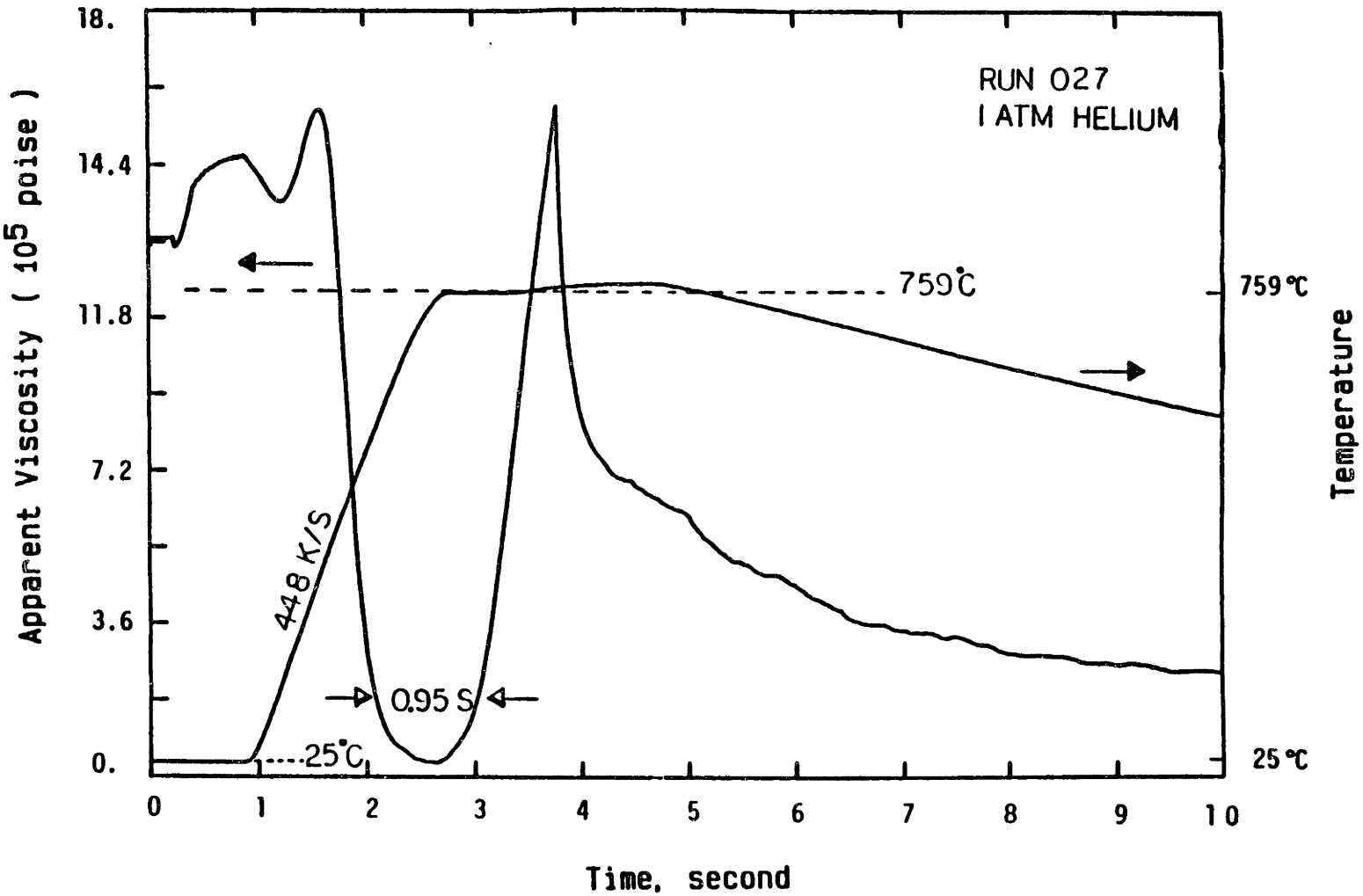

Fig. 6.3.7. Measured apparent viscosity of Pittsburgh seam #8 bituminous coal under rapid heating during 1 atm pyrolysis by a new coal plastometer. (Fong, 1985)

bubbles and the rate of tar cracking in bubbles. The effect of bubble number density on the extent of swelling is discussed in Ch. 6.2.3.

The effect of the rate of the secondary reactions of tar in bubbles on the extent of swelling and other pyrolysis behavior may not be as important as the other two factors. However, if the secondary reactions of tar in bubbles occur rather rapidly while the coal maintains its plasticity, i.e., during the plastic stage, the enhanced growth of bubbles due to the resulting gas formation causes more bubbles to be released from the particle, thus lowering both the number density of bubbles and the amount of gas hold-up. As can be seen from Fig. 6.3.5, the rate of tar conversion to gases, predicted by a single reaction model is slow during heat-up, and most of gases(3) (which contribute to, but do not represent all of, the material denoted 'gases trapped in bubbles', in fig. 6.3.5) are formed after the coal starts to resolidify. Even in the case where the plasticity is maintained after the peak temperature is reached (Fig. 6.4.5), the rate of tar conversion in bubbles is not as fast as would be required to predict observed swelling ratios. Fig. 6.3.8. shows the tar convertion to gases during heat-up when the coal is heated at 1000 °C/sec, calculated using both a single reaction model and a 3-lump model (Serio, 1984). The rate of tar cracking can be seen by looking at the slopes of the curves. The tar conversion rate predicted by the single reaction model is somewhat slower than that predicted by the 3-lump model, which Serio concluded is a better model to describe his data on homogeneous (vapor phase) cracking reactions of freshly formed pyrolyzed tar. Thus, the use of the 3-lump model may improve the model predictions of swelling in some cases, but it also requires treatment of bubbles as something like a CSTR to deal with 3 lumps of tar which have different reactivites. This extra complication is avoided by using the single reaction model.

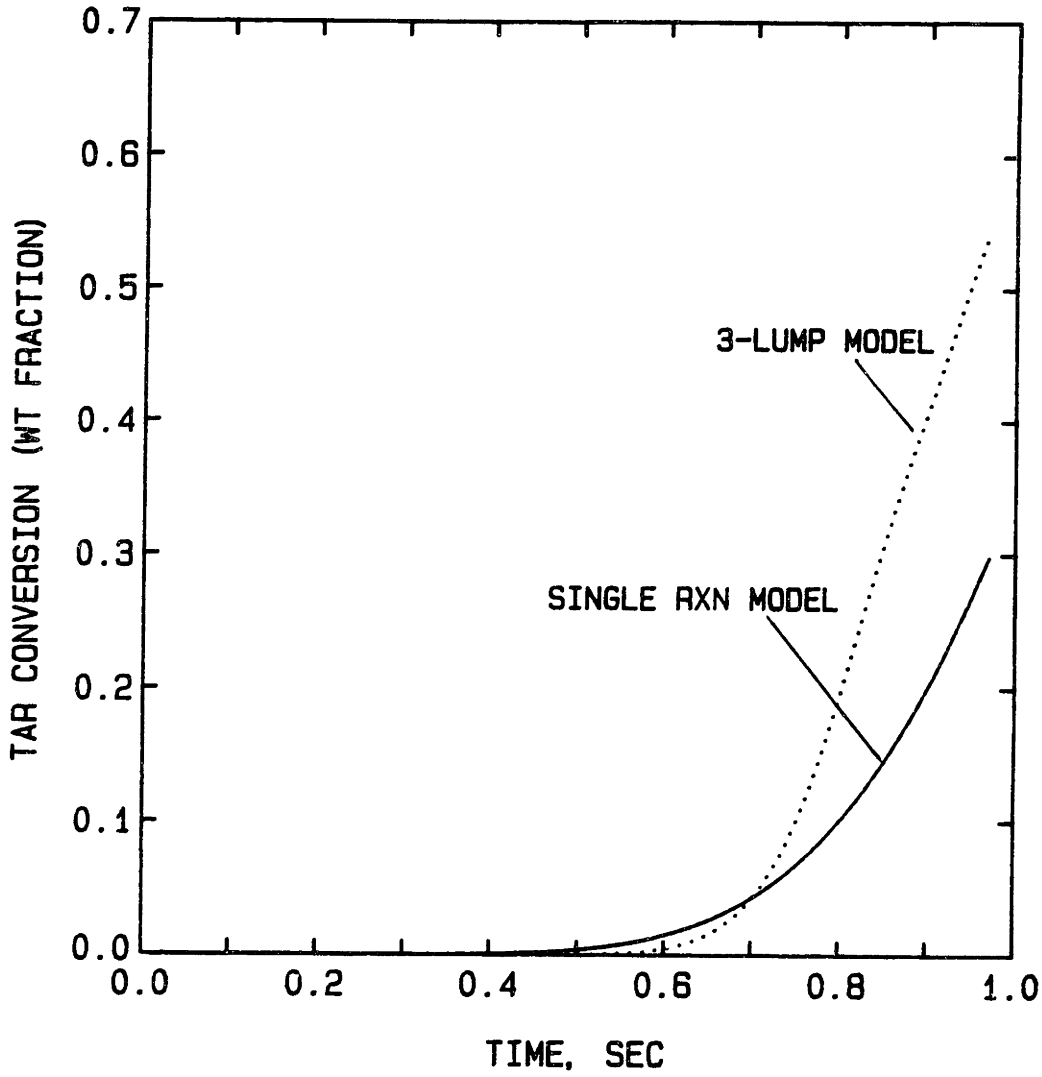

Fig. 6.3.8. Tar conversion during heat-up time, predicted by a single reaction model and a 3-lump model at heating rate 1000°C/s. (Model Reference: Serio, 1984)

6.4. EFFECT OF VAPOR PRESSURE AND VISCOSITY CORRELATIONS ON KINETIC PARAMETERS

6.4.1. Viscosity Correlation

In previous calculations, the temperature dependence of the melt viscosity is included only at low temperatures (< 450°C) to explain the melting of pre-existing metaplast and resolidification at low temperatures. In general, the viscosity of liquids decreases with increasing temperature, even though the rate of decrease is smaller at higher temperatures. To investigate the effect of temperature on the melt viscosity and on the model predictions of volatiles and extract yields, the calculations of the best fitting kinetic parameters were repeated with the viscosity correlation which includes temperature dependence at all temperatures. Again the constant C_v was adjusted to give the minimum predicted viscosity of order 10^4 poise. Table 6.4.1. compares the resulting kinetic parameters and Fig. 6.4.1a and b compare the model predictions with experimental data.

With the new viscosity correlation, the model underpredicts the gas yields at low temperatures as well as at high temperautures. The model also predicts faster depletion of metaplast as a function of a peak temperature. The predicted melt viscosity at the heating rate of 448°C/sec and at the peak temperature of 760°C is plotted as a function of time in Fig. 6.4.2. The viscosity shows a sharp minimum at 1.27 sec (~ 600°C) and the duration of plastic period is much shorter than the one predicted using the other correlation (Fig. 6.3.5) and than the measured value. Even though the formation rate of metaplast is much faster ($k_{o1,m} = 1 \times 10^{13}$, $E_{2,m}$ = 43,759 cal/mole), the higher viscosity at temperatures between 400 and 550 °C inhibits the growth of bubbles and, therefore, the model predicts lower

Table 6.4.1. Effect of viscosity correlation on kinetic parameters: Comparison of kinetic parameters from two viscosity correlations. (A) viscosity model with temperature restriction and (B) without temperature restriction[1].

	(A)[2]	(B)	
$E_{1,m}$	21,690	43,759	cal/mole
$k_{o1,m}$	2.875×10^{6}	1×10^{13}	sec^{-1}
$E_{2,m}$	18,803	25,893	cal/mole
$k_{o2,m}$	2.976×10^{5}	3.476×10^{7}	sec^{-1}
$f_{g,2}$	0.053	0.205	
a_{pore}	0.0757	0.0936	μm
standard error of estimate	0.039	0.046	

1.Melt viscosity:

(A): $$\mu = \frac{1 \times 10^{-10} \exp(45{,}000/RT')}{(1 - \phi)^{-1/3} - 1.0}$$

(B): $$\mu = \frac{1 \times 10^{-7} \exp(45{,}000/RT)}{(1 - \phi)^{-1/3} - 1.0}$$

where ϕ = wt fraction of metaplast
T' = T (K) at temperatures < 450°C
T' = 723 K at temperatures > 450°C

2. Same as listed in Table 6.3.1b.

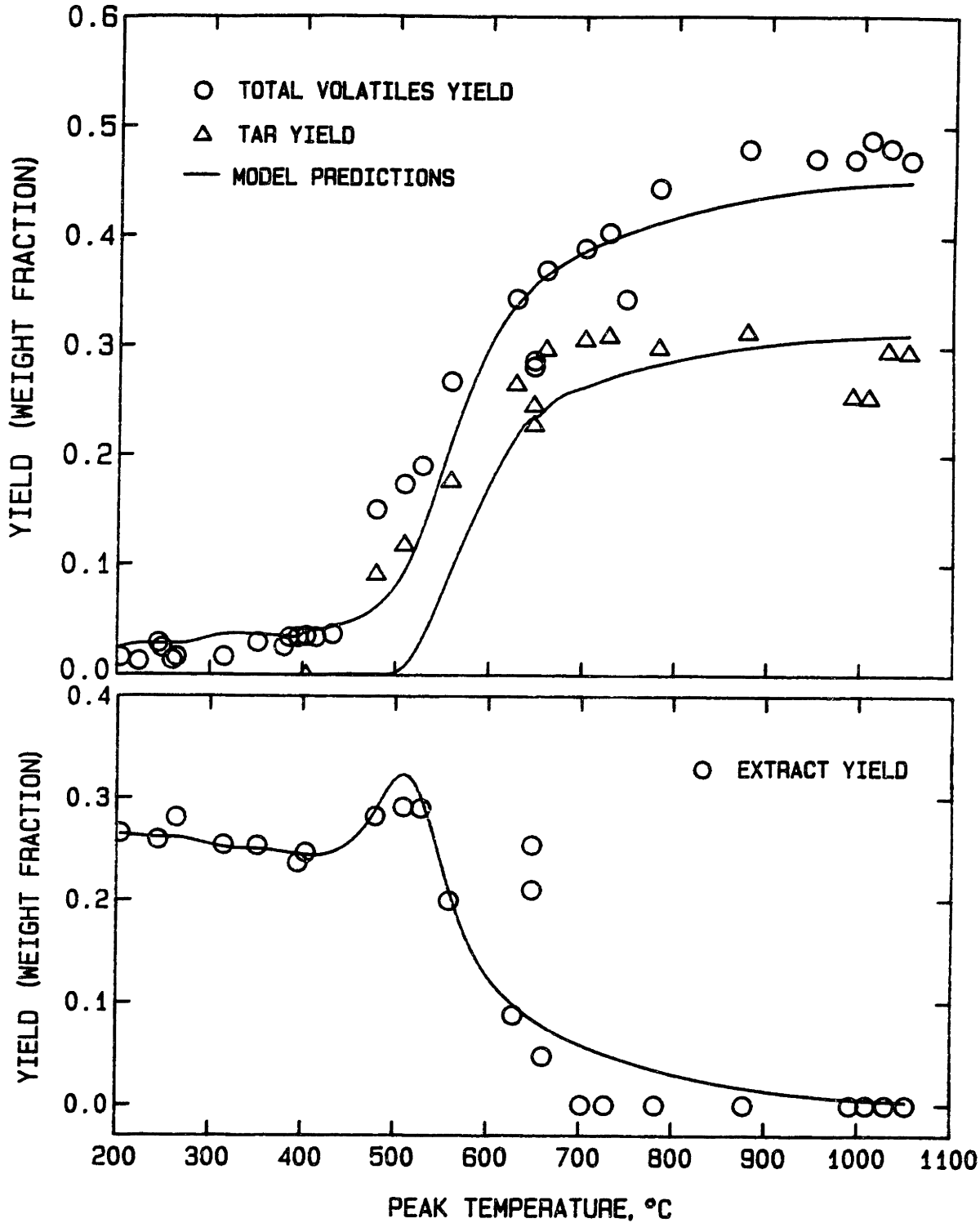

Fig. 6.4.1. Effect of viscosity correlation on the model predictions of total volatiles and tar yields (top), and the yields of extract (bottom). The viscosity correlation has no temperature restrictions and $C_\mu = 10^{-7}$. The model kinetic parameters are listed in Table 6.4.1, Column (B).

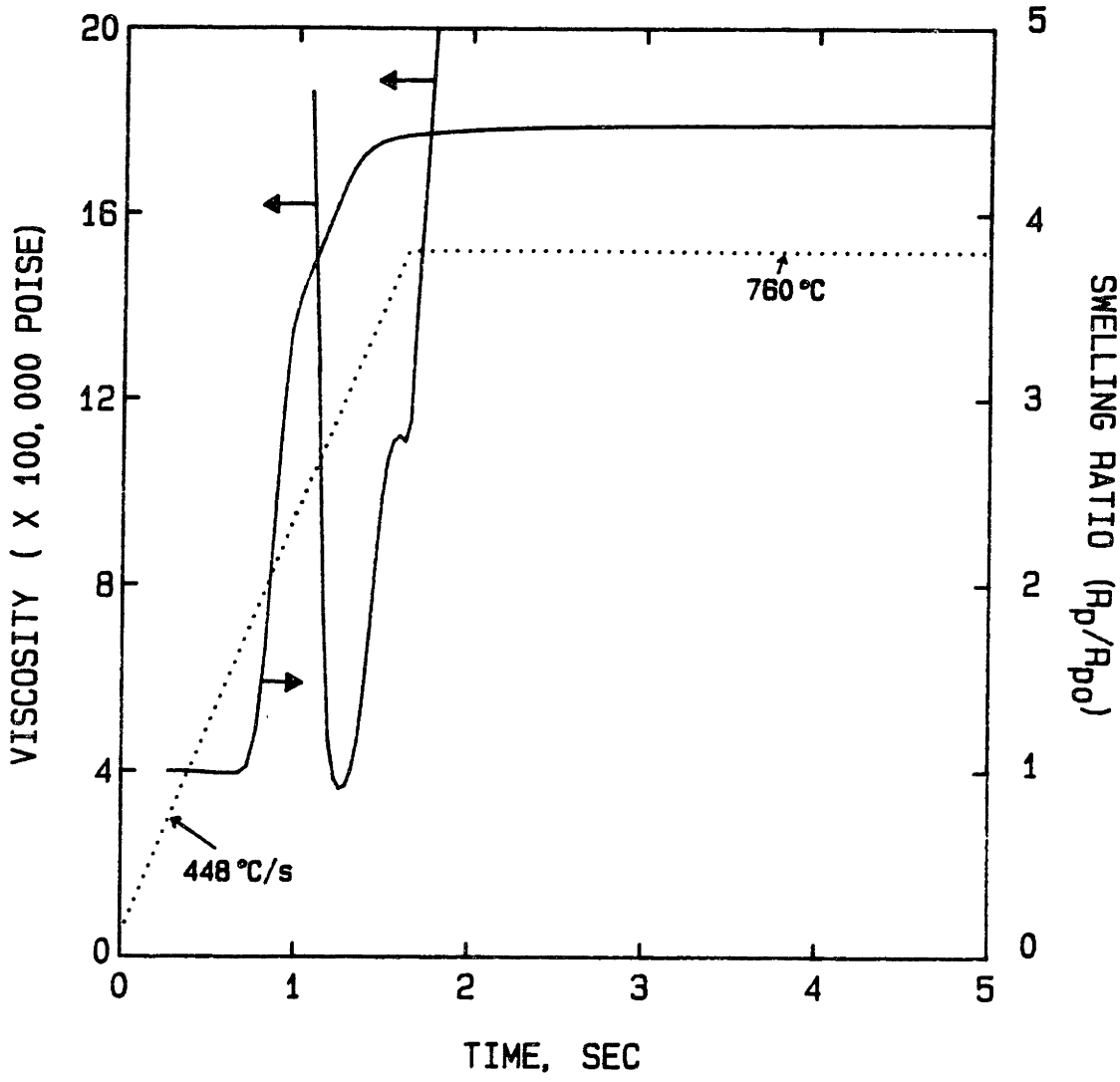

Fig. 6.4.2. Predicted variations in melt viscosity and the swelling ratio during pyrolysis with the viscosity correlation has no temperature restrictions. The model kinetic parameters are listed in Table 6.4.1, Column (B).

volatiles yields.

Comparison of the model predictions which employ the viscosity correlation with no temperature restriction (Fig. 6.4.1a and b) with Fig. 6.3.3a thru c clearly shows that the model with the viscosity correlation which has temperature restrictions gives much better fit to the overall data on volatiles and extract yields. It is encouraging to see that the viscosity correlation which predicts the viscosity variation closer to that of measured experimentally (Fig. 6.3.7) also gives better predictions of volatiles and extract yields.

The prediction of the swelling ratio does not change much with the viscosity correlation. Both correlations give the swelling ratio (R_p/R_{po}) about 4 at the given time-temperature history.

6.4.2. Vapor Pressure Correlation

Even though Maiorella's vapor pressure correlation appears to be more reasonable than the one by Suuberg, it does have a problem of overpredicting vapor pressure at high temperatures which causes most of the metaplast to evaporate into bubbles, thereby leaving a low metaplast concentration in the liquid phase. Therefore, even though the total balance of metaplast and tar in a particle are high, the low metaplast concentration in liquid makes the coal solidify relatively fast, thereby predicting a shorter plastic period and larger gas hold-up in bubbles.

To study the effect of vapor pressure, Suuberg's vapor pressure model (Eq. 5.6-2) is employed and the kinetic parameters are calculated to investigate whether the correlation by Suuberg could fit the experimental data as well as the one by Maiorella. Fig. 6.4.3 plots the model predictions with experimental data and Table 6.4.2 compares the kinetic parameters.

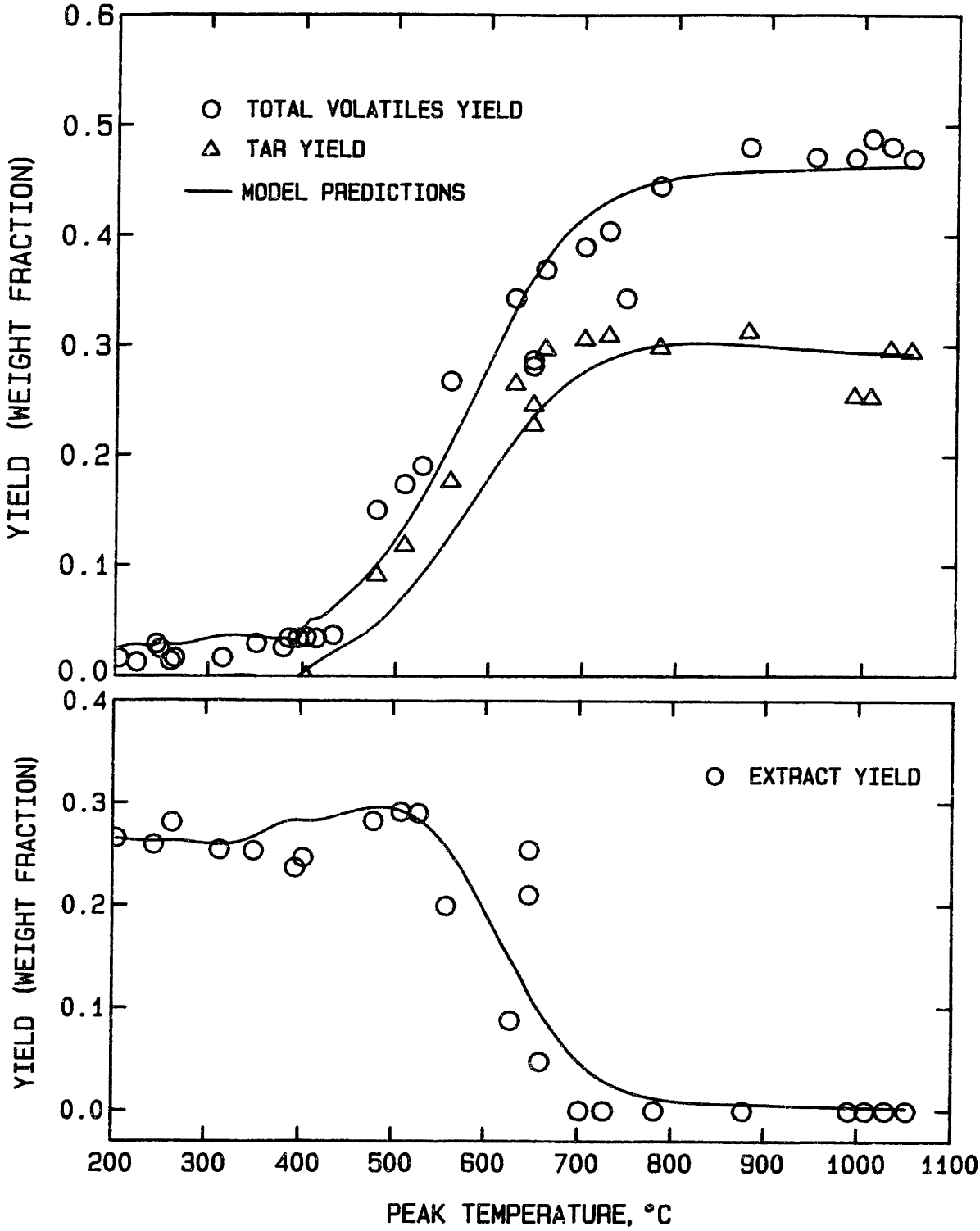

Fig. 6.4.3. Effect of vapor pressure model on the model predictions of total volatiles and tar yields (top), and the yields of extract (bottom). Suuberg's vapor pressure model is employed with kinetic parameters listed in Table 6.4.2, Column (B).

Table 6.4.2. Effect of vapor pressure on kinetic parameters: Comparison of kinetic parameters from two vapor pressure correlations. (A) Maiorella's model and (B) Suuberg's model[1]

	(A)[2]	(B)	
$E_{1,m}$	21,690	16,083	cal/mole
$k_{o1,m}$	2.875×10^6	3.195×10^4	sec^{-1}
$E_{2,m}$	18,803	16,860	cal/mole
$k_{o2,m}$	2.976×10^5	2.964×10^4	sec^{-1}
$f_{g,2}$	0.053	0.284	
a_{pore}	0.0757	0.0799	μm
standard error of estimate	0.0389	0.0394	

1. Maiorella's Model (1978):

$$P_v = 6.311 \times 10^{11} \exp(-561\ MW^{0.474} / T) \quad [dyne/cm^2]$$

Suuberg's Model (1981):

$$P_v = 5.814 \times 10^{9} \exp(-255\ MW^{0.576} / T) \quad [dyne/cm^2]$$

2. Same as listed in Table 6.3.1b.

The resulting kinetic parameters show that the rate of forming the additional amount of metaplast is only slightly faster than that of metaplast decomposition reactions. The initial number density is similar to the case with Maiorella's correlation.

As expected, the model with Suuberg's vapor pressure correlation underpredicts tar yields at temperatures lower than 700°C. The model also underpredicts the gas yield in high peak temperature runs but the model gives a better description of the extract yields at peak temperatures > 600 °C. However, the overall performance is not as good as the one with Maiorella's vapor pressure correlation.

The predicted product distribution during pyrolysis at 1 atm using Suuberg's vapor pressure model is plotted in Fig. 6.4.4. The same time temperature history as in Fig. 6.3.5 was used. In this case, the lower vapor pressure causes more metaplast to remain in the liquid phase and the resolidification occurs due to both secondary reactions in liquid and transport to bubbles and to the outside of the particle. More of the secondary gases are formed from the liquid phase decomposition ($f_{g,2}$ = 0.284) and the amount of gases trapped in bubbles upon resolidification is smaller. The prediction of viscosity (Fig. 6.4.5) is closer to the measured viscosity in the sense that the minimum is reached at ~ 1.5 sec and the period where the viscosity is less than 2×10^5 poise is ~ 0.95 sec. The longer plastic period allows the bubbles to grow to a larger size. Therefore, even though the amount of gases trapped in bubbles is much smaller than in the case with Maiorella's model, the predictions of swelling are similar (of order $R_p/R_{po} = 4$). In this case, the faster rate of tar cracking reactions might have reduced the swelling ratio.

In conclusion, the vapor pressure of metaplast is more reasonably estimated by Maiorella's model at temperatures lower than 600°C and by

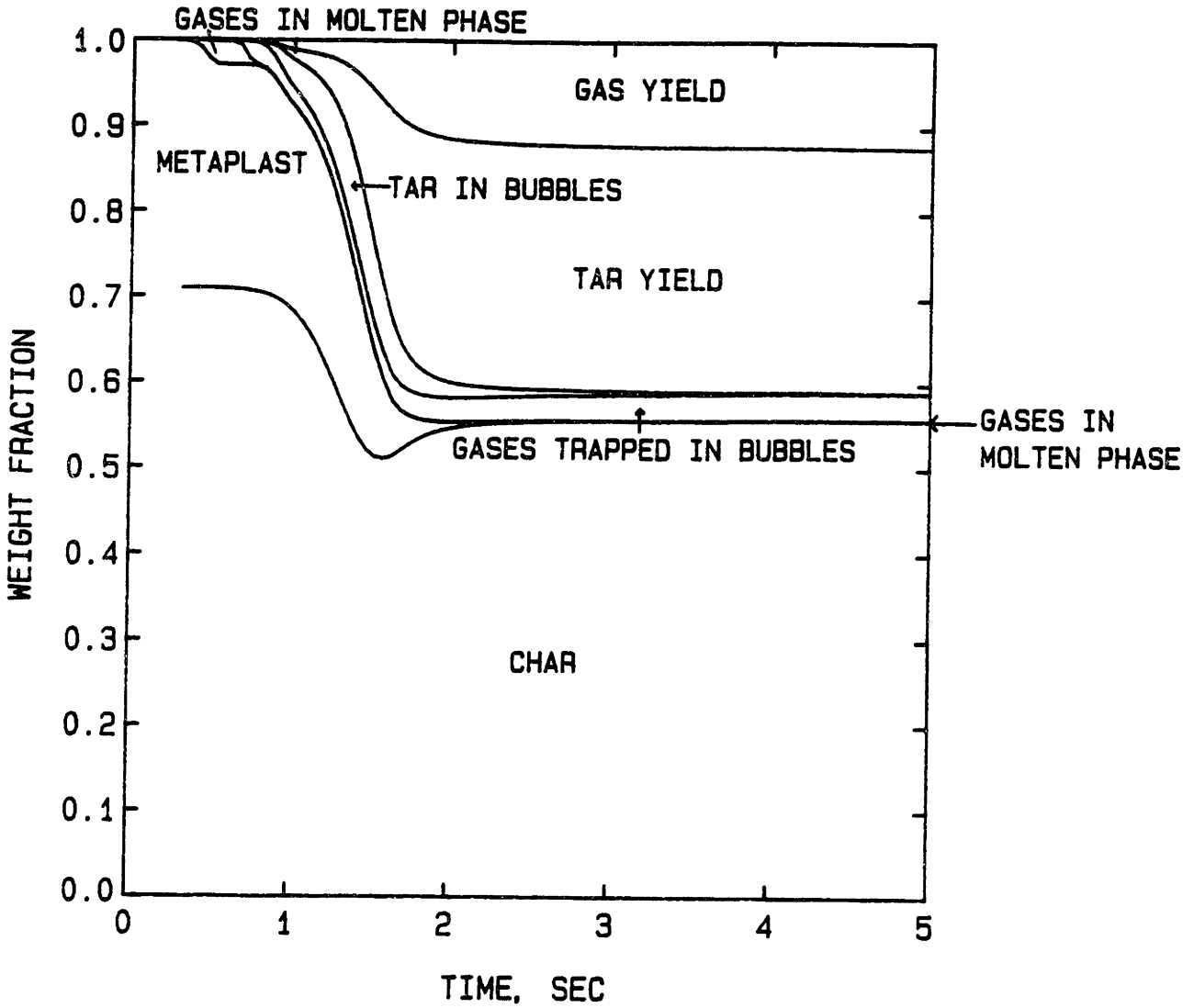

Fig. 6.4.4. Predicted product distribution during coal pyrolysis at 1 atm. (Heating rate = 448°C/s and holding temperature = 760°C). Suuberg's vapor pressure model is employed with kinetic parameters listed in Table 6.4.2, Column (B).

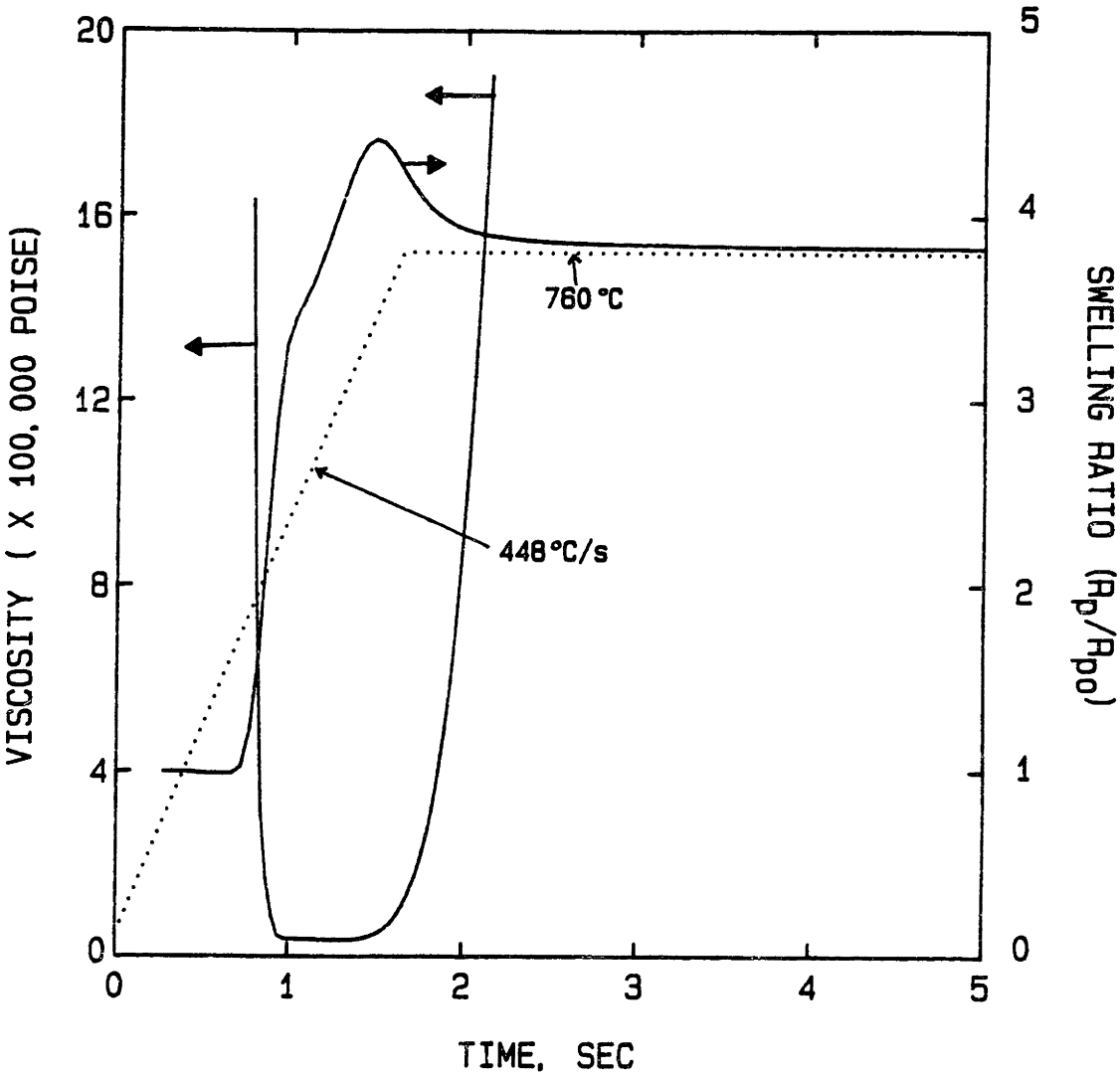

Fig. 6.4.5. Predicted variations in melt viscosity and the swelling ratio during pyrolysis with Suuberg's vapor pressure model and kinetic parameters listed in Table 6.4.2, Column (B).

Suuberg's model at higher temperatures.

6.5. MODEL PREDICTIONS OF PRESSURE, PARTICLE SIZE AND HEATING RATE EFFECT

6.5.1. Pressure Effect

Volatiles yields: It is known that softening coals show stronger pressure effects on volatiles yield than non-softening coals. For example, increasing pressure from vacuum to 100 atm resulted in major reductions in yields of tar and light hydrocarbon liquids from pyrolysis of Pittsburgh No 8 bituminous coal. However, for a Montana lignite similar pressure variations had a much less dramatic effect on weight loss. The predicted volatiles yields and tar yields at different peak temperatures and at 3 different pressures are plotted in Fig. 6.5.1. Unless stated otherwise, the time-temperature history employed in this section to calculate model predictions includes linear heat-up at the heating rate of 1000°C/sec, followed by natural cooling with no holding time at peak temperatures. The cooling period is described by Eq. C-2 in Appendix C. Suuberg's vapor pressure model with kinetic paramerters listed in Table 6.4.2 (B) were used.

As pressure increases, the bubble pressure also increases, while the bubble growth rate is reduced. Since the partial pressure of tar in bubbles is a strong function of temperature but varies little with pressure (Poynting correction is larger at higher pressures), the mole fraction of metaplast in bubbles is lower at higher pressures. Therefore, the relative amount of metaplast transported by bubbles decreases while the relative amount of gases increases. More tar in bubbles is consumed in secondary

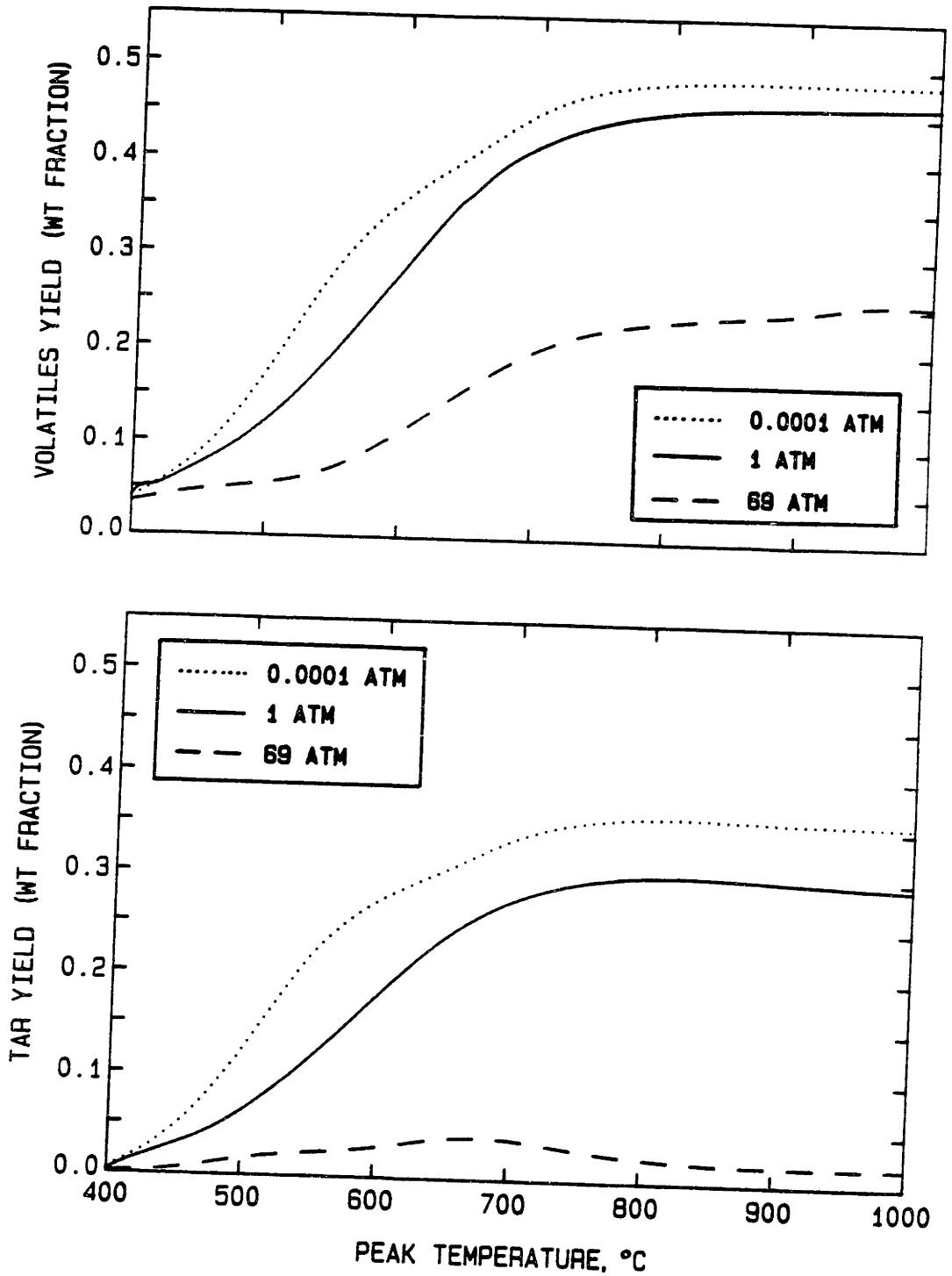

Fig. 6.5.1. **Model predictions of the effect of pressure on total volatiles yields (top) and tar yields (bottom) for pyrolysis of softening coal heated to different peak temperatures.**

reactions and, thus, the total tar yield decreases. This result agrees qualitatively with experimental observations (Howard, 1981).

The predicted tar yields at vacuum are higher than the measured values at peak temperatures between 500 and 700°C as shown in Fig. 6.5.1a. The tar yields at 69 atm are significantly lower than the experimental data (Suuberg, 1977). Thus, while the present model properly predicts the broad trends in observed pressure effects of pressure on pyrolysis yields, exact quantitative predictions of pressure effect requires further analysis and model refinements.

Plasticity: The plasticity of softening coals is known to increase with increasing pressure. The model assumes the same initial number density of 1.87×10^{13} (gm coal)$^{-1}$ at different pressures. With the same initial number density, the amount of metaplast evaporated into bubbles does not vary much with pressure and thus, neither does the liquid phase metaplast concentration. As a result, the model does not predict the differences in plasticity at different pressures. In order to predict the pressure effect on plasticity, one can model the initial number density of bubbles as a function of pressure, for example, a lower initial number density of bubbles at higher pressures. This correction on the initial number density not only makes the model predict the plasticity trends under different pressures, but also helps to improve the predictions of volatiles yields at different pressures.

Other questions that can be raised in the discussion of pressure effects on plasticity is the adequacy of the modeling approach of metaplast formation and the validity of assuming that pyridine extract is representative of metaplast. The model assumes that some metaplast pre-exists in coal, the amount of which is estimated from the yield of pyridine extract

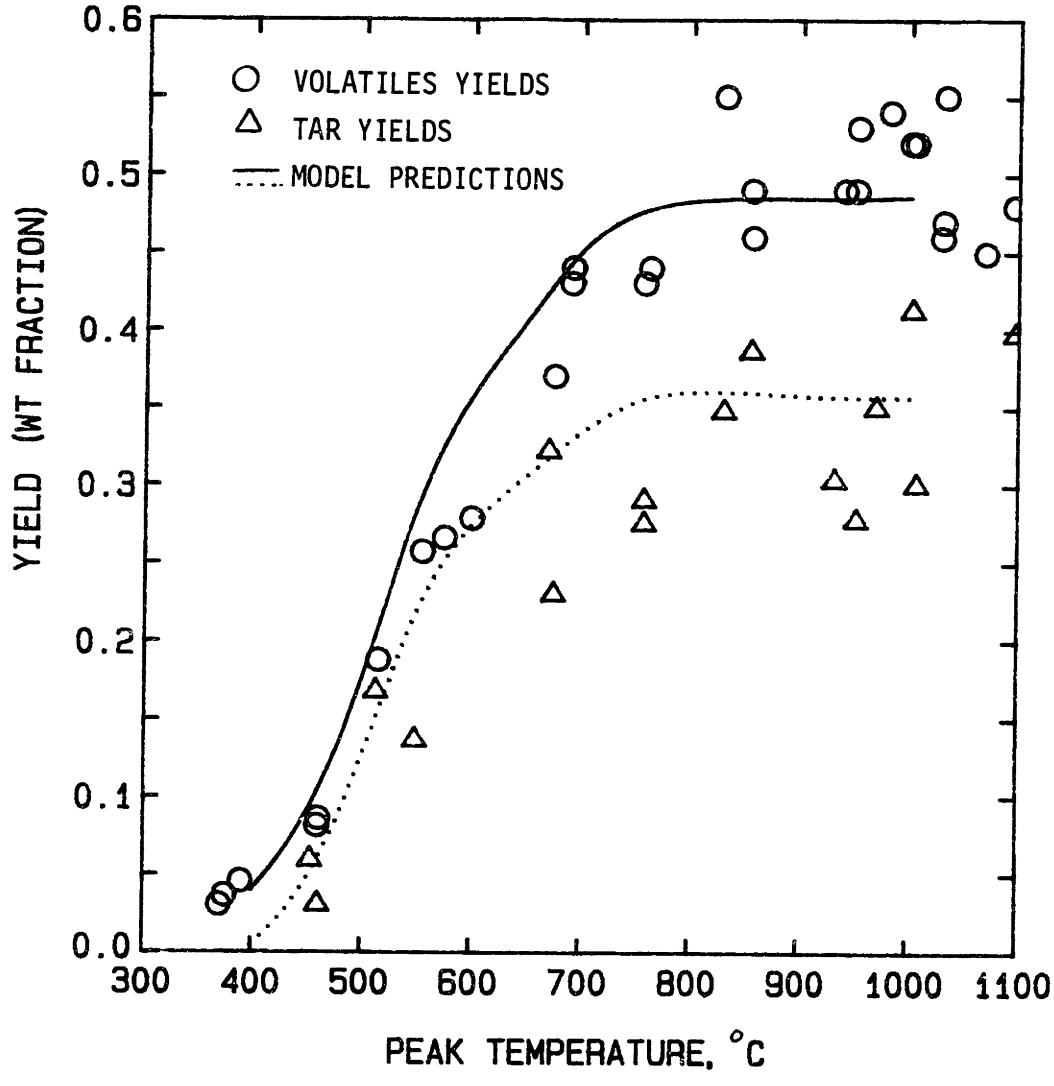

Fig. 6.5.1a. Yields of total volatiles from pyrolysis of Pittsburgh seam bituminous coal heated to different peak temperatures at vacuum (0.0001 atm) with model predictions. Parameters listed in Table 6.4.2 are employed.

of raw (unpyrolyzied) coal. The rest of the metaplast is assumed to be formed by pyrolysis reactions. However, this picture does not explain the fact that the coal does not soften when the initial plasticizer is removed. One explaination would be that the amount of metaplast formed is influenced by the amount of metaplast already present. Then, the ultimate amount of metaplast that formed may vary with the pressure.

According to the molecular weight ranges of tar and pyridine extract, the pyridine extract is a reasonable estimate of metaplast. However, the experimental data on the yields of pyridine extract from the peak temperature pyolysis experiments at 1 atm and at vacuum were quite similar and it is difficult to see from those data the differences in the transient plasticity during pyrolysis. More experimental studies at different time-temperature histories and at different pressures are needed to understand the development of plasticity and to develop the correlation between the melt viscosity and the yield of pyridine extract.

Swelling: The predicted final swelling ratios at different peak temperaures and at 3 pressures are shown in Fig. 6.5.2. Since the model with the same initial number density does not predict an effect of pressure on plasticity, any predicted effects of pressure on swelling ratio reflect the corresponding effects of pressure on volatiles hold-up in bubbles. At 1 atm and vacuum, the final swelling ratio shows a maximum at low peak temperatures, decreases as bubbles are released from the particle, and then starts to increase again at peak temperatures > 700 °C, where the rate of tar cracking in bubbles becomes significantly fast. The model predicts the highest swelling at 1 atm except at around peak temperature of 500 °C at vacuum. At vacuum, since more bubbles are released due to low bubble pressure and the fast growth rate of bubbles, the swelling ratio is indeed

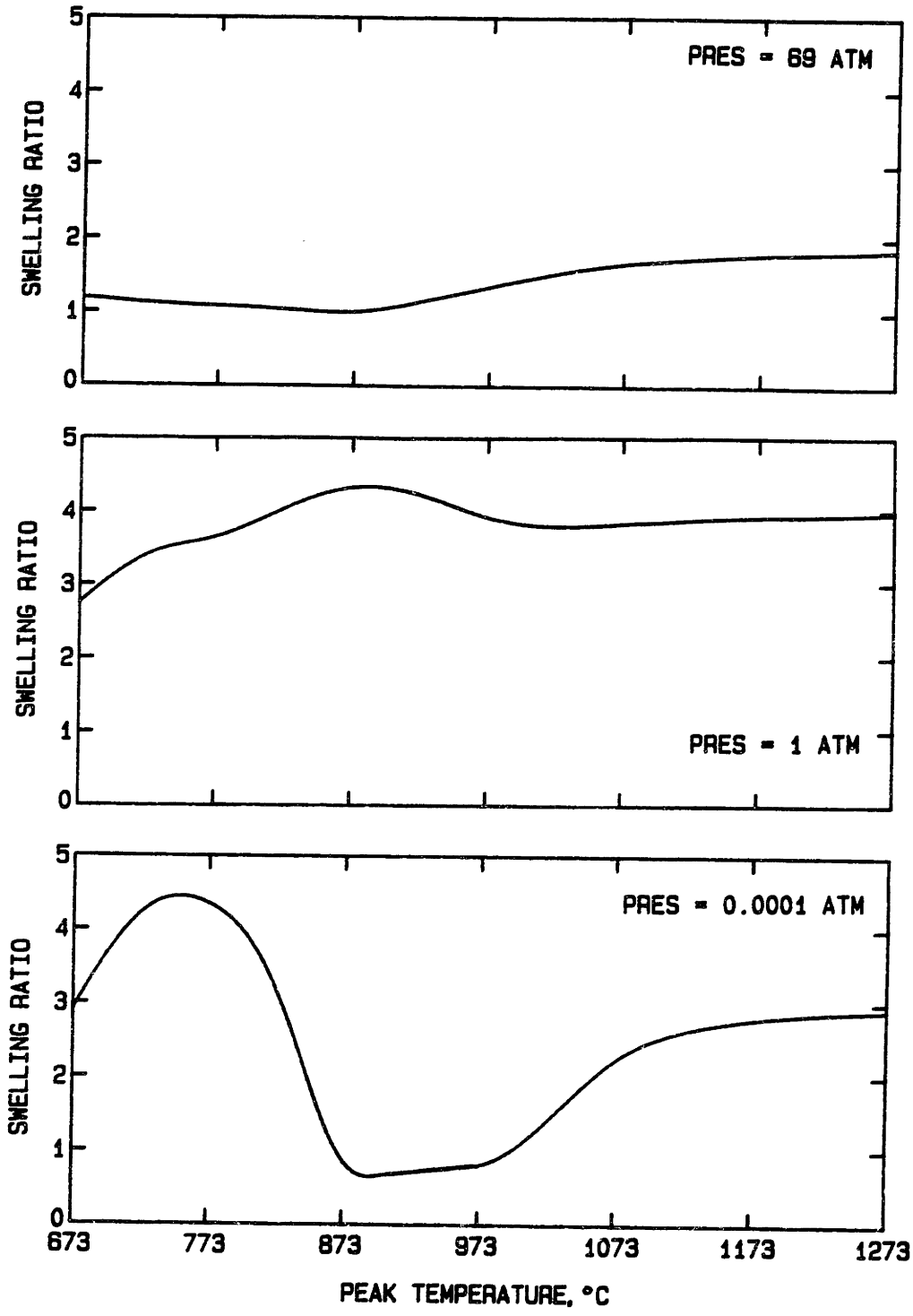

Fig. 6.5.2. Model predictions of swelling ratio as a function of peak temperature at 3 different pressures.

lower except at low temperatures. However, at high pressures, the compression factor dominates and the volume of gases are smaller than that at 1 atm. Thus even though there are more bubbles remaining in a particle, the final swelling ratio is lower than that at 1 atm. Predicted variations in swelling ratio with peak temperature and pressure suggest that there is an optimum peak temperature and pressure which would give the minimum swelling ratio. Again, it should be possible to improve the predictions of swelling when more information on plasticity, vapor pressure of metaplast, and the rate of bubble generation become available.

MW predictions: The number average MW of 1-atm tar varies between 300 and 350 and the number average molecular weight of vacuum tar is about 50 gm/mole higher than that of 1-atm tar. The model can reasonably predict the MW variations of 1-atm tar with peak temperatures, but it is unable to predict the decrease in molecular weight as pressure increases from 0.0001 atm to 1 atm. Evaporation of high MW metaplast at the particle surface is enhanced at low pressures. Even though the model includes this evaporative transport at the particle surface, almost all the metaplast is vaporized into bubbles and leaves the particle via bubble growth and the model prediction does not reflect the enhancement in high MW metaplast yields at low pressures. In the treatment of evaporation process at the particle surface, the model assumes a pseudo-steady state and a partial pressure of metaplast that is in equilibrium with the molten coal. More rigorous treatment of the external transport proceses which handles the unsteady state flux of volatiles at the particle surface may be necessary to predict the decrease in MW with increasing pressure.

The lower molecular weight of the tar from 1 atm pyrolysis may be caused by tar cracking outside the particle. The convective current

observed at 1 atm pyrolysis experiments in a batch screen-heater reactor may circulate the tar through the hot screen and 1-atm tar undergoes more secondary homogeneous cracking reactions. A simple analysis of tar cracking near the hot screen at 1 atm is presented in Appendix D and shows ~ 3 % tar cracking. However, more rigorous analyses, both experimental and theoretical, are necessary to test the above hypothesis.

The model prediction of the MW of extract was less than satisfactory but it does offer an explanation of the trends shown in the 1-atm extract. The MW of extract is related to the number density of bubbles, the vapor pressure of metaplast and the rates of metaplast and tar secondary reactions. At low temperatures, as the low MW metaplast is lost by transport to outside the particle, the average MW of metaplast plus tar increases. As the temperature increases, the metaplast decomposition reactions are faster than that of tar in bubbles, the metaplast in liquid is depleted much faster than tar in bubbles, resulting in the total extractible material consisting of more of the metaplast fractions already evaporated into bubbles and lowering the MW of extract. Again, to understand the molecular weight trends in tar and pyridine extract, more experimental data at different pyrolysis conditions are required in addition to improved understanding of physical properties of softening coals.

6.5.2. Heating Rate Effect

To test the model predictions of heating rate effects on volatiles yields and on the plasticity, the time-temperature history which includes a linear heating period, followed by 5 sec holding at peak temperatures and natural cooling periods was selected. First, the volatiles yields for this time-temperature history are compared with those from peak temperature runs

in Fig. 6.5.3. At low peak temperatures, extended reaction time at the peak temperature causes an additional amount of volatiles to form. At high temperatures (peak temperature >800 °C), however, all pyrolysis reactions are completed during heat-up and neither gas yields nor tar yields were affected by holding time.

The heating rates were varied from 100 °C/s to 1000 °C/s, and the volatiles yields and the temperature range in which the coal maintained its plasticity were calculated. At a low heating rate, more metaplast is consumed in secondary reactions due to the longer residence time at relatively lower temperatures. At a faster heating rate, the coal particles are rapidly brought to tempeatures where the rate of transport is significantly faster and the volatiles yields increase. However, the model predictions of heating rate effects on the volatiles yields were rather small: the total volatiles yields increased by 3.4 % while tar was increased by 2.2 % at the peak temperature of 1000 °C when the heating rate was increased 10-fold. The model predictions of heating rate effects are in agreement with the experimental observations of Suuberg (1977).

It is known that increasing heating rate does not affect the softening point, but does shift the resolidification point to a higher temperature. The model predictions of change in plasticity under different heating rates are plotted as a function of temperature in Fig. 6.5.4. As can be seen, the model predictions are in accord with the expectations.

6.5.3. Particle Size Effect

Fig. 6.5.5 plots total volatiles yield and tar yields from three different sized particles pyrolyzed at different peak temperatures at 1 atm. Since smaller particles have the larger surface area per unit mass available for growing bubbles to be released from the particle, the model

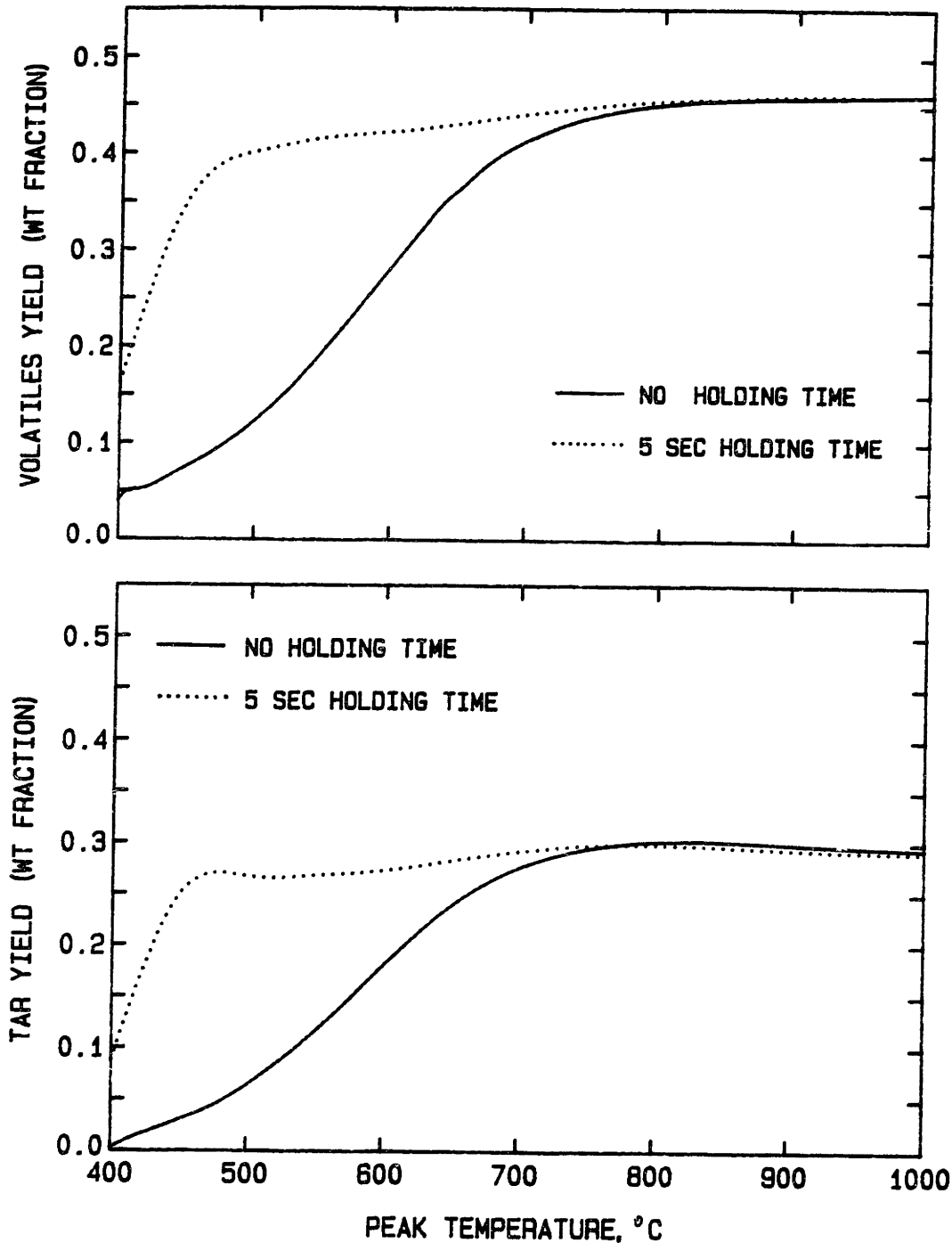

Fig. 6.5.3. Model predictions of the effect of time-temperature history on total volatiles yields (top) and tar yields (bottom).

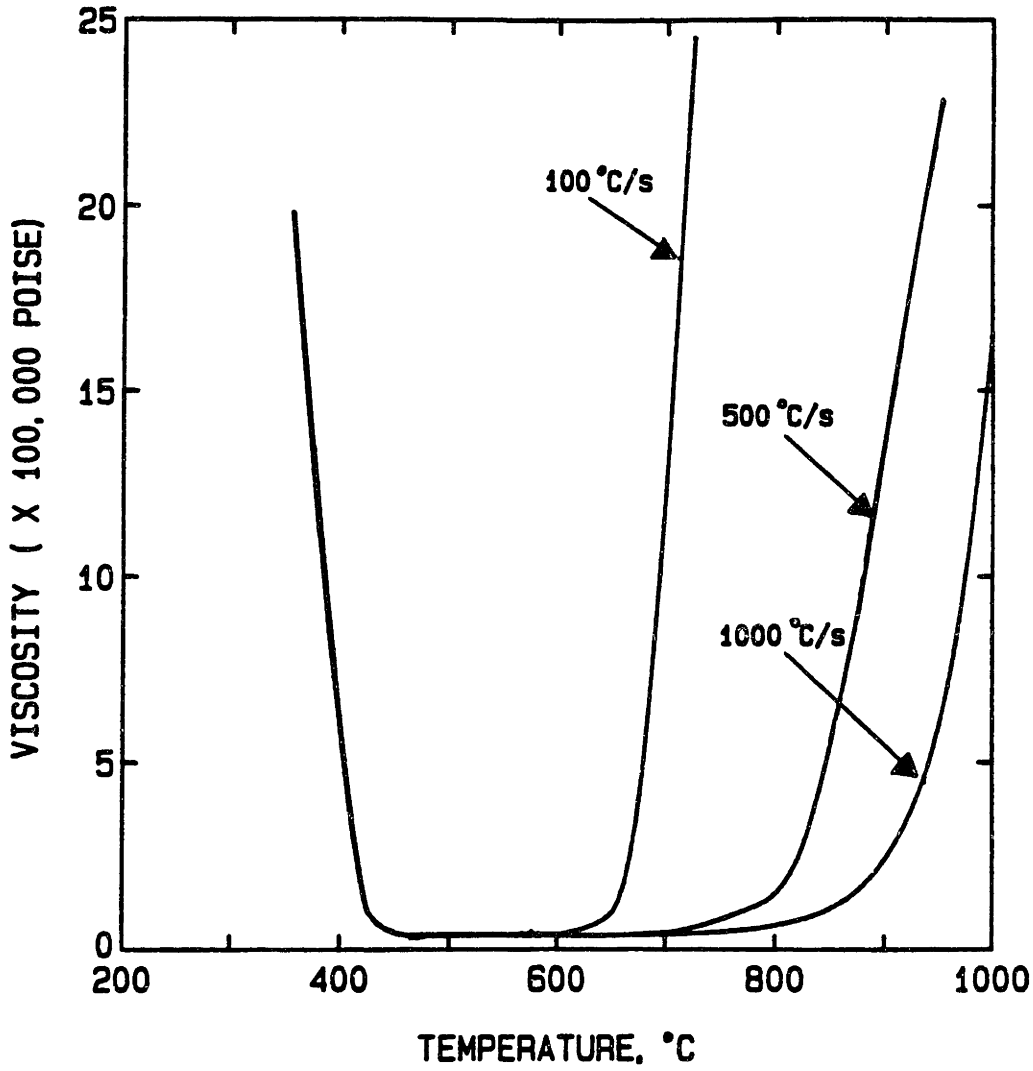

Fig. 6.5.4. Heating rate effect on plastic period as coal is heated to 1000°C at 1 atm at 100°C/s; 500°C/s; and 1000°C/s.

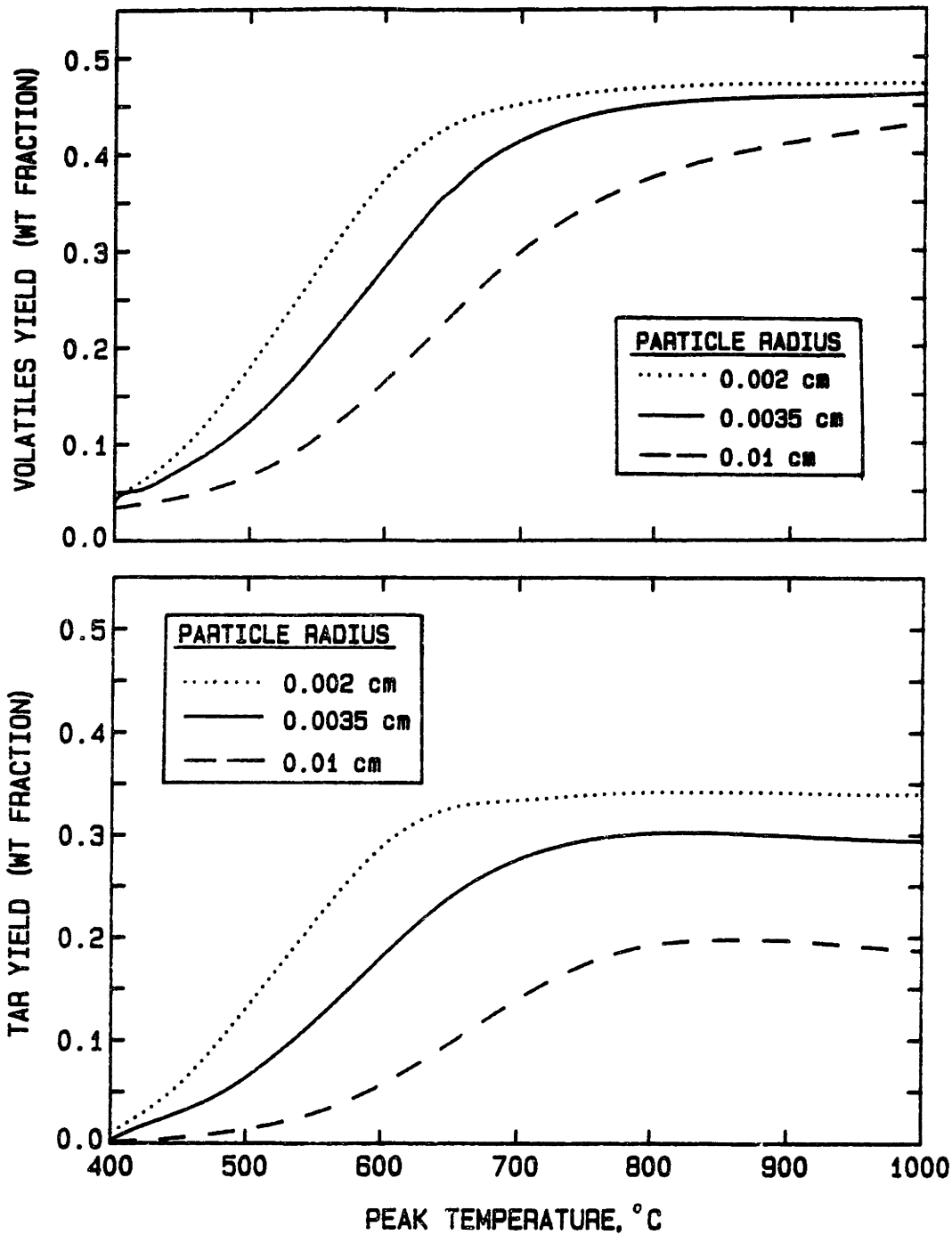

Fig. 6.5.5. Model predictions of the effect of particle size on total volatiles yields (top) and tar yields (bottom).

predicts an increase in volatiles yields as the particle size decreases. Again the model predictions are in agreement with the experimental observations. However, the application of the model is limited to cases with no temperature gradient inside the particle.

6.6 COMPARISON WITH EVAPORATION MODEL

Another transport model for softening coals is the evaporation model (Zacharias, 1979; Suuberg, 1981, 1982), which ignores the transport inside the particle and models tar transport as an evaporative process at the particle surface. Based on the molecular weight data obtained in this thesis, it is concluded that transport inside the particle is much more important than evaporative transport at the particle surface (See Ch. 5.1), and therefore the present model emphasizes the transport inside the particle. The impotant features of the model are summarized in this section by comparing the present model with the evaporation model.

- In modeling the formation of metaplast, some of the metaplast is assumed to pre-exist in the coal, while the evaporation model (and all other models that address this issue) treats all the metaplast as being a result of pyrolysis.
- In the presence of bubbles, volatiles are allowed to be transported via bubbles, as well as via diffusion through the melt. Here, volatiles include both gases and tar, whereas the evaporation model only deals with the transport of tar, and ignores the possibility of tar transport by bubbles.
- The variations in plasticity due to temperature and metaplast concentration, and the viscosity effect on the rate of bubble growth and

the rate of volatiles diffusion to the particle surface are included in the present model, while the evaporation model ignores the increase in mass transport resistance inside the particle as the melt viscosity increases.

- The present model predicts not only the plasticity and volatiles yields but also the extent of swelling, even though the predictions of swelling is more or less in a qualitative stage.
- Both models can predict temperature, pressure, and particle size effect on volatiles yields. However, application of the evaporation model to low pressure pyrolysis is not justified.
- Both models recognized the importance of MWD of tar in modeling transport. However, the evaporation model fails to explain the MW trends with increasing peak temperature and the presence of lower MW metaplast inside the particle at high temperatures, while the present model fails to describe the decrease in the average MW of tar when pressure is increased from 10^{-4} to 1 atm.

7. CONCLUSIONS AND RECOMMENDATIONS

7.1. CONCLUSIONS

The following are the major conclusions of this study:

1. Based on the ranges of molecular weight distribution of tar and pyridine extract, pyridine extract is a reasonable estimate of metaplast remaining in the particle. Just a few percent of extract has MW beyond that of tar. The extract yield of raw coal gives an estimate of the amount of pre-existing metaplast in coal.

2. The number average molecular weights of tar and pyridine extract are much smaller than what is expected from the molecular model of pyolysis tar proposed by Gavalas (MW= 984, 1976). The number average MW of 1-atm tar varies between 300 and 350 and that of extract is between 450 and 550, showing a maximum at peak temperatures around 500 °C. The vacuum tar is usually 50 gm/mole heavier than 1-atm tar, and the MW of vacuum extract does not vary with peak temperature as much as 1-atm extract and stays around 500 gm/mole at temperatures above the softening point.

3. Transport of both gaseous volatiles and tar within molten coal can occur via bubbles in the molten coal.

4. In modeling bubble generation, the application of bubble nucleation theory to molten coal is not justified because of large uncertainties involved in predicting the rate of bubble generation. However, the characteristic time for bubble nucleation is short enough such that bubble generation by the nucleation is not a rate limiting step in the transport model and one can safely assume that any bubbles nucleated are already present at the onset of softening, in addition to those orginating from pores in the solid structure.

5. Only the macropores in solid coal survive through coal softening and serve as initial bubble sites. The size and the typical pore volume of macropores are > 300 A° in diameter and 0.04 cm^3/gm coal, respectively.

6. When the different sized bubbles grow by diffusive influx of volatiles from the molten phase, the smaller bubbles grow faster than larger bubbles and the bubble size distribution grows into a narrow size range. Therefore, the bubble size distribution can be simplified into a single size bubble in the absence of bubble coalescence.

7. Application of the model requires estimating physical properties which are not readily available at present. Among these, the most important parameters are the melt viscosity, the vapor pressure of metaplast and the initial bubble number density and its changes as a function of time:

- Two simple vapor pressure correlations which model the vapor pressure of metaplast as a function of molecular weight and temperature were tested. The model by Maiorella is more suitable to predict the vapor pressure at low temperatures but the model by Suuberg is preferred at high temperatures.
- It is necessary to use a viscosity correlation that predicts well the measured variations in plasticity in order to obtain model predictions of volatiles yields close to the experimental data. The viscosity correlation which models the viscosity as a function of temperature and metaplast concentration at low temperatures and as a function of solely metaplast concentration at high temperatures does a good job of describing the change in plasticity during pyrolysis.
- Not much is understood about the initial bubble number density and

the rate of bubble generation as a function of different pyrolysis conditions. At this stage of the modeling, it seems best to leave the initial number density of bubbles as a fitted parameter and to assume no further bubble generation.

8. The model prediction of the final swelling ratio (R_p/R_{po}) varies between 1 and 4 at a heating rate of 1000 C/s. The swelling ratio is very sensitive to the initial number density, vapor pressure of metaplast, the viscosity of the molten phase and the tar reaction rate in bubbles, and the predictions of swelling cound be improved a great deal with a better understanding of the above properties. However, the model predictions of swelling at different pressures provides following findings:

- In general, low swelling ratios at low pressure, which are expected because faster growth of bubbles results in a loss of a larger number of bubbles.
- At high pressures, even though more bubbles remain in the particle, the swelling ratio is lower because of compression due to the high prssure.

9. Despite the lack of knowledge of many physical properties of molten coal, the modeling of transport in softened coal in terms of bubble motions along with secondary reactions in both bubbles and the liquid phase predicts the trends in volatiles yields, plasticity, and extent of swelling under various temperatures, pressures, particle sizes and heating rates, thereby lending strong support to the picture that bubbles play an important role in intra-particle transport in a softened coal. Improved understanding of the above noted physical and chemical properties will help improve the model predictions.

7.2. Recomendations for Future Work.

The following studies would be of interest for future research:

1. More accurate measurements of time-temperature histories. It is difficult to get accurate time-temperature records from the HP fast response recorder. Use of the Bascom-Turner recorder which gives digitized readings is strongly recommended.

2. Further experimental and theoretical studies of free convection flow observed in pyrolysis experiments at 1 atm and higher pressures. It is important to understand the velocity field due to the convective flow as well as the temperature gradient near the heated screen to calculate the extent of secondary reactions of primary tar necessary for an analysis of apparatus effects on measured volatiles yields. Actual measurements of temperature can be made at different locations within the reactor to provide information on the temperture gradient near the heated screen.

3. More measurements of volatiles yields, the yields of pyridine extracts, and the MWD's of both tar and extract from pyrolysis experiments at different pyrolysis conditions, i.e., different time-temperature histories, different pressures and different coal types including non-softening coals, to answer the following questions:

- How does the ultimate amount of metaplast formed in softened coal vary under different pyrolysis conditions? Can one learn more about mechanisms for the development of plasticity?
- How do the MWD's of tar and extract vary? Are there any systematic correlations between the MWD's of tar and extract and pyrolysis conditions? Do they suggest any new mechanism for transport

processes?

- Do the yields and MWD of extracts reflect the rate and the extent of secondary reactions inside the particle? How do the MWD's of tar and extract vary with the extent of secondary reactions? Is the rate of liquid phase secondary reactions affected by the melt viscosity?

4. Development of the correlation between measured viscosity and the metaplast concentration, estimated by the yield of pyridine extract.

5. Experimental studies of changes in macropore structure and the extent of swelling during pyrolysis to provide improved understanding of bubble generation and the growth at different pyrolysis conditions, especially under fast heating rate.

6. Both experimental and theoretical studies of vapor pressures of known molecular weight tar.

7. Studies of solvent effects on extract yield and MW measurement. Accroding to literature, pyridine is the best choice for experiments measuring both extract yield and MW. However, the yields of pyridine extract may not be the best to represent metaplast.

8. Model improvements by including

- Unsteady state transport of volatiles outside the particle to incorporate the volatile flux delivered by bubbles.
- Chnages in MWD of metaplast due to reploymerization reactions.
- Changes in MWD of tar in bubbles due to cracking reactions.
- Modification of the model of chemical kinetics and transport to deal with currently unexplained phenomema such as the trends in MW of extract and tar, and pressure effect on plasticity.
- Further simplification of the model.

9. Study of bubble coalescence including improving coalescence coefficient and searching for better numerical scheme to incorporate coalescence kinetics into the population balance of bubbles.

10. Extention of the model to the large particles which have temperature gradients inside the particle.

11. Changes of coal geometry from a sphere to a thin slab, which is a more reasonable approximation of the geometry of coals pyrolyzing at pressures higher than 1 atm in a screen heater reactor.

8. REFERENCES

Adair, R. R., E. H. Boult and H. Marsh, "Gasification of a Blast-Furnace Coke. A Study Using Scanning Electron Microscopy," Fuel, Vol. 51, 645 (1983)

Anthony, D. B., "Rapid devolatilization and Hydrogasification of Pulverized Coal," Sc. D. Thesis, Dept. Chem. Eng., M.I.T. Cambridge (1974)

Anthony, D. B. and J. B. Howard, "Coal Devolatilization and Hydrogasification," AIChE J., Vol. 22, 675 (1976)

Arendt, P., "Entgasung und hydrierende Vergasung von Steinkohlen im Druckbereich von 0.1 bis 90 bar bei Aufheizgeachwindigkeiten von 100 bis 1000 K/sec.," Dissertation, University of Aachen (1980)

Attar, A., "Bubble Nucleation in Viscous Material Due to Gas Formation by a Chemical Reaction, Application to Coal Pyrolysis," A.I.Ch.E. J., Vol. 24, 106 (1978)

Audibert, E., Fuel, Vol. 5, 229 (1926)

Badzioch, S., D. R. Gregory, and M. A. Field, Fuel, Vol. 43, 267 (1964)

Badzioch, S., "Thermal Decomposition," B.C.U.R.A. Monthly Bulletin," Vol. 31, No. 4, 193 (1967)

Bangham, D. H., R. E. Franklin, W. Hirst and F. A. P. Maggs, "A Structure Model For Coal Substance," Fuel, Vol. 28, 231 (1949)

Barlow, E. J., and W. E. Langlois, "diffusion of Gas from a Liquid into an Expanding Bubbles," IBM J., 329-337 (1962)

Bird, R. B., W. E. Stuart, and E. L. Lightfoot, Transport Phenomena, John Wiley & Sons, Inc (1960)

Blander, M., D. Hengstenberg, and J. L. Katz, "Bubble Nucleation in n-Pentane, n-Hexane, n-Pentane + Hexadecane Mixtures, and Water," J. Phys. Chem., Vol. 75, 23, 3613, (1971)

Blander, M. and Katz, J. L., "Bubble Nucleation in Liquid," A.I.Ch.E. J., Vol. 21, 833 (1975)

Bockrath, B. C., R. B. LaCount, and R. P. Noceti, "Viscosity of Coal-Derived Liquid," Fuel Processing Technology, Vol. 1, 217 (1977)

Bodzdek, D. and A. Marzed, "Molecular Components of Coal and Coal Structure," Fuel, Vol. 60, 47 (1981)

Brailford, A. D. and R. Bullough, "The rate Theory of Swelling due to Void Growth in Irradiated Materials," J. Nucl. Mat., Vol. 44, 121 (1972)

Briggs, D. E., and P. A. S. Smith, "Studies on the Separation of Coal Extract from Solid Residue in Liquefied Coal," NSF-AER 7515212 (1976)

Bronowski, J., d. Fitzgerald, D. W. Gillings, D. C. Rhys-Jones, "Plastic Properties of Coking Coal," Nature, Vol. 171, 389 (1953)

Brown, H.R. and P. L. Waters, "The Function of Solvent Extraction Products in the Coking Process I - Yields, Properties and Mode of Release of Chloroform Extract," Fuel, Vol. 45, 17 (1966); "The Function of Solvent Extraction Products in the Coking Process II - Theory of the Mechanism of Thermal Softening," Fuel, Vol. 45, 60 (1966)

Brule, M. R., C. T. Lin, L. L. Lee, and K. E. Starling, "Multiparameter Corresponding States Correlation of Coal-Fluid Thermodynamic Properties," AIChE J., Vol. 28, 4, 616 (1982)

Chakrabartty, S. K., and N. Berkowitz, "Properties of Caking Coals; Destruction of Caking Properties by Boron Trifluoride," Fuel, Vol. 51, (1972)

Chandrasekhar S., "Stochastic Problem in Physics and Astronomy," Rev. Mod. Phys., Vol. 15, 141 (1943)

Chao, T. S., H. W. Rutta, and A. C. Smith, Jr., "Reduction Viscosity of Coal Liquefaction Products with Additives," ACS Div. Fuel Chem., Vol. 24, 141 (1979)

Chen, L. H. and C. Y. Wen, "A Model for Coal Pyrolysis," ACS Div. Fuel Chem. Prepr., Vol. 24, 141 (1979)

Cheong, P. H., Oka, M., and Gavalas, G. R., "Modeling and Experimental Studies of Coal Pyrolysis," Presented at NSF Workshop on the Fundemental Organic Chemistry of Coal, Knoxville, Tenn. (1975)

Chermin, H. A. G. and D. W. Van Krevelen, "Chemical Structure and Properties of Coal XVII - Mathematical Model of Coal Pyrolysis," Fuel, Vol. 36, 85 (1957)

Caron, R., "Batch Reactor Manual," Internal report, Dept. Chem. Eng. M.I.T., Cambridge (1979)

Cole, R., "Boiling Nucleation," Adv. Heat Transfer, Vol. 10, 85 (1974)

Culrose, C. C., L. R. Clavenna, and D. Williams, "Technique for Measuring Swelling Tendency and Coke Density for Catalytic Coal Gasification," ACS Div. Fuel. Preprint, 181 (1984)

Dolan, J., "Swelling and Agglomeration Effects for Bituminous Coal in a Lamimar Flow Reactor," B. S. Thesis. M.I.T., Cambridge (1980)

Dormans, H. N. M. and and Van Krevelen, D. W., "Chemical Structure and Properties of Coal XXVII-Composition and Molecular Weight Distribution of Coal Extracts," Fuel, Vol. 39, 373 (1960)

Dryden, I. G. C., "Action of Solvents on Coals at Lower Termperatures II - Mechanixm of Extraction of Coals by Specific Solvents and the Significance of Quantitative Measurements," Fuel, Vol. 30, 145 (1951)

Dryden, I. G. C., "Chemical Constitution and Reactions of Coal," in Chemistry of Coal Utilization, Supplementary Volume, H. H. Lowry Ed., J. Wiley and Sons, NY (1963)

Dryden, I. G. C., and W. K. Joy, "Some Chemical Factors Governing the Plastic Softening of Coals on Heating," Fuel, Vol. 40, (1961)

Dryden, I. G. C., and K. S. Pankhurst, "Plastic Softening of Coking Coals on Heating," Fuel, Vol. 34, (1955)

Edwards, D., C. G. Van de Rostyne, J. Winnick, and J. M. Pausnitz, "Estimation of Vapor Pressures of High Boiling Fractions in Liquified Fossil Fuels Containing Heteroatoms Nitrogen or Sulfur," Ind. Eng. Chem. Proc. Des. Dev., Vol. 24, 138 (1981)

E.P.R.I., Conference on Coal Pyrolysis, Feb. 25-26, Palo Alto, Ca. (1981)

Eckert, E. R. G., and R. M. Drake, Jr. Analysis of Heat and Mass Transfer, Mcgraw-Hill Book Co. (1972)

Essenhigh, R. H. and York, C. G., "Reaction Rates of Single Coal Particles. Influence of Swelling, Shape, and Other Factors," Fuel, Vol. 44, 177 (1965)

Feldmann, H. F., K-D Kiang, and P. M. Yawrsky, "Fluidization Properties of Coal Char," ACS Div. of Fuel, Preprints, Vol. 15, No. 3, 62 (1971)

Fitzgerald, D., "The Kinetics of Coal Carbonization in the Plastic State," Trans. Faraday Soc., Vol. 52, 362 (1956) and Fuel, Vol. 35, 178 (1956)

Fitzgerald, D. and D. W. Van Krevelen, "The Kinetics of Coal Devolatilization," Fuel, Vol. 38, 17 (1959)

Fong, W., Y. F.Khalil, W. A. Peters, and J. B. Howard, "Plastic Behavior of Coal under Rapid-heating High-temperature Conditions," Accepted for presentation in ACS Spring meeting, Miami, Fla., April (1985)

Fong, W., Sc. D. Thesis in preparation, Dept. Chem. Eng., M. I. T., Cambridge, MA (1985)

Frankel, N. a., and A. Acrivos, "On the Viscosity of a Concentrated Suspension of Solid Sphere," Chem. Eng. Sci., Vol. 22, 847 (1967)

Franklin, H. D., "Mineral Matter effects in Coal Pyrolysis and Hydropyrolysis," Ph. D. Thesis, Department of Chemical Engineering, M. I. T., Cambridge, MA (1980)

Franklin, R. E., "A Study of the Fine Structure of Carbonaceous Solids by Meeasurements of True and Apparent Densities. Part I - Coals; and Part II - Carbonized Coals," Trans Faraday Soc. Vol. 45, 274 and 668 (1949)

Frederickson, P., and J. Morris, "Application of High Pressure Liquid Chromatograph to the Analysies of Recycle Solvents from a Bench Scale Continuous Coal Hydrogenation Unit," Report of Australian Coal Industry Research Laboratories, Ltd., No. P. R. 79-6, (1979)

Friedel, R. A., J. L. Shultz, and A. G. Sharkey Jr., "Chemical Composition of Progressive Pyridine Extracts from Coal," Fuel, Vol. 47, 403 (1968)

Friedlander, s. K., and C-S. Wang, "The Self-Preserving Particle Size Distribution for Coagulation by Brownian Motion," J. Colloid and Int. Sci., Vol. 22, 126 (1966)

Gan. H., S. P. Nandi, and P. L. Walker Jr., "Nature of the Porosity in American Coals," Fuel, Vol. 51, 272 (1972)

Gangopadhyay and Margrave, "Thermodynamic Properties of Inorganic Substances (VI. The High Temperature Heat Contents of Chromel-P and Alumel)," J. of Chem. and Engin. Data, Vol. 8, No. 2 (1963)

Gavalas, B. R. and K. Wilks, "Intraparticle Mass Transfer in Coal Pyrolysis," AIChE J., Vol. 26, 201 (1980)

Gavalas, B. R., "Experimental and Modeling Studies of Coal Pyrolysis: Summary of Research Program," Unpublished Report, Div. Chem. and Chem. Eng. Cal. Tech. (1976)

Gelbard, F., Tambour, Y., and Seinfeld, J.H., "Sectional Representations for Simulating Aerosol Dynamics," J. Colloid Interface Sci., Vol. 76, 541 (1980)

Gosch, J., "Rapid Pyrolysis of Sweet Gum Xylan with Applications in Modeling Wood," M. S. Thesis, Dept. Chem. Eng. MIT, Cambridge, Ma (1983)

Graff, R. A., S. Dobner, and A. M. Squires, "Flash hydrogenatin of Coal 1. Experimental Methods and Preliminary Results," Fuel, Vol. 55, 109 (1976)

Gregorey, D. R. and R. F. Littlejohn, "A Survey of Numerical Data on the Thermal Decomposition of Coal," B.C.U.R.A. Mon. Bul., Vol. 29, No. 6, 173 (1965)

Grey, J. A., A. J. Brady, J. R. Cunningham, J. R. Freeman, and G. M. Wilson, "Thermophysical Properties of Coal Liquids:Selected Physical, Chemical, and Thermodynamic Properties of Narrow Boiling Range Coal Liquids," Ind. Eng. Chem. Proc. Des. Dev., Vol. 22, (1983)

Guin, J. A., A. R. Tarrer, W. S. Pitts, and J. W. Prather, "Kinetics and Solubility of Hydrogen in Coal Liquefaction Reactions," in Liquid Fuels from Coal, 133, (1977)

Gulden, M. E., "Migration of Gas Bubbles in Irradiated Uranium Dioxide," J. Nucl. Mat., Vol. 23, 30 (1967)

Hajaligol, M. R. "Rapid Pyrolysis of Cellulose," Ph. D. Thsis, Dept. of Chem. Eng. M.I.T., Cambridge (1980)

Hamilton, L. H., A. G. Ayling and M. Shibaoka, "A New Experimental Device for Pyrolysing Coal Particles under Controlled Conditions over a Wide Range of Heating Rate," Fuel, Vol. 58, 873 (1979)

Hayduk, w., R. Castaneda, H. Bromfield, and R. R. Perras, "Diffusivity of Propane in Normal Paraffin, Chlorobenzene, and Butanol Solvent," AIChE J., Vol. 19, 4, 859 (1973)

Hayduk, W. and S. C. Cheng, "Review of Relation Between Diffusivity and Solvent Viscosity in Dilute Liquid Solutions," Chem. Eng. Sci., Vol. 26, 4, 698 (1973)

Haynes, M. R. and R. Bullough, "The Nucleation and Growth of Fission Gas Bubbles," IAEA-SM-190/15

Haynes, M. R. and m. H. Wood, "On the Rate Theory Model for Fission Gas Behavior in Nuclear Fuel," J. Nucl. Mat., Vol. 59, 293, (1976)

Hays, D. J. W. Patrick, and A. Walker, "Pore Structure Development during Coal Carbonization, 1. Behavior of Single Coals," Fuel, Vol. 53, 297 (1974)

Hirsh, P. B., "X-ray Scattering from Coals," Proc. Roy. Soc. London, A226, 143 (1954)

Hiss, T. G., and E. L. Cussler, "Diffusion in High Viscosity Liquids," AIChE J., Vol. 19, 698 (1973)

Homann, K. H., "Discussion Comment for Article by H. Jinno et al. Sixteenth Symposium (International) on Combustion, Cambridge (1976)

Howard, J. B., "Fundamentals of Coal Pyrolysis and Hydropyrolysis," Chapter 12 in The Chemistry of Coal Utilization - Second supplementary Volume, M. A. Elliot, Ed., J. Wiley and Sons (1981)

Hwang, S-C., L. Tsonopoulos, J. R. Cunningham, and G. W. Wilson, "Density, Viscosity, and Surface Tension of Coal Liquids at High Temperatures and Pressures," Ind. Eng. Chem. Proc. Des. Dev., Vol. 21, 127 (1982)

James, R. K. and A. F. Mills, "Analysis of Coal Particle Pyrolysis," Letters in Heat and Mass Transfer, Vol. 3, 1 (1976)

Juettner, b. and H. C. Howard, "Pyrolysis of Coal - Thermal Decomposition Distillation of Coal in a High Vacuum," Ind. Eng. Chem., Vol. 26, 1115 (1934)

Juntgen, H., and K. H. Van Heek, "Gas Release from Coal as a Function of the Rate of Heating," Fuel, Vol. 47, 103 (1968)

Kagan, Y., "The Kinetics of Boiling of Pure Liquid," Rus. J. Phys. Chem., Vol. 34, No. 1, 42 (1960)

Katz, J. L. and M. Blander, "Condensation and Boiling: Correction to Homogenous Nucleation Theory for Nonideal Gases", J. Col. Int. Sci., Vol. 42, 3, 498 (1973)

Kimber, F. M. and M. D. Gray, "Rapid Devolatilization of Small Coal Particles," Comb. Flame, Vol. 11, 360 (1967a) ; "Measurement of Thermal Decomposition of Low and High Rank Non-Swelling Coals at M.H.D. Temperatures," B.C.U.R.A., Document No. MHD32, (1967b)

Kobayashi, H., "Devolatilization of Pulverized Coal High Temperaure " Ph. D. Thesis, Dept. of Mech. Eng., M.I.T., Cambridge (1976)

Kyte, J. F. A. J. Madden, and E. L. Piret, "Natural-Convection Heat Transfer at Reduced Transfer Pressure," Chem. Eng. Prog., Vol. 49, 12, 653 (1980)

Lee, B. I., and M. G. Kesler, "A Generalized Thermodynamic Correlation Based on Three-Parameter Corresponding States," AIChE J., Vol. 21, 3, 510 (1975)

Lewellen, P. C., "Product Decomposition Effects in Coal Pyrolysis," M. S. Thesis, Dept. of Chem. Eng., M.I.T., Cambridge (1975)

Lightman, P. and P. S. Street, "Microscopical Examination of Heat Treated Pulverized Coal Particles," Fuel, Vol. 47, 7 (1968)

Lin, H-M, H. M. Sebastian, J. J. Simnick, and K-C Chao, "Solubilities of Hydrogen and Methane in Coal Liquids," Ind. Eng. Chem. Process Des. Dev., Vol. 20, 253 (1981); "Gas-Liquid Equilibrium in Binary Mixtures of Methane with n-Decane, benzene, and Toluene," J. Chem. Eng. Data, Vol. 24, 2, 146 (1979)

Lloyd, W. G., Francis, H. F., and Yewell Jr., M. R., "A model for the Isothermal Plastomeric Behavior of Coal," ACS Div. Fuel, Vol. 25, 2, 198 (1980)

Lloyd, W. G. and Others, "Predictors of Plasticity in Bituminous Coals," Final Technical Report DE-FG22-81PC40793, (1984)

Loison, R., A. Paytavy, A. F. Boyer, R. Grillot, "The Plastic Properties of Coal," Chemistry of Coal Utilization, Supplementary Volume, Wiley, New York (1963)

Loison, R. and F. Chauvin, "Pyrolysis Rapidu Du Charbon," Chimie et Industrie, Vol. 91, 269 (1964)

Mackowsky, M. T., and E. M. Wolff, "Microscopic Investigations of Pore Formation during Coking," Coal Science, Advances in Chem. Series #55, 527 (1966)

Maiorella, B. L., "Behavior of Liquid Subbituminous Coal Tars Upon Heating, as it Relates to In-Situ Gasification," B. S. Thesis, Dept. Chem. Eng., M. I. T., Cambridge, MA (1975)

Mason, D. M., and F. C. Schora, Jr, "Coal and Char Formation in Hydrogasification," in Fuel Gasification, ACS Advances in Chemistry Series, No. 69, 18 (1967)

Matsunaga, T., "Gasification of Coals Treated with Non-aqueous Solvent and Swelling Behavior of a Single Coal Particle," Fuel, Vol. 57, 562 (1978)

Mayo, F. R. and N. A. Kirshen, "Comparison of Fractions of Pyridine Extract and Solvent-Refined Coal from Illinois No. 6 Coal," Fuel, Vol. 57, 405 (1978)

Mazumdar, B. K. and M. N. Chaterjee, "Mechanism of Coal Pyrolysis in Relation to Industrial Practice," Fuel, Vol. 52, 11 (1973)

Mcmanamey, W. J., and J. M. Wollen, "The Diffusivity of Carbon Dioxide in Some Organic Liquids at 25 and 50 C," AIChE J., Vol. 19, 667 (1973)

Menster, M., H. J. O'Donnel, S. Ergun, and R. A. Friedel, "Devolitilization of Coal by Rapid Heating," Adv. Chem. Series 131, Coal Gasification, 1, A.C.S., Washington D. C., (1974)

Mills, A. F., R. K. James, and D. Antonink, in Future Energy Production Series, J. C. Denton and N. Afgan, Eds., Hemisphere Publishing Co., Washingtion, D. C. (1976)

Miura, S. and P. L. Silveston, "Changes of Pore Properties during Carbonization of Coking Coal," Carbon, Vol. 18, 93 (1980)

Nazem, F. F., "Rheology of Carbonaceous Mesophase Pitch," Fuel, Vol. 54, 851 (1980)

Neavel, R. C., "Coal Plasticity Mechanism; Inferences from Liquefaction Studies," Symposium on Plasticity and Agglomeration of Coal, U.S. Energy Research and Development Administration, Morgantown, W, Va (1975); Coal Science, Vol. 1, 1, M. L. Gorbaty, J. W. Larsen, and I. Wender, Eds., Academic Press, NY (1982)

Nasakala, N. Y., R. H. Essenhigh, and P. L. Waters Jr., "Characteristics of Chars Produced from Lignites by Pyrolysis at 808 C Following Rapid Heating," Fuel, Vol. 57, 605 (1978)

Niksa, A. "Time-resolved Kinetics of Rapid Coal Develatilization," Ph. D. Thesis, Dept. Chem. Eng., Princeton University, Princeton,(1981)

Ouchi, K., K. Tanimoto, M. Makabe, and H. Itoh, "Retention between Fluidity and Solvent Extraction Yield of Coals," Fuel, Vol. 42, 227 (1983)

Pelofsky, A. H., "Surface Tension-Viscosity Relations for Liquids," J. Chem. Eng. Data, Vol. 11, 3, 394 (1966)

Pierron, E. D. and D. W. Rees, "Solvent Extract and the Plastic Properties of Coal," Div. of the Illinois State Geological Survey, Circular 288 (1960)

Pohl, J. H., Kobayashi, H. and A. F. Sarofim, "The Effect of Temperature and Time on the Swelling of Pulverized Coal Particles," Presented at Combustion Institute Technical Meeting, Boulder, Colorado (1978)

Reid, R., "Some Considerations of Bubble Nucleation from a Super-Heated Pure Liquid," Unpublished paper,Dept.Chem.Eng.M.I.T., Cambridge (1975)

Reid, R., J. Prausnitz, and R. Sherwood, Properties of Gases and Liquids, Third ed. McGraw-Hill Book Company, New York (1979)

Rodes, F. J., "Modeling the Kinetics of tar and Methane Yields from the Pyrolysis and Hydropyrolysis of Coal in a Laminar Flow Reactor," M. S. Thesis, Dept. Chem. Eng. M.I.T., Cambridge, Massachusetts (1981)

Rosenow, W. M. and H. Choi, Heat, Mass, and Momentum Transfer, Series in Engineering of the Physical Sciences, Prentice-Hall (1961)

Rosner, D. and M. Epstein, "Effect of Interface Kinetics, Capllarity and Solute Diffusion on Bubble Growth Rates in Highly Supersaturated Liquids," Chem. Eng. Sci., Vol. 27, 69 (1972)

Russel, W. B., D. A. Saville, and M. I. Greene, "A Modeling for Short Residence Time Hydropyrolysis of Single Coal Particles," AIChE J., Vol. 25, 65 (1979)

Rutger, I. R., "Relative Viscosity and Concentration," Rheologia Acta, Band 2 Heft 4, 305 (1962)

Rutton, P., "Bubble Growth in a Viscous Newtonian Liquid," Chem. Eng. Sci., Vol. 35, 2352 (1980)

Schlichting, H., Boundary Layer Theory, Seventh Ed., McGraw-Hill Series in Mechanical Engineering, McGraw-Hill Book Co. (1979)

Schiller, J. E., B. W. Farnum, and A. C. Smith, Jr., "Reducing Viscosity of Coal Liquefaction Products with Additives," ACS Div. Fuel Chem., Vol. 25, 198 (1980)

Scriven, E., "On the Dynamics of Phase Growth," Chem. Eng. Sci., Vol. 10, 1 (1959)

Sebastian, H. M., H. M. Lin, and K. C. Chao, "Correlation of Solubility of Hydrogen in Hydrocarbon Solvents," AIChE J., Vol. 27, 1, 138 (1981); "Correlation of the Solubility of Methane in Hydrocarbon Solvent," Ind. Eng. Chem. Fundam., Vol. 20, 346 (1981); "Correlation of the Solubility of Carbon Dioxide in Hydrocarbon Solvents," Ind. Eng. Chem. Process Des. Dev., Vol. 20, 508 (1981)

Sebastian, H. M., J. J. Simnick, H-M. Lin, and K-C. Chao, "Gas-Liquid Equilibrium in Binary Mixtures of Methane with Tetralin, Diphenylmethane, and 1-Methylnaphthalene," J. Chem. Eng. Data, Vol. 24, 2, 148 (1979); "Gas-Liquid equilibrium in Mixtures of Carbon Dioxide + Tolune and Carbon Dioxide + m-Xylene," J. Chem. Eng. Data, Vol. 25, 246 (1980)

Serio, M. A., "Secondary Reactions of Tar in Coal Pyrolysis," Ph. D. Thesis, Dept. Chem. Eng., M.I.T., Cambridge, Mass (1984)

Sheomaker, H. D., L. Z. Shock, R. R. Haynes, and S. H. Advani, "Directional Viscoelastic Properties of the Pittsburgh Coal at Elevated temperatures in Compressed Shear," MERC/RI-76/5

Simnick, J. J., H. M. Sebastian, H-M Lin, and K-C Chao, "Solubility of Hydrogen in Toluene at Elevated Temperatures and Pressures," J. Chem. Eng. Data, Vol. 23, 4, 339 (1978)

Singla, P. K., S. Miura, R. R. Hudgins, and P. L. Silveston, "Pore Development during Carbonization of Coals," Fuel, Vol. 62, 645 (1983)

Snyder, L. R., "Determination of Asphalt Molecular Weight Distribution by Gel Permeation Chromatography," Anal. Chem., Vol. 41, 1223 (1969)

Street, P. J., R. P. Weight, and P. Lightman, "Further Investigations of Structural Changes Occuring in Pulverized Coal Particles during Rapid Heating," Fuel, Vol. 48, 343 (1969)

Sung, W. F., "The Study of the Swelling Property of Bituminous Coal," M. S. Thesis, Dept. of Chem. Eng., M.I.T., Cambridge (1978)

Suuberg, E., "Rapid Pyrolysis and Hydropyrolysis of Coal," Sc. D. Thesis, Dept. Chem. Eng., M.I.T., Cambridge (1977)

Tejpar, Z. A., "The Effect of Particle Size on Volatile Release in a Laminar Flow Reactor," B. S. Thesis, Dept. Chem. Eng., M.I.T., Cambridge, Mass (1978)

Toda, Y., "A Study by Density Measurement of Changes in Pore Structures of Coals with Heat Treatment: Part I. Macropore Structure," Fuel, Vol. 52, 36 (1973)

Toda, Y., M. Hatami, S. Toyoda, Y. Yoshida, and H. Honda, "Fine Pore Structure of Carbonized Coals," Carbon, Vol. 8, 565 (1970)

Tucker, A. S. and C. A. Ward, "Critical State of Bubbles in Liquid-Gas System," J. App. Phys., Vol. 46, 11, 4801 (1975)

Tremper, K. K., and J. M. Prausnitz, "Solubility of Inorganic Gases in High-Boiling Hydrocarbon Solvents," J. Chem. Eng. Data, Vol. 21, 3, 295 (1976)

Unger, P. E. and Suuberg, E. M., "Modeling the Devolatilization Behavior of a softening Bituminous Coal," Eighteenth Symposium (International) on Combustion, The Combustion Institute, Pittsburgh, PA 1203 (1981)

Unger, P. E. and E. M. Suuberg, "Internal and External Mass Transfer Limitations in Coal Pyrolysis," ACS Div. Fuel Chem. Prepr., Vol. 28, 4, 278 (1983)

Unger, P. E. and E. M. Suuberg, "Molecular Weight Distribution of Tars Produced by flash Pyrolysis of Coals," Fuel, Vol. 63, 606 (1984)

Van Krevelen, D. W., F. J. Huntjen, and H. N. M. Formans, "Chemical Structure and Properties of Coal XVi - Plastic Behavior on Heating," Fuel, Vol. 35, 462 (1956)

Van Krevelen, D. W., Coal, Elsevier Publishing Co., Armsterdam (1961)

Ward, C. A., A. Balakrishnan, F. C. Hooper, "On the Thermodynamics of Nucleation in Weak Gas-Liquid Solutions," J. Basic Eng., 695 (1970)

Warren, W. B., "Carbonization of Coal," Ind. Eng. Chem., Vol. 27, 72 and 1350 (1935a, b)

Waters, P. L., "Rheological Properties of Coal during the Early Stage of Thermal Softening," Fuel, Vol. 41, 3 (1962)

Wen, C. Y., R, C. Bailie, and W. S. O', "Production of Low Btu Gas Involving Coal Pyrolysis and Gasification," Adv. Chem. Series 131, Coal Gasification, A.C.S., Washignton D. C. (1974)

Wilson, G. M., J. R. H. Johnson, S-C. Hwang, and C. Tsonopoulos, "Volatility of Coal Liquids at High Temperatures and Pressure," Ind. Eng. Chem. Proc. Des. Dev., Vol. 20, 94 (1981); Vol. 22, 636 (1983)

Woods, M. F., G. M. Habberjam, K. Elsworth, and S. Bennett, "The Effect of Maceral Composition on the Binderless Briquetting of Hot Char," Fuel, Vol. 46, 193 (1967)

Yau, Y. D., J. J. Kirkland, and D. P. Bly, Modern Size-Exclusion Liquid Chromatography, Wiley-international, NY (1979)

Zacharias, M. W., "Analysis of Product Yields from Rapid Pyrolysis of Bituminous Coal," M.S. Thesis, Dept. Chem. Eng., M.I.T., Cambridge (1979)

9. APPENDICES

APPENDIX A: CALIBRATION OF GAS CHROMATOGRAPH

Methane is used as the standard calibration gas since it responds to both the thermal conductive detector (TCD) and the flame ionization detector (FID). The response factors of the other gases are defined as the following:

$$R_i = \frac{mg_i}{A_i} \frac{A_{CH_4}}{mg_{CH_4}} \qquad \text{(A-1)}$$

Then,

$$mg_i = R_i \left(\frac{mg_{CH_4}}{A_{CH_4}} A_i \right) \qquad \text{(A-2)}$$

where all symbols are as defined in Chapter 4.2.2. Therefore, by injecting different amount of pure gas samples, the amount of gas injected is correlated with the TCD or FID areas. The response factor, R_i, is obtained from the linear regression model. The response factors of the gas species of interest are summerized in Table A.1.

Table A.1. Response factors for Thermal Conductivity Detector (TCD) and Flame Ionization Detector (FID) on the Sigma 2B and Perkin Elmer 3920B gas chromatograph.

Components	TCD	FID
CH_4	1.0	1.0
C_2H_4	1.299	1.008
C_2H_6	1.290	1.036
C_3H_8	1.384	0.938
C_4H_{10}	1.482	0.839
CO	1.342	-
CO_2	1.789	-
H_2O	1.306	-

APPENDIX B: GPC CALIBRATION

In order to obtain data on the molecular weight distribution of coal tar and pyridine extract of char, Gel Permeation Chromatography has been employed to separate the coal tar according to molecular size. The chromatographic system used was a Waters Associates ALC/GPC 201 Gel Permeation Chromatography systems with 500 Å and 100 Å μ-styragel columns.

Although the approximate molecular weight range for the columns has been determined by the manufacturer and there are standards of known molecular weight available, it is still necessary to calibrate the columns with coal tars since the calibration curve will be unique for the particular tars that are to be studied. Two methods of calibration will be discussed and the result will be compared.

B.1. Calibration Method

The peak position method and the linear calibration method will each be discussed in this section.

For the peak position method, the tar samples need to be fractionated into narrow molecular weight ranges by a large scale preparatory column. Pyridine extracts of char from various pyrolysis experiments are combined and the solvent (pyridine) is evaporated under nitrogen at around 50°C. The dried sample is re-dissolved in Tetrahydrofuran (THF) and fractionated in a preparatory scale column in the Division of Engineering, Brown University. Approximately 60 mg of sample were fractionated into 6 fractions. However, to obtain average retention volumes of fractions from the column to be calibrated, the solvent has to be pyridine, not THF. Therefore, after the

fractionation, THF is evaporated under nitrogen at room temperature and samples are dried in a vacuum oven also at room temperature.

Compared to the peak position method, the linear calibration method has an advantage of not requiring fractionation. Three unfractionated samples were also prepared and used in both calibration methods. Molecular weights of the 6 fractions and 3 unfractionated samples were measured by a Vapor Pressure Osmometer (VPO).

B.1.1. VPO Measurements

A Knauer (model no. 11.00) Vapor Pressure Osmometer was used to determine the molecular weights of samples. Samples were dissolved in dry Pyridine taken from a glove box right before VPO measurements and the same dry solvent was used as a reference solvent. All measurements were made at 60°C and instructions given in the instrument manual were followed closely.

For each sample, the slope of the measured temperature effect versus the concentration of the solution which is extrapolated to zero is calculated:

$$k_i = \frac{\sum_{j=1}^{N} \delta T_j \cdot Conc_j}{\sum_{j=1}^{N} Conc_j^2} \quad \frac{scale \cdot div}{gm/kgm\ solvent}$$

where N is the number of data points, and δT_j is the temperature change due to tar concentration differences. The molecular weight of each sample is obtained by comparing k_i with the standard k.

$$mn_i = \frac{k\ standard}{k_i} \quad \frac{\frac{scale \cdot div}{gm\ mole/kgm\ solvent}}{\frac{scale \cdot div}{gm/kgm\ solvent}} = \frac{gm}{gm\ mole}$$

Benzil (MW = 210) is used as a standard and the accuracy of VPO measurments was checked with Anthracene, which gave 98.6 percent accuracy. The VPO data are summarized in Table B.1.

B.1.2. Peak position Method

The calibration line for GPC columns is established by relating average peak retention volume of each fraction with molecular weight determined from VPO. GPC chromatograms of the fractions and unfractionated samples are shown in Fig. B.1 and Fig. B.2, respectively. The average retention volume of each peak is calculated from the following equation:

$$\bar{V} = \frac{\sum_{j=1}^{N} h_j V_j}{\sum_{j=1}^{N} h_j}$$

where the whole chromatogram is divided into N sections of volume V_1 to V_N respectively, and h_j is the average peak intensity height in section j. The result is summarized in Table B.2.

B.1.3. Linear Calibration Method

The linear approximation of the true calibration line is described by

$$m(v) = D_1 e^{-D_2 v}$$

where D_1 and D_2 are constants and v is the retention volume. Then the number-average molecular weight, Mn, is obtained from the following equation:

$$M_n = \frac{\sum_{j=1}^{N} h_j(V_j)}{\sum_{j=1}^{N} h_j(V_j)/M_j(V_j)} = \frac{\sum_{j=1}^{N} h_j(V_j)}{\sum_{j=1}^{N} h_j(V_j)/D_1 e^{-D_2 V_j}}$$

Table B.1. VPO Data Summary

1-a Fractions and Pure Compounds (Sept. 1983)

		1	2	3	Slope	MW
Frac 1	Conc.[+]	3.9355	1.9560	1.4678		
	ΔT	15.25	4.5152	3.1915	3.4251	582.3
Frac 2	Conc.	3.7453	3.1642	3.0901		
	ΔT	10.0	9.5873	7.6	2.7020	738.1
Frac 3	Conc.	3.7116	2.482	--		
	ΔT	9.1735	6.3926	--	2.5037	796.6
Frac 4	Conc.	4.3700	2.9095	2.1916		
	ΔT	20.46	13.6115	11.126	4.7396	420.8
Frac 5-6	Conc.	6.3822	4.3795	3.2825		
	ΔT	46.475	34.917	23.942	7.4956	266.1
Frac 7-10	Conc.	3.9759	2.6295	1.4450		
	ΔT	42.438	23.851	6.6175	8.9101	223.8
Benzil	Conc.[++]	0.02066	0.01033	0.005335		
	ΔT	41.45	20.8	9.3	1994.4	---
Anthracene	Conc.	4.019	2.2717	1.8342		
	ΔT	44.537	24.543	14.32	11.0509	180.5[+++]

1-b Unfractionated Samples and Benzil (Jan. 1984)

		1	2	3	Slope	MW
Samp 1	Conc.[+]	2.1242	5.42939	3.80491		
	ΔT	11.4	26.472	18.4093	4.90761	430.49
Samp 2	Conc.	5.1848	4.6061	4.9786		
	ΔT	13.43	25.46	22.76	4.65483	453.87
Samp 3	Conc.	2.4871	3.4169	4.0078		
	ΔT	9.0245	13.491	15.422	3.84251	549.82
Benzil	Conc.[++]	0.0053412	0.010529	.020149		
	ΔT	11.96	19.85	41.4	2112.69	---

[+]Conc. 8 gm solute/kgm solvent

[++]Conc. 8 gmole solute/kgm solvent

[+++]98.6 percent accuracy

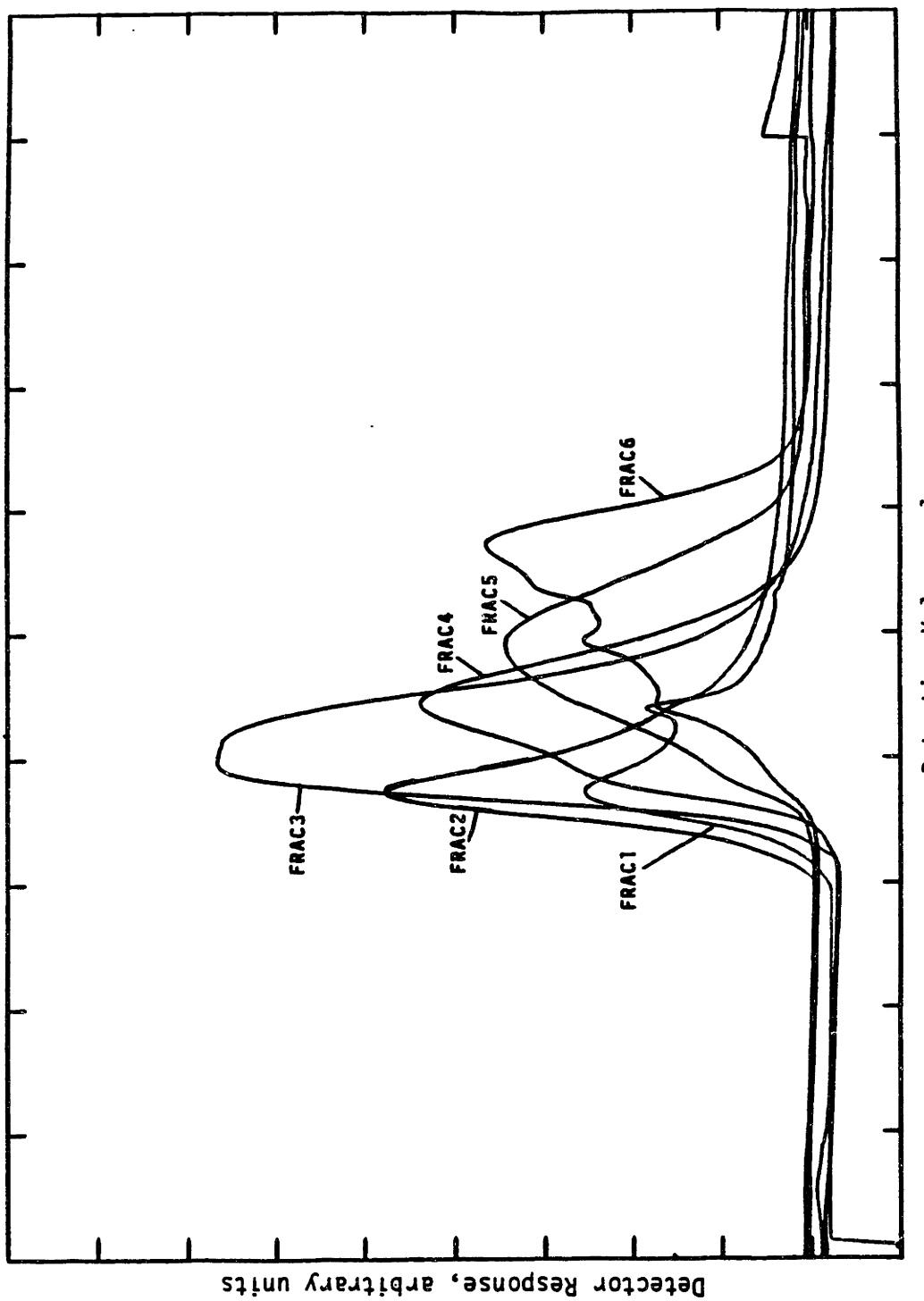

FIG, B.1, GPC CHROMATOGRAM OF 6 FRACTIONS

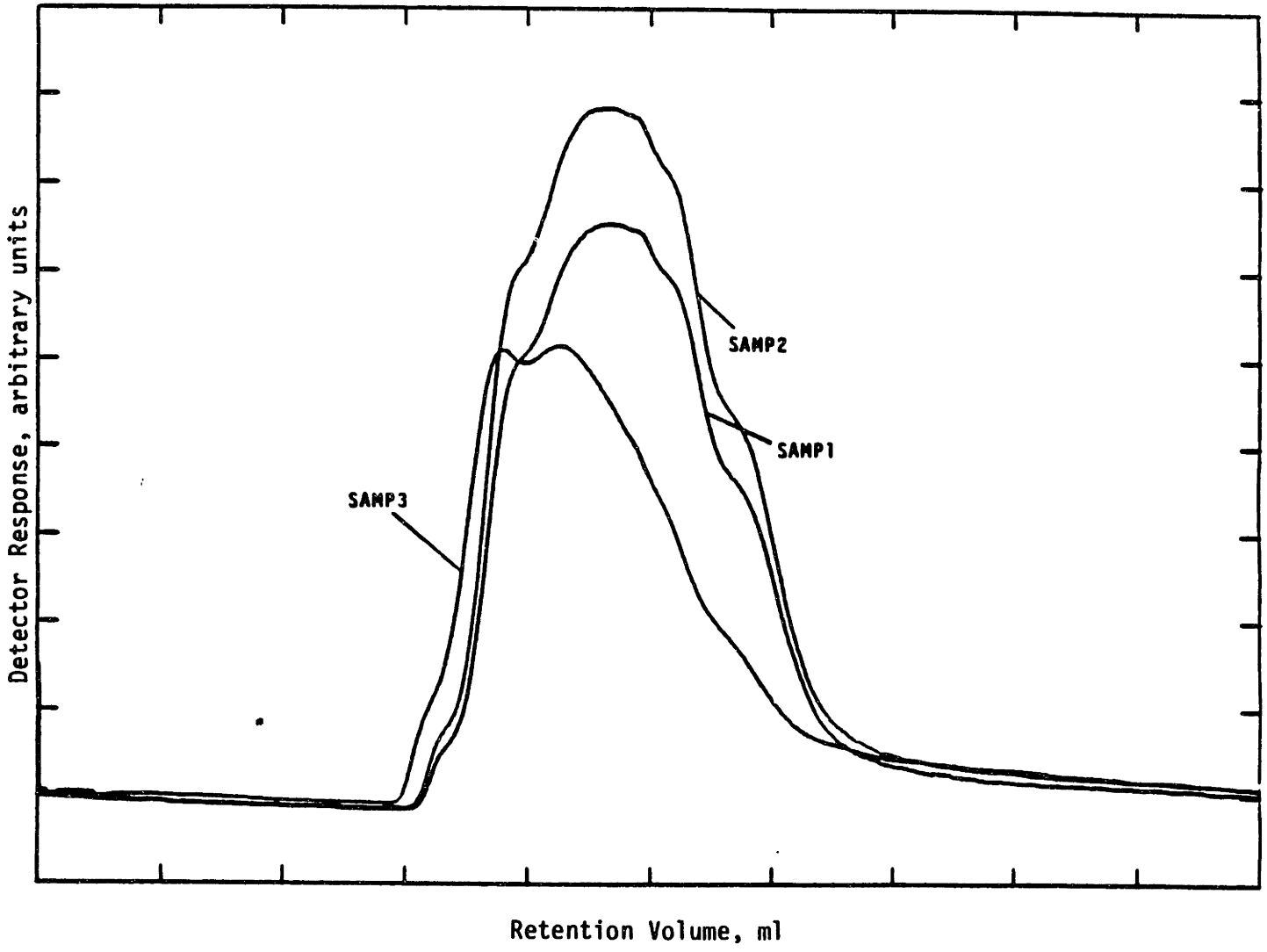

FIG. B.2. GPC CHROMATOGRAM OF 3 SAMPLES

In an improved version, a compensation is provided for the symmetric peak broadening caused by column dispersion effects:

$$M_n = \frac{e^{\frac{1}{2}(D_2\sigma)^2} \sum_{j=1}^{N} h_j(V_j)}{\sum_{j=1}^{N} h_j(V_j)/D_1 e^{-D_2 V_j}}$$

Two known molecular weight samples and σ are required for evaluation of the two constants, D_1 and D_2. However, to increase the precision of the method it is also possible to use more than two sets of data to obtain best fit values of these parameters by the method of least squares. The latter is chosen here.

The instrumental peak broadening, σ, is approximated from the GPC chromatogram of anthracene and is assumed to be independent of retention volume. The number-average molecular weights obtained from VPO are used as input values for Mn and chromatograms of 3 fractions and 3 unfractionated samples were used to determine D_1 and D_2.

B.2. Result and Discussion

Table B.3 summarizes calibration equations obtained from the two calibration methods and molecular weights of fractions calculated from these two equations. Eliminating fraction 3 from the data analysis gives a far better fit to the rest of the data in the peak position method. Calibration lines are plotted in Fig. B.3, and agreement between the two methods is satisfactory. The calibration line from the linear calibration method gives a smaller error in predicting molecular weights of samples and it will be used for analyzing data on coal tar and coal tar extracts.

Table B.3. Calibration Equations and Molecular Weights of Samples Predicted by the Peak Position and Linear Calibration Methods.

3-a. Calibration Equations: log(MW)

Peak Position Method:	-0.1120481 v + 4.3433706	(1)
Linear Calibration Method:	-0.096500 v + 4.1814	(2)

3-b. Molecular Weight of Fractions

	VPO	Eqn (1)	Eqn (2)
Frac 1	582.3	633.762	721.75
Frac 2	738.1	618.23	708.12
Frac 3	796.6	--	602.52
Frac 4	420.8	433.27	521.36
Frac 5-6	266.1	294.03	373.50
Frac 7-10	223.8	213.24	283.77
Samp 1	430.5	296.89	380.55
Samp 2	453.9	300.624	384.69
Samp 3	549.8	406.488	498.27

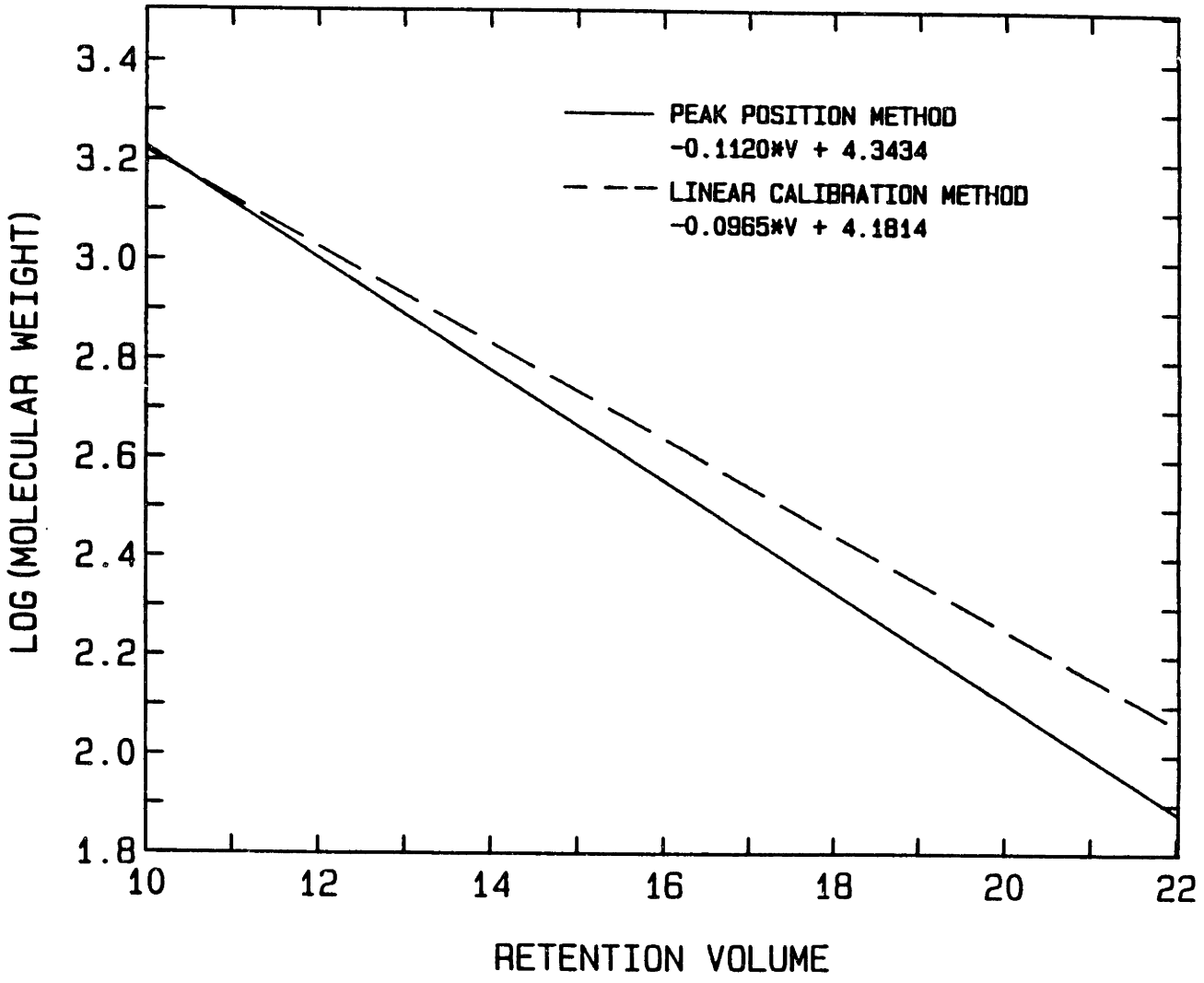

FIG. B.3. COMPARISON OF CALIBRATION METHOD

APPENDIX C:

MODELING HEAT TRANSFER FROM ELECTRICALLY HEATED SCREEN TO COAL PARTICLES

Because of the importance of coal particle time-temperature history in pyrolysis studies, accurate measurements of the coal particle temperature are desired. This appendix presents the derivations to obtain the coal particle temperature as a function of time and the difference between the measurement by a thermocouple and the true coal particle temperature. Heat balances were made on coal particles, thermocouple and the surrounding gas. Resulting non-linear ordinary differential equations were solved numerically.

For the formulation of heat balances, the following assumptions were made;

(1) Spherical coal particles which maintain the shape and size during pyrolysis.

(2) Coal particles form monolayer in a hexagonal close packed arrangements. (See Fig. C.1.a and b)

(3) Spherical thermocouple bead which has the same diameter as the coal particles.

(4) The spacing between the screen folds is the same as the particle diameter.

(5) The screen is flat and is tangent to the particles.

(6) Both the coal particles and thermocouple have no temperature gradient inside the particle. (i.e., Biot No = 0)

The Biot number of the thermocouple bead is on the order of 0.01 and the thermocouple can therefore be treated as a spatially isothermal particle without further arguments. For coal particles, the Biot number is on the order of one. However, the temperature difference between the surface and the center of the particle is around 1 °C at the heating rate of 1000 °C/sec and 10 °C at 10^4 °C/sec due to the small particle size and the

(a)

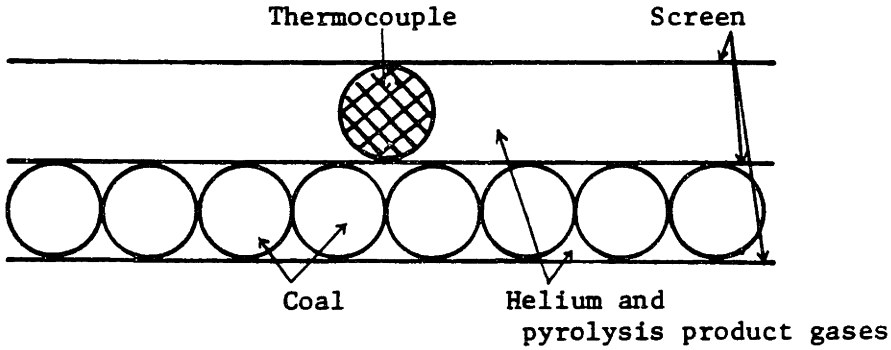

(b)

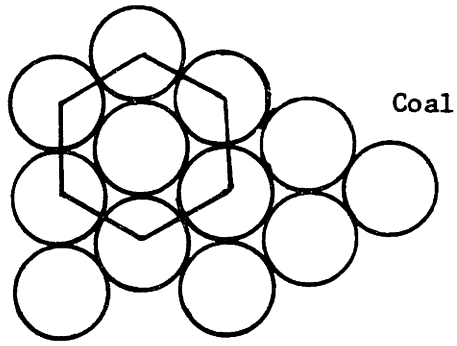

Fig. C.1. Idealized system of screen, thermocouple, and coal particles (a) side view, (b) top view of hexagonal arrangement of coal particles.

coal particle can be also treated as an isothermal particle.

C.1. Heat Balances

Coal Particles

The energy conservation law is applied to a particle:

$$\rho_c C_{p,c} V_c \frac{dT_c}{dt} = A_c h_1 (T_{eq} - T_c) + R_r^{-1} A_c \sigma (T_s^4 - T_c^4) + -\Delta H_r m_o \frac{dV}{dt} \quad \text{(C-1)}$$

where ρ_c = Density of coal

$C_{p,c}$ = Heat capacity of coal

V_c = Volume of a coal particle, constant

A_c = Surface area of a coal particle, constant

h_1 = Heat transfer coefficient from the surrounding gas to coal particles

R_r = Radiative heat transfer resistance

σ = Stefan-Boltzman's

$-\Delta H_R$ = Heat of pyrolysis

m_o = Original mass of a coal particle

dV/dt = Rate of reaction

T_c = Temperature of coal particle

T_s = Temperature of screen

T_g = Temperature of surrounding gas

The second term in the right hand side of Eq. C-1. represents the heat transfer by radiation and the radiative heat transfer resistance, R_r, between two elements 1 and 2 is defined as the following:

$$R_r = \left(\frac{1-\varepsilon_1}{\varepsilon_1 A_1} + \frac{1}{A_1 F_{12}} + \frac{1-\varepsilon_2}{\varepsilon_2 A_2} \right) A_1 \quad \text{(C-2)}$$

where ε_1 is the emissivity of element 1 and F_{12} is a view factor. The area of the screen available for the radiative heat exchange (A_2) is bound in the hexagon shown in Fig. C.1.b ($A_2 = 12\sqrt{3}\ R^2$, including both top and bottom of the screen). The radiation coming out of A_2 is distributed to three particles, one in the center and six one-third particles surrounding the center particle. Then $A_1F_{12} = A_2F_{21} = A_2(1/3)$ and

$$R_r = \frac{1-\varepsilon_c}{\varepsilon_c} + \frac{\pi}{\sqrt{3}} + \frac{1-\varepsilon_s}{\varepsilon_s}\frac{\pi}{3\sqrt{3}} \qquad \text{(C-3)}$$

For the thermocouple, A2 >> A_1, and $F_{12} = 1$. Then R_r becomes $1/\varepsilon_{tc}$.

The last term in Eq. C-1 accounts for the heat of reaction during pyrolysis if there is any significant heat released or absorbed. A simple first order reaction model is used to describe the rate of reaction:

$$\frac{dV}{dt} = k\ (\ V^* - V\ ) = k_o\ e^{-E/RT}\ (\ V^* - V\ ) \qquad \text{(C-4)}$$

where V = Amount of volatiles lost up to time t per unit mass

k_o = Pre-exponential facotr, 1000/sec

E = Activation energy, 12220 cal/mole

V^* = V at t = ∞, 0.4752

The kinetic constants were obtained by fitting volatiles yield data presented in Fig. 4.3.1 (Chapter 4) to a single reaction model. The changes in coal particle density due to pyrolysis is described as follows:

$$\rho_c = \rho_o\ (\ 1 - V\ ) \qquad \text{(C-5)}$$

Screen

The screen is heated by resistance heating and the heat input to the screen is assumed to be constant during heating period. Then the screen tempera-

ture is modeled as a linear function of time:

$$T_s = m\,t + T_o \qquad \text{(C-6)}$$

where m is the heating rate. During cooling period, the screen is cooled naturally due to conduction, convection and radiation:

$$\frac{dT_s}{dt} = a\,(T_s^4 - T_o^4) + b\,(T_s - T_o) \qquad \text{(C-7)}$$

where a and b are constants. Assuming the screen temperature is much larger than that of the surroundings, T_o, The solution to the above equation is

$$T_s = \frac{b/a}{\left(1 + \frac{b}{aT_p^3}\right)\exp(3b(t-t_p)) - 1} \qquad \text{(C-7)}$$

where T_p and t_p are the peak temperature and the time when the peak temperature is reached. Typical values of a and b derived from experimental data are $2.20 \times 10^{-10}\ K^{-3}\ sec^{-1}$ and $6.73 \times 10^{-2}\ sec^{-1}$.

Thermocouple

The energy balance on the thermocouple is

$$\rho_{tc} C_{p,tc} V_{tc} \frac{dT_{tc}}{dt} = A_{tc} h_2 (T_g - T_{tc}) + R_{r,tc}^{-1}\,\sigma\,A_{tc}(T_s^4 - T_{tc}^4) \qquad \text{(C-8)}$$

where ρ_{tc} = Density of thermocouple, constant

$C_{p,tc}$ = Heat capacity of thermocouple

V_{tc} = Volume of thermocouple

A_{tc} = Surface area of thermocouple

h_2 = Heat transfer coefficient from the surrounding gas to thermocouple

$R_{r,tc}$ = Radiative heat transfer resistance, $1/\varepsilon_{tc}$

T_{tc} = Temperature of thermocouple

Gas surrounding coal particles and thermocouple

The third heat balance is made on the gas surrounding the coal particles. The heat balance is applied to the volume enclosed by three coal particles and the screen as shown in Fig. C.1.

$$\rho_g C_{p,g} V_g \frac{dT_g}{dt} = - A_c h_1 (T_c - T_g) + A_s h_3 (T_s - T_g) \qquad (C\text{-}9)$$

$$+ \dot{m}'_{in} C_{p,g} T_c - \dot{m}'_{out} C_{p,g} T_g$$

The convective mass flow into the system defined from coal particles, m_{in}, due to pyrolysis is calculated from the first order reaction model:

$$\dot{m}'_{in} = 3 m_o k_o \exp(-E/RT) (V^* - V) \qquad (C\text{-}10)$$

The pressure build-up due to heating and the accumulaton of product gases causes convective flow out of the system, m_{out}. However, for a simplification, the steady state is assumed ($m_{in} = m_{out}$), and the last two terms in Eq. C-5 become

$$\dot{m}'_{in} C_{p,g} (T_c - T_g) \qquad (C\text{-}11)$$

and to calculate the mass of gases in the volume defined the gas density is evaluated at room temperature and at the system pressure to be consistant with the steady state assumption.

For the gas surrounding the thermocouple, the energy balance is

$$\rho_g C_{p,g} \frac{dT_g'}{dt} = \frac{k_g}{R^2} (T_p - T_g') \qquad \text{(C-12)}$$

In the four heat balances, the only independant variable is time and the rest of the variables are obtained by solving the above equations simultaneously. Due to the differences in heat transfer mechanisms, the separate solutions are worked out for atmospheric pressure and for vacuum.

C.2. Derivation of Heat Transfer Coefficients

At atmospheric and higher pressures

Heat transfer coefficients at atmospheric and higher pressures are derived assuming a conduction layer around a sphere or a plate.

Coal : Assume a thin layer of gas film around a coal particle, the volume of which is the same as the volume of the gas around a particle as shown in Fig. C.1.b. The radius of the outer film surface is 1.436 R and R_{av}, where the temperature is the same as the average temperature of the film is 1.231 R. Then

$$\frac{h_1 R}{k_g} = \frac{1}{1 - \frac{R}{R_{av}}} = 5.329 \qquad \text{(C-13)}$$

Thermocouple : The radius of the outer film surface is ∞ and

$$\frac{h_2 R}{k_g} = 1 \qquad \text{(C-14)}$$

Screen : Again, assume a thin layer of gas film, the volume of which is the same as the gas volume around a coal particle. Assuming a linear temperature profile

$$T = \frac{T_g - T_o}{y_{av}} y + T_o \qquad \text{(C-15)}$$

where $y_{av} = 0.198\ R$. Then the Nusselt number is

$$\frac{h_3 R}{k_g} = \frac{R}{y_{av}} = 5.057$$

To test the uncertainties in the above derivations, the heat transfer coefficients are varied and the sensitivity of the solution to these parameters is discussed in the later section.

Heat transfer coefficients in vacuum (0.0001 atm) pyrolysis

At low pressures, a gas medium loses its identity as a continous fluid and analysis of transfer processes must be based entirely on molecular theory. This flow regime is referred as free molecular. In vacuum pyrolysis, pressures less than 1.495×10^{-3} atm at 1000°C belong to the free molecular regime. The heat transfer coefficient is quite different from that at 1 atm. Assuming undisturbed molecular streams incident on a surface, Rosenow and Choi(1961) derived a heat transfer coefficient for a stagnant medium:

$$h = \left(\frac{R'T}{2}\right)^{1/2} \left(\frac{3}{2} R'\right) \qquad \left[\frac{\text{cal}}{\text{cm}^2\ \text{s}\ ^\circ\text{C}}\right] \qquad \text{(C-17)}$$

where R' is the gas constant per mass. More complicated expressions are

also available in literature(Eckert and Drake, Jr., 1972; Kyte et al., 1953). However, the simple expression shown above gives larger h values than the more complicated expressions and is employed here to test the upper limit contribution of convective heat transfer at low pressures.

C.3. Physical Properties

Thermal diffusivity and conductivity of coal

Badzioch, Gregory and Field(1964) investigated thermal diffusivity and conductivity of several different types of coals. The mean values are expressed as a function of temperature[°C]. For thermal conductivity, k, [cal/cm s C]

$T < 430$°C	5.5×10^{-4}
$430 < T < 610$°C	$(0.0389\ T - 11.22) \times 10^{-4}$
$T > 610$°C	$(0.102\ T - 49.6) \times 10^{-4}$

for thermal diffusivity, $, [cm2/s]

$T < 660$°C	1.2×10^{-3}
$T > 660$°C	$1.66 \times 10^{-4}\ T - 0.108$

Thermal diffusivity and conductivity are plotted as a function of temperature in Figures C.2 and C.3.

Thermal conductivity of helium

The thermal conductivity of helium is obtain from J. of Phys. and Chem. Reference Data, Vol. 3, (1974)

$$k_{he} = 6.525 \times 10^{-7}\ T + 3.672 \times 10^{-4} \qquad [cal/cm\ s\ °C]$$

where T is in °C.

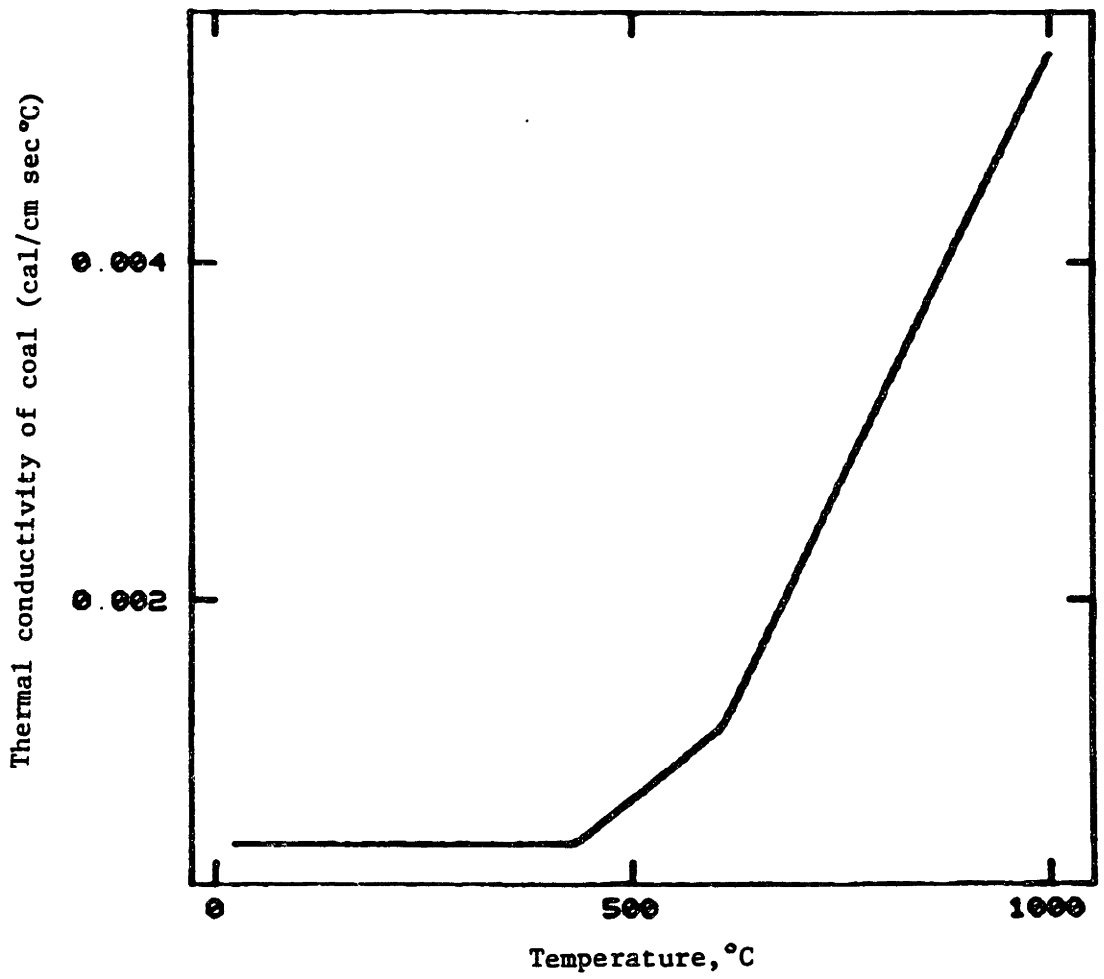

Fig. C.2. Thermal conductivity of coal as a function of temperature

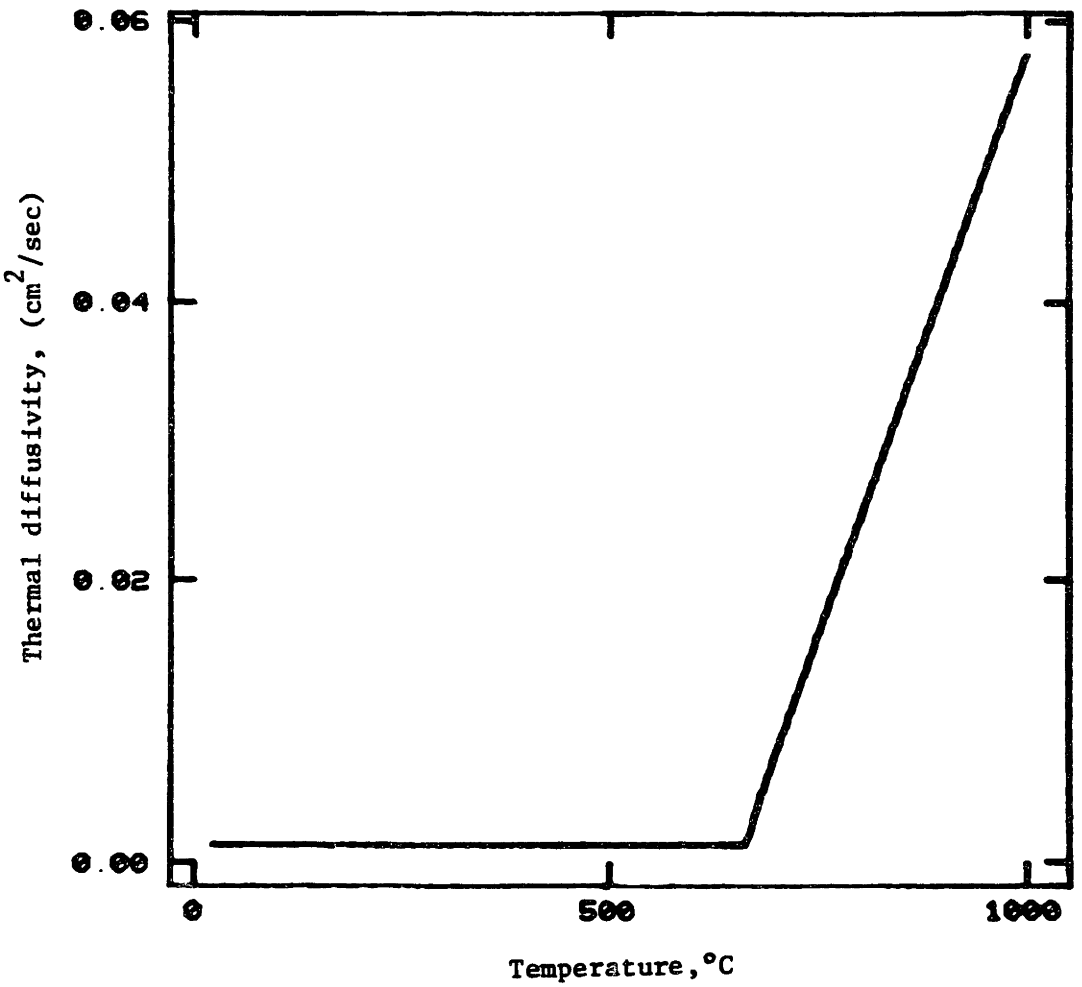

Fig. C.3. Thermal diffusivity of coal as a function of temperature

Heat Capacities

Thermocouple: Assuming the thermocouple bead is made of 50% Chromel and 50% Alumel, $C_{p,tc}$ is

$$C_{p,tc} = 0.09882 + 3.035 \times 10^{-5} T \qquad [cal/gm\ K]$$

where T is in Kelvin (Gangopadhyay and Margrave, 1963).

Coal: The heat capacity of coal is assumed to be the same as graphite;

$$C_{p,c} = 0.2228 + 0.0218\ T - 9.7417 \times 10^{8}/T^{2} \qquad [cal/gm\ K]$$

where T is in Kelvin.

Gases: The coal particles and the thermocouple are surrounded by Helium and the pyrolysis product gases which compose of H_2O, CO_2, CO and light hydrocarbons. The average molecular weight of the product gas is 28 and the heat capacity is

$$C_{p,g} = 0.283 + 1.457 \times 10^{-4}\ T - 4.082 \times 10^{-8}\ T^{2} \quad [cal/gm°C]$$

where T is in°C.

Heat of reactions

The heat of raction, $-\Delta Hr$, is taken as 0, 1.78 and -1.78 Kcal/gm (Suuberg, 1977) and its effect on the coal temperature is studied.

Densities

Gases: Calculated from ideal gas law.

Thermocouple: 8.7 gm/cm^3

Coal: 1.3 gm/cm^3

C.4. Result and Discussion

At 1 atm and higher pressures

At atmospheric and higher pressures, most of the heat transfer is

achieved by the conduction through gases. An order of magnitude analysis shows that the maximum contribution of the radiative heat transfer is ~1 % of the total at high temperatures and thus the radiation terms are neglected in actual calculations. Table C.1 gives the result of calculation at the heating rate of 1000 °C/s with $-\Delta Hr = 0$. The peak temperature of the screen is 1000 °C. During heating, the coal particle temperature is practically the same as the screen temperature and it differs slightly from the thermocouple temperature (by 5 °C the maximum). During the cooling period, the three temperature are all within 1 to 2 °C of each other. The heat transfer from the screen to the gases around the coal particles and the thermocouple is very fast and the gas temperatures are set to be the same as the screen temperature to eliminate the stiffness in the numerical scheme.

The larger temperature lag in the thermocouple from the screen temperature is caused by the differences in the thermal masses (ρCp) of coal and thermocouple and in the heat transfer coefficients. The thermal mass of a chromel-alumel thermocouple is approximately 1.7 times more than that of coal and, thus, it takes longer or takes more energy to heat the thermocouple to the same temperature as the surroundings. Changing the heat transfer coefficient to the coal particles to the same value as the one to the thermocouple ($h_1 = h_2$) reduces the maximum temperature difference between two elements to 3 °C. The heat of reaction is small, and varying $-\Delta H_r$ from -1.78 to 1.78 Kcal/gm makes a small change in coal particle temperature ($\pm$ 2 °C the maximum).

In actual experiments, the screen is not a flat plate and coal particles are not perfect spheres in hexagonal arrangement forming monolayer. Therefore, it is also possible that coal particles are heated by the direct

Table C.1. Time-temperature histories of screen, gases, thermocouple, and coal particles at 1 atm.

HEATING RATE = 0.10000D+04
HEAT OF REACTION= 0.00000D+00

Time	Temperature			
	Coal	Thermo-couple	Gas	Screen
0.50000D-01	0.69484D+02	0.60565D+02	0.70000D+02	0.70000D+02
0.10000D+00	0.11945D+03	0.11109D+03	0.12000D+03	0.12000D+03
0.15000D+00	0.16944D+03	0.16160D+03	0.17000D+03	0.17000D+03
0.20000D+00	0.21942D+03	0.21204D+03	0.22000D+03	0.22000D+03
0.25000D+00	0.26943D+03	0.26242D+03	0.27000D+03	0.27000D+03
0.30000D+00	0.31942D+03	0.31276D+03	0.32000D+03	0.32000D+03
0.35000D+00	0.36945D+03	0.36307D+03	0.37000D+03	0.37000D+03
0.40000D+00	0.41944D+03	0.41334D+03	0.42000D+03	0.42000D+03
0.45000D+00	0.46947D+03	0.46358D+03	0.47000D+03	0.47000D+03
0.50000D+00	0.51945D+03	0.51380D+03	0.52000D+03	0.52000D+03
0.55000D+00	0.56949D+03	0.56401D+03	0.57000D+03	0.57000D+03
0.60000D+00	0.61951D+03	0.61419D+03	0.62000D+03	0.62000D+03
0.65000D+00	0.66957D+03	0.66436D+03	0.67000D+03	0.67000D+03
0.70000D+00	0.71954D+03	0.71452D+03	0.72000D+03	0.72000D+03
0.75000D+00	0.76956D+03	0.76466D+03	0.77000D+03	0.77000D+03
0.80000D+00	0.81962D+03	0.81480D+03	0.82000D+03	0.82000D+03
0.85000D+00	0.86963D+03	0.86492D+03	0.87000D+03	0.87000D+03
0.90000D+00	0.91970D+03	0.91504D+03	0.92000D+03	0.92000D+03
0.95000D+00	0.96973D+03	0.96514D+03	0.97000D+03	0.97000D+03
0.98000D+00	0.99976D+03	0.99521D+03	0.10000D+04	0.10000D+04
0.10300D+01	0.96842D+03	0.97126D+03	0.96830D+03	0.96830D+03
0.10800D+01	0.93945D+03	0.94201D+03	0.93925D+03	0.93925D+03
0.12800D+01	0.84320D+03	0.84528D+03	0.84312D+03	0.84312D+03
0.14800D+01	0.76917D+03	0.77087D+03	0.76910D+03	0.76910D+03
0.16800D+01	0.70942D+03	0.71087D+03	0.70937D+03	0.70937D+03
0.18800D+01	0.65962D+03	0.66085D+03	0.65955D+03	0.65955D+03
0.20800D+01	0.61702D+03	0.61812D+03	0.61697D+03	0.61697D+03
0.22800D+01	0.57991D+03	0.58091D+03	0.57988D+03	0.57988D+03
0.24800D+01	0.54712D+03	0.54802D+03	0.54708D+03	0.54708D+03
0.26800D+01	0.51775D+03	0.51859D+03	0.51773D+03	0.51773D+03
0.28800D+01	0.49122D+03	0.49199D+03	0.49119D+03	0.49119D+03
0.30800D+01	0.46701D+03	0.46773D+03	0.46698D+03	0.46698D+03
0.32800D+01	0.44481D+03	0.44545D+03	0.44475D+03	0.44475D+03
0.34800D+01	0.42422D+03	0.42486D+03	0.42420D+03	0.42420D+03
0.36800D+01	0.40515D+03	0.40572D+03	0.40510D+03	0.40510D+03
0.38800D+01	0.38729D+03	0.38785D+03	0.38727D+03	0.38727D+03
0.40800D+01	0.37056D+03	0.37110D+03	0.37054D+03	0.37054D+03
0.42800D+01	0.35482D+03	0.35533D+03	0.35479D+03	0.35479D+03
0.44800D+01	0.33995D+03	0.34043D+03	0.33992D+03	0.33992D+03
0.46800D+01	0.32584D+03	0.32632D+03	0.32583D+03	0.32583D+03
0.48800D+01	0.31248D+03	0.31292D+03	0.31245D+03	0.31245D+03
0.50800D+01	0.29971D+03	0.30016D+03	0.29970D+03	0.29970D+03
0.52800D+01	0.28758D+03	0.28798D+03	0.28753D+03	0.28753D+03
0.54800D+01	0.27591D+03	0.27632D+03	0.27590D+03	0.27590D+03
0.56800D+01	0.26475D+03	0.26516D+03	0.26474D+03	0.26474D+03
0.58800D+01	0.25406D+03	0.25444D+03	0.25404D+03	0.25404D+03
0.60800D+01	0.24376D+03	0.24414D+03	0.24375D+03	0.24375D+03

conduction from the screen. At 1 atm or higher pressures, however, the gas temperature is the same as the screen temperature and the coal particle temperature is indeed following the screen temperature very closely. Irregularities in geometry of coal particles do not make a significant impact in heat transfer mechanisms.

At low pressures (~0.0001 atm)

The most of heat transfer at very low pressures is by radiation. The contribution of convective heat transfer is approximately 13 % of the total heat transfer at around 400°C of coal particle temperature and becomes smaller at higher temperatures. The result of the calculation at low pressure heat transfer is shown in Table C.2 and Fig. C.4. While the screen temperature increases linearly with time, the temperatures of coal and thermocouple start to increase slowly after 0.5 second and reach the peak temperatures of 867 and 795°C, respectively.

At low pressures, the time-temperature history of each element shows a strong dependence on its physical properties such as density, heat capacity, and emissivity. The larger temperature difference in thermocouple is again due to the larger thermal mass. In the calculations of radiative heat transfer, the values for emissivity of each element are more or less uncertain. Values for emissivities are listed in Table C.2. Assuming blackbody radiation between all elements, $\varepsilon = 1$, increases the peak temperatures of coal and thermocouple to 886 and 859°C, and reduces the temperature difference between coal and thermocouple (See Fig. C.5)

Because of poor conductive heat transfer through the surrounding gas, the direct conduction from the screen may play an important role in heat transfer at low pressures. Niksa (1981) modeled the heat transfer from the electrically heated screen to coal at low pressures by assuming a thin slab

Table C.2. Time-temperature histories of screen, gases, thermocouple, and coal particles at 0.0001 atm.

HEATING RATE = 0.10000D+04
HEAT OF REACTION= 0.00000D+00
EMISSIVITY OF COAL= 0.70
EMISSIVITY OF THERMOCOUPLE= 0.70
EMISSIVITY OF SCREEN= 0.90

Time	Temperature			
	Coal	Thermo-couple	Gas	Screen
0.50000D-01	0.21119D+02	0.20324D+02	0.43296D+02	0.70000D+02
0.10000D+00	0.24554D+02	0.21382D+02	0.68017D+02	0.12000D+03
0.15000D+00	0.30414D+02	0.23326D+02	0.94046D+02	0.17000D+03
0.20000D+00	0.38848D+02	0.26357D+02	0.12146D+03	0.22000D+03
0.25000D+00	0.50051D+02	0.30729D+02	0.15039D+03	0.27000D+03
0.30000D+00	0.64269D+02	0.36758D+02	0.18094D+03	0.32000D+03
0.35000D+00	0.81794D+02	0.44818D+02	0.21329D+03	0.37000D+03
0.40000D+00	0.10297D+03	0.55347D+02	0.24761D+03	0.42000D+03
0.45000D+00	0.12817D+03	0.68849D+02	0.28409D+03	0.47000D+03
0.50000D+00	0.15781D+03	0.85890D+02	0.32302D+03	0.52000D+03
0.55000D+00	0.19229D+03	0.10709D+03	0.36454D+03	0.57000D+03
0.60000D+00	0.23202D+03	0.13312D+03	0.40889D+03	0.62000D+03
0.65000D+00	0.27732D+03	0.16468D+03	0.45631D+03	0.67000D+03
0.70000D+00	0.32843D+03	0.20246D+03	0.50686D+03	0.72000D+03
0.75000D+00	0.38544D+03	0.24714D+03	0.56071D+03	0.77000D+03
0.80000D+00	0.44827D+03	0.29930D+03	0.61776D+03	0.82000D+03
0.85000D+00	0.51668D+03	0.35935D+03	0.67815D+03	0.87000D+03
0.90000D+00	0.59027D+03	0.42745D+03	0.74146D+03	0.92000D+03
0.95000D+00	0.66860D+03	0.50340D+03	0.80783D+03	0.97000D+03
0.98000D+00	0.71750D+03	0.55235D+03	0.84578D+03	0.99161D+03
0.10300D+01	0.78395D+03	0.62458D+03	0.86898D+03	0.96063D+03
0.12300D+01	0.86657D+03	0.77306D+03	0.86631D+03	0.85901D+03
0.14300D+01	0.82238D+03	0.79521D+03	0.80502D+03	0.78161D+03
0.16300D+01	0.76208D+03	0.77196D+03	0.74328D+03	0.71963D+03
0.18300D+01	0.70843D+03	0.73594D+03	0.69040D+03	0.66820D+03
0.20300D+01	0.66250D+03	0.69833D+03	0.64534D+03	0.62443D+03
0.22300D+01	0.62278D+03	0.66261D+03	0.60635D+03	0.58642D+03
0.24300D+01	0.58791D+03	0.62970D+03	0.57204D+03	0.55290D+03
0.26300D+01	0.55687D+03	0.59963D+03	0.54147D+03	0.52296D+03
0.28300D+01	0.52894D+03	0.57215D+03	0.51392D+03	0.49593D+03
0.30300D+01	0.50357D+03	0.54697D+03	0.48887D+03	0.47133D+03
0.32300D+01	0.48033D+03	0.52380D+03	0.46596D+03	0.44875D+03
0.34300D+01	0.45891D+03	0.50237D+03	0.44481D+03	0.42791D+03
0.36300D+01	0.43904D+03	0.48248D+03	0.42516D+03	0.40855D+03
0.38300D+01	0.42053D+03	0.46392D+03	0.40686D+03	0.39049D+03
0.40300D+01	0.40320D+03	0.44655D+03	0.38971D+03	0.37357D+03
0.42300D+01	0.38690D+03	0.43022D+03	0.37358D+03	0.35765D+03
0.44300D+01	0.37153D+03	0.41482D+03	0.35840D+03	0.34263D+03
0.46300D+01	0.35698D+03	0.40026D+03	0.34395D+03	0.32840D+03
0.48300D+01	0.34317D+03	0.38645D+03	0.33027D+03	0.31489D+03
0.50300D+01	0.33002D+03	0.37332D+03	0.31725D+03	0.30203D+03
0.52300D+01	0.31748D+03	0.36080D+03	0.30484D+03	0.28976D+03
0.54300D+01	0.30549D+03	0.34883D+03	0.29296D+03	0.27802D+03
0.56300D+01	0.29399D+03	0.33738D+03	0.28157D+03	0.26678D+03
0.58300D+01	0.28296D+03	0.32639D+03	0.27065D+03	0.25600D+03
0.60300D+01	0.27235D+03	0.31583D+03	0.26015D+03	0.24563D+03

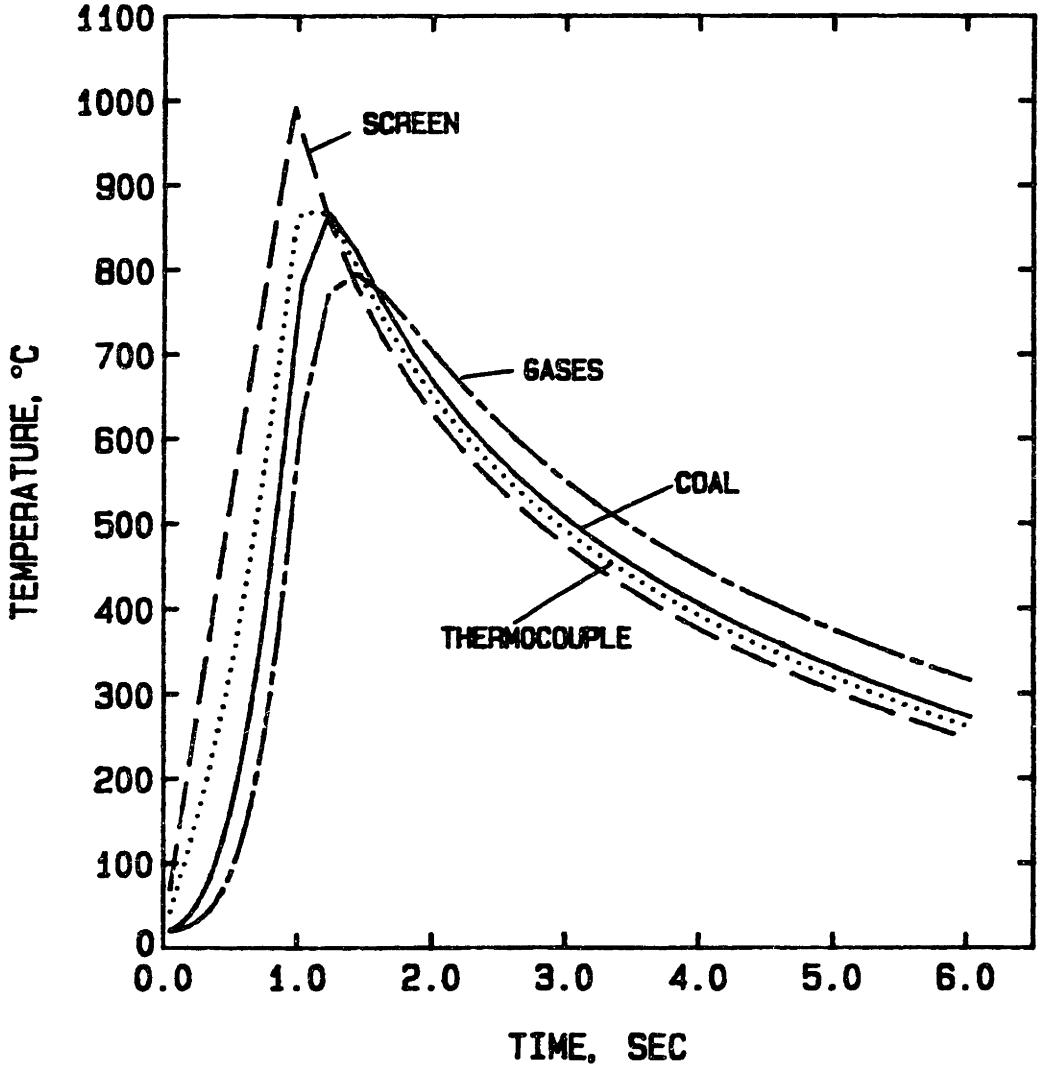

Fig. C.4. Time-temperature histories of screen, gases, thermocouple, and coal particles as heated by radiative heat transfer at 0.0001 atm. (Heating rate of the screen and emissivity of each element are as listed in Table C.2.)

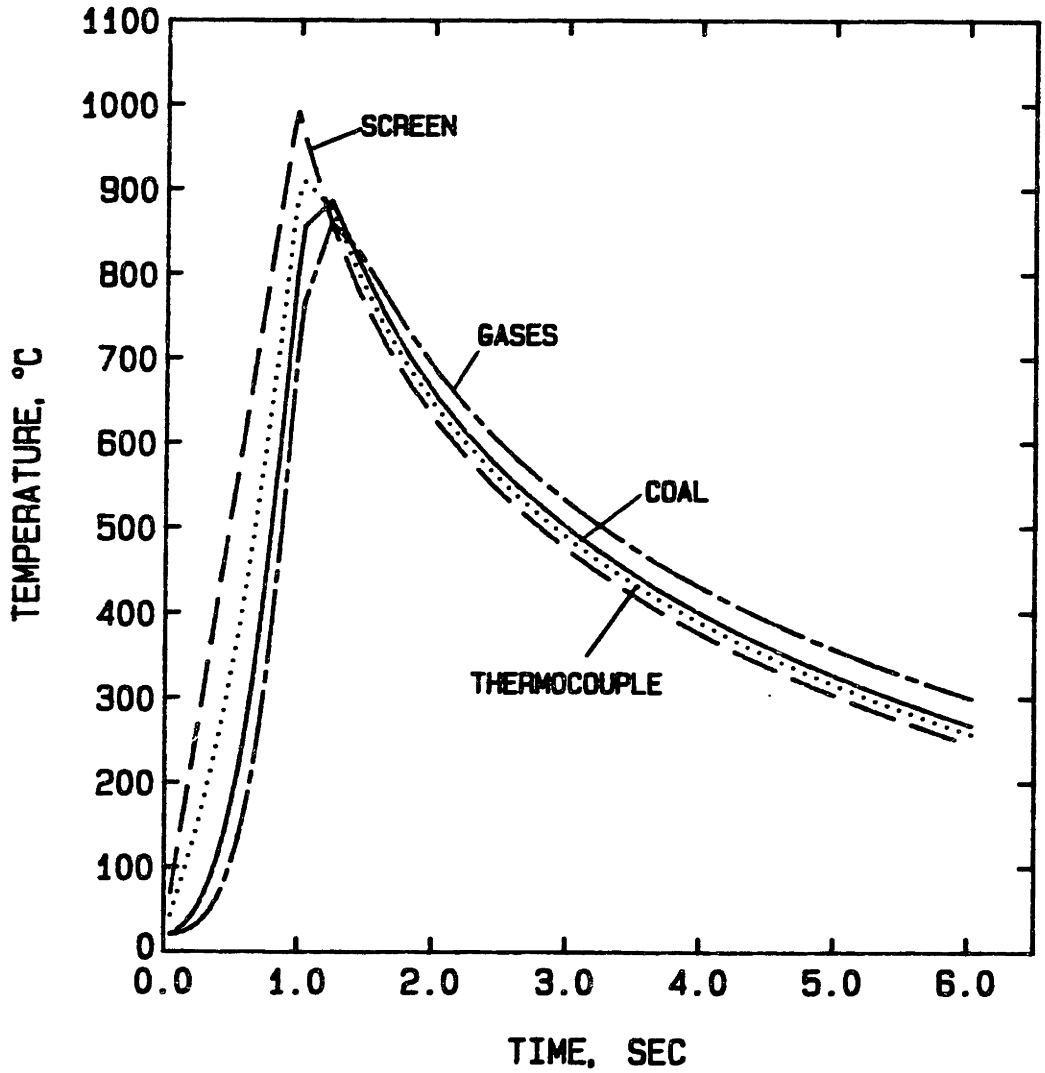

Fig. C.5. Time-temperature histories of screen, gases, thermocouple, and coal particles as heated by blackbody radiation at 0.0001 atm. (Heating rate of the screen = 1000°C/sec)

of coal in contact with the screen. Within the uncertainties of temperature dependant thermal diffusivity of coal, Niksa found that the coal particle temperature lag could reach up to 175°C when the thickness of the slab is 250 μm. He also found that the temperature lag becomes smaller at high temperatures (> 600°C) due to rapidly increasing thermal diffusivity.

In the heating system employed in this work, the power input is preset regardless of the pressure and the thermocouple measures the temperatures in a similar range at both pressures for a given power input. This observation is not possible if the radiation is the only heat transfer mechanism. Therefore, it is possible that the coal and thermocouple are heated directly from the screen and since the thickness of the coal slab is less than 100 μm, the coal temperature in this work is expected to have smaller temperature lag than Niksa have calculated at low temperatures and good agreement with the screen and thermocouple temperature at high temperatures. However, in the case of the thermocouple, the measurements can be made only after the current is cut off and the actual average coal particle temperature is very sensitive to the thickness of the sample. Therefore, there will be more uncertainties in temperatures measured by the thermocouple at this pressure.

C.4. Conclusion

At atmospheric and higher pressures, convective heat transfer from the surrounding gases dominates and the thermocouple and coal particle temperatures are very close. The coal particle temperature is not much affected by either the heat of pyrolysis or the heat transfer coefficients at the heating rate of 1000°C/s.

Under vacuum conditions, the contribution of convective heat transfer is not important and the radiation and the direct condcution from the screen play important roles. The agreement between the coal and thermocouple temperatures depends on physical properties such as thermal prperties and emissivities, and also depends on the thickness of the sample load on the screen.

APPENDIX D: NATURAL CONVECTION FLOW INSIDE THE REACTOR AND THE EXTENT OF TAR CRACKING IN A HOT ZONE NEAR THE SCREEN AT 1 ATM PYROLYSIS

As the screen is heated to a high temperature ($T > 600\,^{o}C$), one can observe convective current carrying volatiles away from the screen at 1 atm or higher pressures. This observation is possible because of the evolution of brown colored tar.

The numerical simulation of this convective flow is very difficult because a rigorous analysis requires three dimentional non-linear momentum balance which is coupled with heat transfer equations. However, the objective here is to obtain the estimates of the thickness of the momentum and thermal boundary layers and, therefore, to estimate the extent of secondary reactions of tar in a hot zone near the screen. This appendix first presents generalized governing equations in a free convection system and then gives simplified solutions to the problem.

In a free convection system, the velocity gradients result entirely from temperature differences and the fluid motion is usually slow if the temperature differences are not too big. Then, one can estimate

$$\nabla P = \mathbf{g}\,\bar{\rho}$$

in which $\bar{\rho}$ is the fluid density at $\bar{T}$ and at the local pressure. The momentum equation becomes

$$\rho\left(\frac{\partial v}{\partial t} + v_x\frac{\partial v}{\partial x} + v_y\frac{\partial v}{\partial y} + v_z\frac{\partial v}{\partial z}\right) = -(\nabla\cdot T) - \rho g\beta(T - \bar{T})$$

and assuming ideal gas, the energy balance becomes

$$\rho C_p\left(\frac{\partial T}{\partial t} + v_x\frac{\partial T}{\partial x} + v_y\frac{\partial T}{\partial y} + v_z\frac{\partial T}{\partial z}\right) = -(\nabla\cdot q) + \frac{DP}{Dt}$$

Now, to describe the convective flow in the vicinity of the heated screen in the batch reactor, assume the following:

(1) Steady-state newtonian fluid

(2) Two dimensional flow; x-axis is the direction parallel to the screen and the center of the screen is the origin of the coordinate as shown in Fig. D.1.

(3) All physical properties of the fluid are constant and evaluated at $\bar{T}$, where $\bar{T}$ is the average of the screen and the ambient temperatures.

Then, the resulting governing equations are (Bird et al., 1960)

$$\frac{\partial v_x}{\partial x} + \frac{\partial v_y}{\partial y} = 0$$

$$\bar{\rho}\left(v_x\frac{\partial v_y}{\partial x} + v_y\frac{\partial v_y}{\partial y}\right) = \mu\left(\frac{\partial^2 v_x}{\partial x^2} + \frac{\partial^2 v_y}{\partial y^2}\right) + \bar{\rho}\bar{g}\bar{\beta}(T - \bar{T})$$

$$\bar{\rho}\, C_p\left(v_x\frac{\partial T}{\partial x} + v_y\frac{\partial T}{\partial y}\right) = k\left(\frac{\partial^2 T}{\partial x^2} + \frac{\partial^2 T}{\partial y^2}\right)$$

B. C.: $x = 0 \quad \frac{\partial v_y}{\partial x} = 0 \quad \frac{\partial T}{\partial x} = 0 \quad v_x = 0$

$y = 0 \quad v_y = 0 \quad v_x = 0 \quad T = T_h$

and assume $x = \pm L \quad v_y = 0 \quad T = T_c$

where L is one half of the width of the screen. Even in the simplified forms, obtaining exact solutions of the above governing equations requires more information on boundary conditions and complicated numerical analyses. Only approximate solutions are attempted here.

In the vicinity of the screen, the flow is affected by the presence of the wall and the velocity is small. Then, one can assume that the buoyancy and the viscous force are in balance. Also assume the following boundary

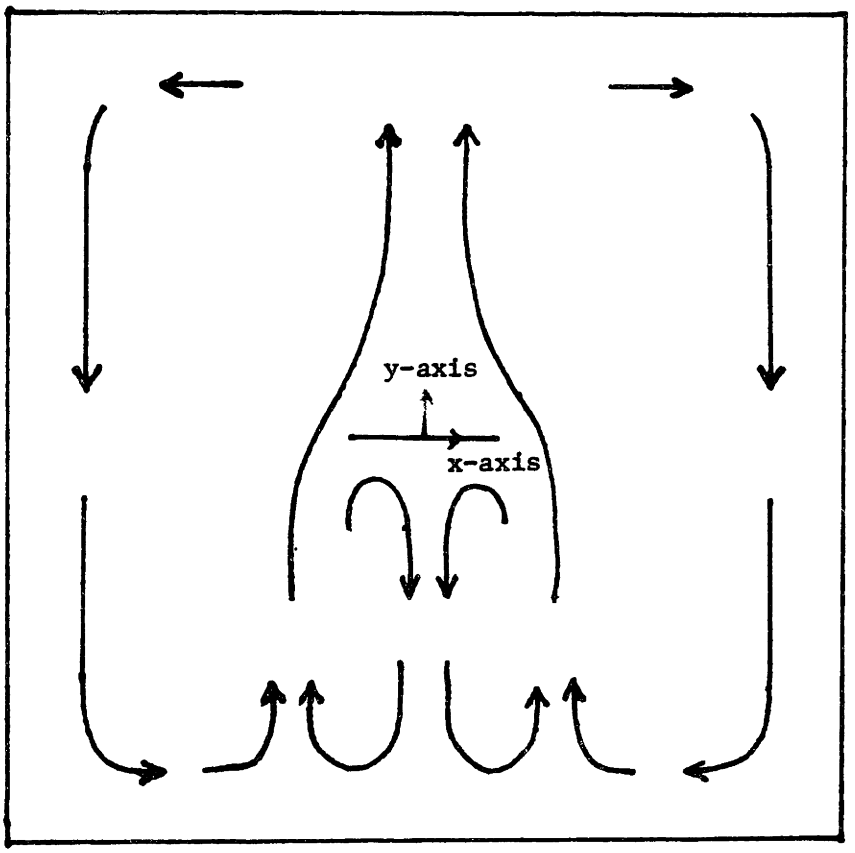

Fig. D.1. The reactor viewed from the narrow end of the screen and hypothesized streamlines of the natural convective flow.

conditions.

$$y = \delta \qquad \frac{\partial v_y}{\partial y} = 0 \tag{D-1a}$$

$$y = \delta \qquad T = T_m \tag{D-1b}$$

and let $$T = -\left[\frac{T_h - T_m}{\delta}\right] y + T_h \tag{D-1c}$$

Then, the momentum equation becomes

$$\frac{\mu}{\rho}\frac{\partial^2 v_y}{\partial y^2} = -g\bar{\beta}\,(T - \bar{T})$$

Substitute T and integrate the above momentum balance twice and then, one obtains v_y and v_y at $y = \delta$.

$$v_y = -\rho g \beta \frac{T_h - T_c}{\mu}\left[\frac{m-1}{2\delta}\left(\frac{1}{3}y^3 - \delta^2 y\right) + \frac{1}{2}\left(\frac{1}{2}y^2 - \delta y\right)\right] \tag{D-2}$$

$$v_y(\delta) = \rho g \beta \frac{T_h - T_c}{\mu}\delta^2\left(\frac{m}{3} - \frac{1}{12}\right) \tag{D-3}$$

where $m = \dfrac{T_m - T_c}{T_h - T_c}$.

Now, apply the energy balance to the region enclosed with $x = \pm L$, $y = 0$, and $y = \delta$ as shown in Fig. D.2.

$$C_p\, v_y(\delta)\,(T_m - T_c) = \frac{k_{he}}{\delta}(T_h - T_m) + \dot{m}_v' C_p\,(T_h - T_m) \tag{D-4}$$

where $\dot{m}_v'$ is the mass flow of volatiles per unit area. For the derivation of $\dot{m}_v'$, the coal particles are assumed to be in hexagonal arrangement forming monolayer as shown in Fig. C.1.b and a single first order reaction model is

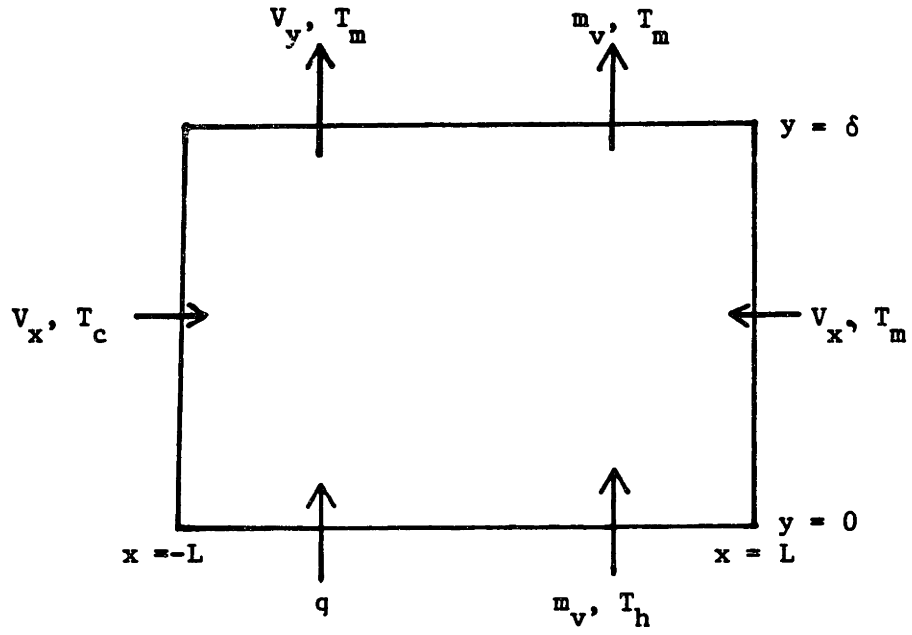

Fig. D.2. Energy balance on the thermal boundary layer of the screen

Table D.1. Thickness of thermal boundary layer (δ), velocity of convective flow ($V_y(\delta)$), and the amount of tar converted for various temperatures at the boundary layer (T_m).

T_m (°C)	δ (cm)	$V_y(\delta)$ (cm/s)	t_c (s)	Tar converted (%)
500.00	2.12908	49.09922	0.04872	2.459
600.00	1.82979	44.87389	0.03734	2.679
700.00	1.59568	38.65563	0.02890	2.858
800.00	1.34765	29.74599	0.02167	2.875
900.00	1.00705	17.38690	0.01443	2.513

used for volatile generation:

$$\dot{m}_v = \rho_{coal} \left(\frac{\pi}{3} R_p\right) k_o \exp(-E/RT_h) (V^* - V)$$

where ρ_{coal} = 1.3 gm/cm^3, R_p = 0.004 cm, k_o = 1000 /sec, E = 12220 cal/gm and V^* = 0.472. Other constants, and k_{he}, are evaluated at $T = (T_h + T_m)/2$ and T_h = 1000°C and T_c = 25°C are used. k_{he} is given in Appendix C and C_p = 1.2425 cal/gm°C. For given T_m, and $v_y(\delta)$ is calculated from Eq's D.3. and D.4. The characteristic time for volatiles to remain in δ is

$$t_c = \frac{\delta}{\frac{\bar{v}_y(\delta)}{2} + \frac{\dot{m}_v}{\rho}}$$

The fraction of tar converted during t_c is

$$\text{tar converted} = 1 - \exp(- t_c \; 996 \exp(-15400/RT))$$

The reaction constants are obtained from the thesis by Serio (1984).

Table D.1 gives the result of calculations at various T_m. T_m = 500°C is chosen as a lower limit of the analysis because the extent of tar cracking below 500°C is not significant. As shown in Table D.1., at T_m = 500°C, the hot zone extends to a few centimeters above the screen and, however, the fraction of primary tar converted is a just a few percent of the total tar evolved. At lower screen temperatures, the fraction of tar converted is even smaller (i.e. at T_h = 800°C, 1 % conversion).

APPENDIX E:

MASS TRANSFER OF VOLATILES INTO A BUBBLE:

DETERMINATION OF MASS TRANSFER COEFFICIENT

The rate of volatiles transport to a bubble is described using film theory of mass transfer (Eq. 5.4-1):

$$\frac{dv}{dt} = 4\pi a \; D_{v,L} \; Sh \; (C - C_{eq}) \qquad (5.4\text{-}1)$$

where $Sh = ha/D_{v,L}$ and v and a are the bubble mass and radius, respectively. To obtain the magnitude of Sh number, a detailed mass balance is made around a single bubble which is surrounded by other bubbles of the same size. Let the concentration of bubbles be N bubbles/cm^3 and let the volatiles formation rate be R(t). The shell balance of mass transfer gives

$$\frac{\partial C}{\partial t} = \frac{D_{v,L}}{r^2} \frac{\partial}{\partial r} r^2 \frac{\partial C}{\partial r} + R(t) - 4\pi a \, D_{v,L} \cdot Sh \cdot (C - C_{eq}) \cdot N \qquad (E\text{-}1)$$

The last term on the right hand side is the sink term due tovolatiles transport to surrounding bubbles. Let

$$f(t) = R(t) + 4\pi a \cdot D_{v,L} \; Sh \cdot C_{eq} \cdot N \qquad (E\text{-}2)$$

$$g(t) = 4\pi a \; D_{v,L} \; Sh \; N \qquad (E\text{-}3)$$

Then the above mass balance and boundary and initial conditions are

$$\frac{\partial C}{\partial t} = \frac{D_{v,L}}{r^2} \frac{\partial}{\partial r} r^2 \frac{\partial C}{\partial r} + f(t) - g(t) \, C \qquad (E\text{-}4)$$

(B. C.) $r = a$ $\quad C = C_{eq}(t)$ (E-4a)

$r = \infty$ $\quad C = C_{\infty}(t)$ (E-4b)

(I. C.) $t = 0$ $\quad C = C_i$ (E-4c)

As r approaches infinity, the mass balance becomes

$$\frac{dC_\infty}{dt} = f(t) - g(t) \cdot C_\infty \qquad \text{(E-5)}$$

and, therefore,

$$C_\infty(t) = e^{-gt} \left(\int_0^t f(t)\, e^{gt}\, dt + C_i \right) \qquad \text{(E-6)}$$

Let $$C = e^{-gt} \left(C' + \int_0^t f\, e^{gt}\, dt \right) \qquad \text{(E-6)}$$

Rewrite Eq's E-4 through E-4c in terms of C':

$$\frac{\partial C'}{\partial t} = \frac{D_{v,L}}{r^2} \frac{\partial}{\partial r} r^2 \frac{\partial C'}{\partial r} \qquad \text{(E-7)}$$

(B. C.) $r = a$ $\quad C' = (C_{eq}(t) - C_\infty(t))\, e^{gt} + C_i$ (E-7a)

$r = \infty$ $\quad C' = C_i$ (E-7b)

(I. C.) $t = 0$ $\quad C' = C_i$ (E-7c)

Assume $(C_{eq}(t) - C_\infty(t))$ - constant and then Eq. E-7 can be solved by Duhamel's superposition integral method. Let $T = D_{v,L}t/a^2$, $g = r/a$, and $K = ga^2/D_{v,L}$. Then the solution to Eq. E-7 is

$$\frac{C' - C_i}{C_{eq} - C_\infty} = y \frac{e^{KT}}{2} \left[e^{-\sqrt{K}(y-1)} \operatorname{erfc}\left(\frac{y-1}{\sqrt{4T}} - \sqrt{KT} \right) + e^{\sqrt{K}(y-1)} \operatorname{erfc}\left(\frac{y-1}{\sqrt{4T}} + \sqrt{KT} \right) \right] \qquad \text{(E-8)}$$

and the flux at the bubble surface is calculated as the following:

$$\left.\frac{\partial C}{\partial r}\right|_{r=a} = e^{-gt} \left.\frac{\partial C'}{\partial r}\right|_{r=a} \qquad \text{(E-9)}$$

$$= \frac{C_\infty(t) - C_{eq}(t)}{a} \left(1 + \sqrt{\frac{ga^2}{D_{v,L}}} \operatorname{erf}(\sqrt{gt}) + \frac{e^{-gt}}{\sqrt{\frac{\pi t D_{v,L}}{a^2}}} \right)$$

and

$$sh = \frac{ha}{D_{v,L}} = 1 + \sqrt{\frac{g\,a^2}{D_{v,L}}}\,\mathrm{erf}(\sqrt{gt}) + \frac{e^{-gt}}{\sqrt{\frac{\pi t\, D_{v,L}}{a^2}}} \qquad \text{(E-10)}$$

Since both the error function and exponential function are bound between 0 and 1, the lower and upper limits of Sherwood number are

$$1 \leq Sh < 1 + \frac{g\,a^2}{D_{v,L}} + \frac{1}{\sqrt{\frac{\pi t\, D_{v,L}}{a^2}}}$$

The reasonable estimate of N and t are

$$\frac{0.04\ \mathrm{cm}^3\ \text{pore volume/ cm}^3\ \text{coal}}{\frac{4\pi}{3}a^3} \quad \text{and} \quad \frac{a^2}{D_{v,L}}$$

Then one can conclude that Sherwood number varies between

$$1 \leq Sh < 2.06$$

APPENDIX F:

SUMMARY OF EXPERIMENTAL DATA

Table F.1. Selected volatiles and pyridine extract yields from 1 atm pyrolysis (Temperature in C and yield in weight %)

Peak Temp	Total wt loss	Tar	Extract	H_2O	CO	CO_2	CH_4	C_2H_4	C_2H_6	C_3'S	C_4+	Mass Balance
172	1.6	-	26.6	-	-	-	-	-	-	-	-	-
210	1.3	-	-	-	-	-	-	-	-	-	-	-
230	1.7	-	28.1	-	-	-	-	-	-	-	-	-
237	2.9	-	25.9	-	-	-	-	-	-	-	-	-
264	1.4	-	21.8	-	-	-	-	-	-	-	-	-
281	2.5	-	-	-	-	-	-	-	-	-	-	-
288	1.7	-	25.4	-	-	-	-	-	-	-	-	-
305	2.9	-	25.3	-	-	-	-	-	-	-	-	-
379	2.6	-	-	-	-	-	-	-	-	-	-	-
381	3.4	-	-	-	-	-	-	-	-	-	-	-
388	3.4	-	23.7	-	-	-	-	-	-	-	-	-
390	3.5	-	24.7	-	-	-	-	-	-	-	-	-
395	3.7	-	22.7	-	-	-	-	-	-	-	-	-
407	3.8	-	-	-	-	-	-	-	-	-	-	-
410	3.2	-	-	-	-	-	-	-	-	-	-	-
410	3.4	-	-	-	-	-	-	-	-	-	-	-
415	3.0	-	-	-	-	-	-	-	-	-	-	-
426	3.1	-	-	-	-	-	-	-	-	-	-	-
475	7.2	-	26.4	-	-	-	-	-	-	-	-	-
485	19.08	-	-	-	-	-	-	-	-	-	-	-
485	15.0	17.6	28.24	5.16	0.12	0.34	0.09	0.04	0.07	0.06	-	108.4
509	17.4	15.7	29.14	4.68	0.14	0.36	0.13	0.05	0.10	0.09	-	103.9
555	26.8	17.7	19.9	7.43	0.26	0.43	0.36	0.15	0.24	0.19	-	99.0
626	34.3	26.6	8.78	-	-	-	-	-	-	-	-	-
635	29.5	-	16.7	-	-	-	-	-	-	-	-	-

Table F.1. continues

635	28.7	22.8	21.0	1.5	–	–	0.16	0.06	0.11	0.13	0.18	96.3
635	28.2	22.9	25.4	1.2	0.49	0.74	0.27	0.10	0.18	0.20	0.33	99.7
645	29.2	–	–	–	–	–	–	–	–	–	–	–
650	28.4	–	–	–	–	–	–	–	–	–	–	–
660	36.9	29.8	4.76	4.59	0.44	0.45	0.74	0.45	0.29	0.41	0.30	100.0
709	39.0	30.7	0.	8.16	1.68	0.50	0.42	0.46	0.54	0.58	0.36	104.6
737	34.3	–	–	–	–	–	–	–	–	–	–	–
755	40.4	31.0	0.	3.58	1.03	0.47	1.16	0.51	0.57	0.50	–	98.4
805	44.5	27.1	0.	5.34	2.19	0.57	0.96	0.65	0.63	0.70	0.40	94.3
875	48.0	28.7	0.	3.7	3.68	1.12	2.49	1.11	0.44	0.63	0.60	94.7
940	47.2	–	0.	–	–	–	–	–	–	–	–	–
1000	47.1	22.0	–	–	–	–	–	–	–	–	–	–
1030	48.1	24.2	0.	2.65	3.19	2.25	2.54	0.92	0.51	0.64	–	89.0
1040	48.8	25.4	–	–	–	–	–	–	–	–	–	–
1100	47.0	29.6	0.	1.41	1.52	0.50	2.18	0.75	0.44	0.04	–	90.0

Table F.2. Selected volatiles and pyridine extract yields from vacuum pyrolysis (Temperature, C and yield, %)

Peak Temp	Total wt loss	Tar	Extract	H_2O	CO	CO_2	CH_4	C_2H_4	C_2H_6	C_3'S	C_4+	Mass Balance
150	1.97	0.	27.6	6.34	0.	0.12	-	-	-	-	-	104.4
240	2.0	0.	27.6	-	-	-	-	-	-	-	-	-
280	3.5	0.	24.9	6.32	0.	0.11	-	-	-	-	-	103.0
280	3.2	0.	23.7	-	-	-	-	-	-	-	-	-
370	3.1	0.	20.2	-	-	-	-	-	-	-	-	-
375	3.7	0.	22.1	7.76	0.06	0.26	-	-	-	-	-	108.0
390	4.6	0.	28.5	-	-	-	-	-	-	-	-	-
460	8.2	6.0	22.1	4.75	0.09	0.20	0.02	0.01	0.	0.	0.	103.0
460	8.6	3.2	26.2	5.56	0.06	0.21	-	-	-	-	-	100.5
515	18.9	16.9	31.7	-	-	-	-	-	-	-	-	-
555	25.8	13.7	28.9	5.05	0.20	0.32	0.14	0.04	0.09	0.11	0.22	94.1
575	26.6	-	20.1	5.14	0.36	0.33	0.18	0.06	0.13	0.12	0.18	114.9
600	27.9	-	15.2	4.67	0.28	0.33	0.22	0.07	0.14	0.13	0.20	113.3
675	37.8	23.1	11.4	6.02	0.74	0.49	0.54	0.14	0.27	0.25	0.29	94.0
690	43.8	32.3	5.6	7.79	0.33	0.58	0.43	0.25	0.37	0.39	0.39	99.5
691	44.2	27.6	4.8	6.30	0.42	0.47	1.03	0.23	0.39	0.38	0.30	92.9
757	43.0	29.1	8.6	5.39	0.59	0.42	0.80	0.24	0.35	0.36	0.47	94.8
762	44.2	20.2	2.5	5.08	0.15	0.49	1.24	0.40	0.47	0.51	0.44	90.9
830	54.8	38.9	0.	3.99	1.01	0.65	1.24	0.47	0.48	0.29	-	92.4
855	48.9	38.7	0.	4.15	0.16	0.54	1.98	0.59	0.56	0.65	0.68	99.0
855	46.5	46.9	0.	7.42	0.19	0.55	2.08	0.64	0.55	0.68	0.57	113.0
940	49.0	30.4	0.	6.63	0.96	0.67	3.14	0.90	0.65	0.89	0.67	95.9
950	43.3	21.9	0.	9.79	1.08	0.57	1.83	0.84	0.62	0.87	0.61	94.8
950	49.2	26.0	0.	5.95	0.93	0.52	2.81	0.98	0.66	0.87	0.74	89.8
950	52.5	27.9	0.	4.86	0.67	0.50	3.36	0.87	0.59	0.78	0.07	86.9
980	44.2	21.4	0.	5.83	3.33	0.96	1.92	1.08	0.66	0.92	1.10	94.2

Table F.2. continues

980	54.3	35.1	0.	9.93	3.63	0.78	1.63	0.77	0.56	0.71	0.52	98.4
990	42.7	20.22	0.	5.92	1.16	0.58	3.24	1.02	0.63	0.91	0.77	91.8
1000	51.9	41.4	0.	-	-	-	-	-	-	-	-	
1005	52.5	30.1	0.	3.65	5.78(inc. CO2)		1.59	0.87	0.58	0.27	0.	90.4
1030	45.8	25.3	-	-	-	-	-	-	-	-	-	-
1030	46.7	-	0.	5.66	5.30(inc. CO2)		1.70	1.20	0.64	0.58	0.	-
1032	54.7	47.9	0.	-	-	-	-	-	-	-	-	-
1096	48.1	39.9	0.	-	-	-	-	-	-	-	-	-

Table F.3. Summary of average molecular weights of tar and pyridine extract from 1 atm pyrolysis where MN = number average MW and MW = weight average MW.

Peak Temp	Tar		Extract	
	MN	MW	MN	MW
25	-	-	441	554
172	-	-	457	574
230	-	-	469	576
288	-	-	466	576
306	-	-	463	583
394	-	-	485	602
475	-	-	501	624
485	303	369	524	639
509	318	382	541	663
530	-	-	570	507
555	329	398	560	701
626	336	404	508	620
660	350	422	540	656
709	338	415	498	606
755	346	427	491	601
805	339	421	485	617
910	329	403	-	-
1040	313	388	-	-
1100	325	401	-	-

Table F.4. Summary of average molecular weights of tar and pyridine extract from vacuum pyrolysis where MN = number average MW and MW = weight average MW.

Peak Temp	Tar		Extract	
	MN	MW	MN	MW
150	-	-	440	562
370a	-	-	482	613
370b	-	-	458	579
375	-	-	426	547
390a	-	-	504	676
390b	-	-	502	665
460	-	-	500	617
460	-	-	479	607
515	361	426	510	627
555a	299	368	-	-
555b	324	388	465	583
575	377	443	-	-
600	379	450	502	613
670	403	480	542	631
675	390	465	461	574
690	390	475	493	600
757	377	452	480	587
760	346	423	512	629
855	356	439	500	595
855	357	439	-	-
940	409	517	482	638
950	388	491	521	694
950	394	501	-	-
990	397	516	-	-
1030	368	471	-	-

* a and b represent two measurement on the same sample.

APPENDIX G:

COMPUTER PROGRAMS AND RESULTS OF CALCULATIONS

G.1. Computer programs and calculation results of best fitting kinetic parameters for a single reaction model

```
C*************************************************************************
C
C                              PROGRAM POWELL
C
c
C    This program gives the best fitting kinetic parameters for a
c    single reaction model.  The original Powell available in the Data
c    General Eclipse computer modified to incorporate the time-temperature
c    history of each pyrolysis experiment. The documentation of the original
c    Powell is also available in the Eclipse computer.  This modified Powell
c    is bound with user provied subroutines calfun, fun, and pplot which
c    are also listed in this section, and with other package routines
c    that the original Powell is bound.  They are found in the directory
c    :userlib:powell:.
c
C*************************************************************************
C
C          M       IS THE NUMBER OF DATA POINTS
C          N       IS THE NUMBER OF UNKNOWNS
C          F       IS A VECTOR OF LENGTH M CONTAINING THE RESIDUAL VALUES
C          X       IS THE VECTOR OF UNKNOWNS
C          E       ABSOLUTE ACCURACY LIMIT VECTOR OF LENGTH N ON THE CHANGE IN
C                  VALUES OF THE UNKNOWNS BETWEEN ITERATIONS
C          ESCALE  PARAMETER LIMITING THE STEP SIZE; NORMALLY X(I) WILL NOT BE
C       CHANGED BY MORE THAN ESCALE*E(I) IN A SINGLE STEP
C       (SUGGESTED VALUE = 1000.)
C          IPRINT  PRINTING INDEX
C          MAXFUN  MAXIMUM LIMIT ON NUMBER OF FUNCTION EVALUATIONS
C          W       STORAGE VECTOR
C
        COMPILER DOUBLE PRECISION
        COMPILER NOSTACK
        PARAMETER NN=10          ;NUMBER OF PARAMETERS
        PARAMETER MM=40          ;NUMBER OF DATA POINTS
        PARAMETER ND=10          ;MAX. # DATA ITEMS/POINT
      DIMENSION E(NN),X(NN),F(MM)
      COMMON/AAA/ W(1330),NDATAS,DATAS(ND,MM)
      COMMON/PARA/EACT,AKO,VSTAR,NCASE
      COMMON/TMTMP/TIM(40),TEM(40),TIMEP(40),TEMPP(40),A(40),B(40),EXPVL(40)
      COMMON/TTP/ITFLAG(40),TIME(20,10),TEMP(20,10)
      COMMON/TEQ/TEFF(40),CALVL(40)
      COMMON/NFIR/NFIRST
C
C
        CALL FOPEN(1, '@DATA')
        CALL FOPEN(4, 'OUT')
        NI=1
        NO=10
        N1=4
```

```
      NFIRST=0.0
      WRITE(N1,101)
      READ FREE(NI) NCASE,M,MAXFUN,IPRINT
      READ FREE(NI) ESCALE
      TYPE NCASE,M,MAXFUN,IPRINT
      TYPE ESCALE
C
      NDATAS=2
C_____________________________________________________________________
C
C     CASE            EACT    AKO     VSTAR   N
C_____________________________________________________________________
C       1             VAR     VAR     VAR     3
C       2             VAR     FIX     VAR     2
C       3             VAR     VAR     FIX     2
C       4             VAR     FIX     FIX     1
C_____ _______________________________________________________________
C
      IF(NCASE .NE. 1) GO TO 11
        N=3
        WRITE(N1,102)N,M
102     FORMAT(//,15X,'NUMBER OF PARAMETERS = ',I3,/,
     1         20X, 'PARAMETER 1: ACTIVATION ENERGY',/,
     2         20X,'PARAMETER 2: LOG(PRE-EXPONENTIAL CONSTANT)',/,
     3         20X,'PARAMETER 3: ULTIMATE YIELD',///,
     4        15X,'NUMBER OF DATA       = ',I3,//)
      GO TO 19
11    IF (NCASE .NE. 2) GO TO 12
        N=2
        TYPE 'FIXED PARAMETER = AKO          ENTER AKO'
        ACCEPT 'AKO=',AKO
        AKO=10.**AKO
        WRITE(N1,152)N,AKO,M
152     FORMAT(//,15X,'NUMBER OF PARAMETERS FIXED =',I3,/,
     1          20X,'PARAMETER 1: ACTIVATION ENERGY',/,
     2          20X,'PARAMETER 2: ULTIMATE YIELD',//,
     3          15X,'PARAMETER FIXED ',/,
     4          20X,'PRE-EXPONENTIAL CONSTANT =',E12.5,///,
     5          15X,'NUMBER OF DATA =',I3,//)
      GO TO 19
12    IF (NCASE .NE. 3) GO TO 13
        N=2
        TYPE 'FIXED PARAMETER = VSTAR       ENTER VSTAR'
        ACCEPT 'VSTAR =',VSTAR
        WRITE(N1,153)N,VSTAR,M
153     FORMAT(//,15X,'NUMBER OF PARAMETERS VARIED =', I3,/,
     1          20X,'PARAMETER 1: ACTIVATION ENERGY',/,
     2          20X,'PARAMETER 2: LOG(PRE-EXPONENTIAL CONSTANT)',//,
     5          15X,'PARAMETER FIXED',/,
     4          20X,'ULTIMATE YIELD =',E12.5,///,
     5          15X,'NUMBER OF DATA =',I3,//)
      GO TO 19
13    N=1
        TYPE 'FIXED PARAMETER = AKO  VSTAR      ENTER AKO VSTAR'
        ACCEPT 'AKO= ',AKO
```

```
      ACCEPT 'VSTAR=',VSTAR
      AKO=10.**AKO
      WRITE(N1,154)N,AKO,VSTAR,M
154   FORMAT(//,15X,'NUMBER OF PARAMETERS VARIED =',I3,/,
     1          20X,'PARAMETER 1:ACTIVATION ENERGY',//,
     2          15X,'PARAMETERS FIXED',/,
     3          20X,'PRE-EXPONENTIAL CONSTANT',E12.5,/,
     4          20X,'ULTIMATE YIELD',E12.5,//,
     5          15X,'NUMBER OF DATA =',I3,//)
19    CONTINUE
C
C
      DO 20 IA=1,N
      READ FREE(NI) X(IA), E(IA)
        TYPE X(IA), E(IA)
20    CONTINUE
C
C
C               IF ITFLAG(TIME-TEMPERATURE FLAG) IS
C               -1: CURVED t-TEMP HISTORY (OCCURED AT LOWER TEMP AT VACUUM)
C                0: TWO LINEAR HEATING (OCCURED AT LOW TEMP AT VACUUM)
C                1: REGULAR LINEAR HEATING
C
      DO 30 I=1,M
      READ FREE (1) ITFLAG(I),M1
              TYPE ITFLAG(I),M1
      IF(ITFLAG(I))21,22,23
21    READ FREE(1) (TIME(J,I),TEMP(J,I),J=1,M1)
      READ FREE(1) TEMPP(I),EXPVL(I)
      TYPE TIME(M1,I),TEMP(M1,I),TEMPP(I),EXPVL(I)
      TEMPP(I)=TEMPP(I) + 273.13
              DO 25 J=1,M1
25            TEMP(J,I)=TEMP(J,I) + 273.13
      GO TO 30
22    READ FREE(1) TIM(I),TEM(I),TIMEP(I),TEMPP(I),A(I),B(I),EXPVL(I)
      TEM(I)=TEM(I) + 273.13
      TEMPP(I)=TEMPP(I) + 273.13
      GO TO 30
23    READ FREE (1) TIMEP(I),TEMPP(I),A(I),B(I),EXPVL(I)
      TEMPP(I)=TEMPP(I) + 273.13
      TYPE TIMEP(I),TEMPP(I),A(I),B(I),EXPVL(I)
30 TYPE M,I
C
C
101   FORMAT(//,20X,27HPOWELL REGRESSION ALGORITHM )
C
      CALL SSQMIN(M,N,F,X,E,ESCALE,IPRINT,MAXFUN,FF,NI,NO)
C
      CALL PPLOT(M,F,N,X)           ;MAKE EPLOT PLOT FILES
      WRITE(N1,103)
103   FORMAT(15X,'DATA POINTS AND CALCULATED RESULTS:',/,
     1          20X,'TEMPP = EXPERIMENTAL PEAK TEMPERATURE',/,
     3          20X,'EXPVL = EXPERIMENTAL YIELD',/,
     4          20X,'CALVL = CALCULATED YIELD',/,
     5          20X,'F     = RESIDUAL',//,
```

```
     6        21X,'TEMPP',5X,'PRES',5X,'EXPVL',5X,'CALVL',5X,'F',//)
C
      DO 40 IA=1,M
      PRES=1.
      IF (IA .LE. 7)PRES=0.0001
      TEMPP(IA)=TEMPP(IA) - 273.13
      WRITE(N1,104) IA,TEMPP(IA),PRES,EXPVL(IA),CALVL(IA),F(IA)
104   FORMAT(15X,'#',I2,':',F9.2,F9.4,F9.2,F9.3,F9.3)
40    CONTINUE
      WRITE(N1,105)FF
105   FORMAT(///,15X,'THE SUM OF THE SQUARES OF RESIDUALS = ',1E12.5)
      WRITE(N1,106)
106   FORMAT(///,15X,'FINAL PARAMETER VALUES:',//)
C
      DO 50 J=1,N
      WRITE(N1,107)J,X(J)
107   FORMAT(20X,'Parameter',I2,':',G16.8)
50    CONTINUE
      READ FREE(1,END=1)I      ;IF READ SUCCESSFUL, SUPRESS CALL TO ANOVA
      IF (I.NE.0) GOTO 1    ;SUPRESS CALL TO ANOVA ONLY IF DATA IS = 0
      WRITE(NO,1002)
1002  FORMAT(/,' Call to ANOVA suppressed by "0" in last line of data file')
      GOTO 7
1     CONTINUE
      TYPE ' '
      WRITE(NO,1000)
1000  FORMAT(' Calling ANOVA.. ',Z)
      CALL ANOVA(N,X,M,F,FF,.0005,10)
7     CONTINUE
C     DO 10 I=1,M
C10         TYPE 'I,F(I)=',I,F(I)
      END
```

```
C*************************************************************************
C
C                          SUBROUTINE CALFUN
C
C*************************************************************************
      COMPILER DOUBLE PRECISION
      COMPILER NOSTACK
      PARAMETER ND=10
      PARAMETER MM=40
      PARAMETER ND1=9
      SUBROUTINE CALFUN(M,N,F,X)
      DIMENSION F(M),X(N)
      COMMON/AAA/ W(1330),NDATAS,DATAS(ND,MM)
      COMMON/PARA/EACT,AKO,VSTAR,NCASE
      COMMON/TMTMP/TIM(40),TEM(40),TIMEP(40),TEMPP(40),A(40),B(40),EXPVL(40)
      COMMON/NFIR/NFIRST
C
      NFIRST=1
      EACT=X(1)
      IF(NCASE.NE.1) GO TO 4
      AKO=10.**X(2)
      VSTAR=X(3)
      GO TO 9
    4 IF(NCASE.NE.2) GO TO 5
        VSTAR=X(2)
      GO TO 9
    5 IF(NCASE.NE.3) GO TO 9
        AKO=10.**X(2)
    9  CONTINUE
      DO 3 I=1,M
        DATAS(1,I)=TEMPP(I)
        DATAS(2,I)=EXPVL(I)
      F(I)=FUN(EACT,AKO,VSTAR,I)-EXPVL(I)
    3 CONTINUE
C
C
      RETURN
      END
```

```
C*************************************************************************
C
C                              SUBROUTINE FUN
C
C*************************************************************************
C
      COMPILER DOUBLE PRECISION
      COMPILER NOSTACK
      FUNCTION FUN(E,AK,VSTAR,I)
        COMMON/TMTMP/TIM(40),TEM(40),TIMEP(40),TEMPP(40),A(40),B(40),EXPVL(40)
        COMMON/TTP/IFLAG(40),TIME(20,10),TEMP(20,10)
        ARR(AK,E,XTEMP)=AK*DEXP(AMAX1(-E/(1.987*XTEMP), -100.))
C
C
        DELT=0.005
C
        SUMKT=0.
        TI=0.
        TE=298.13
        NINT=0
        Y=ARR(AK,E,TE)
C
        IF(IFLAG(I)) 1,2,3
1       J=1
        DO 10 IA=1,10000
        TI=TI + DELT
        IF(TI .GE. 7.)GO TO 40
        NINT=NINT + 1
11      IF (TI .LE. TIME(J,I)) GO TO 12
        J= J + 1
        GO TO 11
12      JN1=J - 1
        TE=(TEMP(J,I)-TEMP(JN1,I))*(TI-TIME(JN1,I))/(TIME(J,I)-TIME(JN1,I))
     1        + TEMP(JN1,I)
        YO=Y
        Y=ARR(AK,E,TE)
        SUMKT=SUMKT + 0.5*(Y + YO)*DELT
10      CONTINUE
        GO TO 40
2       DO 20 IA=1,10000
        TI=TI + DELT
        IF (TI .GE. 6.) GO TO 40
        NINT=NINT + 1
        IF(TI .LE. TIM(I))
     1     TE=(TEM(I)-298.13)*TI/TIM(I) + 298.13
        IF(TI .GT. TIM(I) .AND. TI .LE. TIMEP(I))
     1    TE=(TEMPP(I)-TEM(I))*(TI-TIM(I))/(TIMEP(I)-TIM(I)) + TEM(I)
        IF(TI .GT. TIMEP(I))
     1   TE=((B(I)/A(I))/((1.+B(I)/(A(I)*TEMPP(I)**3))*
     1      EXP(3.*B(I)*(TI-TIMEP(I))) - 1.))**(1./3.)
        Y=YO
        Y=ARR(AK,E,TE)
        SUMKT=SUMKT + 0.5*(Y + YO)*DELT
20      CONTINUE
        GO TO 40
```

```
3       DO 30 IA=1,10000
        TI=TI + DELT
        IF (TI .GE. 6.) GO TO 40
        NINT=NINT + 1
        IF ( TI .LE. TIMEP(I)) TE=(TEMPP(I) - 298.13)*TI/TIMEP(I) + 298.13
        IF ( TI .GT. TIMEP(I))
     1  TE=((B(I)/A(I))/((1.+B(I)/(A(I)*TEMPP(I)**3))*
     1     EXP(3.*B(I)*(TI-TIMEP(I))) - 1.))**(1./3.)
        YO=Y
        Y=ARR(AK,E,TE)
        SUMKT=SUMKT + 0.5*(Y + YO)*DELT
30     CONTINUE
40     CONTINUE
C
        FUN=VSTAR*(1. - EXP(-SUMKT))
C
C
        RETURN
        END
```

```
C*******************************************************************************
C
C                                SUBROUTINE PPLOT
C
C*******************************************************************************
C
      COMPILER DOUBLE PRECISION
      COMPILER NOSTACK
C               ND = NUMBER OF DATA POINT
C               F  = VALUE OF RESIDUALS
C               NP = NUMBER OF UNKNOWNS
C               X  = VECTOR OF UNKNOWNS
        PARAMETER NPAR=10        ;MAX. NO. OF PARAMETERS
        PARAMETER NITEMS=10      ;MAX. # ITEMS PER DATA PT.
        PARAMETER NDATAS=40      ;MAX. # DATA PTS.
        PARAMETER NCUR=50        ;NO. OF ST. LINE SEGMENTS
                                          ;PER CURVE
        SUBROUTINE PPLOT(ND,F,NP,X)
C                       NDIND=NUMBER OF DATA ITEMS PER DATA POINT
C                       D HOLDS THE DATA
        COMMON/AAA/W(1330),NDIND,D(NITEMS,NDATAS)
        COMMON/TMTMP/TIM(40),TEM(40),TIMEP(40),TEMPP(40),A(40),B(40),EXPVL(40)
        COMMON/TTP/ITFLAG(40),TIME(20,10),TEMP(20,10)
        COMMON/TEQ/TEFF(40),CALVL(40)
        COMMON/PARA/EACT,AKO,VSTAR,NCASE
        COMMON/NFIR/NFIRST
        DIMENSION X(NP),F(ND),ITIT(39),DD(NITEMS,10),DDD(NITEMS)
        REAL ITTP(120),IVOL(120)
        NDINDD=NDIND-1
     . TYPE NDINDD
        INDVAR=1
        MFIRST=0
C
C
      TYPE 'Writing data for theory & data plot into file POW.PLT ..'
        CALL FOPEN(2,'POW.PLT')
C
        EACT=X(1)
        IF(NCASE .NE. 1) GO TO 4
        AKO=10.**X(2)
        VSTAR=X(3)
        GO TO 9
4     IF(NCASE .NE. 2) GO TO 5
        VSTAR=X(2)
        GO TO 9
5     IF(NCASE .NE. 3) GO TO 9
        AKO=10.**X(2)
9     CONTINUE
C
C
        WRITE(2,1002)
1002    FORMAT('VOLATILES YIELD VS PEAK TEMPERATURE ',/,
     1         'PEAK TEMPERATURE',/,
     2         'VOLATILES YIELD',/,
     3         'SYMB 0.0',/,
```

```
     4          'YMAX 10.',/,
     5          'YMIN 0.0',/,
     6          'XMAX  600.',/,
     7          'XMIN 0.0',/,
     8          'SYHT 0.1',/,
     9          'XTIC 0.0',/,
     9           '100.,',', -1.0',/,
     9           'YTIC 0.0',/,
     1          '1.,',',-1.0',/,
     2          'END')
C
C    NOW, CALULATE THE YIELD FROM ACTUAL TIME TEMPERATURE HISTORY
C    SNCE THE RESIDUAL VALUES ARE F(I)=CAL(I) - EXPVL(I), CALVL=F + EXPVL
       DO 25 IB=1,ND
25     CALVL(IB)=F(IB) + EXPVL(IB)
C
         DO 30 IC=1,ND
         WRITE(2,1001)TEMPP(IC),EXPVL(IC)
1001     FORMAT(1X,E14.6,',',E14.6)
30       CONTINUE
C
C
                WRITE(2,1003)     ;PEN UP TO NEXT POINT
1003            FORMAT(' 1E32, -1.')
                WRITE(2,1001)ITTP(1),IVOL(1)     ;PLOT FIRST PT. OF CURVE
C
                WRITE(2,1004)
1004            FORMAT(' 1.E32,',',101.0')
         DO 40 IA=1,ND
                WRITE(2,1001)TEMPP(IA),CALVL(IA)         ;PLOT A POINT
40       CONTINUE                          ;END OF J LOOP
50       CALL FCLOSE(2)           ;CLOSE FILE
C
         RETURN
         END
```

```
C*************************************************************************
C
C                              EXAMPLE OF INPUT FILE
C
C*************************************************************************
1,20,1000,1
5000.
30000., 1.
13., 0.001
4.0, 0.001
-1,7                    ;V5D
0.,25., 1.2,124., 1.5,139., 2.7,157., 4.5,153., 6.0,149., 7.5, 140.
157., 1.97
-1,9                       ;V5E
0.,25., 0.4,134., 0.9,187., 1.5,229., 1.8,239., 3.0,234., 4.5,224.,
6.0,209.,7.5,199.
239., 2.0
-1,12             ;V5B
0.,25., 0.9,197., 1.2,241., 1.5,263., 1.8,276., 2.1,281., 2.4,280.,
3.3,276., 3.9,271., 5.4,254., 6.9,236., 8.4,222.
281., 3.46
-1,9              ;V5C
0.,25., 1.2,246., 1.5,259., 1.8,266., 2.1,273., 3.,273., 4.5,259.,
6.,239., 7.5,224.
273., 3.23
-1,10             ;V5F
0.,25., 0.9,307., 1.2,355., 1.5,367., 1.8,372., 2.1,369., 3.,355.,
4.5,319., 6.,295., 7.5,276.
372., 3.08
-1,11             ;V5A
0.,25., 0.9,307., 1.2,343., 1.45,367., 1.95,375., 2.55,369., 3.15,355.,
3.75,341., 4.35,331., 5.85,312., 7.05,280.
375., 3.68
-1,10             ;V5G
0.,25., 0.6,254., 0.9,331., 1.2,360., 1.5,379., 1.8,388., 3.,364.,
4.5,329., 6.,307., 7.5,280.
388., 4.59
1,0
0.2, 175.,  7.19124E-10, -2.24299E-2, 1.626
1,0
0.25, 210.,  10.3806E-10, -3.34748E-2, 1.25
1,0
0.2, 238.,  6.29543E-10, -2.04781E-2, 1.653
1,0
0.15, 237.,  12.8492E-10, -5.91054E-2, 2.91
1,0
0.25, 238.,  14.3310E-10, -7.89890E-2, 2.47
1,0
0.15, 264.,  15.8223E-10, -8.21014E-2, 1.37
1,0
0.3, 293.,  5.59937E-10, -1.55418E-2, 1.657
1,0
0.3, 322.,  3.54142E-10,  0.27279E-2, 2.948
1,0
```

```
0.4, 379.,  6.29711E-10, -1.55190E-2, 2.59
1,0
0.3, 381.,  6.63171E-10, -3.13402E-2, 3.42
1,0
0.3, 388.,  5.28357E-10, -1.05480E-2, 3.43
1,0
0.45, 390.,  4.27660E-10, 0.287905E-2, 3.53
1,0
0.3, 401.,  2.50166E-10,  1.76013E-2, 3.704
1
```

Table G.1.1. 3-best fitting parameters for a single reaction model describing low temperature volatiles yields.

POWELL REGRESSION ALGORITHM

NUMBER OF PARAMETERS = 3
PARAMETER 1: ACTIVATION ENERGY
PARAMETER 2: LOG(PRE-EXPONENTIAL CONSTANT)
PARAMETER 3: ULTIMATE YIELD

NUMBER OF DATA = 20

DATA POINTS AND CALCULATED RESULTS:
TEMPP = EXPERIMENTAL PEAK TEMPERATURE
EXPVL = EXPERIMENTAL YIELD
CALVL = CALCULATED YIELD
F = RESIDUAL

	TEMPP	PRES	EXPVL	CALVL	F
# 1:	157.00	.0001	1.97	1.731	-.239
# 2:	239.00	.0001	2.00	2.809	.809
# 3:	281.00	.0001	3.46	3.242	-.218
# 4:	273.00	.0001	3.23	3.176	-.054
# 5:	372.00	.0001	3.08	3.858	.778
# 6:	375.00	.0001	3.68	3.893	.213
# 7:	388.00	.0001	4.59	3.936	-.654
# 8:	175.00	1.0000	1.63	1.488	-.138
# 9:	210.00	1.0000	1.25	1.614	.364
#10:	238.00	1.0000	1.65	2.083	.430
#11:	237.00	1.0000	2.91	1.821	-1.089
#12:	238.00	1.0000	2.47	1.888	-.582
#13:	264.00	1.0000	1.37	1.920	.550
#14:	293.00	1.0000	1.66	2.531	.874
#15:	322.00	1.0000	2.95	2.858	-.090
#16:	379.00	1.0000	2.59	2.941	.351
#17:	381.00	1.0000	3.42	3.033	-.387
#18:	388.00	1.0000	3.43	3.087	-.343
#19:	390.00	1.0000	3.53	3.153	-.377
#20:	401.00	1.0000	3.70	3.394	-.310

THE SUM OF THE SQUARES OF RESIDUALS = .54069E 01

FINAL PARAMETER VALUES:

Parameter 1: 3872.4485
Parameter 2: .89342586
Parameter 3: 4.4710015

Table G.1.2. 2-best fitting parameters for a single reaction model describing low temperature volatiles yields.

POWELL REGRESSION ALGORITHM

NUMBER OF PARAMETERS FIXED = 2
PARAMETER 1: ACTIVATION ENERGY
PARAMETER 2: ULTIMATE YIELD

PARAMETER FIXED
PRE-EXPONENTIAL CONSTANT = .10000E 14

NUMBER OF DATA = 20

DATA POINTS AND CALCULATED RESULTS:
TEMPP = EXPERIMENTAL PEAK TEMPERATURE
EXPVL = EXPERIMENTAL YIELD
CALVL = CALCULATED YIELD
F = RESIDUAL

	TEMPP	PRES	EXPVL	CALVL	F
# 1:	157.00	.0001	1.97	1.729	-.241
# 2:	239.00	.0001	2.00	2.846	.846
# 3:	281.00	.0001	3.46	2.846	-.614
# 4:	273.00	.0001	3.23	2.846	-.384
# 5:	372.00	.0001	3.08	2.846	-.234
# 6:	375.00	.0001	3.68	2.846	-.834
# 7:	388.00	.0001	4.59	2.846	-1.744
# 8:	175.00	1.0000	1.63	1.583	-.043
# 9:	210.00	1.0000	1.25	2.793	1.543
#10:	238.00	1.0000	1.65	2.846	1.193
#11:	237.00	1.0000	2.91	2.846	-.064
#12:	238.00	1.0000	2.47	2.846	.376
#13:	264.00	1.0000	1.37	2.846	1.476
#14:	293.00	1.0000	1.66	2.846	1.189
#15:	322.00	1.0000	2.95	2.846	-.102
#16:	379.00	1.0000	2.59	2.846	.256
#17:	381.00	1.0000	3.42	2.846	-.574
#18:	388.00	1.0000	3.43	2.846	-.584
#19:	390.00	1.0000	3.53	2.846	-.684
#20:	401.00	1.0000	3.70	2.846	-.858

THE SUM OF THE SQUARES OF RESIDUALS = .14586E 02

FINAL PARAMETER VALUES:

Parameter 1:	26754.818
Parameter 2:	2.8457133

G.2. Computer programs and calculation results for 6-best fitting parameters

```
c*************************************************************************
c
c                        PROGRAM MAINF
c
c
c         Mainf program of the routine for 6 best fitting parameters
c         written for the residual function Eq. 6.3-2 in Ch. 6,  For Eq.
c         6.3-3, calculations of m and f, and the output scheme have to be
c         modified (Not shown here).
c
c         This routine  assumes a single size bubbles and 10 different
c         molecular weight tar which have the same formation and secondary
c         reaction rates.
c
*************************************************************************
          implicit double precision (a - h, o - z)
          implicit integer (i - n)
          logical locsch
          dimension x(6),g(6),bl(6),bu(6),delta(6),hesd(6),hesl(15),
     &              istate(6),iw(2),w(54)
          common/resd/fvecc(77)
          common/tth/ptemp(40),tp,at,bt
          common/yld/mcount(40),yvol(40),ytar(40),ymplast(40)
          common/tar/tmw(10)
          common/con/gcon,gmw,surt,delt,hrate,ao
          common/prop/vcon,visc,dcon,pres,volo,rado,rad,tolo,apore,pvol
          common/rxnc/eg,ept,est,rxng,rxntl,rxnt2,vt,vg,fgl,coalm
          common/ele/ne,nel,pcon,cmden,cden
          common/cnt/ndata,jdata
          external funct, monit, e04jbq
          fexp(x)=dexp(dmaxl(-1.d2,x))
c
c Input data:
c    Initial bubble size, tolerence limit and step size
c    for the integration, and integer flag for input condition
c    minimization routine E04JBF
          read(9,)pres,tolo,delt,itype
c    Molecuar weight of 10 tar components
          read(9,)(tmw(i), i=1,10)
c    constants for viscosity and diffusivity correlations
          read(9,)vcon,dcon
c
c The following parameters are fixed:
          pvol=0.04
          eg=0.26755d5
          rxng=1.d13
          vg=0.028457d0
          vt=0.7
c
c Define constants for fitting routine, e04faf
          read(9, )eta,stepmx,xtol,iprint,maxcal
```

```
c Let x(1)=rxnt1, x(2)=ept, x(3)=rxnt2, x(4)=est, x(5)=fg2, and x(6)=apore
c Define initial guess for  parameters to be obtained and
c Maximum expected change in each iteration
          read(9, )n
          do 5 i=1,n
5         read(9, ) x(i)
c
c Read input data where
c ndata = number of data
c mcount = number of items in a data set. If all data such as gas
c          yield, tar yield, and extract yield are available, m=4 for
           Residual function 6.3-2 and m=3 for 6.3-3 in the main text.
c yvol = total volatiles yield in %
c ytar = tar yield in %
c ymplast = extract yield in %
          read(9, )ndata
          do 10 ia=1,ndata
          read(9, )mcount(ia),ptemp(ia),yvol(ia), ytar(ia), ymplast(ia)
          ptemp(ia)=ptemp(ia) + 273.13
          yvol(ia)=yvol(ia)*0.01
          ytar(ia)=ytar(ia)*0.01
          ymplast(ia)=ymplast(ia)*0.01
10        continue
c
c Define physical constants
c ne=number sections in tar molecular weight
          ne=10
c heating rate and constants for cooling time-temperature history
          hrate=1000.d0
          at=2.1983d-10
          bt=6.7328d-2
c other constants
          coalm=3000.d0
          rado=0.0035d0
          gcon=8.314d7
          gmw=28.d0
          surt=30.d0
          cden=1.3d0
          pcon=gcon/4.187d0
          nel=ne + 1
c
c Calculate the number of residual functions
          m=0
          do 51 ia=1,ndata
c         if(mcount(ia) .ne. 1 ) m=m + 1
51        m=m + mcount(ia)
c
c Define constants required in E04JBF
          lh=n*(n-1)/2
          liw=2
          lw=9*n
          write(6,)'lw=', lw
c         ifail=0
c
c If this is not the first call, use intype = 0
```

```
          if(intype .ne. 1) go to 60
c
c If the first call is made, use of e04hbf is recommended
c at starting point to find suitable differencing intervals
c for numerical derivatives and second derivatives of the residual function.
          call e04hbf(n,funct,x,j,delta,hesl,lh,hesd,f,g,iw,liw,w,lw,ifail)
          write(6, )'function evaluations needed by e04hbf: ',j
c
c e04hbf will assign values to f, the g(j) and the hesd(j), and will have
c set the elements of hesl to zero.  So e04jbf can be entered with
c intype set to 1.
c
c Check whether the hesd(j) indicate that the problem should be rescaled
          big=hesd(1)
          small=hesd(1)
          do 52 ib=2,n
          if(big .lt. hesd(ib)) big=hesd(ib)
          if(small .gt. hesd(ib)) small=hesd(ib)
52        continue
          if(big .lt. 1.d4*small) go to 53
          write(6, )(hesd(j), j=1,n)
          go to 300
c
c For intype = 0 or 2
60        do 61 i=1,n
61        delta(i) = 1.d-10
          if(intype .eq. 0) go to 53
c
c when calculation is constinued from the previous interations.
c values for f and g's have to  be corredted.
          intype=2
          f=0.141884846697582640D+00
          g(1)=   -0.1796760340D-01
          g(2)=    0.3532372205D-01
          g(3)=    0.1255665233D-01
          g(4)=   -0.1203295251D-01
          g(5)=   -0.3022985062D-02
          g(6)=   -0.4218721552D-02
c Assign other input variables.  For detail of these variables,
c please see the manual of the NAG routine e04jbf.
          do 58 ia=1,n
          istate(ia)=ia
          hesd(ia)=1.
          ja=ia*2 - 1
          japl=ja + 1
          jap2=ja + 2
          hesl(jap2)=1.d0
          hesl(ja)=1.d0
58        hesl(japl)=1.d0
c
c Continue setting parameters for e04fcf
53        locsch=.true.
c All variables have the same bound.
          ibound=3
          bl(1)=-1.d0
```

```
          bu(1)=1.d0
          fest=1.d0
          ifail=1
c
c Call the fitting routine
          call e04jbf(n,funct,monit,iprint,locsch,intype,e04jbq,maxcal,
     &               eta,xtol,stepmx,fest,delta,ibound,bl,bu,x,hesl,lh,
     &               hesd,istate,f,g,iw,liw,w,lw,ifail)
          write(6, )'ifail = ', ifail
          if(ifail .ne. 0) go to 200
c
c ------------------------------------------------------------------
c Write the result.
          write(10,101)pres,rado,apore,ao,pvol,vcon,dcon
101       format( '************************ input **************',///,
     &            3x,'pressure                    =',e15.5,'    dyne/cm*cm',/,
     &            3x,'original particle radius =',e15.5,'    cm',/,
     &            3x,'initial pore size          =',e15.5,'    cm',/,
     &            3x,'initial bubble size       =',e15.5,'    cm',/,
     &            3x,'pore volume                =',e15.5,'    cm**3',/,
     &            3x,'constant for viscosity   =',e15.5,/,
     &            3x,'constant for diffusivity =',e15.5,///)
c
          write(10,108)(tmw(i), i=1,10)
108       format(3x, 'Molecular weight of 10 tar compoents',/,2(5e13.5,/),/)
c
          write(10,102)rxng,eg,vg,vt,rxnt1,rxnt2,ept,est,fgl
102       format(10x,'Parameters fixed',//,
     &            3x,'reactin constant for gas  =',e15.5,'    1/sec',/,
     &            3x,'act e for gas formation   =',e15.5,'    cal/mole',/,
     &            3x,'ultimate yield of gas     =',e15.5,'    gm/gm',/,
     &            3x,'ultimate yield of tar     =',e15.5,'    gm/gm',///,
     &            10x,'Parameters varied, final paratmeter values',//,
     &            3x,'reaction constant1 for tar=',e15.5,'    1/sec',/,
     &            3x,'reaction constant2 for tar=',e15.5,'    1/sec',/,
     &            3x,'act E for metaplast formation    =',e15.5,'  cal/mole',/,
     &            3x,'act E for metaplast decomposition=',e15.5,'   cal/mole',/,
     &            3x,'fraction of metaplast converted to gases=',e15.5,///)
c
c
          write(10,103)f
103       format(10x,'square sum of residual functions= ',e12.5,///
     &               20x, 'Comparison with experimental data',//)
c
          ia=1
          write(10,104)
          do 75 jdata=1,ndata
          ptemp(jdata)=ptemp(jdata) - 273.13
          if(mcount(jdata) .eq. 1) go to 71
          if(mcount(jdata) .eq. 2) go to 72
          ja=ia + 1
          caldt=-fvecc(ja) + ytar(jdata)
          cald=-fvecc(ia) + yvol(jdata) - ytar(jdata) + caldt
          write(10,107) ptemp(jdata), cald, yvol(jdata)
          ia=ia + 3
```

```
          go to 75
 71       cald=-fvecc(ia) + yvol(jdata)
          write(10,107) ptemp(jdata), cald, yvol(jdata)
          go to 75
 72       cald=-fvecc(ia) + yvol(jdata)
          write(10,107) ptemp(jdata), cald, yvol(jdata)
          ia=ia + 2
 75       ia=ia + 1
 c
          write(10,105)
          ia=1
          do 85 jdata=1,ndata
          if(mcount(jdata) .eq. 1) go to 85
          if(mcount(jdata) .eq. 2) go to 82
          ia=ia + 1
          cald=-fvecc(ia) + ytar(jdata)
          write(10,107)ptemp(jdata),  cald, ytar(jdata)
          ia=ia + 2
          go to 85
 82       ia=ia + 2
 85       ia=ia + 1
 c
          write(10,106)
          ia=1
          do 95 jdata=1,ndata
          if(mcount(jdata) .eq. 1) go to 95
          if(mcount(jdata) .eq. 2) go to 92
          ia=ia + 2
          cald=-fvecc(ia) + ymplast(jdata)
          write(10,107)ptemp(jdata),  cald, ymplast(jdata)
          ia=ia + 1
          go to 95
 92       ia=ia + 1
          cald=-fvecc(ia) + ymplast(jdata)
          write(10,107)ptemp(jdata), cald, ymplast(jdata)
          ia=ia + 1
 95       ia=ia + 1
 c
 104      format(//,10x,' TOTAL VOLATILES YIELD',//,
     &             8x,'Peak Temp',8x,'Calulated',11x,'Experimental',///)
 105      format(//,10x,' TAR YIELD',//,
     &             8x,'Peak Temp',8x,'Calulated',11x,'Experimental',///)
 106      format(//,10x,' EXTRACT YIELD',//,
     &             8x,'Peak Temp',8x,'Calulated',11x,'Experimental',///)
 107      format(f15.2, f20.7, f20.7)
 c
 300      stop
          end
```

```
c*******************************************************************************
c
c                        SUBROUTINE FUNCT
c
c         Subroutine funct calculate the residual.
c         All variables are as defined in the program SMAIN.
c*******************************************************************************
c
c
          subroutine funct(iflag,n,xc,fc,gc,iw,liw,w,lw)
          implicit double precision (a - h, o - z)
          implicit integer (i - n)
          integer iw,liw,lw,n
          dimension wint(38,18)
          dimension xc(6), w(54), iw(2), gc(6)
          dimension y(38),yp(38),btar(10),alfa(10),ctar(10),ysave(40)
          common/resd/fvecc(100)
          common/tth/ptemp(40),tp,at,bt
          common/yld/mcount(40),yvol(40),ytar(40),ymplast(40)
          common/tar/tmw(10)
          common/con/gcon,gmw,surt,delt,hrate,ao
          common/prop/vcon,visc,dcon,pres,volo,rado,rad,tolo,apore,pvol
          common/rxnc/eg,ept,est,rxng,rxnt1,rxnt2,vt,vg,fg1,coalm
          common/ele/ne,nel,pcon,cmden,cden
          common/cnt/ndata,jdata
          external fcnf
          fexp(x)=dexp(dmax1(-1.d2,x))
c
          m=100
c Convert x's to the actual parameters to be passed onto subroutine fcnf
          rxnt1=10.**(xc(1)*6.5d0 + 6.5d0)
          ept=xc(2)*4.d4 + 4.d4
          rxnt2=10.**(xc(3)*6.5d0 + 6.5d0)
          est=xc(4)*4.d4 + 4.d4
          fg1=(xc(5)*0.25d0) + 0.25d0
          apore=(xc(6)*6.d-6) + 9.d-6
          write(6, )'ept=',ept,'  rxnt1=',rxnt1
          write(6, )'est=',est,'  rxnt2=',rxnt2
          write(6, )'fg1=',fg1,'  apore=',apore
c
          ja=1
          do 100 jdata=1,ndata
c         write(6,)jdata
          if(jdata .ne. 1) go to 20
c
c Define initial conditions for calculations of volatiles yields
          do 15 i=1,ne
          i10=i + 10
          i20=i + 20
          ctar(i)=2.9d-2
          btar(i)=0.d0
          y(i)=2.9d-2
          y(i10)=0.d0
15        y(i20)=0.d0
```

```
          y(38)=1. - 0.29
c
c Calculate total molar density of liquid per gm orig. coal
          cmden=0.d0
          do 11 i=1,ne
11        cmden=cmden + ctar(i)/tmw(i)
          cmden=cmden + y(38)/coalm
c
c v is mass of bubble and v1 is weight of a gas molecule
c initial bubble mass is solely coming from gas
c Initial values for total bubble mass, bubble radius, and
c monomer concentration are
c Assume the same initial number density for all pres
          t=0.0d0
          temp= 298.13
          hcon=2.7924d7*dexp(314.24d0/temp)/cmden
          solub=1./hcon
          v1=28./6.023e23
          bvol=4.187*apore**3
          y(37)=dlog(pvol/(1.3d0*bvol))
          call afunw(apore,temp,ao)
          y(32)=pres*solub
          wmol=pres*bvol*6.023d23/(298.13*gcon)
          bgas=v1*wmol*dexp(y(37))
          y(36)=1.d0
          y(31)=0.029d0
          y(33)=0.d0
          y(34)=0.d0
          y(35)=0.d0
          visc=1.d21
c
c                   calculate the total bubble volume
          volg=4.187*ao**3*dexp(y(37))
          y(38)=1.d0 - bgas - y(32) - 0.29
          volo=(y(38) + 0.29d0)/cden + volg
          rad=rado
          go to 30
c
c
c From the second data point, take an advantage during heat-up time from
c the previous data point.  Initial conditions are defined at the previous
c peak temperature  which is stored under ystore, tsave, rsave, and cmsave.
20        do 25 id=1,38
25        y(id)=ysave(id)
          t=tsave
          rad=rsave
          cmden=cmsave
c
c
30        tp=(ptemp(jdata) - 298.13)/hrate
          tck=tp + 1.d0
c
c Define constant for gear's routine
          neqn=38
          ifail=0
```

```
c
c
c NOW, START THE INTEGRATION
          do 50 ik=1,5000
c
          tol=tolo
          dt=delt
          if(t .gt. tck) dt=delt*2.5d0
          tend=t + dt
          if(tp .gt. t .and. tp .lt. tend) tend=tp
          call d02baf(t,tend,neqn,y,tol,fcnf,wint,ifail)
          if(ifail .ne. 0) go to 302
c
c
          tmplast=0.d0
          do 42 i=1,10
42        tmplast=tmplast + y(i)
c
          if(t .gt. 6.d0) go to 60
          if(y(37) .eq. 0.d0 .and. t .le. tp) go to 43
          if(t .eq. tp) go to 43
          if(tmplast .lt. 1.d-10) go to 60
          if(y(37) .eq. 0.d0) go to 60
          if(t .ne. tp) go to 50
43        do 45 ie=1,38
45        ysave(ie)=y(ie)
          tsave=tp
          rsave=rad
          cmsave=cmden
          if(y(37) .eq. 0.d0) go to 60
          if(tmplast .eq. 1.d-10) go to 60
50        continue
c
c Calculate amount of metaplast remained in particle
60        tmplast=0.d0
          do 61 i=1,10
61        tmplast=tmplast + y(i)
c
c Calculate the particle radius
          brad=ao*y(36)
          cond=tmplast + y(38)
          volg=4.1888*brad**3*dexp(y(37))
          vol=volg + cond/cden
          swell=(vol/volo)**(0.3333)
          rad=rado*swell
c         write(6, ) '     swell =   ',swell
c
c Now, calculate amount of gas and tar in molten coal as well
c as amount of gas formed and released from the particle,
c and total bubble volume
c
c tar yield by diffusion and bubble escape
          btary=0.d0
          dtary=0.d0
          do 70 i=1,ne
```

```
          i10=i + 10
          i20=i + 20
          btary=btary + y(i20)
70        dtary=dtary + y(i10)
c
c Total gas and tar yield
          gasy=y(33) + y(34)
          if(tp .le. 0.375) gasy = y(32)
          ttary=dtary + btary
          chary=y(38)
c
          tvoly=ttary + y(33) + y(34) + y(32)
          px=ptemp(jdata) - 273.13
          write(12,250)px,tvoly
250       format(e12.5,',',e12.5)
c         write(6, )ptemp(jdata),gasy,ttary,tmplast,y(32)
c residual function, fvecc, are
          if(mcount(jdata) .eq. 1) go to 81
          if(mcount(jdata) .eq. 2) go to 82
          fvecc(ja)=yvol(jdata) - ytar(jdata) - gasy
          ja=ja + 1
          fvecc(ja)=ytar(jdata) - ttary
          ja=ja + 1
          fvecc(ja)=ymplast(jdata) - tmplast
          ja=ja + 1
          fvecc(ja)=(1.d0 - yvol(jdata) - ymplast(jdata)) - chary
          go to 100
81        fvecc(ja)=yvol(jdata) - gasy - ttary
          go to 100
82        fvecc(ja)=yvol(jdata) - gasy - ttary
          ja=ja + 1
          fvecc(ja)=ymplast(jdata) - tmplast
          ja=ja + 1
          fvecc(ja)=(1.d0 - yvol(jdata) - ymplast(jdata)) - chary
100       ja=ja + 1
c
c Calculate the residuals.
          fc=0.d0
          do 150 iz=1,m
150       fc=fc + fvecc(iz)**2
          write(6, )'fc  =  ',fc
          go to 300
c
302       write(6, )'ifail from integration package=',ifail
300       return
          end
```

```
c**********************************************************************
c
c                    SUBROUTINE FCNF
c
c         This subroutine calculates the mass balance of volatiles in the
c         molten coal (same as FCNE except  some common statements).
c         For nomenclature, see program SMAIN.
c
c
c**********************************************************************
          subroutine fcnf(t,y,yp)
          implicit double precision (a-h, o-z)
          implicit integer (i - n)
          dimension y(38),yp(38),alfa(10),tsec(10),btar(10),ctar(10),btsec(10)
          common/tth/ptemp(40),tp,at,bt
          common/yld/mcount(40),yvol(40),ytar(40),ymplast(40)
          common/tar/tmw(10)
          common/con/gcon,gmw,surt,delt,hrate,ao
          common/prop/vcon,visc,dcon,pres,volo,rado,rad,tolo,apore,pvol
          common/rxnc/eg,ept,est,rxng,rxnt1,rxnt2,vt,vg,fgl,coalm
          common/ele/ne,nel,pcon,cmden,cden
          common/cnt/ndata, ia
          fexp(x)=dexp(dmax1(-1.d2,x))
c
c
          do 1 i=1,38
          if(y(i) .le. 0.d0) y(i)=0.d0
1         continue
          ysum=0.d0
          do 2 i=1,10
2         ysum=ysum + y(i)
          if (ysum .eq. 0.d0) go to 301
          brad=ao*y(36)
c
c                    Calculate temperature
          if(t .le. tp) temp=hrate*t + 298.13
          if(t .gt. tp) temp=((bt/at)/( (1. + bt/(at*
     &     ptemp(ia)**3))*fexp(3.d0*bt*(t-tp)) - 1.d0))**(1./3.)
c
          if(tp .le. 0.375 ) go to 100
c Calculate tar and gas in bubbles
c which are in equilibrium with molten phase
9         cmdeno=cmden
          con1=(brad**3*dexp(y(37)))/(pcon*cmden*temp)
          do 10 i=1,ne
c Either Suuberg's or Maiorella's vapor pressure model is used and the
c other one is treated as a comment statement.
c         psat1=5.8308d9*exp(-2.55d2*tmw(i)**0.586/temp)
          psat1=6.311d11*dexp(-5.61d2*tmw(i)**0.474/temp)
          if(psat1 .ge. pres) go to 7
          poyf=dexp(tmw(i)*(pres - psat1)/(1.3d0*gcon*temp))
          go to 8
7         poyf=1.d0
8         ckevf=dexp(2.d0*surt*tmw(i)/(brad*gcon*temp*1.3d0))
```

```
            alfa(i)=psat1*con1*poyf*ckevf
            ctar(i)=y(i)/(1.d0 + alfa(i))
            btar(i)=alfa(i)*y(i)/(1.d0 + alfa(i))
 10         continue
 c Calculate total molar density of liquid per gm orig. coal
            cmden=0.d0
            do 11 i=1,ne
 11         cmden=cmden + ctar(i)/tmw(i)
            cmden=cmden + y(38)/coalm
            ck=abs(cmdeno - cmden)/cmden
            if(ck .ge. 1.d-3) go to 9
 c
 c Calculate metaplast weight fraction
            tctar=0.d0
            do 12 i=1,ne
 12         tctar=tctar + ctar(i)
            xtar=tctar/(tctar + y(38))
 c
 c Calculate solubility, viscosity, and diffusivity
            if(xtar .le. 1.d-10)go to 15
            if(temp .le. 723.13)visct=vcon*fexp(45000/(1.987*temp))
            if(temp .gt. 723.13)visct=vcon*fexp(45000/(1.987*723.13))
 c          visct=vcon*fexp(45000/(1.987*temp))
            viscm=1.d0/((1.d0 - xtar)**(-1./3.) - 1.d0)
            visc=visct*viscm
            go to 16
 15         visc=visc
 16         diff=dcon*temp/visc**0.5
            difft=dcon*temp/visc**(2./3.)
            hcon=2.7924d7*dexp(3.1424d2/temp)/cmden
            solub=1./hcon
 c
 c Gas concntration in molten coal and in bubbles
            con2=(brad**3*dexp(y(37))*gmw)/(pcon*solub*temp)
            cmon=y(32)/(1.d0 + con2)
            bgas=con2*y(32)/(1.d0 + con2)
 c
 c Calculate bubble molar density and pressure
            bmden=0.d0
            do 13 i=1,ne
 13         bmden=bmden + btar(i)/tmw(i)
            bmden=(bmden + bgas/gmw)/dexp(y(37))
            pb=bmden*pcon*temp/(brad**3)
 c
 c
 Calculate the particle radius
            cond=tctar + y(38)
            volg=4.1888*brad**3*dexp(y(37))
            vol=volg + cond/cden
            rad=rado*(vol/volo)**(0.3333)
 c
 c Calculate Total Bubble number density
 c Rate of bubble radius growth
            yp(36)=y(36)*(pb -pres - 2.d0*surt/brad)/(4.d0*visc)
 c Balance on log(bubble number density)
```

```
c Calculate amount of bubble escaped
          besc=3.d0*rad**2*yp(36)*ao/rado**3
          if(yp(36) .le. 0.d0) besc=0.d0
          yp(37)=-besc
c
c Balance of gas dissolved in the condensed phase
c Gas formation
          ef1=eg/(1.987*temp)
          yp(35)=rxng*fexp(-ef1)*(vg - y(35))
          if(y(35) .gt. vg)yp(35)=0.d0
c Gas formation from tar cracking both in bubbles and in liquids
          tcovl=0.d0
          tcovg=0.d0
          do 20 i=1,10
          btsec(i)=9.96d2*fexp(-1.54d4/(1.987d0*temp))*btar(i)
          tsec(i)=rxnt2*exp(-est/(1.987*temp))*ctar(i)
          tcovl=tcovl + tsec(i)
20        tcovg=tcovg + btsec(i)
c Monomer escape term
          bltg=(12.56d0*brad*dexp(y(37))*cden)**0.5
          yp(33)=3.d0*bltg*rad**2*diff*cmon/(rado**3)
c         yp(33)=1.5d1*rad*diff*cmon/(rado**3)
          yp(34)=besc*bgas
c
c Then,
          yp(32)=yp(35) - yp(33) - yp(34) + tcovg + fg1*tcovl
c
c For metaplast or tar balance formation
          ft1=ept/(1.987*temp)
          yp(31)=rxnt1*fexp(-ft1)*(0.1d0*vt - y(31))
          if(y(31) .ge. 0.1*vt) yp(31)=0.d0
c
          dgas=pres/(gcon*temp)
          tard=1.013e5*(temp/273.)**1.5/pres
          do 40 i=1,ne
          i10=i + 10
          i20=i + 20
          if (ctar(i) .le. 1.d-38) go to 35
c Rate of tar evaporation
c         psat1=5.8308d9*exp(-2.55d2*tmw(i)**0.586/temp)
          psat1=6.311d11*dexp(-5.61d2*tmw(i)**0.474/temp)
          if(psat1 .ge. pres ) go to 37
          poyf=dexp(tmw(i)*(pres - psat1)/(1.3d0*gcon*temp))
          go to 38
37        poyf=1.d0
38        psat=psat1*poyf
          rlt=rad/(5.d0*difft)
          rgt=(rad*cmden*pres)/(tard*dgas*psat)
          yp(i10)=(1./(rlt + rgt))*(3.d0*rad**2*ctar(i)/(rado**3))
          yp(i20)=besc*btar(i)
          go to 40
35        yp(i10)=0.d0
          yp(i20)=0.d0
40        yp(i)=yp(31) - tsec(i) - yp(i10) - yp(i20) - btsec(i) - yp(35)/10.
c
```

```
c
          form=10.d0*yp(31)
          yp(38)=-form + (1. - fg1)*tcov1
          go to 300
c
c For low temperature runs (peak temp < 400 C),
c assume no mass transfer resistance and no bubbles
100       yp(36)=0.d0
          yp(37)=0.d0
c
c Balance of gas dissolved in the condensed phase
c Gas formation
          ef1=eg/(1.987*temp)
          yp(35)=rxng*fexp(-ef1)*(vg - y(35))
          if(y(35) .gt. vg)yp(35)=0.d0
          yp(33)=0.d0
          yp(34)=0.d0
c
c For metaplast or tar balance
c Formation
          ft1=ept/(1.987*temp)
          yp(31)=rxnt1*fexp(-ft1)*(0.1d0*vt - y(31))
          if(y(31) .ge. 0.1*vt) yp(31)=0.d0
c
          tcov1=0.d0
          do 110 i=1,ne
          i10=i + 10
          i20=i + 20
          tsec(i)=rxnt2*dexp(-est/(1.987*temp))*y(i)
          tcov1=tcov1 + tsec(i)
          yp(i10)=0.d0
          yp(i20)=0.d0
110       yp(i)=yp(31) - yp(35)/10. - tsec(i)
c
c Monomer balance
          yp(32)=yp(35) - fg1*tcov1
c
          yp(38)= - 10.d0*yp(31)
          go to 300
c
301       do 302 i=1,38
302       yp(i)=0.d0
c
c
300       return
          end
```

```
c**********************************************************************
c
c                       SUBROUTINE AFUNW
C
C         This subroutine calculates the radius of a bubble of known mass
c         at a given temperature, pressure, and suface tention of the liquid.
c
c**********************************************************************
          subroutine afunw (apore, temp, ao)
          implicit complex *16 (c-d)
          implicit real *8 (a-b,e-h,o-z),integer *4(i-n)
c
          pres=1.013d6
          surt=30.d0
          gmw=28.d0
          gcon=8.314d7
          p=2.d0*surt/pres
          a=-p**2 /3.d0
          r1=-gcon*temp/(pres*4.187d0)
          v=pres*4.187d0*gmw*apore**3/(gcon*298.d0)
c
          r=r1*v/gmw
          b=(2.d0*p**3 + 27.d0 *r)/27.d0
          e3=(b**2/4.d0 + a**3/27.d0)
          if(e3 .gt. 0.d0)go to 30
          e4=(-e3)**0.5
          c1=cmplx(0.d0,e4)
          go to 40
30 .      e4=e3**0.5d0
          c1=cmplx(e4,0.d0)
40        dummy1=-b/2.d0 + c1
          dummy2=-b/2.d0 - c1
          c2=cexp((clog(dummy1))/3.d0)
          c3=cexp((clog(dummy2))/3.d0)
          d1=c2 + c3
          x11=d1
          ao=x11 - p/3.d0
c
          return
          end
```

```
c*****************************************************************
c
c                        SUBROUTINE MONIT
c
c
c         This routine monitors the iterations of finding best fitting
c         parameters by printing intermediate values.
c
c*****************************************************************
          subroutine monit(n,xc,fc,gc,istate,gpjnrm,cond,posdef,niter,
     &                           nf,iw,liw,w,lw)
          implicit double precision (a-h, o-z)
          implicit integer (i-n)
          logical posdef
          double precision gpjnrm,cond
          integer iw,liw,lw,nf,niter,n
          dimension xc(6),istate(6),gc(6),w(54),iw(2)
c
          write(11,101)
          write(6, )'number of iteration = ',niter
          write(6, )'number of function called = ',nf
          write(6, )'square sum of residuals = ',fc
          write(6, ) 'gpjnrm  =  ', gpjnrm
          write(11, )'number of iteration = ',niter
          write(11, )'number of function called = ',nf
          write(11, )'square sum of residuals = ',fc
          write(11, ) 'gpjnrm  =  ', gpjnrm
          write(11, )'estimated cond of projected hessian: ', cond
c
          write(6, ) 'status'
          do 10 iz=1,n
10        write(6,)istate(iz),xc(iz),gc(iz)
          write(11,102)
          do 20 iz=1,n
20        write(11,103)iz,xc(iz),gc(iz)
c
          if(cond .eq. 0.d0) return
          if(cond .le. 1.d6) go to 21
          write(6, )'estimated condition number of projected Hessian is'
          write(6, )'more than 1.d6'
          go to 30
c
21        write(6, )'estimated cond of projected hessian: ', cond
30        if (.not. posdef)
     &    write(6, )'projected hessian matrix is not positive definite'
          write(6, )'leaving monit'
c
101       format(///)
102       format(/,'Parameters and first derivatives at this iteration',//)
103       format(i15,e20.10,e20.10)
          return
          end
```

****

Example of INPUT file

****

```
1.013d6,  1.d-4, 0.1, 1
169.d0, 270.d0, 330.d0, 386.d0, 447.d0, 519.d0, 609.d0, 727.d0, 892.d0, 1245.d0
1.d-10, 1.d-7
0.5, 1.d0, 1.d-3,  1, 70
6
-0.63674d-2
-0.45775d0
-0.15790d0
-0.52992d0
-0.78798d0
-0.23786d0
32
3,        203.85, 1.626, 0., 26.55
1,        223.26, 1.25, 0., 0.
3,        244.43, 2.91, 0., 25.92
1,        248.53, 2.47, 0., 0.
1,        259.40, 1.37, 0., 0.
3,        264.00, 1.653, 0., 28.10
3,        315.00, 1.657, 0., 25.41
3,        351.50, 2.948, 0., 25.321
1,        379.63, 2.59, 0., 0.
1,        385.56, 3.42, 0., 0.
3,        395.12, 3.43, 0., 23.67
3,        403.55, 3.53, 0., 24.67
1,        414.38, 3.43, 0., 0.
1,        432.38, 3.704, 0., 0.
3,        478.91, 15.04, 9.19, 28.24
3,        509.00, 17.4, 11.85, 29.14
2,        527.90, 19.08, 0., 29.0
3,        558.53, 26.78, 17.72, 19.94
3,        627.77, 34.28, 26.62, 8.78
3,        647.10, 28.70, 24.69, 21.0
3,        647.11, 28.16, 22.90, 25.4
3,        659.59, 36.9, 29.76, 4.76
3,        701.67, 38.96, 30.65, 0.
3,        727.27, 40.43, 30.97, 0.
1,        745.72, 34.3, 0., 0.
3,        781.75, 44.5, 29.93, 0.
3,        877.46, 48.02, 31.34, 0.
1,        948.86, 47.15, 0., 0.
3,        991.00, 47.08, 25.50, 0.
3,        1009.00, 48.84, 25.41, 0.
3,        1029.72, 48.1, 29.70, 0.
3,        1051.76, 47., 29.55, 0.
```

Table G.2.1a. Fitting results with Maiorella's vapor pressure model and the residual function Eq. 6.3-2. Table G.2.1's are employed in Figures 6.3.3's and 6.4.5 thru 6.3.6.

---

pressure	=	0.10130D+07	dyne/cm*cm
original particle radius	=	0.35000D-02	cm
initial pore size	=	0.75729D-05	cm
initial bubble size	=	0.26498D-05	cm
pore volume	=	0.40000D-01	cm**3
constant for viscosity	=	0.10000D-09	
constant for diffusivity	=	0.10000D-06	

Molecular weight of 10 tar compoents

0.16900D+03	0.27000D+03	0.33000D+03	0.38600D+03	0.44700D+03
0.51900D+03	0.60900D+03	0.72700D+03	0.89200D+03	0.12450D+04

Parameters fixed

reactin constant for gas	=	0.10000D+14	1/sec
act e for gas formation	=	0.26755D+05	cal/mole
ultimate yield of gas	=	0.28457D-01	gm/gm
ultimate yield of tar	=	0.70000D+00	gm/gm

Parameters varied, final paratmeter values

reaction constant1 for tar=	0.28748D+07	1/sec	
reaction constant2 for tar=	0.29762D+06	1/sec	
act E for metaplast formation	=	0.21690D+05	cal/mole
act E for metaplast decomposition=		0.18803D+05	cal/mole
fraction of metaplast converted to gases=		0.53004D-01	

square sum of residual functions= 0.14188D+00

Comparison with experimental data

TOTAL VOLATILES YIELD

Peak Temp	Calulated w/o y(32)	Experimental	w/ y(32)
203.85	0.0253175	0.0162600	0.25317D-01
223.26	0.0284219	0.0125000	0.28422D-01
244.43	0.0284413	0.0291000	0.28441D-01
248.53	0.0301472	0.0247000	0.30147D-01
259.40	0.0286470	0.0137000	0.28647D-01
264.00	0.0285021	0.0165300	0.28502D-01
315.00	0.0370164	0.0165700	0.37016D-01
351.50	0.0366343	0.0294800	0.36634D-01
379.63	0.0360485	0.0259000	0.36048D-01
385.56	0.0358759	0.0342000	0.35876D-01
395.12	0.0355512	0.0343000	0.35551D-01
403.55	0.0212840	0.0353000	0.50774D-01
414.38	0.0308530	0.0343000	0.58408D-01
432.38	0.0482879	0.0370400	0.73437D-01
478.91	0.0912327	0.1504000	0.11486D+00
509.00	0.1281190	0.1740000	0.15229D+00
527.90	0.1558730	0.1908000	0.18090D+00
558.53	0.2035101	0.2678000	0.23055D+00
627.77	0.2957889	0.3428000	0.32766D+00

Table G.2.1a continues

647.10	0.3144654	0.2870000	0.34757D+00
647.11	0.3144758	0.2816000	0.34759D+00
659.59	0.3247438	0.3690000	0.35866D+00
701.67	0.3513725	0.3896000	0.38800D+00
727.27	0.3636650	0.4043000	0.40183D+00
745.72	0.3712799	0.3430000	0.41052D+00
781.75	0.3835623	0.4450000	0.42502D+00
877.46	0.4024340	0.4802000	0.45228D+00
948.86	0.4064956	0.4715000	0.46648D+00
991.00	0.4053905	0.4708000	0.47352D+00
1009.00	0.4040868	0.4884000	0.47630D+00
1029.72	0.4019838	0.4810000	0.47935D+00
1051.76	0.3989564	0.4700000	0.48242D+00

TAR YIELD

Peak Temp	Calulated	Experimental
203.85	0.0000000	0.0000000
244.43	0.0000000	0.0000000
264.00	0.0000000	0.0000000
315.00	0.0000000	0.0000000
351.50	0.0000000	0.0000000
395.12	0.0000000	0.0000000
403.55	0.0117578	0.0000000
478.91	0.0702608	0.0919000
509.00	0.1031686	0.1185000
558.53	0.1718410	0.1772000
627.77	0.2561648	0.2662000
647.10	0.2724125	0.2469000
647.11	0.2724215	0.2290000
659.59	0.2809081	0.2976000
701.67	0.2998226	0.3065000
727.27	0.3060389	0.3097000
781.75	0.3103601	0.2993000
877.46	0.2981523	0.3134000
991.00	0.2706180	0.2550000
1009.00	0.2663301	0.2541000
1029.72	0.2616537	0.2970000
1051.76	0.2570457	0.2955000

EXTRACT YIELD

Peak Temp	Calulated	Experimental
203.85	0.2646445	0.2655000
244.43	0.2614337	0.2592000
264.00	0.2613304	0.2810000
315.00	0.2533869	0.2541000
351.50	0.2561745	0.2532100
395.12	0.2659110	0.2367000
403.55	0.2635375	0.2467000
478.91	0.2857140	0.2824000
509.00	0.2840387	0.2914000
527.90	0.2703613	0.2900000
558.53	0.2300243	0.1994000
627.77	0.1345016	0.0878000
647.10	0.1178592	0.2100000
647.11	0.1178515	0.2540000
659.59	0.1089684	0.0476000
701.67	0.0852220	0.0000000
727.27	0.0735005	0.0000000
781.75	0.0536949	0.0000000
877.46	0.0321937	0.0000000
991.00	0.0185697	0.0000000
1009.00	0.0170346	0.0000000
1029.72	0.0154010	0.0000000
1051.76	0.0138063	0.0000000

Table G.2.1b. Product distribution during coal pyrolysis as coal is heated at 448 C/s to 760 C and held there for 5 sec, predicted using parameters from Table G.2.1a.

++++++ Kinetic Constants +++++++

reactin constant for gas	= 0.10000D+14	1/sec
act E for gas formation	= 0.26755D+05	cal/mole
ultimate yield of gas	= 0.28457D-01	gm/gm
reaction constant1 for tar	= 0.28749D+07	1/sec
act e for tar formation	= 0.21690D+05	cal/mole
ultimate yield of tar	= 0.70000D+00	gm/gm
reaction constant2 for tar	= 0.29762D+06	1/sec
act e for tar decomp	= 0.18803D+05	cal/mole
f of metaplast to gases	= 0.53004D-01	

+++++++++ Run Conditions +++++++

pressure	= 0.10130D+07	dyne/cm*cm
original particle radius	= 0.35000D-02	cm
initial bubble size (solid)	= 0.75729D-05	cm
initial bubble size (molten)	= 0.26498D-05	cm
pore volume	= 0.40000D-01	cm**3
heating rate	= 0.44800D+03	C/s
holding time	= 0.50000D+01	sec
constant for viscosity	= 0.10000D-09	
constant for diffusivity	= 0.10000D-06	

Molecular weight of 10 tar compoents

0.16900D+03	0.27000D+03	0.33000D+03	0.38600D+03	0.44700D+03
0.51900D+03	0.60900D+03	0.72700D+03	0.89200D+03	0.12450D+04

1 peak temperature = 0.10331D+04 kelvin

********** output **********

t	temp	char	ctar	cmon	bgas	bmass	ttary	gasy
0.273	0.420530D+03	0.709959D+00	0.289916D+00	0.835298D-04	0.551531D-05	0.570800D-05	0.870969D-10	0.757032D-10
0.323	0.442930D+03	0.709960D+00	0.289472D+00	0.502029D-03	0.303393D-04	0.307358D-04	0.692357D-09	0.226338D-08
0.373	0.465330D+03	0.709961D+00	0.287530D+00	0.234212D-02	0.130863D-03	0.131622D-03	0.416810D-08	0.427548D-07
0.423	0.487730D+03	0.709964D+00	0.281060D+00	0.849202D-02	0.446389D-03	0.447750D-03	0.208662D-07	0.566329D-06
0.473	0.510130D+03	0.709968D+00	0.268672D+00	0.202921D-01	0.102586D-02	0.102817D-02	0.882078D-07	0.484836D-05

Table G.2.1b continues

0.523	0.532530D+03	0.709969D+00	0.261736D+00	0.269248D-01	0.130728D-02	0.131106D-02	0.328627D-06	0.237663D-04
0.573	0.554930D+03	0.709957D+00	0.261386D+00	0.272250D-01	0.131304D-02	0.131933D-02	0.113821D-05	0.760171D-04
0.623	0.577330D+03	0.709909D+00	0.261414D+00	0.268064D-01	0.161676D-02	0.162945D-02	0.365254D-05	0.202450D-03
0.673	0.599730D+03	0.709769D+00	0.261476D+00	0.237025D-01	0.444094D-02	0.450229D-02	0.108753D-04	0.503844D-03
0.723	0.622130D+03	0.709431D+00	0.260549D+00	0.754745D-02	0.200368D-01	0.213026D-01	0.329592D-04	0.110221D-02
0.773	0.644530D+03	0.708677D+00	0.252296D+00	0.131206D-02	0.256942D-01	0.357902D-01	0.141910D-03	0.174785D-02
0.823	0.666930D+03	0.707080D+00	0.234783D+00	0.305335D-03	0.259171D-01	0.544093D-01	0.743853D-03	0.264336D-02
0.873	0.689330D+03	0.703904D+00	0.211278D+00	0.890578D-04	0.246528D-01	0.770729D-01	0.332133D-02	0.430013D-02
0.923	0.711730D+03	0.697983D+00	0.183815D+00	0.326109D-04	0.222311D-01	0.100114D+00	0.109772D-01	0.704231D-02
0.973	0.734130D+03	0.687773D+00	0.161877D+00	0.170104D-04	0.197094D-01	0.117122D+00	0.232181D-01	0.995784D-02
1.023	0.756530D+03	0.671765D+00	0.150111D+00	0.131093D-04	0.186022D-01	0.134181D+00	0.322862D-01	0.116080D-01
1.073	0.778930D+03	0.648738D+00	0.141744D+00	0.111846D-04	0.180937D-01	0.155737D+00	0.408442D-01	0.128910D-01
1.123	0.801330D+03	0.618325D+00	0.133739D+00	0.973045D-05	0.178735D-01	0.182281D+00	0.513982D-01	0.142127D-01
1.173	0.823730D+03	0.581982D+00	0.123752D+00	0.842442D-05	0.178782D-01	0.212467D+00	0.660076D-01	0.157475D-01
1.223	0.846130D+03	0.543688D+00	0.109875D+00	0.724010D-05	0.181386D-01	0.242618D+00	0.862059D-01	0.175698D-01
1.273	0.868530D+03	0.509630D+00	0.915520D-01	0.625376D-05	0.187363D-01	0.267228D+00	0.111891D+00	0.196577D-01
1.323	0.890930D+03	0.486176D+00	0.703147D-01	0.555438D-05	0.197734D-01	0.281262D+00	0.140322D+00	0.218850D-01
1.373	0.913330D+03	0.476644D+00	0.492922D-01	0.519816D-05	0.213364D-01	0.282985D+00	0.166984D+00	0.240550D-01
1.423	0.935730D+03	0.479156D+00	0.315499D-01	0.519380D-05	0.234616D-01	0.274985D+00	0.188284D+00	0.259852D-01
1.473	0.958130D+03	0.487981D+00	0.186801D-01	0.551027D-05	0.261370D-01	0.262399D+00	0.203317D+00	0.275813D-01
1.523	0.980530D+03	0.497562D+00	0.105549D-01	0.610071D-05	0.293429D-01	0.249791D+00	0.213205D+00	0.288459D-01
1.573	0.100293D+04	0.505276D+00	0.596886D-02	0.692599D-05	0.330804D-01	0.239256D+00	0.219614D+00	0.298419D-01
1.623	0.102533D+04	0.510959D+00	0.353485D-02	0.796330D-05	0.373620D-01	0.230913D+00	0.223899D+00	0.306508D-01
1.641	0.103313D+04	0.512575D+00	0.299128D-02	0.837220D-05	0.389826D-01	0.228423D+00	0.225065D+00	0.309022D-01
1.691	0.103313D+04	0.516514D+00	0.238997D-02	0.934987D-05	0.435371D-01	0.221445D+00	0.227992D+00	0.316140D-01
1.741	0.103313D+04	0.519744D+00	0.200329D-02	0.102530D-04	0.477329D-01	0.215308D+00	0.230554D+00	0.323450D-01
1.791	0.103313D+04	0.522490D+00	0.172376D-02	0.110891D-04	0.516127D-01	0.209811D+00	0.232834D+00	0.330945D-01
1.841	0.103313D+04	0.524874D+00	0.150776D-02	0.118652D-04	0.552124D-01	0.204839D+00	0.234876D+00	0.338573D-01
1.891	0.103313D+04	0.526971D+00	0.133433D-02	0.125878D-04	0.585625D-01	0.200308D+00	0.236711D+00	0.346278D-01
1.941	0.103313D+04	0.528836D+00	0.119162D-02	0.132624D-04	0.616889D-01	0.196159D+00	0.238364D+00	0.354009D-01
1.991	0.103313D+04	0.530508D+00	0.107206D-02	0.138938D-04	0.646138D-01	0.192344D+00	0.239855D+00	0.361722D-01
2.041	0.103313D+04	0.532017D+00	0.970429D-03	0.144861D-04	0.673562D-01	0.188823D+00	0.241202D+00	0.369383D-01
2.091	0.103313D+04	0.533386D+00	0.882993D-03	0.150428D-04	0.699327D-01	0.185563D+00	0.242421D+00	0.376962D-01
2.141	0.103313D+04	0.534635D+00	0.806990D-03	0.155671D-04	0.723581D-01	0.182538D+00	0.243526D+00	0.384435D-01
2.191	0.103313D+04	0.535779D+00	0.740337D-03	0.160618D-04	0.746450D-01	0.179723D+00	0.244528D+00	0.391784D-01
2.241	0.103313D+04	0.536830D+00	0.681438D-03	0.165293D-04	0.768050D-01	0.177099D+00	0.245438D+00	0.398993D-01
2.291	0.103313D+04	0.537799D+00	0.629051D-03	0.169717D-04	0.788481D-01	0.174649D+00	0.246266D+00	0.406050D-01
2.341	0.103313D+04	0.538694D+00	0.582194D-03	0.173911D-04	0.807834D-01	0.172358D+00	0.247018D+00	0.412946D-01
2.391	0.103313D+04	0.539524D+00	0.540078D-03	0.177892D-04	0.826192D-01	0.170211D+00	0.247704D+00	0.419672D-01
2.441	0.103313D+04	0.540295D+00	0.502059D-03	0.181675D-04	0.843626D-01	0.168198D+00	0.248329D+00	0.426226D-01
2.491	0.103313D+04	0.541012D+00	0.467610D-03	0.185274D-04	0.860204D-01	0.166307D+00	0.248899D+00	0.432603D-01
2.541	0.103313D+04	0.541680D+00	0.436291D-03	0.188702D-04	0.875984D-01	0.164529D+00	0.249420D+00	0.438802D-01
2.591	0.103313D+04	0.542305D+00	0.407730D-03	0.191971D-04	0.891020D-01	0.162855D+00	0.249896D+00	0.444822D-01
2.641	0.103313D+04	0.542888D+00	0.381612D-03	0.195091D-04	0.905361D-01	0.161278D+00	0.250331D+00	0.450664D-01
2.891	0.103313D+04	0.545308D+00	0.279431D-03	0.208759D-04	0.968077D-01	0.154613D+00	0.252016D+00	0.477270D-01
3.141	0.103313D+04	0.547103D+00	0.209950D-03	0.219824D-04	0.101871D+00	0.149529D+00	0.253116D+00	0.499848D-01
3.391	0.103313D+04	0.548465D+00	0.160833D-03	0.228904D-04	0.106016D+00	0.145581D+00	0.253845D+00	0.518895D-01
3.641	0.103313D+04	0.549517D+00	0.125059D-03	0.236429D-04	0.109446D+00	0.142474D+00	0.254333D+00	0.534920D-01
3.891	0.103313D+04	0.550339D+00	0.983886D-04	0.242714D-04	0.112306D+00	0.140001D+00	0.254664D+00	0.548385D-01
4.141	0.103313D+04	0.550989D+00	0.781390D-04	0.247993D-04	0.114707D+00	0.138013D+00	0.254890D+00	0.559696D-01
4.391	0.103313D+04	0.551507D+00	0.625391D-04	0.252448D-04	0.116731D+00	0.136404D+00	0.255046D+00	0.569201D-01
4.641	0.103313D+04	0.551923D+00	0.503790D-04	0.256220D-04	0.118445D+00	0.135093D+00	0.255153D+00	0.577194D-01
4.891	0.103313D+04	0.552259D+00	0.408080D-04	0.259424D-04	0.119900D+00	0.134019D+00	0.255228D+00	0.583924D-01
5.141	0.103313D+04	0.552532D+00	0.332130D-04	0.262150D-04	0.121138D+00	0.133133D+00	0.255280D+00	0.589599D-01
5.391	0.103313D+04	0.552755D+00	0.271442D-04	0.264474D-04	0.122194D+00	0.132401D+00	0.255317D+00	0.594391D-01
5.641	0.103313D+04	0.552937D+00	0.222655D-04	0.266458D-04	0.123095D+00	0.131792D+00	0.255342D+00	0.598445D-01
5.891	0.103313D+04	0.553087D+00	0.183229D-04	0.268153D-04	0.123865D+00	0.131284D+00	0.255361D+00	0.601882D-01
6.141	0.103313D+04	0.553210D+00	0.151219D-04	0.269601D-04	0.124523D+00	0.130859D+00	0.255373D+00	0.604800D-01
6.391	0.103313D+04	0.553312D+00	0.125124D-04	0.270841D-04	0.125086D+00	0.130502D+00	0.255383D+00	0.607284D-01
6.641	0.103313D+04	0.553397D+00	0.103773D-04	0.271901D-04	0.125568D+00	0.130201D+00	0.255389D+00	0.609403D-01

Table G.2.1c. Changes in viscosity and swelling as a function of time as coal is heated at 448 C/s to 760 C and held there for 5 sec, predicted using parameters from Table G.2.1a.

t	temp	diff	difft	visc	swell
0.273214D+00	0.420530D+03	0.295658D-11	0.122026D-13	0.202309D+15	0.999973D+00
0.323214D+00	0.442930D+03	0.121460D-10	0.789103D-13	0.132985D+14	0.999825D+00
0.373214D+00	0.465330D+03	0.435528D-10	0.426024D-12	0.114154D+13	0.999178D+00
0.423214D+00	0.487730D+03	0.138157D-09	0.195480D-11	0.124628D+12	0.997019D+00
0.473214D+00	0.510130D+03	0.392471D-09	0.774789D-11	0.168945D+11	0.992856D+00
0.523214D+00	0.532530D+03	0.103002D-08	0.276489D-10	0.267301D+10	0.990515D+00
0.573214D+00	0.554930D+03	0.253072D-08	0.904160D-10	0.480828D+09	0.990427D+00
0.623214D+00	0.577330D+03	0.581169D-08	0.270351D-09	0.986833D+08	0.990625D+00
0.673214D+00	0.599730D+03	0.125624D-07	0.746068D-09	0.227912D+08	0.992492D+00
0.723214D+00	0.622130D+03	0.256825D-07	0.191230D-08	0.586796D+07	0.102839D+01
0.773214D+00	0.644530D+03	0.493857D-07	0.451913D-08	0.170327D+07	0.122445D+01
0.823214D+00	0.666930D+03	0.893202D-07	0.984554D-08	0.557520D+06	0.165102D+01
0.873214D+00	0.689330D+03	0.153053D-06	0.199670D-07	0.202849D+06	0.226185D+01
0.923214D+00	0.711730D+03	0.249488D-06	0.378991D-07	0.813822D+05	0.290844D+01
0.973214D+00	0.734130D+03	0.313863D-06	0.509404D-07	0.547100D+05	0.336695D+01
0.102321D+01	0.756530D+03	0.315685D-06	0.508234D-07	0.574306D+05	0.355694D+01
0.107321D+01	0.778930D+03	0.321628D-06	0.515988D-07	0.586528D+05	0.368077D+01
0.112321D+01	0.801330D+03	0.329311D-06	0.527477D-07	0.592122D+05	0.379540D+01
0.117321D+01	0.823730D+03	0.335821D-06	0.536474D-07	0.601665D+05	0.391460D+01
0.122321D+01	0.846130D+03	0.336800D-06	0.533766D-07	0.631145D+05	0.403587D+01
0.127321D+01	0.868530D+03	0.327016D-06	0.508741D-07	0.705394D+05	0.414858D+01
0.132321D+01	0.890930D+03	0.302553D-06	0.454765D-07	0.867130D+05	0.424152D+01
0.137321D+01	0.913330D+03	0.263921D-06	0.375915D-07	0.119759D+06	0.430948D+01
0.142321D+01	0.935730D+03	0.217029D-06	0.287281D-07	0.185894D+06	0.435462D+01
0.147321D+01	0.958130D+03	0.170192D-06	0.206115D-07	0.316937D+06	0.438296D+01
0.152321D+01	0.980530D+03	0.130016D-06	0.142837D-07	0.568759D+06	0.440047D+01
0.157321D+01	0.100293D+04	0.993931D-07	0.990949D-08	0.101819D+07	0.441153D+01
0.162321D+01	0.102533D+04	0.778238D-07	0.709897D-08	0.173581D+07	0.441890D+01
0.164062D+01	0.103313D+04	0.720342D-07	0.638754D-08	0.205699D+07	0.442092D+01
0.169062D+01	0.103313D+04	0.641551D-07	0.547339D-08	0.259327D+07	0.442604D+01
0.174062D+01	0.103313D+04	0.585611D-07	0.484649D-08	0.311237D+07	0.443058D+01
0.179062D+01	0.103313D+04	0.541841D-07	0.436962D-08	0.363552D+07	0.443468D+01
0.184062D+01	0.103313D+04	0.505640D-07	0.398478D-08	0.417471D+07	0.443840D+01
0.189062D+01	0.103313D+04	0.474751D-07	0.366356D-08	0.473563D+07	0.444178D+01
0.194062D+01	0.103313D+04	0.447875D-07	0.338967D-08	0.532104D+07	0.444487D+01
0.199062D+01	0.103313D+04	0.424158D-07	0.315248D-08	0.593273D+07	0.444769D+01
0.204062D+01	0.103313D+04	0.402993D-07	0.294450D-08	0.657225D+07	0.445027D+01
0.209062D+01	0.103313D+04	0.383927D-07	0.276024D-08	0.724123D+07	0.445263D+01
0.214062D+01	0.103313D+04	0.366612D-07	0.259552D-08	0.794139D+07	0.445480D+01
0.219062D+01	0.103313D+04	0.350778D-07	0.244714D-08	0.867451D+07	0.445679D+01
0.224062D+01	0.103313D+04	0.336212D-07	0.231260D-08	0.944241D+07	0.445862D+01
0.229062D+01	0.103313D+04	0.322745D-07	0.218991D-08	0.102469D+08	0.446030D+01
0.234062D+01	0.103313D+04	0.310238D-07	0.207750D-08	0.110897D+08	0.446185D+01
0.239062D+01	0.103313D+04	0.298580D-07	0.197407D-08	0.119726D+08	0.446329D+01
0.244062D+01	0.103313D+04	0.287677D-07	0.187855D-08	0.128973D+08	0.446461D+01
0.249062D+01	0.103313D+04	0.277451D-07	0.179005D-08	0.138655D+08	0.446584D+01
0.254062D+01	0.103313D+04	0.267836D-07	0.170781D-08	0.148790D+08	0.446697D+01
0.259062D+01	0.103313D+04	0.258774D-07	0.163121D-08	0.159393D+08	0.446802D+01
0.264062D+01	0.103313D+04	0.250216D-07	0.155968D-08	0.170482D+08	0.446900D+01
0.289062D+01	0.103313D+04	0.213643D-07	0.126338D-08	0.233847D+08	0.447295D+01
0.314062D+01	0.103313D+04	0.184887D-07	0.104189D-08	0.312247D+08	0.447575D+01
0.339062D+01	0.103313D+04	0.161623D-07	0.870867D-09	0.408606D+08	0.447778D+01
0.364062D+01	0.103313D+04	0.142384D-07	0.735466D-09	0.526488D+08	0.447928D+01
0.389062D+01	0.103313D+04	0.126199D-07	0.626164D-09	0.670193D+08	0.448041D+01
0.414062D+01	0.103313D+04	0.112399D-07	0.536577D-09	0.844859D+08	0.448127D+01
0.439062D+01	0.103313D+04	0.100508D-07	0.462259D-09	0.105659D+09	0.448194D+01
0.464062D+01	0.103313D+04	0.901757D-08	0.400007D-09	0.131260D+09	0.448246D+01
0.489062D+01	0.103313D+04	0.811346D-08	0.347448D-09	0.162143D+09	0.448288D+01
0.514062D+01	0.103313D+04	0.731782D-08	0.302778D-09	0.199318D+09	0.448321D+01
0.539062D+01	0.103313D+04	0.661423D-08	0.264598D-09	0.243978D+09	0.448347D+01
0.564062D+01	0.103313D+04	0.598944D-08	0.231809D-09	0.297535D+09	0.448368D+01
0.589062D+01	0.103313D+04	0.543261D-08	0.203529D-09	0.361654D+09	0.448386D+01
0.614062D+01	0.103313D+04	0.493477D-08	0.179049D-09	0.438304D+09	0.448400D+01
0.639062D+01	0.103313D+04	0.448843D-08	0.157788D-09	0.529811D+09	0.448411D+01
0.664062D+01	0.103313D+04	0.408727D-08	0.139270D-09	0.638917D+09	0.448421D+01

Table G.2.1d. Amount of volatiles formed and changes in bubble radius and bubble number density as a function of time as coal is heated at 448 C/s to 760 C and held there for 5 sec, predicted using parameters from Table G.2.1a.

t	temp	bnden	brad	gasf	tarf
0.273214D+00	0.420530D+03	0.169210D+14	0.264980D-05	0.830994D-04	0.290000D-01
0.323214D+00	0.442930D+03	0.169210D+14	0.264980D-05	0.526352D-03	0.290001D-01
0.373214D+00	0.465330D+03	0.169210D+14	0.264980D-05	0.246680D-02	0.290003D-01
0.423214D+00	0.487730D+03	0.169210D+14	0.264984D-05	0.893219D-02	0.290010D-01
0.473214D+00	0.510130D+03	0.169210D+14	0.265062D-05	0.213147D-01	0.290029D-01
0.523214D+00	0.532530D+03	0.169209D+14	0.265889D-05	0.282450D-01	0.290078D-01
0.573214D+00	0.554930D+03	0.169202D+14	0.271024D-05	0.285974D-01	0.290194D-01
0.623214D+00	0.577330D+03	0.169163D+14	0.298072D-05	0.285974D-01	0.290448D-01
0.673214D+00	0.599730D+03	0.168956D+14	0.443643D-05	0.285974D-01	0.290976D-01
0.723214D+00	0.622130D+03	0.168007D+14	0.109302D-04	0.285974D-01	0.292013D-01
0.773214D+00	0.644530D+03	0.166162D+14	0.213291D-04	0.285974D-01	0.293952D-01
0.823214D+00	0.666930D+03	0.162416D+14	0.342931D-04	0.285974D-01	0.297418D-01
0.873214D+00	0.689330D+03	0.154052D+14	0.503042D-04	0.285974D-01	0.303344D-01
0.923214D+00	0.711730D+03	0.139102D+14	0.679546D-04	0.285974D-01	0.313053D-01
0.973214D+00	0.734130D+03	0.123144D+14	0.823121D-04	0.285974D-01	0.328270D-01
0.102321D+01	0.756530D+03	0.114797D+14	0.891367D-04	0.285974D-01	0.351001D-01
0.107321D+01	0.778930D+03	0.108673D+14	0.940178D-04	0.285974D-01	0.383157D-01
0.112321D+01	0.801330D+03	0.102446D+14	0.989419D-04	0.285974D-01	0.425800D-01
0.117321D+01	0.823730D+03	0.953113D+13	0.104605D-03	0.285974D-01	0.478055D-01
0.122321D+01	0.846130D+03	0.872167D+13	0.111152D-03	0.285974D-01	0.536074D-01
0.127321D+01	0.868530D+03	0.787164D+13	0.118290D-03	0.285974D-01	0.592960D-01
0.132321D+01	0.890930D+03	0.707255D+13	0.125381D-03	0.285974D-01	0.640616D-01
0.137321D+01	0.913330D+03	0.640590D+13	0.131696D-03	0.285974D-01	0.673357D-01
0.142321D+01	0.935730D+03	0.590556D+13	0.136750D-03	0.285974D-01	0.690900D-01
0.147321D+01	0.958130D+03	0.555723D+13	0.140466D-03	0.285974D-01	0.697801D-01
0.152321D+01	0.980530D+03	0.532373D+13	0.143062D-03	0.285974D-01	0.699655D-01
0.157321D+01	0.100293D+04	0.516700D+13	0.144858D-03	0.285974D-01	0.699968D-01
0.162321D+01	0.102533D+04	0.505780D+13	0.146136D-03	0.285974D-01	0.699999D-01
0.164062D+01	0.103313D+04	0.502715D+13	0.146499D-03	0.285974D-01	0.700000D-01
0.169062D+01	0.103313D+04	0.494777D+13	0.147448D-03	0.285974D-01	0.700000D-01
0.174062D+01	0.103313D+04	0.487501D+13	0.148330D-03	0.285974D-01	0.700000D-01
0.179062D+01	0.103313D+04	0.480732D+13	0.149160D-03	0.285974D-01	0.700000D-01
0.184062D+01	0.103313D+04	0.474401D+13	0.149946D-03	0.285974D-01	0.700000D-01
0.189062D+01	0.103313D+04	0.468466D+13	0.150691D-03	0.285974D-01	0.700000D-01
0.194062D+01	0.103313D+04	0.462897D+13	0.151398D-03	0.285974D-01	0.700000D-01
0.199062D+01	0.103313D+04	0.457665D+13	0.152068D-03	0.285974D-01	0.700000D-01
0.204062D+01	0.103313D+04	0.452746D+13	0.152705D-03	0.285974D-01	0.700000D-01
0.209062D+01	0.103313D+04	0.448116D+13	0.153311D-03	0.285974D-01	0.700000D-01
0.214062D+01	0.103313D+04	0.443755D+13	0.153886D-03	0.285974D-01	0.700000D-01
0.219062D+01	0.103313D+04	0.439644D+13	0.154433D-03	0.285974D-01	0.700000D-01
0.224062D+01	0.103313D+04	0.435766D+13	0.154953D-03	0.285974D-01	0.700000D-01
0.229062D+01	0.103313D+04	0.432107D+13	0.155448D-03	0.285974D-01	0.700000D-01
0.234062D+01	0.103313D+04	0.428650D+13	0.155918D-03	0.285974D-01	0.700000D-01
0.239062D+01	0.103313D+04	0.425383D+13	0.156367D-03	0.285974D-01	0.700000D-01
0.244062D+01	0.103313D+04	0.422293D+13	0.156793D-03	0.285974D-01	0.700000D-01
0.249062D+01	0.103313D+04	0.419370D+13	0.157200D-03	0.285974D-01	0.700000D-01
0.254062D+01	0.103313D+04	0.416603D+13	0.157587D-03	0.285974D-01	0.700000D-01
0.259062D+01	0.103313D+04	0.413981D+13	0.157956D-03	0.285974D-01	0.700000D-01
0.264062D+01	0.103313D+04	0.411497D+13	0.158308D-03	0.285974D-01	0.700000D-01
0.289062D+01	0.103313D+04	0.400850D+13	0.159838D-03	0.285974D-01	0.700000D-01
0.314062D+01	0.103313D+04	0.392576D+13	0.161053D-03	0.285974D-01	0.700000D-01
0.339062D+01	0.103313D+04	0.386073D+13	0.162025D-03	0.285974D-01	0.700000D-01
0.364062D+01	0.103313D+04	0.380913D+13	0.162808D-03	0.285974D-01	0.700000D-01
0.389062D+01	0.103313D+04	0.376785D+13	0.163441D-03	0.285974D-01	0.700000D-01
0.414062D+01	0.103313D+04	0.373463D+13	0.163956D-03	0.285974D-01	0.700000D-01
0.439062D+01	0.103313D+04	0.370774D+13	0.164376D-03	0.285974D-01	0.700000D-01
0.464062D+01	0.103313D+04	0.368587D+13	0.164719D-03	0.285974D-01	0.700000D-01
0.489062D+01	0.103313D+04	0.366802D+13	0.165001D-03	0.285974D-01	0.700000D-01
0.514062D+01	0.103313D+04	0.365339D+13	0.165233D-03	0.285974D-01	0.700000D-01
0.539062D+01	0.103313D+04	0.364137D+13	0.165424D-03	0.285974D-01	0.700000D-01
0.564062D+01	0.103313D+04	0.363147D+13	0.165583D-03	0.285974D-01	0.700000D-01
0.589062D+01	0.103313D+04	0.362328D+13	0.165714D-03	0.285974D-01	0.700000D-01
0.614062D+01	0.103313D+04	0.361650D+13	0.165822D-03	0.285974D-01	0.700000D-01
0.639062D+01	0.103313D+04	0.361088D+13	0.165912D-03	0.285974D-01	0.700000D-01
0.664062D+01	0.103313D+04	0.360621D+13	0.165988D-03	0.285974D-01	0.700000D-01

Table G.2.2a. Fitting results with Maiorella's vapor pressure model and the residual function Eq. 6.3-3. Table G.2.2's are employed in Figure 6.3.4.

---

pressure	=	0.10130D+07	dyne/cm*cm
original particle radius	=	0.35000D-02	cm
initial pore size	=	0.75568D-05	cm
initial bubble size	=	0.26415D-05	cm
pore volume	=	0.40000D-01	cm**3
constant for viscosity	=	0.10000D-09	
constant for diffusivity	=	0.10000D-06	

Molecular weight of 10 tar compoents

0.16900D+03	0.27000D+03	0.33000D+03	0.38600D+03	0.44700D+03
0.51900D+03	0.60900D+03	0.72700D+03	0.89200D+03	0.12450D+04

Parameters fixed

reactin constant for gas	=	0.10000D+14	1/sec
act e for gas formation	=	0.26755D+05	cal/mole
ultimate yield of gas	=	0.28457D-01	gm/gm
ultimate yield of tar	=	0.70000D+00	gm/gm

Parameters varied, final paratmeter values

reaction constant1 for tar=	0.19045D+09	1/sec	
reaction constant2 for tar=	0.17552D+06	1/sec	
act E for metaplast formation	=	0.27354D+05	cal/mole
act E for metaplast decomposition=		0.17915D+05	cal/mole
fraction of metaplast converted to gases=		0.18835D-01	

square sum of residual functions= 0.14331D+00

Comparison with experimental data

TOTAL VOLATILES YIELD

Peak Temp	Calulated w/o y(32)	Experimental	w/ y(32)
203.85	0.0253200	0.0162600	0.25320D-01
223.26	0.0284277	0.0125000	0.28428D-01
244.43	0.0284546	0.0291000	0.28455D-01
248.53	0.0301625	0.0247000	0.30163D-01
259.40	0.0286696	0.0137000	0.28670D-01
264.00	0.0285288	0.0165300	0.28529D-01
315.00	0.0371461	0.0165700	0.37146D-01
351.50	0.0369832	0.0294800	0.36983D-01
379.63	0.0367446	0.0259000	0.36745D-01
385.56	0.0366755	0.0342000	0.36675D-01
395.12	0.0365461	0.0343000	0.36546D-01
403.55	0.0206371	0.0353000	0.49480D-01
414.38	0.0300166	0.0343000	0.56768D-01
432.38	0.0474295	0.0370400	0.71423D-01
478.91	0.0955710	0.1504000	0.11646D+00
509.00	0.1409102	0.1740000	0.16132D+00
527.90	0.1715242	0.19[illegible]000	0.19248D+00
558.53	0.2130429	0.2678000	0.23618D+00
627.77	0.2828241	0.3428000	0.31257D+00
647.10	0.2996414	0.2870000	0.33104D+00
647.11	0.2996509	0.2816000	0.33105D+00
659.59	0.3095729	0.3690000	0.34200D+00

Table G.2.2a continues

701.67	0.3377624	0.3896000	0.37346D+00
727.27	0.3516030	0.4043000	0.38911D+00
745.72	0.3603460	0.3430000	0.39907D+00
781.75	0.3746194	0.4450000	0.41568D+00
877.46	0.3971319	0.4802000	0.44635D+00
948.86	0.4029224	0.4715000	0.46183D+00
991.00	0.4026682	0.4708000	0.46934D+00
1009.00	0.4017350	0.4884000	0.47228D+00
1029.72	0.4000416	0.4810000	0.47548D+00
1051.76	0.3974706	0.4700000	0.47869D+00

TAR YIELD

Peak Temp	Calulated	Experimental
203.85	0.0000000	0.0000000
244.43	0.0000000	0.0000000
264.00	0.0000000	0.0000000
315.00	0.0000000	0.0000000
351.50	0.0000000	0.0000000
395.12	0.0000000	0.0000000
403.55	0.0113250	0.0000000
478.91	0.0746801	0.0919000
509.00	0.1161406	0.1185000
558.53	0.1835388	0.1772000
627.77	0.2484845	0.2662000
647.10	0.2632711	0.2469000
647.11	0.2632793	0.2290000
659.59	0.2716613	0.2976000
701.67	0.2931472	0.3065000
727.27	0.3016603	0.3097000
781.75	0.3104837	0.2993000
877.46	0.3035949	0.3134000
991.00	0.2796542	0.2550000
1009.00	0.2757528	0.2541000
1029.72	0.2714647	0.2970000
1051.76	0.2672135	0.2955000

EXTRACT YIELD

Peak Temp	Calulated	Experimental
203.85	0.2645227	0.2655000
244.43	0.2608684	0.2592000
264.00	0.2602451	0.2810000
315.00	0.2489064	0.2541000
351.50	0.2464971	0.2532100
395.12	0.2488248	0.2367000
403.55	0.2470253	0.2467000
478.91	0.2865096	0.2824000
509.00	0.2854788	0.2914000
527.90	0.2652576	0.2900000
558.53	0.2161301	0.1994000
627.77	0.1353136	0.0878000
647.10	0.1206597	0.2100000
647.11	0.1206526	0.2540000
659.59	0.1122046	0.0476000
701.67	0.0879879	0.0000000
727.27	0.0756983	0.0000000
781.75	0.0547513	0.0000000
877.46	0.0321620	0.0000000
991.00	0.0182270	0.0000000
1009.00	0.0166806	0.0000000
1029.72	0.0150452	0.0000000
1051.76	0.0134544	0.0000000

Table G.2.2b. Product distribution during coal pyrolysis as coal is heated at 448 C/s to 760 C and held there for 5 sec, predicted using parameters from Table G.2.2a.

```
++++++ Kinetic  Constants +++++++

reactin constant for gas  =     0.10000D+14     1/sec
act E for gas formation   =     0.26755D+05     cal/mole
ultimate yield of gas     =     0.28457D-01     gm/gm
reaction constant1 for tar=     0.19045D+09     1/sec
act e for tar formation   =     0.27354D+05     cal/mole
ultimate yield of tar     =     0.70000D+00     gm/gm
reaction constant2 for tar=     0.17552D+06     1/sec
act e for tar decomp      =     0.17915D+05     cal/mole
f of metaplast to gases   =     0.18835D-01

+++++++++  Run Conditions  +++++++

pressure                  =     0.10130D+07     dyne/cm*cm
original particle radius  =     0.35000D-02     cm
initial bubble size (solid)=     0.75568D-05     cm
initial bubble size (molten)=    0.26415D-05     cm
pore volume     =           0.40000D-01     cm**3
heating rate =      0.44800D+03     C/s
holding time =      0.50000D+01     sec
constant for viscosity    =     0.10000D-09
constant for diffusivity  =     0.10000D-06



 Molecular weight of 10 tar compoents
0.16900D+03  0.27000D+03  0.33000D+03  0.38600D+03  0.44700D+03
0.51900D+03  0.60900D+03  0.72700D+03  0.89200D+03  0.12450D+04


1   peak temperature          =     0.10331D+04     kelvin


************************* output ***************
```

t	temp	char	ctar	cmon	bgas	bmass	ttary	gasy
0.273	0.420530D+03	0.709960D+00	0.289916D+00	0.835375D-04	0.549916D-05	0.569127D-05	0.870968D-10	0.758336D-10
0.323	0.442930D+03	0.709962D+00	0.289470D+00	0.502079D-03	0.302508D-04	0.306460D-04	0.692351D-09	0.226728D-08
0.373	0.465330D+03	0.709968D+00	0.287524D+00	0.234237D-02	0.130483D-03	0.131240D-03	0.416800D-08	0.428283D-07
0.423	0.487730D+03	0.709982D+00	0.281043D+00	0.849291D-02	0.445104D-03	0.446461D-03	0.208648D-07	0.567294D-06
0.473	0.510130D+03	0.710012D+00	0.268629D+00	0.202940D-01	0.102296D-02	0.102526D-02	0.881927D-07	0.485639D-05

Table G.2.2b continues

0.523	0.532530D+03	0.710069D+00	0.261638D+00	0.269259D-01	0.130369D-02	0.130746D-02	0.328493D-06	0.238030D-04
0.573	0.554930D+03	0.710172D+00	0.261177D+00	0.272229D-01	0.130959D-02	0.131586D-02	0.113720D-05	0.761178D-04
0.623	0.577330D+03	0.710337D+00	0.260997D+00	0.267987D-01	0.161252D-02	0.162516D-02	0.364597D-05	0.202631D-03
0.673	0.599730D+03	0.710564D+00	0.260706D+00	0.236963D-01	0.442335D-02	0.448430D-02	0.108383D-04	0.503880D-03
0.723	0.622130D+03	0.710792D+00	0.259248D+00	0.756831D-02	0.199711D-01	0.212233D-01	0.327334D-04	0.110115D-02
0.773	0.644530D+03	0.710805D+00	0.250379D+00	0.131673D-02	0.256101D-01	0.355799D-01	0.139814D-03	0.174294D-02
0.823	0.666930D+03	0.710035D+00	0.232396D+00	0.306838D-03	0.257882D-01	0.538767D-01	0.725467D-03	0.262465D-02
0.873	0.689330D+03	0.707314D+00	0.208992D+00	0.896227D-04	0.244725D-01	0.761132D-01	0.321440D-02	0.424117D-02
0.923	0.711730D+03	0.700563D+00	0.182647D+00	0.327826D-04	0.219968D-01	0.991854D-01	0.106283D-01	0.690835D-02
0.973	0.734130D+03	0.686683D+00	0.163174D+00	0.169929D-04	0.193677D-01	0.117598D+00	0.227323D-01	0.976013D-02
1.023	0.756530D+03	0.662113D+00	0.155886D+00	0.129572D-04	0.180386D-01	0.138360D+00	0.321864D-01	0.114068D-01
1.073	0.778930D+03	0.623971D+00	0.153881D+00	0.108071D-04	0.171764D-01	0.167195D+00	0.421535D-01	0.127536D-01
1.123	0.801330D+03	0.572802D+00	0.152155D+00	0.898390D-05	0.164472D-01	0.204419D+00	0.563487D-01	0.142308D-01
1.173	0.823730D+03	0.516351D+00	0.144706D+00	0.725405D-05	0.158258D-01	0.244856D+00	0.780626D-01	0.159821D-01
1.223	0.846130D+03	0.470042D+00	0.126908D+00	0.579877D-05	0.154971D-01	0.277635D+00	0.107451D+00	0.179227D-01
1.273	0.868530D+03	0.448665D+00	0.998362D-01	0.482570D-05	0.157427D-01	0.292945D+00	0.138720D+00	0.197937D-01
1.323	0.890930D+03	0.453194D+00	0.704515D-01	0.436792D-05	0.167182D-01	0.290417D+00	0.164524D+00	0.213732D-01
1.373	0.913330D+03	0.470371D+00	0.457031D-01	0.431766D-05	0.183586D-01	0.278436D+00	0.182812D+00	0.226381D-01
1.423	0.935730D+03	0.487773D+00	0.280322D-01	0.455309D-05	0.205345D-01	0.264965D+00	0.195508D+00	0.236820D-01
1.473	0.958130D+03	0.501391D+00	0.165806D-01	0.501131D-05	0.231933D-01	0.252887D+00	0.204524D+00	0.245768D-01
1.523	0.980530D+03	0.511348D+00	0.964853D-02	0.567354D-05	0.263497D-01	0.242642D+00	0.210969D+00	0.253519D-01
1.573	0.100293D+04	0.518522D+00	0.568105D-02	0.653634D-05	0.300364D-01	0.234143D+00	0.215586D+00	0.260263D-01
1.623	0.102533D+04	0.523775D+00	0.346177D-02	0.760014D-05	0.342797D-01	0.227125D+00	0.218952D+00	0.266232D-01
1.641	0.103313D+04	0.525284D+00	0.297326D-02	0.801807D-05	0.358906D-01	0.224970D+00	0.219912D+00	0.268178D-01
1.691	0.103313D+04	0.529005D+00	0.241672D-02	0.903041D-05	0.404399D-01	0.218748D+00	0.222399D+00	0.273870D-01
1.741	0.103313D+04	0.532098D+00	0.204778D-02	0.996953D-05	0.446587D-01	0.213167D+00	0.224649D+00	0.279923D-01
1.791	0.103313D+04	0.534752D+00	0.177651D-02	0.108417D-04	0.485795D-01	0.208096D+00	0.226700D+00	0.286292D-01
1.841	0.103313D+04	0.537073D+00	0.156428D-02	0.116531D-04	0.522315D-01	0.203452D+00	0.228573D+00	0.292910D-01
1.891	0.103313D+04	0.539128D+00	0.139204D-02	0.124096D-04	0.556409D-01	0.199179D+00	0.230282D+00	0.299710D-01
1.941	0.103313D+04	0.540965D+00	0.124892D-02	0.131166D-04	0.588304D-01	0.195234D+00	0.231841D+00	0.306631D-01
1.991	0.103313D+04	0.542618D+00	0.112799D-02	0.137787D-04	0.618202D-01	0.191579D+00	0.233264D+00	0.313621D-01
2.041	0.103313D+04	0.544115D+00	0.102445D-02	0.143999D-04	0.646282D-01	0.188186D+00	0.234561D+00	0.320636D-01
2.091	0.103313D+04	0.545479D+00	0.934817D-03	0.149840D-04	0.672700D-01	0.185028D+00	0.235744D+00	0.327639D-01
2.141	0.103313D+04	0.546725D+00	0.856498D-03	0.155340D-04	0.697595D-01	0.182084D+00	0.236824D+00	0.334598D-01
2.191	0.103313D+04	0.547870D+00	0.787512D-03	0.160529D-04	0.721091D-01	0.179334D+00	0.237809D+00	0.341490D-01
2.241	0.103313D+04	0.548924D+00	0.726318D-03	0.165431D-04	0.743299D-01	0.176760D+00	0.238709D+00	0.348293D-01
2.291	0.103313D+04	0.549897D+00	0.671709D-03	0.170070D-04	0.764319D-01	0.174350D+00	0.239531D+00	0.354990D-01
2.341	0.103313D+04	0.550798D+00	0.622718D-03	0.174466D-04	0.784241D-01	0.172088D+00	0.240282D+00	0.361567D-01
2.391	0.103313D+04	0.551635D+00	0.578564D-03	0.178636D-04	0.803145D-01	0.169963D+00	0.240969D+00	0.368014D-01
2.441	0.103313D+04	0.552413D+00	0.538608D-03	0.182598D-04	0.821105D-01	0.167966D+00	0.241598D+00	0.374320D-01
2.491	0.103313D+04	0.553137D+00	0.502319D-03	0.186366D-04	0.838186D-01	0.166085D+00	0.242173D+00	0.380481D-01
2.541	0.103313D+04	0.553814D+00	0.469255D-03	0.189954D-04	0.854448D-01	0.164313D+00	0.242700D+00	0.386492D-01
2.591	0.103313D+04	0.554447D+00	0.439042D-03	0.193374D-04	0.869946D-01	0.162642D+00	0.243183D+00	0.392349D-01
2.641	0.103313D+04	0.555039D+00	0.411361D-03	0.196636D-04	0.884730D-01	0.161064D+00	0.243626D+00	0.398049D-01
2.891	0.103313D+04	0.557501D+00	0.302551D-03	0.210915D-04	0.949390D-01	0.154366D+00	0.245352D+00	0.424214D-01
3.141	0.103313D+04	0.559334D+00	0.228071D-03	0.222459D-04	0.100159D+00	0.149225D+00	0.246490D+00	0.446649D-01
3.391	0.103313D+04	0.560729D+00	0.175173D-03	0.231921D-04	0.104432D+00	0.145216D+00	0.247249D+00	0.465726D-01
3.641	0.103313D+04	0.561809D+00	0.136512D-03	0.239759D-04	0.107967D+00	0.142048D+00	0.247760D+00	0.481876D-01
3.891	0.103313D+04	0.562655D+00	0.107612D-03	0.246302D-04	0.110915D+00	0.139518D+00	0.248108D+00	0.495516D-01
4.141	0.103313D+04	0.563325D+00	0.856188D-04	0.251798D-04	0.113388D+00	0.137480D+00	0.248347D+00	0.507025D-01
4.391	0.103313D+04	0.563860D+00	0.686403D-04	0.256436D-04	0.115474D+00	0.135826D+00	0.248512D+00	0.516734D-01
4.641	0.103313D+04	0.564290D+00	0.553797D-04	0.260364D-04	0.117239D+00	0.134475D+00	0.248626D+00	0.524928D-01
4.891	0.103313D+04	0.564638D+00	0.449230D-04	0.263700D-04	0.118738D+00	0.133365D+00	0.248706D+00	0.531848D-01
5.141	0.103313D+04	0.564921D+00	0.366109D-04	0.266541D-04	0.120014D+00	0.132449D+00	0.248761D+00	0.537700D-01
5.391	0.103313D+04	0.565152D+00	0.299581D-04	0.268963D-04	0.121102D+00	0.131689D+00	0.248801D+00	0.542655D-01
5.641	0.103313D+04	0.565342D+00	0.246019D-04	0.271031D-04	0.122030D+00	0.131057D+00	0.248828D+00	0.546857D-01
5.891	0.103313D+04	0.565498D+00	0.202674D-04	0.272798D-04	0.122823D+00	0.130529D+00	0.248848D+00	0.550427D-01
6.141	0.103313D+04	0.565626D+00	0.167437D-04	0.274310D-04	0.123502D+00	0.130086D+00	0.248862D+00	0.553466D-01
6.391	0.103313D+04	0.565733D+00	0.138676D-04	0.275604D-04	0.124082D+00	0.129713D+00	0.248872D+00	0.556058D-01
6.641	0.103313D+04	0.565821D+00	0.115118D-04	0.276711D-04	0.124579D+00	0.129399D+00	0.248879D+00	0.558272D-01

Table G.2.2c. Changes in viscosity and swelling as a function of time as coal is heated at 448 C/s to 760 C and held there for 5 sec, predicted using parameters from Table G.2.2a.

t	temp	diff	difft	visc	swell
0.273214D+00	0.420530D+03	0.295658D-11	0.122026D-13	0.202309D+15	0.999973D+00
0.323214D+00	0.442930D+03	0.121460D-10	0.789098D-13	0.132986D+14	0.999825D+00
0.373214D+00	0.465330D+03	0.435522D-10	0.426016D-12	0.114157D+13	0.999178D+00
0.423214D+00	0.487730D+03	0.138151D-09	0.195470D-11	0.124638D+12	0.997019D+00
0.473214D+00	0.510130D+03	0.392432D-09	0.774687D-11	0.168979D+11	0.992856D+00
0.523214D+00	0.532530D+03	0.102978D-08	0.276403D-10	0.267426D+10	0.990516D+00
0.573214D+00	0.554930D+03	0.252945D-08	0.903558D-10	0.481308D+09	0.990429D+00
0.623214D+00	0.577330D+03	0.580591D-08	0.269993D-09	0.988798D+08	0.990628D+00
0.673214D+00	0.599730D+03	0.125393D-07	0.744240D-09	0.228751D+08	0.992487D+00
0.723214D+00	0.622130D+03	0.256022D-07	0.190434D-08	0.590482D+07	0.102807D+01
0.773214D+00	0.644530D+03	0.491484D-07	0.449019D-08	0.171976D+07	0.122233D+01
0.823214D+00	0.666930D+03	0.887360D-07	0.975978D-08	0.564885D+06	0.164458D+01
0.873214D+00	0.689330D+03	0.151952D-06	0.197758D-07	0.205798D+06	0.224944D+01
0.923214D+00	0.711730D+03	0.248327D-06	0.376640D-07	0.821455D+05	0.289265D+01
0.973214D+00	0.734130D+03	0.315267D-06	0.512445D-07	0.542236D+05	0.335400D+01
0.102321D+01	0.756530D+03	0.323486D-06	0.525049D-07	0.546941D+05	0.355042D+01
0.107321D+01	0.778930D+03	0.340344D-06	0.556405D-07	0.523795D+05	0.368724D+01
0.112321D+01	0.801330D+03	0.362419D-06	0.599345D-07	0.488879D+05	0.382403D+01
0.117321D+01	0.823730D+03	0.381890D-06	0.636781D-07	0.465257D+05	0.396895D+01
0.122321D+01	0.846130D+03	0.385576D-06	0.639245D-07	0.481564D+05	0.410445D+01
0.127321D+01	0.868530D+03	0.361706D-06	0.581942D-07	0.576577D+05	0.420890D+01
0.132321D+01	0.890930D+03	0.313167D-06	0.476160D-07	0.809350D+05	0.427735D+01
0.137321D+01	0.913330D+03	0.256068D-06	0.361075D-07	0.127217D+06	0.431988D+01
0.142321D+01	0.935730D+03	0.203028D-06	0.262840D-07	0.212417D+06	0.434753D+01
0.147321D+01	0.958130D+03	0.158317D-06	0.187167D-07	0.366262D+06	0.436653D+01
0.152321D+01	0.980530D+03	0.122668D-06	0.132177D-07	0.638934D+06	0.437991D+01
0.157321D+01	0.100293D+04	0.957343D-07	0.942612D-08	0.109750D+07	0.438949D+01
0.162321D+01	0.102533D+04	0.762899D-07	0.691302D-08	0.180631D+07	0.439653D+01
0.164062D+01	0.103313D+04	0.709449D-07	0.625907D-08	0.212065D+07	0.439856D+01
0.169062D+01	0.103313D+04	0.637476D-07	0.542708D-08	0.262653D+07	0.440391D+01
0.174062D+01	0.103313D+04	0.585165D-07	0.484157D-08	0.311712D+07	0.440885D+01
0.179062D+01	0.103313D+04	0.543723D-07	0.438987D-08	0.361039D+07	0.441344D+01
0.184062D+01	0.103313D+04	0.509144D-07	0.402163D-08	0.411745D+07	0.441772D+01
0.189062D+01	0.103313D+04	0.479406D-07	0.371153D-08	0.464412D+07	0.442169D+01
0.194062D+01	0.103313D+04	0.453343D-07	0.344496D-08	0.519346D+07	0.442537D+01
0.199062D+01	0.103313D+04	0.430196D-07	0.321245D-08	0.576737D+07	0.442880D+01
0.204062D+01	0.103313D+04	0.409425D-07	0.300732D-08	0.636740D+07	0.443197D+01
0.209062D+01	0.103313D+04	0.390626D-07	0.282464D-08	0.699501D+07	0.443492D+01
0.214062D+01	0.103313D+04	0.373487D-07	0.266062D-08	0.765170D+07	0.443766D+01
0.219062D+01	0.103313D+04	0.357764D-07	0.251233D-08	0.833906D+07	0.444021D+01
0.224062D+01	0.103313D+04	0.343259D-07	0.237745D-08	0.905869D+07	0.444257D+01
0.229062D+01	0.103313D+04	0.329816D-07	0.225412D-08	0.981218D+07	0.444477D+01
0.234062D+01	0.103313D+04	0.317306D-07	0.214085D-08	0.106012D+08	0.444682D+01
0.239062D+01	0.103313D+04	0.305622D-07	0.203639D-08	0.114272D+08	0.444873D+01
0.244062D+01	0.103313D+04	0.294676D-07	0.193973D-08	0.122920D+08	0.445050D+01
0.249062D+01	0.103313D+04	0.284392D-07	0.185000D-08	0.131970D+08	0.445216D+01
0.254062D+01	0.103313D+04	0.274708D-07	0.176649D-08	0.141438D+08	0.445371D+01
0.259062D+01	0.103313D+04	0.265568D-07	0.168856D-08	0.151341D+08	0.445515D+01
0.264062D+01	0.103313D+04	0.256925D-07	0.161569D-08	0.161695D+08	0.445650D+01
0.289062D+01	0.103313D+04	0.219861D-07	0.131264D-08	0.220808D+08	0.446208D+01
0.314062D+01	0.103313D+04	0.190581D-07	0.108490D-08	0.293866D+08	0.446617D+01
0.339062D+01	0.103313D+04	0.166819D-07	0.908395D-09	0.383549D+08	0.446921D+01
0.364062D+01	0.103313D+04	0.147124D-07	0.768293D-09	0.493109D+08	0.447152D+01
0.389062D+01	0.103313D+04	0.130529D-07	0.654972D-09	0.626467D+08	0.447330D+01
0.414062D+01	0.103313D+04	0.116360D-07	0.561938D-09	0.788316D+08	0.447468D+01
0.439062D+01	0.103313D+04	0.104137D-07	0.484644D-09	0.984234D+08	0.447577D+01
0.464062D+01	0.103313D+04	0.935034D-08	0.419809D-09	0.122083D+09	0.447664D+01
0.489062D+01	0.103313D+04	0.841888D-08	0.364995D-09	0.150592D+09	0.447733D+01
0.514062D+01	0.103313D+04	0.759831D-08	0.318350D-09	0.184874D+09	0.447789D+01
0.539062D+01	0.103313D+04	0.687197D-08	0.278435D-09	0.226020D+09	0.447834D+01
0.564062D+01	0.103313D+04	0.622639D-08	0.244116D-09	0.275320D+09	0.447871D+01
0.589062D+01	0.103313D+04	0.565056D-08	0.214488D-09	0.334293D+09	0.447901D+01
0.614062D+01	0.103313D+04	0.513534D-08	0.188817D-09	0.404736D+09	0.447925D+01
0.639062D+01	0.103313D+04	0.467309D-08	0.166503D-09	0.488766D+09	0.447946D+01
0.664062D+01	0.103313D+04	0.425736D-08	0.147051D-09	0.588883D+09	0.447963D+01

Table G.2.2d. Amount of volatiles formed and changes in bubble radius and bubble number density as a function of time as coal is heated at 448 C/s to 760 C and held there for 5 sec, predicted using parameters from Table G.2.2a.

t	temp	bnden	brad	gasf	tarf
0.273214D+00	0.420530D+03	0.170294D+14	0.264150D-05	0.830994D-04	0.290000D-01
0.323214D+00	0.442930D+03	0.170294D+14	0.264150D-05	0.526352D-03	0.290000D-01
0.373214D+00	0.465330D+03	0.170294D+14	0.264150D-05	0.246680D-02	0.290000D-01
0.423214D+00	0.487730D+03	0.170294D+14	0.264154D-05	0.893219D-02	0.290002D-01
0.473214D+00	0.510130D+03	0.170294D+14	0.264231D-05	0.213147D-01	0.290006D-01
0.523214D+00	0.532530D+03	0.170293D+14	0.265056D-05	0.282450D-01	0.290020D-01
0.573214D+00	0.554930D+03	0.170286D+14	0.270173D-05	0.285974D-01	0.290061D-01
0.623214D+00	0.577330D+03	0.170247D+14	0.297107D-05	0.285974D-01	0.290172D-01
0.673214D+00	0.599730D+03	0.170039D+14	0.441880D-05	0.285974D-01	0.290451D-01
0.723214D+00	0.622130D+03	0.169090D+14	0.108737D-04	0.285974D-01	0.291105D-01
0.773214D+00	0.644530D+03	0.167249D+14	0.212037D-04	0.285974D-01	0.292548D-01
0.823214D+00	0.666930D+03	0.163537D+14	0.340438D-04	0.285974D-01	0.295553D-01
0.873214D+00	0.689330D+03	0.155290D+14	0.498692D-04	0.285974D-01	0.301486D-01
0.923214D+00	0.711730D+03	0.140521D+14	0.673423D-04	0.285974D-01	0.312576D-01
0.973214D+00	0.734130D+03	0.124564D+14	0.816751D-04	0.285974D-01	0.332130D-01
0.102321D+01	0.756530D+03	0.115958D+14	0.886749D-04	0.285974D-01	0.364348D-01
0.107321D+01	0.778930D+03	0.109159D+14	0.940536D-04	0.285974D-01	0.413088D-01
0.112321D+01	0.801330D+03	0.101588D+14	0.999946D-04	0.285974D-01	0.478900D-01
0.117321D+01	0.823730D+03	0.925553D+13	0.107143D-03	0.285974D-01	0.554844D-01
0.122321D+01	0.846130D+03	0.829032D+13	0.115019D-03	0.285974D-01	0.625157D-01
0.127321D+01	0.868530D+03	0.743697D+13	0.122348D-03	0.285974D-01	0.672969D-01
0.132321D+01	0.890930D+03	0.680425D+13	0.128107D-03	0.285974D-01	0.694158D-01
0.137321D+01	0.913330D+03	0.637021D+13	0.132267D-03	0.285974D-01	0.699390D-01
0.142321D+01	0.935730D+03	0.606529D+13	0.135314D-03	0.285974D-01	0.699977D-01
0.147321D+01	0.958130D+03	0.584243D+13	0.137615D-03	0.285974D-01	0.700000D-01
0.152321D+01	0.980530D+03	0.567756D+13	0.139361D-03	0.285974D-01	0.700000D-01
0.157321D+01	0.100293D+04	0.555491D+13	0.140686D-03	0.285974D-01	0.700000D-01
0.162321D+01	0.102533D+04	0.546186D+13	0.141707D-03	0.285974D-01	0.700000D-01
0.164062D+01	0.103313D+04	0.543452D+13	0.142010D-03	0.285974D-01	0.700000D-01
0.169062D+01	0.103313D+04	0.536155D+13	0.142824D-03	0.285974D-01	0.700000D-01
0.174062D+01	0.103313D+04	0.529252D+13	0.143603D-03	0.285974D-01	0.700000D-01
0.179062D+01	0.103313D+04	0.522681D+13	0.144352D-03	0.285974D-01	0.700000D-01
0.184062D+01	0.103313D+04	0.516424D+13	0.145072D-03	0.285974D-01	0.700000D-01
0.189062D+01	0.103313D+04	0.510474D+13	0.145765D-03	0.285974D-01	0.700000D-01
0.194062D+01	0.103313D+04	0.504822D+13	0.146428D-03	0.285974D-01	0.700000D-01
0.199062D+01	0.103313D+04	0.499459D+13	0.147064D-03	0.285974D-01	0.700000D-01
0.204062D+01	0.103313D+04	0.494373D+13	0.147673D-03	0.285974D-01	0.700000D-01
0.209062D+01	0.103313D+04	0.489552D+13	0.148254D-03	0.285974D-01	0.700000D-01
0.214062D+01	0.103313D+04	0.484982D+13	0.148810D-03	0.285974D-01	0.700000D-01
0.219062D+01	0.103313D+04	0.480651D+13	0.149341D-03	0.285974D-01	0.700000D-01
0.224062D+01	0.103313D+04	0.476545D+13	0.149849D-03	0.285974D-01	0.700000D-01
0.229062D+01	0.103313D+04	0.472653D+13	0.150333D-03	0.285974D-01	0.700000D-01
0.234062D+01	0.103313D+04	0.468962D+13	0.150796D-03	0.285974D-01	0.700000D-01
0.239062D+01	0.103313D+04	0.465461D+13	0.151238D-03	0.285974D-01	0.700000D-01
0.244062D+01	0.103313D+04	0.462141D+13	0.151660D-03	0.285974D-01	0.700000D-01
0.249062D+01	0.103313D+04	0.458989D+13	0.152063D-03	0.285974D-01	0.700000D-01
0.254062D+01	0.103313D+04	0.455998D+13	0.152447D-03	0.285974D-01	0.700000D-01
0.259062D+01	0.103313D+04	0.453157D+13	0.152815D-03	0.285974D-01	0.700000D-01
0.264062D+01	0.103313D+04	0.450458D+13	0.153166D-03	0.285974D-01	0.700000D-01
0.289062D+01	0.103313D+04	0.438829D+13	0.154700D-03	0.285974D-01	0.700000D-01
0.314062D+01	0.103313D+04	0.429725D+13	0.155928D-03	0.285974D-01	0.700000D-01
0.339062D+01	0.103313D+04	0.422531D+13	0.156914D-03	0.285974D-01	0.700000D-01
0.364062D+01	0.103313D+04	0.416797D+13	0.157712D-03	0.285974D-01	0.700000D-01
0.389062D+01	0.103313D+04	0.412196D+13	0.158359D-03	0.285974D-01	0.700000D-01
0.414062D+01	0.103313D+04	0.408481D+13	0.158887D-03	0.285974D-01	0.700000D-01
0.439062D+01	0.103313D+04	0.405467D+13	0.159319D-03	0.285974D-01	0.700000D-01
0.464062D+01	0.103313D+04	0.403010D+13	0.159672D-03	0.285974D-01	0.700000D-01
0.489062D+01	0.103313D+04	0.401000D+13	0.159963D-03	0.285974D-01	0.700000D-01
0.514062D+01	0.103313D+04	0.399351D+13	0.160203D-03	0.285974D-01	0.700000D-01
0.539062D+01	0.103313D+04	0.397993D+13	0.160401D-03	0.285974D-01	0.700000D-01
0.564062D+01	0.103313D+04	0.396872D+13	0.160565D-03	0.285974D-01	0.700000D-01
0.589062D+01	0.103313D+04	0.395945D+13	0.160702D-03	0.285974D-01	0.700000D-01
0.614062D+01	0.103313D+04	0.395177D+13	0.160815D-03	0.285974D-01	0.700000D-01
0.639062D+01	0.103313D+04	0.394538D+13	0.160909D-03	0.285974D-01	0.700000D-01
0.664062D+01	0.103313D+04	0.394007D+13	0.160987D-03	0.285974D-01	0.700000D-01

Table G.2.3a. Effect of viscosity correlation on kinetic parameters. Table G.2.1's are employed in Figures 6.4.1. and 6.4.2.

********** input **********

pressure	=	0.10130D+07	dyne/cm*cm
original particle radius	=	0.35000D-02	cm
initial pore size	=	0.93559D-05	cm
initial bubble size	=	0.36108D-05	cm
pore volume	=	0.40000D-01	cm**3
constant for viscosity	=	0.10000D-06	
constant for diffusivity	=	0.10000D-06	

Molecular weight of 10 tar compoents

0.16900D+03 0.27000D+03 0.33000D+03 0.38600D+03 0.44700D+03
0.51900D+03 0.60900D+03 0.72700D+03 0.89200D+03 0.12450D+04

Parameters fixed

reactin constant for gas	=	0.10000D+14	1/sec
act e for gas formation	=	0.26755D+05	cal/mole
ultimate yield of gas	=	0.28457D-01	gm/gm
ultimate yield of tar	=	0.70000D+00	gm/gm

Parameters varied, final paratmeter values

reaction constant1 for tar=		0.10000D+14	1/sec
reaction constant2 for tar=		0.34765D+08	1/sec
act E for metaplast formation	=	0.43759D+05	cal/mole
act E for metaplast decomposition=		0.25893D+05	cal/mole
fraction of metaplast converted to gases=		0.20461D+00	

square sum of residual functions= 0.22828D+00

Comparison with experimental data

TOTAL VOLATILES YIELD

Peak Temp	Calulated w/o y(32)	Experimental	w/ y(32)
203.85	0.0253222	0.0162600	0.25322D-01
223.26	0.0284314	0.0125000	0.28431D-01
244.43	0.0284597	0.0291000	0.28460D-01
248.53	0.0301678	0.0247000	0.30168D-01
259.40	0.0286944	0.0137000	0.28694D-01
264.00	0.0285409	0.0165300	0.28541D-01
315.00	0.0370755	0.0165700	0.37075D-01
351.50	0.0365929	0.0294800	0.36593D-01
379.63	0.0356388	0.0259000	0.35639D-01
385.56	0.0353248	0.0342000	0.35325D-01
395.12	0.0347026	0.0343000	0.34703D-01
403.55	0.0012218	0.0353000	0.40141D-01
414.38	0.0016880	0.0343000	0.41287D-01
432.38	0.0025333	0.0370400	0.44051D-01
478.91	0.0047655	0.1504000	0.61785D-01
509.00	0.0166489	0.1740000	0.93708D-01
527.90	0.0435596	0.1908000	0.13064D+00
558.53	0.1245476	0.2678000	0.21085D+00
627.77	0.2716554	0.3428000	0.33773D+00

Table G.2.3a continues

647.10	0.2931216	0.2870000	0.35565D+00
647.11	0.2931312	0.2816000	0.35566D+00
659.59	0.3040710	0.3690000	0.36483D+00
701.67	0.3302614	0.3896000	0.38716D+00
727.27	0.3416515	0.4043000	0.39703D+00
745.72	0.3488325	0.3430000	0.40323D+00
781.75	0.3613785	0.4450000	0.41381D+00
877.46	0.3880389	0.4802000	0.43419D+00
948.86	0.4024301	0.4715000	0.44332D+00
991.00	0.4090095	0.4708000	0.44686D+00
1009.00	0.4114420	0.4884000	0.44804D+00
1029.72	0.4139884	0.4810000	0.44919D+00
1051.76	0.4164220	0.4700000	0.45021D+00

TAR YIELD

Peak Temp	Calulated	Experimental
203.85	0.0000000	0.0000000
244.43	0.0000000	0.0000000
264.00	0.0000000	0.0000000
315.00	0.0000000	0.0000000
351.50	0.0000000	0.0000000
395.12	0.0000000	0.0000000
403.55	0.0000143	0.0000000
478.91	0.0007786	0.0919000
509.00	0.0078501	0.1185000
558.53	0.0930412	0.1772000
627.77	0.2176264	0.2662000
647.10	0.2351062	0.2469000
647.11	0.2351139	0.2290000
659.59	0.2437782	0.2976000
701.67	0.2634775	0.3065000
727.27	0.2714375	0.3097000
781.75	0.2842552	0.2993000
877.46	0.2994155	0.3134000
991.00	0.3088312	0.2550000
1009.00	0.3097093	0.2541000
1029.72	0.3105656	0.2970000
1051.76	0.3113177	0.2955000

EXTRACT YIELD

Peak Temp	Calulated	Experimental
203.85	0.2646833	0.2655000
244.43	0.2614984	0.2592000
264.00	0.2613368	0.2810000
315.00	0.2519115	0.2541000
351.50	0.2500017	0.2532100
395.12	0.2452246	0.2367000
403.55	0.2443071	0.2467000
478.91	0.2875552	0.2824000
509.00	0.3236566	0.2914000
527.90	0.3019929	0.2900000
558.53	0.2093627	0.1994000
627.77	0.0980669	0.0878000
647.10	0.0842848	0.2100000
647.11	0.0842785	0.2540000
659.59	0.0769844	0.0476000
701.67	0.0581431	0.0000000
727.27	0.0493589	0.0000000
781.75	0.0343493	0.0000000
877.46	0.0165685	0.0000000
991.00	0.0059054	0.0000000
1009.00	0.0049326	0.0000000
1029.72	0.0039872	0.0000000
1051.76	0.0031586	0.0000000

Table G.2.3b. Product distribution during coal pyrolysis as coal is heated at 448 C/s to 760 C and held there for 5 sec, predicted using parameters from Table G.2.3a.

++++++ Kinetic Constants +++++++

reactin constant for gas	= 0.10000D+14	1/sec
act E for gas formation	= 0.26755D+05	cal/mole
ultimate yield of gas	= 0.28457D-01	gm/gm
reaction constant1 for tar	= 0.10000D+14	1/sec
act e for tar formation	= 0.43759D+05	cal/mole
ultimate yield of tar	= 0.70000D+00	gm/gm
reaction constant2 for tar	= 0.34765D+08	1/sec
act e for tar decomp	= 0.25893D+05	cal/mole
f of metaplast to gases	= 0.20461D+00	

+++++++++ Run Conditions +++++++

pressure	= 0.10130D+07	dyne/cm*cm
original particle radius	= 0.35000D-02	cm
initial bubble size (solid)	= 0.93559D-05	cm
initial bubble size (molten)	= 0.36108D-05	cm
pore volume	= 0.40000D-01	cm**3
heating rate	= 0.44800D+03	C/s
holding time	= 0.50000D+01	sec
constant for viscosity	= 0.10000D-06	
constant for diffusivity	= 0.10000D-06	

Molecular weight of 10 tar compoents

0.16900D+03	0.27000D+03	0.33000D+03	0.38600D+03	0.44700D+03
0.51900D+03	0.60900D+03	0.72700D+03	0.89200D+03	0.12450D+04

1 peak temperature = 0.10331D+04 kelvin

********** output **********

t	temp	char	ctar	cmon	bgas	bmass	ttary	gasy
0.273	0.420530D+03	0.709959D+00	0.289917D+00	0.817790D-04	0.724555D-05	0.750411D-05	0.927726D-12	0.199146D-11
0.323	0.442930D+03	0.709959D+00	0.289473D+00	0.492360D-03	0.399264D-04	0.404584D-04	0.735391D-11	0.596420D-10
0.373	0.465330D+03	0.709959D+00	0.287532D+00	0.230031D-02	0.172461D-03	0.173480D-03	0.441429D-10	0.112828D-08
0.423	0.487730D+03	0.709960D+00	0.281065D+00	0.834940D-02	0.588893D-03	0.590721D-03	0.220318D-09	0.149621D-07
0.473	0.510130D+03	0.709961D+00	0.268679D+00	0.199679D-01	0.135328D-02	0.135637D-02	0.928166D-09	0.128179D-06

Table G.2.3b continues

0.523	0.532530D+03	0.709967D+00	0.261740D+00	0.265408D-01	0.171149D-02	0.171651D-02	0.344625D-08	0.628428D-06
0.573	0.554930D+03	0.709981D+00	0.261367D+00	0.269753D-01	0.163180D-02	0.163969D-02	0.119041D-07	0.200685D-05
0.623	0.577330D+03	0.710015D+00	0.261319D+00	0.270729D-01	0.154060D-02	0.155257D-02	0.380984D-07	0.528603D-05
0.673	0.599730D+03	0.710093D+00	0.261212D+00	0.271686D-01	0.146063D-02	0.147824D-02	0.112728D-06	0.125838D-04
0.723	0.622130D+03	0.710246D+00	0.261000D+00	0.272709D-01	0.139477D-02	0.142006D-02	0.309955D-06	0.279362D-04
0.773	0.644530D+03	0.710500D+00	0.260625D+00	0.273900D-01	0.135466D-02	0.139055D-02	0.797106D-06	0.586848D-04
0.823	0.666930D+03	0.710798D+00	0.260089D+00	0.275279D-01	0.137812D-02	0.143009D-02	0.192952D-05	0.117822D-03
0.873	0.689330D+03	0.710763D+00	0.259666D+00	0.276252D-01	0.159337D-02	0.167715D-02	0.442680D-05	0.228526D-03
0.923	0.711730D+03	0.709117D+00	0.260422D+00	0.272272D-01	0.256601D-02	0.275423D-02	0.973752D-05	0.435345D-03
0.973	0.734130D+03	0.702473D+00	0.264907D+00	0.228834D-01	0.791729D-02	0.884948D-02	0.216129D-04	0.830018D-03
1.023	0.756530D+03	0.683546D+00	0.273793D+00	0.877818D-02	0.238566D-01	0.323031D-01	0.704343D-04	0.147318D-02
1.073	0.778930D+03	0.640763D+00	0.285214D+00	0.226992D-02	0.338793D-01	0.690716D-01	0.382781D-03	0.226387D-02
1.123	0.801330D+03	0.568322D+00	0.293039D+00	0.670089D-03	0.414047D-01	0.132020D+00	0.223377D-02	0.368036D-02
1.173	0.823730D+03	0.493126D+00	0.257721D+00	0.204698D-03	0.494795D-01	0.228987D+00	0.125371D-01	0.738875D-02
1.223	0.846130D+03	0.471844D+00	0.172963D+00	0.710542D-04	0.552260D-01	0.294521D+00	0.450040D-01	0.155622D-01
1.273	0.868530D+03	0.502524D+00	0.932360D-01	0.344616D-04	0.572005D-01	0.287273D+00	0.904011D-01	0.264964D-01
1.323	0.890930D+03	0.535431D+00	0.447650D-01	0.228646D-04	0.570415D-01	0.254369D+00	0.128551D+00	0.368261D-01
1.373	0.913330D+03	0.557521D+00	0.195226D-01	0.184598D-04	0.561037D-01	0.222917D+00	0.154857D+00	0.451282D-01
1.423	0.935730D+03	0.570747D+00	0.801954D-02	0.167522D-04	0.552131D-01	0.198594D+00	0.171407D+00	0.511805D-01
1.473	0.958130D+03	0.578437D+00	0.347676D-02	0.161999D-04	0.546806D-01	0.180601D+00	0.181879D+00	0.555550D-01
1.523	0.980530D+03	0.583345D+00	0.175744D-02	0.161195D-04	0.544098D-01	0.166412D+00	0.189355D+00	0.590795D-01
1.573	0.100293D+04	0.586942D+00	0.101258D-02	0.162002D-04	0.541992D-01	0.154124D+00	0.195529D+00	0.623416D-01
1.623	0.102533D+04	0.589819D+00	0.625790D-03	0.163219D-04	0.539263D-01	0.142842D+00	0.201055D+00	0.656067D-01
1.641	0.103313D+04	0.590701D+00	0.534492D-03	0.163650D-04	0.538059D-01	0.139079D+00	0.202870D+00	0.667641D-01
1.691	0.103313D+04	0.592888D+00	0.425832D-03	0.161449D-04	0.536296D-01	0.129751D+00	0.207167D+00	0.697166D-01
1.741	0.103313D+04	0.594663D+00	0.351236D-03	0.160587D-04	0.537018D-01	0.122581D+00	0.210263D+00	0.720909D-01
1.791	0.103313D+04	0.596145D+00	0.296621D-03	0.160457D-04	0.539070D-01	0.116828D+00	0.212603D+00	0.740762D-01
1.841	0.103313D+04	0.597408D+00	0.254847D-03	0.160755D-04	0.541863D-01	0.112075D+00	0.214431D+00	0.757805D-01
1.891	0.103313D+04	0.598500D+00	0.221853D-03	0.161314D-04	0.545071D-01	0.108062D+00	0.215894D+00	0.772711D-01
1.941	0.103313D+04	0.599455D+00	0.195149D-03	0.162033D-04	0.548502D-01	0.104618D+00	0.217087D+00	0.785930D-01
1.991	0.103313D+04	0.600300D+00	0.173118D-03	0.162853D-04	0.552038D-01	0.101624D+00	0.218073D+00	0.797779D-01
2.041	0.103313D+04	0.601052D+00	0.154662D-03	0.163732D-04	0.555605D-01	0.989937D-01	0.218900D+00	0.808490D-01
2.091	0.103313D+04	0.601725D+00	0.139003D-03	0.164645D-04	0.559154D-01	0.966624D-01	0.219598D+00	0.818238D-01
2.141	0.103313D+04	0.602332D+00	0.125576D-03	0.165573D-04	0.562655D-01	0.945812D-01	0.220193D+00	0.827160D-01
2.191	0.103313D+04	0.602882D+00	0.113959D-03	0.166504D-04	0.566088D-01	0.927114D-01	0.220704D+00	0.835366D-01
2.241	0.103313D+04	0.603382D+00	0.103828D-03	0.167429D-04	0.569440D-01	0.910225D-01	0.221146D+00	0.842942D-01
2.291	0.103313D+04	0.603838D+00	0.949316D-04	0.168342D-04	0.572703D-01	0.894896D-01	0.221529D+00	0.849962D-01
2.341	0.103313D+04	0.604256D+00	0.870715D-04	0.169239D-04	0.575872D-01	0.880926D-01	0.221864D+00	0.856487D-01
2.391	0.103313D+04	0.604639D+00	0.800888D-04	0.170118D-04	0.578944D-01	0.868146D-01	0.222157D+00	0.862566D-01
2.441	0.103313D+04	0.604993D+00	0.738549D-04	0.170975D-04	0.581920D-01	0.856415D-01	0.222415D+00	0.868245D-01
2.491	0.103313D+04	0.605319D+00	0.682647D-04	0.171811D-04	0.584800D-01	0.845616D-01	0.222643D+00	0.873560D-01
2.541	0.103313D+04	0.605621D+00	0.632315D-04	0.172624D-04	0.587586D-01	0.835648D-01	0.222844D+00	0.878543D-01
2.591	0.103313D+04	0.605901D+00	0.586832D-04	0.173413D-04	0.590278D-01	0.826423D-01	0.223023D+00	0.883224D-01
2.641	0.103313D+04	0.606161D+00	0.545591D-04	0.174180D-04	0.592881D-01	0.817868D-01	0.223182D+00	0.887628D-01
2.891	0.103313D+04	0.607220D+00	0.387580D-04	0.177672D-04	0.604629D-01	0.783127D-01	0.223759D+00	0.906172D-01
3.141	0.103313D+04	0.607983D+00	0.283450D-04	0.180640D-04	0.614514D-01	0.758093D-01	0.224099D+00	0.920275D-01
3.391	0.103313D+04	0.608547D+00	0.211795D-04	0.183155D-04	0.622844D-01	0.739518D-01	0.224306D+00	0.931204D-01
3.641	0.103313D+04	0.608972D+00	0.160895D-04	0.185285D-04	0.629878D-01	0.725433D-01	0.224436D+00	0.939792D-01
3.891	0.103313D+04	0.609297D+00	0.123845D-04	0.187089D-04	0.635827D-01	0.714570D-01	0.224518D+00	0.946615D-01
4.141	0.103313D+04	0.609548D+00	0.963495D-05	0.188618D-04	0.640865D-01	0.706078D-01	0.224572D+00	0.952083D-01
4.391	0.103313D+04	0.609745D+00	0.756231D-05	0.189914D-04	0.645137D-01	0.699366D-01	0.224607D+00	0.956500D-01
4.641	0.103313D+04	0.609900D+00	0.597975D-05	0.191013D-04	0.648760D-01	0.694011D-01	0.224630D+00	0.960090D-01
4.891	0.103313D+04	0.610022D+00	0.475839D-05	0.191946D-04	0.651835D-01	0.689703D-01	0.224645D+00	0.963027D-01
5.141	0.103313D+04	0.610120D+00	0.380725D-05	0.192737D-04	0.654446D-01	0.686214D-01	0.224656D+00	0.965441D-01
5.391	0.103313D+04	0.610199D+00	0.306081D-05	0.193407D-04	0.656661D-01	0.683370D-01	0.224663D+00	0.967435D-01
5.641	0.103313D+04	0.610262D+00	0.247110D-05	0.193976D-04	0.658541D-01	0.681039D-01	0.224668D+00	0.969091D-01
5.891	0.103313D+04	0.610313D+00	0.200250D-05	0.194458D-04	0.660136D-01	0.679118D-01	0.224671D+00	0.970471D-01
6.141	0.103313D+04	0.610355D+00	0.162822D-05	0.194867D-04	0.661488D-01	0.677527D-01	0.224673D+00	0.971627D-01
6.391	0.103313D+04	0.610389D+00	0.132791D-05	0.195212D-04	0.662633D-01	0.676205D-01	0.224675D+00	0.972599D-01
6.641	0.103313D+04	0.610417D+00	0.108597D-05	0.195505D-04	0.663603D-01	0.675099D-01	0.224676D+00	0.973419D-01

Table G.2.3d. Amount of volatiles formed and changes in bubble radius and bubble number density as a function of time as coal is heated at 448 C/s to 760 C and held there for 5 sec, predicted using parameters from Table G.2.3a.

t	temp	bnden	brad	gasf	tarf
0.273214D+00	0.420530D+03	0.897340D+13	0.361080D-05	0.830992D-04	0.290000D-01
0.323214D+00	0.442930D+03	0.897340D+13	0.361080D-05	0.526352D-03	0.290000D-01
0.373214D+00	0.465330D+03	0.897340D+13	0.361080D-05	0.246680D-02	0.290000D-01
0.423214D+00	0.487730D+03	0.897340D+13	0.361080D-05	0.893219D-02	0.290000D-01
0.473214D+00	0.510130D+03	0.897340D+13	0.361080D-05	0.213147D-01	0.290000D-01
0.523214D+00	0.532530D+03	0.897340D+13	0.361081D-05	0.282450D-01	0.290000D-01
0.573214D+00	0.554930D+03	0.897340D+13	0.361088D-05	0.285974D-01	0.290001D-01
0.623214D+00	0.577330D+03	0.897340D+13	0.361123D-05	0.285974D-01	0.290004D-01
0.673214D+00	0.599730D+03	0.897338D+13	0.361276D-05	0.285974D-01	0.290016D-01
0.723214D+00	0.622130D+03	0.897334D+13	0.361888D-05	0.285974D-01	0.290065D-01
0.773214D+00	0.644530D+03	0.897317D+13	0.364117D-05	0.285974D-01	0.290236D-01
0.823214D+00	0.666930D+03	0.897260D+13	0.371635D-05	0.285974D-01	0.290796D-01
0.873214D+00	0.689330D+03	0.897078D+13	0.395781D-05	0.285974D-01	0.292476D-01
0.923214D+00	0.711730D+03	0.896491D+13	0.473695D-05	0.285974D-01	0.297160D-01
0.973214D+00	0.734130D+03	0.894446D+13	0.744049D-05	0.285974D-01	0.309251D-01
0.102321D+01	0.756530D+03	0.888530D+13	0.149986D-04	0.285974D-01	0.337786D-01
0.107321D+01	0.778930D+03	0.877726D+13	0.264333D-04	0.285974D-01	0.397139D-01
0.112321D+01	0.801330D+03	0.854474D+13	0.420325D-04	0.285974D-01	0.497469D-01
0.117321D+01	0.823730D+03	0.795963D+13	0.635468D-04	0.285974D-01	0.614763D-01
0.122321D+01	0.846130D+03	0.687426D+13	0.880698D-04	0.285974D-01	0.685724D-01
0.127321D+01	0.868530D+03	0.569507D+13	0.109239D-03	0.285974D-01	0.699593D-01
0.132321D+01	0.890930D+03	0.477281D+13	0.125230D-03	0.285974D-01	0.700000D-01
0.137321D+01	0.913330D+03	0.413388D+13	0.136841D-03	0.285974D-01	0.700000D-01
0.142321D+01	0.935730D+03	0.371668D+13	0.144930D-03	0.285974D-01	0.700000D-01
0.147321D+01	0.958130D+03	0.343900D+13	0.150636D-03	0.285974D-01	0.700000D-01
0.152321D+01	0.980530D+03	0.322962D+13	0.155157D-03	0.285974D-01	0.700000D-01
0.157321D+01	0.100293D+04	0.304675D+13	0.159288D-03	0.285974D-01	0.700000D-01
0.162321D+01	0.102533D+04	0.287345D+13	0.163386D-03	0.285974D-01	0.700000D-01
0.164062D+01	0.103313D+04	0.281419D+13	0.164833D-03	0.285974D-01	0.700000D-01
0.169062D+01	0.103313D+04	0.266830D+13	0.168507D-03	0.285974D-01	0.700000D-01
0.174062D+01	0.103313D+04	0.255677D+13	0.171433D-03	0.285974D-01	0.700000D-01
0.179062D+01	0.103313D+04	0.246759D+13	0.173854D-03	0.285974D-01	0.700000D-01
0.184062D+01	0.103313D+04	0.239404D+13	0.175909D-03	0.285974D-01	0.700000D-01
0.189062D+01	0.103313D+04	0.233201D+13	0.177687D-03	0.285974D-01	0.700000D-01
0.194062D+01	0.103313D+04	0.227880D+13	0.179246D-03	0.285974D-01	0.700000D-01
0.199062D+01	0.103313D+04	0.223253D+13	0.180630D-03	0.285974D-01	0.700000D-01
0.204062D+01	0.103313D+04	0.219186D+13	0.181867D-03	0.285974D-01	0.700000D-01
0.209062D+01	0.103313D+04	0.215580D+13	0.182983D-03	0.285974D-01	0.700000D-01
0.214062D+01	0.103313D+04	0.212359D+13	0.183994D-03	0.285974D-01	0.700000D-01
0.219062D+01	0.103313D+04	0.209462D+13	0.184916D-03	0.285974D-01	0.700000D-01
0.224062D+01	0.103313D+04	0.206844D+13	0.185759D-03	0.285974D-01	0.700000D-01
0.229062D+01	0.103313D+04	0.204465D+13	0.186534D-03	0.285974D-01	0.700000D-01
0.234062D+01	0.103313D+04	0.202296D+13	0.187249D-03	0.285974D-01	0.700000D-01
0.239062D+01	0.103313D+04	0.200310D+13	0.187909D-03	0.285974D-01	0.700000D-01
0.244062D+01	0.103313D+04	0.198486D+13	0.188521D-03	0.285974D-01	0.700000D-01
0.249062D+01	0.103313D+04	0.196805D+13	0.189090D-03	0.285974D-01	0.700000D-01
0.254062D+01	0.103313D+04	0.195253D+13	0.189620D-03	0.285974D-01	0.700000D-01
0.259062D+01	0.103313D+04	0.193816D+13	0.190113D-03	0.285974D-01	0.700000D-01
0.264062D+01	0.103313D+04	0.192482D+13	0.190575D-03	0.285974D-01	0.700000D-01
0.289062D+01	0.103313D+04	0.187062D+13	0.192482D-03	0.285974D-01	0.700000D-01
0.314062D+01	0.103313D+04	0.183156D+13	0.193891D-03	0.285974D-01	0.700000D-01
0.339062D+01	0.103313D+04	0.180261D+13	0.194954D-03	0.285974D-01	0.700000D-01
0.364062D+01	0.103313D+04	0.178074D+13	0.195768D-03	0.285974D-01	0.700000D-01
0.389062D+01	0.103313D+04	0.176396D+13	0.196399D-03	0.285974D-01	0.700000D-01
0.414062D+01	0.103313D+04	0.175092D+13	0.196894D-03	0.285974D-01	0.700000D-01
0.439062D+01	0.103313D+04	0.174070D+13	0.197284D-03	0.285974D-01	0.700000D-01
0.464062D+01	0.103313D+04	0.173262D+13	0.197595D-03	0.285974D-01	0.700000D-01
0.489062D+01	0.103313D+04	0.172620D+13	0.197842D-03	0.285974D-01	0.700000D-01
0.514062D+01	0.103313D+04	0.172105D+13	0.198041D-03	0.285974D-01	0.700000D-01
0.539062D+01	0.103313D+04	0.171692D+13	0.198201D-03	0.285974D-01	0.700000D-01
0.564062D+01	0.103313D+04	0.171358D+13	0.198331D-03	0.285974D-01	0.700000D-01
0.589062D+01	0.103313D+04	0.171088D+13	0.198436D-03	0.285974D-01	0.700000D-01
0.614062D+01	0.103313D+04	0.170868D+13	0.198522D-03	0.285974D-01	0.700000D-01
0.639062D+01	0.103313D+04	0.170689D+13	0.198592D-03	0.285974D-01	0.700000D-01
0.664062D+01	0.103313D+04	0.170543D+13	0.198649D-03	0.285974D-01	0.700000D-01

Table G.2.3c. Changes in viscosity and swelling as a function of time as coal is heated at 448 C/s to 760 C and held there for 5 sec, predicted using parameters from Table G.2.3a.

t	temp	diff	difft	visc	swell
0.273214D+00	0.420530D+03	0.934953D-13	0.122026D-15	0.202309D+18	0.999973D+00
0.323214D+00	0.442930D+03	0.384091D-12	0.789104D-15	0.132984D+17	0.999825D+00
0.373214D+00	0.465330D+03	0.137727D-11	0.426027D-14	0.114153D+16	0.999179D+00
0.423214D+00	0.487730D+03	0.436894D-11	0.195483D-13	0.124625D+15	0.997020D+00
0.473214D+00	0.510130D+03	0.124112D-10	0.774806D-13	0.168940D+14	0.992860D+00
0.523214D+00	0.532530D+03	0.325722D-10	0.276492D-12	0.267296D+13	0.990515D+00
0.573214D+00	0.554930D+03	0.800244D-10	0.904102D-12	0.480874D+12	0.990394D+00
0.623214D+00	0.577330D+03	0.183739D-09	0.270267D-11	0.987293D+11	0.990389D+00
0.673214D+00	0.599730D+03	0.396995D-09	0.745410D-11	0.228213D+11	0.990381D+00
0.723214D+00	0.622130D+03	0.812366D-09	0.191297D-10	0.586487D+10	0.990364D+00
0.773214D+00	0.644530D+03	0.158301D-08	0.460146D-10	0.165776D+10	0.990338D+00
0.823214D+00	0.666930D+03	0.295190D-08	0.104418D-09	0.510456D+09	0.990308D+00
0.873214D+00	0.689330D+03	0.529359D-08	0.225005D-09	0.169572D+09	0.990329D+00
0.923214D+00	0.711730D+03	0.918744D-08	0.464324D-09	0.600124D+08	0.990759D+00
0.973214D+00	0.734130D+03	0.155839D-07	0.929630D-09	0.221919D+08	0.995049D+00
0.102321D+01	0.756530D+03	0.260530D-07	0.182614D-08	0.843213D+07	0.103790D+01
0.107321D+01	0.778930D+03	0.432444D-07	0.355419D-08	0.324442D+07	0.121747D+01
0.112321D+01	0.801330D+03	0.712704D-07	0.685396D-08	0.126417D+07	0.162693D+01
0.117321D+01	0.823730D+03	0.108227D-06	0.118536D-07	0.579297D+06	0.227945D+01
0.122321D+01	0.846130D+03	0.136609D-06	0.160261D-07	0.383631D+06	0.296810D+01
0.127321D+01	0.868530D+03	0.144444D-06	0.171135D-07	0.361552D+06	0.344582D+01
0.132321D+01	0.890930D+03	0.140188D-06	0.163055D-07	0.403892D+06	0.372017D+01
0.137321D+01	0.913330D+03	0.128014D-06	0.143262D-07	0.509030D+06	0.387319D+01
0.142321D+01	0.935730D+03	0.112170D-06	0.119157D-07	0.695895D+06	0.395840D+01
0.147321D+01	0.958130D+03	0.998172D-07	0.101189D-07	0.921379D+06	0.400874D+01
0.152321D+01	0.980530D+03	0.947831D-07	0.937176D-08	0.107019D+07	0.404323D+01
0.157321D+01	0.100293D+04	0.949712D-07	0.932608D-08	0.111521D+07	0.407082D+01
0.162321D+01	0.102533D+04	0.974524D-07	0.958155D-08	0.110699D+07	0.409468D+01
0.164062D+01	0.103313D+04	0.985686D-07	0.970361D-08	0.109858D+07	0.410230D+01
0.169062D+01	0.103313D+04	0.878209D-07	0.831915D-08	0.138393D+07	0.411988D+01
0.174062D+01	0.103313D+04	0.796414D-07	0.730242D-08	0.168280D+07	0.413211D+01
0.179062D+01	0.103313D+04	0.730981D-07	0.651363D-08	0.199755D+07	0.414110D+01
0.184062D+01	0.103313D+04	0.676847D-07	0.587853D-08	0.232986D+07	0.414797D+01
0.189062D+01	0.103313D+04	0.630944D-07	0.535306D-08	0.268120D+07	0.415336D+01
0.194062D+01	0.103313D+04	0.591287D-07	0.490922D-08	0.305291D+07	0.415768D+01
0.199062D+01	0.103313D+04	0.556524D-07	0.452821D-08	0.344621D+07	0.416120D+01
0.204062D+01	0.103313D+04	0.525695D-07	0.419689D-08	0.386226D+07	0.416411D+01
0.209062D+01	0.103313D+04	0.498096D-07	0.390571D-08	0.430213D+07	0.416654D+01
0.214062D+01	0.103313D+04	0.473193D-07	0.364753D-08	0.476688D+07	0.416859D+01
0.219062D+01	0.103313D+04	0.450569D-07	0.341689D-08	0.525759D+07	0.417033D+01
0.224062D+01	0.103313D+04	0.429898D-07	0.320949D-08	0.577535D+07	0.417182D+01
0.229062D+01	0.103313D+04	0.410914D-07	0.302192D-08	0.632132D+07	0.417310D+01
0.234062D+01	0.103313D+04	0.393400D-07	0.285142D-08	0.689670D+07	0.417422D+01
0.239062D+01	0.103313D+04	0.377177D-07	0.269572D-08	0.750273D+07	0.417519D+01
0.244062D+01	0.103313D+04	0.362095D-07	0.255297D-08	0.814074D+07	0.417603D+01
0.249062D+01	0.103313D+04	0.348029D-07	0.242160D-08	0.881211D+07	0.417678D+01
0.254062D+01	0.103313D+04	0.334870D-07	0.230029D-08	0.951826D+07	0.417743D+01
0.259062D+01	0.103313D+04	0.322527D-07	0.218795D-08	0.102607D+08	0.417801D+01
0.264062D+01	0.103313D+04	0.310921D-07	0.208361D-08	0.110410D+08	0.417852D+01
0.289062D+01	0.103313D+04	0.261831D-07	0.165695D-08	0.155693D+08	0.418036D+01
0.314062D+01	0.103313D+04	0.223772D-07	0.134387D-08	0.213156D+08	0.418144D+01
0.339062D+01	0.103313D+04	0.193342D-07	0.110590D-08	0.285535D+08	0.418210D+01
0.364062D+01	0.103313D+04	0.168457D-07	0.920307D-09	0.376126D+08	0.418251D+01
0.389062D+01	0.103313D+04	0.147754D-07	0.772685D-09	0.488910D+08	0.418279D+01
0.414062D+01	0.103313D+04	0.130298D-07	0.653427D-09	0.628690D+08	0.418297D+01
0.439062D+01	0.103313D+04	0.115417D-07	0.555872D-09	0.801255D+08	0.418309D+01
0.464062D+01	0.103313D+04	0.102619D-07	0.475248D-09	0.101357D+09	0.418318D+01
0.489062D+01	0.103313D+04	0.915322D-08	0.408050D-09	0.127398D+09	0.418324D+01
0.514062D+01	0.103313D+04	0.818681D-08	0.351642D-09	0.159251D+09	0.418329D+01
0.539062D+01	0.103313D+04	0.734005D-08	0.304005D-09	0.198112D+09	0.418332D+01
0.564062D+01	0.103313D+04	0.659483D-08	0.263564D-09	0.245416D+09	0.418334D+01
0.589062D+01	0.103313D+04	0.593645D-08	0.229078D-09	0.302871D+09	0.418336D+01
0.614062D+01	0.103313D+04	0.535281D-08	0.199553D-09	0.372517D+09	0.418338D+01
0.639062D+01	0.103313D+04	0.483390D-08	0.174186D-09	0.456787D+09	0.418339D+01
0.664062D+01	0.103313D+04	0.437133D-08	0.152323D-09	0.558577D+09	0.418340D+01

Table G.2.4a. Effect of vapor pressure model on kinetic parameters. Suuberg's vapor pressure model is employed instead of Maiorellas's model. Table G.2.4's are employed in Figures 6.4.3. thru 6.4.5.

********** input **********

pressure	=	0.10130D+07	dyne/cm*cm
original particle radius	=	0.35000D-02	cm
initial pore size	=	0.79934D-05	cm
initial bubble size	=	0.28685D-05	cm
pore volume	=	0.40000D-01	cm**3
constant for viscosity	=	0.10000D-09	
constant for diffusivity	=	0.10000D-06	

Molecular weight of 10 tar compoents

0.16900D+03	0.27000D+03	0.33000D+03	0.38600D+03	0.44700D+03
0.51900D+03	0.60900D+03	0.72700D+03	0.89200D+03	0.12450D+04

Parameters fixed

reactin constant for gas	=	0.10000D+14	1/sec
act e for gas formation	=	0.26755D+05	cal/mole
ultimate yield of gas	=	0.28457D-01	gm/gm
ultimate yield of tar	=	0.70000D+00	gm/gm

Parameters varied, final paratmeter values

reaction constant1 for tar=		0.31945D+05	1/sec
reaction constant2 for tar=		0.29641D+05	1/sec
act E for metaplast formation	=	0.16083D+05	cal/mole
act E for metaplast decomposition=		0.16860D+05	cal/mole
fraction of metaplast converted to gases=		0.28440D+00	

square sum of residual functions= 0.14254D+00

Comparison with experimental data

TOTAL VOLATILES YIELD

Peak Temp	Calulated w/o y(32)	Experimental	w/ y(32)
203.85	0.0252962	0.0162600	0.25296D-01
223.26	0.0283807	0.0125000	0.28381D-01
244.43	0.0283602	0.0291000	0.28360D-01
248.53	0.0300557	0.0247000	0.30056D-01
259.40	0.0285251	0.0137000	0.28525D-01
264.00	0.0283593	0.0165300	0.28359D-01
315.00	0.0364885	0.0165700	0.36489D-01
351.50	0.0354442	0.0294800	0.35444D-01
379.63	0.0339528	0.0259000	0.33953D-01
385.56	0.0335289	0.0342000	0.33529D-01

Table G.2.4a continues

395.12	0.0327455	0.0343000	0.32745D-01
403.55	0.0160277	0.0353000	0.47265D-01
414.38	0.0222380	0.0343000	0.51959D-01
432.38	0.0336109	0.0370400	0.62060D-01
478.91	0.0708749	0.1504000	0.10069D+00
509.00	0.1031272	0.1740000	0.13530D+00
527.90	0.1274121	0.1908000	0.16156D+00
558.53	0.1730140	0.2678000	0.21070D+00
627.77	0.2941207	0.3428000	0.33203D+00
647.10	0.3265252	0.2870000	0.36107D+00
647.11	0.3265413	0.2816000	0.36108D+00
659.59	0.3452861	0.3690000	0.37731D+00
701.67	0.3923118	0.3896000	0.41715D+00
727.27	0.4096167	0.4043000	0.43211D+00
745.72	0.4181144	0.3430000	0.43980D+00
781.75	0.4278692	0.4450000	0.44956D+00
877.46	0.4311813	0.4802000	0.45822D+00
948.86	0.4277666	0.4715000	0.46053D+00
991.00	0.4251933	0.4708000	0.46189D+00
1009.00	0.4239829	0.4884000	0.46247D+00
1029.72	0.4225131	0.4810000	0.46313D+00
1051.76	0.4208441	0.4700000	0.46381D+00

TAR YIELD

Peak Temp	Calulated	Experimental
203.85	0.0000000	0.0000000
244.43	0.0000000	0.0000000
264.00	0.0000000	0.0000000
315.00	0.0000000	0.0000000
351.50	0.0000000	0.0000000
395.12	0.0000000	0.0000000
403.55	0.0054746	0.0000000
478.91	0.0468640	0.0919000
509.00	0.0725752	0.1185000
558.53	0.1273145	0.1772000
627.77	0.2148591	0.2662000
647.10	0.2359880	0.2469000
647.11	0.2359985	0.2290000
659.59	0.2478149	0.2976000
701.67	0.2769336	0.3065000
727.27	0.2880096	0.3097000
781.75	0.3004786	0.2993000
877.46	0.3005962	0.3134000
991.00	0.2943834	0.2550000
1009.00	0.2937528	0.2541000
1029.72	0.2931378	0.2970000
1051.76	0.2925981	0.2955000

EXTRACT YIELD

Peak Temp	Calulated	Experimental
203.85	0.2649627	0.2655000
244.43	0.2625900	0.2592000
264.00	0.2632973	0.2810000
315.00	0.2594526	0.2541000
351.50	0.2671015	0.2532100
395.12	0.2832825	0.2367000
403.55	0.2827689	0.2467000
478.91	0.2959030	0.2824000
509.00	0.2923877	0.2914000
527.90	0.2839200	0.2900000
558.53	0.2571626	0.1994000
627.77	0.1476307	0.0878000
647.10	0.1148058	0.2100000
647.11	0.1147898	0.2540000
659.59	0.0955726	0.0476000
701.67	0.0467936	0.0000000
727.27	0.0291140	0.0000000
781.75	0.0119497	0.0000000
877.46	0.0061606	0.0000000
991.00	0.0036234	0.0000000
1009.00	0.0032870	0.0000000
1029.72	0.0029210	0.0000000
1051.76	0.0025575	0.0000000

Table G.2.4b. Product distribution during coal pyrolysis as coal is heated at 448 C/s to 760 C and held there for 5 sec, predicted using parameters from Table G.2.4a.

+++++ Kinetic Constants +++++++

reactin constant for gas =	0.10000D+14	1/sec
act E for gas formation =	0.26755D+05	cal/mole
ultimate yield of gas =	0.28457D-01	gm/gm
reaction constant1 for tar=	0.31945D+05	1/sec
act e for tar formation =	0.16083D+05	cal/mole
ultimate yield of tar =	0.70000D+00	gm/gm
reaction constant2 for tar=	0.29641D+05	1/sec
act e for tar decomp =	0.16860D+05	cal/mole
f of metaplast to gases =	0.28440D+00	

+++++++++ Run Conditions +++++++

pressure =	0.10130D+07	dyne/cm*cm
original particle radius =	0.35000D-02	cm
initial bubble size (solid)=	0.79934D-05	cm
initial bubble size (molten)=	0.28685D-05	cm
pore volume =	0.40000D-01	cm**3
heating rate =	0.44800D+03	C/s
holding time =	0.50000D+01	sec
constant for viscosity =	0.10000D-09	
constant for diffusivity =	0.10000D-06	

Molecular weight of 10 tar compoents

0.16900D+03	0.27000D+03	0.33000D+03	0.38600D+03	0.44700D+03
0.51900D+03	0.60900D+03	0.72700D+03	0.89200D+03	0.12450D+04

peak temperature = 0.10331D+04 kelvin

********** output **********

t	temp	char	ctar	cmon	bgas	bmass	ttary	gasy
0.273	0.420530D+03	0.709957D+00	0.289918D+00	0.832225D-04	0.592773D-05	0.596640D-05	0.820008D-10	0.723608D-10
0.323	0.442930D+03	0.709953D+00	0.289478D+00	0.500164D-03	0.326065D-04	0.326748D-04	0.647772D-09	0.216356D-08
0.373	0.465330D+03	0.709944D+00	0.287547D+00	0.233350D-02	0.140643D-03	0.140757D-03	0.387397D-08	0.408702D-07
0.423	0.487730D+03	0.709921D+00	0.281102D+00	0.846154D-02	0.479766D-03	0.479947D-03	0.192678D-07	0.541429D-06
0.473	0.510130D+03	0.709873D+00	0.268762D+00	0.202220D-01	0.110258D-02	0.110285D-02	0.809497D-07	0.463616D-05

Table G.2.4b continues

0.523	0.532530D+03	0.709777D+00	0.261918D+00	0.268413D-01	0.140519D-02	0.140560D-02	0.299861D-06	0.227352D-04
0.573	0.554930D+03	0.709597D+00	0.261726D+00	0.271560D-01	0.141151D-02	0.141211D-02	0.103303D-05	0.727702D-04
0.623	0.577330D+03	0.709275D+00	0.262010D+00	0.267442D-01	0.173668D-02	0.173779D-02	0.329847D-05	0.193994D-03
0.673	0.599730D+03	0.708727D+00	0.262487D+00	0.235305D-01	0.472239D-02	0.472725D-02	0.975356D-05	0.483190D-03
0.723	0.622130D+03	0.707830D+00	0.263177D+00	0.749137D-02	0.202879D-01	0.203781D-01	0.272853D-04	0.106064D-02
0.773	0.644530D+03	0.706417D+00	0.263637D+00	0.140340D-02	0.258890D-01	0.267105D-01	0.797118D-04	0.171762D-02
0.823	0.666930D+03	0.704261D+00	0.262267D+00	0.368044D-03	0.262285D-01	0.301106D-01	0.276193D-03	0.268229D-02
0.873	0.689330D+03	0.701065D+00	0.256487D+00	0.118358D-03	0.250623D-01	0.366601D-01	0.112699D-02	0.450728D-02
0.923	0.711730D+03	0.696449D+00	0.247485D+00	0.476813D-04	0.227142D-01	0.444408D-01	0.401717D-02	0.752507D-02
0.973	0.734130D+03	0.689975D+00	0.240222D+00	0.283945D-04	0.205721D-01	0.500590D-01	0.914291D-02	0.105381D-01
1.023	0.756530D+03	0.681218D+00	0.237422D+00	0.246157D-04	0.201068D-01	0.555216D-01	0.135745D-01	0.122045D-01
1.073	0.778930D+03	0.669804D+00	0.236137D+00	0.232346D-04	0.203432D-01	0.622533D-01	0.181109D-01	0.136362D-01
1.123	0.801330D+03	0.655478D+00	0.235122D+00	0.222974D-04	0.210011D-01	0.705647D-01	0.235126D-01	0.152650D-01
1.173	0.823730D+03	0.638220D+00	0.233415D+00	0.213933D-04	0.220349D-01	0.805452D-01	0.304491D-01	0.173141D-01
1.223	0.846130D+03	0.618367D+00	0.229874D+00	0.204042D-04	0.234219D-01	0.919513D-01	0.397508D-01	0.200019D-01
1.273	0.868530D+03	0.596705D+00	0.223207D+00	0.192907D-04	0.250908D-01	0.103984D+00	0.524600D-01	0.235898D-01
1.323	0.890930D+03	0.574495D+00	0.212227D+00	0.180548D-04	0.268899D-01	0.115169D+00	0.696826D-01	0.283736D-01
1.373	0.913330D+03	0.553380D+00	0.196225D+00	0.167317D-04	0.285896D-01	0.123528D+00	0.921904D-01	0.346247D-01
1.423	0.935730D+03	0.535162D+00	0.175289D+00	0.153856D-04	0.299369D-01	0.127191D+00	0.119826D+00	0.424810D-01
1.473	0.958130D+03	0.521454D+00	0.150408D+00	0.140963D-04	0.307494D-01	0.125228D+00	0.151039D+00	0.518214D-01
1.523	0.980530D+03	0.513297D+00	0.123326D+00	0.129464D-04	0.310041D-01	0.118156D+00	0.182981D+00	0.621928D-01
1.573	0.100293D+04	0.510848D+00	0.961804D-01	0.120068D-04	0.308524D-01	0.107705D+00	0.212355D+00	0.728644D-01
1.623	0.102533D+04	0.513299D+00	0.710464D-01	0.113264D-04	0.305485D-01	0.960251D-01	0.236578D+00	0.830048D-01
1.641	0.103313D+04	0.515030D+00	0.630823D-01	0.111553D-04	0.304546D-01	0.920164D-01	0.243552D+00	0.862735D-01
1.691	0.103313D+04	0.521239D+00	0.461700D-01	0.106609D-04	0.299781D-01	0.792167D-01	0.258867D+00	0.944616D-01
1.741	0.103313D+04	0.527640D+00	0.336777D-01	0.102873D-04	0.294168D-01	0.693542D-01	0.268515D+00	0.100767D+00
1.791	0.103313D+04	0.533300D+00	0.246034D-01	0.100371D-04	0.289701D-01	0.619894D-01	0.274548D+00	0.105514D+00
1.841	0.103313D+04	0.537974D+00	0.180580D-01	0.988070D-05	0.286607D-01	0.564891D-01	0.278361D+00	0.109073D+00
1.891	0.103313D+04	0.541704D+00	0.133478D-01	0.979153D-05	0.284694D-01	0.523391D-01	0.280812D+00	0.111753D+00
1.941	0.103313D+04	0.544630D+00	0.995620D-02	0.974958D-05	0.283708D-01	0.491649D-01	0.282420D+00	0.113784D+00
1.991	0.103313D+04	0.546910D+00	0.750708D-02	0.974046D-05	0.283418D-01	0.466997D-01	0.283498D+00	0.115340D+00
2.041	0.103313D+04	0.548687D+00	0.573013D-02	0.975393D-05	0.283634D-01	0.447548D-01	0.284236D+00	0.116546D+00
2.091	0.103313D+04	0.550079D+00	0.443280D-02	0.978274D-05	0.284214D-01	0.431967D-01	0.284753D+00	0.117493D+00
2.141	0.103313D+04	0.551178D+00	0.347821D-02	0.982170D-05	0.285044D-01	0.419295D-01	0.285123D+00	0.118246D+00
2.191	0.103313D+04	0.552054D+00	0.276934D-02	0.986714D-05	0.286044D-01	0.408841D-01	0.285393D+00	0.118854D+00
2.241	0.103313D+04	0.552762D+00	0.223746D-02	0.991641D-05	0.287151D-01	0.400099D-01	0.285594D+00	0.119352D+00
2.291	0.103313D+04	0.553339D+00	0.183381D-02	0.996767D-05	0.288319D-01	0.392697D-01	0.285747D+00	0.119765D+00
2.341	0.103313D+04	0.553818D+00	0.152371D-02	0.100196D-04	0.289518D-01	0.386359D-01	0.285865D+00	0.120112D+00
2.391	0.103313D+04	0.554218D+00	0.128243D-02	0.100714D-04	0.290722D-01	0.380876D-01	0.285958D+00	0.120409D+00
2.441	0.103313D+04	0.554558D+00	0.109220D-02	0.101222D-04	0.291916D-01	0.376090D-01	0.286032D+00	0.120664D+00
2.491	0.103313D+04	0.554849D+00	0.940253D-03	0.101719D-04	0.293089D-01	0.371878D-01	0.286091D+00	0.120886D+00
2.541	0.103313D+04	0.555101D+00	0.817296D-03	0.102201D-04	0.294233D-01	0.368144D-01	0.286140D+00	0.121082D+00
2.591	0.103313D+04	0.555321D+00	0.716547D-03	0.102666D-04	0.295342D-01	0.364813D-01	0.286181D+00	0.121255D+00
2.641	0.103313D+04	0.555514D+00	0.633006D-03	0.103113D-04	0.296415D-01	0.361825D-01	0.286214D+00	0.121410D+00
2.891	0.103313D+04	0.556212D+00	0.371049D-03	0.105089D-04	0.301201D-01	0.350601D-01	0.286320D+00	0.121991D+00
3.141	0.103313D+04	0.556641D+00	0.238632D-03	0.106674D-04	0.305095D-01	0.343335D-01	0.286372D+00	0.122370D+00
3.391	0.103313D+04	0.556924D+00	0.162052D-03	0.107946D-04	0.308256D-01	0.338361D-01	0.286399D+00	0.122633D+00
3.641	0.103313D+04	0.557120D+00	0.114068D-03	0.108971D-04	0.310830D-01	0.334827D-01	0.286414D+00	0.122823D+00
3.891	0.103313D+04	0.557260D+00	0.823991D-04	0.109802D-04	0.312937D-01	0.332248D-01	0.286422D+00	0.122964D+00
4.141	0.103313D+04	0.557362D+00	0.607136D-04	0.110479D-04	0.314667D-01	0.330326D-01	0.286427D+00	0.123071D+00
4.391	0.103313D+04	0.557437D+00	0.454466D-04	0.111034D-04	0.316094D-01	0.328869D-01	0.286431D+00	0.123153D+00
4.641	0.103313D+04	0.557494D+00	0.344612D-04	0.111490D-04	0.317273D-01	0.327750D-01	0.286433D+00	0.123217D+00
4.891	0.103313D+04	0.557538D+00	0.264157D-04	0.111866D-04	0.318251D-01	0.326879D-01	0.286434D+00	0.123267D+00
5.141	0.103313D+04	0.557571D+00	0.204363D-04	0.112176D-04	0.319063D-01	0.326196D-01	0.286435D+00	0.123308D+00
5.391	0.103313D+04	0.557597D+00	0.159370D-04	0.112434D-04	0.319738D-01	0.325654D-01	0.286435D+00	0.123340D+00
5.641	0.103313D+04	0.557618D+00	0.125155D-04	0.112647D-04	0.320301D-01	0.325221D-01	0.286435D+00	0.123366D+00
5.891	0.103313D+04	0.557634D+00	0.988945D-05	0.112825D-04	0.320770D-01	0.324872D-01	0.286436D+00	0.123387D+00
6.141	0.103313D+04	0.557646D+00	0.785764D-05	0.112973D-04	0.321162D-01	0.324590D-01	0.286436D+00	0.123404D+00
6.391	0.103313D+04	0.557657D+00	0.627430D-05	0.113096D-04	0.321490D-01	0.324359D-01	0.286436D+00	0.123419D+00
6.641	0.103313D+04	0.557665D+00	0.503256D-05	0.113199D-04	0.321763D-01	0.324170D-01	0.286436D+00	0.123431D+00

Table G.2.4c. Changes in viscosity and swelling as a function of time as coal is heated at 448 C/s to 760 C and held there for 5 sec, predicted using parameters from Table G.2.4a.

t	temp	diff	difft	visc	swell
0.273214D+00	0.420530D+03	0.295659D-11	0.122027D-13	0.202307D+15	0.999973D+00
0.323214D+00	0.442930D+03	0.121462D-10	0.789117D-13	0.132981D+14	0.999825D+00
0.373214D+00	0.465330D+03	0.435544D-10	0.426045D-12	0.114145D+13	0.999178D+00
0.423214D+00	0.487730D+03	0.138170D-09	0.195504D-11	0.124605D+12	0.997018D+00
0.473214D+00	0.510130D+03	0.392554D-09	0.775008D-11	0.168874D+11	0.992856D+00
0.523214D+00	0.532530D+03	0.103046D-08	0.276649D-10	0.267068D+10	0.990513D+00
0.573214D+00	0.554930D+03	0.253278D-08	0.905144D-10	0.480043D+09	0.990425D+00
0.623214D+00	0.577330D+03	0.582002D-08	0.270868D-09	0.984009D+08	0.990633D+00
0.673214D+00	0.599730D+03	0.125927D-07	0.748467D-09	0.226817D+08	0.992638D+00
0.723214D+00	0.622130D+03	0.258256D-07	0.192652D-08	0.580312D+07	0.102985D+01
0.773214D+00	0.644530D+03	0.504509D-07	0.464955D-08	0.163211D+07	0.122757D+01
0.823214D+00	0.666930D+03	0.940917D-07	0.105530D-07	0.502410D+06	0.164970D+01
0.873214D+00	0.689330D+03	0.167506D-06	0.225197D-07	0.169354D+06	0.225344D+01
0.923214D+00	0.711730D+03	0.286234D-06	0.455186D-07	0.618286D+05	0.288585D+01
0.973214D+00	0.734130D+03	0.375904D-06	0.647906D-07	0.381409D+05	0.329387D+01
0.102321D+01	0.756530D+03	0.387559D-06	0.668099D-07	0.381046D+05	0.344062D+01
0.107321D+01	0.778930D+03	0.401117D-06	0.692673D-07	0.377099D+05	0.353997D+01
0.112321D+01	0.801330D+03	0.415903D-06	0.720088D-07	0.371226D+05	0.364326D+01
0.117321D+01	0.823730D+03	0.431299D-06	0.748932D-07	0.364765D+05	0.376189D+01
0.122321D+01	0.846130D+03	0.446306D-06	0.776899D-07	0.359425D+05	0.389567D+01
0.127321D+01	0.868530D+03	0.459411D-06	0.800462D-07	0.357410D+05	0.403769D+01
0.132321D+01	0.890930D+03	0.468605D-06	0.814944D-07	0.361471D+05	0.417535D+01
0.137321D+01	0.913330D+03	0.471564D-06	0.815038D-07	0.375124D+05	0.429246D+01
0.142321D+01	0.935730D+03	0.466001D-06	0.795792D-07	0.403206D+05	0.437310D+01
0.147321D+01	0.958130D+03	0.450139D-06	0.753913D-07	0.453059D+05	0.440678D+01
0.152321D+01	0.980530D+03	0.423254D-06	0.689152D-07	0.536684D+05	0.439244D+01
0.157321D+01	0.100293D+04	0.386099D-06	0.605119D-07	0.674753D+05	0.433920D+01
0.162321D+01	0.102533D+04	0.340947D-06	0.508895D-07	0.904386D+05	0.426322D+01
0.164062D+01	0.103313D+04	0.323950D-06	0.474153D-07	0.101708D+06	0.423471D+01
0.169062D+01	0.103313D+04	0.276931D-06	0.384689D-07	0.139177D+06	0.415648D+01
0.174062D+01	0.103313D+04	0.235995D-06	0.310804D-07	0.191647D+06	0.409026D+01
0.179062D+01	0.103313D+04	0.201206D-06	0.251268D-07	0.263650D+06	0.403742D+01
0.184062D+01	0.103313D+04	0.171976D-06	0.203816D-07	0.360891D+06	0.399635D+01
0.189062D+01	0.103313D+04	0.147560D-06	0.166178D-07	0.490200D+06	0.396475D+01
0.194062D+01	0.103313D+04	0.127231D-06	0.136376D-07	0.659363D+06	0.394049D+01
0.199062D+01	0.103313D+04	0.110332D-06	0.112776D-07	0.876819D+06	0.392179D+01
0.204062D+01	0.103313D+04	0.962892D-07	0.940557D-08	0.115121D+07	0.390726D+01
0.209062D+01	0.103313D+04	0.846166D-07	0.791691D-08	0.149073D+07	0.389587D+01
0.214062D+01	0.103313D+04	0.749008D-07	0.672869D-08	0.190255D+07	0.388684D+01
0.219062D+01	0.103313D+04	0.667952D-07	0.577576D-08	0.239232D+07	0.387958D+01
0.224062D+01	0.103313D+04	0.600104D-07	0.500707D-08	0.296385D+07	0.387367D+01
0.229062D+01	0.103313D+04	0.543065D-07	0.438280D-08	0.361914D+07	0.386879D+01
0.234062D+01	0.103313D+04	0.494857D-07	0.387188D-08	0.435863D+07	0.386471D+01
0.239062D+01	0.103313D+04	0.453857D-07	0.345017D-08	0.518170D+07	0.386126D+01
0.244062D+01	0.103313D+04	0.418742D-07	0.309892D-08	0.608720D+07	0.385830D+01
0.249062D+01	0.103313D+04	0.388439D-07	0.280358D-08	0.707398D+07	0.385574D+01
0.254062D+01	0.103313D+04	0.362083D-07	0.255285D-08	0.814131D+07	0.385351D+01
0.259062D+01	0.103313D+04	0.338975D-07	0.233797D-08	0.928913D+07	0.385154D+01
0.264062D+01	0.103313D+04	0.318555D-07	0.215209D-08	0.105182D+08	0.384979D+01
0.289062D+01	0.103313D+04	0.243757D-07	0.150623D-08	0.179637D+08	0.384335D+01
0.314062D+01	0.103313D+04	0.195414D-07	0.112174D-08	0.279509D+08	0.383926D+01
0.339062D+01	0.103313D+04	0.160997D-07	0.866375D-09	0.411788D+08	0.383649D+01
0.364062D+01	0.103313D+04	0.135053D-07	0.685415D-09	0.585197D+08	0.383454D+01
0.389062D+01	0.103313D+04	0.114771D-07	0.551727D-09	0.810300D+08	0.383313D+01
0.414062D+01	0.103313D+04	0.985092D-08	0.450040D-09	0.109991D+09	0.383209D+01
0.439062D+01	0.103313D+04	0.852231D-08	0.370986D-09	0.146959D+09	0.383131D+01
0.464062D+01	0.103313D+04	0.742081D-08	0.308473D-09	0.193824D+09	0.383072D+01
0.489062D+01	0.103313D+04	0.649682D-08	0.258355D-09	0.252876D+09	0.383026D+01
0.514062D+01	0.103313D+04	0.571424D-08	0.217717D-09	0.326884D+09	0.382991D+01
0.539062D+01	0.103313D+04	0.504605D-08	0.184452D-09	0.419186D+09	0.382963D+01
0.564062D+01	0.103313D+04	0.447162D-08	0.157000D-09	0.533803D+09	0.382942D+01
0.589062D+01	0.103313D+04	0.397485D-08	0.134187D-09	0.675567D+09	0.382925D+01
0.614062D+01	0.103313D+04	0.354304D-08	0.115111D-09	0.850272D+09	0.382911D+01
0.639062D+01	0.103313D+04	0.316599D-08	0.990742D-10	0.106486D+10	0.382901D+01
0.664062D+01	0.103313D+04	0.283542D-08	0.855274D-10	0.132762D+10	0.382892D+01

Table G.2.4d. Amount of volatiles formed and changes in bubble radius and bubble number density as a function of time as coal is heated at 448 C/s to 760 C and held there for 5 sec, predicted using parameters from Table G.2.4a.

t	temp	bnden	brad	gasf	tarf
0.273214D+00	0.420530D+03	0.143887D+14	0.286850D-05	0.830993D-04	0.290002D-01
0.323214D+00	0.442930D+03	0.143887D+14	0.286850D-05	0.526352D-03	0.290007D-01
0.373214D+00	0.465330D+03	0.143887D+14	0.286850D-05	0.246680D-02	0.290019D-01
0.423214D+00	0.487730D+03	0.143887D+14	0.286854D-05	0.893219D-02	0.290047D-01
0.473214D+00	0.510130D+03	0.143887D+14	0.286938D-05	0.213147D-01	0.290107D-01
0.523214D+00	0.532530D+03	0.143886D+14	0.287832D-05	0.282450D-01	0.290228D-01
0.573214D+00	0.554930D+03	0.143879D+14	0.293381D-05	0.285974D-01	0.290455D-01
0.623214D+00	0.577330D+03	0.143844D+14	0.322625D-05	0.285974D-01	0.290864D-01
0.673214D+00	0.599730D+03	0.143654D+14	0.479567D-05	0.285974D-01	0.291566D-01
0.723214D+00	0.622130D+03	0.142800D+14	0.116587D-04	0.285974D-01	0.292724D-01
0.773214D+00	0.644530D+03	0.141148D+14	0.225663D-04	0.285974D-01	0.294565D-01
0.823214D+00	0.666930D+03	0.137821D+14	0.361039D-04	0.285974D-01	0.297396D-01
0.873214D+00	0.689330D+03	0.130425D+14	0.528916D-04	0.285974D-01	0.301611D-01
0.923214D+00	0.711730D+03	0.117429D+14	0.712620D-04	0.285974D-01	0.307700D-01
0.973214D+00	0.734130D+03	0.105061D+14	0.847980D-04	0.285974D-01	0.316245D-01
0.102321D+01	0.756530D+03	0.996182D+13	0.902678D-04	0.285974D-01	0.327890D-01
0.107321D+01	0.778930D+03	0.955752D+13	0.942343D-04	0.285974D-01	0.343296D-01
0.112321D+01	0.801330D+03	0.910296D+13	0.986395D-04	0.285974D-01	0.363057D-01
0.117321D+01	0.823730D+03	0.853233D+13	0.104145D-03	0.285974D-01	0.387580D-01
0.122321D+01	0.846130D+03	0.781478D+13	0.111130D-03	0.285974D-01	0.416940D-01
0.127321D+01	0.868530D+03	0.694277D+13	0.119892D-03	0.285974D-01	0.450726D-01
0.132321D+01	0.890930D+03	0.593905D+13	0.130676D-03	0.285974D-01	0.487925D-01
0.137321D+01	0.913330D+03	0.486229D+13	0.143669D-03	0.285974D-01	0.526897D-01
0.142321D+01	0.935730D+03	0.379990D+13	0.158957D-03	0.285974D-01	0.565499D-01
0.147321D+01	0.958130D+03	0.284407D+13	0.176462D-03	0.285974D-01	0.601383D-01
0.152321D+01	0.980530D+03	0.206160D+13	0.195823D-03	0.285974D-01	0.632429D-01
0.157321D+01	0.100293D+04	0.147545D+13	0.216274D-03	0.285974D-01	0.657192D-01
0.162321D+01	0.102533D+04	0.106842D+13	0.236616D-03	0.285974D-01	0.675218D-01
0.164062D+01	0.103313D+04	0.961842D+12	0.243406D-03	0.285974D-01	0.679988D-01
0.169062D+01	0.103313D+04	0.737301D+12	0.261022D-03	0.285974D-01	0.689367D-01
0.174062D+01	0.103313D+04	0.598397D+12	0.275345D-03	0.285974D-01	0.694350D-01
0.179062D+01	0.103313D+04	0.509971D+12	0.286640D-03	0.285974D-01	0.696998D-01
0.184062D+01	0.103313D+04	0.451661D+12	0.295420D-03	0.285974D-01	0.698405D-01
0.189062D+01	0.103313D+04	0.411923D+12	0.302201D-03	0.285974D-01	0.699153D-01
0.194062D+01	0.103313D+04	0.384038D+12	0.307435D-03	0.285974D-01	0.699550D-01
0.199062D+01	0.103313D+04	0.363955D+12	0.311490D-03	0.285974D-01	0.699761D-01
0.204062D+01	0.103313D+04	0.349143D+12	0.314653D-03	0.285974D-01	0.699873D-01
0.209062D+01	0.103313D+04	0.337981D+12	0.317144D-03	0.285974D-01	0.699932D-01
0.214062D+01	0.103313D+04	0.329397D+12	0.319126D-03	0.285974D-01	0.699964D-01
0.219062D+01	0.103313D+04	0.322667D+12	0.320723D-03	0.285974D-01	0.699981D-01
0.224062D+01	0.103313D+04	0.317295D+12	0.322026D-03	0.285974D-01	0.699990D-01
0.229062D+01	0.103313D+04	0.312933D+12	0.323104D-03	0.285974D-01	0.699995D-01
0.234062D+01	0.103313D+04	0.309335D+12	0.324006D-03	0.285974D-01	0.699997D-01
0.239062D+01	0.103313D+04	0.306323D+12	0.324771D-03	0.285974D-01	0.699998D-01
0.244062D+01	0.103313D+04	0.303769D+12	0.325427D-03	0.285974D-01	0.699999D-01
0.249062D+01	0.103313D+04	0.301576D+12	0.325995D-03	0.285974D-01	0.700000D-01
0.254062D+01	0.103313D+04	0.299673D+12	0.326492D-03	0.285974D-01	0.700000D-01
0.259062D+01	0.103313D+04	0.298007D+12	0.326930D-03	0.285974D-01	0.700000D-01
0.264062D+01	0.103313D+04	0.296536D+12	0.327320D-03	0.285974D-01	0.700000D-01
0.289062D+01	0.103313D+04	0.291183D+12	0.328756D-03	0.285974D-01	0.700000D-01
0.314062D+01	0.103313D+04	0.287839D+12	0.329669D-03	0.285974D-01	0.700000D-01
0.339062D+01	0.103313D+04	0.285596D+12	0.330289D-03	0.285974D-01	0.700000D-01
0.364062D+01	0.103313D+04	0.284027D+12	0.330726D-03	0.285974D-01	0.700000D-01
0.389062D+01	0.103313D+04	0.282897D+12	0.331042D-03	0.285974D-01	0.700000D-01
0.414062D+01	0.103313D+04	0.282066D+12	0.331276D-03	0.285974D-01	0.700000D-01
0.439062D+01	0.103313D+04	0.281445D+12	0.331451D-03	0.285974D-01	0.700000D-01
0.464062D+01	0.103313D+04	0.280974D+12	0.331584D-03	0.285974D-01	0.700000D-01
0.489062D+01	0.103313D+04	0.280613D+12	0.331686D-03	0.285974D-01	0.700000D-01
0.514062D+01	0.103313D+04	0.280334D+12	0.331765D-03	0.285974D-01	0.700000D-01
0.539062D+01	0.103313D+04	0.280117D+12	0.331827D-03	0.285974D-01	0.700000D-01
0.564062D+01	0.103313D+04	0.279946D+12	0.331876D-03	0.285974D-01	0.700000D-01
0.589062D+01	0.103313D+04	0.279812D+12	0.331914D-03	0.285974D-01	0.700000D-01
0.614062D+01	0.103313D+04	0.279705D+12	0.331944D-03	0.285974D-01	0.700000D-01
0.639062D+01	0.103313D+04	0.279619D+12	0.331968D-03	0.285974D-01	0.700000D-01
0.664062D+01	0.103313D+04	0.279551D+12	0.331988D-03	0.285974D-01	0.700000D-01

G.3. Model predictions and computer programs of the model under various time-temperature histories, pressures, and particle sizes

```
**********************************************************************
c
c                          PROGRAM MMAIN
c
c         This program gives the model predictions of volatiles yields,
c         metaplast inventory, and final swelling ratio. This main program
c         is desinged such that several peak temperature runs or extended
c         time temperature runs are used as input and the model predictions
c         are listed as a function of peak temperatures.
c
c         This routine assumes a single size bubbles and 10 different
c         molecular weight tar which have the same formation and secondary
c         reaction rates. This main program calls for subroutines FCNE and
c         AFUNW, and a NAG integration routine d02baf.
c         Subroutine AFUNW is listed in Appendix G.2.
c
----------------------------------------------------------------------
c
c                    Nomenclature
c
c bmden = number of moles in a bubble
c brad = bubble radius, dimensional
c bgas = total mass of gases in bubbles
c btar(i) = total mass of tar i in bubbles
c btary = yield of tar via bubbles
c cmden = molar density of the condensed phase/gm. orig coal
c cmon = concentration of gases dissoved in molten coal
c ctar(i) = total mass of metaplast i in molten phase
c diff = diffusivity of gases in molten coal
c difft = diffusivity of metaplast vapor in molten coal
c dtary = yields of tar due to diffusion
c gasy = total gas yield
c gcon, gcont = gas constant
c gmw = average molecular weight of gases
c hcon = Henry's law constant of gases
c rad = particle radius as a function of time
c rado = original particle radius
c t = time
c tctar = total amount of metaplast in molten coal
c temp = temperature
c visc = viscosity of molten coal
c vol = volume of a particle
c vol = total volume of bubbles
c xtar = mass fraction of metaplast in molten coal
c y(1)-y(10) = ctar(i) + btar(i)
c y(11)-y(20) = amount of tar yield due to diffusion
c y(21)-y(30) = amount of tar yield due to bubble transport
c y(31) = amount of tar(i) formed
c y(32) = bgas + cmon
c y(33) = amount of gas yield due to diffusion
c y(34) = amount of gas yield due to bubble motion
```

```
c y(35) = amount of gas formed
c y(36) = bubble radius, dimensionless, brad/ao
c y(37) = ln(bubble number density)
*************************************************************************
      implicit double precision (a - h, o - z)
      implicit integer (i - n)
      dimension y(38),w(38,18),btar(10),alfa(10),ctar(10)
      common/tar/tmw(10)
      common/con/gcon,wmw,surt,delt,hrate,ptemp,tck,temp,ao
      common/prop/vcon,dcon,visc,pres,volo,rado,at,bt,tp,tpl
      common/rxnc/eg,ept,est,rxng,rxntl,rxnt2,vt,vg,fgl,coalm
      common/ele/ne,nel,pcon,cmden
      external fcne
      fexp(x)=dexp(dmaxl(-1.d2,x))
c
c
c                read initial bubble size, pore volume, heating rate,
c                holding time, and delt and tolo for integration routine.
      read(9,)apore,hrate,tpe,delt,tolo
c                Read pressure, initial particle size and constants for
c                viscosity and diffusivity correlations
      read(9,)pres,rado,vcon,dcon
      pvol=0.04
c
c
c                Define kinetic constants
c                They are derived from the 6-parameter fitting routine
c                using Suuberg's vapor pressure correlation.
c                For low temperature gas formation:
      eg=0.26755d5
      rxng=1.d13
      vg=0.28457d-1
c                For metaplast formation
      ept=0.160825d5
      rxntl=0.319454d5
      vt=0.7d0
c                For metaplast decomposition
      est=0.168602d5
      rxnt2=0.296412d5
c                For high temperature gas formation
      fgl=0.2844025
c
c                Define molecular weight for 10 metaplast components
      tmw(1)=1.69d2
      tmw(2)=2.70d2
      tmw(3)=3.30d2
      tmw(4)=3.86d2
      tmw(5)=4.47d2
      tmw(6)=5.19d2
      tmw(7)=6.09d2
      tmw(8)=7.27d2
      tmw(9)=8.92d2
      tmw(10)=1.245d3
c
c                Define phsical constants and number of section in tar
```

```
c                   molecular weight(ne)
          gcon=8.314d7
          wmw=28.d0
          coalm=3.d3
          surt=30.d0
          cden=1.3d0
          pcon=gcon/4.187d0
          ne=10
          ne1=ne + 1
c
c                   Define constants for cooling time-temperature history
          at=2.1983d-10
          bt=6.7328d-2
c
          write(10,101)pres,rado,apore,pvol,hrate,tpe,vcon,dcon
c         write(10,102)(tmw(i), i=1,10)
          write(10,103)
c
c                   Read peak temperature
200       read(9,)ptemp,tadd,istop
c
c                   Define initial conditions
          do 15 i=1,ne
          i10=i + 10
          i20=i + 20
          ctar(i)=0.029d0
          btar(i)=0.d0
          y(i)=0.029d0
          y(i10)=0.d0
15        y(i20)=0.d0
c
c                   Assume the same initial number density for all pres.
c                   v is mass of bubble and v1 is weight of a gas molecule.
c                   Initial bubble mass is solely coming from gas. Then
c                   initial values for total bubble mass, bubble radius, and
c                   monomer concentration ar
e
          temp= 398.13
          solub=6.55d-12*dexp(-45.16/temp)
          v1=28./6.023e23
          bvols=4.187*apore**3
          wmol=pres*bvols*6.023d23/(298.13*gcon)
          visc=1.d21
          y(31)=0.029d0
          y(32)=pres*solub
          y(33)=0.d0
          y(34)=0.d0
          y(35)=0.d0
          y(36)=1.d0
          y(37)=dlog(pvol/(1.3d0*bvols))
          bgas=v1*wmol*dexp(y(37))
c
c                   define initial bubble size
          call afunw(apore, pres, temp,ao)
          write(6, ) 'ao =    ',ao
```

```
c
c                    calculate the total bubble volume
      volg=4.187*ao**3*dexp(y(37))
c
c
      y(38)=0.71d0 - bgas - y(32)
      cmden=y(38)/coalm
      do 16 i=1,ne
16    cmden=cmden + ctar(i)/tmw(i)
      volo=(y(38) + 0.29d0)/cden + volg
      write(6, )'volg=    ',volg,'cond=    ',y(38),y(37)
c
c
      rad=rado
      t=(temp - 298.13)/hrate
      tpl=(ptemp - 298.13)/hrate
      tp=tpl + tpe
      twrite=tp + 1.d0
      tstop=tp + tadd
c
c                 Define constant for integration's routine
      neqn=38
      ifail=0
c
c                 NOW, START THE INTEGRATION
      do 100 ik=1,1000
c
      dt=delt
      if( t .gt. twrite ) dt=5.d0*delt
      tol=tolo
      tend=t + dt
      if( t .lt. tpl .and. tend .gt. tpl ) tend=tpl
c
      call d02baf(t,tend,neqn,y,tol,fcne,w,ifail)
      if(ifail .eq. 1)write(6,)'ifail = 1'
      if(ifail .eq. 2)go to 302
      if(ifail .eq. 3)go to 303
      if(ifail .eq. 4)go to 304
c
c
      do 41 i=1,38
      if(y(i) .le. 0.d0) y(i)=0.d0
41    continue
      if(y(37) .le. 0.d0) go to 50
      if(t .gt. tstop) go to 50
100   continue
c
50    brad=ao*y(36)
      bnun=dexp(y(37))
      cden=1.3d0
c
c                 Calculate tar and gas in bubbles
c                 which are in equilibrium with molten phase
59    cmdeno=cmden
      conl=(brad**3*dexp(y(37)))/(pcon*cmden*temp)
```

```
      do 60 i=1,ne
      psat1=5.8308d9*fexp(-2.55d2*tmw(i)**0.586/temp)
      if(psat1 .ge. pres) go to 57
      poyf=dexp(tmw(i)*(pres - psat1)/(1.3d0*gcon*temp))
      go to 58
57    poyf=1.d0
58    ckevf=dexp(surt*tmw(i)*2.d0/(1.3d0*gcon*temp*brad))
      alfa(i)=psat1*con1*poyf*ckevf
      ctar(i)=y(i)/(1.d0 + alfa(i))
      btar(i)=alfa(i)*y(i)/(1.d0 + alfa(i))
60    continue
c
c                Calculate total molar density of liquid and bubble pressure
      cmden=0.d0
      do 61 i=1,ne
61    cmden=cmden + ctar(i)/tmw(i)
      cmden=cmden + y(38)/coalm
      ck=abs(cmdeno - cmden)/cmden
      if(ck .ge. 1.d-3) go to 59
c
c                Now, calculate amount of gas and tar in molten coal as well
c                as amount of gas formed and released from the particle,
c                and total bubble volume
c
c                tar yield by diffusion and bubble escape
c                and amount of metaplast remaining in the particle
      tctar=0.d0
      btary=0.d0
      dtary=0.d0
      tmplast=0.d0
      do 70 i=1,ne
      i10=i + 10
      i20=i + 20
      tctar=tctar + ctar(i)
      tmplast=tmplast + y(i)
      btary=btary + y(i20)
70    dtary=dtary + y(i10)
c
c                total gas and tar yield
      gasy=y(32) + y(33) + y(34)
      ttary=dtary + btary
      voly=ttary + gasy
c
c                Calculate number average MW of tar and metaplast
      amwt1=0.d0
      amwm1=0.d0
      do 62 i=1,ne
      i10=i + 10
      i20=i + 20
      amwt1=amwt1 + (y(i10) + y(i20))/tmw(i)
62    amwm1=amwm1 + y(i)/tmw(i)
      amwt=ttary/amwt1
      amwm=tmplast/amwm1
c
c                Calculate the particle radius
```

```
          cond=tctar + y(38)
          volg=4.1888*brad**3*bnun
          vol=volg + cond/cden
          swell=(vol/volo)**(0.3333)
          rad=rado*swell
c
c
c                   Write the result
          write(10,105)ptemp,voly,ttary,tmplast,y(38),amwm,amwt,swell
          write(6,)ptemp
c
          if (istop .ne. 0) go to 200
          go to 300
c
302       write(6, )'ifail = 2      stop'
          stop
303       write(6, )'ifail = 3      stop'
          stop
304       write(6, )'ifail = 4      stop'
c
101       format( //////////,'++++++++  Run Conditions  +++++++',//,
     &          3x,'pressure                  =',e15.5,'    dyne/cm*cm',/,
     &          3x,'original particle radius =',e15.5,'    cm',/,
     &          3x,'initial bubble size =',e15.5,'    cm',/,
     &          3x,'pore volume    =          ',e12.5,'    cm**3',/,
     &          3x,'heating rate = ',e15.5,'    C/s',/,
     &          3x,'holding time = ',e15.5,'     sec',/,
     &          3x,'constant for viscosity   =',e15.5,/,
     &          3x,'constant for diffusivity =',e15.5,///)
102      format(///,3x, 'Molecular weight of 10 tar compoents',/,
     &             2(5e13.5,/),//)
103       format(3x,'************************ output ***************',///,
     &     7x,'ptemp',10x,'voly',10x,'tary',10x,'mplast',10x,'char',11x,'MNm',
     &     12x,'MNt',10x,'swell',///)
105       format(8e15.5)
c
c
300       stop
          end
```

```
c*************************************************************************
c
c                              SUBROUTINE FCNE
C
C       This subroutine calculates mass balance of volatiles in molten
c       coal and is called by Main programs MMAIN and SMAIN.
c       Variables are as defined in MMAIN
c
c*************************************************************************
        subroutine fcne(t,y,yp)
        implicit double precision (a-h, o-z)
        implicit integer (i - n)
        dimension y(38),yp(38),alfa(10),tsec(10),btar(10),ctar(10),btsec(10)
        common/tar/tmw(10)
        common/rxnc/eg,ept,est,rxng,rxntl,rxnt2,vt,vg,fgl,coalm
        common/prop/vcon,dcon,visc,pres,volo,rado,at,bt,tp,tpl
        common/con/gcon,wmw,surt,delt,hrate,ptemp,tck,temp,ao
        common/ele/ne,nel,pcon,cmden
        fexp(x)=dexp(dmaxl(-1.d2,x))
c
c
        do 1 i=1,38
        if(y(i) .le. 0.d0) y(i)=0.d0
1       continue
        brad=ao*y(36)
        if (brad .eq. 0.d0) go to 300
c
c                 Calculate temperature
        if(t .le. tpl) temp=hrate*t + 298.13
        if(t .gt. tpl .and. t .le. tp) temp=ptemp
        if(t .gt. tp) temp=((bt/at)/( (1. + bt/(at*ptemp**3))
     &                        *fexp(3.d0*bt*(t-tp)) - 1.d0))**(1./3.)
c
        cden=1.3d0
c
c                 Calculate tar and gas in bubbles
c                 which are in equilibrium with molten phase
9       cmdeno=cmden
        conl=(brad**3*dexp(y(37)))/(pcon*cmden*temp)
        do 10 i=1,ne
        psatl=5.8308d9*exp(-2.55d2*tmw(i)**0.586/temp)
        if(psatl .ge. pres) go to 7
        poyf=dexp(tmw(i)*(pres - psatl)/(1.3d0*gcon*temp))
        go to 8
7       poyf=1.d0
8       ckevf=dexp(2.d0*surt*tmw(i)/(brad*gcon*temp*1.3d0))
        alfa(i)=psatl*conl*poyf*ckevf
        ctar(i)=y(i)/(1.d0 + alfa(i))
        btar(i)=alfa(i)*y(i)/(1.d0 + alfa(i))
10      continue
c                 Calculate total molar density of liquid and bubble pressure
        cmden=0.d0
        do 11 i=1,ne
```

```
11      cmden=cmden + ctar(i)/tmw(i)
        cmden=cmden + y(38)/coalm
        ck=abs(cmdeno - cmden)/cmden
        if(ck .ge. 1.d-3) go to 9
c
c                Calculate tar concentration
        tctar=0.d0
        do 12 i=1,ne
12      tctar=tctar + ctar(i)
        xtar=tctar/(tctar + y(38))
c
c                Calculate solubility, viscosity, and diffusivity
        if(xtar .le. 0.)go to 15
        if(temp .le. 723.13)visct=vcon*fexp(45000/(1.987*temp))
        if(temp .gt. 723.13)visct=vcon*fexp(45000/(1.987*723.13))
c       visct=vcon*fexp(45000/(1.987*temp))
        viscm=1.d0/((1.d0 - xtar)**(-1./3.) - 1.d0)
        visc=visct*viscm
        go to 16
15      visc=visc
16      diff=dcon*temp/visc**0.5
        difft=dcon*temp/visc**(2./3.)
c
        hcon=2.7924d7*fexp(314.24/temp)/cmden
        solub=1./hcon
c               gas concntration in molten coal and in bubbles
        con2=(brad**3*dexp(y(37))*wmw)/(pcon*solub*temp)
        cmon=y(32)/(1.d0 + con2)
        bgas=con2*y(32)/(1.d0 + con2)
c
c               Calculate bubble pressure
        bmden=0.d0
        do 13 i=1,ne
13      bmden=bmden + btar(i)/tmw(i)
        bmden=(bmden + bgas/wmw)/dexp(y(37))
        pb=bmden*pcon*temp/(brad**3)
c
c               Calculate the particle radius
        cond=tctar + y(38)
        volg=4.1888*brad**3*dexp(y(37))
        vol=volg + cond/cden
        rad=rado*(vol/volo)**(0.3333)
c
c               Calculate Total Bubble number density
c               Rate of bubble radius growth
        yp(36)=y(36)*(pb -pres - 2.d0*surt/brad)/(4.d0*visc)
c               Balance on log(bubble number density)
c               Calculate amount of bubble escaped
        besc=3.d0*rad**2*yp(36)*ao/rado**3
        if(yp(36) .le. 0.d0) besc=0.d0
        yp(37)=-besc
c
c               balance of gas dissolved in the condensed phase
c               gas formation
        fg11=eg/(1.987*temp)
```

```
      yp(35)=rxng*fexp(-fg11)*(vg - y(35))
      if(y(35) .gt. vg)yp(35)=0.d0
c                gas formation from tar cracking both
c                in bubbles and in liquids
      tcovl=0.d0
      tcovg=0.d0
      do 20 i=1,10
      btsec(i)=9.96d2*fexp(-1.54d4/(1.987d0*temp))*btar(i)
      tsec(i)=rxnt2*exp(-est/(1.987*temp))*ctar(i)
      tcovl=tcovl + tsec(i)
20    tcovg=tcovg + btsec(i)
c                monomer escape term
      bltg=(12.56d0*brad*dexp(y(37))*cden)**0.5
      yp(33)=3.d0*bltg*rad**2*diff*cmon/(rado**3)
c     yp(33)=1.5d1*rad*diff*cmon/(rado**3)
      yp(34)=besc*bgas
c
c                Then,
      yp(32)=yp(35) - yp(33) - yp(34) + tcovg + fg1*tcovl
c
c                for metaplast or tar balance
c                formation
      ft1=ept/(1.987*temp)
      yp(31)=rxnt1*fexp(-ft1)*(0.1d0*vt - y(31))
      if(y(31) .ge. 0.1*vt) yp(31)=0.d0
c
      dgas=pres/(gcon*temp)
      tard=1.013e5*(temp/273.)**1.5/pres
      do 40 i=1,ne
      i10=i + 10
      i20=i + 20
      if (ctar(i) .le. 1.d-38) go to 35
c                rate of tar evaporation
      psat1=5.8308d9*exp(-2.55d2*tmw(i)**0.586/temp)
c     psat1=6.311d11*dexp(-5.61d2*tmw(i)**0.474/temp)
      if(psat1 .ge. pres) go to 37
      poyf=dexp(tmw(i)*(pres - psat1)/(1.3d0*gcon*temp))
      go to 38
37    poyf=1.d0
38    psat=psat1*poyf
      rlt=rad/(5.d0*difft)
      rgt=(rad*cmden*pres)/(tard*dgas*psat)
      yp(i10)=(1./(rlt + rgt))*(3.d0*rad**2*ctar(i)/(rado**3))
      yp(i20)=besc*btar(i)
      go to 40
35    yp(i10)=0.d0
      yp(i20)=0.d0
40    yp(i)=yp(31) - tsec(i) - yp(i10) - yp(i20) - btsec(i) - 0.1d0*yp(35)
c
      form=10.d0*yp(31)
      yp(38)=-form + (1. - fg1)*tcovl
c
c
300   return
      end
```

```
**************************************************************************
c
c                          PROGRAM SMAIN
C
C       Program SMAIN is a main program which calculates concentrations
c       of pyrolysis products inside a particle, volatiles yields,
c       metaplast balance, plasticity and the extent of swelling as a
c       function of time during coal pyrolysis under a given time-temperature
c       history.
c
c       This routine also assumes a single size bubbles and 10 different
c       molecular weight tar which have the same formation and secondary
c       reaction rates.  SMAIN calls for subroutines FCNE and AFUNW.
c
**************************************************************************
        implicit double precision (a - h, o - z)
        implicit integer (i - n)
        dimension y(38),w(38,18),btar(10),alfa(10),ctar(10)
        common/tar/tmw(10)
        common/con/gcon,wmw,surt,delt,hrate,ptemp,tck,temp,ao
        common/prop/vcon,dcon,visc,pres,volo,rado,at,bt,tp,tpl
        common/rxnc/eg,ept,est,rxng,rxntl,rxnt2,vt,vg,fgl,coalm
        common/ele/ne,nel,pcon,cmden
        external fcne
        fexp(x)=dexp(dmaxl(-1.d2,x))
c
c
c                  read initial bubble size, pore volume, heating rate,
c  .               holding time, and delt and tolo for integration routine.
        read(9,)apore,pvol,hrate,tpe,delt,tolo
c                  Read pressure, initial particle size and constants for
c                  viscosity and diffusivity correlations, other constants
c                  needed for controlling output statements.
        read(9,)pres,rado,vcon,dcon,jwrite,xdeltl,xdelt
c                  Read peak temperature
        read(9,)ptemp,tadd
c
c
c                  Define kinetic constants
c                  They are derived from the 6-parameter fitting routine
c                  using Suuberg's vapor pressure model.
c                  For low temperature gas formation:
        eg=0.26755d5
        rxng=1.d13
        vg=0.28457d-1
c                  For metaplast formation
        ept = 0.160825d5
        rxntl = 0.319454d5
        vt=0.7d0
c                  For metaplast decomposition
        est = 0.168602d5
        rxnt2 = 0.296412d5
c                  For high temperature gas formation
        fgl = 0.2844025d0
```

```
c
c                  Define molecular weight for 10 metaplast components
      tmw(1)=1.69d2
      tmw(2)=2.70d2
      tmw(3)=3.30d2
      tmw(4)=3.86d2
      tmw(5)=4.47d2
      tmw(6)=5.19d2
      tmw(7)=6.09d2
      tmw(8)=7.27d2
      tmw(9)=8.92d2
      tmw(10)=1.245d3
c
c                  Define phsical constants and number of section in tar
c                  molecular weight(ne)
      gcon=8.314d7
      wmw=28.d0
      coalm=3.d3
      surt=30.d0
      cden=1.3d0
      pcon=gcon/4.187d0
      ne=10
      nel=ne + 1
c
c                  Define constants for cooling time-temperature history
      temp=398.13
      at=2.1983d-10
      bt=6.7328d-2
c
c                  Calculate ao for given apore, pres, and temperature.
      call afunw (apore, pres, temp, ao)
      write(10,101)rxng,eg,vg,rxnt1,ept,vt,rxnt2,est,fgl,
     &                pres,rado,apore,ao,pvol,hrate,tpe,vcon,dcon
      write(10,102)(tmw(i), i=1,10)
      write(10,103)ptemp
      write(10,104)
      write(11,105)
      write(12,106)
c
c                  Define initial conditions
      do 15 i=1,ne
      i10=i + 10
      i20=i + 20
      ctar(i)=0.029d0
      btar(i)=0.d0
      y(i)=0.029d0
      y(i10)=0.d0
15    y(i20)=0.d0
c
c                  Assume the same initial number density for all pres
c                  v is mass of bubble and vl is weight of a gas molecule.
c                  Initial bubble mass is solely coming from gas and then
c                  initial values for total bubble mass, bubble radius, and
c                  monomer concentration are
      temp= 398.13
```

```
      solub=6.55d-12*dexp(-45.16/temp)
      vl=28./6.023e23
      bvol=4.187*apore**3
      wmol=pres*bvol*6.023d23/(298.13*gcon)
      visc=1.d21
      y(31)=0.029d0
      y(32)=pres*solub
      y(33)=0.d0
      y(34)=0.d0
      y(35)=0.d0
      y(36)=1.d0
      y(37)=dlog(pvol/(1.3d0*bvol))
      bgas=vl*wmol*dexp(y(37))
c
c                calculate the total bubble volume
      volg=4.187*ao**3*dexp(y(37))
c
c
      y(38)=0.71d0 - bgas - y(32)
      cmden=y(38)/coalm
      do 16 i=1,ne
16    cmden=cmden + ctar(i)/tmw(i)
      volo=(y(38) + 0.29d0)/cden + volg
      write(6, )'volg=    ',volg,'cond=    ',y(38),y(37)
c
c
      rad=rado
      t=(temp - 298.13)/hrate
      tpl=(ptemp - 298.13)/hrate
      tp=tpl + tpe
      twritel=tpl + 1.d0
      twrite=tp + 1.d0
      tstop=tp + tadd
c
c                Define constant for integration routine
      neqn=38
      ifail=0
      ja=0
c
c                NOW, START THE INTEGRATION
      do 100 ik=1,1000
      ja=ja + 1
c
      dt=delt
      if( t .gt. twritel) dt=xdeltl*delt
      if( t .gt. twrite ) dt=xdelt*delt
      tol=tolo
      tend=t + dt
      if( t .lt. tpl .and. tend .gt. tpl ) tend=tpl
c
      call d02baf(t,tend,neqn,y,tol,fcne,w,ifail)
      if(ifail .eq. 1)write(6,)'ifail = 1'
      if(ifail .eq. 2)go to 302
      if(ifail .eq. 3)go to 303
      if(ifail .eq. 4)go to 304
```

```
c
      if(ja .ne. jwrite ) go to 87
c
      do 41 i=1,38
      if(y(i) .le. 0.d0) y(i)=0.d0
41    continue
      if(y(37) .le. 0.d0) go to 300
c
      brad=ao*y(36)
      bnun=dexp(y(37))
      cden=1.3d0
c
c               Calculate tar and gas in bubbles
c               which are in equilibrium with molten phase
59    cmdeno=cmden
      conl=(brad**3*dexp(y(37)))/(pcon*cmden*temp)
      do 60 i=1,ne
      psatl=5.8308d9*fexp(-2.55d2*tmw(i)**0.586/temp)
      if(psatl .ge. pres) go to 57
      poyf=dexp(tmw(i)*(pres - psatl)/(1.3d0*gcon*temp))
      go to 58
57    poyf=1.d0
58    ckevf=dexp(2.d0*surt*tmw(i)/(brad*gcon*temp*1.3d0))
      alfa(i)=psatl*conl*poyf*ckevf
      ctar(i)=y(i)/(1.d0 + alfa(i))
      btar(i)=alfa(i)*y(i)/(1.d0 + alfa(i))
60    continue
c
c               Calculate total molar density of liquid and bubble pressure
      cmden=0.d0
      do 61 i=1,ne
61    cmden=cmden + ctar(i)/tmw(i)
      cmden=cmden + y(38)/coalm
      ck=abs(cmdeno - cmden)/cmden
      if(ck .ge. 1.d-3) go to 59
c
c               Calculate tar concentration
      tctar=0.d0
      do 62 i=1,ne
      i10=i + 10
      i20=i + 20
62    tctar=tctar + ctar(i)
      xtar=tctar/(tctar + y(38))
c
c               Calculate solubility, viscosity, and diffusivity
      hcon=2.7924d7*dexp(3.1424d2/temp)/cmden
      solub=1./hcon
      if(xtar .le. 0.)go to 65
      if(temp .le. 723.13)visct=vcon*fexp(45000/(1.987*temp))
      if(temp .gt. 723.13)visct=vcon*fexp(45000/(1.987*723.13))
c     visct=vcon*fexp(45000/(1.987*temp))
      visc=visct/((1.d0 - xtar)**(-1./3.) - 1.)
      go to 66
65    visc=visc
66    diff=dcon*temp/visc**0.5
```

```
      difft=dcon*temp/visc**(2./3.)
c
c                gas concentration in molten coal and in bubbles
      con2=(brad**3*dexp(y(37))*wmw)/(pcon*solub*temp)
      cmon=y(32)/(1.d0 + con2)
      bgas=con2*y(32)/(1.d0 + con2)
c
c                Calculate the particle radius
      cond=tctar + y(38)
      volg=4.1888*brad**3*bnun
      vol=volg + cond/cden
      swell=(vol/volo)**(0.3333)
      rad=rado*swell
c
c                Calculate total bubble mass, tar concentration and
c                bubble volume.
      bmass=0.d0
      do 50 i=1,ne
50    bmass=bmass + btar(i)
      bmass=bmass + bgas
c
c                Now, calculate amount of gas and tar in molten coal as well
c                as amount of gas formed and released from the particle,
c                and total bubble volume
c
c                tar yield by diffusion and bubble escape
      btary=0.d0
      dtary=0.d0
      do 70 i=1,ne
      i10=i + 10
      i20=i + 20
      btary=btary + y(i20)
70    dtary=dtary + y(i10)
c
c               total gas and tar yield
      gasy=y(33) + y(34)
      ttary=dtary + btary
c
c
      write(10,107)t,temp,y(38),tctar,cmon,bgas,bmass,ttary,gasy
      write(11,108)t,temp,diff,difft,visc,swell
      write(12,109)t,temp,bnun,brad,y(35),y(31)
c     write(14,110)t,temp
c     write(14,111)(btar(i), i=1,10)
c     write(14,112)(ctar(i), i=1,10)
c     write(14,113)(y(i),i=11,20)
c     write(14,114)(y(i),i=21,30)
c     write(14,115)y(33),y(34)
      ja=0
      write(6,)t,temp
c
c
87    if(t .gt. tstop) go to 300
100   continue
      go to 300
```

```
c
302       write(6, )'ifail = 2      stop'
          stop
303       write(6, )'ifail = 3      stop'
          stop
304       write(6, )'ifail = 4      stop'
c
101       format( '************************* input *************',///,
     &          3x,'++++++ Kinetic  Constants +++++++',//,
     &          3x,'reactin constant for gas  =',e15.5,'    1/sec',/,
     &          3x,'act E for gas formation   =',e15.5,'    cal/mole',/,
     &          3x,'ultimate yield of gas     =',e15.5,'    gm/gm',/,
     &          3x,'reaction constantl for tar=',e15.5,'    1/sec',/,
     &          3x,'act e for tar formation   =',e15.5,'    cal/mole',/,
     &          3x,'ultimate yield of tar     =',e15.5,'    gm/gm',/,
     &          3x,'reaction constant2 for tar=',e15.5,'    1/sec',/,
     &          3x,'act e for tar decomp      =',e15.5,'    cal/mole',/,
     &          3x,'f of metaplast to gases   =',e15.5,//,
     &          3x,'++++++++  Run Conditions  +++++++',//,
     &          3x,'pressure                  =',e15.5,'    dyne/cm*cm',/,
     &          3x,'original particle radius =',e15.5,'    cm',/,
     &          3x,'initial bubble size (solid)=',e15.5,'    cm',/,
     &          3x,'initial bubble size (molten)=',e15.5,'    cm',/,
     &          3x,'pore volume    =          ',e12.5,'    cm**3',/,
     &          3x,'heating rate = ',e15.5,'    C/s',/,
     &          3x,'holding time = ',e15.5,'     sec',/,
     &          3x,'constant for viscosity   =',e15.5,/,
     &          3x,'constant for diffusivity =',e15.5,///)
102       format(///,3x, 'Molecular weight of 10 tar compoents',/,
     &             2(5e13.5,/),//)
103       format('1',3x,'peak temperature         =',e15.5,'    kelvin',///)
104       format(3x,'************************* output ***************',///,
     &    7x,'t',10x,'temp',9x,'char',10x,'ctar',10x,'cmon',10x,'bgas',
     &    10x,'bmass',10x,'ttary',10x,'gasy',///)
105       format(3x,'************************* output ***************',///,
     &    12x,'t',13x,'temp',11x,'diff',11x,'difft',12x,'visc',
     &    11x,'swell',///)
106       format(3x,'************************* output ***************',///,
     &    12x,'t',13x,'temp',10x,'bnden',11x,'brad',12x,'gasf',
     &    12x,'tarf',///)
107       format(f6.3, 8e15.6)
108       format(6e16.6)
109       format(6e16.6)
110       format(2e20.6)
111       format('Tar Balance',/,'In Bubbles',10e12.5)
112       format('In  Liquid',10e12.5)
113       format('Tar dif Y ',10e12.5)
114       format('tar bub y ',10e12.5)
115       format('gas yield diffusion=',e12.5,/,
     &          'gas yield bubbly=',e12.5,////)
c
c
300       stop
          end
```

Table G.3.1. Model predictions of pyrolysis product yields, number average MW's of tar and extract, and final swelling ratio as a function of peak tempeature. Kinetic parameters with Suuberg's vapor pressure model is employed (Table G.2.4a). Table G.3.1's are employed in Figures 6.5.1 thru 6.5.5.

Table G.3.1a. Base case

```
+++++++++  Run Conditions  +++++++

    pressure                  =     0.10130D+07     dyne/cm*cm
    original particle radius =     0.35000D-02     cm
    initial bubble size =     0.79934D-05     cm
    pore volume     =              0.40000D-01     cm**3
    heating rate =      0.10000D+04     C/s
    holding time =      0.00000D+00      sec
    constant for viscosity    =     0.10000D-09
    constant for diffusivity =     0.10000D-06


    ************************ output ***************
```

ptemp	voly	tary	mplast	char	MNm	MNt	swell
0.67313D+03	0.37803D-01	0.42109D-02	0.29016D+00	0.67200D+00	0.41229D+03	0.28750D+03	0.27455D+01
0.72313D+03	0.65187D-01	0.25036D-01	0.30176D+00	0.63302D+00	0.41478D+03	0.32192D+03	0.34097D+01
0.77313D+03	0.11522D+00	0.62655D-01	0.30180D+00	0.58295D+00	0.40870D+03	0.35798D+03	0.36523D+01
0.82313D+03	0.18845D+00	0.11577D+00	0.27135D+00	0.54017D+00	0.40117D+03	0.35412D+03	0.40251D+01
0.87313D+03	0.27681D+00	0.17889D+00	0.20018D+00	0.52298D+00	0.40098D+03	0.32962D+03	0.43184D+01
0.92313D+03	0.35772D+00	0.23727D+00	0.11273D+00	0.52951D+00	0.41615D+03	0.30815D+03	0.42209D+01
0.97313D+03	0.40938D+00	0.27491D+00	0.49755D-01	0.54083D+00	0.41626D+03	0.30119D+03	0.39145D+01
0.10231D+04	0.43522D+00	0.29399D+00	0.20239D-01	0.54450D+00	0.35856D+03	0.30215D+03	0.37896D+01
0.10731D+04	0.44680D+00	0.30138D+00	0.10366D-01	0.54280D+00	0.28451D+03	0.30481D+03	0.38302D+01
0.11231D+04	0.45136D+00	0.30136D+00	0.75436D-02	0.54106D+00	0.25152D+03	0.30647D+03	0.38848D+01
0.11731D+04	0.45348D+00	0.29835D+00	0.60449D-02	0.54044D+00	0.24023D+03	0.30710D+03	0.39172D+01
0.12231D+04	0.45517D+00	0.29530D+00	0.48115D-02	0.53998D+00	0.23423D+03	0.30742D+03	0.39432D+01
0.12731D+04	0.45688D+00	0.29306D+00	0.37318D-02	0.53935D+00	0.22958D+03	0.30772D+03	0.39704D+01

Table G.3.1b. Effect of pressure: pres = 0.0001 atm

+++++++++ Run Conditions +++++++

pressure = 0.10130D+03 dyne/cm*cm
original particle radius = 0.35000D-02 cm
initial bubble size = 0.79934D-05 cm
pore volume = 0.40000D-01 cm**3
heating rate = 0.10000D+04 C/s
holding time = 0.00000D+00 sec
constant for viscosity = 0.10000D-09
constant for diffusivity = 0.10000D-06

********** output **********

ptemp	voly	tary	mplast	char	MNm	MNt	swell
0.67313D+03	0.39200D-01	0.53184D-02	0.28883D+00	0.67197D+00	0.41260D+03	0.29533D+03	0.29206D+01
0.72313D+03	0.87724D-01	0.47947D-01	0.28101D+00	0.63127D+00	0.43380D+03	0.28911D+03	0.42445D+01
0.77313D+03	0.17599D+00	0.12610D+00	0.24809D+00	0.57592D+00	0.46197D+03	0.30880D+03	0.43470D+01
0.82313D+03	0.28426D+00	0.21872D+00	0.19157D+00	0.52417D+00	0.52701D+03	0.30728D+03	0.31653D+01
0.87313D+03	0.35718D+00	0.27358D+00	0.14201D+00	0.50081D+00	0.58536D+03	0.30313D+03	0.86311D+00
0.92313D+03	0.40553D+00	0.30634D+00	0.96495D-01	0.49798D+00	0.62045D+03	0.30212D+03	0.84920D+00
0.97313D+03	0.45051D+00	0.33651D+00	0.42265D-01	0.50723D+00	0.64213D+03	0.30598D+03	0.82161D+00
0.10231D+04	0.47537D+00	0.35368D+00	0.89974D-02	0.51564D+00	0.63923D+03	0.31001D+03	0.14204D+01
0.10731D+04	0.48303D+00	0.35960D+00	0.22151D-02	0.51475D+00	0.46157D+03	0.31260D+03	0.22370D+01
0.11231D+04	0.48495D+00	0.35997D+00	0.12053D-02	0.51384D+00	0.26019D+03	0.31398D+03	0.26308D+01
0.11731D+04	0.48512D+00	0.35845D+00	0.11236D-02	0.51376D+00	0.22117D+03	0.31453D+03	0.27949D+01
0.12231D+04	0.48524D+00	0.35718D+00	0.98104D-03	0.51377D+00	0.21093D+03	0.31476D+03	0.28695D+01
0.12731D+04	0.48559D+00	0.35654D+00	0.77101D-03	0.51364D+00	0.20479D+03	0.31488D+03	0.29126D+01

Table G.3.1c. Effect of pressure: pres = 69 atm

++++++++ Run Conditions +++++++

pressure = 0.69897D+08 dyne/cm*cm
original particle radius = 0.35000D-02 cm
initial bubble size = 0.79934D-05 cm
pore volume = 0.40000D-01 cm**3
heating rate = 0.10000D+04 C/s
holding time = 0.00000D+00 sec
constant for viscosity = 0.10000D-09
constant for diffusivity = 0.10000D-06

********** output **********

ptemp	voly	tary	mplast	char	MNm	MNt	swell
0.67313D+03	0.35417D-01	0.13061D-02	0.29252D+00	0.66963D+00	0.41105D+03	0.33171D+03	0.11892D+01
0.72313D+03	0.48000D-01	0.64227D-02	0.31602D+00	0.63355D+00	0.41244D+03	0.32647D+03	0.11194D+01
0.77313D+03	0.73698D-01	0.17034D-01	0.33210D+00	0.59178D+00	0.41478D+03	0.32652D+03	0.10364D+01
0.82313D+03	0.11275D+00	0.29676D-01	0.31637D+00	0.56845D+00	0.41627D+03	0.33120D+03	0.10088D+01
0.87313D+03	0.15984D+00	0.39502D-01	0.25042D+00	0.58731D+00	0.41383D+03	0.34048D+03	0.10366D+01
0.92313D+03	0.19983D+00	0.39716D-01	0.15538D+00	0.64236D+00	0.39695D+03	0.35400D+03	0.11592D+01
0.97313D+03	0.22250D+00	0.31439D-01	0.77021D-01	0.69805D+00	0.34484D+03	0.36572D+03	0.13640D+01
0.10231D+04	0.23269D+00	0.23502D-01	0.35903D-01	0.72897D+00	0.26273D+03	0.36659D+03	0.15531D+01
0.10731D+04	0.23889D+00	0.19911D-01	0.20065D-01	0.73861D+00	0.20587D+03	0.35945D+03	0.16765D+01
0.11231D+04	0.24442D+00	0.18974D-01	0.13936D-01	0.73921D+00	0.18549D+03	0.35255D+03	0.17517D+01
0.11731D+04	0.24974D+00	0.18982D-01	0.10033D-01	0.73779D+00	0.17919D+03	0.34828D+03	0.17969D+01
0.12231D+04	0.25438D+00	0.19203D-01	0.70872D-02	0.73610D+00	0.17638D+03	0.34543D+03	0.18300D+01
0.12731D+04	0.25814D+00	0.19407D-01	0.48402D-02	0.73459D+00	0.17463D+03	0.34325D+03	0.18572D+01

Table G.3.1d. Effect of heating rate: heating rate = 1000 C/s and holding time = 5 sec

+++++++++ Run Conditions +++++++

pressure = 0.10130D+07 dyne/cm*cm
original particle radius = 0.35000D-02 cm
initial bubble size = 0.79934D-05 cm
pore volume = 0.40000D-01 cm**3
heating rate = 0.10000D+04 C/s
holding time = 0.50000D+01 sec
constant for viscosity = 0.10000D-09
constant for diffusivity = 0.10000D-06

********** output **********

ptemp	voly	tary	mplast	char	MNm	MNt	swell
0.67313D+03	0.16206D+00	0.88491D-01	0.29069D+00	0.54721D+00	0.40681D+03	0.35465D+03	0.38821D+01
0.72313D+03	0.35291D+00	0.25003D+00	0.13925D+00	0.50781D+00	0.34892D+03	0.38932D+03	0.40339D+01
0.77313D+03	0.40347D+00	0.26674D+00	0.47363D-01	0.54913D+00	0.31642D+03	0.34034D+03	0.42818D+01
0.82313D+03	0.41722D+00	0.26752D+00	0.81029D-02	0.57464D+00	0.26639D+03	0.30944D+03	0.38356D+01
0.87313D+03	0.42377D+00	0.27277D+00	0.18718D-02	0.57432D+00	0.20838D+03	0.29910D+03	0.35788D+01
0.92313D+03	0.43303D+00	0.28255D+00	0.88454D-03	0.56605D+00	0.19232D+03	0.29771D+03	0.35883D+01
0.97313D+03	0.44289D+00	0.29188D+00	0.48602D-03	0.55659D+00	0.18727D+03	0.30014D+03	0.37049D+01
0.10231D+04	0.45102D+00	0.29763D+00	0.22617D-03	0.54872D+00	0.18499D+03	0.30353D+03	0.38308D+01
0.10731D+04	0.45621D+00	0.29881D+00	0.77137D-04	0.54368D+00	0.18335D+03	0.30615D+03	0.39290D+01
0.11231D+04	0.45884D+00	0.29671D+00	0.18167D-04	0.54111D+00	0.18196D+03	0.30752D+03	0.39957D+01
0.11731D+04	0.46018D+00	0.29380D+00	0.27803D-05	0.53978D+00	0.18046D+03	0.30804D+03	0.40390D+01
0.12231D+04	0.46118D+00	0.29172D+00	0.26921D-06	0.53878D+00	0.17905D+03	0.30825D+03	0.40661D+01
0.12731D+04	0.46204D+00	0.29062D+00	0.16068D-07	0.53793D+00	0.17774D+03	0.30836D+03	0.40825D+01

Table G.3.1e. Effect of heating rate: heating rate = 500 C/s and holding time = 5 sec

+++++++ Run Conditions +++++++

pressure = 0.10130D+07 dyne/cm*cm
original particle radius = 0.35000D-02 cm
initial bubble size = 0.79934D-05 cm
pore volume = 0.40000D-01 cm**3
heating rate = 0.50000D+03 C/s
holding time = 0.50000D+01 sec
constant for viscosity = 0.10000D-09
constant for diffusivity = 0.10000D-06

********** output **********

ptemp	voly	tary	mplast	char	MNm	MNt	swell
0.67313D+03	0.16288D+00	0.88938D-01	0.29013D+00	0.54695D+00	0.40675D+03	0.35481D+03	0.38810D+01
0.72313D+03	0.35367D+00	0.25023D+00	0.13784D+00	0.50846D+00	0.34819D+03	0.38939D+03	0.40336D+01
0.77313D+03	0.40345D+00	0.26630D+00	0.46529D-01	0.54999D+00	0.31420D+03	0.34080D+03	0.42847D+01
0.82313D+03	0.41693D+00	0.26701D+00	0.80949D-02	0.57494D+00	0.26245D+03	0.31045D+03	0.38617D+01
0.87313D+03	0.42333D+00	0.27203D+00	0.19686D-02	0.57466D+00	0.20764D+03	0.30061D+03	0.36250D+01
0.92313D+03	0.43152D+00	0.28037D+00	0.92842D-03	0.56751D+00	0.19244D+03	0.29942D+03	0.36336D+01
0.97313D+03	0.43882D+00	0.28658D+00	0.48261D-03	0.56066D+00	0.18706D+03	0.30129D+03	0.37276D+01
0.10231D+04	0.44317D+00	0.28836D+00	0.20434D-03	0.55659D+00	0.18407D+03	0.30312D+03	0.38164D+01
0.10731D+04	0.44500D+00	0.28710D+00	0.62039D-04	0.55490D+00	0.18175D+03	0.30397D+03	0.38771D+01
0.11231D+04	0.44586D+00	0.28555D+00	0.12771D-04	0.55409D+00	0.17985D+03	0.30426D+03	0.39136D+01
0.11731D+04	0.44650D+00	0.28477D+00	0.16806D-05	0.55346D+00	0.17805D+03	0.30437D+03	0.39331D+01
0.12231D+04	0.44698D+00	0.28446D+00	0.13914D-06	0.55298D+00	0.17649D+03	0.30442D+03	0.39429D+01
0.12731D+04	0.44730D+00	0.28435D+00	0.70621D-08	0.55266D+00	0.17516D+03	0.30445D+03	0.39479D+01

Table G.3.1f. Effect of heating rate: heating rate = 100 C/s and holding time = 5 sec

+++++++++ Run Conditions +++++++

pressure = 0.10130D+07 dyne/cm*cm
original particle radius = 0.35000D-02 cm
initial bubble size = 0.79934D-05 cm
pore volume = 0.40000D-01 cm**3
heating rate = 0.10000D+03 C/s
holding time = 0.50000D+01 sec
constant for viscosity = 0.10000D-09
constant for diffusivity = 0.10000D-06

********** output **********

ptemp	voly	tary	mplast	char	MNm	MNt	swell
0.67313D+03	0.17002D+00	0.93023D-01	0.28501D+00	0.54494D+00	0.40630D+03	0.35563D+03	0.38910D+01
0.72313D+03	0.36008D+00	0.25238D+00	0.12693D+00	0.51295D+00	0.34218D+03	0.38920D+03	0.40485D+01
0.77313D+03	0.40477D+00	0.26520D+00	0.40584D-01	0.55461D+00	0.29705D+03	0.34441D+03	0.43083D+01
0.82313D+03	0.41689D+00	0.26613D+00	0.86038D-02	0.57447D+00	0.23691D+03	0.32047D+03	0.40762D+01
0.87313D+03	0.42209D+00	0.26874D+00	0.30155D-02	0.57486D+00	0.20332D+03	0.31498D+03	0.39816D+01
0.92313D+03	0.42505D+00	0.26959D+00	0.13841D-02	0.57353D+00	0.19268D+03	0.31460D+03	0.39850D+01
0.97313D+03	0.42641D+00	0.26909D+00	0.55125D-03	0.57301D+00	0.18659D+03	0.31482D+03	0.40049D+01
0.10231D+04	0.42714D+00	0.26885D+00	0.16004D-03	0.57267D+00	0.18218D+03	0.31493D+03	0.40166D+01
0.10731D+04	0.42747D+00	0.26879D+00	0.31473D-04	0.57246D+00	0.17882D+03	0.31496D+03	0.40214D+01
0.11231D+04	0.42760D+00	0.26878D+00	0.39773D-05	0.57237D+00	0.17633D+03	0.31496D+03	0.40231D+01
0.11731D+04	0.42764D+00	0.26878D+00	0.29706D-06	0.57233D+00	0.17436D+03	0.31496D+03	0.40236D+01
0.12231D+04	0.42765D+00	0.26878D+00	0.12303D-07	0.57231D+00	0.17288D+03	0.31496D+03	0.40238D+01
0.12731D+04	0.42766D+00	0.26878D+00	0.26280D-09	0.57231D+00	0.17177D+03	0.31496D+03	0.40238D+01

Table G.3.1g. Effect of particle size: particle size = 0.0020 cm

+++++++++ Run Conditions +++++++

pressure = 0.10130D+07 dyne/cm*cm
original particle radius = 0.20000D-02 cm
initial bubble size = 0.79934D-05 cm
pore volume = 0.40000D-01 cm**3
heating rate = 0.10000D+04 C/s
holding time = 0.00000D+00 sec
constant for viscosity = 0.10000D-09
constant for diffusivity = 0.10000D-06

********** output **********

ptemp	voly	tary	mplast	char	MNm	MNt	swell
0.67313D+03	0.43909D-01	0.10374D-01	0.28418D+00	0.67188D+00	0.41392D+03	0.32165D+03	0.26099D+01
0.72313D+03	0.96152D-01	0.56736D-01	0.27250D+00	0.63131D+00	0.41874D+03	0.35479D+03	0.31221D+01
0.77313D+03	0.18027D+00	0.13060D+00	0.24355D+00	0.57615D+00	0.41119D+03	0.38181D+03	0.32838D+01
0.82313D+03	0.27924D+00	0.21321D+00	0.19570D+00	0.52503D+00	0.40597D+03	0.37604D+03	0.35593D+01
0.87313D+03	0.37454D+00	0.28803D+00	0.12631D+00	0.49911D+00	0.43763D+03	0.34906D+03	0.34680D+01
0.92313D+03	0.43175D+00	0.32574D+00	0.65243D-01	0.50297D+00	0.52574D+03	0.32684D+03	0.25088D+01
0.97313D+03	0.45353D+00	0.33386D+00	0.28098D-01	0.51834D+00	0.57856D+03	0.31675D+03	0.16900D+01
0.10231D+04	0.46465D+00	0.33873D+00	0.87233D-02	0.52659D+00	0.56082D+03	0.31415D+03	0.18242D+01
0.10731D+04	0.47016D+00	0.34202D+00	0.24044D-02	0.52740D+00	0.40042D+03	0.31468D+03	0.21698D+01
0.11231D+04	0.47209D+00	0.34257D+00	0.12075D-02	0.52667D+00	0.24761D+03	0.31562D+03	0.23995D+01
0.11731D+04	0.47246D+00	0.34151D+00	0.10017D-02	0.52651D+00	0.21097D+03	0.31613D+03	0.25137D+01
0.12231D+04	0.47263D+00	0.34049D+00	0.83010D-03	0.52651D+00	0.20078D+03	0.31637D+03	0.25700D+01
0.12731D+04	0.47294D+00	0.33997D+00	0.63134D-03	0.52639D+00	0.19492D+03	0.31650D+03	0.26027D+01

Table G.3.1h. Effect of particle size: particle size = 0.001 cm

++++++++ Run Conditions +++++++

pressure = 0.10130D+07 dyne/cm*cm
original particle radius = 0.10000D-01 cm
initial bubble size = 0.79934D-05 cm
pore volume = 0.40000D-01 cm**3
heating rate = 0.10000D+04 C/s
holding time = 0.00000D+00 sec
constant for viscosity = 0.10000D-09
constant for diffusivity = 0.10000D-06

********** output **********

ptemp	voly	tary	mplast	char	MNm	MNt	swell
0.67313D+03	0.34525D-01	0.90776D-03	0.29339D+00	0.67205D+00	0.41070D+03	0.23132D+03	0.28816D+01
0.72313D+03	0.46180D-01	0.56335D-02	0.31996D+00	0.63383D+00	0.40971D+03	0.25769D+03	0.37481D+01
0.77313D+03	0.68147D-01	0.13779D-01	0.34498D+00	0.58684D+00	0.40372D+03	0.29226D+03	0.41308D+01
0.82313D+03	0.10681D+00	0.29265D-01	0.34295D+00	0.55020D+00	0.39287D+03	0.29524D+03	0.46642D+01
0.87313D+03	0.16485D+00	0.56745D-01	0.29374D+00	0.54138D+00	0.37573D+03	0.28643D+03	0.52186D+01
0.92313D+03	0.23437D+00	0.96553D-01	0.21150D+00	0.55410D+00	0.35060D+03	0.28256D+03	0.56402D+01
0.97313D+03	0.29897D+00	0.13971D+00	0.13509D+00	0.56591D+00	0.31852D+03	0.28669D+03	0.58538D+01
0.10231D+04	0.34702D+00	0.17374D+00	0.86504D-01	0.56644D+00	0.28953D+03	0.29339D+03	0.59334D+01
0.10731D+04	0.37825D+00	0.19271D+00	0.60472D-01	0.56124D+00	0.27271D+03	0.29826D+03	0.60026D+01
0.11231D+04	0.39780D+00	0.19841D+00	0.45975D-01	0.55619D+00	0.26586D+03	0.30026D+03	0.61059D+01
0.11731D+04	0.41181D+00	0.19674D+00	0.35027D-01	0.55313D+00	0.26212D+03	0.30059D+03	0.61966D+01
0.12231D+04	0.42295D+00	0.19221D+00	0.26393D-01	0.55063D+00	0.25960D+03	0.30058D+03	0.62452D+01
0.12731D+04	0.43212D+00	0.18693D+00	0.19605D-01	0.54824D+00	0.25751D+03	0.30080D+03	0.62567D+01

Table G.3.2. Model predictions of variations in coal plasticity during pyrolysis at different heating rate. Kinetic parameters with Suuberg's vapor pressure model are employed. Table G.3.2's are employed in Fig. 6.5.4.

Table G.3.2a. Heating rate = 1000 C/s and holding time 5 sec.

t	temp	diff	difft	visc	swell
0.150000D+00	0.448130D+03	0.165372D-10	0.118617D-12	0.734320D+13	0.999885D+00
0.200000D+00	0.498130D+03	0.229599D-09	0.382102D-11	0.470700D+11	0.997453D+00
0.250000D+00	0.548130D+03	0.194273D-08	0.638147D-10	0.796058D+09	0.990561D+00
0.300000D+00	0.598130D+03	0.119136D-07	0.695760D-09	0.252060D+08	0.991084D+00
0.350000D+00	0.648130D+03	0.557146D-07	0.529751D-08	0.135327D+07	0.111934D+01
0.400000D+00	0.698130D+03	0.207373D-06	0.298097D-07	0.113336D+06	0.207155D+01
0.450000D+00	0.748130D+03	0.377134D-06	0.646648D-07	0.393517D+05	0.316504D+01
0.500000D+00	0.798130D+03	0.399439D-06	0.683245D-07	0.399251D+05	0.346897D+01
0.550000D+00	0.848130D+03	0.426862D-06	0.731525D-07	0.394775D+05	0.367267D+01
0.600000D+00	0.898130D+03	0.456478D-06	0.784839D-07	0.387113D+05	0.389862D+01
0.650000D+00	0.948130D+03	0.480249D-06	0.824769D-07	0.389766D+05	0.414313D+01
0.700000D+00	0.998130D+03	0.484059D-06	0.819349D-07	0.425184D+05	0.433704D+01
0.750000D+00	0.104813D+04	0.453057D-06	0.738015D-07	0.535211D+05	0.440697D+01
0.800000D+00	0.109813D+04	0.383058D-06	0.580944D-07	0.821825D+05	0.435656D+01
0.850000D+00	0.114813D+04	0.288954D-06	0.393045D-07	0.157879D+06	0.426119D+01
0.900000D+00	0.119813D+04	0.196307D-06	0.231426D-07	0.372510D+06	0.418553D+01
0.950000D+00	0.124813D+04	0.124791D-06	0.124784D-07	0.100035D+07	0.414400D+01
0.975000D+00	0.127313D+04	0.992652D-07	0.913633D-08	0.164494D+07	0.413241D+01
0.102500D+01	0.127313D+04	0.710159D-07	0.584588D-08	0.321391D+07	0.411809D+01
0.107500D+01	0.127313D+04	0.557625D-07	0.423479D-08	0.521268D+07	0.410924D+01
0.112500D+01	0.127313D+04	0.460798D-07	0.328390D-08	0.763350D+07	0.410307D+01
0.117500D+01	0.127313D+04	0.391721D-07	0.264450D-08	0.105631D+08	0.409850D+01
0.122500D+01	0.127313D+04	0.338839D-07	0.217955D-08	0.141175D+08	0.409501D+01
0.127500D+01	0.127313D+04	0.296582D-07	0.182489D-08	0.184271D+08	0.409227D+01
0.132500D+01	0.127313D+04	0.261853D-07	0.154568D-08	0.236391D+08	0.409010D+01
0.137500D+01	0.127313D+04	0.232738D-07	0.132089D-08	0.299233D+08	0.408836D+01
0.142500D+01	0.127313D+04	0.207967D-07	0.113684D-08	0.374764D+08	0.408696D+01
0.147500D+01	0.127313D+04	0.186645D-07	0.984159D-09	0.465277D+08	0.408581D+01
0.152500D+01	0.127313D+04	0.168123D-07	0.856143D-09	0.573442D+08	0.408488D+01
0.157500D+01	0.127313D+04	0.151911D-07	0.747871D-09	0.702375D+08	0.408411D+01
0.162500D+01	0.127313D+04	0.137629D-07	0.655628D-09	0.855702D+08	0.408347D+01
0.167500D+01	0.127313D+04	0.124982D-07	0.576554D-09	0.103765D+09	0.408294D+01
0.172500D+01	0.127313D+04	0.113730D-07	0.508407D-09	0.125312D+09	0.408250D+01
0.177500D+01	0.127313D+04	0.103681D-07	0.449406D-09	0.150783D+09	0.408214D+01
0.182500D+01	0.127313D+04	0.946731D-08	0.398118D-09	0.180839D+09	0.408183D+01
0.187500D+01	0.127313D+04	0.865754D-08	0.353374D-09	0.216250D+09	0.408157D+01
0.192500D+01	0.127313D+04	0.792758D-08	0.314217D-09	0.257908D+09	0.408136D+01
0.197500D+01	0.127313D+04	0.726798D-08	0.279851D-09	0.306844D+09	0.408118D+01
0.202500D+01	0.127313D+04	0.667067D-08	0.249614D-09	0.364256D+09	0.408102D+01
0.227500D+01	0.127313D+04	0.440538D-08	0.143556D-09	0.835176D+09	0.408055D+01
0.252500D+01	0.127313D+04	0.296202D-08	0.845591D-10	0.184743D+10	0.408033D+01
0.277500D+01	0.127313D+04	0.201812D-08	0.506958D-10	0.397970D+10	0.408023D+01
0.302500D+01	0.127313D+04	0.138923D-08	0.308136D-10	0.839836D+10	0.408019D+01
0.327500D+01	0.127313D+04	0.964278D-09	0.189370D-10	0.174318D+11	0.408017D+01
0.352500D+01	0.127313D+04	0.673916D-09	0.117449D-10	0.356889D+11	0.408016D+01
0.377500D+01	0.127313D+04	0.473721D-09	0.734074D-11	0.722270D+11	0.408015D+01
0.402500D+01	0.127313D+04	0.334657D-09	0.461859D-11	0.144726D+12	0.408015D+01
0.427500D+01	0.127313D+04	0.237443D-09	0.292273D-11	0.287493D+12	0.408015D+01
0.452500D+01	0.127313D+04	0.169112D-09	0.185898D-11	0.566759D+12	0.408015D+01
0.477500D+01	0.127313D+04	0.120853D-09	0.118774D-11	0.110976D+13	0.408015D+01
0.502500D+01	0.127313D+04	0.866280D-10	0.761939D-12	0.215938D+13	0.408015D+01
0.527500D+01	0.127313D+04	0.622649D-10	0.490569D-12	0.418079D+13	0.408015D+01
0.552500D+01	0.127313D+04	0.448643D-10	0.316892D-12	0.805272D+13	0.408015D+01

Table G.3.2b. Heating rate = 500 C/s and holding time 5 sec.

t	temp	diff	difft	visc	swell
0.300000D+00	0.448130D+03	0.165285D-10	0.118534D-12	0.735089D+13	0.999771D+00
0.400000D+00	0.498130D+03	0.227554D-09	0.377571D-11	0.479199D+11	0.995579D+00
0.500000D+00	0.548130D+03	0.194194D-08	0.637801D-10	0.796705D+09	0.990438D+00
0.600000D+00	0.598130D+03	0.119367D-07	0.697562D-09	0.251084D+08	0.992627D+00
0.700000D+00	0.648130D+03	0.559078D-07	0.532201D-08	0.134394D+07	0.125520D+01
0.800000D+00	0.698130D+03	0.207538D-06	0.298413D-07	0.113156D+06	0.244802D+01
0.900000D+00	0.748130D+03	0.381719D-06	0.657152D-07	0.384120D+05	0.337254D+01
0.100000D+01	0.798130D+03	0.411343D-06	0.710527D-07	0.376478D+05	0.360479D+01
0.110000D+01	0.848130D+03	0.444834D-06	0.772876D-07	0.363521D+05	0.386915D+01
0.120000D+01	0.898130D+03	0.470405D-06	0.816927D-07	0.364530D+05	0.417159D+01
0.130000D+01	0.948130D+03	0.466827D-06	0.794180D-07	0.412499D+05	0.438024D+01
0.140000D+01	0.998130D+03	0.414833D-06	0.666963D-07	0.578933D+05	0.438021D+01
0.150000D+01	0.104813D+04	0.318412D-06	0.461156D-07	0.108355D+06	0.422992D+01
0.160000D+01	0.109813D+04	0.209033D-06	0.259061D-07	0.275980D+06	0.408231D+01
0.170000D+01	0.114813D+04	0.120579D-06	0.122565D-07	0.906641D+06	0.400421D+01
0.180000D+01	0.119813D+04	0.673595D-07	0.555944D-08	0.316380D+07	0.397425D+01
0.190000D+01	0.124813D+04	0.415326D-07	0.287805D-08	0.903113D+07	0.396287D+01
0.200000D+01	0.127313D+04	0.293500D-07	0.179965D-08	0.188160D+08	0.395757D+01
0.210000D+01	0.127313D+04	0.226950D-07	0.127727D-08	0.314693D+08	0.395440D+01
0.220000D+01	0.127313D+04	0.180515D-07	0.941294D-09	0.497418D+08	0.395236D+01
0.230000D+01	0.127313D+04	0.146078D-07	0.709835D-09	0.759579D+08	0.395099D+01
0.240000D+01	0.127313D+04	0.119644D-07	0.543954D-09	0.113231D+09	0.395007D+01
0.250000D+01	0.127313D+04	0.988800D-08	0.421878D-09	0.165779D+09	0.394943D+01
0.260000D+01	0.127313D+04	0.822990D-08	0.330295D-09	0.239307D+09	0.394899D+01
0.270000D+01	0.127313D+04	0.688912D-08	0.260572D-09	0.341522D+09	0.394867D+01
0.280000D+01	0.127313D+04	0.579418D-08	0.206871D-09	0.482793D+09	0.394845D+01
0.290000D+01	0.127313D+04	0.489286D-08	0.165117D-09	0.677048D+09	0.394830D+01
0.320000D+01	0.127313D+04	0.300285D-08	0.861166D-10	0.179754D+10	0.394804D+01
0.370000D+01	0.127313D+04	0.139190D-08	0.308924D-10	0.836627D+10	0.394791D+01
0.420000D+01	0.127313D+04	0.669680D-09	0.116466D-10	0.361419D+11	0.394789D+01
0.470000D+01	0.127313D+04	0.330574D-09	0.454362D-11	0.148322D+12	0.394788D+01
0.520000D+01	0.127313D+04	0.166314D-09	0.181809D-11	0.585985D+12	0.394788D+01
0.570000D+01	0.127313D+04	0.849161D-10	0.741929D-12	0.224784D+13	0.394788D+01
0.620000D+01	0.127313D+04	0.438696D-10	0.307558D-12	0.842206D+13	0.394788D+01
0.670000D+01	0.127313D+04	0.228825D-10	0.129136D-12	0.309555D+14	0.394788D+01
0.720000D+01	0.113785D+04	0.145311D-10	0.731762D-13	0.613159D+14	0.394788D+01
0.770000D+01	0.969344D+03	0.144490D-10	0.766108D-13	0.450072D+14	0.394788D+01

Table G.3.2c. Heating rate = 100 C/s and holding time 5 sec.

t	temp	diff	difft	visc	swell
0.1500000D+01	0.448130D+03	0.164627D-10	0.117905D-12	0.740981D+13	0.998905D+00
0.2000000D+01	0.498130D+03	0.222400D-09	0.366211D-11	0.501668D+11	0.990866D+00
0.2500000D+01	0.548130D+03	0.194680D-08	0.639933D-10	0.792728D+09	0.990589D+00
0.3000000D+01	0.598130D+03	0.120455D-07	0.706050D-09	0.246570D+08	0.103024D+01
0.3500000D+01	0.648130D+03	0.570869D-07	0.547219D-08	0.128900D+07	0.184761D+01
0.4000000D+01	0.698130D+03	0.215958D-06	0.314664D-07	0.104504D+06	0.324224D+01
0.4500000D+01	0.748130D+03	0.412320D-06	0.728317D-07	0.329219D+05	0.364697D+01
0.5000000D+01	0.798130D+03	0.434106D-06	0.763431D-07	0.338030D+05	0.407392D+01
0.5500000D+01	0.848130D+03	0.397851D-06	0.665998D-07	0.454448D+05	0.438951D+01
0.6000000D+01	0.898130D+03	0.284896D-06	0.418603D-07	0.993814D+05	0.432338D+01
0.6500000D+01	0.948130D+03	0.152302D-06	0.178369D-07	0.387545D+06	0.413293D+01
0.7000000D+01	0.998130D+03	0.637161D-07	0.548617D-08	0.245401D+07	0.405166D+01
0.7500000D+01	0.104813D+04	0.282682D-07	0.182639D-08	0.137478D+08	0.403246D+01
0.8000000D+01	0.109813D+04	0.156711D-07	0.818935D-09	0.491028D+08	0.402688D+01
0.8500000D+01	0.114813D+04	0.910651D-08	0.391266D-09	0.158956D+09	0.402483D+01
0.9000000D+01	0.119813D+04	0.511589D-08	0.178811D-09	0.548487D+09	0.402410D+01
0.9500000D+01	0.124813D+04	0.267650D-08	0.743593D-10	0.217464D+10	0.402387D+01
0.1000000D+02	0.127313D+04	0.131512D-08	0.286415D-10	0.937164D+10	0.402381D+01
0.1050000D+02	0.127313D+04	0.660990D-09	0.114455D-10	0.370984D+11	0.402380D+01
0.1180000D+02	0.127313D+04	0.117470D-09	0.114361D-11	0.117460D+13	0.402380D+01
0.1430000D+02	0.127313D+04	0.490972D-11	0.165876D-13	0.672407D+15	0.402380D+01

G.4. Computer programs for calculations of coal-screen tempeatures.

```
C*************************************************************************
C
C                          PROGRAM ATMTC
C
C*************************************************************************
          implicit double precision (A-H,O-Z)
        dimension Y(4),W(4,18)
        common/PROC/S,PTEMP,R,ERXN,CRXN,VSTAR
        common/PROP/DCOALO,HRXN,A1,B1
        external fcn
C
C  VARIABLES ARE
C  TC=TEMPERATURE OF COAL PARTICLES
C  THE=TEMPERATURE OF SURROUNDING GAS, I.E. HELIUM
C  TTC=TEMPERATURE OF THERMOCOUPLE
C  TS=SCREEN TEMPERATURE
C  TOO=INITIAL TEMPERATURE
C  R=RADIUS OF COAL PARTICLE AND THERMOCOUPLE
C  S=HEATING RATE
C  DT=TIME INCREMENT
          read(9,) S,HRXN,DT,TOL
          read(9, )ERXN,CRXN,VSTAR
        R=0.0035
        PTEMP=1000.
        A1=2.20E-10
        B1=6.73E-2
        DCOALO=1.3
        TOO=20.
          write(2,101) S,HRXN
101     format(3x,'     HEATING RATE = ',e12.5,/,
     &         3x,'     HEAT OF REACTION= ',e12.5,///)
          write(2,102)
102     format(7x,'T',11x'TC',9x,'TTC',10x,'THE',10x,'TS',10x,'VOLA',///)
C
C  INITIAL CONDITIONS ARE
        do 10 I=1,3
10      Y(I)=TOO
        Y(4)=0.
C
          tp=(PTEMP - 20.)/S
        T=0.
        N=4
          ifail=0
          DTO=DT
C
C
C  CCCCCCCCCCCCC  DO LOOP CCCCCCCCCCCCCCCCCCCCCCCCCCCCCCCCCCCCCCCCCCCCCCC
        do 100 I=1,200
        TEND=T + DT
          if(T .lt. tp .and. TEND .gt. tp) TEND=tp
          if(T .gt. tp) DT = 4.*DTO
C
          call d02baf(T,TEND,N,Y,TOL,fcn,W,ifail)
          write(6,)T,ifail
          write(6,)TOL
          if (TOL .le. 0) TOL=-TOL
        TC=Y(1)
        TTC=Y(2)
        TS=Y(3)
        THE=TS
```

```
      THE1=TS
      VOAL=Y(4)
C
      write(2,105) T,TC,TTC,THE,TS,VOAL
105   format(3x,6e12.5)
      if (T .gt. 6.) go to 200
100   continue
C
C
200     stop
        end
```

```
C ***************************************************************************
C
C                       SUBROUTINE FCN
C
C ***************************************************************************
C ***BOUND WITH MAIN PROGRAM ATMTC
C     THIS PROGRAM CALCULATES DERIVATIVES OF THEMPERATURES
C     TO BE CALCULATED
C
          subroutine fcn(T,Y,YP)
          implicit double precision(A-H, O-Z)
          dimension Y(4),YP(4)
          common/PROC/S,PTEMP,R,ERXN,CRXN,VSTAR
          common/PROP/DCOALO,HRXN,A1,B1
C
C       DEFINE TC,TTC, TS, THE INTERSMS OF Y'S
        TC=Y(1)
        TTC=Y(2)
        TS=Y(3)
        VOAL=Y(4)
          THE=TS
          THE1=TS
C
C  DEFINE PYSICAL CONSTANTS
C  THERMAL CONDUTIVITY OF HELIUM
        HEK=6.525E-7*THE + 3.672E-4
C  HEAT TRANSFER COEFFICIENTS ARE
        H1=5.329*HEK/R
        H2=1.*HEK/R
        H3=5.5057*HEK/R
C
C   HEAT CAPACITIES ARE
C   COAL
        CPC=0.2228 + 2.18d-4*(TC + 273.13) - 9.7417d3/(TC + 273.13)**2
C   THERMOCOUPLE
        CPTC=0.09882 + 3.035d-5*(TTC + 273.13)
c
C   DENSITIES ARE
        DCOAL=DCOALO*(1. - Y(4))
        DTTC=8.7
        DHE=1.1451D-3
        TP=(PTEMP - 20.)/S
C
C   NOW CALCULATE TEMPERATUERES
        YP(4)=CRXN*dexp(-ERXN/(1.987*(TC + 273.13)))*(VSTAR - Y(4))
        YP(1)=(3.*H1*(THE - TC)/R + DCOALO*YP(4)*(-HRXN))/(DCOAL*CPC)
        YP(2)=(3.*H2*(THE1 - TTC)/R)/(DTTC*CPTC)
        YP(3)=S
        if(T .gt. TP) YP(3)=-A1*(TS + 273.13)**4 - B1*(TS + 273.13)
C
C
          return
          end
```

```
C*************************************************************************************
C
C                          PROGRAM VTC
C
C*************************************************************************************
          implicit double precision (A-H,O-Z)
        dimension Y(5),W(5,18)
        common/PROC/S,PTEMP,R,ERXN,CRXN,VSTAR
        common/PROP/DCOALO,HRXN,A1,B1
        common/rad/ec,etc,es,sig
        external vfcn
C
C  VARIABLES ARE
C  TC=TEMPERATURE OF COAL PARTICLES
C  THE=TEMPERATURE OF SURROUNDING GAS, I.E. HELIUM
C  TTC=TEMPERATURE OF THERMOCOUPLE
C  TS=SCREEN TEMPERATURE
C  TOO=INITIAL TEMPERATURE
C  R=RADIUS OF COAL PARTICLE AND THERMOCOUPLE
C  S=HEATING RATE
C  DT=TIME INCREMENT
          read(8,) S,HRXN,DT,TOL
          read(8, )ERXN,CRXN,VSTAR
          read(8, )ec,etc,es
        R=0.0035
        PTEMP=1000.
        A1=2.20E-10
        B1=6.73E-2
        DCOALO=1.3
        sig= 1.354e-12
        TOO=20.
          write(2,101) S,HRXN,ec,etc,es
101     format(3x,'     HEATING RATE = ',e12.5,/,
     &         3x,'     HEAT OF REACTION= ',e12.5,/,
     &         3x,'     EMISSIVITY OF COAL= ',F5.2,/,
     &         3x,'     EMISSIVITY OF THERMOCOUPLE= ',F5.2,/,
     &         3x,'     EMISSIVITY OF SCREEN= ',F5.2,///)
          write(2,102)
102     format(7x,'T ',11x'TC ',9x,'TTC ',10x,'THE ',10x,'TS ',10x,'VOL ',///)
C
C  INITIAL CONDITIONS ARE
        do 10 I=1,4
10      Y(I)=TOO
        Y(5)=0.
        DTO=DT
C
        T=0.
          tp=(PTEMP - TOO)/S
        N=5
          ifail=0
C
C
C  CCCCCCCCCCCCC  DO LOOP CCCCCCCCCCCCCCCCCCCCCCCCCCCCCCCCCCCCCCCCCCCCCCCCCCC
        do 100 I=1,200
          if(T .gt. tp) DT=DTO*4.0
        TEND=T + DT
          if(T .lt. tp .and. TEND .gt. tp) TEND=tp
```

```
C
          call d02baf(T,TEND,N,Y,TOL,vfcn,W,ifail)
          write(6,)ifail
          write(6,)TOL
          if(TOL .lt. 0) TOL=-TOL
        TC=Y(1)
        TTC=Y(2)
        TS=Y(3)
        THE=Y(4)
        VOAL=Y(5)
C
        write(2,105) T,TC,TTC,THE,TS,VOAL
105     format(3x,6e12.5)
        if (T .gt. 6.) go to 200
100     continue
C
C
200       stop
          end
```

```
C ***************************************************************************
C
C                        SUBROUTINE VFCN
C
C ***************************************************************************
C ***BOUND WITH MAIN PROGRAM ATMTC
C     THIS PROGRAM CALCULATES DERIVATIVES OF THEMPERATURES
C     TO BE CALCULATED
C
          subroutine vfcn(T,Y,YP)
          implicit double precision(A-H, O-Z)
          dimension Y(5),YP(5)
          common/PROC/S,PTEMP,R,ERXN,CRXN,VSTAR
          common/PROP/DCOALO,HRXN,A1,B1
          common/rad/ec,etc,es,sig
C
C       DEFINE TC,TTC, TS, THE INTERSMS OF Y'S
        TC=Y(1)
        TTC=Y(2)
        TS=Y(3)
        THE=Y(4)
        THE1=THE
        VOAL=Y(5)
C
C   Absolute temperatures are
          ATC=TC + 273.13
          ATTC=TTC + 273.13
          ATS=TS + 273.13
          ATHE=THE + 273.13
C
C  DEFINE PYSICAL CONSTANTS
C  THERMAL CONDUTIVITY OF HELIUM
       HEK=6.525E-7*THE + 3.672E-4
C  HEAT TRANSFER COEFFICIENTS ARE
       H1=6.6063E-3/ATHE**0.5
       H2=H1
       H3=H1
C
C   HEAT CAPACITIES ARE
C   COAL
       CPC=0.2228 + 2.18d-4*ATC - 9.7417d3/ATC**2
C   THERMOCOUPLE
       CPTC=0.09882 + 3.035d-5*ATTC
C   SURROUNDING GASES
       CPHE=0.283 + 1.457D-4*THE - 4.082d-8*THE**2
C
C   DENSITIES ARE
       DCOAL=DCOALO*(1. - Y(5))
       DTTC=8.7
       DHE=1.1451D-3
       TP=(PTEMP - 25.)/S
C
C   RADIATIVE HEAT TRANSFER RESISTANCES ARE
         Rc=(1.-ec)/ec + 1.8138 + 0.6046*(1.-es)/es
         Rtc=1./etc
C
C   NOW CALCULATE TEMPERATUERES
```

```
      YP(5)=CRXN*dexp(-ERXN/(1.987*ATC))*(VSTAR - Y(5))
      YP(1)=(3.*H1*(THE - TC)/R + DCOALO*YP(5)*(-HRXN) +
     &       3.*sig*(ATS**4 - ATC**4)/(R*Rc))/(DCOAL*CPC)
      YP(2)=(3.*H2*(THE1 - TTC)/R + 3.*sig*(ATS**4 - ATTC**4)/(R*Rtc))/
     &       (DTTC*CPTC)
      YP(3)=S
      if(T .gt. TP) YP(3)=-A1*ATS**4 - B1*ATS
      YP(4)=(-H1*4.5873*(THE - TC)/R + 1.5291*H3*2.529*(TS - THE)/R +
     &       1.5291*YP(5)*DCOALO)/(DHE*CPHE)
C
C
        return
        end
```